Acta GEODAETICA, GEOPHYSICA et MONTANISTICA

ACADEMIAE SCIENTIARUM HUNGARICAE

ADIUVANTIBUS
G. BARTA
J. VERŐ
J. ZAMBÓ
REDIGIT
A. TÁRCZY-HORNOCH

AKADÉMIAI KIADÓ, BUDAPEST

TOMUS 14
FASCICULI 1—2
1979

ACTA GEODAETICA, GEOPHYSICA et MONTANISTICA

Academiae Scientiarum Hungaricae

A Magyar Tudományos Akadémia Föld- és Bányászati Tudományok Osztályának folyóirata

Szerkesztőség: H-9400 Sopron, Múzeum u. 6.
Kiadja az Akadémiai Kiadó, 1054 Budapest, Alkotmány utca 21.

Az *Acta Geodaetica, Geophysica et Montanistica* eredeti tanulmányokat közöl a geodézia, geofizika és a bányászati tudományok tárgyköréből, angol, német, francia vagy orosz nyelven. Félévenként jelenik meg, évi egy, kb. 400—500 oldalas kötetet alkotva.

Megrendelhető az Akadémiai Kiadónál (1363 Budapest Pf. 24.), a külföld részére pedig a „Kultura" Külkereskedelmi Vállalatnál (1389 Budapest 62, P.O.B. 149).

Acta Geodaetica, Geophysica et Montanistica is a semiannual review of the Hungarian Academy of Sciences, publishing papers on geodesy, geophysics and minings in English, German, French or Russian.

Editorial Office: H-9400 Sopron, Múzeum u. 6.

Subscription: $ 36.00 per year.

Orders may be placed with "Kultura" Foreign Trading Company (1389 Budapest 62, P.O.B. 149) or its representatives abroad.

ACTA GEODAETICA, GEOPHYSICA et MONTANISTICA

ACADEMIAE SCIENTIARUM HUNGARICAE

ADIUVANTIBUS

G. BARTA, J. VERŐ, J. ZAMBÓ

REDIGIT

A. TÁRCZY-HORNOCH

TOMUS 14

AKADÉMIAI KIADÓ, BUDAPEST
1979

ACTA GEODAETICA, GEOPHYSICA et MONTANISTICA

ACADEMIAE SCIENTIARUM HUNGARICAE

ADIUVANTIBUS

G. BARTA, J. VERŐ, J. ZAMBÓ

REDIGIT

A. TÁRCZY-HORNOCH

TOMUS 14

AKADÉMIAI KIADÓ, BUDAPEST
1979

INDEX

Halmos, F.: Geodynamical evaluation of Doppler satellite observations 3

Rinner, K.: Geodetic work and projects at the observatory of Graz—Lustbühel 17

Groten, E.: On variations of geocentric positions with time 31

Hein, G.—Groten, E.: On the use of bandwidth and profile reduction in combination solutions of satellite altimetry 59

Schaab, H.: Investigation of the geoid in Europe by the collocation method 71

Мозжухин, О. А.: Учет рефракции в нивелировании на основе метеорологических измерений 81

Ferencz, Cs.: A possibility of using quasi-single-frequency Doppler — Faraday measurements — A proposal 93

Mentes, Gy.: Development of horizontal pendulum recordings 101

Závoti, J.: Ideas on the practical application of collocation 111

Lichtenegger, H.: Formelsysteme zur Berechnung der Sonnenephemeriden 125

Bácsatyai, L.: Zur Frage der Planung der Höhennetze, mit Rücksicht auf die Erdkrustenbewegungs-Untersuchungen 135

Tárczy-Hornoch, A.—Verő-Hetényi, M.: Adjustment of quadrilaterals computed from electromagnetic distance measurements encumbered by temperature and other meteorological effects 141

Szeidovitz, Gy.: Amplitude and velocity of seismic waves excited by weight dropping ... 149

Metzger, J.: Variations telluriques lentes observées à M'Bour (Sénégal) 155

Csomor, D.—Kiss, Z.—Szeidovitz, Gy.: Dynamics of seismic waves caused by blastings in mines 171

Лебедев, Т. С.—Корчин, В. А.: Упругие характеристики минерального вещества в термобарических условиях земнях недр 181

Märcz, F.: Quasi-periodic variations of ionospheric absorption with characteristic changes during a solar cycle 227

Albu. I.—Mituch, E.—Posgay, K.—Aric, K.—Gutdeutsch, R.: Deutung der refraktionsseismischen Messungen auf dem östlichen Abschnitt des Alpenlängsprofiles 237

Bobok, E.: Investigation of capillary-gravity waves in a thin non-Newtonian film flow by potential-theory method 247

Патварош, Й.: Определение основых парометров эксплуатации скважинами линз боксита в случае конкуренции разносным карьером 257

Balla, L.—Meggyes, T.: On the weighted linearization 267

Boldizsár, T.: Non-electric use of geothermal energy in Hungary 289

Zambó, J.: Über die theoretischen Grundlagen der Wegstreckentrassierung 299

Recensio

Atanasiu, G.: Opere alese (Selected works) — *Wallner, Á.* 311

Asszonyi, Cs.—Kapolyi, L.—Richter, R.: Laboratory determination of rock characteristics. I. Uniaxial compression tests 313

Asszonyi, Cs.—Kapolyi, L.—Huszár, I.: II. Determination of rock characteristics using rheological creep investigation 341

Asszonyi, Cs.—Huszár, I.—Richter, R.: III. Determination of rock characteristics using relaxation tests 361

Asszonyi, Cs.—Huszár, I.—Kapolyi, L.: IV. Triaxial facture tests 379

Recensio

Energetics of geological processes (Eds: S. K. Saxena—S. Bhattacharji) — *A. Ádám* 403

Halmos, F.: Some problems of the connection of networks deduced from satellite observations and of terrestrial networks 405

Hristov, W. K.: Ausgleichung einer mehrmals beobachteten Nivellierungsstrecke nach Bedingungen 417

Bobok, E.—Somosvári, Zs.: Mechanical erosion in flow channels of rocks 421

Patvaros, J.: Feasibility of combined mining technological systems in production of mineral massifs 437

Patvaros, J.: Die Anwendungsmöglichkeiten der Bohrloch-Abbautechnologie bei der Gewinnung der heimischen Bauxitvorkommen 449

Recensio

Moritz, H.—Sünkel, H.: Approximation methods in geodesy — *F. Halmos* 473

Acta Geodaet., Geophys. et Montanist. Acad. Sci. Hung. Tomus 14 (1—2), pp. 3—16 (1979)

GEODYNAMICAL EVALUATION OF DOPPLER SATELLITE OBSERVATIONS

F. HALMOS

DOCTOR OF TECHN. SCIENCES
GEODETIC AND GEOPHYSICAL RESEARCH INSTITUTE OF THE HUNGARIAN ACADEMY OF SCIENCES, SOPRON

[Manuscript received March 14, 1977]

The paper investigates the accuracy and evaluation methods of Doppler satellite observations from a geodynamical point of view. A semi-dynamical method is presented for the adjustment of Doppler shifts which takes the coordinates and velocity vectors of the satellite positions into account in addition to the orbit parameters. The formulas are also deduced for the determination of single points and for the computation of several points together. The number of unknown parameters to be taken into account is analysed and possibilities for the reduction of unknowns are treated. A short analysis of accuracy is also given. In the final part, the paper summarizes the results of practical observations and their reliability from a geodynamical point of view.

1. Introduction

The problems in plate tectonics connect the geodesy with the solution of geodynamical problems. The description of movements is a geodetical task which cannot be separated from the interpretation of plate tectonics. While the classical surveying methods reach a relative accuracy of 10^{-6} on lengths of 50—80 km, the relative accuracy of up-to-date geodetical methods is about 10^{-7} in distances of 1000—5000 km. A greater problem is the determination of relative coordinates in a terrestrial or geocentric system, as tne centre of the coordinates and the orientation of the axis change in time (polar motion). Therefore a task of the near future is to create the theoretical principles of four-dimensional geodesy on a dynamical basis. In spite of the possibility to determine relative height differences with levelling between very distant points with great accuracy (± 3—4 cm per 1000 km), the absolute height determination (e.g. geoid height relative to a reference ellipsoid) is uncertain to several meters due to a difference of sea levels. Therefore the determination of the position on the reference surface is much more accurate than the determination of the elevation component perpendicular to that surface. The continuous control of the initial data of the coordinate system necessitates a world-wide network of observatories for the unambiguous, correct solution of geodynamical problems with astronomical, geophysical and geodetic observations.

For a solution of these problems, observations of the Doppler shift of radiowaves emitted from satellites can be used with success [1]. Lately these measurements reached an accuracy which enables their use for a high-accuracy determination of the components of polar motion [2, 3] in addition to the construction of continental networks and to the determination of the gravity field of the Earth [4].

In the following a solution will be presented which ensures the determination of the change of the relative position with greater accuracy for the study of geodynamical changes, in the framework of a semi-dynamical model.

2. Initial formulas for the geodetical use of Doppler satellite observations

For a determination of the gravity field of the Earth, of the parameters of the Earth and of the relative position of points, first of all the problems of the system of coordinates must be solved. Generally, a geocentric system is used with the commonly used orientation (Fig. 1), where the position of the point in space is given in function of the time t with the basic formula of satellite geodesy:

$$\vec{r}_S(t) = \vec{R}_B(t) + \vec{S}(t) \tag{1}$$

where $\vec{r}_S(t)$ is the spatial geocentric location of the satellite position, S, $\vec{R}_B(t)$ is the geocentric location of the terrestrial observing station, $\vec{S}(t)$ are the topocentric coordinates of the satellite position S in the moment t. Eq. 1 can also be written as:

$$\vec{r}_S(t) = \int_{t_0}^{t} (t - \tau)\, \vec{F}(\tau)\, \mathrm{d}\tau + (t - t_0)\, \dot{\vec{r}}(t_0) + \vec{r}(t_0) =$$

$$= f(t_0;\ \vec{\alpha}_0, \vec{\alpha}_1;\ W_1 \ldots W_n)\,, \tag{2}$$

where the integration constants are the position coordinates and velocity vectors of the satellite ($\vec{r}/t_0$), $\dot{\vec{r}}(t_0)$, and $f(t_0; \vec{\alpha}_0, \vec{\alpha}_1)$) in the moment t_0, $F(\tau)$ means the force function (i.e. effects due to the gravity field of the Earth) in a moment t, $\vec{\alpha}_0$ is the time function of the position vector, $\vec{\alpha}_1$ that of the velocity vector. $W_1 \ldots W_n$ are the parameters of the gravity field. The latter enable, as known, to express the potential of the gravity field W:

$$W = U + T = \frac{kM}{r}\left[1 + \sum_{n=2}^{n_0}\sum_{m=0}^{n}\left(\frac{a}{n}\right)^n \bar{P}_{nm} \sin \Phi \cdot \right.$$

$$\left. \cdot\, (\bar{C}_{nm} \cos m\lambda + \bar{S}_{nm} \sin m\lambda)\right] + \frac{1}{2}(\omega^2 r^2 \cos^2 \Phi) + \iint_{\Sigma} \frac{\Phi}{l}\, d\Sigma\,, \tag{3}$$

where r (radius), Φ, λ mean the geocentric coordinates of the point, k is the gravity constant, M is the mass of the Earth, a is the average equatorial radius when approximating the shape of the Earth by a rotational ellipsoid, $\bar{P}_{nm}$ is the Legendre function of degree n and order m, ω is the angular velocity of the Earth, $\bar{C}_{nm}$ and $\bar{S}_{nm}$ are the normal harmonic coefficients (beginning with the degree n_c). These are therefore terms describing the known part of the potential of the gravity field of the Earth (U). The potential perturbation T is expressed with the method of the simple surface method with unknown density Φ, by

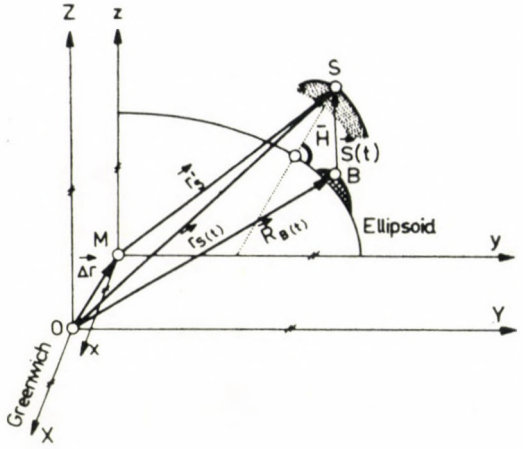


Fig. 1

expanding the surface elements $d\Sigma$ to the whole surface of the Earth, l is the distance of the point with the coordinates r, Φ, λ from the centre of the surface element $d\Sigma$.

Thus, one gets a dynamical model which can be used on the basis of satellite observations for the determination both of terrestrial points and of the gravity field and parameters of the Earth. It should be remarked that the potential harmonics $\bar{C}_{nm}$, $\bar{S}_{nm}$ are in functional connection with the Keplerian elements of the satellite orbit ($\Omega, \omega, i, \ldots$).

3. The use of Doppler observations for a semi-dynamical determination of point positions

The positions of the satellite orbit are given in an inertial system of coordinates. If the observations are carried out in an interval less than 2 weeks, the three-axial geocentric coordinate system can also be used for the description of satellite positions.

In case of integrated Doppler satellite observations the Doppler shift is between the frequencies emitted by the transmitted f_S and received by the receiver f_B:

$$\frac{f_S - f_B}{f_S}$$

which can be used for the determination of the change in distance between transmitter and receiver (ds/dt), i.e. of the velocity $\dot{s}$:

$$\frac{f_S - f_B}{f_S} = -\frac{1}{c}\frac{d}{dt}(|\vec{R}_{B(t)} - \vec{r}_{S(t)}|) + df\,, \tag{4}$$

where c is the velocity of light, t is the time, $\vec{R}_{B_{(t)}}$ the position vector of the terrestrial station, $\vec{r}_{S_{(t)}}$ that of the satellite, and df unites the effects of the ionospheric and tropospheric refractions, of the delay due to the wave propagation, of the timing error (e.g. clock) and of the gravity field. If the carrier frequency f_B is subtracted from the correct reference frequency f_R and then integrated between the moments t_0, t_1 then the distance differences $s_1 - s_0$ can be received (Fig. 2):

$$s_1 = s_0 + \frac{c}{f_S} \Delta N - \frac{c}{f_S} (f_R - f_S)(t_1 - t_0) + \sum_1^5 df \ . \tag{5}$$

From this:

$$N = \int_{t_0}^{t_1} (f_R - f_B)\, dt = \int_{t_0}^{t_1} \left(f_R - f_S + f_S \frac{r}{c} \right) dt =$$

$$= (f_R - f_S)(t_1 - t_0) + f_S (s_1 - s_0) \frac{1}{c} \ . \tag{6}$$

The initial distance s_0 appears in each transit as unknown, or the equations are written for the distance differences $s_1 - s_0$. The latter is not advantageous, as due to the too acute intersections of the distance vectors, the mathematical connections can be ill-conditioned.

Taking into account that in a satellite transit many (at least 100—150) Doppler shifts can be recorded, there is a possibility for an adjustment of the superfluous measurements from which the most probable position vectors (station coordinates) can be deduced. The distance s_1 can be expressed with the geocentric coordinates as unknowns, taking into account the known values in Eq. 6, the unknown distance s_0 and the corrections df. Good approximative values are available for all unknowns, therefore a multiple iteration is seldom necessary.

3.1 *Evaluation of Doppler observations*

It is known that the satellites for the emission of radiowaves (at present 6) transmit their positional data with an accuracy of about 20 m immediately. The US Naval Surface Weapons Center publishes the data of the orbit adjustment of 2 satellites based on Doppler satellite observations of 20 stations, distributed rather uniformly on the surface of the Earth. The ephemerides (position data, e.g. 3 coordinates and 3 velocity vectors in certain time intervals) are given with an accuracy of about 2 m. In possession of these data, several adjustment methods can be used [5, 6, 7, 8].

The determination of a single point, and the translocation (relative determination of the position of two or more points) can be carried out without any restrictions about the orbit of the satellite. The common orbital determination of spatial satellite positions can be made by the methods of short arc mode or

mechanical method, by the translocation method with short arc mode, by the simultaneous method and by the semi-dynamical method [9, 10, 11, 12, 13].

The basis of the semi-dynamical method is the inclusion of data about the satellite orbit and positions into the dynamical model by using fictitious corrections with appropriate weights. If the given ephemerides contain e.g. Keplerian orbital elements, the three-dimensional geocentric coordinates can be immediately computed from them [14].

In order to obtain the model, let us use Eq. 6. According to Fig. 2, the distance s_1 connects the surface station B with the satellite position S_1:

$$s_1 = \{(X_{S_1} - X_B)^2 + (Y_{S_1} - Y_B)^2 + (Z_{S_1} - Z_B)^2\}^{\frac{1}{2}} . \tag{7}$$

Attributing a correction v_s to s_1, and corrections δX, δY, δZ to the preliminary coordinates X, Y, Z, the correction equation is, where the correction δs_0 of the unknown s_0 according to Eq. 5, further the changes of the correction terms are taken into account:

$$v_{s_1} = \delta s_0 + \frac{X'_S - X_{B,0}}{s_{1,0}} (\delta X_S - \delta X_B) + \frac{Y'_S - Y_{B,0}}{s_{1,0}} (\delta Y_S - \delta Y_B) + \\ + \frac{Z'_S - Z_{B,0}}{s_{1,0}} (\delta Z_S - \delta Z_B) + \Sigma \delta f + l_1 , \tag{8}$$

where $s_{0,0}$ is the initial distance, δs_0 is the change of the approximate values, $\Sigma \delta f$ is the change of the different correction coefficients in the course of the adjustment, X'_S, Y'_S, Z'_S are the known satellite positional coordinates, $X_{B,0}$, $Y_{B,0}$, $Z_{B,0}$ the preliminary coordinates of the observing stations, δX, δY, δZ the changes of them in the adjustment. The free term l_1 contains the values corresponding to the right-hand approximations of Eq. 8, further the approxi-

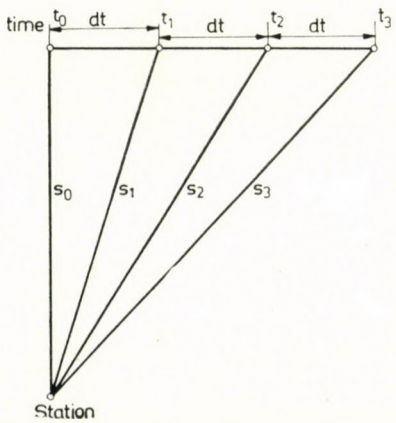


Fig. 2

mate distance $s_{1,0}$ computed from the approximative coordinates ($l_1 = s_1' - s_{1,0} + s_{0,0}$). Here s_1' is the measured value, $s_{1,0}$ the value computed from the approximative coordinates. As the satellite positions X_S, Y_S, Z_S are supposed to be known, the corrections $\delta X_S = v_{X_S} \ldots$ are introduced:

$$v_{s_1} = \delta s_0 + \Sigma \delta f + \frac{X_S' - X_{B,0}}{s_{1,0}} (v_{X_{S_1}} - \delta X_B) +$$

$$+ \frac{Y_S' - Y_{B,0}}{s_{1,0}} (v_{Y_S} - \delta Y_B) + \frac{Z_S' - Z_{B,0}}{s_{1,0}} (v_{Z_S} - \delta Z_B) + l_1 . \qquad (9)$$

As the final aim is the determination of the δX_B, δY_B, δZ_B unknown changes of the terrestrial stations within the adjustment, therefore the corrections v are not needed. The corrections in the equations are all different, therefore they can be united in a fictitious correction $\underline{\lambda}$. In matrix formulation the coefficients δX, δY, δZ in Eq. 9 are denoted by $\mathbf{a}$, and the correction $\mathbf{v}_{s_1}$, $\mathbf{v}_{X_S}$:

$$\mathbf{v}_{s_1} - \mathbf{a}\mathbf{v}_{X_S} = -\underline{\lambda} \quad \text{or} \quad \mathbf{A}\mathbf{v} = -\underline{\lambda}, \qquad (10)$$

where $\mathbf{a}$ symbolizes the diagonal matrix of the coefficients of $\mathbf{v}_{X_S}$ in Eq. 9. If a variance $\mathbf{Q}_{s_1 s_1}$ is attributed to $\mathbf{s}_1$, and $\mathbf{Q}_{X_S X_S}$ to $\mathbf{v}_{X_S}$ then the variance-covariance matrix of the $\underline{\lambda}$ fictitious corrections is:

$$\mathbf{Q}_{\lambda\lambda} = \mathbf{Q}_{s_1 s_1} + \mathbf{a}^2 \mathbf{Q}_{X_S X_S} = \mathbf{A}\mathbf{Q}\mathbf{A}^T . \qquad (11)$$

The method of the solution is supposed in the following as known. If one has good approximate values for the corrections $\delta\mathbf{f}$, then by correcting the measurement data by them, the change $\delta\mathbf{f}$ can be eliminated from the adjustment. It should be remarked that at present the model errors of the adjustment methods, and the incorrect mathematical and physical description of the correctional unknowns cause the greatest regular and irregular errors in the computed results. The solution presented here is a more rigorous solution than those published hitherto.

3.11 *The semi-dynamical solution*

In case of very precise ephemerides, the satellite positions $\mathbf{X}_S$ can be supposed as known. Let us denote them by $\mathbf{X}_S'$. The corrections $\mathbf{v}_{X_S}$ and the changes $\delta\mathbf{X}_S$ are attributed to them simultaneously. In that case in matrix form:

$$\mathbf{X}_S = \mathbf{X}_S' + \mathbf{v}_{X_S} + \delta\mathbf{X}_S . \qquad (12)$$

If the initial time t_0 is the centre of the satellite crossing, then in any time t is valid that $t - t_0 = \bar{t}$. In function of the latter, a polynomial can be written

for all point-like positions of the satellite (advantageously an orthogonal polynomial), which must be fulfilled by the satellite positions $\mathbf{X}_S$ [15, 10, 11].

$$\mathbf{X}_{S_t} = \mathbf{X}_{S_0} + \dot{\mathbf{X}}_S \bar{t} + \frac{1}{2} \ddot{\mathbf{X}}_S \bar{t}^2 + \ldots = \underline{\alpha}_0 + \underline{\alpha}_1 \bar{t} + \underline{\alpha}_2 \bar{t}^2 + \ldots \tag{13}$$

By introducing approximate values (with indices 0) and changes:

$$\begin{aligned} \mathbf{X}_{S_t} &= \mathbf{v}_{X_S} + \delta\mathbf{X}_S + \delta\dot{\mathbf{X}}_S \bar{t} + \frac{1}{2} \ddot{\mathbf{X}}_S \bar{t}^2 + \\ &+ \left\{ \mathbf{X}'_{S_0} + \mathbf{X}_{S,0} \bar{t} + \frac{1}{2} \ddot{\mathbf{X}}_{S0} \bar{t}^2 + \ldots \right\} = \\ &= \mathbf{v}_{X_S} + \underline{\delta\alpha}_0 + \underline{\delta\alpha}_1 \bar{t} + \underline{\delta\alpha}_2 \bar{t}^2 + \\ &+ \left\{ \underline{\alpha}_{0.0} + \underline{\alpha}_{1,0} \bar{t} + \underline{\alpha}_{2.0} \bar{t}^2 + \ldots . \right\} . \end{aligned} \tag{14}$$

$\underline{\lambda}_1$, $\underline{\alpha}_0$, $\underline{\alpha}_1$, $\underline{\alpha}_2$, $\underline{\delta\alpha}_0$, $\underline{\delta\alpha}_1$, $\underline{\delta\alpha}_2$ are matrices.

Substituting Eq. 14 into Eq. 9 one gets in a more detailed form:

$$\begin{aligned} v_{S_1} &- \frac{X_S - X_B}{s_1} v_{X_{S_1}} + \frac{Y_S - Y_B}{s_1} v_{Y_{S_1}} + \frac{Z_S - Z_B}{s_1} v_{Z_{S_1}} = \delta s_0 + \Sigma\delta f + \\ &+ \frac{X_{S_1} - X_B}{s_1} (-\delta X_B) + \frac{Y_{S_1} - Y_B}{s_1} (-\delta Y_B) + \frac{Z_{S_1} - Z_B}{s_1} (-\delta Z_B) + \\ &+ \frac{X_{S_1} - X_B}{s_1} \delta\alpha_0 + \frac{Y_{S_1} - Y_B}{s_1} \delta\beta_0 + \frac{Z_{S_1} - Z_B}{s_1} \delta\gamma_0 + \\ &+ \frac{X_{S_1} - X_B}{s_1} \bar{t}\delta\alpha_1 + \frac{Y_{S_1} - Y_B}{s_1} \bar{t}\delta\beta_1 + \frac{Z_{S_1} - Z_B}{s_1} \bar{t}\delta\gamma_1 + \\ &+ \frac{X_{S_1} - X_B}{s_1} \bar{t}^2\delta\alpha_2 + \frac{Y_{S_1} - Y_B}{s_1} \bar{t}^2\delta\beta_2 + \frac{Z_{S_1} - Z_B}{s_1} \bar{t}^2\delta\gamma_2 + \\ &+ \left\{ s'_1 - s_{1,0} + s_{0,0} \right\} , \end{aligned} \tag{15}$$

where $s_{i,0}$ is the approximate distance determined from the satellite positional coordinate according to the polynomial approximation and from the station coordinates s'_1 is the distance according to function 5 from the observations with the approximate reductions.

If we introduce the notation

$$\frac{X_S - X_B}{s_1} = a \,, \quad \frac{Y_S - Y_B}{s_1} = b \,, \quad \frac{Z_S - Z_B}{s_1} = c \quad \text{for:}$$

$$\begin{aligned} v_{S_1} &- a v_{X_{S_1}} - b v_{Y_{S_1}} - c v_{Z_{S_1}} = \delta s_0 + \Sigma\delta f - a\delta X_B - b\delta Y_B - c\delta Z_B + \\ &+ a\delta\alpha_0 + b\delta\beta_0 + c\delta\gamma_0 + a\bar{t}\delta\alpha_1 + b\bar{t}\delta\beta_1 + c\bar{t}\delta\gamma_1 + a\bar{t}^2\delta\alpha_2 + \\ &+ b\bar{t}^2\delta\beta_2 + c\bar{t}^2\delta\gamma_2 + (s'_1 - s_{1,0} + s_{0,0}) . \end{aligned} \tag{16}$$

By introducing the matrix notation $\mathbf{v}_{s_1} - \mathbf{a}\mathbf{v}_{X_{s_1}} = -\underline{\lambda}_1$, the known $\mathbf{Q}_{\lambda_1\lambda_1}$ variance-covariance matrix can be used.

If the time measurements get also a correction $\mathbf{v}_{\bar{t}}$, the left- hand side of Eq. 15 will be:

$$\mathbf{v}_{s_1} + \dot{\mathbf{s}}_1\mathbf{v}_{\bar{t}} - \mathbf{a}\mathbf{v}_{X_{s_1}} = -\underline{\lambda}_1 \,, \tag{17a}$$

where $\dot{\mathbf{s}}_1$ is the value of the velocity. The variance-covariance matrix is:

$$\mathbf{Q}_{\lambda_1\lambda_1} = \mathbf{Q}_{s_1s_1} + \mathbf{s}_1^2\mathbf{Q}_{\bar{t}\bar{t}} + \mathbf{a}^2\mathbf{Q}_{X_{s_1}X_{s_1}} \,. \tag{17b}$$

If the velocities $\dot{\mathbf{X}}_S$ are also supposed to be known and they get also corrections, then in addition to Eq. 12, the substitution

$$\dot{\mathbf{X}}_S = \dot{\mathbf{X}}'_S + \mathbf{v}_{X_S} + \delta\dot{\mathbf{X}}_S = \underline{\alpha}_1 + \mathbf{v}_{\alpha_1} + \underline{\delta\alpha}_1 \tag{12a}$$

must also be made. $\mathbf{v}_{X_S}$ and $\dot{\mathbf{v}}_{X_S}$ unites the positional random errors, $\delta\mathbf{X}_S$, $\delta\dot{\mathbf{X}}_S$ the model errors. Thus one gets from Eq. 15:

$$\begin{aligned} &v_{s_1} - av_{X_{s_1}} - bv_{Y_{s_1}} - cv_{Z_{s_1}} - a\bar{t}v_{\alpha_1} - b\bar{t}v_{\beta_1} - c\bar{t}v_{\gamma_1} = \delta s_0 + \\ &+ \Sigma\delta f - a\delta X_B - b\delta Y_B - c\delta Z_B + a\delta\alpha_0 + b\delta\beta_0 + c\delta\gamma_0 + \\ &+ a\bar{t}\delta\alpha_1 + b\bar{t}\delta\beta_1 + c\bar{t}\delta\gamma_1 + a\bar{t}^2\delta\alpha_2 + b\bar{t}^2\delta\beta_2 + c\bar{t}^2\delta\gamma_2 + l_1 \,. \end{aligned} \tag{15'}$$

Instead of Eq. 17 one has, introducing here also the fictitious corrections $\underline{\lambda}_1$:

$$\mathbf{v}_{s_1} - \mathbf{a}\mathbf{v}_{Xs_1} - \mathbf{a}\bar{t}\mathbf{v}_{\alpha_1} = -\underline{\lambda}_1 \tag{17a'}$$

taking into account that:

$$\mathbf{Q}_{\lambda_1\lambda_1} = \mathbf{Q}_{s_1s_1} + \mathbf{a}^2\mathbf{Q}_{Xs_1Xs_1} + \mathbf{a}^2\bar{t}^2\mathbf{Q}_{\alpha_1\alpha_1} \,. \tag{17b'}$$

Eq. 17a has the following form:

$$\mathbf{v}_{s_1} + \dot{\mathbf{s}}\mathbf{v}_{\bar{t}} - \mathbf{a}\mathbf{v}_{Xs_1} - \mathbf{a}\bar{t}\mathbf{v}_{\alpha_1} = -\underline{\lambda}_1 \tag{17a''}$$

and by taking this into account in Eq. 17b:

$$\mathbf{Q}_{\lambda_1\lambda_1} = \mathbf{Q}_{s_1s_1} + \mathbf{s}_1^2\mathbf{Q}_{\bar{t}\bar{t}} + \mathbf{a}^2\mathbf{Q}_{X_{s_1}X_{s_1}} + \mathbf{a}^2\,\bar{t}^2\,\mathbf{Q}_{\alpha_1\alpha_1} . \tag{17b''}$$

Let us analyse the coefficients and unknowns from the point of view of matrix constuction:

$$\begin{array}{ccccccccccccccc} \textcircled{0} & & \textcircled{1} & & \textcircled{2} & & \textcircled{3} & & & & \textcircled{4} & & & & \\ -\underline{\lambda}_1 & = & \delta\mathbf{s}_0 & + & \delta\mathbf{f} & - & \mathbf{a}\delta\mathbf{X}_B & & + & & \mathbf{a} & \underline{\delta\alpha}_0 & & + & \\ (1,\ 1) & & (1,\ 1) & & (1,\ 1) & & (1,\ 3) & (3,\ 1) & & & (1,\ 3) & (3,\ 1) & & & \\ & & \textcircled{5} & & & & & \textcircled{6} & & & & \textcircled{7} & & & \\ + & & \mathbf{a} & \bar{t} & \underline{\delta\alpha}_1 & + & \mathbf{a} & \bar{t}^2 & \underline{\delta\alpha}_2 & + & l_1 & & & & \\ & & (1,\ 3) & (3,\ 3) & (3,\ 1) & & (1,\ 3) & (3,\ 3) & (3,\ 1) & & (1,\ 1) & & & & \end{array} \tag{18}$$

where (0) is fictitious correction,

(1) the change of the initial distance for each crossing, its coefficient is $\mathbf{B}^{(1)}$,

(2) the changes of the corrections, being in good approximation equal to zero; their coefficient is $\mathbf{B}^{(2)}$,

(3) the coordinates of the terrestrial station, with the coefficient $\mathbf{B}^{(3)}$,

(4) the changes of the satellite coordinates in the moment t_0 with the coefficient $\mathbf{B}^{(4)}$,

(5) the changes of the satellite velocities with the coefficients $\mathbf{B}^{(5)}$,

(6) the changes of the satellite accelerations with the coefficients $\mathbf{B}^{(6)}$,

(7) the free term of the equation.

3.12 *The construction of the normal equations*

Up to now, the correction equations have been written for general observation equations. During a crossing, 100—150 Doppler shifts can be measured, where all unknowns are constant with the exception of the corrections $\mathbf{v}$, $\underline{\lambda}$, only the coefficients change when including the new measurements. If the coefficients are distinguished with figure brackets when departing from a single measurement in case of all observations from the station 1 and by imagining the unit matrix $\mathbf{E} = 1$, beside $\underline{\lambda}_1$ one has:

$$\mathbf{E}\underline{\lambda}_i = \left\{\mathbf{B}_1^{(1)}\right\} \delta\mathbf{s}_{0,1} + \left\{\mathbf{B}_1^{(2)}\right\} \delta\mathbf{f}_1 + \left\{\mathbf{B}_1^{(3)}\right\} \delta\mathbf{X}_1 + \\ + \left\{\mathbf{B}_1^{(4)}\right\} \underline{\delta\alpha}_0 + \left\{\mathbf{B}_1^{(5)}\right\} \underline{\delta\alpha}_1 + \left\{\mathbf{B}_1^{(6)}\right\} \underline{\delta\alpha}_2 + \left\{\mathbf{l}_1\right\}. \tag{19}$$

The same is in case of the i-th terrestrial station observing the same crossing:

$$\mathbf{E}\underline{\lambda}_i = \left\{\mathbf{B}_i^{(1)}\right\} \delta\mathbf{s}_{0,1} + \left\{\Sigma\mathbf{B}_i^{(2)}\right\} \delta\mathbf{f}_i + \left\{\mathbf{B}_i^{(3)}\right\} \delta\mathbf{X}_i + \\ + \left\{\mathbf{B}_i^{(4)}\right\} \underline{\delta\alpha}_0 + \left\{\mathbf{B}_i^{(5)}\right\} \underline{\delta\alpha}_1 + \left\{\mathbf{B}_i^{(6)}\right\} \underline{\delta\alpha}_2 + \left\{\mathbf{l}_i\right\}. \tag{20}$$

As not only one, but several crossings are naturally included in the determination, the crossings are distinguished by Roman numbers as indices (i.e. there is a third index beside the index i and the index of the orbital parameter, denoting the number of the crossing). Let us unite the orbital parameters for a crossing in a common unknown ($\underline{\delta\alpha}$), its coefficient will be $\mathbf{B}_i^{(4)}$. In case of several crossings, the variance-covariance matrix belonging to $\underline{\lambda}_{ij}$ is:

$$\left\{\mathbf{Q}_{\lambda_i\lambda_i}\right\} = \left\{\mathbf{A}_i\right\} \mathbf{Q}_i \left\{\mathbf{A}_i\right\}^T \tag{21}$$

According to the notations used hitherto, the stations B will be denoted by 1, 2, . . ., i, . . . N;

the satellite crossings I, II, . . ., k, . . . ν;

the point-like positions of the satellite by 0, 1, 2, . . ., j, . . . n.

Let us suppose that Doppler measurements are made from the terrestrial station B during k crossings (it can happen that some stations do not make any

measurements during certain crossings; in such cases after each interruption in a crossing a new initial distance δs_0 should be introduced as unknown). The values $\delta s_{0,i}$, $\delta \mathbf{f}_i$ and $\delta \mathbf{X}_i$ change for each observing station. According to Fig. 1, the origin of the coordinate system ($\mathbf{X}_0$) is introduced as unknown (its coefficient is $\frac{\partial \mathbf{r}}{\partial \mathbf{x}}$). Let its change in the adjustment be $\delta \mathbf{X}_0$, and its coefficient $\{\mathbf{B}_{ik}^{(5)}\}$. In that case one gets an undetermined system of equations (free adjustment), which can be solved if the 6 conditions referring to 3-dimensional networks are added [6, 16, 17]. The first group of the normal equations is taking into account the variance-covariance matrix (22).

If the unknowns which occur only in data of one transit ($\delta \mathbf{s}_{01}$, $\delta \mathbf{f}_1$, $\underline{\delta \alpha}_1$) are united in a common unknown $\delta \mathbf{X}_1$, and its coefficient is denoted by $\mathbf{B}^{(1)}$, then one gets the matrix (23).

The normal equations of the other stations can be written similarly. The unknowns are most advantageously grouped so that the unknowns of one transit and one station should be next to each other. Thus e.g. the connecting unknowns of several stations observing the same transit are the common orbital parameters ($\underline{\delta \alpha}$). The unknown changes of the station coordinates shall be included into the row following $\delta \underline{\mathbf{X}}_1$. If the observations of another group of stations for other transits should also be included into the adjustment, taking the common origin of the coordinate system into account, a normal matrix similarly to Eq. 23 is valid. That means that the minor matrix is repeated always meaning a cyclic repetition on the computer, thus being advantageous. In that case all equations are united by the common unknown $\delta \mathbf{X}_0$ of the change of the origin [6].

The six supplementary equations to the free adjustment matrix found so (singular matrix) can be obtained by the following method [18]: if the normal matrix of the first group is denoted by $\mathbf{N}$, and its unknowns by $\mathbf{X}$, the free terms by $\mathbf{L}$, then:

$$\begin{bmatrix} \mathbf{N} & \mathbf{K}^T \\ \mathbf{K} & \mathbf{0} \end{bmatrix} \begin{bmatrix} \mathbf{X} \\ \overline{\mathbf{X}} \end{bmatrix} + \begin{bmatrix} \mathbf{L} \\ \mathbf{0} \end{bmatrix} = \mathbf{0} \tag{24}$$

where

$$\mathbf{K} = \left[\begin{array}{ccc|ccc|ccc} 1 & 0 & 0 & 1 & 0 & 0 & 1 & 0 & 0 \\ 0 & 1 & 0 & 0 & 1 & 0 & 0 & 1 & 0 \\ 0 & 0 & 1 & 0 & 0 & 1 & 0 & 0 & 1 \\ 0 & Z_1 & -Y_1 & 0 & Z_2 & -Y_2 & 0 & Z_N & -Y_N \\ -Z_1 & 0 & X_1 & -Z_2 & 0 & X_2 & -Z_N & 0 & X_N \\ Y_1 & -X_1 & 0 & Y_2 & -X_2 & 0 & Y & -X_N & 0 \end{array}\right]. \tag{25}$$

and the supplementary unknowns are $\overline{\mathbf{X}}$. For the determination of the variance-covariance matrix after the adjustment, a simple method has been presented

$$
\begin{array}{llllll}
\left[\mathbf{B}^{(1)T}\mathbf{Q}_{\lambda\lambda}^{-1}\mathbf{B}^{(1)}\right]_{1,\mathrm{I}}\delta\mathbf{s}_{01,\mathrm{I}}+ & & +\left[\mathbf{B}^{(1)T}\mathbf{Q}_{\lambda\lambda}^{-1}\mathbf{B}^{(2)}\right]_{1,\mathrm{I}}\delta\mathbf{f}_{1,\mathrm{I}}+ & & +\left[\mathbf{B}^{(1)T}\mathbf{Q}_{\lambda\lambda}^{-1}\mathbf{B}^{(4)}\right]_{1,\mathrm{I}}\underline{\delta\boldsymbol{\alpha}_1}+ & +\left[\mathbf{B}^{(1)T}\mathbf{Q}_{\lambda\lambda}^{-1}\mathbf{B}^{(3)}\right]_{1,\mathrm{I}}\delta\mathbf{X}_1+\left[\mathbf{B}^{(1)T}\mathbf{Q}_{\lambda\lambda}^{-1}\mathbf{B}^{(3)}\right]_{1,\mathrm{I}}\delta\mathbf{X}_0+\left[\mathbf{B}^{(1)T}\mathbf{Q}_{\lambda\lambda}^{-1}\mathbf{I}\right]_{1,\mathrm{I}}=\mathbf{0}\\
\left[\mathbf{B}^{(1)T}\mathbf{Q}_{\lambda\lambda}^{-1}\mathbf{B}^{(1)}\right]_{1,\mathrm{II}}\delta\mathbf{s}_{01,\mathrm{II}}+ & & +\left[\mathbf{B}^{(1)T}\mathbf{Q}_{\lambda\lambda}^{-1}\mathbf{B}^{(2)}\right]_{1,\mathrm{II}}\delta\mathbf{f}_{1,\mathrm{II}}+ & & +\left[\mathbf{B}^{(1)T}\mathbf{Q}_{\lambda\lambda}^{-1}\mathbf{B}^{(4)}\right]_{1,\mathrm{II}}\underline{\delta\boldsymbol{\alpha}_2}+ & +\left[\mathbf{B}^{(1)T}\mathbf{Q}_{\lambda\lambda}^{-1}\mathbf{B}^{(3)}\right]_{1,\mathrm{II}}\delta\mathbf{X}_1+\left[\mathbf{B}^{(1)T}\mathbf{Q}_{\lambda\lambda}^{-1}\mathbf{B}^{(5)}\right]_{1,\mathrm{II}}\delta\mathbf{X}_0+\left[\mathbf{B}^{(1)T}\mathbf{Q}_{\lambda\lambda}^{-1}\mathbf{I}\right]_{1,\mathrm{II}}=\mathbf{0}\\
\vdots & & & & & \vdots\\
 & \left[\mathbf{B}^{(1)T}\mathbf{Q}_{\lambda\lambda}^{-1}\mathbf{B}^{(4)}\right]_{1,k}\delta\mathbf{s}_{01,k}+ & & +\left[\mathbf{B}^{(1)T}\mathbf{Q}_{\lambda\lambda}^{-1}\mathbf{B}^{(2)}\right]_{1,k}\delta\mathbf{f}_{1,k}+ & & +\left[\mathbf{B}^{(1)T}\mathbf{Q}_{\lambda\lambda}^{-1}\mathbf{B}^{(4)}\right]_{1,k}\underline{\delta\boldsymbol{\alpha}_k}+\left[\mathbf{B}^{(1)T}\mathbf{Q}_{\lambda\lambda}^{-1}\mathbf{B}^{(3)}\right]_{1,k}\delta\mathbf{X}_1+\left[\mathbf{B}^{(1)T}\mathbf{Q}_{\lambda\lambda}^{-1}\mathbf{B}^{(3)}\right]_{1,k}\delta\mathbf{X}_0+\left[\mathbf{B}^{(1)T}\mathbf{Q}_{\lambda\lambda}^{-1}\mathbf{I}\right]_{1,k}=\mathbf{0}\\
\left[\mathbf{B}^{(1)T}\mathbf{Q}_{\lambda\lambda}^{-1}\mathbf{B}^{(2)}\right]_{1,\mathrm{I}}\delta\mathbf{s}_{01,\mathrm{I}}+ & & +\left[\mathbf{B}^{(2)T}\mathbf{Q}_{\lambda\lambda}^{-1}\mathbf{B}^{(2)}\right]_{1,\mathrm{I}}\delta\mathbf{f}_{1,\mathrm{I}}+ & & +\left[\mathbf{B}^{(2)T}\mathbf{Q}_{\lambda\lambda}^{-1}\mathbf{B}^{(4)}\right]_{1,\mathrm{I}}\underline{\delta\boldsymbol{\alpha}_1}+ & +\left[\mathbf{B}^{(2)T}\mathbf{Q}_{\lambda\lambda}^{-1}\mathbf{B}^{(3)}\right]_{1,\mathrm{I}}\delta\mathbf{X}_1+\left[\mathbf{B}^{(2)T}\mathbf{Q}_{\lambda\lambda}^{-1}\mathbf{B}^{(5)}\right]_{1,\mathrm{I}}\delta\mathbf{X}_0+\left[\mathbf{B}^{(2)T}\mathbf{Q}_{\lambda\lambda}^{-1}\mathbf{I}\right]_{2,\mathrm{I}}=\mathbf{0}\\
\left[\mathbf{B}^{(1)T}\mathbf{Q}_{\lambda\lambda}^{-1}\mathbf{B}^{(2)}\right]_{1,\mathrm{II}}^{T}\delta\mathbf{s}_{01,\mathrm{II}}+ & & +\left[\mathbf{B}^{(2)T}\mathbf{Q}_{\lambda\lambda}^{-1}\mathbf{B}^{(2)}\right]_{1,\mathrm{II}}\delta\mathbf{f}_{1,\mathrm{II}}+ & & +\left[\mathbf{B}^{(2)T}\mathbf{Q}_{\lambda\lambda}^{-1}\mathbf{B}^{(4)}\right]_{1,\mathrm{II}}\underline{\delta\boldsymbol{\alpha}_2}+ & +\left[\mathbf{B}^{(2)T}\mathbf{Q}_{\lambda\lambda}^{-1}\mathbf{B}^{(3)}\right]_{1,\mathrm{II}}\delta\mathbf{X}_1+\left[\mathbf{B}^{(2)T}\mathbf{Q}_{\lambda\lambda}^{-1}\mathbf{B}^{(5)}\right]_{1,\mathrm{II}}\delta\mathbf{X}_0+\left[\mathbf{B}^{(2)T}\mathbf{Q}_{\lambda\lambda}^{-1}\mathbf{I}\right]_{1,\mathrm{II}}=\mathbf{0}\\
\vdots & & & & & \vdots\\
 & \left[\mathbf{B}^{(1)T}\mathbf{Q}_{\lambda\lambda}^{-1}\mathbf{B}^{(2)}\right]_{1,k}^{T}\delta\mathbf{s}_{01,k}+ & & +\left[\mathbf{B}^{(1)T}\mathbf{Q}_{\lambda\lambda}^{-1}\mathbf{B}^{(1)}\right]_{1,k}\delta\mathbf{f}_{1,k}+ & & +\left[\mathbf{B}^{(2)T}\mathbf{Q}_{\lambda\lambda}^{-1}\mathbf{B}^{(4)}\right]_{1,k}\underline{\delta\boldsymbol{\alpha}_k}+\left[\mathbf{B}^{(2)T}\mathbf{Q}_{\lambda\lambda}^{-1}\mathbf{B}^{(3)}\right]_{1,k}\delta\mathbf{X}_1+\left[\mathbf{B}^{(2)T}\mathbf{Q}_{\lambda\lambda}^{-1}\mathbf{B}^{(5)}\right]_{1,k}\delta\mathbf{X}_0+\left[\mathbf{B}^{(2)T}\mathbf{Q}_{\lambda\lambda}^{-1}\mathbf{I}\right]_{1,k}=\mathbf{0}\\
\left[\mathbf{B}^{(2)T}\mathbf{Q}_{\lambda\lambda}^{-1}\mathbf{B}^{(4)}\right]_{1,\mathrm{I}}^{T}\delta\mathbf{s}_{01,\mathrm{I}}+ & & +\left[\mathbf{B}^{(2)T}\mathbf{Q}_{\lambda\lambda}^{-1}\mathbf{B}^{(4)}\right]_{1,\mathrm{I}}^{T}\delta\mathbf{f}^{1,\mathrm{I}}+ & & +\left[\mathbf{B}^{(4)T}\mathbf{Q}_{\lambda\lambda}^{-1}\mathbf{B}^{(4)}\right]_{1,\mathrm{I}}\underline{\varrho\boldsymbol{\alpha}_1}+ & +\left[\mathbf{B}^{(4)T}\mathbf{Q}_{\lambda\lambda}^{-1}\mathbf{B}^{(3)}\right]_{1,\mathrm{I}}\delta\mathbf{X}_1+\left[\mathbf{B}^{(4)T}\mathbf{Q}_{\lambda\lambda}^{-1}\mathbf{B}^{(5)}\right]_{1,\mathrm{I}}\delta\mathbf{X}_0+\left[\mathbf{B}^{(4)T}\mathbf{Q}_{\lambda\lambda}^{-1}\mathbf{I}\right]_{1,\mathrm{I}}=\mathbf{0}\\
\left[\mathbf{B}^{(1)T}\mathbf{Q}_{\lambda\lambda}^{-1}\mathbf{B}^{(4)}\right]_{1,\mathrm{II}}^{T}\delta\mathbf{s}_{01,\mathrm{II}}+ & & +\left[\mathbf{B}^{(2)T}\mathbf{Q}_{\lambda\lambda}^{1}\mathbf{B}^{(4)}\right]_{1,\mathrm{II}}^{T}\delta\mathbf{f}_{1,\mathrm{II}}+ & & +\left[\mathbf{B}^{(4)T}\mathbf{Q}_{\lambda\lambda}^{-1}\mathbf{B}^{(4)}\right]_{1,\mathrm{II}}\underline{\delta\boldsymbol{\alpha}_2}+ & +\left[\mathbf{B}^{(4)T}\mathbf{Q}_{\lambda\lambda}^{-1}\mathbf{B}^{(3)}\right]_{1,\mathrm{II}}\delta\mathbf{X}_1+\left[\mathbf{B}^{(4)T}\mathbf{Q}_{\lambda\lambda}^{-1}\mathbf{B}^{(5)}\right]_{1,\mathrm{II}}\delta\mathbf{X}_0+\left[\mathbf{B}^{(4)T}\mathbf{Q}_{\lambda\lambda}^{-1}\mathbf{I}\right]_{1,\mathrm{II}}=\mathbf{0}\\
\vdots & & & & & \vdots\\
 & \left[\mathbf{B}^{(1)T}\mathbf{Q}_{\lambda\lambda}^{-1}\mathbf{B}^{(4)}\right]_{1,k}^{T}\delta\mathbf{s}_{01,k}+ & & +\left[\mathbf{B}^{(2)T}\mathbf{Q}_{\lambda\lambda}^{-1}\mathbf{Q}^{(4)}\right]_{1,\mathrm{II}}\delta\mathbf{f}_{1,k}+ & & +\left[\mathbf{B}^{(4)T}\mathbf{Q}_{\lambda\lambda}^{-1}\mathbf{B}^{(4)}\right]_{1,k}\underline{\delta\boldsymbol{\alpha}_k}+\left[\mathbf{B}^{(4)T}\mathbf{Q}_{\lambda\lambda}^{-1}\mathbf{B}^{(3)}\right]_{1,k}\delta\mathbf{X}_1+\left[\mathbf{B}^{(4)T}\mathbf{Q}_{\lambda\lambda}^{-1}\mathbf{B}^{(5)}\right]_{1,k}\delta\mathbf{X}_0+\left[\mathbf{B}^{(4)T}\mathbf{Q}_{\lambda\lambda}^{-2}\mathbf{I}\right]_{1,k}=\mathbf{0}\\
\left[\mathbf{B}^{(1)T}\mathbf{Q}_{\lambda\lambda}^{-1}\mathbf{B}^{(5)}\right]_{1,\mathrm{I}}^{T}\delta\mathbf{s}_{01,\mathrm{I}}+\left[\mathbf{B}^{(1)T}\mathbf{Q}_{\lambda\lambda}^{-1}\mathbf{B}^{(3)}\right]_{1,\mathrm{II}}^{T}\delta\mathbf{s}_{01,\mathrm{II}}+\ldots+\left[\mathbf{B}^{(1)T}\mathbf{Q}_{\lambda\lambda}^{-1}\mathbf{B}^{(3)}\right]_{1,k}^{T}\delta\mathbf{s}_{01,k}+\left[\mathbf{B}^{(2)T}\mathbf{Q}_{\lambda\lambda}^{-1}\mathbf{B}^{(3)}\right]_{1,\mathrm{I}}^{T}\delta\mathbf{f}_{1,\mathrm{I}}+\left[\mathbf{B}^{(2)T}\mathbf{Q}_{\lambda\lambda}^{-1}\mathbf{B}^{(3)}\right]_{1,\mathrm{II}}^{T}\delta\mathbf{f}_{1,\mathrm{II}}+\ldots+\left[\mathbf{B}^{(2)T}\mathbf{Q}_{\lambda\lambda}^{-1}\mathbf{B}^{(3)}\right]_{1,k}^{T}\delta\mathbf{f}_{1,k}+\left[\mathbf{B}^{(2)T}\mathbf{Q}_{\lambda\lambda}^{-1}\mathbf{B}^{(4)}\right]_{1,\mathrm{I}}^{T}\underline{\delta\boldsymbol{\alpha}_1}+\left[\mathbf{B}^{(2)T}\mathbf{Q}_{\lambda\lambda}^{-1}\mathbf{B}^{(4)}\right]_{1,\mathrm{II}}^{T}\underline{\delta\boldsymbol{\alpha}_2}+\ldots+\left[\mathbf{B}^{(2)T}\mathbf{Q}_{\lambda\lambda}^{-1}\mathbf{B}^{(4)}\right]_{1,k}^{T}\underline{\varrho\boldsymbol{\alpha}_k}+\left[\mathbf{B}^{(3)T}\mathbf{Q}_{\lambda\lambda}^{-1}\mathbf{B}^{(3)}\right]_{1}\delta\mathbf{X}_1+\left[\mathbf{B}^{(3)T}\mathbf{Q}_{\lambda\lambda}^{-1}\mathbf{B}^{(5)}\right]_{1}\delta\mathbf{X}_0+\left[\mathbf{B}^{(3)T}\mathbf{Q}_{\lambda\lambda}^{-1}\mathbf{I}\right]_{1}=\mathbf{0}\\
\left[\mathbf{B}^{(1)T}\mathbf{Q}_{\lambda\lambda}^{-1}\mathbf{B}^{(5)}\right]_{1,\mathrm{I}}^{T}\delta\mathbf{s}_{01,\mathrm{I}}+\left[\mathbf{B}^{(1)T}\mathbf{Q}_{\lambda\lambda}^{-1}\mathbf{B}^{(5)}\right]_{1,\mathrm{II}}^{T}\delta\mathbf{s}_{01,\mathrm{II}}+\ldots+\left[\mathbf{B}^{(1)T}\mathbf{Q}^{-1}\mathbf{B}^{(5)}\right]_{1,k}^{T}\delta\mathbf{s}_{01,k}+\left[\mathbf{B}^{(1)T}\mathbf{Q}_{\lambda\lambda}^{-1}\mathbf{B}^{(5)}\right]_{1,\mathrm{I}}^{T}\delta\mathbf{f}_{1,\mathrm{I}}+\left[\mathbf{B}^{(2)T}\mathbf{Q}_{\lambda\lambda}^{-1}\mathbf{B}^{(5)}\right]_{1,\mathrm{II}}^{T}\delta\mathbf{f}_{1,\mathrm{II}}+\ldots+\left[\mathbf{B}^{(2)T}\mathbf{Q}_{\lambda\lambda}^{1}-\mathbf{B}^{(5)}\right]_{1,k}^{T}\delta\mathbf{f}_{1,k}+\left[\mathbf{B}^{(2)T}\mathbf{Q}_{\lambda\lambda}^{-1}\mathbf{B}^{(4)}\right]_{1,\mathrm{I}}^{T}\underline{\delta\boldsymbol{\alpha}_1}+\left[\mathbf{B}^{(2)T}\mathbf{Q}_{\lambda\lambda}^{-1}\mathbf{B}^{(5)}\right]_{1,\mathrm{II}}^{T}\underline{\delta\boldsymbol{\alpha}_2}+\ldots+\left[\mathbf{B}^{(2)T}\mathbf{Q}_{\lambda\lambda}^{-1}\mathbf{B}^{(5)}\right]_{1,k}^{T}\underline{\delta\boldsymbol{\nu}_k}+\left[\mathbf{B}^{(3)T}\mathbf{Q}_{\lambda\lambda}^{-1}\mathbf{B}^{(5)}\right]_{1}\delta\mathbf{X}_1+\left[\mathbf{B}^{(5)T}\mathbf{Q}_{\lambda\lambda}^{-1}\mathbf{B}^{(5)}\right]_{4}\delta\mathbf{X}_0+\left[\mathbf{B}^{(5)T}\mathbf{Q}_{\lambda\lambda}^{-1}\mathbf{I}\right]_{1}=\mathbf{0}
\end{array}
\tag{22}
$$

$$
\begin{aligned}
&\left[\overline{\mathbf{B}}^{(1)T}\mathbf{Q}_{\lambda\lambda}^{-1}\mathbf{B}^{(1)}\right]_{1,\mathrm{I}}\delta\overline{\mathbf{X}}_{\mathrm{I}} && && +\left[\overline{\mathbf{B}}^{(1)T}\mathbf{Q}_{\lambda\lambda}^{-1}\mathbf{B}^{(3)}\right]_{1,\mathrm{I}}\delta\mathbf{X}_1+\left[\overline{\mathbf{B}}^{(1)T}\mathbf{Q}_{\lambda\lambda}^{-1}\mathbf{B}^{(5)}\right]_{1,\mathrm{I}}\delta\mathbf{X}_0+\left[\overline{\mathbf{B}}^{(1)T}\mathbf{Q}_{\lambda\lambda}^{-1}\mathbf{1}\right]_{1,\mathrm{I}}=\mathbf{0}\\
&\left[\overline{\mathbf{B}}^{(1)T}\mathbf{Q}_{\lambda\lambda}^{-1}\mathbf{B}^{(1)}\right]_{1,\mathrm{II}}\delta\overline{\mathbf{X}}_{\mathrm{II}} && && +\left[\overline{\mathbf{B}}^{(1)T}\mathbf{Q}_{\lambda\lambda}^{-1}\mathbf{B}^{(3)}\right]_{1,\mathrm{II}}\delta\mathbf{X}_1+\left[\overline{\mathbf{B}}^{(1)T}\mathbf{Q}_{\lambda\lambda}^{-1}\mathbf{B}^{(5)}\right]_{1,\mathrm{II}}\delta\mathbf{X}_0+\left[\overline{\mathbf{B}}^{(1)T}\mathbf{Q}_{\lambda\lambda}^{-1}\mathbf{1}\right]_{1,\mathrm{II}}=\mathbf{0}\\
&\qquad\vdots\\
&\left[\overline{\mathbf{B}}^{(1)T}\mathbf{Q}_{\lambda\lambda}^{-1}\mathbf{B}^{(1)}\right]_{1,k}\delta\overline{\mathbf{X}}_k && && +\left[\overline{\mathbf{B}}^{(1)T}\mathbf{Q}_{\lambda\lambda}^{-1}\mathbf{B}^{(3)}\right]_{1,k}\delta\mathbf{X}_1+\left[\overline{\mathbf{B}}^{(1)T}\mathbf{Q}_{\lambda\lambda}^{-1}\mathbf{B}^{(5)}\right]_{1,k}\delta\mathbf{X}_0+\left[\overline{\mathbf{B}}^{(1)T}\mathbf{Q}_{\lambda\lambda}^{-1}\mathbf{1}\right]_{1,k}=\mathbf{0} \qquad (23)\\
&\left[\overline{\mathbf{B}}^{(1)T}\mathbf{Q}_{\lambda\lambda}^{-1}\mathbf{Q}^{(3)}\right]_{1,\mathrm{I}}^{T}\delta\overline{\mathbf{X}}_{\mathrm{I}}+\left[\overline{\mathbf{B}}^{(1)T}\mathbf{Q}_{\lambda\lambda}^{-1}\mathbf{B}^{(3)}\right]_{1,\mathrm{II}}^{T}\delta\overline{\mathbf{X}}_{\mathrm{II}}+\cdots+\left[\overline{\mathbf{B}}^{(1)T}\mathbf{Q}_{\lambda\lambda}^{-1}\mathbf{B}^{(3)}\right]_{1,k}^{T}\delta\overline{\mathbf{X}}_k+\left[\overline{\mathbf{B}}^{(3)T}\mathbf{Q}_{\lambda\lambda}^{-1}\mathbf{B}^{(3)}\right]_{1}\delta\mathbf{X}_1+\left[\overline{\mathbf{B}}^{(3)T}\mathbf{Q}_{\lambda\lambda}^{-1}\mathbf{B}^{(5)}\right]_{1}\delta\mathbf{X}_0+\left[\overline{\mathbf{B}}^{(3)T}\mathbf{Q}_{\lambda\lambda}^{-1}\mathbf{1}\right]_{1}=\mathbf{0}\\
&\left[\overline{\mathbf{B}}^{(1)T}\mathbf{Q}_{\lambda\lambda}^{-1}\mathbf{B}^{(5)}\right]_{1,\mathrm{I}}^{T}\delta\overline{\mathbf{X}}_{\mathrm{I}}+\left[\overline{\mathbf{B}}^{(1)T}\mathbf{Q}_{\lambda\lambda}^{-1}\mathbf{B}^{(5)}\right]_{1,\mathrm{II}}^{T}\delta\overline{\mathbf{X}}_{\mathrm{II}}+\cdots+\left[\overline{\mathbf{B}}^{(1)T}\mathbf{Q}_{\lambda\lambda}^{-1}\mathbf{B}^{(5)}\right]_{1,k}^{T}\delta\overline{\mathbf{X}}_k+\left[\overline{\mathbf{B}}^{(3)T}\mathbf{Q}_{\lambda\lambda}^{-1}\mathbf{B}^{(5)}\right]_{1}^{T}\delta\mathbf{X}_1+\left[\overline{\mathbf{B}}^{(5)T}\mathbf{Q}_{\lambda\lambda}^{-1}\mathbf{B}^{(5)}\right]_{1}\delta\mathbf{X}_0+\left[\overline{\mathbf{B}}^{(5)T}\mathbf{Q}_{\lambda\lambda}^{-1}\mathbf{1}\right]_{1}=\mathbf{0}.
\end{aligned}
$$

[6], though it should be remarked that any program solving the generalized inverses assures the unique solution of the problem. A solution with a system of coordinates according to the conditions 25 ensures an optimal variance-covariance matrix in case of the given configuration and observations (i.e. this is a solution of mass centre).

3.13 *Accuracy analysis of the data*

On the basis of the given ephemerides a smoothing of the orbit can be carried out, i.e. the coefficients of Eq. 13 can be determined from the orbital data. For sake of simplicity let us denote them by Roman letters $\mathbf{a}_0$, $\mathbf{a}_1$, $\mathbf{a}_2$ [10]. These can be compared with the computed coefficients $\underline{\alpha}_0$, $\underline{\alpha}_1$, $\underline{\alpha}_2$, ... According to the experiences the difference of $\mathbf{a}_0$ and $\underline{\alpha}_0$, of $\mathbf{a}_1$ and $\underline{\alpha}_1$ can be neglected [6, 19]. If the mathematical model is good then the deviations in the higher-order terms cannot be great either, only amounts which are allowed by the random measurement errors. The values $\mathbf{a}_0$, $\mathbf{a}_1$, $\mathbf{a}_2$ can be essentially regarded as theoretical orbital values according to the Keplerian laws. Thus taking the difference of second-order terms of the two polynomials from the orbital data and from the adjustment one gets the model errors of the computational formulas used. In order to check whether model errors or random errors are present, one uses the variance-covariance matrix of the difference on the basis of the variance-covariance matrix of the coefficients. If the latter is in its absolute value less than the difference determined from the two equations, then a model error must be supposed.

3.14 *Computation demand of the semi-dynamical method*

The lowest demand of computations emerges in the simple point determination method.

If the observations of several transits and stations are adjusted together, then the number of unknowns increases significantly. Thus the following unknowns appear if the transit of 100 satellites are measured at 4 stations, in each transit with the measurement of 100 Doppler shifts, if one introduces 9 path parameters:

$3 \times 4 = 12$ station coordinates,
$9 \times 100 = 900$ orbital parameters,
$4 \times 5 \times 100 = 2000$ correction unknowns,
$4 \times 100 = 400$ initial unknown distances,
$1 \times 3 = 3$ unknowns for the origin of the coordinates.

The number of the correctional unknowns can be significantly reduced if the approximative values can be accepted as final ones (e.g. drift in respect of a

time etalon). In that case the number of the remaining model unknowns is 1315. Using appropriate submatrices (partitioning) the solution can be carried out with a medium-capacity computer.

4. Results of Doppler satellite observations and their geodynamical aspects

Several experiments have been made for the geodetic use of Doppler satellite observations. This short summary tries to show the accuracy levels of the methods used hitherto. From among them, only the most important ones shall be mentioned.

BROWN [5] reported data of the short orbital sector adjustment from 5 North-American stations, using 15 satellite transits, where the average coordinate deviations were 0.91 m, 0.21 m and 0.23 m. The errors of the simple point determination are about five times of those when adjusting many points together.

If the Doppler observations are arranged optimally, an analysis of the model errors to be expected has been given in [6]. From the results presented there it is clear that by making observations in a network from 20—25 stations with 4 instruments during 20—25 days, a mean square error of the coordinates of ± 0.5 m can be ensured.

SIGL [20] reported recently on the experimental observations of the European satellites ESRO and EDOC. The mean square coordinate errors were in the first case

$$\mu_X = \pm 0.8 \text{ m}, \qquad \mu_Y = \pm 1.0 \text{ m}, \qquad \mu_Z = \pm 0.7 \text{ m},$$

and in the second case

$$\mu_X = \pm 0.3 \text{ m}, \qquad \mu_Y = \pm 0.6 \text{ m}, \qquad \mu_Z = \pm 0.4 \text{ m}.$$

KOUBA and BOAL [7] examined the mean square errors of coordinate differences between those from terrestrial surveying measurements and those by satellite observations, using 3 cases with 6 stations, and 30—60 satellite transits. The Φ, λ and h values are the following: | 0.02 | — | 0.19 | m; | 0.09 | — — | 0.13 | m; | 0.46 | — | 1.39 | m. The average of the mean square errors is: $\pm 0.10 - 0.22$ m, $\pm 0.17 - 0.22$ m, $\pm 0.14 - 0.31$ m. Two Doppler observations have also been compared. The mean square errors in Φ, λ and h are ± 0.21 m, ± 0.15 m, ± 0.05 m. The mean square errors on the coordinates in a Canadian network consisting of 200 stations (with distances between the stations of 200 — 500 km) are: ± 0.60 m, ± 0.43 m, ± 0.54 m.

In the Canadian network further 300 stations have been recently determined with Doppler observations [21]. The average distance of the stations is 300 km. The mean square errors of the coordinates are ± 0.6 m, ± 0.8 m and ± 1.2 m. The number of the satellite observations was 30. In Canada Doppler observations are widely used in the practice.

ANDERLE [22] determined recently polar motions of 60 cm with a mean square error of ± 25 cm.

MOOSE [23] investigated the possibilities of the stiffening of first- and second-order geodetic networks at distances of 250 km with the help of Doppler points in the US network. He found that the positional and orientation errors decrease with the square root of the number of Doppler points. The scale error is inversely proportional with the distance between Doppler stations. The stiffening points deduced from Doppler observations substitute the azimuths and base lines of the network. A common adjustment of geodetical surface measurements and Doppler observations ensures a mean square point error of ± 0.5 m.

Taking into account the present accuracy of Doppler satellite observations, it can be stated that for geodynamical purposes, motions with velocities around 5 cm/year can be determined only with measurements in a longer space of time (10—15 years). It can be supposed that in case of relative position determinations the accuracy can be increased and motions of some cm/year can be determined in shorter time intervals.

It is clear that the importance of Doppler satellite observations in geodynamics consists in the future not only in investigation of polar motions, but also in the study of motion of terrestrial points. This will be the case if the Doppler satellite observation will have an accuracy superior to the present one.

Taking into account that the motions of terrestrial points are bound to certain coordinate systems, at first the basic theoretical problems of the reference system must be studied together with the accuracy problems of their practical determination (polar motions, temporal variations of the gravity field, temporal variations of the origin of the reference system in respect to the mass center of the Earth, etc.). As long as these problems are not cleared by theoretical investigations and by data of different kinds of up-to-date observatories, the changes of the positions determined by up-to-date geodynamical observations have a relative character. In order to ensure the determination of absolute motions (these are best approximated up to now by data deduced from satellite geodetic or cosmical geodetic observations), a more close cooperation of astronomical, geodetical, geophysical and geological investigations is necessary.

REFERENCES

1. ANDERLE, R. I.: Transformation of terrestrial survey data to Doppler satellite datum. *Journal of Geophysical Research*, 79 (1974), 5319—5331.
2. ANDERLE, R. I.: Determination of polar motion from satellite observations. *Geophys. Surv.* (1973), 147—161.
3. CAPITAINE, N.: Resultats de l'expérience TRAPOL détermination du pole par des observations Doppler en une seule station. *Géodésie de Spatiale, Paris, Bull.* No. 9 (1973).
4. KOCH, K. R.: Earth's gravity field and station coordinates from Doppler data, satellite triangulation and gravity anomalies. NOAA Technical Report No. 62. Rockville, Md. 1974.

5. BROWN, D. C.: Doppler surveying with the JMR-1 receiver. *Bulletin Géodésique*, 50 (1976), 9—25.
6. HALMOS, F.: Methodical problems of the geodetical use of Doppler satellite observations. Seminar on Satellite Geodesy, Sopron, Hungary, 1976. *Geodézia és Kartográfia* (in press).
7. KOUBA, J.—BOAL, J. D.: The Canadian Doppler satellite network. Int. Geodetic Symposium on Satellite Doppler Positioning, New Mexico, 1976. Presented paper.
8. WELLS, D. E.: Doppler satellite control. Technical Report 29. New Brunswick, 1974.
9. BROWN, D. C.—TROTTER, J. E.: SAGA, A Computer Program for Short Arc Geodetic Adjustment of Satellite Observations. 1969, AFCRL.
10. WOLF, H.: Computation of satellite triangulation by fitting of the orbit. Deutsche Geodätische Kommission, Reihe B., Nr. 153 (1967).
11. HALMOS, F.—KÁDÁR, I.—KARSAY, F.: The evaluation of asynchronous and synchronous satellite observations by orthogonal polynomials. Fifteenth Meeting of the Commission for Multilateral Cooperation between the Academies of Sciences of the Socialis Countries Dealing with the Problems "Scientific Researches Using Observations of Artificial Satellites of the Earth", Bucharest, 7—13, June 1970, No. 11, 115—148.
12. KOUBA, J.—WELLS, D. E.: Semi-dynamical Doppler satellite positioning. *Bulletin Géodésique*, 50 (1976), 27—42.
13. ANDERLE, R. I.: Error model for geodetic positions derived from Doppler satellite observations. *Bulletin Géodésique*, 50 (1976), 43—77.
14. KAULA, W. M.: Theory of Satellite Geodesy. Blaisdell Publ. Comp., London, 1966.
15. BROWN, D. C.—TROTTER, G.: Precise determination of geodetic positions by the method of continuous traces. Air Force Cambridge Research Laboratory. Melbourne, 1967.
16. MEISSL, P.: Zusammenfassung und Ausbau der inneren Fehlertheorie eines Punkthaufens. Deutsche Geodätische Kommission, Reihe A, No. 61, München, 1969.
17. MUELLER, I. I.—GELDER, B. H.—KUMAR, M.: Error analysis for the proposed close grid geodynamic satellite measurement system (CLOGEOS). OSU Dep. of Geodetic Science, Report No. 230 (1975).
18. RINNER, K.—KILLIAN, P.—MEISSL, P.: Beiträge zur Theorie der geodätischen Netze im Raum. Deutsche Geodätische Kommission, Reihe A, No. 61, München, 1969.
19. EHRNSPERGER, W.: Numerische Erfahrungen bei der Berechnung von Bahnparametern für die räumliche Glättung bei Short Arcs. Bayerische Komm. f. Erdmessung, H. 32, 1974.
20. SIGL, R.: Aktuelle Aufgaben der Satellitengeodäsie. *Z. f. Vermessungswesen*, (1977), 20—40.
21. WELLS, D. E.—KRAKIWSKY, E. I.—THOMSON, D. B.: Review of Doppler satellite positioning in Canada. *Bulletin Géodésique*, 50 (1976), 307—321.
22. ANDERLE, R. I.: Polar motion determined by Doppler satellite observations. *Bulletin Géodésique*, 50 (1976) 377—390.
23. MOOSE, R. E.: Effect of Geoceiver observations. NOAA Technical Report No. 66, Rockville, Md. 1976.

ГЕОДИНАМИЧЕСКАЯ ОБРАБОТКА ДОППЛЕРОВСКИХ СПУТНИКОВЫХ НАБЛЮДЕНИЙ

Ф. ХАЛМОШ

РЕЗЮМЕ

В статье рассматриваются точность и методы обработки допплеровских спутниковых наблюдений с геодинамической точки зрения. Задается полудинамический метод для уравнения допплеровских сдвигов, который кроме параметров орбиты учитывает и координаты, и вектор скоростей положения спутника. Формулы выведены также для определения отдельных пунктов, а также совместного определения нескольких пунктов. Анализируется число учитываемых неизвестных параметров. Исследуются возможности для уменьшения числа неизвестных. Кратко анализируется и точность. В последней части подытоживаются результаты практических наблюдений и их надежность с геодинамической точки зрения.

Acta Geodaet., Geophys. et Montanist. Acad. Sci. Hung. Tomus 14 (1—2), pp. 17—29 (1979)

GEODETIC WORK AND PROJECTS AT THE OBSERVATORY OF GRAZ-LUSTBÜHEL

K. RINNER

TECHNISCHE UNIVERSITÄT, GRAZ, AUSTRIA

[Manuscript received August 31, 1977]

An observatory has been constructed at Lustbühel near Graz, Austria, where, among others, geodetic observations of satellites are made with a BMK 75 camera and a Doppler, measuring equipment (Marconi). The observatory is described here, its activities are reported on, and the objectives of the station are explained. Graz-Lustbühel will be the Austrian geodynamic station to take part in international projects for determining geodetic and physical parameters of earth and their variations.

1. Description of the observatory

The observatory at Graz-Lustbühel was completed in December 1976. Research equipments of the Institutes of Astronomy, Meteorology and Geophysics, National Surveying and Photogrammetry, Telecommunication Engineering and Wave Propagation of the Universities in Graz and of the Institute for Space Research of the Austrian Academy of Sciences are accommodated at this observatory.

The observatory is situated on a grassy hill 491 m above sea level, about 5 km east of the centre of the town of Graz (200,000 inhabitants). The area of about 2 hectares is screened off from the town by a group of 20 m high trees, in the other directions the view is unhindered.

The observatory has two domes mounted on a flat roof for astronomic and geodetic observations and below them, in two floors, office and laboratory rooms. Figs 1a, b, c show the situation of the observatory and its building structure.

In the western dome a BMK 75 camera Zeiss, (Oberkochen) is installed for making direction observations to geodetic satellites as well as for directions of small planets of the earth. The eastern dome is intended to

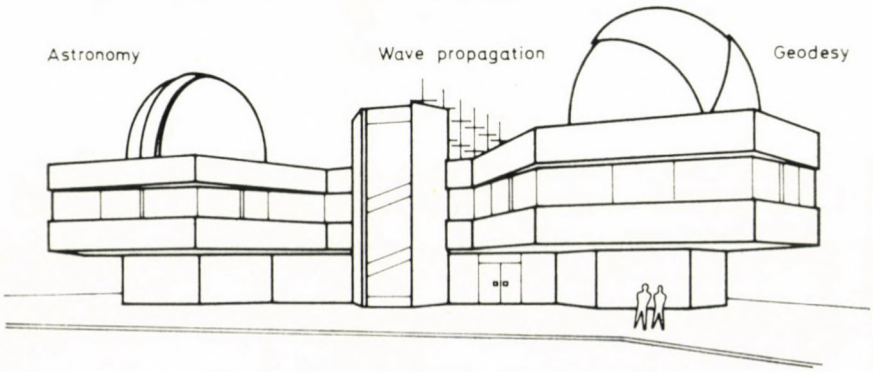


Fig. 1a. Space observatory Graz-Lustbühel

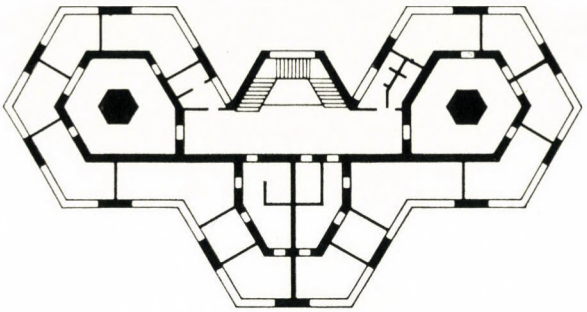


Fig. 1b. Horizontal projection, scale 1 : 250

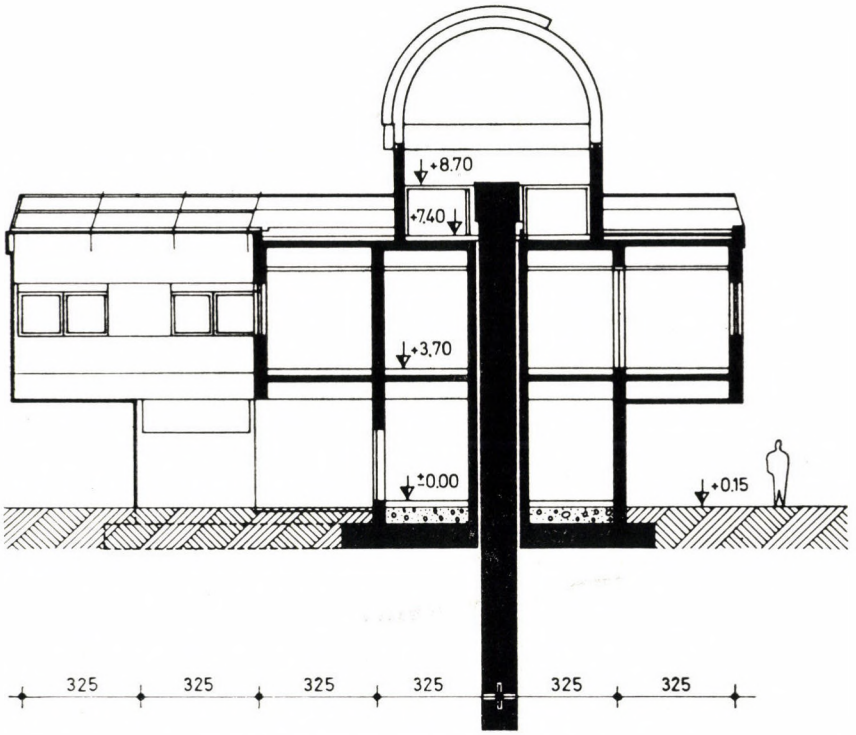


Fig. 1c. Intersection, scale 1 : 125

special astronomic work such as the observation of small celestial bodies of the solar system and position determinations (for practising). Between the two domes there are aerials for the geodetic Doppler measuring apparatus. A PSK II stereocomparator Zeiss, (Oberkochen) with automatic recording is available for measuring image coordinates.

The Institute of Meteorology and Geophysics has installed radar and Doppler sets for stationary satellites and for satellites revolving around the

earth to obtain data on the electron density and on the structure of the ionosphere and to study models therefore.

The Institute of Telecommunication, Engineering and Wave Propagation is concerned with telecommunication satellites and the propagation of long and superlong waves. For the former task a ground station with a 3 m parabolic mirror was erected for frequencies of 10 GHz. It is used for studying the properties of telecommunication transmission via satellites for radio and TV within national and international projects. Refined propagation models and, in conjunction with rocket experiments, structural problems of the ionosphere are investigated with the aid of a receiving station for long and superlong waves (20 to 100 kHz). The cesium frequency standard (accuracy ± 1 sec) acquired for this purpose is available to all institutes.

At the Graz-Lustbühel observatory scientists of various disciplines of various scientific institutions are working on occasional tasks and using the research equipment jointly. This form of scientific cooperation, being new to Austria, has been instigated by a shortness of research facilities. The overcoming of traditional particularism must be regarded as an "Austrian miracle" and is rather promising for the future. The joint use of instruments, laboratories and office rooms, a cooperation in carrying out research projects and a permanent exchange of experience by the various institutes make expect a high degree of economic efficiency for the new facilities.

2. Geodetic objectives

The geodetic section of the Graz-Lustbühel observatory is established to study problems of scientific geodesy, particularly satellite geodesy. Besides, it is planned to work out suggestions for applying the latest geodetic findings to the practical work of the Austrian surveying authorities. This should be effected through cooperation in international geodetic projects, in the observation and analysis of data, as well as by contributions of theory and operating techniques. Of course, the geodetic objectives of the Graz-Lustbühel observatory are bound to the general trends of development in geodetic research.

It is still the task of geodesy to carry out the geometric description, distribution and representation of the earth's surface and of natural and artificial objects thereon, and to determine the parameters of the earth's gravity field. But there is also an increasing demand for determining the variations of these quantities as a function of time and the variation trends.

The geodetic statements are derived from information (measuring data) determined by geometric measurements (angles, distances directions), astronomic measurements (longitude, latitude, azimuth), and gravimetric measurements (gravity values, gradients) as well as techniques of remote sensing (photogrammetry, radar-grammetry). Processing this information is carried

out (increasingly) by automatic systems with the use of increasingly complex mathematical and physical models. By increasing the accuracy of measuring data and reducing the time for obtaining and processing them it will (in many cases) be possible to repeat the geodetic statement of short intervals, thus determining variations of the state variables as a function of time as well as the respective trends. Therefore, geodesy can also make statements on global and local phenomena of motion in the earth's crust, thus providing contributions to study the dynamic behaviour of the earth, determining deformations of natural and artificial objects, early recognizing changes in our environment, and avoiding catastrophes.

For this task, integral systems are needed for obtaining and processing data, including various methods of eliminating systematic influences. They should be used to establish a system of control points of maximum accuracy that is superior to the former control systems and also includes operative satellites of high accuracy. From these points it will be possible define local variations and to determine geodetic fundamentals for studying national problems of geodynamics and geophysics. The objective is speeding up geodetic statement and increasing its accuracy; the final objective will be real-time reporting.

Any country may take part in this development; international cooperarion that is required already now, will become even stronger in the future. Natutally, countries with geodetic tradition such as Austria will have to fulfill a special task: they will have to make their data available to the developing countries and consult them in founding their own systems.

The geodetic tasks are, however, different for developing and traditional countries. In the developing countries it will be necessary to establish as quickly as possible, with the aid of integrated self-controlling systems, control points as a basis for subsequent geodetic operations for economy, technology and administration. This will conveniently be done in development phases based on each other. In the 1st phase, operative satellite systems will be mainly used. In the 2nd phase, completion will be carried out by terrestrial techniques and geodetic inertial systems. In the 3rd phase, methods of aerotriangulation and radar-grammetry will be applied and the system of control points currently integrated, completed and improved. In the 4th phase, the desired final state will be achieved by joint adjustment of all measuring data.

As a rule, the countries with geodetic tradition already dispose of control points for position, height and gravity values. In these countries it will be necessary to determine, in another (5th) phase, control points of higher accuracy to take account of the dynamic and tectonic behaviour of earth. The required nets of zeroth order are connected to global geostations and secured by national geostations. Also for this task, integral methods of terrestrial and satellite geodesy will be used. Permanent observations at the geostations and, at certain intervals, repeat observations for the connecting nets should be made.

By this demand the national surveying authorities will be faced with new tasks. They will mean the beginning of a new phase aiming at intensifying the geodetic, astronomic and gravimetric measurements and defining the geoid as a basis for reducing the measured quantities and as a contribution to geophysical exploration.

Scientific geodesy will have to develop systems by which measuring and computing procedures should be automatized and the reporting effected in the shortest possible time. To eliminate systematic error influences, integral systems will be sought making possible a thorough control by the simultaneous application of different measuring and computing systems or by mathematical self-calibration.

With these systems geodesy will be able to keep on exercising its control function in the field of geosciences, economy and technology. Its statements will serve, also in the future, as bases for the statements of other disciplines. Geodesy will keep on acting as a "notary public of earth" enjoying the confidence of geosciences and geotechnology.

From these general statements follow the general directions for the geodetic objectives of the Graz-Lustbühel observatory:

a) The observatory is to be a station within a world system of geostations controlling the dynamic behaviour of earth by means of geodetic techniques.

b) The observatory is to take part, for Austria, in international research projects. Corresponding to the position of Austria as a neutral country, participation will be likewise desirable in eastern and western projects.

c) The observatory is to carry out permanent measurement to satellites, to establish the terrestrial geodetic connection to geostations in neighbouring countries, and to repeat all these at intervals of about 10 years.

d) Starting from the observatory a net of zeroth order is planned superior to the Austrian national net of 1st order. From this net detailed nets will be deduced for tectonically active areas to be measured at certain time intervals.

e) The experience and results obtained at the observatory are to be used to improve the structure of the geodetic nets in Austria and to forecast the local behaviour of the earth's crust.

f) The equipment of the observatory and the results obtained there should be made available to developing countries as a contribution of Austria to the geodetic development.

3. Activities performed to date

At present, direction measurements are being made at the geostation of Graz-Lustbühel with a ballistic camera (BMK 75) as well as Doppler measurements with the (Marconi-) measuring equipment for GEOS C and the TRANET

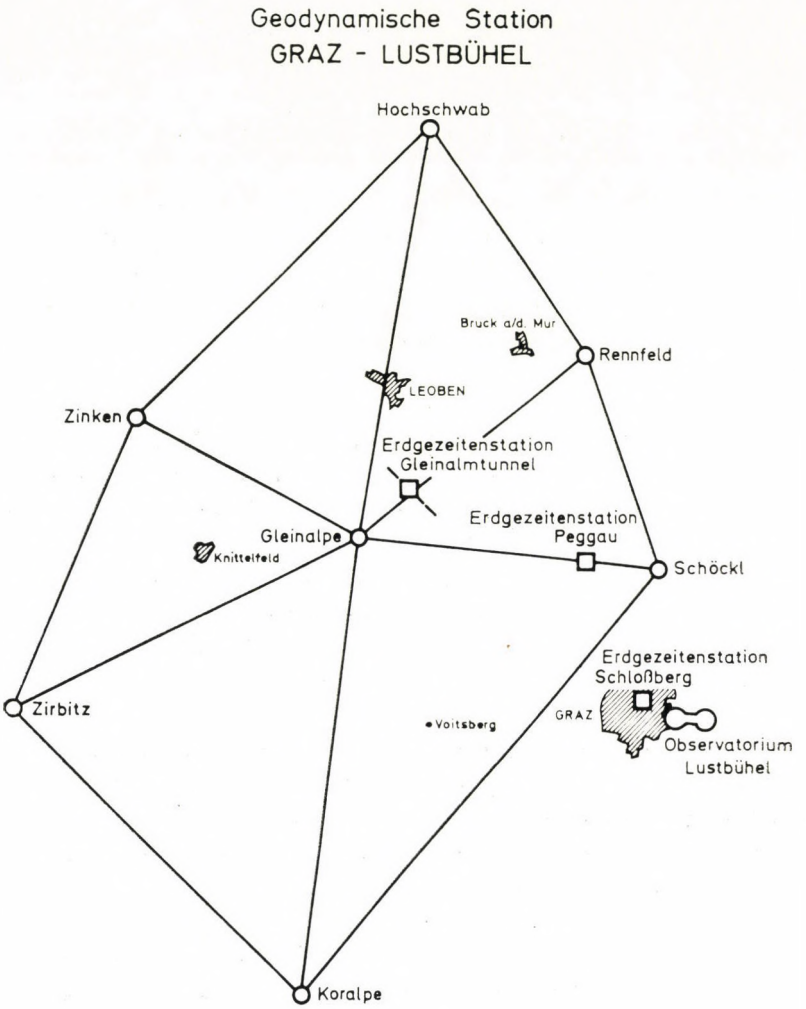


Fig. 2

system. They are complemented by the recording of terrestrial tides at two stations near the observatory, a three-dimensional test net (Styria) in the farthersurroundings, and preparatory work for later laser and interferometric measurements (see Fig. 2).

3.1 *Photographic direction finding*

Optical direction finding to satellites by photographic connection to fixed stars at present cannot exceed an accuracy of 1 ppm; it provides, however, the orientation of the terrestrial system in the superior astronomic equatorial system. Besides, it offers the advantage of using the numerous information of

astronomy and of introducing — beside a refraction theory — no further assumptions on the structure of earth or space. The directions found are (in conjunction with time measurements) absolutely oriented in space. They correspond to gyro-directions in terrestrial geodesy, making possible an orientation to the meridian plane and the rotational axis of earth, thus supporting terrestrial statements in spite of lower measuring accuracy, or to pendulum measurements determining the level of gravimeter measurements more accurate by one or two powers of ten. In spite of the higher accuracy of laser, Doppler or interferometric distances, the potential of space-oriented directions is at least equivalent for the formation of geometric nets.

Therefore, methods of direction finding to satellites by photographic connection to fixed stars will be required in the future, too, for supporting and controlling superior dynamic systems.

The efficiency of BMK of the 1st generation was investigated and proved in the PAGEOS project. An increased accuracy of statement may be expected from further improvements of the apparatus and the utilization of the experiences.

The BMK 75 is equipped with an ASTRO-TOPAR object lens (focal length 750 mm) and a maximum relative aperture of 1 : 2.5. The image size is 18×18 cm, the plates can be exchanged automatically. The camera is mounted parallactically according to the Zeiss-Coudé refractor system, the sidereal resetting is effected with the aid of a control device. With a 1 : 2.5 relative aperture it is possible to observe satellites of 8th and stars of 16th magnitude. The camera contains an eight-disc rotating shutter, the mean opening time is recorded and registered with a resolution of 10 μ/sec. The camera is also equipped with a device for the follow-up of comets.

Test observations on the satellites EXPLORER 19, KOSMOS 44, PAGEOS (rest piece), RADCAT and SALYJUT 4, with sidereal resetting and

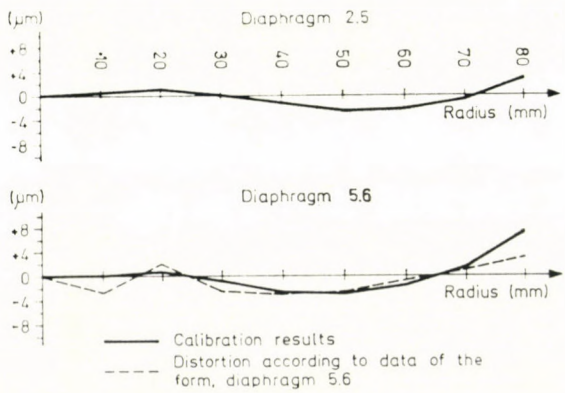


Fig. 3. BMK 75: Radial distortion

exposure times of more than 30 sec, yielded optimum imaging of stars of magnitude 6.5. Distortion was defined from star observations with 1 : 2.5 and 1 : 5.6 diaphragms and compared with data of the firm (Zeiss). The result represented in Fig. 3 shows a maximum distortion of 3 μm.

To find out the full capacity of the BMK series (40 and 75), the measurements in a BMK test net were agreed with the German Geodetic Research Institute in Munich with stations in Berlin, Bonn, Wettzell and Graz. The Polish Academy of Sciences agreed to a project of connecting the stations at Graz and Borowiec and of taking part in a short-arc project. Cooperation in Interkosmos



simultaneous with:	number
Brüssel	10
Kopenhagen	9
Meudon	7
Straßburg	35
Bordeaux	6
Nizza	10
Goult	4
Braunschweig	22
Frankfurt	59
Karlsruhe	16
Berlin	14
Meppen	1
München	42
Athen	40
Delft	10
San Fernando	8
Lovoa	7
Zimmerwald	30
Edinburgh	5
Malvern	36
Tromsö	8
Madrid	33
Oslo	4
Bonn	0
Triest	13
Mailand	0
Catania	19
Brindisi	7
Cagliari	9
Spitzbergen	1
Reykjavik	1
Hvar (Zagreb)	2
Sum	465

Fig. 4

projects was suggested by Graz and agreed to by the USSR Academy of Sciences.

Before erecting the Graz-Lustbühel observatory an auxiliary equipment (BEK $1\,f = 300$ mm) was used to make a total of 393 observations of the satellites ECHO 1, 2 and PAGEOS including the reduction of 215 simultaneous observations. The directions obtained were made available to the West European satellite programme of IAG and the short-arc programme of the University at Uppsala (Sweden) (see Fig. 4).

3.2 *Doppler measurements*

Methods of position finding by means of Doppler measurements to satellites with known orbital data are already of great importance for developing and traditional countries.

As in a single point positioning, the orbital data errors are fully reflected, accuracy will be low (1 to 2 m) even if precise orbital data are used. The accuracy of point positioning is greatly increased by methods of simultaneous multi-

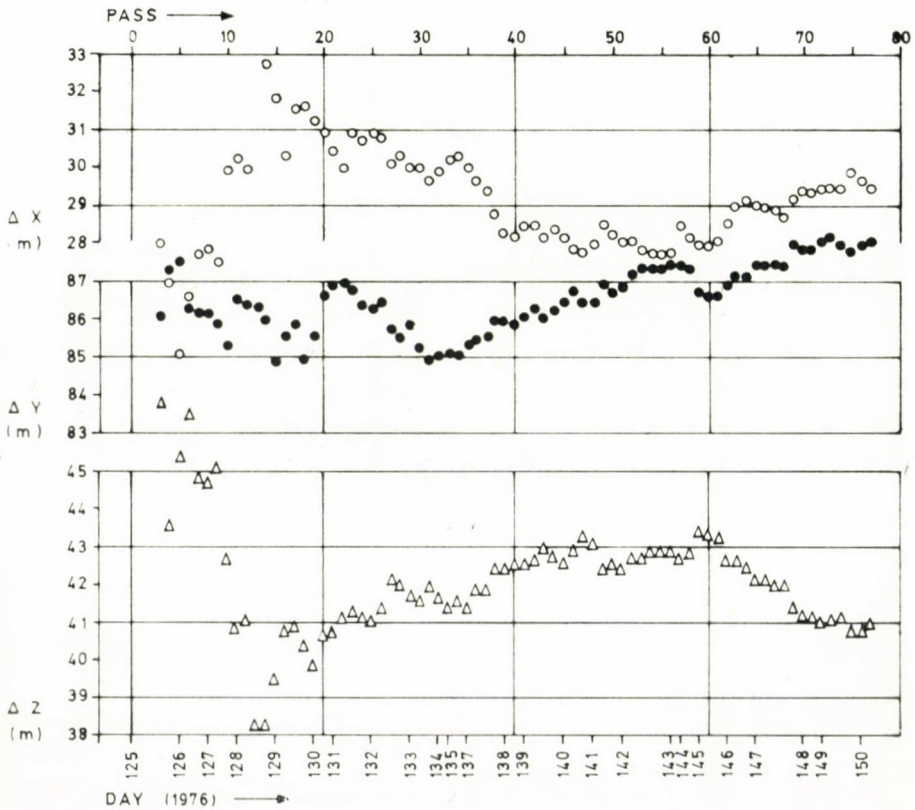


Fig. 5a. Satellite 19, broadcast ephemeris, 77 passes

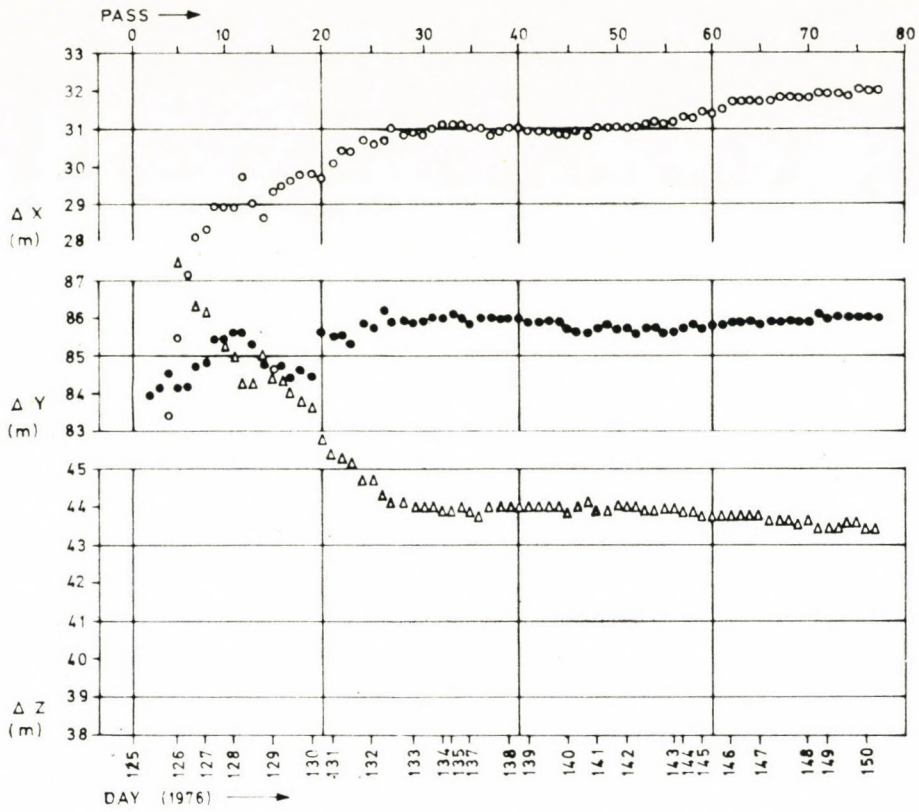


Fig. 5b. Satellite 19, precise ephemeris, 77 passes

location since orbital parameters are not used at all or only for centering short orbit parts (short arc). These methods are, therefore, supposed to bring an increase in position accuracy to a few dm. As the Austrian terrestrial triangulation crosses the Alps rising up to 4,000 m and may, therefore, be systematically distorted by refraction influences and deflections from the vertical, it seems reasonable to provide detection of these systematic error influences by superior Doppler measurements. Besides, contributions to solving geodynamic problems of the Alps may be expected from repeat measurements.

For the reasons mentioned the Graz-Lustbühel observatory takes part in the 2nd European Doppler campaign EDOC 2, and will subsequently take part in a German—Austrian Doppler campaign DŐDOC serving structural improvements of the Federal German and Austrian nets. Theoretical studies and analyses of the measuring techniques and results are intended.

At the Graz-Lustbühel station single point positioning was carried out with precise and broadcast ephemerides of the TRANET satellites during the months of May and June 1976. The results are compiled in Table I and graphically represented in Figs 5a to c.

Table I

Doppler-single point positioning (Graz-Lustbühel, point L2)

A) *Precise ephemeris, satellite No. 19*

	Day No.	Passes	ΔX	ΔY	ΔZ
May 5th—30th, 1976	126—132	25	30.6 ± 1.3	85.7 ± 0.7	44.6 ± 1.0
	132—142	25	30.0 ± 1.0	85.3 ± 0.5	44.4 ± 0.8
	142—151	27	32.0 ± 1.1	86.0 ± 0.6	43.9 ± 0.9
	126—151	77	32.0 ± 0.6	86.0 ± 0.3	43.4 ± 0.5
	126—151	77	29.5 ± 0.9	88.1 ± 0.5	41.0 ± 0.7*

B) *Broadcast ephemeris, all satellites (Nos 12, 13, 14, 19, 20)*

	Day No.	Passes	ΔX	ΔY	ΔZ
May 5th—June 30th, 1976	126—132	100	29.5 ± 0.7	85.0 ± 0.4	44.9 ± 0.6
	132—139	99	28.6 ± 0.7	85.7 ± 0.4	49.1 ± 0.6
	139—147	100	30.2 ± 0.8	85.7 ± 0.4	47.5 ± 0.6
	147—155	100	28.7 ± 0.7	89.7 ± 0.4	45.3 ± 0.6
	155—167	100	28.7 ± 0.7	85.5 ± 0.4	49.8 ± 0.5
	167—175	100	31.3 ± 0.7	87.1 ± 0.4	47.4 ± 0.5
	175—182	82	29.3 ± 0.8	84.3 ± 0.4	51.0 ± 0.6
	126—182	650	29.9	86.5	44.5

C) *Broadcast ephemeris, single satellites*

	Sat. No.	Passes	ΔX	ΔY	ΔZ
May—June, 1976	12	140	31.8 ± 0.6	84.8 ± 0.3	44.0 ± 0.5
	13	115	31.7 ± 0.7	85.5 ± 0.4	43.1 ± 0.6
	14	91	26.6 ± 0.8	86.3 ± 0.4	47.3 ± 0.6
	19	151	29.6 ± 0.6	88.3 ± 0.3	43.1 ± 0.5
	19	77	29.5 ± 0.9	88.1 ± 0.5	41.0 ± 0.7
	20	80	27.5 ± 0.8	87.2 ± 0.4	47.4 ± 0.7

* See Table IC

$$X = 4\,194\,400 + \Delta X$$
$$Y = 1\,162\,600 + \Delta Y$$
$$Z = 4\,647\,200 + \Delta Z$$

Table IA shows the coordinates obtained with the precise ephemerides of satellite 19 and the GEODOP programme (J. KOUBA) for the whole period of May as well as the values obtained in subsequent weeks. The internal accuracy of the Y and Z components is relatively high and lies above the accuracy of the X components.

Table 1B shows the results obtained in May and June with the use of all satellites with broadcast ephemerides. Here, the values are determined from all measurements and from the values obtained in subsequent weeks. The internal deviations are greater, the differences from the precise ephemerides increase in X up to 2 m.

Table IC shows the values obtained for the different satellites (Nos. 12—20) with the broadcast ephemerides. Again, there are great differences from the mean values for all satellites and the values computed with the precise ephemerides.

A graphic representation (Figs 5a to c) shows — after a run-in time of a few days — a relatively high internal accuracy but systematic deviations.

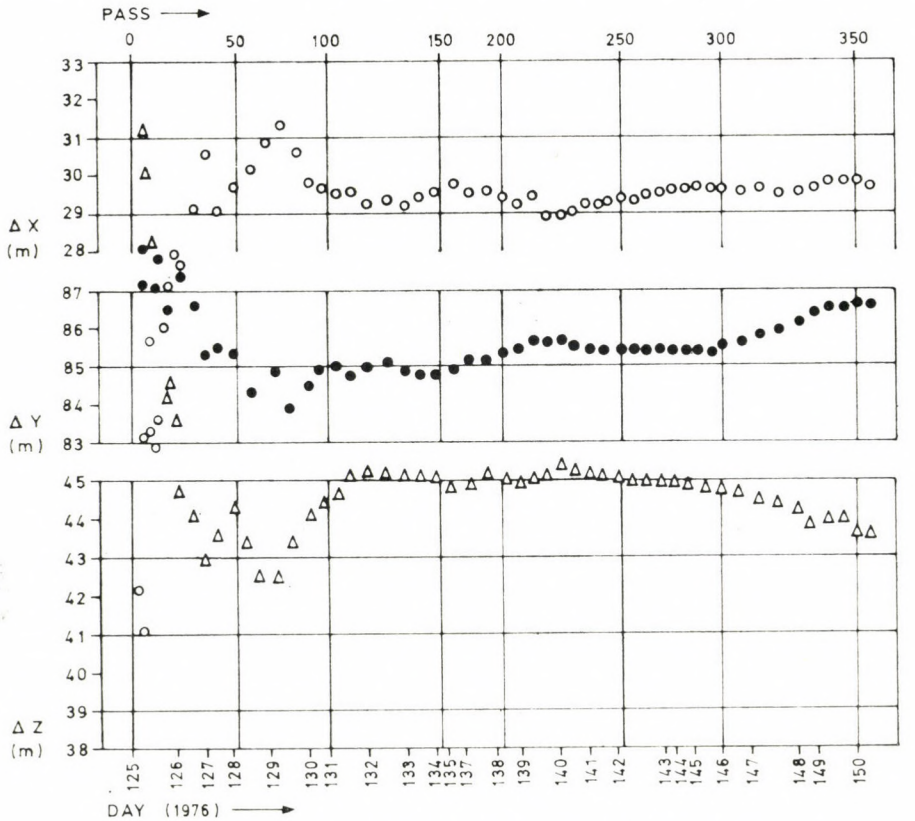


Fig. 5c. Five satellites, broadcast ephemeris, 350 passes

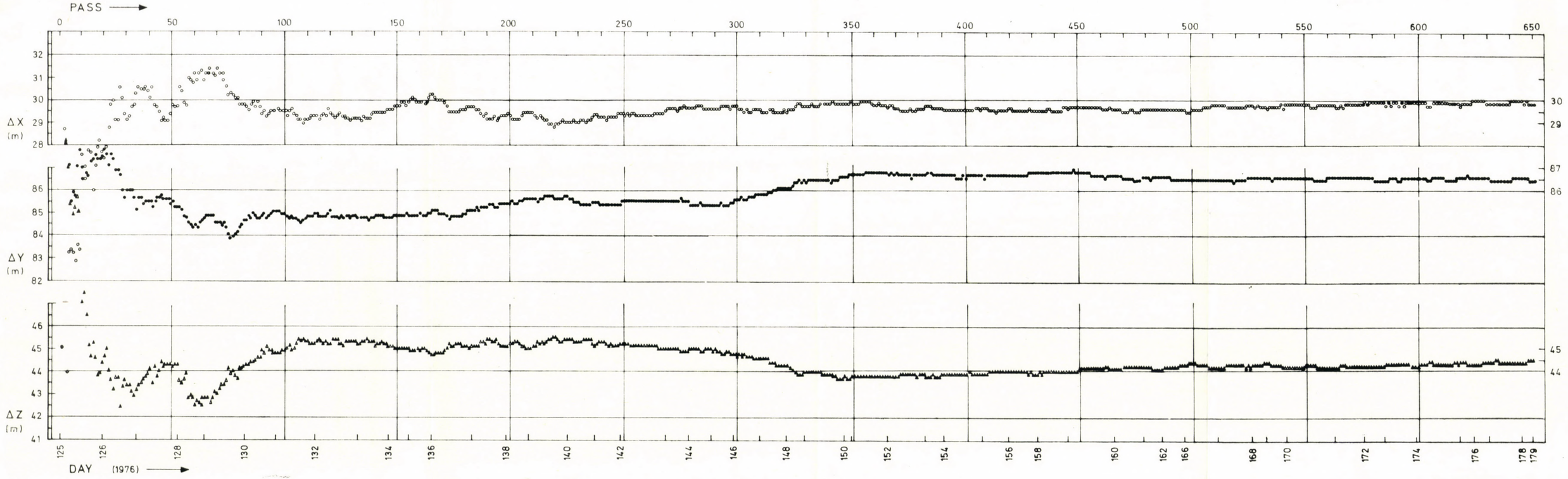


Fig. 5d. Five satellites, broadcast ephemeris, 650 passes

3.3 *Astronomic and tidal measurements*

The dynamic behaviour of the earth is also described by the movements of the vector of vertical. The direction of the vector of vertical is determined by astronomic measurements, its amount by gravity measurements; the variations of both are determined by terrestrial tide recordings. To determine these variations three terrestrial tidal stations were established near the Graz-Lustbühel observatory where recordings are made with a horizontal pendulum (Verbaandert-Melchior) and a gravimeter (North American Geodynamics). For recording the dynamic behaviour of the earth, a test net (Styria) with a radius of about 100 km was established near Graz. Laser and microwave distances as well as horizontal and zenith directions were measured in it. In each of the seven points of the net the longitude, the latitude, and azimuths were determined by astronomic measurements so that the net formed with measured data can be computed free from any hypothesis. The shape of the geoid of the area is to be defined by additional astronomic and gravimetric measurements; hints as to possible movements are to be obtained from repeat measurements.

4. Final remarks

The construction of the observatory was financed by the Austrian Federal Ministry of Science and Research. The research equipment was paid for by the Fund for the Promotion of Scientific Research and by the Municipality of Graz. The measurements with BMK 75 were made by Dipl. Ing. G. Chesi, the Doppler measurements by Dr. P. Pesec. The latter also made the numerical computations for this report.

ГЕРДЕЗИЧЕСКИЕ РАБОТЫ И ПРОЕКТ В ОБСЕРВАТОРИИ ГРАЦ—ЛУСТБЮХЕЛ

К. РИННЕР

РЕЗЮМЕ

В Австрии, недалеко от города Грац, в Лустбюхеле была создана обсерватория, где среди других, проводятся спутниковые наблюдения при помощи камеры BMK 75 и допплеровским прибором фирмы Маркони. В статье описываются обсерватория, ее деятельность и оборудование станции. Эта обсерватория будет геодинамической станцией Австрии, принимающей участие в международных работах для определения геодезических и физических параметров Земли и их вариаций.

Acta Geodaet., Geophys. et Montanist. Acad. Sci. Hung. Tomus 14 (1—2), pp. 31—57 (1979)

ON VARIATIONS OF GEOCENTRIC POSITIONS WITH TIME

E. GROTEN

INSTITUT FÜR PHYSIKALISCHE GEODÄSIE, TECHNISCHE HOCHSCHULE, DARMSTADT

[Manuscript received September 5, 1977]

Space geodesy techniques as lunar and satellite ranging yield the opportunity to detect variations of the geocenter with respect to a "pseudo-earth-fixed-reference" frame. The order of magnitude of geocenter shifts is estimated for movements of terrestrial fluid masses. The precise definition of the geocenter (mass center of the earth) is discussed.

In view of high-precision geodesy and of reconciliation of classical geoid definitions with modern concepts, problems inherent in the classical geoidal concept are pointed out.

1. Introduction

The precise determination of the instantaneous geocenter and, consequently, of instantaneous *geocentric* positions is a most difficult problem. In dealing with centimeter accuracy it is, therefore, tried to use *relative* positioning, as, e.g., in the SAFE-Programme. On the other hand, whenever orbital computation enters directly into the solution of high-precision geodesy problems, the *absolute* positioning is not avoidable. Moreover, it seems that the absolute location of the geocenter is indeed feasible with accuracy better than ± 5 m, as at present, as soon as some additional careful consideration is combined with the more accurate tracking techniques.

However, the aim of the present investigation is less practical but rather a theoretical one related to the well known condition

$$\lim_{r \to \infty} (Tr^2) = 0 \,,$$

where T = disturbing potential and $r = |\mathbf{r}|$ = absolute value of radius vector. The above condition is fulfilled for an ellipsoid whose center is situated at the *geocenter* and whenever, in addition, the ellipsoidal mass equals the mass of the earth. The equality of masses has been considered in many recent investigations. Similarly the second condition

$$\lim_{r \to \infty} (Tr) = \text{const}$$

which is fulfilled whenever the rotational axes coincide has recently gained a lot of interest; both conditions together imply regularity of T at infinity.

By "geocenter" we mean the mass center of the earth. It is used as basic reference in the present paper. In contrast, the earth's gravity center which differs remarkably from the mass center only in strongly heterogeneous grav-

ity fields is less important. Rather the *gravity* center (= barycenter) *of the earth—moon system* is important for orbital motion of the earth. But for tidal and similar work the difference *mass* center—barycenter *of the earth* is not of interest, at present.

In linear theory the geocenter is usually supposed to coincide with the instantaneous axis of rotation. Even though this assumption is a good approximation applied throughout the main part of the present context, it is not fulfilled by the real earth. A few hints on this topic at the end of the present investigation seem to be in order.

Even though the regularity at infinity is a basic hypothesis in dealing with the geodetic boundary value problem as, e.g., discussed by HOERMANDER [12], the boundary value problem is usually assumed to be stable. However, this fact has been questioned by several authors; we assume that *slight* deviations from the aforementioned conditions for regularity at infinity do *not strongly* affect solutions of the geodetic boundary value problem.

In dealing with the rotating earth we are used to rely upon a set of axes where (1) the axis of rotational momentum, (2) the axis of maximum moment of inertia, and (3) the instantaneous rotation axis are important. But the figure axis (FA) does not coincide in reality with the axis of maximum moment of inertia of a *deformable* earth. Therefore, from the geodetic viewpoint it can either be dismissed or it could rather be assumed to coincide with the CIO to which the semiminor axis of the ellipsoid of reference is usually related by applying corresponding polar motion corrections to astronomical observations. In

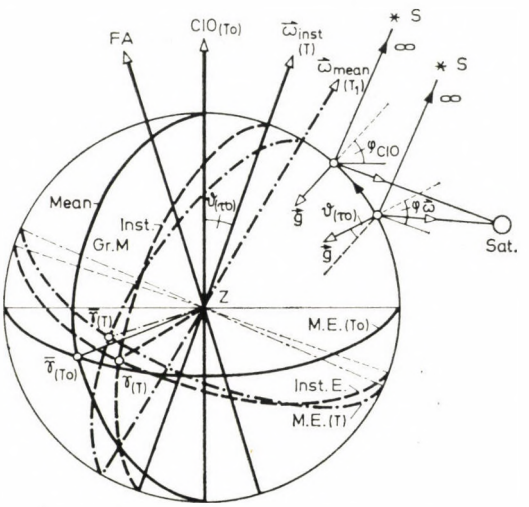


Fig. 1. Rotation axes and latitudes; mean axes referred to different epochs (T_i) and latitude variations $\theta(\tau)$ for $\tau = T_k - T_i$; note that polar motion difference $\theta(\tau) \neq \Phi_{\vec{\omega}} - \Phi_{CIO}$; on a deformable earth $\theta(\tau_0) = \theta(T - T_0)$

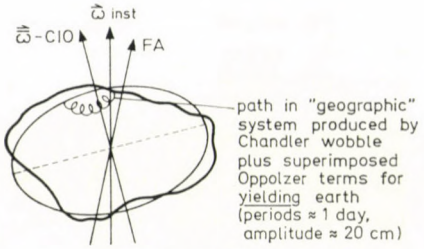


Fig. 2. Axes of rotation where ellipsoidal mean equator (broken line) is related to CIO whereas figure axis (FA) and instantaneous axis $\vec{\omega}_{inst}$ are related to the earth

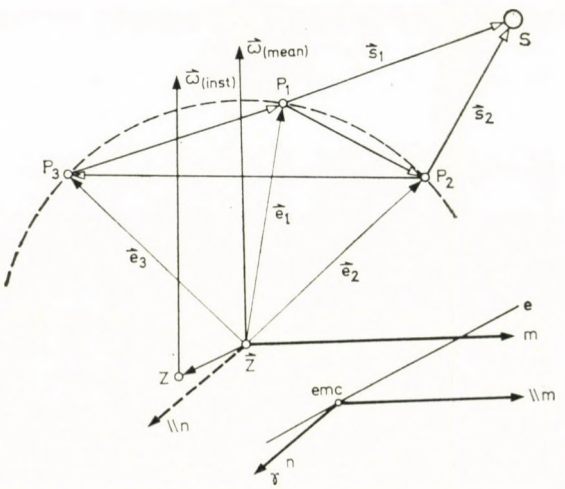


Fig. 3. Earth reference frame consisting of three stations P_i ($i = 1, 2, 3$), $\underline{z}$ = instantaneous geocenter, $\bar{Z}$ = mean geocenter, emc = earth—moon center with ecliptic e

Fig. 2 we still stick to the previous concept of CIO $\neq$ FA. But in Fig. 3 it is replaced by the concept based on a geohedron where FA is dismissible.

Motions of the geocenter relative to the earth surface do *not directly* affect astrogeodetic positioning but can be detected, at least in principle, from satellite tracking. In contrast, polar motion implies variations of local plumb line direction and, therefore, affects classical *as well as* satellite positioning; the latter are usually not related to the local plumb line. But changes of the geocenter imply variations of poles and equator; the poles are related to the meridians and longitudes, whereas from the equator the latitudes are reckoned; consequently, there is an *indirect* influence of variations of the geocenter.

Since atmosphere and seas, i.e. the fluid earth, change the moments of inertia with time, *the axis of maximum moment of inertia is not fixed to the body.* Polar migration together with tectonic motion, etc. implies additional variations of the axis of figure of the earth. The *instantaneous axis of rotation* is, of course,

not fixed to the earth because of polar motion. As *CIO and mean Greenwich meridian* depend on the observation stations from which they are derived (BIH, IPMS) and those stations are not supposed to be fixed in relation to the earth body, *neither CIO nor mean Greenwich longitude* ($\lambda \doteq 0$) *are truly fixed to the earth*; they are *conventional* references. The determination and definition of an earth-fixed system is a complicated problem for high-precision geodesy; variations of location of geocenter are difficult to determine, so *relative* determination of geodetic stations is straightforward. If geocenter motion with time, as necessary with high-precision orbital analysis is considered, then even more sophisticated considerations are in order. But *theoretical* consequences for the earth rotation are *not* considered in the present paper.

The above conditions for regularity at infinity are, however, not strictly fulfilled in practice because even if the volume V' of the ellipsoid E is the same as the volume V of the earth (which is not identical with the volume of the geoid!) there is usually a difference in mass

$$\delta M = M - M'$$

where M and M' are the masses of the earth and the ellipsoid, respectively. If the center of inertia of the ellipsoid Z' does not coincide with the center of the earth Z (which is not identical with the center of the geoid), then the second above condition is not fulfilled. As the geoid is always connected with mass transport which changes the potential (the only exception is RUDZKI's[1] reduction) Z' and Z will almost never coincide and

$$\lim_{r \to \infty} (r^2 T) = 0$$

will only hold approximately; deviations are, however, small in practical application.

In Fig. 2 it is shown that the semiminor axis of the ellipsoid is usually defined by the CIO. Now BURSA (1969) and LAMBECK [15] have shown that variations in absolute gravity are of an order of magnitude which *at present* does not yet affect geoid computation. This implies that also the first condition of regularity at infinity is nearly fulfilled. In this connection it should be emphasized again that the Love constants (k, h) characterizing the deformation of the elastic earth are only crude approximate values even with a centrifugal potential of degree two (in terms of spherical harmonics) because LOVE's (1911) model is a spherical one having radial distribution of elastic parameters.[2] The generalizations by KAULA (1968) and by GROTEN (1969) differ substantially, as KAULA takes indirect effects into account, whereas GROTEN considers [$k(\varphi, \lambda)$, $h(\varphi, \lambda)$] as purely formal generalization of the Love constants,

[1] But he changes the total mass.
[2] The real irregularities of the earth lead to (h, k) being location-dependent.

taking into account the heterogeneity of the earth's body (similarly to formal use of osculating orbital elements in orbital computations).

The precise determination of geocentric position **r** is extremely difficult; at present this can be achieved with accuracy of a few meters. Nevertheless, the determinations of variations of **r** with time are necessary in the near future with much higher accuracy. Therefore, at the Torun Symposium 1974, we had proposed to determine the deviations of the instantaneous geocenter from its mean position. For this purpose some additional investigations are necessary in order to supplement our previous results.

The most important points in detecting positional variations of the geocenter, using recent methods as ranging, etc., are:

(1) *variations* of the position of the geocenter are observed purely geometrically and no longer dynamically; the determination of those variations is more precise than the dynamical determination of the geocenter position itself;

(2) using any *geodetic* coordinate system as discussed in our previous paper we have a pseudo-earth-fixed system (perhaps defined by three tracking stations) in contrast to the *astronomical* system which is defined by sets of longitudal or polar tracking sites (of BIMP, ILS, etc.) in which coordinate systems the positions of the other observational stations are not fixed but rather have time-dependent station vectors.

On the other hand, it should be kept in mind that the center of the earth–moon system does not coincide with the terrestrial mass center. Consequently, in dealing with *inertial systems* it should be realized that the ecliptic is defined by the center of the earth moon system, and the point of Aries is no longer in the equatorial plane which is perpendicular to the earth rotation axis and goes through the mass center of the earth. But there are no practical implications of the above definitions as shown in Fig. 1, as reductions are readily made for the shift from one system into the other whenever necessary (see Fig. 3). Consequently: *since distances play a role now in precise geodesy as, e.g. in lunar ranging, the classical concept of spherical astronomy is no longer sufficient!*

By its very definition the ecliptic moves around the geocenter O (even if O is supposed to be stationary) together with the earth moon center. The celestial equator is supposed to be defined by $(\vec{\omega}, 0)$ whereas the *terrestrial* equator plane might be defined by stars CIO and O; this definition is not sufficient and together with the vernal equinox is fundamentally based on the *spherical astronomy concept*; in contrast, *geodetic* and *astronomical* equators are defined by stations having geodetic and astronomical latitudes equal to zero, respectively; consequently, there exists no astronomical equatorial *plane*; with earth's satellites the terrestrial equator *plane* might be considered as an average of the *astronomical* equator "surface"; a non-stationary geocenter implies time-dependent astronomical latitudes and, therefore, necessitates a more precisely defined "equivalent" to the *geographical* equator as defined by WOOLARD

and CLEMENCE, (1966); it coincides with the *geodetic* equator of an ellipsoid centered at O; but this ellipsoid does not necessarily coincide with a *mean* earth ellipsoid for time-varying O.

2. Determination of geocentric positions

In considering a nonstationary geocenter we can distinguish two different types of motions of the geocenter: (1) *slow* variations of positions due to ice melting and corresponding variations of sea level, mass shifts in the earth's interior as convective flow in the outer core, and those due to flow in the asthenosphere and due to sudden earthquakes; further, mass variations in connection with tectonic plate motion; (2) more or less *periodic* mass variations in the atmosphere, in seas due to wind and tides (it can be presumed that body tides do not produce remarkable deformations of the earth which are connected with asymmetric mass shift).

Neither by radiointerferometry (astronomical methods like VLBI) nor by satellite or lunar laser ranging those mass center variations are presently observable because those variations produce only geocenter variations of the order of a few centimeters or even less within time spans of one year or so.

Consequently, at least part of them is of the order of the variations of "terrestrial reference systems". For there is no earth-fixed reference system, the variations of pseudo-earth-fixed systems are, of course, due to variations of positions as well as observational errors at those stations which take part in ILS and IPMS observation programmes, respectively. As any *wobble* (in the terrestrial system) is *always* associated with a corresponding *nutation* (referred to a "space-fixed" system) we need to consider both events in spite of the fact that the system "fixed in space" is basically an inertial system the *realization* of which is still more difficult and far away than its precise *definition*. Even though observations of planetoids, very long base line interferometry (VLBI) of galaxies, etc. might essentially contribute to improving the parameters of inertial systems, the motion of the ecliptic and the equinox and galactic problems still imply a lot of uncertainties.

The incorporation of ranging to planets and satellites (including the moon) in astronomy brings up some difficulties in dealing with the concept of spherical astronomy where translations of directions are supposed to be without influence. But if distances are taken into account the motion of the geocenter, of the earth–moon system, etc. with respect to a terrestrial system is of interest because the (terrestrial) equator is defined by the geocenter and the mean axis of rotation of the earth, i.e. CIO.

The deficiencies of lunar theory imply well known trouble not only in basic astronomical quantities but also in the lunar position with respect to

the earth. And if the lunar coordinates (α, δ) are used in relation to positions and locations on the earth then the instantaneous geocenter location is of interest. Because of the above mentioned deficiencies the (relative) accuracy of satellite ranging of ± 15 cm implies accuracy of the lunar center location of ± 40 cm.

On the other hand, laser ranging and Doppler methods which are basically independent of the (α, δ)-system, need at least one absolute direction in most applications in space; for instance, a zero meridian is needed for computation in a terrestrial system when the Doppler results are related to geodetic networks. Geometric applications of lunar ranging yield station separation from the instantaneous rotation axis of the earth. Thus, in most applications radio methods and astronomical observations are interrelated and corresponding references and their interrelations are important.

With small variations of the geocenter the deviations of the *instantaneous* geocenter, to which orbital computations are referred, from any conventional mean geocenter do not imply remarkable orbital perturbations since orbital perturbations are, in general, smaller than the variations of the geocenter about its mean location.

With a rigid earth we get the variations $\Delta\mathbf{r}$ of the instantaneous geocenter with respect to the earth (see Fig. 4).

$$\Delta\mathbf{r} = \mathbf{r}(t_1) - \mathbf{r}(t_2) = \mathbf{r}'(t_1) - \mathbf{r}'(t_2)\,. \tag{1}$$

This relation holds only for a satellite which does not change its location in an "earth-fixed-reference system" i.e. an ideally geostationary satellite which cannot really exist. In practice there is always "proper motion" $\Delta\mathbf{r}'$ of the geo-

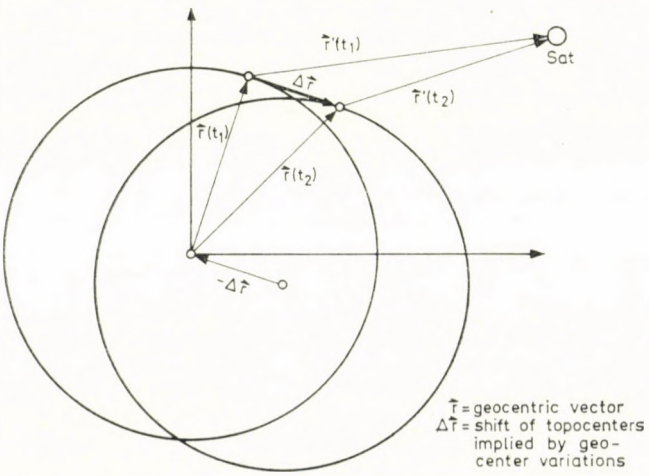


Fig. 4. Variation $\Delta\vec{r}$ of the rigid terrestrial surface with respect to the geocenter as obtained from ranging

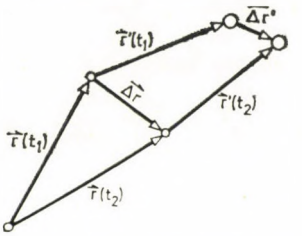


Fig. 5. Determination of geocenter variations $\vec{\Delta r}$ from satellite ranging $\vec{r}'(t)$, taking into account satellite motion $\vec{\Delta r}'$ whenever known precisely

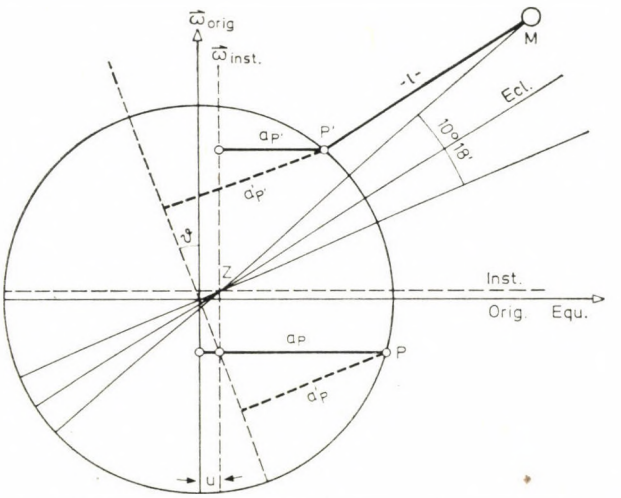


Fig. 6. Separation of polar motion from geocenter variations using space methods. The coincidence of instantaneous geocenter Z with the instantaneous rotation axis is presupposed

stationary or other satellite. In Fig. 5 it is realized that when $\Delta\mathbf{r}'$ is known then, of course, $\Delta\mathbf{r}$ can be deduced.

Whereas in the pseudo-inertial system (α, δ) there is still a lot of difficulties, to be mentioned below, the main difficulty in the pseudo-earth-fixed system is the separation of polar motion and geocenter location variation. If only one tracking station is available motion of the geocenter orthogonal to the instantaneous axis of rotation $\vec{\omega}$ is hardly detectable; with several stations we are better off.

With VLBI-stations (for controlling the motion of tracking stations relative to each other) together with laser ranging (to the moon and satellites) polar motion, geocenter shifts parallel to the equator plane and relative station location variations can be found. Fig. 6 shows that with LLR (lunar laser ranging) stations on the same meridian at high (positive or negative) latitudes we are able to separate motions of the pole from those of the geocenter whenever there are two stations at longitude difference $\Delta\lambda \doteq 90°$.

From this viewpoint the separation of geocenter motion parallel to the $\vec{\omega}$-axis is more difficult because the small corresponding variations in range $l \to l'$ to the moon are difficult to observe in any case.

High accuracy in tracking geocenter motion could be achieved in making laser range measurements to a polar as well as to an equatorial satellite.

One may, of course, ask to what extent geocenter variations are of interest if they might be of the same order of magnitude as the variations of the pseudo-earth-fixed system.

But it seems that in high-precision work many parts of our present terrestrial reference system need to be revised. The axis of maximum moment of inertia is no longer fixed to the earth; since the figure axis is no longer identical with that axis in case of a deformable earth, it has to be replaced by a system as given in Fig. 3. The CIO being a conventional reference to which geodetic observations are referred could be considered as a good substitute of the figure axis but only to some extent because of its conventional character. And, moreover, a spherical harmonic expansion of the geopotential referred to CIO has, of course, non-zero terms for ($n = 1$, $m = 2$). If, in addition, we could assume that the instantaneous geocenter is no longer a point on the instantaneous $\vec{\omega}$-axis, then a lot of problems is arising in precise orbital computations. Moreover, the Newtonian part of the geopotential V is no longer harmonic because $V = V(\mathbf{r}, t)$, even when tidal deformations, etc. are eliminated. The dynamic determination of polar and geocentric positions in this connection will always be inferior to the determination by geometric means, i.e. according to Fig. 4.

In orbital computations *apparent* non-inertial effects arise in addition to those presently obtained.

One may suppose that seasonal and periodic variations of polar position are much greater than corresponding shifts of the geocenter. The equatorial wandering of the *meteorological* low-pressure zone which strongly affects UT 1 is a good example. Because of symmetry the corresponding seasonal variations of geocenter are indeed small. STOLZ [20] in his recent investigations found geocenter variations due to meteorology which are also surprisingly small.

3. The deviations of the real earth parameters from those of the geoid

It is well known that with origin at the instantaneous geocenter we get the potential

$$V = \frac{k^2 M}{r}\left(1 - \sum_{n=2}^{\infty}\sum_{m}^{n}\left(\frac{a}{r}\right)^{n+1}\left[J_n^m R_n^m + K_n^m S_n^m\right]\right), \qquad (2)$$

where a = equatorial radius

$r = |\mathbf{r}|$ = geocentric distance

J_n^m, K_n^m = harmonic coefficients of degree n and order m
$R_n^m = P_n^m \cos m\lambda$
$S_n^m = P_n^m \sin m\lambda$
(φ, λ) = geographic position in spherical coordinates (r, φ, λ)
k^2M = terrestrial gravitational constant.

If the origin does not coincide with the geocenter we have, in addition,

$$\begin{aligned} -aJ_1^0 &= z_0 \\ -aJ_1^1 &= x_0 \\ -aK_1^1 &= y_0 \end{aligned} \tag{3}$$

where $\mathbf{r}_0(x_0, y_0, z_0)$ is the "geocentric vector".

In a similar way the deviation of the axis of maximum moment of inertia is obtained for the geoid with respect to the one of the (real) earth:

$$-\begin{Bmatrix} E \\ D \end{Bmatrix} \frac{1}{k^2Ma^2} \begin{Bmatrix} \Delta J_2^1 \\ \Delta K_2^1 \end{Bmatrix} \tag{4}$$

where ΔJ_2^1, ΔK_2^1 are the differences in harmonics (2, 1) between geoid and real earth and E, D are the corresponding "products of inertia". On taking the numerical values of harmonics of the topography as obtained by VENING–MEINESZ (cit. [17]) we can readily estimate E, D, $\mathbf{r}_0$, etc.

The difference in volume between the real earth and the geoid is readily estimated from the zero degree harmonics of the topographic heights

$$h = \Sigma h_n \tag{5}$$

of the "lithosphere" where on terms of *normalized* Legendre polynomials [17]

$$\bar{P}_n^m = \frac{P_n^m}{N_n^m} \tag{6}$$

with

$$N_n^m = \left(\frac{2}{2n+1} \frac{(n+m)!}{(n-m)!} \right)^{1/2} \tag{7}$$

gives

$$h_0 = -3348 + 3679 = 331 \text{ [m]}. \tag{8}$$

The corresponding term in BALMINO et al.'s [1] *fully normalized* development reads

$$\bar{h}_0 = \frac{1}{4\pi} \iint h(\Phi, \lambda)\, d\sigma = -2300 + 2520 = +220 \text{ [m]}. \tag{9}$$

When the total mass of the geoid is supposed to be known, being the same as the mass of the "solid" earth,[3] we can differentiate the well known relation [11]

[3] "solid" = solid plus liquid earth without atmosphere.

$$a = \frac{k^2 M}{W^0}\left(1 + \frac{f}{3} + \frac{m}{3}\right) \tag{10}$$

where f = flattening
m = $\omega^2 a/\gamma_a$ of Clairaut's formula
ω = rotation speed of the earth
γ_a = normal gravity at the equator
a = equatorial radius
U^0, W^0 = gravity potential on the ellipsoid and geoid, resp.,

as

$$\delta a = -\frac{W}{\gamma_a} + \frac{a}{3}\delta f\,; \tag{11}$$

this relation yields the change in potential corresponding to a change in radius a. Even though the classical definition of W^0 (using the geoid) is fully equivalent to MOLODENSKY's definition (without geoid), neither h_0 nor W^0 are well known quantities because of the unknown deviations of levelling zero references from mean sea level so that [11]

$$W^0 - U^0 = \delta W = R\Delta g_0 + \gamma N_0 \quad \text{and} \quad \delta a = N_0 + \frac{a}{3}df \tag{12}$$

for geoid heights $N = \Sigma N_n$ and $\Delta g = \Sigma \Delta g_n$ is only of limited actual interest, at least for high-precision work at the present time. When δf is considered it should be noticed that for the "lithosphere" the coefficient of K_2^0 is of the following order [17][4]

$$a_2^0 = 744 - 636 = 108 \text{ [m]}.$$

Consequently, the geoidal flattening is slightly different from the flattening of the real earth as obtained from J_2 of satellite orbits.

However, it should be clearly kept in mind that there is an additional difference between both flattenings which is due to the fact J_2 as found from orbit analysis is related to solid earth plus atmosphere, whereas surface gravity is related to the solid earth according to present computational methods. With BALMINO et al. we get

$$\bar{a}_2^0 = 106 \text{ m}\,.$$

At this occasion a clarification seems to be in order: The earth ellipsoid as determined from satellite harmonics is not identical with the best fitting ellipsoid because J_2 is related to the solid earth (including sea) *plus* the atmosphere; strictly speaking J_2 must be time-dependent as the atmospheric mass

[4] With LEDERSTEGER's, i.e. HOFSOMMER's and POTTER's, normalization there is a remarkable difference between his and BALMINO's second-degree zonal coefficient of as much as $a_2 = a_2/\sqrt{2} \to 41$ m.

distribution varies with time. Moreover, the mass center as obtained from terrestrial gravity does not coincide with the moving center of the earth ellipsoid determined from satellite data; the terrestrial mass center is mainly affected by motion within the solid earth and its fluid part, so it is less movable than the center of earth plus atmosphere.

4.

4.1 *The geocenter in the classical geoid approach*

MORITZ (HEISKANEN—MORITZ, 1968) has pointed out the reconciliation of the modern theory by ARNOLD, BJERHAMMAR and MOLODENSKY'S with the classical theory as explained by JUNG [13]. Nevertheless, when dealing with accuracy of ten centimeters or so in co-geoid determinations some problems arise which previously were thought to be unimportant.

At present, the low-degree harmonics of gravity are mainly obtained from satellite geodesy (k^2M, J_2, . . .) or from combination solutions of satellite with terrestrial data. In any case, coordinates are now related to CIO (as z-axis) so that the coefficients C_2^1 and S_2^1 of the potential are not zero. At the IAU meeting in Torun (1974) we had pointed out several other difficulties and previously unobserved aspects arising with the application of the classical geoid computation some of which will be explained below in more detail.

Whenever gravity anomalies are combined with satellite harmonics in view of the *modern* theory where

$$\Delta g_p = g_p - \gamma_Q \tag{13}$$

with p = surface station
Q = point on the telluroid corresponding to P
g_p = gravity at P
γ_Q = γ at Q

problems do not arise. In contrast, with the *classical* definition of Δg on the co-geoid difficulties are faced because the perturbing potential T is usually obtained at the geoid ($r = R$) from

$$T = \sum_n T_n = R \sum_n \Delta g_n/(n-1) \,. \tag{14}$$

Whenever the harmonics of degree $n = 1$ in the topographic heights are unequal to zero, the center of *any* co-geoid (except RYDZKI's) is different from the geocenter.[5] Even though for the free-air anomaly in the *modern* theory $\Delta g_1 = 0$, this term is unequal to zero in the *classical* theory as free-air anomalies are only an approximation of the condensation anomalies[6] after HELMERT; for otherwise the co-geoid is no longer a free boundary surface. Consequently, the

normal potential needs to contain a first-degree term in the classical theory which is *specific* for any gravity reduction and is readily obtained from h_1 of $h = \Sigma h_n$, i.e. the first-degree term of the topographic height h (above sea level). From the geometric viewpoint this implies an *eccentric-level ellipsoid* with respect to the geocenter. Whenever the center of this eccentric ellipsoid coincides

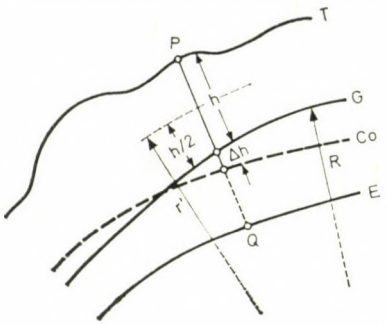


Fig. 7. Effect of gravity reduction as found from single layer concept; Co = co-geoid, E = ellipsoid, T = topographic surface, G = geoid, h = orthometric height, Δh = separation of geoid from co-geoid, R = radius vector of geoid at P, Q = image of P on E, $r' = R + h/2$

with the center of the *co-geoid* then $\Delta g_1 = 0$ for any *specific* type of anomaly (say isostatic, condensation, etc.). But even though this effect is small when the total mass M of the earth is not changed, i.e. masses removed above the co-geoid are stored inside, the corresponding shift of the cogeoid center is of interest; at present, it is certainly mainly of academic interest.

As a consequence, the indirect effect must also contain a first-degree term for any of the above mentioned types of gravity anomalies; this will be seen below. But since the successive approximation process as described by JUNG in evaluating the separation between the co-geoid and the earth's surface is usually replaced by a single-step computation (also in the gravity reduction) the indirect effect does not fully compensate the mass removal in reducing gravity g. These facts are readily explained, using a spherical model where the topography is represented by a single layer density

$$\sigma = \Sigma\, Y_n \tag{15}$$

on the sphere of radius $r = R$.

The potential produced at P (r) by a single layer on a sphere of radius r' of density $\delta = \Sigma Yn = \Sigma h_n \cdot P$ (see Fig. 7), where $\varrho = 2.67$ cgs, reads [4]

$$V(P) = 4\pi k^2 r' \,\Sigma \frac{Yn}{2n+1}\left(\frac{r'}{r}\right)^{n+1} \tag{16}$$

[5] For $W_1 = 0$ with the real earth in a geocentric system (W = geopotential).
[6] Implying mass shift.

and

$$\left(\frac{\partial V}{\partial r}\right)_P = 4\pi k^2 \Sigma \frac{n+1}{2n+1} Y_n \left(\frac{r'}{r}\right)^{n+2} \tag{17}$$

Further, if in conventional gravity reductions $\partial g/\partial h = \partial\gamma/\partial h + \partial \Delta g/\partial h$ is replaced by $\partial\gamma/\partial h$ we neglect

$$\left(\frac{\partial \Delta g}{\partial h}\right)_{r=R} = \frac{-1}{R} \Sigma(n+2)\, \Delta g_n \tag{18}$$

and, consequently, there arises an error of

$$\frac{\partial \Delta g}{\partial h} \cdot h = \frac{-1}{R} \Sigma(n+2)\, \Delta g_n \cdot h_n . \tag{19}$$

If, however, $\Delta g_1 = 0$, the latter formula *does not contain* a first-degree term even if $h_1 \neq 0$. This implies that the free air correction will *not* contribute to a shift of the geoid center with respect to the geocenter.[7] But since $h_1 \neq 0$, any removal of topographic masses above the geoid $r = R$ according to eq. (15) will produce a shift. Even if, according to the condensation anomaly or the isostatic concept, the removed masses are restored at (or below) the geoid or co-geoid there is a corresponding shift of the mass center. The corresponding effect is readily estimated for a storing at $r = R$ from (16)

$$\left(\frac{\partial V}{\partial r}\right)_P = 4\pi k^2 \Sigma \frac{n+1}{2n+1} Y_n \left[\left(\frac{r'}{r}\right)^{n+2} - \left(\frac{R}{r}\right)^{n+2}\right]. \tag{20}$$

The indirect effect Δh corresponding to simple *removal* is, of course, at $r = R$, equal to

$$\left(\frac{V}{\gamma}\right)_{r=R} = \frac{4\pi k^2 R}{\gamma} \Sigma \frac{Y_n}{2n+1} \left(\frac{r'}{R}\right)^{n+1} \tag{21}$$

and in the *restoring* case

$$\left(\frac{V}{\gamma}\right)_{r=R} = \frac{4\pi k^2 R}{\gamma} \Sigma \frac{Y_n}{2n+1} \left[\left(\frac{r'}{R}\right)^{n+1} - 1\right]. \tag{22}$$

From

$$\Delta g = \frac{1}{r} \Sigma(n-1) \left(\frac{R}{r}\right)^{n+1} T_n \tag{23}$$

it is realized that the change of $N = T/\gamma$ produced by (19) is, at $r = R$,

$$\frac{T_n}{\gamma} = \frac{R \Delta g_n}{\gamma(n-1)} \tag{24}$$

[7] Note that usually γ does not contain a first-order term.

or
$$\frac{4\pi Rk^2}{\gamma}\sum\frac{(n+1)}{(n-1)(2n+1)}Y_n\left[\left(\frac{r'}{r}\right)^{n+2}-\underbrace{\left(\frac{R}{R}\right)^{n+2}}_{=1}\right]. \tag{25}$$

When gravity is transferred down to the co-geoid we have, of course, reduced gravity

$$\Delta g \doteq \Sigma\Delta g_n = g_P - \frac{\partial g}{\partial n}(h+\Delta h) - \gamma_Q \tag{26}$$

where Δh is given by (21) and (20), respectively.

Consequently, (24) is not (but almost) identical with (21). The factor

$$\frac{n+1}{n-1} \to 1 \text{ for } n \to \infty \tag{27}$$

means that whenever gravity is *not* reduced down to the co-geoid (instead of the geoid) there is an error affecting mainly the low harmonics.

In dealing with the separation of the geoid center from the geocenter only the *first*-degree coefficients are important which, according to VENING—MEINESZ, are

m	cos-term $[m]$	sin-term $[m]$
0	$+945-867=78$	—
1	$+1188-1052=136$	$+800-646=154$

With BALMINO's full normalization we find accordingly

m	cos-term $[m]$	sin-term $[m]$
0	$639-615=24$	—
1	$591-523=68$	$409-334=75$

MORITZ's [19] integral equation approach is of interest in this connection. He shows that for the regularized geoid there is basically no secondary indirect effect in the integral equation approach. The contradiction to JUNG's reasoning in his article on the figure of the earth in Flügges Encyclopedia of Physics is only an apparent one; MORITZ reduces the gravity reduction to basically algebraic transformations.

As far as condensation anomaly is concerned, in this connection LEDERSTEGER [17] has shown that the interpretation of free-air reduction in terms of condensation anomalies leads to *smaller* geoid heights.

4.2 *Some numerical considerations*

From N_1 of $N = T/\gamma = \Sigma N_n$ we can, in theory, get the coordinates of the mass center of a reference body like a co-geoid with respect to origin, using [11]

$$N_1 = x_0 \sin\theta \cos\lambda + y_0 \sin\theta \sin\lambda + z_0 \cos\theta$$

where spherical harmonics $P_1^1 = \sin\theta$, $P_1^0 = \cos\theta$; consequently, the latter equation is written as

$$N_1(\theta, \lambda) = z_0 P_1^0 + (x_0 \cos\lambda + y_0 \sin\lambda)\, P_1^1$$

which means that the coordinates $r_0(x_0, y_0, z_0)$ are simply the harmonic coefficients of degree $n = 1$ for N. For practical applications where Δg is involved, formula (3) together with (16) is appropriate.

a) Bouguer-anomalies:

This type of Δg is seldom used in geoid computation but is usually incorporated in the isostatic anomaly. As MORITZ has shown, the flat approximation of Bouguer's reduction does not remove correctly the masses outside the geoid. In order to get some idea of the Bouguer-approach, let us summarize a few results of the investigation. Only the order of magnitude seems to be of interest and in that context the discrepancies between BOLMINO's and LEDER-

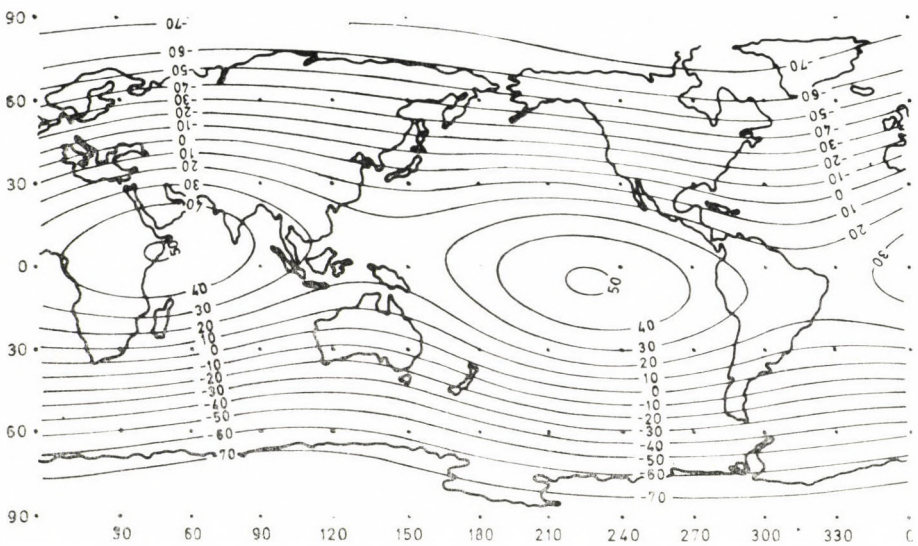


Fig. 8. δN [cm] $= \sum_0^3 \delta N_n$

STEGER's data are found to be mostly small when in addition to the above normalization factor the normalization factors of fully normalized harmonics

$$\sqrt{2n+1}\; P_n^0 = P_n^0 \quad \text{and} \quad P_n^m = \sqrt{\frac{1}{2(2n+1)}\,\frac{(n+m)!}{(n-m)!}}\, P_n^m$$

$$(m \neq 0)$$

are considered. On applying again the surface coating formula (16) as an approximation we get at $r = R$

$$V_n = 4\pi k^2 R Y_n/(2n+1)$$

with

$$k^2 = 66.7 \cdot 10^{-9}\ \text{cm}^3\ \text{g}^{-1}\ \text{sec}^{-2}$$
$$k^2 M = 3.9860 \cdot 10^{20}\ \text{cm}^3\ \text{sec}^{-2}$$
$$Y_n = h_n \cdot \varrho = h_n \cdot 2.7\ \text{g cm}^{-2}$$
$$4\pi k^2 R = 535\ \text{cm}^4\ \text{g}^{-1}\ \text{sec}^{-2};$$

we end up with

$$\mathbf{r}_0\ [\text{m}] = \begin{pmatrix} -39.2 \\ -44.4 \\ -31.8 \end{pmatrix}$$

on applying (3) and LEDERSTEGER's data. Using the value

$$v_0 = 1.083.319.780.000 \cdot 10^{12}\ \text{km}^3$$

as volume of the earth (this is really the volume of the international ellipsoid of 1924) and BALMINO's zero-degree term of the topography, we end up with the ratio

$$\frac{v_g - v_0}{v_0} = 1.035 \cdot 10^{-4}$$

where v_g = volume of the geoid. This value holds for any geoid–co-geoid and does not depend on the specific gravity reduction.

The relative change of mass is about $0.766 \cdot 10^{-4}$.

With BALMINO's second-degree zonal term for the topography we get

$$\Delta J_2 \doteq 0.97 \cdot 10^{-6}$$

using again the surface coating approximation. Then $\Delta J_2/J_2$ is of the order of 10^{-3}.

When the tilt of the axis of maximum moment of inertia due to the full Bouguer correction is considered, we show this fact best by V_2^1/V_2^0; for the cosine-term we obtain

$$V_2^1/V_2^0 = 0.322 \cdot 10^{-12}$$

and for the sine-term

$$V_2^1/V_2^0 = 0.714 \cdot 10^{-11}$$

where the conventional cosine-coefficient of V_2^1 is $2.26 \cdot 10^{-7}$ and the corresponding sine-term is about $4.97 \cdot 10^{-6}$.

With isostatic anomalies where the total mass is conserved there are much smaller deviations of the model from the real earth.

b) Free-air reduction:

In contrast to LEVALLOIS' or JEFFREYS' ideas the classical concept of free-air reduction is based on a transfer of observed stations on to the geoid. As was stated above, there is no contribution to a shift of the geocenter, axes of inertia, etc., unless the mass transportation (condensation) is considered.

In comparison to $\mathbf{r}_0$ in *a)* the shift is very small and depends on the type of condensation. Since there is always a geocenter shift due to condensation we could ask for model effects according to eq. (19).

But from

$$V = \sum_n \frac{Y_n}{r^{n+1}} \rightarrow \frac{-\partial V}{\partial r} = \sum_n \frac{Y_n(n+1)}{r^{n+2}}$$

we get at $r = R$

$$V_n = \frac{R\delta g_n}{n+1}$$

and with $\delta g_1 = 10$ mgal we obtain

$$V_1 = 3.2 \cdot 10^{-6} \text{ sec}^{-2} \text{ cm}^2$$

thus

$$\frac{V}{k^2 M} = 32.6 \text{ m};$$

this value varies, of course, linearly with δg_1.

5. The first-degree harmonics in Stokes' formula

Let us start from the spherical harmonic formula for Stokes' integral

$$T = \Sigma T_n = R\Sigma \frac{\Delta g_n}{n-1} \tag{28}$$

which is a special case of the generalized Stokes' formula as

$$T(r, \theta, \lambda) = \Sigma \left(\frac{R}{r}\right)^{n+1} T_n(\theta, \lambda) \tag{29}$$

$$= R\Sigma \left(\frac{R}{r}\right)^{n+1} \frac{\Delta g_n}{n-1}.$$

Consequently, for $n = 1$, we get

$$T_1 = R\Delta g_1/0$$

which implies that T_1 cannot be determined from Δg_1 because *any value of* T_1 *is compatible with any* Δg_1*-values.*

HEISKANEN and MORITZ [11], therefore, consider the coordinates of the center of the geoid (ellipsoid) with respect to the geocenter as integration constants (which can always be supposed to be zero)

$$\mathbf{r}_0 = \begin{Bmatrix} x_0 \\ y_0 \\ z_0 \end{Bmatrix} = \vec{\mathbf{0}} .$$

But previously the question was posed whether $\Delta g_1 \neq 0$ produced remarkable distortions. The impact of first-degree harmonics in the gravity field on the solution of the geodetic boundary value problem was mentioned, e.g., in [3]. In the strict sense Stokes' formula is only valid for $\Delta g_1 = \Delta g_0 = 0$ [11]. But even under purely formal aspects the balancing of the gravity field does not imply any real improvement as even a very small value of $\Delta g_1 \neq 0$ will yield

$$T_1 = \frac{\Delta g_1}{0} \to \infty .$$

Note that $n = 1$ and not $n \to 1$; however, the latter statement is not important for stable boundary value problems in practice.

This is realized on inspecting the most general formulation of T_1 with $\mathbf{r}_0$ = center of ellipsoid and $\mathbf{r}_0$ = center of mass of the earth (i.e. geocenter) differing from coordinate origin

$$T_1 = \frac{k^2 M}{R^2} [(z_0' - z_0)\, P_{10}(\cos\theta) + (x_0' - x_0)\, P_{11}(\cos\theta)\cos\lambda + \tag{30}$$

$$+ (y_0' - y_0) P_{11}(\cos\theta)\sin\lambda]$$

where $T_1 \to \infty$ results from an *arbitrary* finite Δg_1 according to

$$T_1 = \frac{R \cdot \Delta g_1}{0} \to \infty .$$

But only for $(\mathbf{r}_0' - \mathbf{r}_0) \to \infty$ can this expression become infinite. It is well known that the first-degree term vanishes whenever the coordinate system and mass center of the mass producing the potential field coincide. As a consequence, *regularity at infinity* (see, e.g. KELLOGG) as defined by MOLODENSKY et al.

$$\lim_{r \to \infty} (rT) = \text{const}$$

$$\lim_{r \to \infty} (r^2 T) = 0$$

plays a *significant role in dealing with* $\Delta g_n \to N_n$ *transformations.* The latter formula implies that $r^2 T$ is *bounded in absolute value* which holds whenever the

centers of inertia as well as the (total) masses of earth and ellipsoid are the same. The limes (rT) is related to the coincidence of the axes of rotation and is not of primary interest here. The direct relation of (r^2T) to the boundary condition of physical geodesy in spherical approximation

$$\Delta g = -\frac{\partial T}{\partial r} - \frac{2}{r} T \tag{31}$$

is directly seen on multiplying it by r^2. Then

$$r^2 \Delta g = -r^2 \frac{\partial T}{\partial r} - rT = \frac{\partial}{\partial r}(r^2 T) \tag{32}$$

and after integration in space

$$r^2 T = \Sigma \left(\frac{R}{r}\right)^{n+1} T_n = \int r^2 \Delta g dr = \int r\Sigma(n-1)\left(\frac{R}{r}\right)^{n+1} \times$$
$$\times T_n \, dr = R \int r\Sigma \left(\frac{R}{r}\right)^{n+1} \Delta g_n \, dr \,. \tag{33}$$

By splitting off the first and second harmonics on the right side of the latter equation we get the "modified" Poisson kernel [11] as

$$V = \frac{r^2 - R^2}{l^3} - \frac{1}{r} - \frac{3R}{r^2} \cos \psi \,, \tag{34}$$

where $r^2 - R^2/l^3$ in Poisson's kernel and r^{-2} correspond to the zero-degree term, whereas $3R/r^2 \cos \psi$ corresponds to the first-degree term. On integrating

$$\int_r^\infty r \sum_{n=2}^{\infty} \left(\frac{R}{r}\right)^{n+1} dr = \int_r^\infty rV dr \tag{35}$$

we finally come up with Stokes' well known function; details of integration are found in [11]. One could think of retaining the term of degrees zero and one in the function V, i.e. V equals Poisson's kernel $= (r^2 - R^2)l^{-3}$ but in *that case the regularity at infinity gets lost* because

$$\lim_{r \to \infty} Tr^2 \neq 0 \,.$$

Now, whenever a product $F \cdot V$ is expanded in a series of spherical harmonics as

$$F \cdot V = \Sigma F_n \, \Sigma V_n \rightarrow \text{on integrating} \rightarrow \Sigma V_n \, F_n$$

then, on removing V_0 and V_1 from $\sum_n V_n$ the orthogonality condition is of practical impact in the series. Therefore, we *need not anticipate* that even a very small Δg_1-term in $\Sigma \Delta g_n$ would imply a $T_1 \rightarrow \infty$ according to

$$R \frac{\Delta g_1}{1-1} \rightarrow T_1 \,.$$

Rather, the regularity at infinity is destroyed, so the integral $\int_r^\infty$ is no longer bounded and a *rigorous* solution becomes impossible. In so far a small Δg_1 does not distort completely the computation of the geoid.

6. Tidal effects

6.1 *Sea tides*

According to the classical theory of tides where a harmonic expansion of the tidal potential of degree $n = 2$ is used there is no part of *equilibrium* tides which might produce variations of the location of the geocenter. But as CARTWRIGHT [6] has shown, there is at least one constituent M_1 in the *(dynamic)* ocean tides of the Atlantic Ocean which leads to small asymmetric deformations implying periodic geocenter shifts. But these dislocations are, of course, extremely small since the sea tide amplitudes are not remarkable for M_1.

On the other hand, there are harmonics of degrees $n = 1$ and $m = 2$, which produce small variations of the principal axes of inertia and of the mass center of the earth, respectively. The diurnal K_1 and the semidiurnal constituent M_2 are those waves of the sea tides which are presently best known. In [10] we have seen that for the Atlantic $O_1 \simeq K_1$ in amplitude and phase. This relation holds approximately for the whole globe, to some extent. Thus, in the whole we may state that $K_1 + O_1$ is of the order of magnitude of 2 K_1 in phase and amplitude. The zero-, first- and second-degree terms obtained from

Table I

	n	m	$v = 0°$		$v = 90°$	
			cos-term	sin-term	cos-term	sin-term
	0	0	+0.3526	—	+0.4919	—
	1	0	+0.4012	—	+0.2278	—
	1	1	+0.3053	−0.9230	+0.7055	−0.3148
M_2	2	0	+0.9585	—	−4.3260	—
	2	1	−1.8673	−0.5542	+0.8670	−0.3785
	2	2	−1.5662	+8.4919	+7.8476	+2.8099
	0	0	+0.2484	—	+0.1862	—
	1	0	+0.5226	—	−2.8160	—
	1	1	+0.1300	+0.3368	+0.5602	+0.6859
K_1	2	0	+0.2360	—	−0.9382	—
	2	1	−2.2131	+0.4907	+3.5447	+4.9609
	2	2	+2.3573	+0.4816	−0.8783	−2.6258

our above mentioned harmonic analysis of K_1 and M_2 sea tidal constituents are given in Table I in terms of fully normalized spherical harmonics. It needs to be pointed out that for theoretical reasons there must not be a zero- degree term in the sea tide expansion. Consequently, those values in Table I might be considered as indicators of the errors inherent in that expansion.

Therefore, it should be noticed that coefficients of degree one as well as those of terms (2, 1) and (2, 2) are relatively large in comparison to (0, 0). This means that the variation of equatorial ellipticity inherent in (2, 2) and change in direction of the axis of maximum moment of inertia are indeed significant. The effects due to (2, 1) terms are less than ten times as big, i.e. 1 or 2 cm at best. In evaluating the data in Table I we have used the following quantities:

χ = phase lag with respect to Greenwich zero time,
v = Greenwich phase of equilibrium,
H = tidal amplitude [cm] $= H\cos(v - \chi)$.

Now, with

$$H = \sum_n H_n = \sum_{n,m} (H_n^m \cos m\lambda + h_n^m \sin m\lambda)\ P_n^m \tag{36}$$

we get in fully normalized form

$$H\cos\chi = \sum_{n,m} (\bar{A}_n^m \cos m\lambda + \bar{B}_n^m \sin m\lambda)\ \bar{P}_n^m \tag{37}$$

$$H\sin\chi = \sum_{n,m} (\bar{C}_n^m \cos m\lambda + \bar{D}_n^m \sin m\lambda)\ \bar{P}_n^m\ , \tag{38}$$

where $\bar{A}_n^m$, $\bar{B}_n^m$, $\bar{C}_n^m$ and $\bar{D}_n^m$ are the fully normalized coefficients given in Table I; the corresponding power spectra were given by (GROTEN and BRENNECKE (1973, 1974).

On applying again formula (15) we get for the potential coefficients at station P at $r = R$

$$V(P) = 4\pi k^2 R \Sigma\, Y_n/(2n + 1) \tag{39}$$

and, therefore, the corresponding variations of potential coefficients for $n = 1$ as

$$-\bar{J}_1^0 = 4\pi\varrho\, R^3 \left\{ \begin{matrix} \bar{A}_1^0 \\ \bar{C}_1^0 \end{matrix} \right\} \Big/ (M(2n + 1)) \tag{40}$$

$$-\bar{J}_1^1 = 4\pi\varrho\, R^3 \left\{ \begin{matrix} \bar{A}_1^1 \\ \bar{C}_1^1 \end{matrix} \right\} \Big/ (M(2n + 1)) \tag{41}$$

$$\bar{K}_1^1 = 4\pi\varrho\, R^3 \left\{ \begin{matrix} \bar{B}_1^1 \\ \bar{D}_1^1 \end{matrix} \right\} \Big/ (M(2n + 1)) \tag{42}$$

where $\varrho = 1.03$ cgs (density of sea water), $M =$ terrestrial mass; with $v = 0^0$ and 90°, respectively and $\chi = 0°$, we get geocenter variations (for all coefficients) which are less than one millimeter.

6.2 *Atmospheric tides*

The diurnal planetary wave is very small; the greatest semidiurnal wave W_2^2 corresponding to the sectorial harmonics P_2^2 has a maximum amplitude of 1.5 mbar [14]. Regional and aperiodical air pressure variations may be greater by a factor of ten; the tides excited by gravitation and temperature variation are greatest at high altitudes. Nevertheless, we have to expect only small dislocation of the geocenter because atmospheric tides comply much better with the theory than oceanic tides do. In comparison, the aperiodic variations in the lower atmosphere are much greater. But because of regional extent of such "lows" and "highs" they can only be represented by very high spherical harmonics expansion. Therefore they usually do not affect geocenter positions.

7. Topography of sea surface

Since the sea surface deviates from the geoid results of sea gravimetry need to be corrected for $H =$ separation of sea surface from the geoid in terms of an additional free-air correction:

$$\delta g = 0.3086 \; H = 0.3086 \sum_n H_n = a \cdot H \,, \tag{44}$$

where H_n is the spherical harmonic of degree n. On expanding LISITZIN's wellknown data of sea surface topography variations h in terms of spherical harmonics we found with

$$\bar{h} = \frac{1}{O} \int_0 \int h do \tag{45}$$

where $O =$ ocean surface and do is an infinitesimal element of O, i.e. the integral in (45) is the world wide average of h *in ocean areas*; for degrees 1 to 3 the results are given in Table II.

There (again) fully normalized coefficients for

$$H = h - \bar{h} = \Sigma H_n \tag{46}$$

are shown. The corrections to geoid undulations δN are then found from Bruns' formula

$$\delta N = \frac{R}{\gamma} a \sum_{n=2}^{35} H_n/(n-1) \tag{47}$$

Table II

	cos-term [cm]	sin-term [cm]
$n = 1$		
$m = 0$	+7.710	—
$m = 1$	−17.690	+4.994
$n = 2$		
$m = 0$	−16.245	—
$m = 1$	−0.181	+4.306
$m = 2$	−0.398	+3.308
$n = 3$		
$m = 0$	+0.575	—

δN is given in a forthcoming paper by GROTEN and BRENNECKE for the whole world. These data are the corrections which need be applied to a terrestrial geoid. But since, at present, most geoids are evaluated from a combination of satellite harmonics for $n \leq 16$, we also give in the last mentioned paper δN for degrees ($12 \leq n \leq 35$). The latter results seem to be most appropriate for correcting actual geoids.

It is, of course, impossible to evaluate the first-order coefficients of the geoid corrections δN. But using a surface coating of density $\varrho = 1.03$ times H we get from formula (16) the corresponding potential effect

$$\delta V_n(P) = 4\pi k^2 R H_n \varrho/(2n + 1), \tag{48}$$

and e.g., for $n = 1$

$$\delta V_1(P) = \frac{4}{3} \pi k^2 R H_1 \varrho. \tag{49}$$

It is found to affect the geocenter by less than 1 mm in any case.

8. Conclusions

The above statements concerning the (2, 1) terms of the potential affect primarily the axis of maximum moment of inertia, i.e. the "previous" figure axis of the earth; they consequently induce a *slight* wobble whenever affecting the position of the figure axis with respect to the instantaneous axis of rotation. Since, in general, the wobbling of the earth is a question which still seems to be open [5], those slight effects discussed in the present paper do not yet imply consequences for present observation accuracies.

On combining the results found by STOLZ [20] with ours we conclude that variations of geocentric positions due to physical events like variations of

fluid masses are not as big as is often assumed. Consequently, determination of geocentric positions may be considered as *stationary within centimeter range* and measurements of geocentric station vectors over longer time spans might improve the accuracy and can yield bias-free estimates within centimeter range. The motion of the mean equinox does not yet seems to be fully explained because of deficiencies in determining the motion of the ecliptic; with the feasibility of distances the spherical astronomy concept is, in addition, insufficient even in the modern definition of the ecliptic.

In general, the consideration of effects producing coordinate variations and deviations <30 cm is problematic, at least at present; for precession and — mainly — nutation terms are presently determined with accuracies of a few decimeters over longer time spans. Consequently, the "nutation" in a space fixed framework corresponding to the terrestrial Chandler wobble is not yet considered at present. On the other hand, the above discussed motion of the geocenter is of relatively short period but also of small amplitudes.

In dealing with a deformable earth, the axis of figure is no longer uniquely defined if it is assumed non-coincident with the axis of maximum moment of inertia. The latter axis changes its position with respect to the earth's surface in case of moving masses as, e.g., fluid masses and tectonic plates. The angle between rotational momentum and $\vec{\omega}$ (inst.) is supposed to be of the order of 1.7 cm (GAPOSCHKIN, 1972); this "sway" can be neglected in view of uncertainties in the other axis position. But it becomes clear that the identification of CIO with the "conventional axis of figure", as done by GROTEN [8], makes sense to some extent. The "polyhedron" mentioned above is, however, not dismissible in high-precision work.

The identification of the figure axis with CIO is justified by geodetic practice where the ellipsoidal minor axis is supposed to coincide with CIO in reducing latitude observations. Only in that case a purely geometrical concept (ellipsoidal figure) of axes is in order.

Since the astronomical equator and the equinox are connected with the solar system through the declinations of planets and the positions of sun and moon based fundamentally on NEWCOMB's and HILL-BROWN's theories, respectively, the ordinary spherical astronomy is to be revised in view of directions which are no longer free to translation. This implies that the ecliptic which, on neglecting planetary forces, moves around the earth—moon barycenter as shown in Fig. 3, can no longer be shifted arbitrarily in such a way that the plane of ecliptic passes through the center of the "Gaussian directions sphere" ("Richtungskugel").

The motion of the geocenter is found to be so small that today the separation of the instantaneous rotation axis from the terrestrial mass center cannot be of any remarkable influence. When going into details we need, of course, to keep in mind that the barycenter ($\doteq$ gravity center) of the earth is different

from the mass center to which $\vec{\omega}$ is basically related. The barycenter is shifted due to the lunisolar, planetary attraction, etc.

Elementary cases of systems of rotating bodies and of bodies for time-varying moments of inertia corresponding to the real earth are dealt with in textbooks like MAGNUS [22]. But our results may corroborate that those cases are not of primary concern in our cases today.

The classical concept of Stokes' boundary value problem involves a number of difficulties in dealing with high-precision geodesy. Even though a few corresponding effects (like tilt of axis of maximum moment of inertia due to mass transport, etc.) are *not* yet relevant, with increasing accuracy of measurements the *conceptual* difficulties prevail and, e.g., the unknown discrepancies between geoid and real earth become significant. Thus, Stokes' concept is only useful as a zero approximation of the free boundary value problem.

BROSCHE and SÜNDERMANN [16] who considered the *integrated* sea tide effect came up with a 2 cm amplitude in an M_4-type wave as a result of M_2. With global elasticity we arrive at about 20 cm instead of the before mentioned value of 1.7 cm.

With uncertainties of about $\pm 0.01''$ in nutations we end up with errors no less than 30 cm in data referred to celestial systems which are still enlarged by proper motion, etc. So, with very long arcs at present a lot of difficulties arise; also in non-celestial systems — like the geographical one — where nutations are without primary effect, due to difficulties in handling very long orbital arcs, sufficient accuracy is not yet obtained at present; corresponding difficulties which arise even with shorter arcs are seen, e.g., in [25].

REFERENCES

1. BALMINO, G.—LAMBECK, K.—KAULA, W. M.: A spherical harmonic analysis of the earth's topography. *J. Geophys. Res.*, 78(1973), 478—480.
2. BENDER, P. L.: Prospects for rapid realization of a quasi earth fixed coordinate system, IAU Colloq. 28, Torun/Poland, B. Kolazek and G. Weiffenbach eds, 297—302, Warszawa 1975.
3. BJERHAMMAR, A.: On the gravity field of the earth, *Ann. Acad. Sci. Fenn.* A III 61, 43—53, Helsinki, (1961).
4. BOMFORD, G.: Geodesy. Clarendon Press, Oxford 3rd ed. 1971.
5. CAPITAINE, N.: Total effect of any Nearly-Diurnal Wobble of the earth's axis of rotation in latitude and time observations. Application to the Paris Astrolabe observations from 1956.6 to 1973.8. *Geophys. J. R. astr. Soc.*, 43(1975), 573—588.
6. CARTWRIGHT, D. E.: A subharmonic linear tide in the seas off western Europe. *Nature*, 257, (1975) 277.
7. EICHHORN, H.: Astronomy of Star Positions. Frederick Ungar. Publ. Co., New York 1974.
8. GROTEN, E.: Some problems related to geodetic datum definition for terrestrial measurements, IAU Colloq. 28, Torun/Poland, B. Kolazek and G. Weiffenbach eds, 247—259, Warszawa 1975.
9. GROTEN, E.: Zur Definition astrogeodätischer Koordinatensysteme. *Z. Vermessungswesen* 101(1976), 25—37.
10. GROTEN, E.—BRENNECKE, J. : Global sea tide effects of O_1 and K_1 constituents in earth tide gravity observations. *Rev. Ital. Geof.*, 23(1974), 133—136.

11. HEISKANEN, W. A.—MORITZ, H.: Physical Geodesy. Freeman Co., San Francisco 1967.
12. HOERMANDER, L.: The boundary problems of physical geodesy, The Royal Inst. of Technology, Division of Geodesy, Stockholm 1975.
13. JUNG, K.: Figur der Erde, Handb. der Geophysik, S. Flügge ed. vol. XLVII Geophysik I. Springer Verlag Berlin 1956.
14. KERTZ, W.: Atmosphärische Gezeiten, Handb. d. Physik, S. Flügge ed., Band Geophysik II, 928—978, Springer Verlag, Berlin 1957.
15. LAMBECK, K.: Temporal variation of rotational origin in the absolute value of gravity. *Studia geophys. et geod.*, 17(1973), 269—272.
16. BROSCHE, P.—SÜNDERMANN, J.: Effects of oceanic tides on the rotation of the earth, (Manuskript) Univ. of Bonn. 1976.
17. LEDERSTEGER, K.: Handbuch der Vermessungskunde V, Jordan, Eggert, Kneißl (eds), Stuttgart 1969.
18. MATHER, R.: Reference coordinate system requirements for geodesy and ocean dynamics, IAU Colloq. 28, Torun/Poland, *B. Kolazek* and *G. Weiffenbach* eds, 93—114, Warszawa 1975.
19. MORITZ, H.: Eine Integralgleichung des Geoides, *Gerlands Beitr. Geophysik*, 70 (1961)
20. STOLZ, A.: Changes in the position of the geocentre due to seasonal variations in air masses and ground water. *Geophys. J. Roy. Astr. Soc.*, 44(1976) 19—26.
21. VEIS, G.: Precise aspects of terrestrial and celestial reference frames, SAO Special Report 123, Cambridge 1963.
22. MAGNUS, K.: Kreisel, Theorie und Anwendungen. Springer, Berlin 1971.
23. WOOLARD, E. W.: Theory of the rotation of the earth around its center of mass, Astron. Papers XV, I, U.S. Govt. Printing Office, Wash. 1953
24. WOOLARD, E. W.: Spherical Astronomy, Academic Press, New York 1966.
25. DUNN, P. J.—SMITH, D. E.—KOLENKIEWICZ, R.: The measurement of latitude, time and height variations of laser tracking station. *JGR*, 82(1977), 895—897.

ИЗМЕНЕНИЕ ВО ВРЕМЕНИ ГЕОЦЕНТРИЧЕСКОГО ПОЛОЖЕНИЯ

Э. ГРОТЕН

РЕЗЮМЕ

Такие методы пространственной геодезии, как измерение расстояний до Луны или до спутников, позволяют выявлять изменения геоцентра в системе относимости, зафиксированной в теле «псевдо-Земли». Порядок перемещения геоцентра оценивается на основе движения террестрических жидкостных масс. В статье рассфатривается и точное определение геоцентра (центра массы Земли).

С точки зрения высокоточной геодезии и сопоставления классических определений геоида с современными представлениями автор указывает на некоторые проблемы классического понятия геоида.

Acta Geodaet., Geophys. et Montanist. Acad. Sci. Hung. Tomus 14 (1—2), pp. 59—69 (1979)

ON THE USE OF BANDWIDTH AND PROFILE REDUCTION IN COMBINATION SOLUTIONS OF SATELLITE ALTIMETRY*

G. HEIN—E. GROTEN

INSTITUT FÜR PHYSIKALISCHE GEODÄSIE, TECHNISCHE HOCHSCHULE, DARMSTADT

[Manuscript received September 5, 1977]

When gravity material on land is combined with altimeter data in oceanic areas the collocation or adjustment approaches lead to large, sparse occupied normal equation matrices. By using graph-theoretical methods for reducing the bandwidth and profile of a sparse matrix, the time-consuming elimination process to get the unknowns can be shortened significantly.

In testing different bandwidth and profile reduction algorithms at some examples first experiences are pointed out. The use of other possibilities to minimize storage and time is discussed.

1. Introduction

Beside conventional triangulation and modern triangulation-trilateration systems data processing in satellite altimetry is a typical example where large sparse symmetric matrices arise. This case is quite similar to — or can be considered as part of — T. KRARUP's "integrated geodesy". With altimeter data processing orbital tracking information and dense gravity material *on land* is combined with altimeter data in oceanic areas. Whenever, in addition, other terrestrial data on land and/or seaborne or airborne information over the oceans is incorporated in the adjustments, collocation and mixed boundary value problem approaches (having signal and error covariances mainly depending on data location separation) lead to normal equation systems where special sparse matrix techniques are useful. GROTEN and SCHAAB [14] have discussed global solutions of that kind where gradiometry, gravimetry and altimetry data were applied in combined solutions. But in refined applications of global types "stripe" and "spots" solutions are of main practical impact. Such solutions are of primary importance along coast lines with sea data and continental geodetic material put together and crosscorrelation of errors affects only limited parts of the sea and land areas, respectively. But because of irregular shapes of coastal lines instead of banded matrices, sparse systems arise.

Handling with *large* sets of linear equations, we look for systems with a large number of unknowns, e.g. several thousands. The new adjustment of the North American Horizontal Datum requires, e.g. the computation of approximately 500 000 unknowns simultaneously [3].

* Paper submitted to the "International Symposium on Satellite Geodesy", Budapest, Hungary, June 28th—July 1st, 1977.

In view of the sparsity of such normal equation matrices special techniques to minimize storage and computer time are necessary. So we can try to verify the methods in strategies which (tend to) get optimal

(i) numbering of the unknowns (before the adjustment)

(ii) reordering of the normal equation matrix to produce special structures (e.g. banded forms)

(iii) elimination processes (e.g. minimum "fill-in").

Optimal numbering of the unknowns to get a special structure of the normal equation matrix can be found in problems of analytical photogrammetry, e.g. in bundle adjustments [12, 16] but also in geodesy [29]. GERGEN [8] investigated sorting techniques in trigonometric net adjustments based on the relative positions of points on the earth's surface. The unknowns were rearranged into blocks bordered by geographic latitude and longitude. The resulting normal equation matrix was neither minimum band width nor minimum fill-in but it tended to near minimum conditions by this simple procedure.

The Stuttgart group especially concerned with nonlinear adjustment [15] propagated a four-step factorization scheme consisting of optimal ordering, symbolic factorization, numerical factorization and solution. The ordering algorithms (sorting the rows by increasing or minimal length) do not produce banded matrices but minimize approximately the number of additional nonzero elements ("fill-ins") which are introduced by the factorization [28].

Our American colleagues plan to use in the adjustment procedure for the North American Datum an algorithm for reducing the bandwidth of the normal equation matrix and the Helmert–Wolf blocking technique to partition the system into blocks of about 2000 unknowns [6, 17].

In the last years several authors were concerned with storing methods and solution of large geodetic nets, e.g. ASHKENAZI [1], HAAG [16], SCHMITT [29].

The aim of our work is to investigate the structures of the normal equation matrices arising in combination solutions proposed by GROTEN [13] and GROTEN, and SCHAAB [14] and to discuss the possibilities in solving such large systems. In particular, we are concerned with methods for reducing the *bandwidth* and/or *profile* of symmetric, positive definite matrices.

The problem can be stated mathematically in the following way:

The linear algebraic normal equation system

$$\mathbf{N}\mathbf{x} = \mathbf{c}\,, \tag{1}$$

where $\mathbf{N} = (n_{ij})$ a sparse symmetric and positive definite matrix, is to be ordered by row and column permutations into the permuted linear system

$$\mathbf{P}\mathbf{N}\mathbf{P}^T(\mathbf{P}\mathbf{x}) = \mathbf{P}\mathbf{c}\,. \tag{2}$$

Variant 1. Bandwidth minimization

We want to determine a minimum bandwidth b which is defined by

$$b(\mathbf{N}) = \max \{|i - j| : n_{ij} \neq 0\} . \tag{3}$$

Variant 2. Profile reduction

We want to reduce the profile of the $n \times n$ sparse matrix $\mathbf{N}$.

Set $f_i = \min \{j : n_{ij} \neq 0\}$ for $i = 1, 2, \ldots, n$
and let $d_i = i - f_i$.

The profile is then defined to be

$$p = \sum_{i=1}^{n} d_i . \tag{4}$$

Due to the fact that the applied algorithms are found by graph theory, we will briefly point out the basic definitions and theorems for the reader who is not familiar with this part of mathematical science.

2. Remarks on graph theory

2.1 *Definitions*

The following definitions can be found in textbooks on graph theory, e.g. NOLTEMEIER [27] or in books on sparse matrix techniques, e.g. TEWARSON [31].

Definition 1

If $\mathbf{V}\{v_1, v_2, \ldots, v_n\}$ is a finite nonempty set and $\mathbf{E} \subseteq \{\{v_i, v_k\},\ v_i,\ v_k \in V\}$ is a collection of unordered pairs of elements of $\mathbf{V}$, then $\Omega = (\mathbf{V}, \mathbf{E})$ is a *finite undirected graph.*

Remarks

We call the elements of $\mathbf{V} = \mathbf{V}(\Omega)$ the *vertices* and the elements of $\mathbf{E} = \mathbf{E}(\Omega)$ the *edges*. The edges v_i and v_k are said to be *adjacent* if $\{v_i, v_k\} \in \mathbf{E}$. The *degree* of a node v_i (vertex) is the number of edges adjacent to it. See, for example Fig. 1.

A *path* of length k is a sequence of edges $\{v_0, v_1\}, \{v_1, v_2\}, \ldots, \{v_{k-1}, v_k\}$ such that $v_i = v_j$ implies $i = j$. If there is a path connecting each pair of vertices then the graph Ω is connected. We call the shortest path from one vertex v_i to another v_j the *distance* between vertices v_i and v_j.

Definition 2

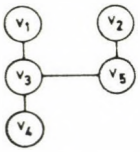
If $\mathbf{V} = \{v_1, v_2 \ldots, v_n\}$ is the set of vertices of a graph $\Omega = (\mathbf{V}, \mathbf{E})$ with $n \geq 1$, then the graph is a *tree* if only at least one of the following statements holds:

(i) Ω is weakly constrained and $| \mathbf{E} | = n - 1$

(ii) Ω contains no cycle, that means $\mathbf{E} \subseteq \{\{v_i, v_k\} : v_i \neq v_k\}$, and $| \mathbf{E} | = n - 1$.

Remarks

In connection with the problem of bandwidth minimization the *level structure* $\mathfrak{L}(\Omega)$ or also named the spanning tree of Ω (**V**, **E**) is important.



$\Omega = \Omega$ (V, E)

$V = [v_1, v_2, v_3, v_4, v_5]$

$E = [[v_1, v_3], [v_2, v_5], [v_3, v_5], [v_3, v_4]]$

Fig. 1

Definition 3

A level structure $\mathfrak{L}(\Omega)$ of a graph $\Omega = (\mathbf{V}, \mathbf{E})$ is the partition of the set of vertices $\mathbf{V}(\Omega) = \{v_1, v_2, \ldots, v_n\}$ into levels $L_1, L_2, \ldots, L_k$ such that all vertices belonging to level L_i have the distance 1 to the vertices of the level L_{i-1} and do not belong to level L_{i-2}.

Remarks

In such a way a *spanning tree* is defined. The nodes belonging to level L_i have the distance i from the foot of tree or starting point which in general is a vertex of minimum degree. The number $k = k(\mathfrak{L})$ is called the *length* of the level structure, and the width $w = w(\mathfrak{L})$ is defined by

$$w(\mathfrak{L}) = \max |L_i| \,. \tag{5}$$

The rooted level structure at a vertex $\mathbf{V}(\Omega)$ is

$$\mathfrak{L}(V) = \{L_0(V),\ L_1(V), \ldots, L_k(V)\} \,,$$

where $L_0(V) = \{V\}$, and $L_i(V)$ is the set of those vertices of level $L_{i-1}(V)$ not yet assigned to a level.

2.2 *On the use of graph theory in geodetic problems*

Graph theory becomes more and more important in the analysis of geodetic nets (see for example the early work by KOROBKOV [22—25] or quite recently the application in optimization of geodetic networks [20]).

In so far, we want to point out the correspondence between matrices and graphs. Each structure of a symmetric quadratic matrix $\mathbf{N} = (n_{ik})$ (e.g. normal equation matrix) can be associated by an unoriented graph $\Omega(\mathbf{N}, \mathbf{E})$ with $\mathbf{V} = \{v_1, v_2 \ldots, v_n\}$ as the numbers of rows or columns, respectively, and the set $\mathbf{E}$ consisting of the pairs $\{v_i, v_k\}$ which stand for the connection of an element $n_{ik} \neq 0$ in row i and column k. The size of the elements is not of interest.

In Fig. 2 the structure of the matrix belonging to the graph in Fig. 1 is outlined.

$$\mathbf{N} = \begin{bmatrix} x & o & x & x & o \\ o & x & x & o & o \\ x & x & x & o & x \\ x & o & o & x & o \\ o & o & x & o & x \end{bmatrix}$$

Fig. 2

Of significance to the methods of bandwidth and profile reduction is the fact that permuting the rows and columns by $\mathbf{P}$ [(see eg. (2)] corresponds to renumbering the vertices of a graph.

The permutation matrix $\mathbf{P} = (p_{ij})$ consists of elements $p_{ij} = 1$ interchanging the unknown i by the unknown j and the corresponding rows, respectively. If $p_{ij} = 0$ or $p_{ii} = 1$, no interchange is to be performed.

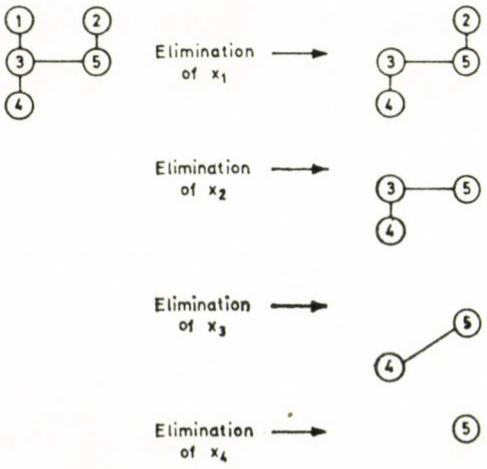


Fig. 3

By graph theory the structures of a matrix during the particular steps of the elimination process by GAUSS or CHOLESKY can be described in a simple way. On eliminating the unknown x_i, the graph of the remaining system arises by

(i) eliminating the node (vertex) v_i and all adjacent edges containing v_i and

(ii) connecting all vertices v_k having the distance 1 from v_i by pairs. Every new edge specifies "fill-ins".

In Fig. 3 the elimination process of the matrix given in Fig. 2 is shown.

In general, the fill-ins should be a minimum which corresponds to a minimum of new edges in the graph-theoretical approach stated above [7, 18]. In so far the elimination process of the matrix in Fig. 2 becomes an optimum if we change the sequence in Fig. 3 into $x_1 - x_2 - x_4 - x_3 - x_5$.

Another application of graph theory, however never used in geodesy, is given by the error analysis of sparse matrices [2, 4].

On showing the basic concepts of graph theory, we will outline now the methods used for reducing the bandwidth and profile of a matrix.

3. Bandwidth minimization and profile reduction

3.1 *Basic concepts*

The several strategies to minimize storage and computer time are verified in chapter 1. Reordering strategies during the elimination process for minimizing the fill-ins (group iii) as described by SCHEK et al. [28] are preferable in case of strong networks where the band of the resulting normal matrix is large and a lot of null-elements are within the band. Such methods have the property to determine the local minimum for each elimination step. The global minimum for the elimination process cannot be reached in practice but the methods tend to get it.

However, the large adjustment problems with more than, say, 10 000 unknowns seem to require satisfactory structures of the normal equation matrix [31]. So the most important structure in geodetic and photogrammetric adjustments is the band form. The elimination time is proportional $n \cdot b^2$ (n = number of unknowns and b defined by (3)). The storage capacity is of the dimension $n \cdot (b + 1)$ disregarding the null-elements within the band. However, in case of *profile* reduction the variable band storage mode as described by JENNINGS [19] is preferable.

3.2 *Algorithms*

Of the several algorithms published in the last years we used the probably most widely known one by CUTHILL, and MCKEE [5], the recently published method by GIBBS et al. [10] as well as the newest algorithm by GIBBS [9]. By

comparison, the mentioned algorithms seem to be the only ones which are useful in practice today [11]. In the following we briefly describe the methods by graph theory.

3.21 *CM-algorithm* [5]

The algorithm consists of a direct method of renumbering the nodes of the graph associated with the symmetric matrix **N** in increasing order of degree. It corresponds to the generation of a spanning tree in level-by-level fashion as noted by definition (3) of 2.1. A weak point is the search for a starting node which in general is a vertex of minimum degree. There are some modifications of this algorithm in the mathematical literature. So the bandwidth is improved by renumbering the label sequence in the *reverse* way [26].

3.22 *GPS-algorithm* [10]

This ordering algorithm is significantly faster than the CM-algorithm and preferable — like CM — in case of *bandwidth minimization*. The basic concept lies in the choice of the endpoint of a *pseudodiameter u, v* or also called *pseudo-peripheral nodes* as starting nodes. There are a pair of vertices that are at nearly maximal distance apart. In a second step the rooted level structures L_w, L_v generated by the iterative procedure to find the pseudo-peripheral nodes are used to partition the set of vertices into levels in such a way that the level width is nearly minimized. The vertices are numbered then level by level beginning at the (pseudo-) peripheral node of lower degree.

3.23 *G-algorithm* [9]

In a recent comparison GIBBS et al. [11] found that KING's algorithm [21] most often produces the best *profile* but it sometimes shows an erratic behavior. To combine the better features of the GPS-algorithm concerning computation time and starting notes with the above mentioned characteristic of the KING-algorithm in producing best profile, GIBBS [9] presented a new "hybrid" algorithm which uses the pseudo-peripheral nodes as starting nodes and renumbers the generated level structure according KING's strategy. Test results proved that the G-algorithm is superior to GPS in *reducing profile*. However, the performance takes more time.

There has been just published in the geodetic literature another method for profile reduction called "banker's algorithm" [30]. Comparing it with the reverse CM, its superiority was concluded. Unfortunately, there is no comparison between the described algorithms (GPS, G) and banker's algorithm.

4. Investigated examples

As already mentioned, we wanted to investigate the structures of the normal equation matrices arising by combining altimeter data in oceanic areas and gravity material on land as proposed by GROTEN [13] and GROTEN and

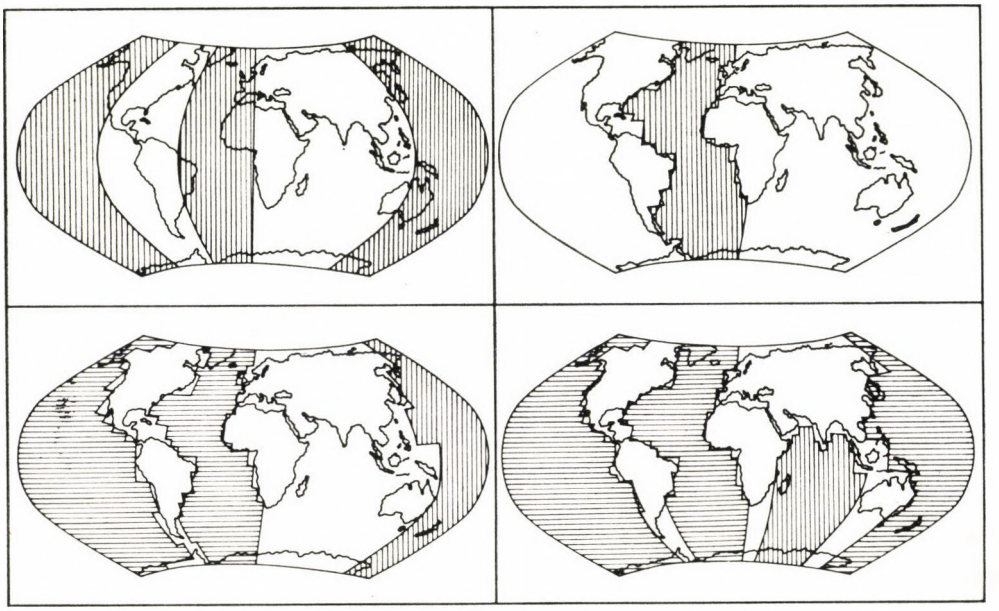
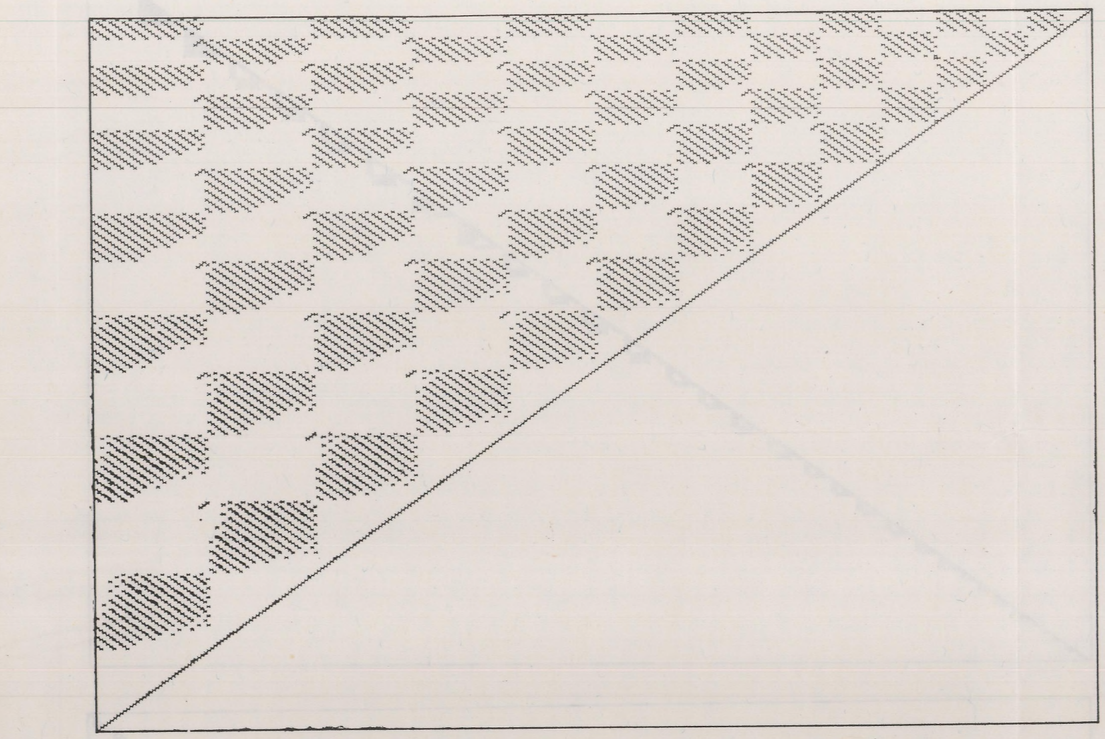


Fig. 4. Simple combination models (▤, ▥ altimeter data, □ Δg-data)

SCHAAB [14]. The approach is based on a determination of the set of harmonic coefficients of any orthogonal series, using the original function as well as its derivatives.

Considering that the presently available altimeter data are restricted to a few profiles in local areas combinations as shown in Fig. 4 or similar forms are of interest. We have dealt in our examples with a division of the earth in 5-by-5-degree blocks and $(n, m) = 18$ as the degree and order of spherical harmonics. The sparse matrices (see Figs 5—7) arise by the fact that in consequence of the size of certain elements (in relation to the size of the elements on the main diagonal) a lot of elements can be neglected and set equal to zero without loss of accuracy of the result. Otherwise, the solution of the fully occupied systems is questionable for large (n, m) in consideration of computer time. So it was the aim of our investigations to look for satisfied structures in renumbering the normal equation matrices by the described algorithms.

The results concerning values of profile, bandwidth and computer time are summarized in Table I. For three matrices of the investigated cases stated



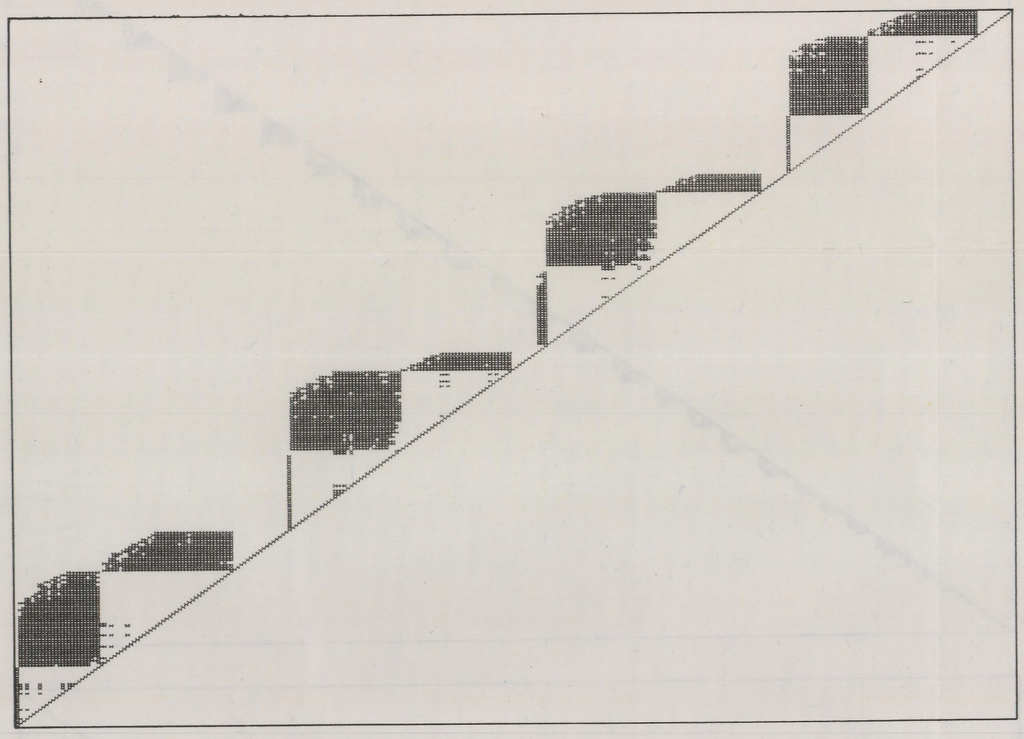
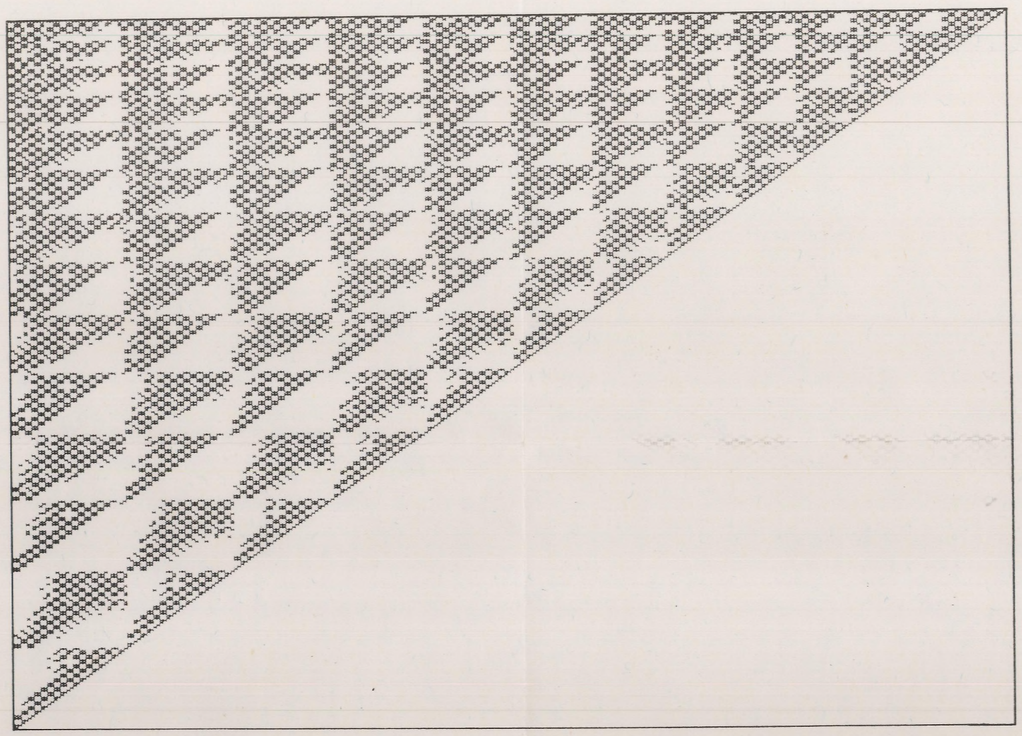


Fig. 5. Matrix structures. Left: original, middle: reordered by GPS, right: reordered by G



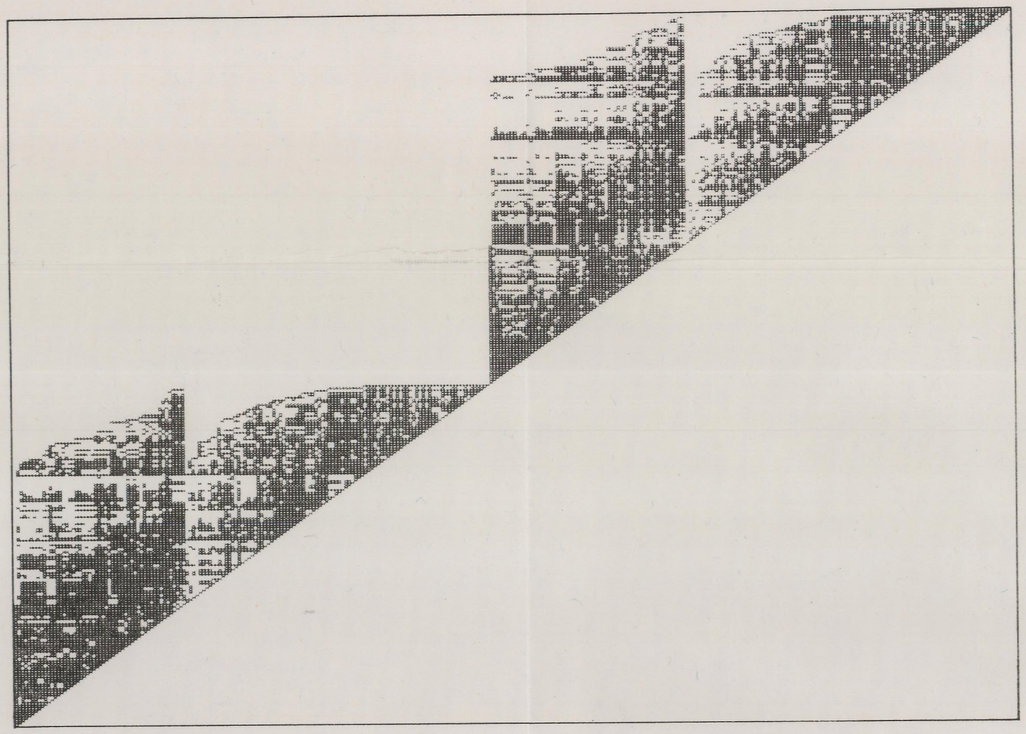
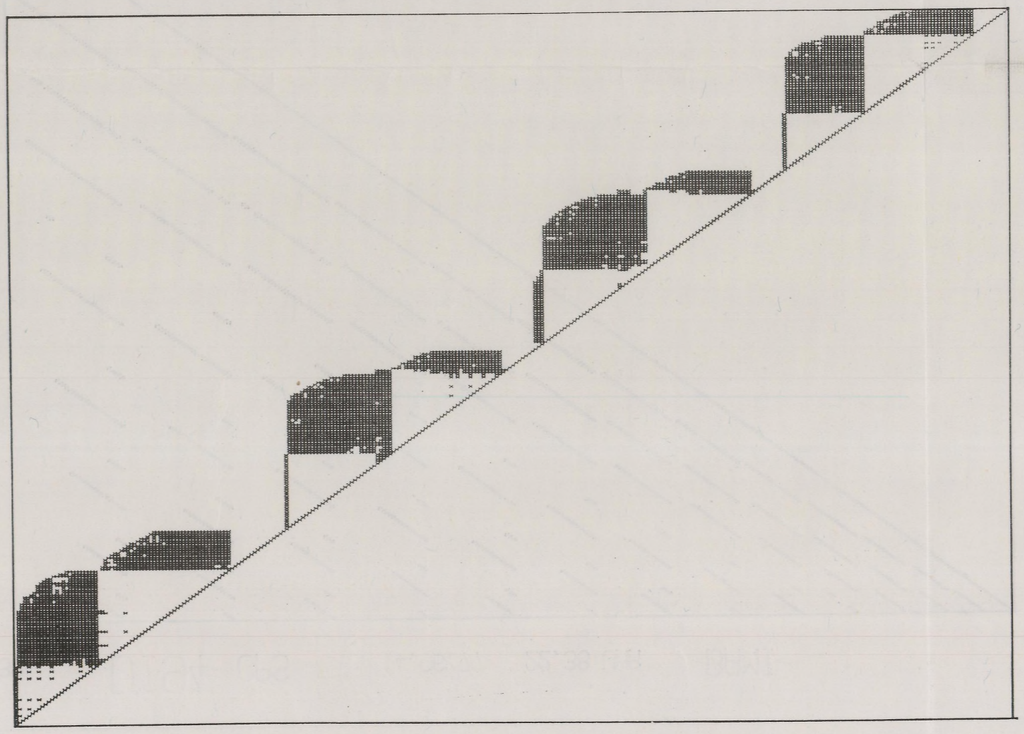
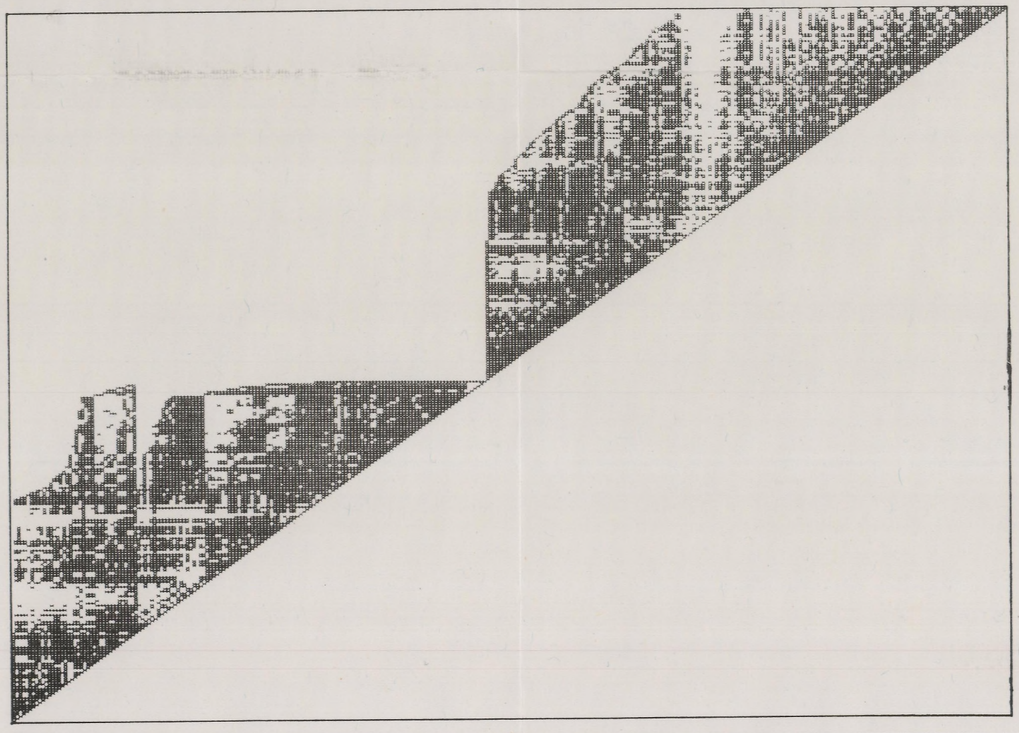


Fig. 6. Matrix structures. Left: original, middle: reordered by GPS, right: reordered by G





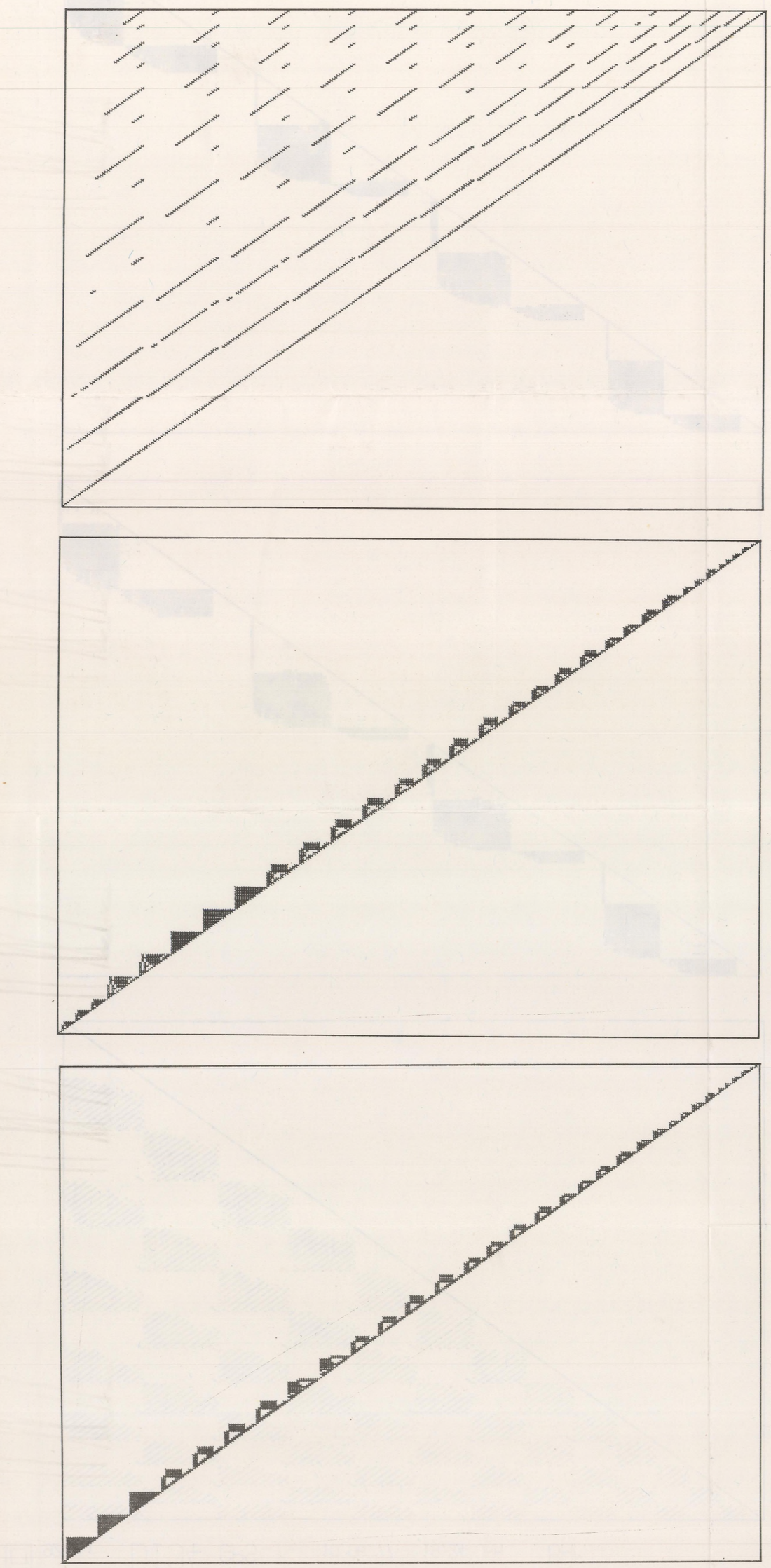


Fig. 7. Matrix structures. Left: original, middle: reordered by GPS, right: reordered by G

Table I

Bandwith, profile and computer time of the investigated examples

Order of matrix n	Original bandwidth	Original profile	Number of non-null elements	Bandwidth after reordering	GPS-algorithm		G-algorithm		
					profile after reordering	CPU-time* (in seconds)	bandwidth after reordering	profile after reordering	CPU-time* (in seconds)
308	307	45.631	19 514	170	30 756	0.98	181	30 671	31.79
308	307	45 574	11 858	144	15 935	2.75	109	14 932	12.29
308	307	45 757	13 238	127	20 295	1 29	104	18 608	7.97
308	307	45 536	10 608	58	9 415	0.76	55	9 273	1.62
308	299	36 772	13 422	174	23 243	1.80	245	20 539	40.25
308	273	28 827	2 580	28	1 815	0.27	29	1 827	0.49
308	273	28 857	2 676	13	1 358	0.41	13	1 356	0.41
308	307	46 908	27 438	131	20 073	1.03	118	18 823	18.54
308	307	46 955	32 270	148	21 637	10.42	120	20 481	26.73

* Computations are performed on an IBM-Computer model 370/168 (OPT = 1)

above graphical plots are shown in Figs 5—7 to demonstrate the different renumbering. In all examples the most widely used CM-algorithm (not listed in Table I; see also a previous publication*) took more computation time than the GPS-algorithm. Additionally, the bandwidth produced by GPS was less, and in view of the fact that the original matrices often could be reordered into several *independent* submatrices (see Figs 5—7), it was necessary to take more than one starting point when using CM because of independent graphs.

In respect of the computation time the GPS-algorithm is also superior to the G-algorithm although the last produces the best profile. The computation time is about $1.0 \times n \exp(1.3)$ for GPS (n = order of matrix) for the matrices arisen in the investigated combination solutions which seems to be less than stated in [11].

It can be concluded that using GPS satisfied matrix structures are produced in the approach proposed by GROTEN [13]. The results give the occasion for further investigations of the method in order to prepare it for practical purposes. The G-algorithm is not of practical interest concerning our problem because of the higher computation time. The improvement in profile is not significant.

* HEIN, G., GROTEN, E. (1977) On the Use of Bandwidth Minimization in Geodetic and Photogrammetric Problems. Paper presented at CERN-Workshop "Processing of Special Large Matrices for Geodesy—Interpretation of the Results", Genfeva, 1st—4th March 1977.

REFERENCES

1. ASHKENAZI, V.: The Adjustment and Analysis of Very Large Networks. *Canad. Surv.* 28(1974), 653—662.
2. BAUER, F. L.: Computational Graphs and Rounding Error. *SIAM J. Numer. Anal.*, 11(1974), 87—96.
3. BOSSLER, J. D.: The New Adjustment of the North American Horizontal Datum, *EOS* 57(1976), 557—562.
4. BUNCH, J. R.: Analysis of Sparse Elimination. *SIAM J. Numer. Anal.*, 11(1974), 847—872.
5. CUTHILL, E.—MCKEE, V.: Reducing the Bandwidth of Sparse Symmetric Matrices, Proc. of 24th National Conference, ACM, 1969, 157—172.
6. DRACUP, J. F.—GERGEN, J. G.: The Least Squares Adjustment of Large Geodetic Networks. *Boll. geod. sci. aff.*, 23(1974), 261—275.
7. DUFF, I. S.: On the Number of Nonzeros Added when Gaussian Elimination is Performed on Sparse Random Matrices. *Math. Comp.*, 28(1974), 219—230.
8. GERGEN, J. G.: The Importance of Ordering Systems of Geodetic Normal Equations. *Canad. Surv.*, 28(1974), 672—676.
9. GIBBS, N. E.: Algorithm 509: A Hybrid Profile Reduction Algorithm. *ACM Trans. on Mathem. Software* 2(1976), 378—387.
10. GIBBS, N. E.—POOLE, W. G.—STOCKMEYER, P. K.: An Algorithm for Reducing the Bandwidth and Profile of a Sparse Matrix. *SIAM J. Numer. Anal.*, 13(1976), 236—250.
11. GIBBS, N. E.—POOLE, W. G.—STOCKMEYER, P. K.: A Comparison of Several Bandwidth and Profile Reduction Algorithms. *ACM Trans. on Math. Software*, 2(1976), 322—330.
12. GLASER, G. H.—SALIBA, M. S.: Application of Sparse Matrices to Analytical Photogrammetry. Sparse Matrices and their Application, *D. J. Rose* and *R. A. Willoughby*, eds, Plenum Press, New York, 1972, 135—146.
13. GROTEN, E.: Some Numerical Investigations on Combination Solutions in "Beiträge zur gravimetrischen Geodäsie und Gezeitenforschung", DGK, Reihe B, Nr. 217(1976), 99—127.
14. GROTEN, E.—SCHAAB, H.: On the Combination of Gravity, Gradiometry and Altimetry. Paper presented at Primer Congresso de Geodesia, Maracaibo, Dec. 1975.
15. GRÜNDIG, L.: Die Berechnung vorgespannter Teil- und Hängenetze unter Berücksichtigung ihrer topologischen und physikalischen Eigenschaften und der Ausgleichungsrechnung, DGK, Reihe C, Nr. 216, (1976).
16. HAAG, K.: Die photogrammetrische Bündelausgleichung und die Auflösung großer Normalgleichungssysteme. DGK, Reihe C, Nr. 232, (1977).
17. HANSON, B. H.: Applications of Normal Equation Reordering and Helmert Blocking to the New Adjustment of the North American Datum (abstract). *EOS* 56(1974), 1105.
18. HSIEH, H. Y.—GHAUSI, M. S.: A Probabilistic Approach to Optimal Pivoting and Predicting of Fill-In for Random Sparse Matrices. *IEEE Trans. Circuit Theory CT*, 19(1972), 329—336.
19. JENNINGS, A.: A Compact Storage Scheme for the Solution of Symmetric Linear Simultaneous Equations. *Computer Journal*, 9(1977), 281—285.
20. KELM, R.: Zur analytischen Optimierung geodätischer Netze: Allgemeine Analyse bis zur Entwicklung der Minoren- und Graphenmethode, DGK, Reihe C, Nr. 220 (1976).
21. KING, I. P.: An Automatic Reordering Scheme for Simultaneous Equations Derived from Network Analysis. *Int. J. Numer. Methods Engrg.* 2(1970) 523—533.
22. KOROBKOV, S. A.: Application of the Theory of Graphs to Problems in the Analysis of Geodetic Nets. *Geod.* and *Aerophot.* (1965), 75—83.
23. KOROBKOV, S. A.: Construction and Transformation of Graphs of Normal Equation Systems. *Geod. a. Aerophot.* (1966), 92—99.
24. KOROBKOV, S. A.: Computation of Oriented Graphs. *Geod.* and *Aerophot.* (1966) 258—263.
25. KOROBKOV, S. A.: Determining Weighting Factors by Transforming Graphs. *Geod. a. Aerophot.*, 1968, 7—14.
26. LIU, W.-H.—SHERMAN, A. H.: Comparative Analysis of the Cuthill-McKKee and the Reverse Cuthill-McKKee Ordering Algorithms for Sparse Matrices. *SIAM J. Numer. Anal.*, 13 (1976), 198—213.
27. NOLTEMEIER, H.: Graphentheorie mit Algorithmen und Anwendungen. Walter de Gruyter, Berlin, New York, 1976.
28. SCHEK, H. J.—SCHAUER, U.—STEIDLER, F.: The Adjustment of Large Geodetic Networks by Sparse Matrix Techniques, Report TR 76.07004, IBM Heidelberg Scientific Center

29. Schmitt, G.: Speichertechnische und numerische Probleme bei der Auflösung großer geodätischer Normalgleichungssysteme, DGK, Reihe C, Nr. 195 (1973).
30. Snay, R. A.: Reducing the Profile of Sparse Symmetric Matrices. *Bull. Geod.*, 50(1976), 341—352.
31. Tewarson, R. P.: Sparse Matrices, Acad. Press, New York 1973.

ОБ ИСПОЛЬЗОВАНИИ РЕДУКЦИЙ ШИРОТЫ ПОЛОС И ПРОФИЛЯ В КОМБИНИРОВАННЫХ РЕШЕНИЯХ СПУТНИКОВОЙ АЛЬТИМЕТРИИ

Г. ХЕЙН—Э. ГРОТЕН

РЕЗЮМЕ

Если гравитационный материал на местности комбинировать с высотными данными на океанах, то коллокация или уравнивание приводит к большим, редко заполненным матрицам нормальных уравнений. При помощи методо теории графов для редукции широты полос и профиля редко заполенной матрицы время для элиминации неизвестных может быть существенно уменьшено.

Первые эксперименты в исследовании различных алгорифмов для редукции широты полос и профиля показаны на нескольких числовых примерах. Рассматриваются и другие возможности для минимализации места для хранения и времени.

Acta Geodaet., Geophys. et Montanist. Acad. Sci. Hung. Tomus 14 (1—2), pp. 71—79 (1979)

INVESTIGATION OF THE GEOID IN EUROPE BY THE COLLOCATION METHOD

H. SCHAAB

INSTITUT FÜR PHYSIKALISCHE GEODÄSIE, TECHNISCHE HOCHSCHULE DARMSTADT ,FRG

[Manuscript received September 5, 1977]

For the reduction of the geometric and natural observations from the topography to their appropriate reference surfaces the precise knowledge of the deflections of the vertical and the geoid undulation are necessary.

By the comparison of global and relative geoid heights in Europe the accuracy was examined and systematic deviations were detected. Different weights of the observations and the correlations between them were taken into account.

The collocation method was used by applying different covariance functions.

1. The astrogeodetic method

With HELMERT's astrogeodetic method we can determine a local geoid for an area like the European continent. For the computations we must know the components of the deflections of the vertical ξ and η. The deflection components are obtained by comparing the astronomic and geodetic coordinates of identical points

$$\xi = \Phi - \varphi, \quad \eta = (\Lambda - \lambda) \cos \varphi = (A - \alpha) \cot \varphi; \tag{1}$$

on integrating [8]

$$N_B - N_A = - \int_A^B (\xi \cos \alpha + \eta \sin \alpha) \, ds \tag{2}$$

we get the difference of the astrogeodetic geoid heights of the two points A and B which are connected by the line $\overline{AB}$ whose azimuth is α.

The geodetic coordinates refer to a certain reference ellipsoid as a computational surface. The positioning of this ellipsoid is achieved by the selection of an initial point P_1 for which the deflection components and the geoid height can be arbitrarily chosen.

The reduction of the geometric observations from the topography to the reference ellipsoid presupposes an iteration procedure because for the reduction of the horizontal angles and distances the deflections of the vertical and the geoid heights must be known beforehand. The orientation of the triangulation net is determined by taking into consideration the Laplace equation:

$$\Delta\alpha = \eta \tan \varphi + (\xi \sin \alpha - \eta \cos \alpha) \cot z \, . \tag{3}$$

The astrogeodetic datum ED 1950 was established in the years after World War II. From the existing European triangulation net only chains were selected and adjusted. As the reference surface the ellipsoid from Hayford was used with its main axis $a = 6\ 37\ 8388$ m and the flattening $f = 1./297$. The orientation of the network was achieved by carrying out a least-squares adjustment by which the sum of the squares of the deflection components becomes a minimum [17, 18]

$$\Sigma(\xi^2 + \eta^2) = \text{minimum} .$$

This adjustment yielded a coherent system of the deflections of the vertical. The deflection components at the initial point P_1 (Potsdam, HELMERT—TOWER) assumed the values

$$\xi_1 = 3{\cdot}36'' \qquad \eta_1 = 1{\cdot}78'' .$$

On this basis many geoid sections were evaluated. BOMFORD [1] brought these sections together and in regions were new data were available he corrected and expanded his European Geoid. At the initial point he chose the geoid undulation $N_1 = 0$m. LEVALLOIS and MONGE [10] completed BOMFORD's geoid in the Balkanic area and extended it preponderantly into the Mediterranean sea area.

2. The gravimetric method

By the generalized Stokes formula

$$N = N_0 + \frac{R}{4\pi G}\int_\sigma\int \Delta g\, S(\psi)\, d\sigma . \tag{4}$$

geoid undulations are obtained which refer to a reference ellipsoid whose center coincides with the geocenter. The scale constant ([8], p. 101)

$$N_0 = \frac{k\delta M}{RG} - \frac{\delta W}{G} \tag{5}$$

results from the potential and mass differences δW and δM between the reference ellipsoid and the earth. By this way S. VINCENT and J. G. MARSH [16] determined a detailed global gravimetric geoid with an accuracy of about ± 2 m in the European area. For the computation they used (i) gravity anomalies Δg_S from the GSFC earth model GEM-8 and (ii) 37125 gravimetrically determined $1^\circ \times 1^\circ$ mean values Δg_T. The geoid heights refer to an ellipsoid with a semimajor axis $a = 6\ 37\ 8142$ m and flattening $f = 1./298.255$. The product of the gravitational constant and the mass of the earth has the value $kM = 3.986009 \times 10^{20}$ cm^{3}sec^{-2}.

3. Comparison of the astrogeodetic geoid in the ED-50 system with the global GEM-8 geoid

For the comparison with the European section of the gravimetric geoid we must transform the astrogeodetic geoid undulations into a geocenter position. We can carry out the transformation using the 7 transformation parameter solution, 3 translations (x_0, y_0, z_0), 3 rotations $(\varepsilon, \psi, \omega)$ and a scale correction (dm) determined with satellite-derived station coordinates [6].

To get more possibilities for comparison we used an alternative method ([8], p. 213). We fitted together the whole European astrogeodetic geoid and the gravimetric geoid and also some parts of the ED-50 geoid and the corresponding sections of the global geoid together. This was done in a way, that the sum of the squares of the undulation differences became a minimum

$$\sum_i (N_a^i - N_g^i)^2 = \text{minimum} . \tag{6}$$

N_a^i are the astrogeodetic geoid heights transformed to the global system and N_g^i are the gravimetric undulations.

We assumed that the Laplace equation (3) is fulfilled and restricted ourselves therefore to regard only the three shift parameters x_0, y_0, z_0. For their determination we used the parametric case of the least-squares collocation $(AX \neq 0)$ and obtained therefore simultaneously at the same time

(1) the parameters for the shift of the astrogeodetic reference ellipsoid to its absolute position

(2) a check of the astrogeodetic geoid if we assume that the gravimetric undulations have a constant accuracy of about ± 2 m in Europe

(3) a combined gravimetric—astrogeodetic geoid. The basic equations are exposed by MORITZ (1972).

$$x = AX + s + n . \tag{7}$$

In our case this equation is replaced by

$$N_a' = x_0 \cos\varphi \cos\lambda + y_0 \cos\varphi \sin\lambda + z_0 \sin\varphi + Ng + n . \tag{8}$$

N_a' is the astrogeodetic geoid height transformed to the parameters (a, f) of the gravimetric reference ellipsoid by the term given in MOLODENSKY et al. ([13], p. 15)

$$\delta N_M = -\frac{a}{\overline{RN}} \delta a + \frac{b\,\overline{RN}}{a} \sin^2\varphi\, \delta f. \tag{9}$$

$\overline{RN}$ is the normal radius of curvature and δa and δf are the differences of the main semiaxis and the flattening between the Hayford ellipsoid and the ellipsoid used by VINCENT and MARSH.

The shift parameters $X = (x_0, y_0, z_0)^T$ are determined by using the terminology from MORITZ (1972)

$$X = (A^T \mathbf{C}^{-1} A)^{-1} A^T \mathbf{C}^{-1} \boldsymbol{x} . \tag{10}$$

$\mathbf{C}$ is the covariance matrix $\mathbf{C}_{N_a N_a}$ of the astrogeodetic geoid heights N_a which is equal to the sum of the covariance matrices $\mathbf{C}_{N_g N_g}$ and $\mathbf{C}_{n_a n_a}$ of the gravimetric undulations (which represent the signal s) and the noise of the astrogeodetic undulations.

$$\mathbf{C}_{N_a N_a} = \mathbf{C}_{N_g N_g} + \mathbf{C}_{n_a n_a} . \tag{11}$$

The European area has a radius of a few degrees only, the corresponding part of the local covariance function is needed. Because the geoid undulations are not so strongly correlated with the topography as the free-air anomalies, we determined empirical covariance functions which are given in Figs 1a and 1b. We made sure that the astrogeodetic undulations have a zero average by performing different trend eliminations.

In GROTEN and SCHAAB [5] we compared dynamically derived GEM-6 station coordinates with their corresponding coordinates in the ED-50 system and obtained a scale correction of $dm = -2.89$ ppm. This correction yields a change of the main semi-axis of the reference ellipsoid used by LERCH et al. ([9], p. 68) of $\delta a = -18.5$ m resulting in $a = 6\ 378\ 136.5$ m.

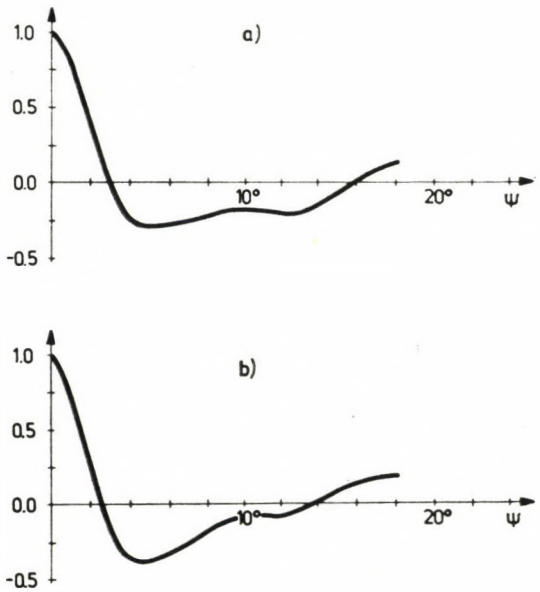


Fig. 1. Empirically determined covariance function of the geoid undulations in Europe. Trend polynomials of the 3rd degree (a) and of the 4th degree (b) were eliminated

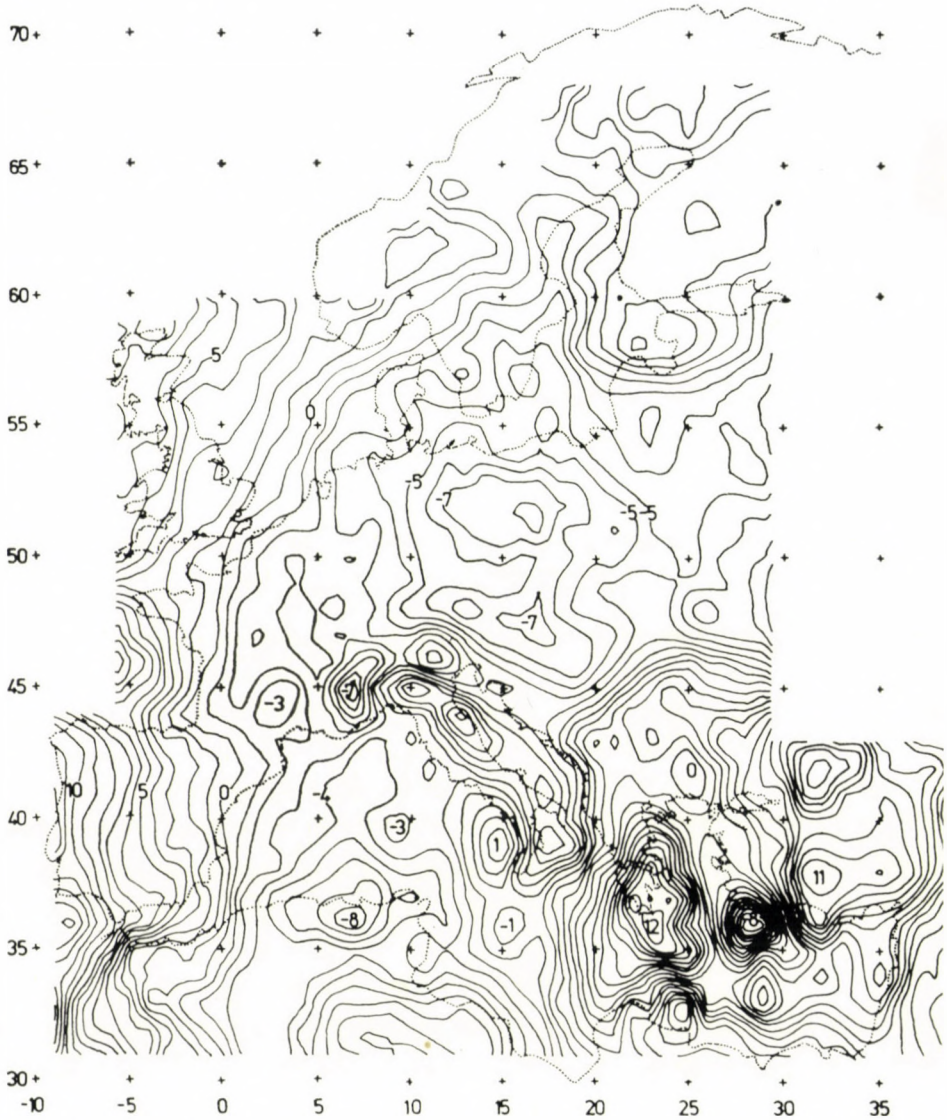


Fig. 2. Discrepancies remaining after fitting together the whole astrogeodetic and the gravimetric geoid

In our computations we used for the product of the earth mass and the gravitational constant the value $kM = 3.986005 \cdot 10^{20}\text{cm}^3$ given by MORITZ ([14], p. 403). We changed therefore the scale of the gravimetric geoid by about $dm = -1$ ppm. If we assume that there exists no difference between the potential of the reference ellipsoid and the earth we obtain by equation (5): $N_0 = \delta a = -6.4$ m. The main semi-axis assumes then a value of $a = 6\,378\,135.6$ m which is in very good agreement with the value computed above!

We divided the geoids in different regions. In a first approach we fitted together the whole astrogeodetic geoid with the gravimetric geoid. By this approach we used all 1500 $1^\circ \times 1^\circ$ undulations of both systems. The discrepancies obtained are show in Fig. 2.

To get a possibility for the detection of distortions we fitted together in the further approaches also the parts of the geoids (Table I).

The translation parameters got by these fits vary strongly. Hence, there must exist systematic distortions.

For seperation we took into consideration the discrepancies between the geoid heights after the transformation. We can remark (Table I) that they will become smaller when also the geoid sections become smaller. This implies that the systematic distortions lost their influence on the optimal fitting.

The translation parameters show a different behaviour. Let us have a look on the first five approaches. First of all, we obtained improved translation parameters by compareing them with the results using satellitederived station coordinates [6]. It is interesting in this sense that the translation parameters we got by carrying out the geoid fit ((2) in Table I) agree completely with the values obtained by the comparison of Doppler station coordinates with the ED-50 coordinates.

The following two approaches ((4) and (5) in Table I) yield a little worthier results. By this consideration the geoid regions became smaller and the limitations of the sections approached the initial point of the astrogeodetic geoid. So we can say that there is some systematic error of the gravimetric geoid in Central Europe possibly caused by the lack of free air anomalies in the eastern countries.

Table I

No.	Geoid sections fitter together	Limitations				Translation parameters			Discrepancies remaining after the geoid fit
		φ_1	φ_2	λ_1	λ_2	x_0	y_0	z_y	
		(degree)				(meter)			(meter)
1	Whole astrogeodetic geoid	68	31	−9	40	82	127	116	5—12 (see Fig. 2)
2	West and Central Europe	59	44	−6	30	79	109	122	2—6
3	Central Europe	55	45	0	20	86	104	115	1—3
4	France and FRG	52	47	−2	14	83	92	116	1—3
5	FRG	55	47	6	14	87	83	114	0—1
6	Mediterranean Sea	44	31	−9	40	65	128	138	6—14
7	Eastern Mediterranean	43	31	15	40	71	140	131	5—11
8	Western Mediterranean	44	31	−9	15	77	85	128	4—8
9	France	53	43	−2	7	81	96	119	1—3
10	England	59	50	−6	2	63	69	136	1
11	Scandinavia	68	55	6	30	61	124	130	1—3

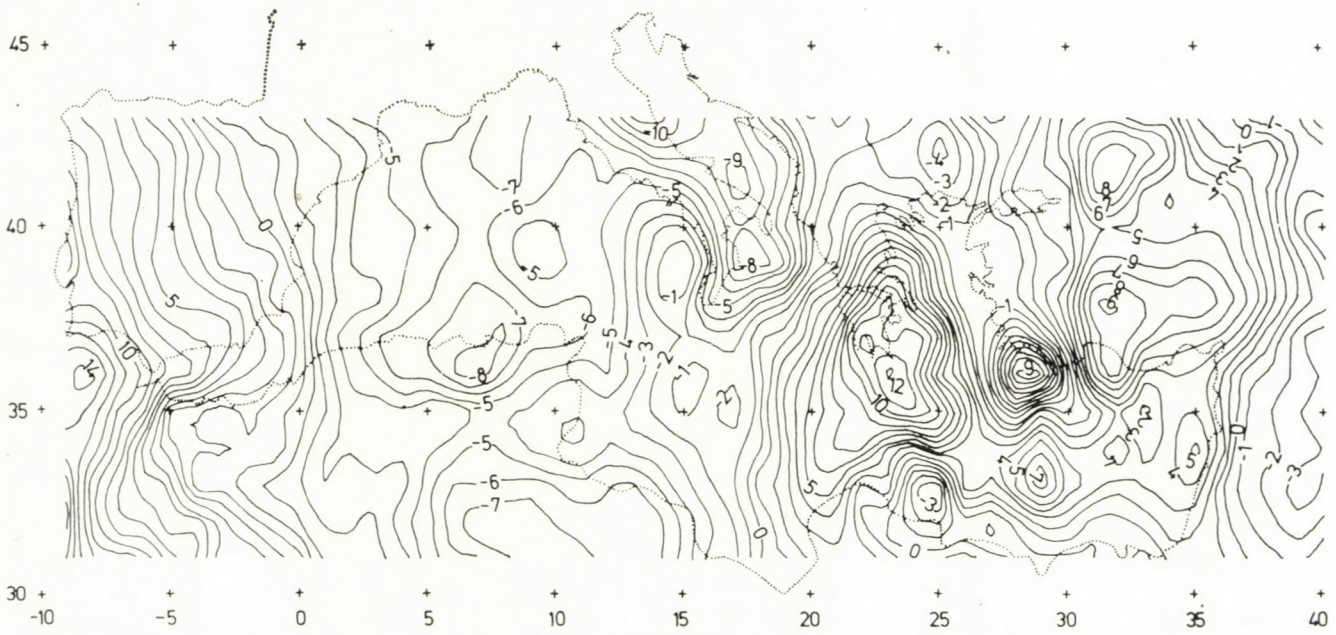


Fig. 3. Discrepancies remaining after fitting together the geoid heights of the Mediterranean area

But the systematic distortions of the astrogeodetic geoid in the Mediterranean area in England and in Scandinavia with amounts up to 10 meters are overwhelming.

Therefore, we have to do some investigations for the computation of a new geoid, by combining all available data, maybe by using collocation.

REFERENCES

1. BOMFORD, G.: The astrogeodetic geoid in Europe and connected areas 1971. Appendix to Mrs. I. FISCHER's report for Study, Group V-29, International Union of Geodesy and Geophysics General Assembly, Moscow 1971.
2. BRENNECKE, J.—GROTEN, E.—RUMMEL, E.—SCHAAB, H.: Variationen zum Geoid in Deutschland, DGK, Reihe A, Heft Nr. 83, München 1975.
3. GROTEN, E.: Absolute orientation of an astrogeodetic geoid section and its correlation with geophysical data. *Studia Geophysica et Geodetica*, Praha 14, 1970.
4. GROTEN, E.: Problems related to absolute orientation of geodetic systems. Paper presented at the IAG Symp. "Redefinition of North American Geodetic Datum", Fredericton (Canada), May 1974.
5. GROTEN, E.—SCHAAB, H.: On the accuracy of astrogeodetic geoid heights. *Boll. di Geodezia e Science Affini*, March, 1975.
6. GROTEN, E.—SCHAAB, H.: Alternative determination of geodetic datum shifts. Paper presented at 3rd International Symp. "Geodesy and Physics of the Earth", Weimar, October 1976.
7. GROTEN, E.—SCHAAB, H.: On the scaling of the geoid. 1977.
8. HEISKANEN, W. A.—MORITZ, H.: Physical Geodesy, W. H. Freeman and Co., San Francisco and London, 1967.
9. LERCH, F. J.—WAGNER, C. A.—RICHARDSON, J. A.—BROWND, J. E.: Goddard earth models (5 and 6). Goddard Space Flight Center, X 921—74—145 Greenbelt, Maryland, 1974.
10. LEVALLOIS, H. J.—MONGE, H.: Le géoide Européen, version 1975, presented at the 16th Gen. Ass. of IUGG, Sept. 1975.
11. MEISSL, P.: Distortions of terrestrial networks caused by geoid errors. Proceedings of the Fifth Symp. on Mathematical Geodesy, Florence, 1972.
12. MEISSL, P.: The Strength of Continental Terrestrial Networks. Paper presented at the IAG Symp. "Redefinition of North American Geodetic Datum". Fredericton (Canada) May 1974.
13. MOLODENSKY, M. S.—EREMEEV, V. F.—YURKINA, M. I.: Methods for study of the external gravitational field and figure of the earth. Israel Program for Scientific Translations, Jerusalem, 1962.
14. MORITZ, H.: Fundamental geodetic constants. *Bulletin Géodésique*, No. 118, 1975.
15. THOMSON, D. B.—NASSAR, M. M.—MERRY, C. L.: Distortions of Canadian geodetic networks due to the neglect of deflections of the vertical and geoidal heights. Paper presented at the IAG Symp. "Redefinition of North American Geodetic Datum". Fredericton (Canada), May 1974.
16. VINCENT, S.—MARSH, J. G.: Goddard Space Flight Center Global detailed Gravimetric Geoid. Presented at the 16th Gen. Ass. of IUGG, Sept. 1975.
17. WOLF, H.: Die Lotabweichungsausgleichung für das Zentraleuropäische Netz. Veröff. Inst. Erdm. Nr. 6, Bamberg, 1949.
18. WOLF, H.: Die angenäherte Bestimmung des Geoids mittels astronomischen Nivellements im Bereich des Zentraleuropäischen Netzes. Veröff. Inst. Erdm. Nr. 6, Bamberg, 1949.

ИССЛЕДОВАНИЕ ГЕОИДА В ЕВРОПЕ МЕТОДОМ КОЛЛОКАЦИИ

Х. ШААБ

РЕЗЮМЕ

Для редукции геометрических и природных наблюдений с целью получения соответствующей поверхности относимости из топографической, необходимо точно знать уклонение отвеса и высоту геоида.

На основе сравнения глобальных и относительных высот геоида в Европе была исследована точность и выведены систематические отклонения. Различные веса наблюдений и корреляции между ними были учтены.

Метод коллокации был применен при различных ковариационных функциях.

Acta Geodaet., Geophys. et Montanist. Acad. Sci. Hung. Tomus 14 (1—2), pp. 81—91 (1979)

УЧЕТ РЕФРАКЦИИ В НИВЕЛИРОВАНИИ НА ОСНОВЕ МЕТЕОРОЛОГИЧЕСКИХ ИЗМЕРЕНИЙ

О. А. МОЗЖУХИН

ГОРЬКОВСКИЙ ИНЖЕНЕРНО-СТРОИТЕЛЬНЫЙ ИНСТИТУТ

[Поступило 15 октября 1977 г.]

Обосновывается «метеорологический» способ учета рафракции в нивелировании, использующий фактическое распределение физических параметров приземного слоя атмосферы на момент геодезических измерений. Рассматриваются особенности методики определения температурного градиента на высоте 1 м, лежащей в основе способа. Приводятся примеры определения поправок за счет влияния рефракции. Рассмотрены ограничения в применении метода.

1. Введение

Одна из важнейших проблем современной геодезии состоит в преодолении ограничений, вызванных влиянием атмосферной рефракции.

Существует два основных направления исследований в этой области. Первое из них предполагает использование статистических характеристик физических параметров атмосферы для установления условий, при которых рефракция оказывает наименьшее влияние, а также с целью получения поправок за рефракцию.

Второе направление заключается в использовании фактического распределения физических параметров атмосферы на момент геодезических наблюдений. Суть его состоит в определении поправок, устраняющих влияние атмосферных помех. При этом возможны инструментальный (посредством рефрактометров) и «метеорологический» методы решения задачи. Автор сосредоточил свои усилия на последнем направлении, предполагающим определение поправок на основе метеорологических измерений. В данной работе получили дальнейшее развитие рассмотренные ранее [6, 7, 8] способы учета рефракции применительно к определению превышений методом тригонометрического и геометрического нивелирования, выполняемого через точку (из середины).

2. Рефракция в одностороннем нивелировании

Погрешность за счет влияния рефракции при одностороннем нивелировании и нормальных условиях атмосферы ($p_0 = 1000$ мб, $T_0 = 288°K$) выражается зависимостью [8]

$$r = 0{,}5S^2 \left(0{,}0342 - \frac{\gamma_1}{\bar{Z}}\right) \cdot 10^{-6}, \qquad (1)$$

где S — расстояние от инструмента до цели, γ_1 — градиент температуры воздуха на высоте 1 м, $\bar{Z}$ — репрезентативная высота.

В том случае, если реальные условия измерений отличаются от нормальных, вычисляемый по формуле (1) результат следует умножить на коэффициент

$$C = 78{,}96\frac{p}{T^2}, \tag{2}$$

где p и T — фактические значения давления и температуры воздуха. Постоянный множитель в формуле (2) вычислен для «эффективной» длины световой волны $\lambda = 0{,}56$ мкм.

Во влажном воздухе для вычисления множителя C принимается во внимание виртуальная температура

$$T_v = T + \Delta T_v, \tag{3}$$

где ΔT_v — виртуальный добавок, вычисляемый по формуле

$$\Delta T_v = 0{,}378T\frac{e}{p}. \tag{4}$$

Здесь e — упругость водяного пара, мб.

Без учета виртуального добавка расчет по формуле (2) окажется завышенным на 1, 2 и 3% при температурах воздуха соответственно 15, 25 и 35°С.

Если не учитывать поправочный множитель C, то расчет по формуле (1) будет сопровождаться ошибкой, занижающей результат на 10—15% при температурах воздуха, превышающих 20°С.

3. Определение температурного градиента

Для определения градиентов γ_1 с целью учета рефракции в геодезических измерениях было предложено [7] воспользоваться разработанной ранее методикой [4], в соответствии с которой γ_1 определяется на основе показаний аспирационного психрометра по формуле

$$\gamma_1 = \beta\frac{T_0 - T_2}{\ln\dfrac{200}{Z_0'}} \quad °C. \tag{5}$$

Параметры $\Delta T_2 = T_0 - T_2$ и Z_0' находят посредством специально составленных эмпирических номограмм по температуре и влажности воздуха, исправленным поправками за инерционность тепло- и влагообмена в суточном и сезонном ходе. Для получения поправок составлены специальные таблицы, куда

входят по аргументам T_2 (измеренная температура на высоте $Z = 2$ м) и дате измерений (число, месяц, время суток).

Поправочный коэффициент β, характеризующий отличие фактических профилей температуры от логарифмических, вычисляют по формуле

$$\beta = (1 - Ri_1)^{-\frac{1}{4}}.$$

Или, пользуясь разложением функции в ряд, напишем

$$\beta = 1 + \frac{1}{4} Ri_1 + \frac{5}{32} Ri_1^2. \tag{6}$$

В последних выражениях Ri_1 — число Ричардсона, рассчитанное для высоты 1 м, являющееся характеристикой степени термодинамической устойчивости атмосферы. Величину Ri_1 можно получить на графике рис. 1 по исправленной поправками температуре T_2' и влажности воздуха e_2 [5].

При равновесной температурной стратификации ($\gamma_1 = 0{,}01$°C/м) $\beta = 1$. По мере роста неустойчивости ($Ri < 0$) множитель β уменьшается до 0,9, а в условиях устойчивости ($Ri > 0$) возрастает до 1,1. Таким образом, если принять $\beta = 1$, то систематическая ошибка в определении γ_1 может достигать примерно 10%.

Величина γ_1 возрастает с общим увеличением температуры воздуха и уменьшается по мере степени насыщения его водяными парами. При температурах воздуха менее 30°C градиенты γ_1 не превышают, как правило, 0,3°C/м. Однако в сухом и жарком климате величина их может достигать 1°C/м и более. К такому заключению нетрудно придти из рассмотрения эмпирических

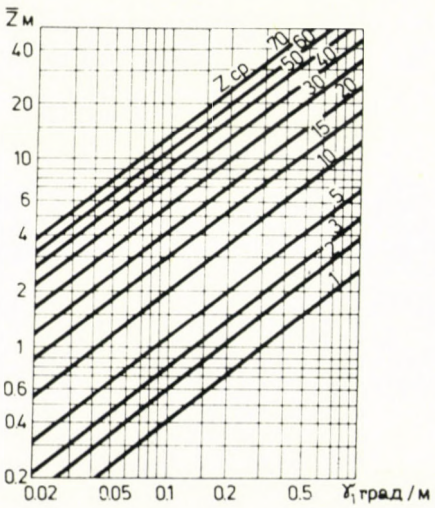


Рис. 1. Зависимость Ri_1 от температуры и влажности на высоте 2 м

графиков для определения ΔT_2 [7]. Заметим, что знак градиента считается положительным, когда температура воздуха уменьшается с высотой.

По данным Брокса [2] градиент температуры на произвольной высоте приземного слоя выражается зависимостью вида

$$\gamma_Z = \gamma_1 Z^b , \tag{7}$$

где b — безразмерная величина, примерно равная -1, зависящая от термодинамической устойчивости атмосферы. При сверхравновесных условиях $b = -1{,}04 \pm 0{,}02$. В условиях инверсии среднее значение b равно $-0{,}9$ и имеет больший размах отклонений [1].

Коэффициенты, b в последней формуле и β в формуле (5), играют одинаковую роль. Поэтому при подстановке выражения (5) в (7) правомерно принять $\beta = 1$. С другой стороны, при использовании формулы (5) с учетом выражения (6) для вычисления градиента γ_Z становится справедливой зависимость

$$\gamma_Z = \frac{\gamma_1}{Z} . \tag{8}$$

Градиент γ_1 может быть также найден по формуле

$$\gamma_1 = 0{,}5\beta \frac{T_n - T_2}{\ln \dfrac{200}{Z_0}} , \tag{9}$$

где T_n — температура подстилающей поверхности, Z_0 — коэффициент шероховатости, выбираемый из таблиц [4] по виду подстилающей поверхности, T_2 — температура воздуха на высоте 2 м. В том случае, если температуру воздуха измеряют в интервале высот от 1 до 10 м, то коэффициент в формуле (9) может изменяется от 0,45 до 0,55.

Процесс определения γ_1 по формуле (9) легко поддается автоматизации, что связано с измерением разности температуры $\Delta T = T_n - T_2$ в двух точках, разнесенных на расстояние 2 м.

Методика расчета по формуле (5) удобна тем, что для определения градиента γ_1 достаточно снять показания аспирационного психрометра. Кроме этого, имеется возможность воспользоваться данными срочных наблюдений температуры и влажности, получаемых на стационарных метеорологических станциях.

Рассмотренная методика позволяет находить γ_1 над открытой земной поверхностью. При геодезическом нивелировании в заселенной местности для определения γZ над лесом представляется возможным воспользоваться формулой

$$\gamma_Z = \beta \frac{T_1 - T_2}{Z \ln \dfrac{Z_2 - Z_B}{Z_1 - Z_B}}, \tag{10}$$

где Z_B — высота слоя вытеснения, которую с некоторым приближением можно принять равной 2/3 средней высоты древостоя. T_1 и T_2 — показания температуры на высотах Z_1 и Z_2. Аналогичным образом рассчитывают градиенты, когда в качестве подстилающей поверхности могут быть густые посевы сельскохозяйственных культур (пшеницы, кукурузы, хлопчатника и т. п.).

4. Определение репрезентативной высоты

В простейшем случае, характерном для геометрического нивелирования, в качестве $\bar{Z}$ в формуле (1) представляется возможным [8] воспользоваться средним между обратными значениями высоты инструмента и отсчетом на рейке.

При тригонометрическом нивелировании среднюю высоту визирного луча над подстилающей поверхностью Z_{cp} можно определить по снятому с карты профилю методом численного интегрирования по формуле Симпсона [6], которая, однако, отличается от $\bar{Z}$. Последнюю можно найти из уравнения (1), если γ_1 и r измерены. В этом случае, отложенные по координатным осям $\lg Z$ и $\lg \gamma_1$ при постоянном Z_{cp} экспериментальные данные располагаются примерно вдоль одной прямой, определяемой уравнением вида

$$\bar{Z} = a\, \gamma_1^b. \tag{11}$$

На рис. 2 приведена эмпирическая номограмма для определения репрезентативной высоты $\bar{Z}$ по известным значениям γ_1 и Z_{cp}, построенная по измерениям вертикальных углов в Подмосковье [3] между пунктами с из-

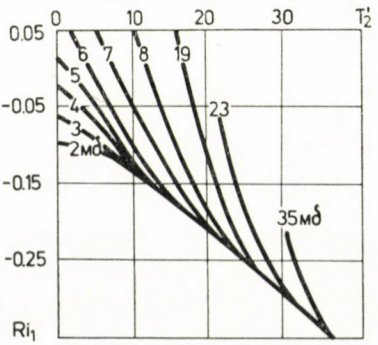


Рис. 2. Эмпирическая номограмма для определения $\bar{Z}$ по γ_1 и Z_{cp}

вестными отметками. Было использовано три характерных направления со средними высотами 2,4; 12,5 и 32 м, что позволило по способу наименьших квадратов найти неизвестные a и b и ипостроить номограмму (рис. 2) с заданным шагом.

5. Высота слоя автоконвекции Z^0

Если величина второго члена в круглых скобках формулы (1) не превышает градиент автоконвекции (0,0342°С/м), то погрешность за рефракцию имеет положительный знак. В противном случае — отрицательный.

Отрицательная рефракция образуется в дневное время летом в слое автоконвекции высотой

$$Z^\circ = \frac{\gamma_1}{0{,}0342}, \tag{12}$$

прилегающем к земной поверхности. Высота этого слоя составляет в полуденные часы летом на территории Средней Европы примерно 5—10 м.

6. Определение поправок за рефракцию при нивелировании через точку (из середины)

Поскольку при геодезическом нивелировании погрешность за рефракцию возрастает пропорционально квадрату расстояния, то это существенно ограничивает возможности применения метода. При нивелировании из середины влияние рефракции в значительной мере компенсируется и в превышение входит систематическая погрешность, равная разности ошибок за рефракцию при нивелировании в одном и другом направлениях

$$\Delta r = r_1 - r_2. \tag{13}$$

В соответствии с формулой (1) погрешность Δr может быть вызвана неравенством сторон $S_1 \neq S_2$ и репрезентативных высот $\bar{Z}_1 \neq \bar{Z}_2$. При геометрическом нивелировании из середины, когда равенство $S_1 = S_2$ соблюдено, рефракция определяется неравенством высот на переднем и заднем расстояниях от нивелира до реек [8]. При тригонометрическом нивелировании из середины, когда визирный луч проходит на более значительной высоте относительно подстилающей поверхности, влияние рефракции определяется первой из отмеченных причин. Тогда, подставляя в соотношение (13) вместо r_1 и r_2 их значения из выражения (1) и полагая при этом, что $S_1 \neq S_2$, а $\bar{Z} = 0{,}5\,(\bar{Z}_1 + \bar{Z}_2)$, получим

$$\Delta r = 0{,}5\,\Delta S(S_1+S_2)\left(0{,}0342 - \frac{\gamma_1}{Z}\right)\cdot 10^{-6}. \tag{14}$$

Последняя формула позволяет вводить поправки за рефракцию при определении превышений методом тригонометрического нивелирования из середины. Как видим, погрешность пропорциональна лишь разности квадратов сторон, что свидетельствует в пользу этого метода по сравнению с односторонним нивелированием.

Преимущества нивелирования методом из середины очевиды в том случае, если визирный луч проходит в слое, где рефракция имеет или положительные, или отрицательные значения. Однако, могут возникнуть условия, при которых погрешности за рефракцию при нивелировании в одном и другом направлениях имеют разные знаки, что влечет за собой увеличение результирующей погрешности.

При геометрическом нивелировании подобные условия возникают в утренние и вечерние периоды наблюдений, когда происходит смена в состоянии распределения температуры воздуха с высотой. Зарождаясь у земли задолго до захода Солнца, слой инверсии увеличивается со временем по высоте вплоть до восхода Солнца. В утренние часы инверсия интенсивно размывается как снизу, так и сверху. Вследствии этого, как утром, но преимущественно вечером, возникают условия для появления существенных ошибок за рефракцию при $\gamma_1 \approx 0$ [8]. При тригонометрическом нивелировании из середины могут возникнуть условия, когда визирный луч проходит в одном направлении выше слоя Z°, а в другом ниже его, что по понятным причинам усугубляет действие рефракции на результат измеряемого превышения. При одностороннем нивелировании может быть так, что высота инструмента Z_1 окажется меньше Z^0, а репрезентативная высота $\bar{Z}$ больше (либо наоборот: $Z_1 > Z^0$ и $\bar{Z} < Z^0$). Расчет поправок по формуле (1) в этом случае также не приводит к успеху.

Таким образом, для уверенного введения поправок за рефракцию по формулам (1) или (14) необходимо, чтобы траектория распространения визирного луча находилась выше или внутри слоя Z^0, то есть соблюдалось условие: $Z_1, \bar{Z} > Z^0$ или $Z_1, \bar{Z} < Z^0$. Наличие этих условий определяется расчетом по формуле (12).

7. Экспериментальная проверка эффективности учета рефракции на основе метеорологических измерений

Для проверки теоретических расчетов воспользуемся материалами экспериментальных исследований земной рефракции в геодезическом нивелировании, содержащимися в работе[3].

В табл. I сопоставлены систематические погрешности за рефракцию $\Delta r_г$ и $\Delta r_м$ (графы 8, 9), полученные нивелированием методом из середины с пункта высотой 14,1 м между двумя другими, удаленными от наблюдателя на

Таблица I

№№ пп	время	γ_1 °C/м	$\bar{Z}$ м	Z° м	r_1 мм	r_2 мм	Δr_Γ мм	Δr_M мм	δ мм
1	2	3	4	5	6	7	8	9	10
1	12—56	0,19	9,5	5,6	820	263	547	565	18
2	13—22	0,20	9,5	5,9	760	270	490	522	32
3	15—40	0,18	9,3	5,3	806	390	416	606	190
4	16—18	0,13	8,0	3,8	665	298	367	715	348
5	18—18	0,00	0,0	0,0	2460	770	1690	1420	—270
6	18—44	0,00	0,0	0,0	2920	830	2090	1420	—670
среднее					1403,5	470,2	933,3	874,7	—58,6

расстояния 16,86 и 7,25 км. В графах 6 и 7 указаны ошибки за рефракцию, полученные при одностороннем нивелировании в одном и другом направлениях и вычисленные по формуле

$$r = \frac{\delta Z'' \cdot S}{\varrho''},$$

где $\delta Z'' = Z_T - Z_U$ — разность между теоретическим и измеренным значениями зенитного расстояния (угол рефракции). Теоретические зенитные расстояния Z_T были вычислены по известным отметкам конечных пунктов, найденным геометрическим нивелированием.

Если превышение передавать через точку (методом из середины), то ошибка за рефракцию в значительной мере компенсируется, так как результирующая погрешность равна разности из нивелирования «назад» и «вперед». Ввиду того, что первое «плечо» примерно в два с половиной раза превышает второе, то поэтому ошибка r_1 значительно больше r_2 и разности $\Delta r_г$ велики. Для исключения последних вычислены поправки (графа 9) по формуле (14). Градиенты γ_1 находили при этом по температуре и влажности воздуха на основе описанной в п. 3. методики. В последней графе табл. I указаны расхождения между «геодезическими» погрешностями $\Delta r_г$ и «метеорологическими» поправками $\Delta r_м$. Как видим, среднее отклонение δ из шести измерений составило около 6 см при передаче превышения между пунктами, удаленными на расстояние 24 км. Заметим при этом, что в практике одностороннего геодезического нивелирования при передаче высот на расстояния порядка 10 км и при использовании «стандартного» коэффициента рефракции $\sim 0{,}15$ погрешности около 1 м не составляют исключения, на что указывают также данные граф 6 и 7.

Из табл. I видно, что с уменьшением градиента γ_1 точность расчета $\Delta r_м$ падает, так как возрастают неопределенности в нахождении репрезентативной высоты с помощью номограммы рис. 2.

В приведенном эксперименте как высота инструмента, так и высота $\bar{Z}$ (графа 4) значительно превышают высоту слоя Z^0 (графа 5), что позволило воспользоваться изложенной методикой.

Аналогично приведенным в табл. I, были сделаны вычисления между остальными пятью пунктами [3], находящимися на расстояниях от 11 до 30 км, которые включали 151 измерение δ. Это позволило оценить погрешность передачи высот с точностью 0,1—0,2 м при $S \sim 10$ км м 0,3—0,4 м при $S \sim 25$—30 км.

В табл. II представлен расчет величин $\Delta r_г$ и $\Delta r_м$ в случае, когда визирный луч не выходил за пределы слоя Z^0. Наблюдения проводились при вы-

Табзица II

Время	γ_1 °C/м	Z^0 м	Пункты №2—№1				
			r_1 мм	r_2 мм	$\Delta r_Г$ мм	$\Delta r_М$ мм	δ мм
1	2	3	4	5	6	7	8
10—30	0,34	10,0	—59	—21	—38	—43	—5
10—58	0,35	10,2	—67	—18	—49	—43	6
11—22	0,36	10,5	—63	—19	—44	—42	2
13—03	0,45	13,2	—73	—20	—53	—41	11
13—33	0,48	14,0	—50	—18	—32	—38	—6
14—01	0,48	14,0	—63	—11	—52	—38	14
15—34	0,47	13,7	—55	—17	—38	—41	—3
15—58	0,46	13,4	—50	—17	—33	—42	—9
16—20	0,45	13,2	—38	—14	—24	—42	—18
среднее			—57,5	—17,2	—40,3	—41,2	—0,9

Время	γ_1 °C/м	Z^0 м	Пункты №3—№2				
			r_1 мм	r_2 м	$\Delta r_Г$ мм	$\Delta r_М$ мм	δ мм
1	2	3	9	10	11	12	13
10—30	0,34	10,0	—96	—59	—37	—52	—15
10—56	0,35	10,2	—111	—67	—44	—51	—7
11—22	0,36	10,5	—108	—63	—45	—51	—6
13—03	0,45	13,2	—132	—73	—49	—52	7
13—33	0,48	14,0	—100	—50	—50	—52	—2
14—01	0,48	14,0	—113	—63	—50	—52	—2
15—34	0,47	13,7	—88	—55	—33	—52	—19
15—58	0,46	13,4	—74	—50	—24	—51	—26
16—20	0,45	13,2	—69	—38	—31	—51	—20
среднее			—99,0	—57,6	—41,4	—51,5	—10,0

соте инструмента 2,4 м на пункте 1, 2, 3, удаленные на расстояния 0,5; 1,0 и 1,5 км. Величины вызванных рефракцией ошибок соответственно составили в среднем из 9 измерений —17,2; —57,5; —99,0 мм. При этом их разности (графы 6,11) оказались примерно равными. После введения поправок получены средние значения ошибок —0,9 мм и —10 мм при передаче превышений на расстояния 1,5 км и 2,5 км из одной стоянки инструмента.

Таким образом, представленные экспериментальные данные показывают, что предложенная методика введения поправок приводит к практически полному исключению систематического влияния рефракции из результатов нивелирования, выполняемого методом из середины. Соответствующие расчеты были выполнены и для случаев, когда траектория распространения визирного луча располагалась одновременно по обе стороны от уровня Z^0. Как и следовало ожидать, попытки введения поправок за рефракцию на основе градиентных измерений температуры успеха в этих случаях не имели.

8. Заключение

При определении превышений методом из середины происходит частичная компенсация погрешностей за рефракцию, если визирный луч распространяется выше слоя автоконвекции Z^0 или внутри его. Погрешности за рефракцию возникают в этом случае за счет неравенства репрезентативных высот Z и расстояний S на участках от наблюдателя до пунктов визирования. При этом в геометрическом нивелировании погрешности за рефракцию вызваны преимущественно первой причиной, в тригонометрическом — второй. Предложенная методика позволяет исключить влияние рефракции из результатов измерений при условии соблюдения известных ограничений, определяемых высотой уровня Z^0.

ЛИТЕРАТУРА

1. Bahnert, G.: Bestimmung und Verwendung vertikaler Temperaturgradienten. *Vermessungstechnik*, 20(1972), 172—175.
2. Brocks, K.: Die Lichtstrahlkrümmung in Bodennähe. *Deutsche Hydrogr. Z.*, 3(1950), 241—248.
3. ИЗОТОВ, А. А.—ПЕЛЛИНЕН, Л. П.: Исследование земной рефракции и методов геодезического нивелирования. Труды ЦНИИГАиК, 1955 вып. 102, 176 с.
4. КОНСТАНТИНОВ, А. Р.: Испарение в природе. *Л., Гидрометеоиздат*, 1968, 532 с.
5. КОНСТАНТИНОВ, А. Р.—АСТАХОВА, Н. И.—ЛИВЕНКО, А. А.: Методы расчета испарения с сельскохозяйственных полей. *Л., Гидрометеоиздат*, 1971.
6. МОЗЖУХИН, О. А: Определение коэффициента рефракции способом метеорологических измерений. *Геодезия и картография*, 1976, № 12, 27—32.
7. Mozžuchin, O. A.: Erfassung des Einflusses der bodennahen Luftschicht bei geodätischen Messungen. *Vermessungstechnik*, 25(1977), 152—154.
8. Mozžuchin, O. A.: Die nivellitische Refraktion und die Methoden ihrer Berücksichtigung. *Vermessungstechnik*, 25(1977), 335—338.

CORRECTION OF LEVELLING BY REFRACTION DETERMINED FROM METEOROLOGICAL MEASUREMENTS

O. A. MOZZHUKHIN

SUMMARY

Author introduces the "meteorological" method of correcting the levelling by refraction data, whereby the distribution of the physical parameters of the near-surface atmosphere in the moment of the geodetic survey has been taken into account. He investigates the methodological characteristics of the determination of the temperature gradient and this is the basis of the method. The determinations of the refraction corrections are shown on examples. The limits of the application of the method are also discussed.

Acta Geodaet., Geophys. et Montanist. Acad. Sci. Hung. Tomus 14 (1—3), pp. 93—99 (1979)

A POSSIBILITY OF USING QUASI-SINGLE-FREQUENCY DOPPLER—FARADAY MEASUREMENTS

A PROPOSAL

CS. FERENCZ

INTERCOSMOS COUNCIL ACCAD. SCI, HUNG.

[Manuscript received October 19, 1977]

As nowadays polarization measurements became equivalent to frequency shift measurements, when the characteristics of the medium are investigated by means of radio waves, the combined measurement and analysis of both the Doppler shift and the Faraday rotation are proposed. Thus, in case of navigational and quick geodetical measurements, it would be sufficient to have a single satellite transmitter sending a plane-polarized and coherently modulated beacon signal.

In the domain of basic research and of practical applications (navigation, geodesy, geophysics, etc.) both Doppler shift [1] and Faraday rotation [2] measurements show important traditions as well as an actual use. More exactly, we are dealing here with the determination of frequency (Doppler shift), polarization and amplitude (Faraday rotation) of a well or sufficiently well known electromagnetic signal. We know that in case of an application of satellite techniques the value of frequency change of a signal emitted (re-emitted, reflected,etc.) by a satellite and observable by a ground receiving station is determined by the relative movement and actual position of the emitter and receiver, by the gravity field, the nature of the traversed medium, characteristics of the circuits (transmitter, oscillators, etc.) used, etc. [3, 4]. According to this the so-called Doppler shift thus obtained is used for navigation, geodetic measurements, tracking of space objects [10, 11], geophysical [12] and space physics measurements, etc. by means of suitable computing procedures [3—9, etc.]. The wide-spread application was motivated by the high accuracy of frequency measurements — today the accuracy is better than 10^{-12} —, by the relatively simple way of producing a measuring signal with high frequency-stability and the possibility of the theoretical treatment of frequency shifts. At the same time we have to deal with the ever returning problem that it is not sufficient to carry out measurements on a single frequency [3, 4, 6].

It is also known that in an anisotropic medium such as the magnetoionic medium found generally in space research (Earth's ionosphere, solar corona, etc.) the polarization of a plane-polarized electromagnetic signal will rotate. This is partly due to the anisotropy of the medium — as it is widely known [2, 13] — partly to the strong inhomogeneous fronts [14, 15]. Thus the polarization measurements were widely applied — among others — in geophysics [16, 17], space physics [2] and astronomy as well. It is an advantage of the method that a plane-polarized signal can be emitted very easily, a single frequency measurement can also be evaluated, the results refer immediately to

the medium [2, 13, 15] and depend in a simply separable way on the position of the transmitting aerial. A problem has been represented, however, by the low accuracy of polarimeters.

1. New possibilities for measuring technics

During recent years a very serious technical progress was encountered both in Doppler experiments and Faraday measurements — more closely in the field of beacon measurements in general [18]. The "group-delay" method increased in a significant manner the applicability and accuracy of the frequency and phase-change measurements. In addition, there appeared such signals on board which are modulated by an exact frequency and are coherent with the carrier one. E.g., in the case of ATS-6 the beacon transmitters were modulated by coherent signals of 100 kilocycle and 1 megacycle and so a "sideband signal" of an exactly known frequency and phase could also be used in the measurements.

On the other hand, a significant technological progress was encountered also in the field of polarimeters [19]. By means of two perpendicularly positioned, plane-polarized and highly balanced aerials and up-to-date semiconductor switches (PIN-diodes) a type of polarimeter could be constructed, which, beside its simplicity and cheapness, is able to measure the polarization with an error less than 0.5°, i.e.

$$\delta\left(\frac{\Delta\alpha_{\mathrm{POL}}}{\alpha_{\mathrm{POL}}}\right) \approx 10^{-3} < 10^{-2},$$

supposed it has been set precisely electronically. In addition, the system does not hinder the use of the received signal for any other purposes.

Thus the polarization measurements became equivalent to the frequency shift measurements when investigating the characteristics of the medium transversed. And what is more, the system mentioned furnishes the amplitude of the signal with a maximum error of a few tenth of decibels [19]. Taking these into account from the point of view of research it is definitely practical to apply a complex measuring method using several kinds of measurements instead of a single method. On the other hand, the progress mentioned above makes it obvious that apparently also in the customary application fields a significant technical simplification can be obtained. This is the aim of the proposal to be described in detail in what follows, based on the measuring-technical progress outlined above.

2. The proposed method

The new technique to be described provides, in principle, an opportunity for the combined measurement and analysis of both the Doppler shift and Faraday rotation. Thus, in case of navigational and (perhaps) quick geodetical measurements it would be sufficient to receive a single satellite transmitter sending a plane-polarized and coherently modulated beacon signal, and in general there would be no need to receive two coherent frequencies being strongly different one from the other, as it is necessary today. Let us give here some details.

With the Doppler measurement the quantities to be observed according to customary notations are:

$$\Delta f(f_0) = \left(\sum_i \Delta f_i\right) + \left(\sum_{k=1}^{n} \frac{\Delta f_k}{f_0^k}\right) , \tag{1}$$

where $\Delta f_i \sim f_0$ and $n = 1$ or 3 yields sufficient accuracy. As it is well known, f_0 is the carrier frequency, the term $(\sum_k \Delta f_k / f_0^k)$ contains the effect of the ionosphere, while

$$\sum_i \Delta f_i = \Delta f_{\mathrm{GEO}} + \Delta f_{\mathrm{TRO}} + \Delta f_{\mathrm{STR}} + \Delta f_{\mathrm{OSC}} + \dots , \tag{2}$$

where Δf_{GEO} is the geometrical term giving the geodetic and navigational information, Δf_{TRO} is the influence of the troposphere to be corrected by atmospheric model, Δf_{STR} is the effect of the atmospheric motions [5] which is negligible in our case, Δf_{OSC} is the frequency error of the transmitting oscillator of the satellite, which is either negligible or it can be compensated by means of well known methods.

During the measurement at the given moment we have to eliminate [6] by all means, as a propagation correction in (1) (in case of a position finding measurement), the quantities

$$\frac{\Delta f_1}{f_0} \text{ and perhaps } \frac{\Delta f_3}{f_0^3} \text{ too.}$$

It is well known [6, etc.] that

$$\begin{aligned}
&\frac{\Delta f_1}{f_0} = -K_1 \frac{1}{f_0} \frac{d}{dt} \int_{g(t)} N(\bar{\mathbf{r}})\, ds , && K_1 = \frac{e^2}{8\pi^2 \varepsilon_0 m} ; \\
&\frac{\Delta f_2}{f_0^2} = \pm K_2 \frac{1}{f_0^2} \frac{d}{dt} \int_{g(t)} N(\bar{\mathbf{r}})\, \bar{H}(\bar{\mathbf{r}})\, d\bar{s} , && K_2 = \frac{|e|^3 \mu_0}{8\pi^2 \varepsilon_0 m^2} ; \\
&\frac{\Delta f_3}{f_0^3} = f_0 \frac{d}{dt} \left[\int_{g(t)} n_{\mathrm{ion}} \left(\frac{1}{f_0^4} \right) ds \right] + \frac{1}{f_0^3} \left\{ f_0^4 \frac{d}{dt} \left[\int_{g(t)} n(\bar{\mathbf{r}})\, ds - \int_{p(t)} n(\bar{\mathbf{r}})\, ds \right] \right\} .
\end{aligned} \tag{3}$$

It can be seen that $K_2 = K_1 \mid e \mid \mu_0/m$. In (3) $g(t)$ denotes the phase path, $p(t)$ the straight line between emitter and receiver, ds is a path element, t is the time, $\bar{\mathbf{r}}$ the position vector, N the electron density, $\bar{H}$ the magnetic field, e the electron charge, m the electron mass, ε_0 and μ_0 the permittivity and permeability of vacuum, respectively, n is the refractive index. It is also known [6] that in $\Delta f_3/f_0^3$ the first (refraction) term is negligible and at best it is only the second term to be taken into account which is connected with the curved path propagation [6, 20]. If we compute the first two terms along the curved path, we introduce a negligible error both from navigational and geodetical point of view, the latter being based on adjusting a great number of measurements in most practical applications.

The Faraday rotation gives, in the well-known manner [2, 13],

$$\Omega = K_2 \frac{1}{f_0^2} \int_{g(t)} N(\bar{\mathbf{r}})\, \bar{H}(\bar{\mathbf{r}})\, \bar{ds}\,, \tag{4}$$

where Ω is uncertain by an amount of $K_0 2\pi$ in case of an actual measurement, and K_0 is a positive integer. Therefore, in the following we consider a differential measurement [13]:

$$\Delta\Omega = \left[\frac{1}{f_0^2} - \frac{1}{(f_0 + f_m)^2}\right] K_2 \int_{g(t)} N(\bar{\mathbf{r}})\, \bar{H}(\bar{\mathbf{r}})\, \bar{ds}\,, \tag{5}$$

where $\bar{H}(\bar{\mathbf{r}})\bar{ds}$ should be $2H_s ds$ in the following and f_m is the modulation frequency superimposed on f_0 and coherent with it. Then we have

$$\Delta\Omega = \frac{(f_0 + f_m)^2 - f_0^2}{(f_0 + f_m)^2} \cdot \frac{K_2}{f_0^2} \int_{g(t)} N H_s\, ds = K_\Delta \Omega(f_0) \tag{6}$$

where the meaning of $\Omega(f_0)$ is evident from (4). Since we can obviously suppose that $f_m \ll f_0$ (18) we can write

$$K_\Delta = \frac{(f_0 + f_m)^2 - f_0^2}{(f_0 + f_m)^2} \simeq 2\frac{f_m}{f_0}\,. \tag{7}$$

Of course, K_Δ is always to be determined with the accuracy corresponding to the accuracy of the polarimeter. At the same time (6) and (7) show that $\Delta\Omega$ can be measured with a sufficient accuracy in the meter-band already in case of a modulation frequency of 1 megacycle.

Now let us measure $\Delta\Omega$ according to (6) and the Doppler shift on the carrier f_0 — (1), (3). From $\Delta\Omega(t)$ thus obtained we get

$$\Omega(f_0) = \frac{\Delta\Omega(t)}{K_\Delta}\,. \tag{8}$$

Using the H_s model in the customary manner [2, 13, 16, 17, etc.] and, in case of a more accurate geodetic computation, combining it with iterative techniques [21, 22, etc.], we get

$$\Omega(f_0) = \frac{K_2}{f_0^2} \widetilde{H}_s \int_{g(t)} N ds \,, \tag{9}$$

where $\widetilde{H}_s$ is an average value obtained from the model. Hence

$$\int_{g(t)} N ds = \frac{f_0^2}{K_2 \widetilde{H}_s} \left[\frac{\Delta\Omega(t)}{K_\Delta} \right] . \tag{10}$$

On the basis of (10) we can correct the $\Delta f(f_0)$ Doppler curve measured on f_0 for the ionospheric propagation, since we have

$$\begin{aligned} \frac{\Delta f_1}{f_0} &\cong - \frac{m}{|e|\,\mu_0} \frac{f_0}{K_\Delta \widetilde{H}_s} \frac{d[\Delta\Omega(t)]}{dt} , \\ \frac{\Delta f_2}{f_0^2} &= \pm \frac{1}{K_\Delta} \frac{d[\Delta\Omega(t)]}{dt} , \\ \frac{\Delta f_3}{f_0^3} &\cong \frac{1}{f_0^3} \left\{ f_0^4 \frac{d\,[\text{curved ray path}]}{dt} \right\} + \mathcal{O}(N) . \end{aligned} \tag{11}$$

Using (11) in the correction of $\Delta f(f_0)$ in the usual way used at present, we have a Doppler-data at our disposal, which is suitable for a position determination as accurate as it can be achieved with a double-frequency Doppler measurement [4].

3. Conclusions

According to these considerations it seems that, when applying a have with a special demodulator, appropriate to receive single carrier frequency and equipped with a switching-mode polarimeter, and a satellite beacon transmitter with a single frequency, coherent modulation, we can obtain navigational or geodetical measuring possibilities of the same accuracy as with the double-frequency Doppler method. In case of need the error of $\widetilde{H}_s$ can be corrected also by means of a computer built in the equipment, applying well known methods [21, 22, etc.].

Thus we think that an experimental testing of the method proposed is advisable.

Application possibilities could be as follows:

Position finding measurements. The use of a single frequency seems especially to be practical for then avigation and in general in surveying and in other mobile (e.g. military) services.

If we execute the measurement on two carrier frequencies simultaneously we shall be able to directly measure the curvature of the propagation path. This can assure more precise ionospheric observations and geodetical data nearly as accurate as could be obtained with the three-frequency Doppler method. In the course of practical use other fields of application can emerge, of course.

Finally, a joint evaluation of frequency- and polarization-change measurements may be practical in searching for earth resources too [23, 24].

REFERENCES

1. KRAMAR, E.: A Historical Survey of the Application of the Doppler Principle for Radio Navigation. IEEE Trans. on Aerosp. and El. Syst.; *AES-8*, (1972), 258.
2. SWENSON, G. W.: The Utilisation of Ionosphere Beacon Satellites; NASA Goddard S.F.C.; X-250—62—32, 1962.
3. DRAHOS, D.—FERENCZ, Cs.—FERENCZ, I.—HORVÁTH, F.—TARCSAI, Gy.: Some Theoretical Contributions Concerning Doppler Geodetical Measurements. *Space Res.*, X(1970), 43.
4. FERENCZ, Cs.—FERENCZ, I.—TARCSAI, Gy.: Refraction Problems and Wave Propagation in Doppler Geodetical Measurements. *Nablj. I.S.Z.*, 9(1970), 361.
5. FERENCZ, Cs.—TARCSAI, Gy.: Refraction Effects due to Moving Media in Doppler Measurements. *Space Res.*, XII(1972), 595.
6. ÁRKOS, I. F.: Notes on the curved path propagation (in Hungarian); Felsőfokú Földmérési Technikum. *Tudományos Közlemények*, 1(1970), 119.
7. VONBUN, F. O.—KAHN, W. D.: Tracking Systems, their Mathematical Models and their Errors, Part I. Theory; NASA Goddard S.F.C., N63—10177, 1962.
8. KAHN, W. D.—VONBUN, F. O.: Tracking Systems, their Mathematical Models and their Errors, Part II. Least Squares Treatment; NASA Goddard S.F.C.; N67—13175, 1966.
9. COOLEY, J. L.: Tracking Systems, their Mathematical Models and their Errors. Program Description; NASA Goddard S.F.C., N64—28931, 1964.
10. KRUGER, B.: A Critical Review of the Use of Doppler Frequency for Range and Range Rate Measurements; NASA Goddard S.F. C.; N66—19449, 1965.
11. IZSÁK, I. G.: Orbit Determination from Simultaneous Doppler-Shift Measurements; Smithsonian Inst. Astr. Obs. Spec. Rep. No. *38*, Cambridge, Mass., 1960.
12. GEORGES, T. M.: HF Doppler Studies of Traveling Ionospheric Disturbances. *J. of Atm. and Terr. Phys.*, 30(1968), 735.
13. HOUMINER, Z.: Determination of the Ionospheric Electron Content and its Horizontal Gradient, by means of Satellite Signals. *Isr. J. of Techn.*, 4(1966), 63.
14. LEVY, G. S.—SATO, T.—SEIDEL, B. L.—STELZRIED, C. T.—OHLSON, J. E.—RUSCH, W. V. T.: Pioneer 6: Measurements of Transient Faraday Rotation Phenomena Observed during Solar Occultation. *Science*, 166(1969), 596.
15. FERENCZ, Cs.: Electromagnetic Wave Propagation in Inhomogeneous Media: The Analysis of the Rotation of Polarization and the Application of the Principle of Modified Ray Tracing. *Acta Technica Acad. Sci. Hung.* (in press)
16. HUNTER, A. N.: Faraday Rotation of the 136 MHz Transmission from the Geostationary Satellite "Canary Bird" Observed at Nairobi. *Radio Sci.*, 4(1969), 811.
17. TITHERIDGE, J. E.,—HERON, M. L.: Second-Order Effects in the Faraday Rotation of Satellite Signals. *Radio Sci.*, 6(1971), 567.
18. DA ROSA, A. V.: Recent Results from Satellite Beacon Measurements. *Space Res.*, XIV (1974), 209.
19. ANTONIADIS, D. A.: A Novel Method for Measuring the Polarization Angle of Satellite Radio Waves; IEEE Trans. on Aerosp. and El. Syst.; *AES-10* (1974), 510.
20. TUCKER, A. J.—FANNIN, B. M.: Analysis of Ionospheric Contributions to the Doppler Shift of CW Signal from the Artificial Earth Satellites. *J. of Geophys. Res.*, 73(1968), 4325.
21. GARRIOTT, O. K.: The Determination of Ionospheric Electron Content and Distribution from Satellite Observations, I. and II. *J. of Geophys. Res.*, 65(1960), 1139.

22. Hame, T. G.—Stuart, W. D.: The Electron Content and Distribution in the Ionosphere. *Proc. IRE*, 48(1960), 1786.
23. Rouse, J. W.: On Radio Science Techniques for Remote Sensing; COSPAR Approaches to Earth Survey Problems through Use of Space Techniques. ed. P. Bock; 29, Akademie-Verlag, Berlin, 1974.
24. Special Joint Issue on Radio Oceanography; IEEE Trans. on Ant. and Prop.; *AP-25*, No. 1, 1977.

ОДНА ВОЗМОЖНОСТЬ ПРИМЕНЕНИЯ КВАЗИ-ОДНОЧАСТОТНЫХ ДОППЛЕРОВО-ФАРАДЕЙСКИХ НАБЛЮДЕНИЙ

Ч. ФЕРЕНЦ

РЕЗЮМЕ

При изучении среды при помощи радиоволн в наши дни стали равноценными измерения поляризации и сдвига частот, поэтому автор предлагает комбинированный метод измерения допплеровского сдвига и ротации Фарадея. Так в случае навигационных и быстрых геодезических измерений было бы достаточно иметь единственный спутник-датчик, излучающий плоско-поляризованный и когерентно модулированный направленный сигнал.

Acta Geodaet., Geophys. et Montanist. Acad. Sci. Hung. Tomus 14 (1—2), pp. 101—109 (1979)

DEVELOPMENT OF HORIZONTAL PENDULUM RECORDINGS

GY. MENTES

GEODETIC AND GEOPHYSICAL RESEARCH INSTITUTE OF THE HUNGARIAN ACADEMY OF SCIENCES, SOPRON

[Manuscript received November 29, 1977]

The paper deals with the problems of the development of pendulum recordings. It describes the photoelectric compensation method which can be used instead of photorecording with pendulums of traditional construction. A detailed description is given of a new horizontal pendulum, type HI-175, with Zöllner suspension and supplied with a capacitive transducer.

In respect of the up-to-date data processing, it is advisable to alter the horizontal pendulums with Zöllner suspension used for earth tides recording so that the output signal is either digitized, or easy to digitize. Having stored the digitized output signals, e.g. on magnetic tape, the measured data can be directly processed on a computer. Thus, the disadvantages of the photographic recording on a drum can be eliminated, where a beam of light was reflected from the mirror fixed on the pendulum arm and projected to the photographic paper on a drum rotating around its horizontal axis. The records became visible only after the development of the photographic paper. In order to get the necessary optical amplification, a beam path of about 4—5 m and so a rather large room was needed and the checking and adjusting of the instruments had to be done in the dark.

To produce the output signals in digitized form, it is necessary to transform the mechanical rotation of the pendulum arm, i.e. an angle into an electric signal by means of a signal converter. Several signal converters are known in measurement technics which transform mechanical displacements into electric signals.

Those to be used for horizontal pendulums can be selected on the basis of the following main criteria:

1. The reaction force of the signal converter to the pendulum should be negligible with respect to the effect of the tidal forces turning the pendulum arm.
2. The characteristics of the signal converter should be unambiguous and linear within the measuring range.
3. The noise sensitivity of the converter should be small.
4. Its temperature dependence should be small.
5. It should not be sensitive for overloading.

The more important methods usable for the transformation of the rotation angle of the pendulum arm into electric signal are outlined in this paper. Those will be discussed in more details which were tried in our Institute.

The traditional photographic recording on a drum can be transformed into a photoelectrical recording by applying some kind of photosensitive element, like photoelectric cell, photoresistance or photodiode instead of the drum with photopaper and by recording the current. Its operation principle is the following: In consequence of a rotation of the pendulum arm, the illuminated surface of the photoelectric element will change and so will the current, too. The advantage of this method is its high sensitivity, but it has the trouble that the temperature dependence and aging of the photoelectric element as well as the instability of the illumination cause disadvantageous influences on the measurement. These troubles can considerably be decreased by differential coupling of two photoelectric elements.

The errors of the photoelectric elements can almost totally be eliminated by the so-called photoelectric compensation method. Figure 1 shows an equipment built on this principle; it has been manufactured from a commercial two-channel compensograph. Records of this instrument are shown in Fig. 2. The main point of this method can be understood from Fig. 3. The light falls on two photoresistances coupled into a bridge. The bridge is balanced when the illuminated surfaces of both photoresistances are equal and the output voltage is zero. In case of a displacement of the light beam the bridge becomes unbalanced, there is an output voltage on the bridge. A servo-amplifier detects and amplifies this voltage so that it can control a servo-motor. The photoresistances mounted on a slide are moved by the servo-motor till the bridge is balanced again. By means of a writing mechanism on the slide of the photoresistances or of a potentiometric teletransmitter the displacement of the light beam, i.e., the angular rotation of the pendulum arm can be recorded or teletransmitted and digitized with an analog digital converter.

The common advantage of the photoelectric methods is that the converter does not react on the pendulum arm and the traditional pendulums can be applied for photoelectric recording without any change in their mechanical construction. Their disadvantage is, however, that they need large and dark rooms and thus their handling is wearisome. These disadvantages can be totally eliminated by means of capacitive or inductive transducers. Since the latter has a greater reactive effect, it is more suitable to apply capacitive transducers. A detailed description can be found in [4] and [5]. Among capacitive transducers, the differential condenser fulfills best the above mentioned criteria, its production and handling is easy, it has linear characteristics in a wide range and a very small reactive effect to the pendulum arm.

The force acting between the electrodes of a simple capacitive transducer can be calculated from the following formula [2]:

$$F = -\frac{dW_e}{dX} = -\frac{1}{2} U^2 \frac{dC}{dX}, \tag{1}$$

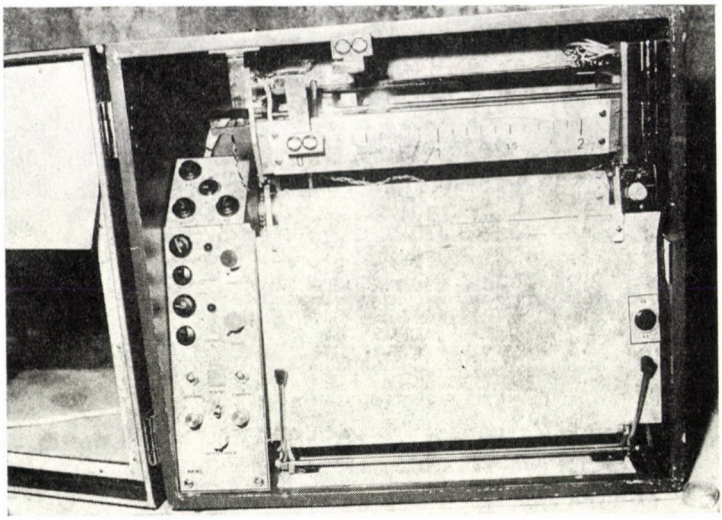


Fig. 1

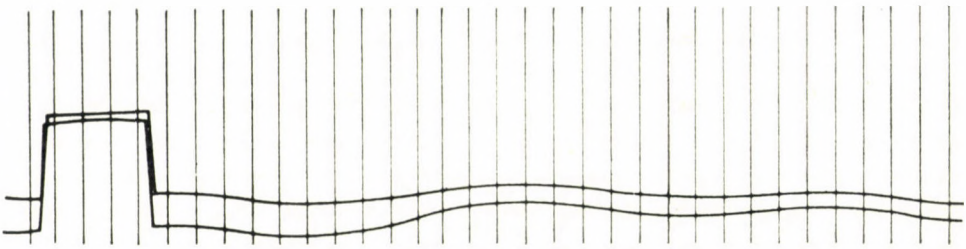


Fig. 2

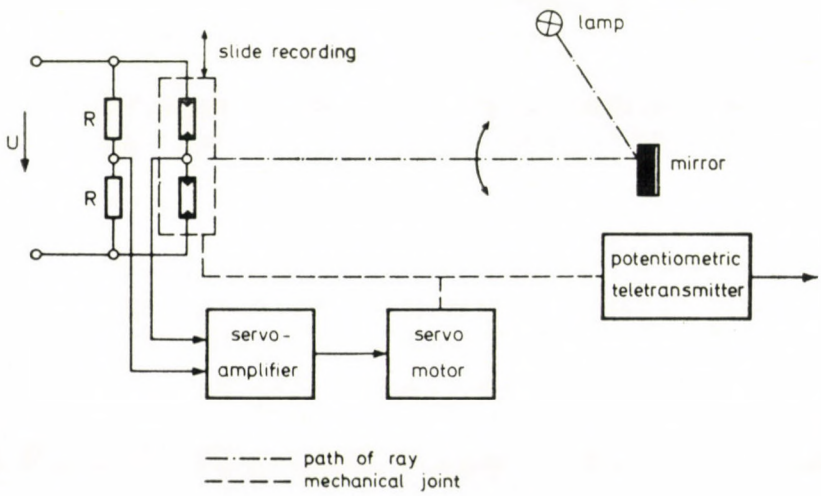


Fig. 3

where

W_e = the electrostatic energy stored in the condenser
C = the capacity of the transducer
U = the voltage switched to the electrodes of the condenser
X = the variable parameter of the transducer (e.g. electrode distance).

In case of a differential condenser the force acting on the pendulum arm is only the result of the asymmetry between the capacities — since the forces of the two condensers compensate each other — and hence extremely small. Therefore, the moment resulting from the reactive forces can be neglected beside the moment of the tidal forces acting on the pendulum arm [3].

In case of a differential condenser the measurement can be made in an oscillator circuit or in an unbalanced bridge. A possible arrangement of the oscillator circuit is presented in Fig. 4. In case of a movement of the central plate of the differential condenser fixed on the pendulum arm, the frequencies of the two oscillators change oppositely. The differential frequency can be produced by mixing the signals of the two oscillators. After amplifying and forming the signal with the differential frequency, the impulses can be counted and the result displayed or stored on a digital recorder. At the same time a potential proportional to the number of impulses can be obtained and analogously recorded by standardizing the impulses and leading them through an integrator circuit. The advantage of the method is the direct frequency output which enables an undisturbed transmission of the output signal to great distances due to its low noise sensitivity. Further, the uncertainty of the measurement is less here than in case of voltage or current measurements. The output signal is easy to digitize.

The measuring method in an unbalanced bridge circuit will be discussed in connection with the following description of the instrument type HI 175 built in our Institute.

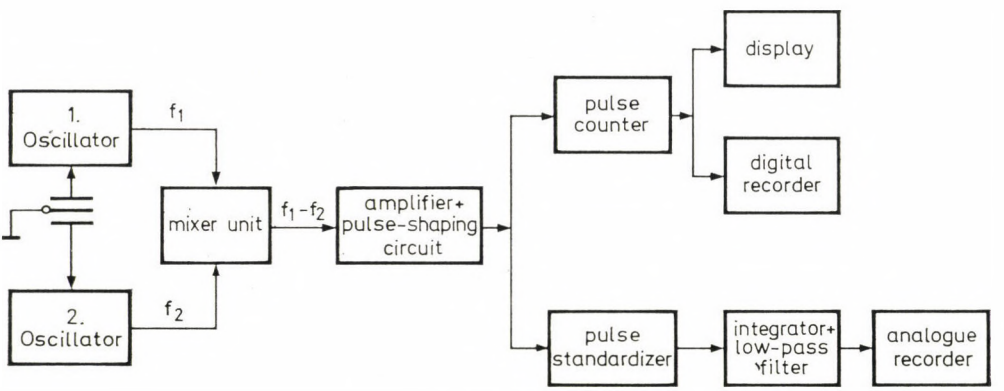


Fig. 4

In spite of the advantages of the oscillator circuit, we have constructed our instrument by using an unbalanced bridge. The reason is that an analogous output is also demanded due to the illustrativeness of the analogous signal and in consequence of problems of digitizing. The analogous output

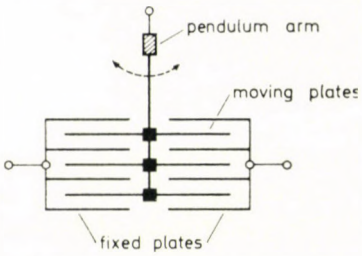


Fig. 5

does not, however, mean any inconvenience for digitizing, since commercial A—D converters are available for such purposes.

The main part of the instrument is the differential condenser; at its construction we strived at great capacity and small weight. In order to secure a relatively great movement for the pendulum arm beside the relatively great capacity of the condenser, the surface of the plates facing in the condenser are enlarged by applying three sheets. The distance between the facing plates is 1 mm, that enables a reliable function and an easy handling. The theoretical scheme of the differential condenser can be seen in Fig. 5, the inner construction of the instrument on a photo (Fig. 6). The differential condenser has been com-

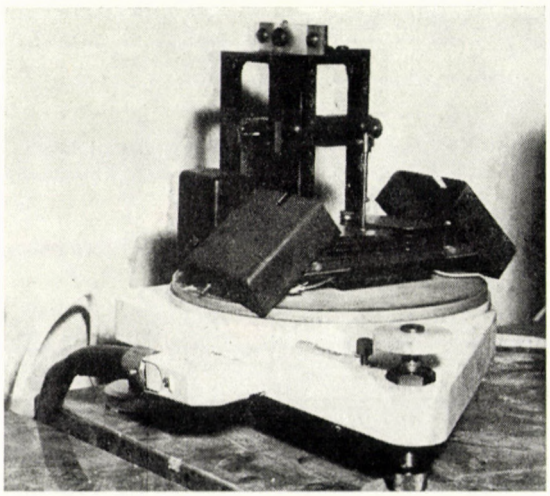


Fig. 6

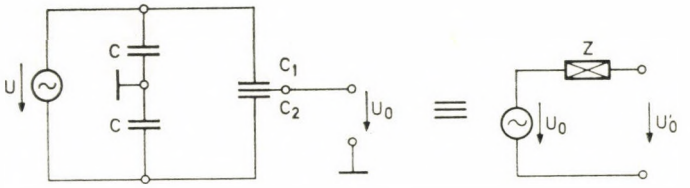


Fig. 7

pleted with two capacitances of equal value to a bridge circuit, as can be seen in Fig. 7 together with its electrical substitution scheme. The idle output voltage of the bridge circuit is:

$$U_0 = \frac{U}{2} \cdot \frac{C_2 - C_1}{C_2 + C_1}, \tag{2}$$

where U is the supply voltage of the bridge.

The absolute value of the output impedance of the bridge is:

$$Z_0 = \frac{1}{\omega}\left[\frac{1}{C_1 + C_2} + \frac{1}{2C}\right] \tag{3}$$

where $\omega = 2\pi f$ is the circular frequency of the supply voltage of the bridge. It is visible from Eq. (2) that the sensitivity of the bridge can be increased by the increase of the supply voltage of the bridge, but this is limited by the increase of the effects calculable from Eq. (1). The output impedance can be decreased by increasing the frequency of the supply voltage.

According to these considerations, 20 V was chosen as supply voltage of the bridge and 12.5 kHz for its frequency, and so it was possible to decrease the output impedance to a few $k\Omega$-s. In consequence of the AC supply, changes of the spurious capacities can cause disturbances, therefore, their constant value is secured by shielding. In order that the own capacity of the shielded wire should not load the output of the transducer, the preamplifier has been placed into the pendulum casing near to the transducer. The shielding pot taken off and the closed shield casing of the preamplifier can be well distinguished in Fig. 6. The remaining parts of the electronics are placed into a separated box. The function of the instrument is the following (see Fig. 8).

The supply voltage of the bridge is produced by a sine-wave oscillator with great amplitude stability, since the output voltage of the bridge is according to Eq. (2) directly proportional to the supply voltage and a change of the supply voltage would cause errors in the measurements. The same oscillator produces the reference signal for the phase-sensitive rectifier, too.

The output voltage of the bridge is detected by an amplifier having a high input and a low output resistance. This secures against an overloading of the

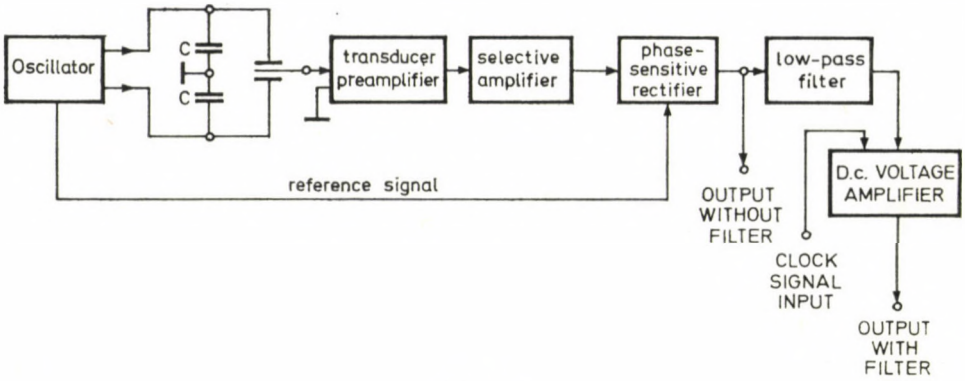


Fig. 8

output of the bridge and enables that the output voltage of the bridge will be transmitted on small impedance to the separate electronical units, to ensure a lower noise-sensitivity. The selective amplifier which follows the pre-amplifier is a two-stage amplifier. Its first stage is a narrow band filter for 50 Hz, its task is to suppress network disturbances. The second stage is an amplifier with a band pass filter, transmitting only the 12.5 kHz signals coming from the transducer. The phase-sensitive rectifier enables the sign-correct measurement of the deviation of the pendulum arm from its central position. Its output is at the same time an unfiltered output, since this signal contains yet the self-swingings of the pendulum arm. This output is necessary for the measurement of the swinging time of the pendulum, e.g. in case of a pendulum calibration with the swinging time when mounting the pendulum. The phase-sensitive rectifier is followed by a low-pass filter for filtering of the self-swinging of the pendulum. The filter characteristics are shown in Fig. 9. A filtering is necessary

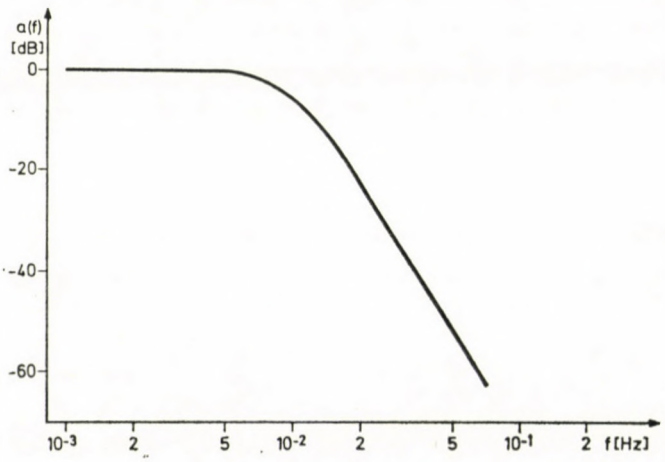


Fig. 9

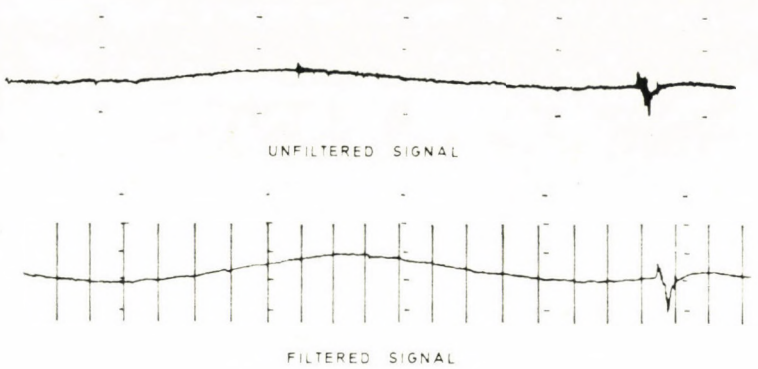


Fig. 10

for apossible further amplification of the signal. Namely, earth movements independent of the earthtides also excite the pendulum and increase very much the amplitude of the self-swinging of the pendulum, and that would blast the next amplifier. The low-pass filter is followed by an integrating DC voltage amplifier; the output signal of the filter comes to one of its inputs, while to the other comes a clock signal. Thus, time marks are picks superposed to the recorded curve.

Two records are shown in Fig. 10. One is unfiltered, the other the same as taken from the filtered output. By comparing the two curves, we can see on the unfiltered output the self-swingings of the pendulum which are caused by soil unrest.

Figure 11 presents the complete measuring equipment. In the centre, there are the two horizontal pendulums with Zöllner suspension (their inner

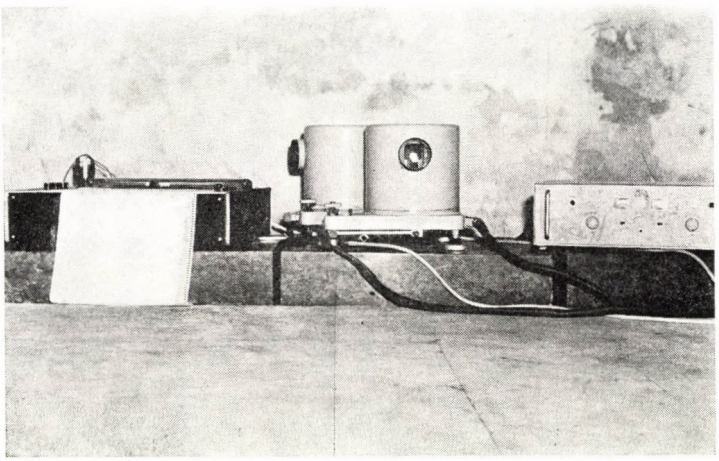


Fig. 11

construction was shown in Fig. 6). For the sake of control a mirror fixed on the pendulum arm allows a traditional recording, too. On the right-hand side a box contains the electronic units of the two channels. At the left-hand side we can see the recorder. The calibration of the pendulum is made with a crapaudine.

The advantage of the instrument is its small place need. There is no long light way, i.e. need for a relatively great room. The recorder can be placed at a relatively great distance from the pendulums, so their control as well as the change of the records can be done without entering into the pendulum chamber. Consequently, the disturbing factors of the recording are decreased.

The described methods enable the recording of the earthtides on a digital way. Since digitizing always means some loss in information, there can arise problems in certain cases (leaps on the curve) with the play-back of the original curve. That is why many people trust even now more in analogous records than in digital ones. These problems, however, can be eliminated by correct sampling methods and by the development of a corresponding processing algorithm.

REFERENCES

1. Alpár, Gy.: Investigations to the development of Zöllner-suspension horizontal pendulums. *Acta Geod. Geoph. et Mont. Hung.*, 10(1975), 329—338.
2. Fodor, Gy.: Elméleti elektrotechnika (Theoretical electrotechnics). Vol. I.Tankönyvkiadó, Budapest 1970.
3. Grave, H. F.: Elektrische Messung nichtelektrischer Größen. Akademische Verlagsgesellschaft Geest und Portig K. G. Leipzig 1962.
4. Mittelstrass, G.: Konstruktionsprinzipien von Horizontaleinfachpendeln. Wissenschaftliche Arbeiten der Lehrstühle für Geodäsie, Photogrammetrie und Kartographie an der Technischen Hochschule Hannover, Nr. 26, 1968.
5. Rohrbach, Chr.: Handbuch für elektrisches Messen mechanischer Größen. VDI-Verlag GmbH Düsseldorf 1967.
6. TSZMK: Ipari folyamatok méréstechnikája és műszerei I/1 (Measuring technics and instruments of industrial processes). Jelátalakítók (Transducers). Tankönyvkiadó, Budapest 1971.

ДАЛЬНЕЙШЕЕ РАЗВИТИЕ РЕГИСТРАЦИИ НАКЛОНОМЕРОМ

ДЬ. МЕНТЕШ

РЕЗЮМЕ

В статье рассматриваются проблемы дальнейшего развития регистрации наклономерами. Подробно излагается фотоэлектрический компенсационный метод, который вместо фоторегистрации может быть применен к существующим уже наклономерам. Далее, подробно рассматривается наклономер с подвеской Цёллнера, снабженный разработанным в последнее время емкостным преобразователем типа HI-175.

Acta Geodaet., Geophys. et Montanist. Acad. Sci. Hung. Tomus 14 (1—2), pp. 111—124 (1979)

IDEAS ON THE PRACTICAL APPLICATION OF COLLOCATION

J. ZÁVOTI

GEODETIC AND GEOPHYSICAL RESEARCH INSTITUTE OF THE HUNGARIAN ACADEMY OF SCIENCES, SOPRON

[Manuscript received November 30, 1977]

The present paper analyses the collocation method being a synthesis of adjustment and prediction methods. Using stochastic simulation, the different numerical solutions of these methods, i.e. collocation and traditional adjustment, are compared.

Nowadays, "least-squares" collocation has already a very significant international literature. It is extensively used in physical geodesy, in the evaluation of satellite observations and in photogrammetry.

Objectives of this report are to show the basic characteristics of the method of collocation and to provide a relatively exact view of conditions of its application. Investigations of MORITZ [11, 12, 13], WOLF [20], KRARUP [10] and KAULA [8] referring to this field are summarized and completed by some remarks from the theory of stochastic processes.

Using the method of stochastic simulation, a test has been carried out to determine with what precision are the starting parameters of the model — in a given special case — given back by collocation.

1. Basis of collocation

The bases of "least-squares" collocation model are surveyed without the claim of completeness (details can be found in the study of MORITZ [13]).

The basic equation using denotations of MORITZ is:

$$\mathbf{y} = \mathbf{A}\mathbf{x} + \mathbf{s}' + \mathbf{n}\,, \tag{1.1}$$

where $\mathbf{A}_{NM}$ is a given matrix,
$\mathbf{x}_{M,1}$ is the vector of unknowns,
$\mathbf{n}_{N,1}$ is the so-called "noise" vector,
$\mathbf{s}'_{N,1}$ is the so-called "signal" vector and
$\mathbf{y}_{N,1}$ is the vector of measurement.

The measurements consist of a systematic part (trend) and random parts. The following obvious questions arise in relation to this model:

What do the notations "signal" and "noise" mean?

What do we know about them?

How can we estimate them?

How can the informations on them improve accuracy of our model?

Let us initially adopt that the signal has the following properties:

a) it may vary continuously (it may exist at points other than the discrete measuring points),

b) any one of its values is of unpredictable, arbitrary nature.

These conditions are practically equivalent to the definition of stochastic processes (a detailed survey e.g. in [4]). Thus the signal may be considered as a stochastic process. Under this condition the study of our model requires the statistical knowledge of nonnumerably innumerable random variables. It is an extremely difficult work. For applicability of this model additional restrictions must be taken:

$$M[\mathbf{s}'] = \mathbf{0} \qquad M[\mathbf{n}] = \mathbf{0} \tag{1.2}$$

(our condition is also the existence of mean values).

It must be noted that the stochastic signal is not a process of Gaussian character by all means (c.f. MORITZ [12]).

The question is what degree of freedom do we have in choosing the stochastic process to be applied. (In the case of a given problem the situation is reversed: the signal — provided that there is any — should be selected, filtered and its statistical characteristics should be determined and classified.) Stationarity of the process is desirable even for the sake of (1.2) alone; on the other hand, prediction — considered as one of the advantages of collocation — in the theory of collocation has been elaborated for the case of stationary processes under limiting conditions.

Let us now assume that we wish to estimate the signal

$$\mathbf{s} = [s_1, s_2, \ldots s_K]^T \tag{1.3}$$

at an arbitrary number of points which may be different from the measured points. Let us form the following vector:

$$\mathbf{v} = [s_1, s_2, \ldots s_K, s'_1 + n_1, s'_2 + n_2, \ldots s'_N + n_N]^T \tag{1.4}$$

where K is the number of the predicted points,

N is the number of points measured,

and let

$$\mathbf{R}_{N,K+N} = [\mathbf{0}_{N,K}, \mathbf{E}_{N,N}] \,, \tag{1.5}$$

where each element of the matrix $\mathbf{0}$ is zero and $\mathbf{E}$ is the unit matrix.

The model (1.1) can be formally described as follows:

$$\mathbf{Ax} + \mathbf{Rv} - \mathbf{y} = \mathbf{0} \,. \tag{1.6}$$

The covariance matrix $\mathbf{Q}$ of vector $\mathbf{v}$ may be written as a partitioned matrix:

$$\mathbf{Q}_{K+N,K+N} = \begin{bmatrix} \mathbf{C}_{ss} & \mathbf{C}_{sy} \\ \mathbf{C}_{ys} & \mathbf{C}_{yy} \end{bmatrix}, \tag{1.7}$$

where $\mathbf{C}_{ss} = \mathrm{cov}(\mathbf{s}, \mathbf{s}) = M[\mathbf{s}\mathbf{s}^T]$ denotes the covariance matrix of the signal vector $\mathbf{s}$ and $\mathbf{C}_{sy} = \mathrm{cov}(\mathbf{s}, \mathbf{y}) = M[\mathbf{s}(\mathbf{s}' + \mathbf{n})^T]$ denotes the crosscovariance matrix between the signal vector $\mathbf{s}$ and the measurement vector $\mathbf{y}$.

For the crosscovariance matrix of the measurement vector $\mathbf{y}$ and the signal vector $\mathbf{s}$, the following connection is obviously true:

$$\mathbf{C}_{ys} = \mathbf{C}_{sy}^T$$

$$\mathbf{C}_{yy} = \mathrm{cov}(\mathbf{y}, \mathbf{y}) = M[(\mathbf{y} - \mathbf{A}\mathbf{x})(\mathbf{y} - \mathbf{A}\mathbf{x})^T] =$$

$$= M[(\mathbf{s}' + \mathbf{n})(\mathbf{s}' + \mathbf{n})^T] = M[\mathbf{s}'\mathbf{s}'^T] +$$

$$+ M[\mathbf{n}\mathbf{s}'^T] + M[\mathbf{s}'\mathbf{n}^T] + M[\mathbf{n}\mathbf{n}^T] .$$

Assuming that signal and noise are uncorrelated

$$M[\mathbf{n}\,\mathbf{s}'^T] = \mathbf{0}$$

$$M[\mathbf{s}'\,\mathbf{n}^T] = \mathbf{0} . \tag{1.8}$$

Hence the covariance matrix of the measurement vector may be transformed into the simple form

$$\mathbf{C}_{yy} = \mathbf{C}_{s's'} + \mathbf{C}_{nn} \tag{1.9}$$

where $\mathbf{C}_{s's'}$ is the covariance matrix of the signal vector $\mathbf{s}'$ obtained at the measuring points,

$\mathbf{C}_{nn}$ is the covariance matrix of the noise vector $\mathbf{n}$ occurring at the measuring points.

Now we are looking for the minimum of the expression

$$\mathbf{v}^T\,\mathbf{Q}^{-1}\,\mathbf{v} . \tag{1.10}$$

The solution is well known [20]; and the unknown parameters are:

$$\mathbf{x} = (\mathbf{A}^T\,\mathbf{C}_{yy}^{-1}\,\mathbf{A})^{-1}\,\mathbf{A}^T\,\mathbf{C}_{yy}^{-1}\,\mathbf{y} . \tag{1.11}$$

Formally, the solution is in accordance with the relation obtained by traditional adjustment but with the essential difference that it can be produced on the basis of the covariance matrix $\mathbf{C}_{yy}$ (1.9) of measurements.

Predicting the signal vector $\mathbf{s}$ to be estimated (1.3) we obtain [20]:

$$\mathbf{s} = \mathbf{C}_{sy}\mathbf{C}_{yy}^{-1}(\mathbf{y} - \mathbf{A}\mathbf{x}) . \tag{1.12}$$

Let $\mathbf{w}_{K,1}$ denote the values to be estimated at an arbitrary point K. At the non-measuring points, the predicted value of $\mathbf{w}$ (so-called complete signal) is given [20] by:

$$\mathbf{w} = \mathbf{B}\mathbf{x} + \mathbf{s}\,, \tag{1.13}$$

where $\mathbf{B}_{KN}$ is a given, so-called prediction matrix.

The estimated quantities $\mathbf{w}$ consist of a systematic part and a random signal.

The accuracy of the estimated quantities $\mathbf{x}$, $\mathbf{s}$ and $\mathbf{w}$ can be characterized by the following matrices (review and demonstration in details may be found in the report of MORITZ [12]):

$$\begin{aligned}
\mathbf{K}_{xx} &= (\mathbf{A}^T\,\mathbf{C}_{yy}^{-1}\,\mathbf{A})^{-1} \\
\mathbf{K}_{ss} &= \mathbf{C}_{ss} - \mathbf{C}_{sy}\,\mathbf{C}_{yy}^{-1}\,\mathbf{C}_{ys} + \mathbf{C}_{sy}\,\mathbf{C}_{yy}^{-1}\,\mathbf{A}\mathbf{K}_{xx}\,\mathbf{A}^T\,\mathbf{C}_{yy}^{-1T}\,\mathbf{C}_{sy}^T \\
\mathbf{K}_{ww} &= \mathbf{K}_{ss} + \mathbf{B}\mathbf{K}_{xx}\,\mathbf{B}^T - \mathbf{B}\mathbf{K}_{xx}\,\mathbf{A}^T\,\mathbf{C}_{yy}^{-1T}\,\mathbf{C}_{sy}^T - \mathbf{C}_{yy}^{-1}\,\mathbf{A}\mathbf{K}_{xx}\,\mathbf{B}^T\,,
\end{aligned} \tag{1.14}$$

where $\mathbf{K}_{xx}$, $\mathbf{K}_{ss}$, $\mathbf{K}_{ww}$ represent the covariance matrices of the estimated values $\mathbf{x}$, $\mathbf{s}$ and $\mathbf{w}$, respectively.

The connection between random variables $\mathbf{x}$ and $\mathbf{s}$ is expressed by the error-crosscovariance matrix $\mathbf{K}_{xs}$:

$$\mathbf{K}_{xs} = -\mathbf{K}_{xx}\,\mathbf{A}^T\,\mathbf{C}_{yy}^{-1T}\,\mathbf{C}_{sy}^T\,. \tag{1.15}$$

2. Collocation in case of one dimension

The problem of one-dimensional interpolational is one of the most important basic cases of collocation. The measured values $y(t_i)$ $(i = 1, 2, \ldots N)$ consist of the following components:

$$y(t_i) = m(t_i) + s'(t_i) + n(t_i) \qquad i = 1, 2, \ldots N\,, \tag{2.1}$$

where $m(t_i)$ is the unknown deterministical function,

$s'(t_i)$ are the measured values of one realization of the stochastic process $s(t)$, taken at points $(i = 1, 2, \ldots N)$,

$n(t_i)$ is the random independent measuring error $(i = 1, 2, \ldots N)$.

On the basis of the measured values $y(t_i)$ $(i = 1, 2, \ldots N)$ we intend to draw some conclusions referring to the function $m(t)$.

We are looking for the function $m(t)$ in the following form:

$$m(t) = \sum_{k=1}^{M} a_k\, t^{k-1} \tag{2.2}$$

where a_k $(k = 1, 2, \ldots M)$ are unknown coefficients. Our task is to estimate the coefficients a_k $(k = 1, 2, \ldots M)$ by means of introducing the following denotations:

$$\mathbf{x} = [a_1, a_2, \ldots a_M]^T$$
$$\mathbf{y} = [y(t_1), y(t_2), \ldots y_N(t)]^T$$
$$\mathbf{s}' = [s'(t_1), s'(t_2), \ldots s'(t_N)^T$$
$$\mathbf{n} = [n(t_1), n(t_2), \ldots n(t_N)]^T$$

$$\mathbf{A} = \begin{bmatrix} 1 & t_1 & t_1^2 \ldots t_1^{M-1} \\ 1 & 1_2 & t_2^2 \ldots t_2^{M-1} \\ \vdots & \vdots & \vdots \quad \vdots \\ 1 & t_N & t_N^2 \ldots t_N^{M-1} \end{bmatrix} . \tag{2.3}$$

The problem (2.1) can be written in matrix form:

$$\mathbf{y} = \mathbf{Ax} + \mathbf{s}' + \mathbf{n} . \tag{2.4}$$

One of the most interesting fields of application of collocation is the problem of prediction. The most probable values $y(t)$ must be given at an arbitrary point t of the time axis by taking the known or suspected characteristics of the stochastic process $s(t)$ into account. These characteristics may be parameters of quantity (e.g. average, deviation, etc.) or parameters of quality, too, to which one can conclude somehow (e.g. stationarity).

The covariance function provides the basis of collocation, by means of which a method is given to estimate the predicted values $y(t)$. Illustratively, the covariance function characterizes the extent of change of the stochastic relation between the different elements of the process.

Let us make an estimation at the points $[t_1^*, t_2^*, \ldots t_k^*]$ on the time axis for the values

$$\mathbf{s}^* = [s(t_1^*), s(t_2^*), \ldots s(t_k^*)] , \tag{2.5}$$
$$\mathbf{y}^* = [y(t_1^*), y(t_2^*), \ldots y(t_k^*)] ,$$

in case of model (2.1). On the basis of (1.13) it can be done in the following way:

$$\mathbf{y}^* = \mathbf{Bx} + \mathbf{s}^* , \tag{2.6}$$

where $\mathbf{x}$ is identical with the $\mathbf{x}$ in the connection (2.3) and

$$\mathbf{B} = \begin{bmatrix} 1 & t_1^* & t_1^{*2} \ldots t_1^{*M-1} \\ 1 & t_2^* & t_1^{*2} \ldots t_2^{*M-1} \\ \vdots & \vdots & \vdots \quad \vdots \\ 1 & t_K^* & t_K^{*2} \ldots t_K^{*M-1} \end{bmatrix} .$$

It is visible that this problem corresponds to the model communicated in paragraph 1.

Further investigations of our model will be carried out by means of the method of stochastic simulation.

Stochastic simulation is employed in more and more fields of sciences, as it makes it possible to solve very difficult practical problems. Mathematical background of the method consists of mathematical analysis, theory of probability and statistics, numerical methods; stochastic models are simulated by computational means. As the first step we must construct such a stochastic model for the given problem, the parameters of which correspond to the unknown quantities in the model. Then observations are performed regarding the stochastic model and the parameters in question are determined by statistical estimation from the results obtained. In many cases the exact mathematical description of the stochastic model itself is not possible, and it can yield only an approximation of the original phenomenon in a certain way. Generally, the simplifications and approximations are unavoidable because we do not know perfectly the real process or the fundamentals of the computer that set limits to the exact realization of the process.

3. Stochastic simulation

Let us investigate the distribution of estimations obtained from the one-dimensional collocation model in certain given cases. The example of simulation constructed for the model is the following:

Let us start with the concrete

$$m(t) = t^3 - 13t^2 + 52t - 10 \tag{3.1}$$

third-degree polynomial, considering it as a deterministical component (trend) in the model. Let us choose such a stochastic process as a signal which satisfies the restrictions mentioned above and for which the covariance function is known. These conditions are satisfied by the following stochastic process:

$$s(t) = \alpha \sin\left(\frac{2\pi}{T} t + \varphi\right) \tag{3.2}$$

where α denotes the same given constant in case of every realization of the process (amplitude of the process),

T denotes a similarly known constant (period-time of process),

φ denotes the phase angle which is a random variable with uniform distribution in the interval $[0, 2\pi]$.

Under these conditions the random process $s(t)$ is not only stationary but ergodic, too (it can be found e.g. in [9]).

It can be easily verified that the condition (1.2) too, is fulfilled. It can be proved that $M[\sin \varphi] = M[\cos \varphi] = 0$, therefore

$$M[s(t)] = \alpha \sin \frac{2\pi}{T} tM[\cos \varphi] + \alpha \cos \frac{2\pi}{T} tM[\sin \varphi] = 0 . \tag{3.3}$$

Let us determine the covariance function $C(t, r)$ of the process $s(t)$; on the basis of (3.3) it can be written:

$$\begin{aligned} C(t, r) &= M[s(t)s(t + r)] - M[s(t)]M[s(t + r)] = \\ &= M[s(t)s(t + r)] . \end{aligned} \tag{3.4}$$

In our case $C(t, r)$ can be determined directly, too:

$$\begin{aligned} C(t, r) &= M\left[\alpha \sin \left(\frac{2\pi}{T} t + \varphi\right) \alpha \sin \left\{\frac{2\pi}{T} (t + r) + \varphi\right\}\right] = \\ &= \frac{\alpha^2}{2} \cos \frac{2\pi}{T} r - \frac{\alpha^2}{2} \cos \left(\frac{4\pi}{T} t + \frac{2\pi}{T} r\right) M[\cos 2\varphi] + \\ &\quad + \frac{\alpha^2}{2} \sin \left(\frac{4\pi}{T} t + \frac{2\pi}{T} r\right) M[\sin 2\varphi] = \\ &= \frac{\alpha^2}{2} \cos \frac{2\pi}{T} r \end{aligned} \tag{3.5}$$

as it can be readily seen that $M[\cos 2\varphi] = M[\sin 2\varphi] = 0$.

It can be seen that the covariance function of the stochastic process $s(t)$ depends on r only — in accordance with the stationarity of stochastic process $s(t)$.

Let us have observations at the points t_i $(i = 1, 2, \ldots 10)$ distributed uniformly in the interval $[0, 10]$ (these points are contained in Table I).

Table I

t_1	t_2	t_3	t_4	t_5	t_6	t_7	t_8	t_9	t_{10}
0.7	1.8	3.1	3.9	4.6	5.5	7.3	8.2	9.4	10.0

The structure of observations corresponds to the relation (2.1):

$$\begin{aligned} y(t_i) &= t_i^3 - 13t_i^2 + 52t_i - 10 + \alpha \sin \left(\frac{2\pi}{T} t_i + \varphi\right) + n(t_i) \\ & i = 1, 2, \ldots 10 \end{aligned} \tag{3.6}$$

where $n(t_i)$ is a given output of an independent random variable with normal distribution N (0, 1) for each t_i $(i = 1, 2, \ldots 10)$.

The stochastic process $s(t)$ takes place continuously in time but observations can be done only at discrete points of time, although in principle the observations can be made as frequently as desired.

Let us create a series of realizations of the stochastic process $s(t)$ with given amplitude, period time, in the combinations given in Table II by the method of FREIBERGER and GRENANDER [3]. Table III involves the realization occurring at the measurement points of the stochastic process $s(t)$ simulated at points of time t_k $(k - 1)\delta$ $(k = 1, 2, \ldots 101; = 0.1)$ in cases corresponding to Table II.

Table II

Amplitude α \ Period time T	1	2.5	5
1	(1, 1)	(1, 2.5)	(1, 5)
2.5	(2.5, 1)	(2.5, 2.5)	(2.5, 5)
5	(5, 1)	(5, 2.5)	(5, 5)

In such a way we can determine the values $y(t_i)$ $(i = 1, 2, \ldots 10)$ on the basis of (3.6) which can be considered as measurement values. The physical contents correspond to the model of collocation: the measurements contain a trend and the measurement error is divided into two components. The measurements $y(t_i)$ $(i = 1, 2, \ldots 10)$ are evaluated by a method of collocation separately [the matrix $\mathbf{C}_{s's'}$ in the connection (1.9) can be derived from the covariance function (3.5); on the basis of (3.6) the matrix $\mathbf{C}_{nn}$ is a matrix of unity] and by means of the conventional least-squares method separately.

The question is, knowing the statistical characteristics of signal $s(t)$ (the given theoretical covariance function), whether the method of collocation provides more precise and more reliable results than the traditional method of least-squares. Quantitative characteristics can be evaluated according to the way how the two methods reproduce the coefficients of the original polynomial. The results are summarized in Table IV and Table V. (In reality one could draw general conclusions for each case concerning the statistical characteristics of estimation from several realizations only. Our intention here is merely to show what kind of estimations occur in case of a single realization.)

By means of relation (2.6) we can predict at non-measured points of time $t_1^* = 0.0$, $t_2^* = 2.0$, $t_3^* = 5.0$, $t_4^* = 6.0$, too, the values $\mathbf{y}^*$ modified by the signal. The predicted values corresponding to the single cases are shown in Table VI. Substance of the exhibited method of collocation is made clear in Fig. 1, which refers to the case (5, 5) given in Table II.

Table III

Signals

	(1, 1)	(2.5, 1)	(5, 1)	(1, 2.5)	(2.5, 2.5)	(5, 2.5)	(1, 5)	(2.5, 5)	(5, 5)
$s(t_1)$	−0.951	0.940	4.996	0.946	2.499	−4.888	−0.996	1.167	−4.965
$s(t_2)$	−0.752	−1.538	−4.999	0.041	0.916	4.753	0.128	2.405	−0.463
$s(t_3)$	0.611	1.682	4.589	−0.762	−1.089	−1.730	0.947	−1.808	−3.489
$s(t_4)$	−0.388	−2.013	4.886	0.295	1.660	−3.370	0.902	1.534	4.887
$s(t_5)$	0.684	2.303	1.472	0.839	−0.951	4.220	−0.377	2.381	−2.798
$s(t_6)$	0.149	2.438	−4.303	−0.617	−2.448	−4.018	0.159	2.497	−3.415
$s(t_7)$	0.111	2.429	4.695	0.818	−2.129	−0.959	0.181	2.384	−4.557
$s(t_8)$	0.868	−0.645	−1.231	0.979	2.496	−4.692	−0.900	2.169	3.049
$s(t_9)$	−0.303	2.225	−3.846	−0.190	2.482	4.999	0.999	2.444	1.182
$s(t_{10})$	−0.985	2.451	4.205	0.993	1.700	3.364	−0.529	2.473	−4.282

Table IV

Exact value	(1, 1)	(2.5, 1)	(5, 1)	(1, 2.5)	(2.5, 2.5)	(5, 2.5)	(1, 5)	(2.5, 5)	(5, 5)
−10	−10.953	−10.399	−5.476	−8.374	−6.655	−12.312	−11.629	−8.647	−10.270
52	52.328	53.953	48.897	50.799	50.068	55.094	53.455	51.266	50.863
−13	−12.992	−13.545	−12.272	−12.753	−12.762	−13.895	−13.300	−12.750	−12.746
1	0.996	1.038	0.953	0.986	0.996	1.063	1.017	0.983	0.984

Table V

Least-squares method

Exact value	(1, 1)	(2.5, 1)	(5, 1)	(1, 2.5)	(2.5, 2.5)	(5, 2.5)	(1, 5)	(2.5, 5)	(5, 5)
−10	−11.155	−9.914	−8.086	−8.546	−6.291	−16.597	−11.784	−7.907	−15.409
52	52.290	51.892	52.325	50.922	50.204	58.110	53.529	50.873	54.359
−13	−12.963	−12.918	−13.178	−12.778	−12.828	−14.515	−13.306	−12.703	−13.353
1	0.994	0.995	1.014	0.987	0.999	1.102	1.017	0.981	1.016

Table VI

Predicted values

(1, 1)	(2.5, 1)	(5, 1)	(1, 2.5)	(2.5, 2.5)	(5, 2.5)	(1, 5)	(2.5, 5)	(5, 5)
−10.952	−12.084	−12.193	−8.263	−8.841	−10.129	−11.766	−8.218	−10.456
49.703	49.948	54.133	50.253	49.873	54.596	50.262	50.711	46.575
50.381	48.823	54.547	50.153	46.940	50.874	50.164	52.238	48.144
50.429	48.248	55.121	50.119	51.114	44.003	49.875	52.909	45.330

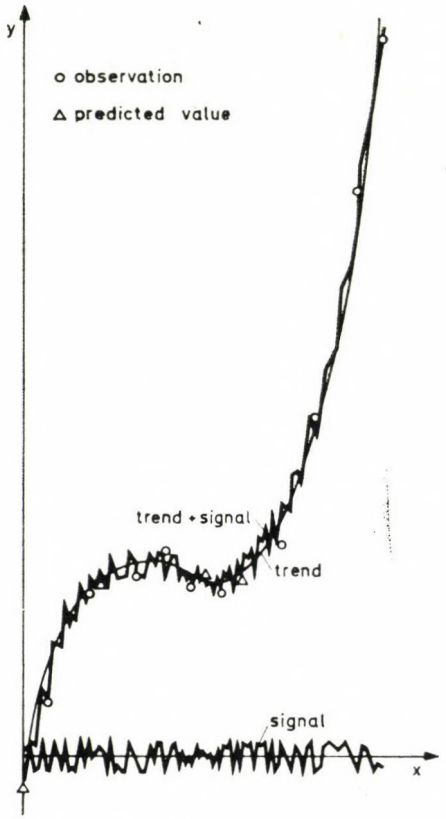


Fig. 1

4. Remarks

The problem raised in the previous paragraph cannot be decided generally. Even if consequently executing the method of collocation, we do not get essentially more satisfying results than with the method of least-squares which requires less mathematical apparatus [we carried out the error calculations (1, 3), (1, 15), too].

The effectiveness of the equalization method is a very complex problem. If we make use of more information of the distribution of measurements during the equalization then the method is generally more effective but it necessitates more difficult computation and the accuracy of calculation decreases because of complexity, which causes the worsening of accuracy of estimation.

When applying the method of collocation, the correct choice of the covariance function requires great care. The statistical characteristics of the signal (the stochastic process) are existing independently of us; when describing a natural phenomenon, we try to draw conclusions on its parameters by methods

of estimation only. We can increase the efficiency of collocation by selecting the appropriate method of estimation. There are other covariance functions beside the "usual" functions

$$C_1(r) = ke^{-a^2r}, \qquad C_2(r) = 1/(1 + r^2/b^2), \qquad C_3(r) = a^{b^r}.$$

The selection of the covariance function is determined by the character of the problem on the basis of the results of estimation methods.

The selection of the measuring points is a separate problem: how should the measurements of a number n (which should be possibly a minimum) be distributed, how many measurements should be carried out in a point in order to obtain a good estimate of the coefficients? A further problem is to choose the number of degree of the approximation polynomial.

These problems raise many mathematical difficulties. Even if a part of the questions are solved in principle, frequently serious numerical objections occur in the course of execution.

Computations were performed on a computer of type HP 2100 A of the Geodetic and Geophysical Research Institute of the Hungarian Academy of Sciences by means of a programme package developed for this very purpose.

REFERENCES

1. Buslenko, N. P.: Simulation of Complicated Systems. Műszaki Könyvkiadó, Budapest, 1972.
2. Csáki, F.: Dynamics of Controlling. Akadémiai Kiadó, Budapest, 1974.
3. Freiberger, W.—Grenander, U.: Probability and Statistics. Springer-Verlag, New York, 1971.
4. Gihman, I. I.—Szkorohod, A. V.: An Introduction to the Theory of Stochastic Processes. Műszaki Könyvkiadó, Budapest, 1975.
5. Gotthardt, E.: Einführung in die Ausgleichungsrechnung. Wichmann, Karlsruhe, 1968.
6. Grafarend, E.: Geodetic stochastic processes. Bibliographisches Institut AG, Zürich, 1975.
7. Hannan, E. J.: Time Series Analysis. Methuen and Co. Ltd., London, 1960.
8. Kaula, W. M.: Statistical and harmonic analysis of gravity. *J. Geophys. Research*, 64 (12), 1959.
9. Korn, G. A.—Korn, T. M.: Mathematical Handbook for Engineers. Műszaki Könyvkiadó, Budapest, 1975.
10. Krarup, T.: A contribution to the mathematical foundation of physical geodesy. Danish Geodetic Institute, Copenhagen, 44, 1968.
11. Moritz, H.: Least-squares estimation in physical geodesy. Reports of the Department of Geodetic Science, 130, 1970.
12. Moritz, H.: Advanced least-squares methods. Reports of the Department of Geodetic Science, 175, 1972.
13. Moritz, H.: Stepwise and sequential collocation. Reports of the Department of Geodetic Science, 203, 1973.
14. Lauritzen, S.: The probabilistic background of some statistical methods in physical geodesy. Danish Geodetic Institute, Copenhagen, 1971.
15. Reza, F. H.: An Introduction to Information Theory. McGraw Hill Book Co., New York 1962.
16. Rényi, A.: Wahrscheinlichkeitsrechnung. Deutscher Verlag der Wissenschaften, Berlin 1962.
17. Rosenblatt, M.: Time Series Analysis. John Wiley and Sons, New York, 1963.

18. SCHREJDER, JU. A.: Die Monte-Carlo-Methode. B. G. Teubner Verlagsgesellschaft, Leipzig, 1964.
19. WIENER, N.: Time Series. The M.I.T. Press, Cambridge, 1970.
20. WOLF, H.: Prädiktion und Punktausgleichung. *Zschr. für Vermessungswesen*, 94, 1969.

СООБРАЖЕНИЯ О ПРАКТИЧЕСКОМ ПРИМЕНЕНИИ МЕТОДА КОЛЛОКАЦИИ

Й. ЗАВОТИ

РЕЗЮМЕ

Настоящая статья посвящена методу коллокации, который является синтезом уравнивания и метода предикции. С помощью стохастической симуляции были сравнены различные вычислительные методы решения названных методов, т. е. метода коллокации и традиционный метод уравнения.

Acta Geodaet., Geophys. et Montanist. Acad. Sci. Hung. Tomus 14 (1—2), pp. 125—133 (1979)

FORMELSYSTEME ZUR BERECHNUNG DER SONNENEPHEMERIDEN

H. LICHTENEGGER

INSTITUT FÜR LANDESVERMESSUNG UND PHOTOGRAMMETRIE,
TECHNISCHE UNIVERSITÄT GRAZ

[Eingegangen am 5. Dezember 1977]

Die Formelsysteme zur Berechnung der Sonnenephemeriden werden so dargestellt, daß sie auch für den Praktiker ohne astronomische Vorkenntnisse anwendbar sind.
Die theoretischen Ausführungen werden durch ein numerisches Beispiel ergänzt.

1. Vorbemerkung

In der ingenieurgeodätischen Praxis treten häufig Aufgaben auf, zu deren Lösung unter anderem die Richtungskoordinaten (Azimut, Zenitdistanz) der Sonne benötigt werden.

Aus der Erfahrung des Verfassers seien einige Problemstellungen angeführt:

a) bei der Planung von Gebäuden, insbesonders von Hochhäusern, ist aus rechtlichen Grundsätzen die Beschattung der angrenzenden Grundstücke zu beachten,

b) zur Dimensionierung der Beleuchtung bei Tunneleinfahrten ist die jeweilige Sonneneinstrahlung in bezug auf die Tunnelachse von Bedeutung,

c) aus Schattenlängen und -richtungen können Beweissicherungen, etwa aus photographischen Aufnahmen von Verkehrsunfällen, gewonnen werden,

d) die optimale Ausrichtung von Sonnenkollektoren zur Energiegewinnung bedarf der Vorausberechnung der scheinbaren Sonnenbahn,

e) da die Orientierung von historischen Kulturdenkmälern (Kirchen, Tempel usw.) häufig aus Beobachtung des Sonnenauf- oder -unterganges erfolgte, tritt im archäologisch-architektonischen Bereich das Problem auf, aus der Orientierung der Bauwerke auf die Epoche deren Errichtung zu schließen,

f) aus Sonnenbeobachtungen können astronomische Azimute irdischer Ziele abgeleitet werden. Es sei auf die Methode in [6] hingewiesen, deren Lösung bei Kenntnis der Deklination der Sonne das Azimut einer Mire voraussetzungslos (ohne Zeitmessung oder Kenntnis astronomischer Standpunktsparameter) ergibt.

Daneben werden Sonnenkoordinaten bei den verschiedensten wissenschaftlichen Problemstellungen (Berechnung der Gezeitenwirkung, Zenitdistanz der Sonne als Parameter von dynamischen Temperaturen usw.) benötigt.

Die Koordinaten der Sonne sind in den astronomischen Jahrbüchern oder Ephemeridentafeln (etwa [3]) verzeichnet, oder können mit Hilfe von

Tabellen und Tafeln [1, 2] oder bereitgestellten Programmen [5] berechnet werden.

Für die Anwendung in der Praxis jedoch erscheint es sinnvoll, die hiefür verwendeten Formelsysteme anzugeben, um einerseits unabhängig von Tabellen zu sein und andererseits die Koordinaten für beliebige, auch historische Epochen, mit Hilfe einfacher Tischrechner bestimmen zu können.

2. Problemstellung

Gesucht sind die scheinbaren (apparent) Richtungskoordinaten der Sonne bezogen auf das himmelsfeste Äquatorsystem, d.h. Rektaszension α, Deklination δ, sowie der Abstand der Erde von der Sonne zu beliebigen Epochen.

Mit Hilfe dieser Größen können durch einfache Transformationen unter Verwendung der jeweiligen Ortsparameter (geographische Breite und Länge) das Azimut a und die Zenitdistanz z der Sonne abgeleitet werden (etwa [7]).

Die Formelsysteme sollen eine Genauigkeit von maximal $\pm 0''1$ in den Sonnenkoordinaten gewährleisten. Für geringere Genauigkeitsansprüche soll die Möglichkeit einer Vereinfachung bestehen.

3. Lösungsansatz

3.1 *Mittlere Größen*

Zur Lösung des gestellten Problems wird vorerst von mittleren Größen im Sonnensystem ausgegangen. Diese Größen beschreiben eine ungestörte, gleichförmige Bewegung einer ideellen Sonne, des Mondes und der Planeten. Sie beziehen sich auf das mittlere ekliptikale Koordinatensystem der jeweiligen Epoche. Es sind dies:

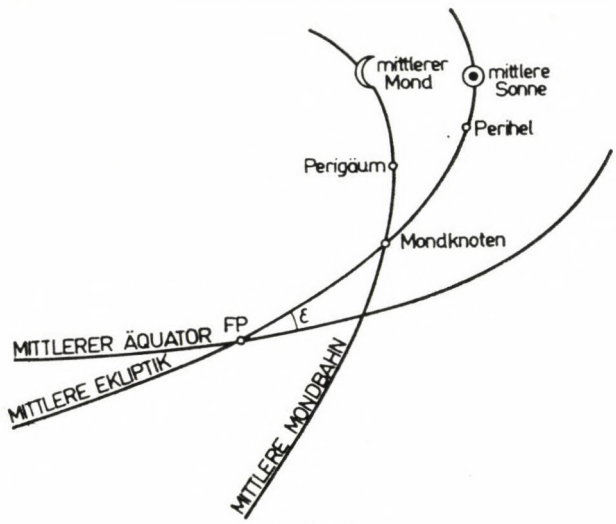


Abb. 1

Symbol	Größe	Definition
L	Sonne-FP	mittlere geometrische Länge der Sonne
B	$B = 0$	mittlere ekliptikale Breite der Sonne
g	Sonne-Perihel	mittlere Anomalie der Sonne
ε		mittlere Schiefe der Ekliptik
e		mittlere Erdbahnexzentrizität
c	$c = 1.496 \cdot 10^8$ km	mittlerer Erdbahnradius
L'	Mond-Knoten-FP	mittlere Länge des Mondes
g'	Mond-Perigäum	mittlere Anomalie des Mondes
Ω	Knoten-FP	mittlere Knotenlänge des Mondes
D_i	$D_i = L + 180° - L_i$	mittlere Elongation der Planeten in bezug auf die Erde, d.h. Differenz der mittleren Länge der Erde und der mittleren Länge der Planeten

3.2 *Korrekturglieder*

Um die ekliptikalen Koordinaten der wahren Sonne bezogen auf den wahren Frühlingspunkt (apparent coordinates) zu erhalten, sind Korrekturen an die mittleren Größen anzubringen:

$\lambda = L + \Sigma dL_i$ apparent ekliptikale Länge der wahren Sonne
$\beta = B + \Sigma d\beta_i$ apparent ekliptikale Breite der wahren Sonne
$\bar{\varepsilon} = \varepsilon + \Sigma d_\varepsilon$ apparent ekliptikale Schiefe
$r = c + \Sigma dr$ wahre Entfernung der Sonne

dL_1 langperiodische Störungen der mittleren Länge
dL_2 Korrektur auf elliptische Bahn (Flächensatz)
dL_3 Störglieder der Planeten
dL_4 Störglieder des Mondes
dL_5 Korrektur zufolge Nutation in Länge
dL_6 Korrektur zufolge jährlicher Aberration

$d\beta_1$ Störglieder des Mondes
$d\beta_2$ Störglieder der Planeten

$d\varepsilon$ Korrektur zufolge Nutation in Schiefe

dr_1 Korrektur auf elliptische Bahn
dr_2 Störglieder des Mondes und der Planeten

4. Formelsystem

4.1 *Mittlere Größen*

$$
\begin{aligned}
L &= 279°69668 + 36\,000°76892\ \mathrm{T} + 0°00030\ \mathrm{T}^2 \\
B &= 0° \\
g &= 358°47583 + 35\,999°04975\ \mathrm{T} + 0°00015\ \mathrm{T}^2 - \ldots \\
\varepsilon &= 23°45229 - 0°01301\ \mathrm{T} - \ldots \\
e &= 0.0167510 - 0.0000418\ \mathrm{T} - 0.0000001\ \mathrm{T}^2
\end{aligned}
$$

$$
\begin{aligned}
L' &= 270°43 + 481\,267°88\ \mathrm{T} - \ldots \\
g' &= 296°10 + 477\,198°85\ \mathrm{T} + \ldots \\
\Omega &= 259°18 - 1\,934°14\ \mathrm{T} + \ldots
\end{aligned}
$$

$$
\begin{aligned}
D_1 &= 63°1 + 22\,518°4\ \mathrm{T} + \ldots \text{ Venus (Supplement der Elongation)} \\
D_2 &= 193°1 + 34\,777°3\ \mathrm{T} + \ldots \text{ Saturn} \\
D_3 &= 166°0 + 16\,859°1\ \mathrm{T} + \ldots \text{ Mars} \\
D_4 &= 221°7 + 32\,964°5\ \mathrm{T} + \ldots \text{ Jupiter}
\end{aligned}
$$

(Die übrigen Planeten können für die angestrebte Genauigkeit außer Betracht bleiben!)

T Anzahl der Julianischen Jahrhunderte zu 36 525 (Ephemeriden)-Tagen seit der Epoche 1900, Jänner 0^d5 ET (der Zusammenhang zwischen Ephemeridenzeit ET und Weltzeit UT ist bekanntlich gegeben durch ET = UT + ΔT, ΔT z. Z. $\sim 49^s$).

4.2 *Korrekturglieder*

$$
\begin{aligned}
dL_1 &= 6''40 \sin(231°2 + 20°2\ \mathrm{T}) + 1''88 \sin(57°2 + 150°3\ \mathrm{T}) + \\
&\quad + 0''27 \sin(32° + 119°\ \mathrm{T}) + 0''20 \sin(316° + 893°\ \mathrm{T}) + \ldots
\end{aligned}
$$

$$
\begin{aligned}
dL_2 &= \left(2e - \frac{1}{4}e^3\right) \sin g + \frac{5}{4}e^2 \sin(2g) + \frac{13}{12}e^3 \sin(3g) + \ldots = \\
&= (1°91946 - 0°00479\ \mathrm{T} - 0°00001\ \mathrm{T}^2) \sin g + \\
&\quad + (0°02009 - 0°00010\ \mathrm{T}) \sin(2g) + 0°00029 \sin(3g) + \ldots
\end{aligned}
$$

(Vor der Berechnung von dL_2 ist g um dL_1 zu korrigieren!)

$$
dL_3 = \underset{\text{Planeten}}{\Sigma\Sigma}\ s \cos(aD + bg + k)
$$

s	Amplitude	siehe Tabelle I
a, b	ganzzahlige Koeffizienten	
k	Phasenwinkel	
D	mittlere Elongation des betrachteten Planeten	
g	mittlere Anomalie der Sonne	

Tabelle I

Planetenstörungen in Länge

$s[''']$	a	b	$k[°]$	$s[''']$	a	b	$k[°]$
			VENUS				MARS
4.84	1	0	90.00	0.27	1	0	90.60
5.53	2	0	90.12	2.04	2	0	89.76
0.67	3	0	270.41	0.13	3	0	273.00
0.21	4	0	89.80	1.77	2	−1	306.27
0.08	5	0	270.10	0.58	4	−2	185.82
2.50	2	−1	257.75	0.50	4	−1	316.94
1.56	3	−1	77.96	0.43	3	−1	317.70
1.02	3	−2	50.85	0.20	5	−2	185.50
0.15	5	−3	34.10	0.15	6	−2	185.00
0.15	4	−2	227.40	0.11	7	−3	53.30
0.14	4	−1	79.00	0.10	6	−3	53.90
0.12	5	−2	229.80	0.09	5	−1	139.30
0.12	2	1	90.70	0.05	8	−3	52.50
0.08	1	1	87.50	0.06	9	−4	282.60
0.07	1	−1	358.80				JUPITER
			SATURN	7.21	1	0	91.09
0.42	1	0	90.34	2.73	2	0	270.25
0.11	2	0	270.10	0.16	3	0	265.20
0.32	1	−1	259.22	2.60	1	−1	174.77
0.11	2	−1	273.10	1.61	2	−1	292.60
				0.56	3	−1	177.31
				0.21	3	−2	193.20
				0.16	1	1	110.20
				0.08	4	−2	83.90
				0.07	1	−2	187.90
				0.07	2	−2	75.70
				0.07	2	1	263.90

$$dL_4 = 6''45 \sin D_M + 0''18 \sin(D_M + g') - 0''42 \sin(D_M - g') - 0''06 \sin(D_M + g) + 0''17 \sin(D_M - g) + \ldots$$

$$D_M = L' - L$$

$$dL_5 = -17''24 \sin \Omega + 0''21 \sin(2\Omega) + 0''07 \sin g' - 0''20 \sin(2L') - 1''27 \sin(2L) + 0''13 \sin g - 0''05 \sin(2L + g) + \ldots$$

$$dL_6 = -(20''47 + 0''34 \cos g)$$

$$d\beta_1 = 0''58 \sin (L' - \Omega) - 0''05 \sin (L' - \Omega - g') + \ldots$$

$$d\beta_2 = \underset{\text{Planeten}}{\Sigma\Sigma}\, s \cos (aD + bg + k) \quad \text{(Tabelle II)}$$

Tabelle II

Planetenstörungen in Breite

$s['']$	a	b	$k[°]$
			VENUS
0.21	3	−1	64.50
0.09	1	−1	64.60
0.07	2	−1	244.80
0.03	4	−1	65.40
0.03	1	1	116.00
0.02	2	1	295.00
			JUPITER
0.17	2	−1	268.00
0.02	1	−2	0.00

$$d\varepsilon = 9''21 \cos \Omega - 0''09 \cos (2\Omega) + 0''55 \cos (2L) + 0''09 \cos (2L') + \ldots$$

$$r = c\left[1 + \frac{e^2}{2} - \left(e - \frac{3}{8} e^3\right) \cos g - \left(\frac{e^2}{2} - \frac{e^4}{3}\right) \cos (2g)\right] - \ldots] =$$

$$= 1.0001 - 0.0168 \cos g - 0.0001 \cos (2g) - \ldots$$

Bei den Korrekturen der Länge werden Terme $<0''05$, bei denen der Breite solche $<0''02$ vernachlässigt.

4.3 *Transformationsformeln*

a) Ekliptik — → Äquatorsystem

$$\cos \delta \cos \alpha = \cos \beta \cos \lambda$$
$$\cos \delta \sin \alpha = \cos \beta \sin \lambda \cos \bar{\varepsilon} - \sin \beta \sin \bar{\varepsilon}$$
$$\sin \delta = \cos \beta \sin \lambda \sin \bar{\varepsilon} + \sin \beta \cos \bar{\varepsilon}$$

b) Äquator — → Horizontsystem

$$\sin z \cos a = \cos \delta \cos t \sin \varphi - \sin \delta \cos \varphi$$
$$\sin z \sin a = \cos \delta \sin t$$

$\cos z = \cos \delta \cos t \cos \varphi + \sin \delta \sin \varphi$

$t = \mathrm{ET} - \Delta\mathrm{T} + \Delta\lambda \pm 12^{\mathrm{h}} + L + dL_5 \cos \varepsilon + dL_6 - \alpha - 0.002738\, \Delta\mathrm{T}$

φ = geographische Breite

t = Stundenwinkel der wahren Sonne bezogen auf Ortsmeridian mit einem Längenunterschied von $\Delta\lambda$ östlich von Greenwich.

5. Numerisches Beispiel

Zur Veranschaulichung der theoretischen Formeln soll folgendes Zahlenbeispiel dienen. Gesucht seien die äquatorialen scheinbaren Koordinaten der Sonne zur Epoche 1978, Sept. 1. um 0^{h} ET. Zum Vergleich sind bei den Ergebnissen die aus dem astronomischen Jahrbuch [3] folgenden Werte angegeben.

Da seit der Epoche 1900 Jänner, $0^{\mathrm{d}}5$ 28 732.5 Tage bis zur angegebenen Epoche verflossen sind, ergibt sich

$$\mathrm{T} = 0.786\,652\,9774$$

5.1 *Mittlere Größen*

L	= 159°80893	L'	= 141°24	D_1	= 137°3
g	= 237°23541	g'	= 206°00	D_2	= 190°8
ε	= 23°44206	Ω	= 177°68	D_3	= 108°3
				D_4	= 233°3

5.2 *Korrekturglieder*

dL_1	= −5″70	$d\beta_1$	= −0″39
dL_2	= −1°59270	$d\beta_2$	= −0″14
dL_3	= 9″81		
dL_4	= −2″17	$d\varepsilon$	= −8″85
dL_5	= 0″18		
dL_6	= −20″29		

5.3 *Scheinbare ekliptikale Koordinaten*

	Berechnung	Astronomical Ephemeris
λ	158°12′40″25	158°12′40″29
β	−0″53	−0″49
$\bar{\varepsilon}$	23°26′22″56	23°26′22″53
r	1.0092	1.0092

5.4 *Scheinbare äquatoriale Koordinaten*

Berechnung	Astronomical Ephemeris
α $10^h39^m26^s16$	$10^h39^m26^s17$
δ $8°29'26''6$	$8°29'26''6$

t_0 $11^h58^m57^s51$ ($\Delta T = 49^s$)

(Stundenwinkel bezogen auf Greenwich).

6. Computerprogram

Für den Rechner Olivetti P 652 am Institut des Verfassers wurde ein Programm erstellt, das nach Eingabe der gewünschten Epoche die ekliptikalen und äquatorialen Koordinaten der Sonne nebst weiteren Hilfsgrößen (Nutation in Länge und Schiefe, Zeitgleichung, Korrektur auf Sternzeit Greenwich usw.) berechnet. Auf eine Publikation der Befehlsfolge wird verzichtet, doch wird das Programm auf Magnetkarten samt Dokumentation allen Interessenten zur Verfügung gestellt.

7. Schlußbemerkung

Das angegebene Formelsystem gewährleistet eine Genauigkeit von etva $\pm 0''1$ in den äquatorialen Sonnenkoordinaten. Werden geringere Genauigkeiten gewünscht, ergeben sich beträchtliche Vereinfachungen. Zum Beispiel genügt die Berücksichtigung der Korrektur dL_2 an den mittleren Größen, um eine Genauigkeit von etwa $\pm 30''$ zu erzielen. In diesem Fall können die Sonnenkoordinaten mit Hilfe eines Tischrechners ohne Zuhilfenahme astronomischer Tafeln in wenigen Minuten berechnet werden.

SCHRIFTTUM

1. Newcomb, S.: Tables of the motion of the earth on its axis and around the sun. Astronomical Papers, Vol. VI, Part 1, Washington, 1895.
2. Meeus, J.: Tables of Moon and Sun. Kesselberg Sterrenwacht, Belgium 1962.
3. Nautical Almanac Office: The Astronomical Ephemeris for 1978. Her Majesty's Stationery Office, London 1977.
4. Nautical Almanac Office: Explanatory Supplement to the Astronomical Ephemeris. Her Majesty's Stationery Office, London, 1973.
5. Heitz, S.: Mathematische Modelle der geod. Astronomie. DGK A, Heft 85, München 1976.
6. Lichtenegger, H.: A Method of Astronomic Azimuth Determination. Mittlg. d. geod. Inst. der TU Graz, Folge 20, 1975.
7. Lichtenegger, H.—Rinner, K.: Sphärische Astronomie, Grundlagen. Spkriptenreferat der Hochschülerschaft der TU Graz, Graz, 1977.
8. Bartels, J.: Gezeitenkräfte. Handbuch der Physik, Band XLVIII, Geophysik II, Springer Verlag, Heidelberg 1957.

СИСТЕМЫ ФОРМУЛ ДЛЯ ВЫЧИСЛЕНИЯ ЭФЕМЕРИД СОЛНЦА

Х. ЛИХТЕНЕГГЕР

РЕЗЮМЕ

Системы формул для вычисления эфемерид Солнца представляются ввиде, пригодном и для практикантов без астрономических знаний.

Теоретические выводы илюстрируются на числовом примере.

Acta Geodaet., Geophys. et Montanist. Acad. Sci. Hung. Tomus 14 (1—2), pp. 135—140 (1979)

ZUR FRAGE DER PLANUNG DER HÖHENNETZE, MIT RÜCKSICHT AUF DIE ERDKRUSTENBEWEGUNGS-UNTERSUCHUNGEN

L. BÁCSATYAI

KANDIDAT DER TECHN. WISSENSCHAFTEN
GEODÄTISCHES UND GEOPHYSIKALISCHES
FORSCHUNGSINSTITUT DER UNGARISCHEN AKADEMIE DER WISSENSCHAFTEN, SOPRON

[Eingegangen am 20. April 1978]

Es werden allgemeine Bemerkungen zur Planung der geodätischen Netze zwecks Erdkrustenbewegungs-Untersuchungen gemacht. Im weiteren wird im Falle linearer Bewegungsmodelle eine für den zwischen Wiederholungsmessungen benötigten minimalen Zeitabschnitt abgeleitete Formel in Abhängigkeit von der Messungszahl, der Meßgenauigkeit und der Anzahl der Wiederholungsmessungen für Höhennetze angegeben. Dabei werden die Größe der zu erwartenden absoluten Punktbewegungen sowie das Ausmaß und die Konfiguration des Höhennetzes als unveränderlich betrachtet. Die Formel wird für das Präzisionsnivellementsnetz Ungarns angewendet. Aus den erhaltenen Ergebnissen werden entsprechende Schlußfolgerungen gezogen.

1. Der Zweck der im Laufe der Erdkrustenbewegungs-Untersuchungen durchgeführten geodätischen Messungen ist die Bestimmung der Bewegungstendenzen der Erdoberfläche (der Erdkruste) mit Hilfe vielfacher Wiederholungsmessungen sowie der gemeinsamen Ausgleichung spezieller geodätischer Netze. Aus der Natur der geodätischen Netze folgt, daß die horizontalen bzw. vertikalen Bewegungskomponenten nur in diskreten, entsprechend ausgewählten, nach bestimmten Gesichtspunkten gezeichneten Punkten der Erdoberfläche registrierbar sind. So bedeutet die Feststellung der Bewegungstendenzen irgendeines beliebigen Teiles der Erde die Bestimmung der sich auf das diskrete Punktfeld beziehenden Bewegungsfunktion.

Hier stößt man gleich auf zwei, charaktermäßig unterschiedliche Schwierigkeiten, die einander ergänzen. Die erste ist, daß man zur Zeit über keinen zusammenhängenden großen, z. B. regionalen Flächenteil verfügt, zu dem bereits mehr als eine völlige und moderne Wiederholungsmessung durchgeführt worden wäre. Dabei ist noch die erste Messung ausnahmslos auf andere Zwecke gerichtet, die Wiederholungsmessung wurde nur für die Bestimmung der Vertikalkomponenten aus Nivellementsnetzen durchgeführt; in den meisten Fällen diente sogar die zweite Messung einem anderen Zweck. Das ist nicht überraschend, den die Tätigkeit der Geodäsie auf diesem Gebiet nur auf etwa zwei Jahrzehnte zurückblickt. Die zweite Schwierigkeit liegt darin, daß man über die Natur der Bewegungsfunktion fast keinerlei Vorstellung hat. Die Bewegungsfunktion kann als Polynom erster, zweiter, sogar mehrerer Ordnung oder in beliebiger anderer Form angenähert werden, es scheint aber dabei unvermeidlich, systematische, sogenannte Modellfehler zu begehen. Als eine Möglichkeit, diese in Betracht zu ziehen, soll die Kollokationsmethode, die neben

den in der traditionellen Methode der kleinsten Quadrate behandelten zufälligen Messungsfehlern (noise) auch die Modellfehler (signal) berücksichtigen kann [1], erwähnt werden. Die Vorteile dieser Methode können aber nicht widerspruchslos beurteilt werden [2, 3].

Es scheint überflüssig zu sein, über die Bestimmungsmöglichkeiten der Bewegungsfunktion zu sprechen, solange kine entsprechende Anzahl von Wiederholungsmessungen der Netze verfügbar ist. Die im ganzen Messungskomplex, bei der Organisierung der Planung einzelner Messungen auftretenden Parameter können streng nur mit Hilfe der Vorkenntnis der Ausgleichsprozedur (Ausgleichsmodell) erhalten werden. Daraus geht die Gegenwirkung beider Probleme hervor: einerseits sind die Messungen auf lange Zeitperiode für ein gedankliches Ausgleichsmodell zu planen, andererseits würde die mathematische Strenge in Kenntnis der ganzen Messungsdatenmenge die Anwendung des gedanklichen Ausleichungsmodells erfordern.

Es ist natürlicherweise nicht zu erwarten, daß während einer langen Zeitperiode (z. B. eines Jahrhunderts) die Ausgleichungstheorie sich nicht weiterentwickelt, daher darf — im späteren — die Anwendung eines anderen Modells, statt des ursprünglich geplanten gedanklichen Ausgleichsmodells, kein Hindernis bedeuten. Deshalb reicht es aus, bei der Planung aus der einfachen Modellvorstellung auszugehen (da eine kompliziertere keine größere Wahrscheinlichkeit hat) und auf den möglichen Modellfehler zu verzichten. Das endgültige Ausgleichsmodell soll — im Besitz der Menge der Messungsdaten — der Zukunft überlassen werden. Im folgenden motiviert diese Tatsache auch weitere Vereinfachungen.

Die Qualität jeder Methode wird von der Praxis aus gerechtfertigt. Darauf ist im Falle der Erdkrustenbewegungen noch lange zu warten, so dürfen die ausgearbeiteten Methoden an den für die Untersuchung größenordnungsmäßig größerer technogener Bewegungen gestalteten Netzen getestet werden.

2. Die Frage der Planung geodätischer Netze kann mit der Feststellung der wichtigsten Netz-Parameter in engen Zusammenhang gestellt werden. Als solche Parameter können z. B. die Meßgenauigkeit, die Messungszahl, die Anzahl der Wiederholungsmessungen, der Zeitabschnitt zwischen je zwei Wiederholungsmessungen, die Größe der zu erwartenden Bewegungen sowie das Ausmaß des Netzes (Anzahl der Punkte, geometrische Konfiguration) genannt werden [4, 5]. Wird ein funktionaler Zusammenhang zwischen den Parametern festgesetzt, so bleibt die Anzahl der Parameterkombinationen noch unendlich. Fixiert man aber einige der Parameter, so wird der Kreis der Parameterkombinationen in Abhängigkeit von den fixierten Parametern eingeengt. Für uns ist der Zeitabschnitt zwischen Wiederholungsmessungen am interessantesten, der in Abhängigkeit von Messungszahl, Meßgenauigkeit und Anzahl der Wiederholungsmessungen ausgedrückt werden kann. In diesem Falle werden die Größe

der zu erwartenden Bewegungen sowie das Ausmaß und die Konfiguration des Netzes als unveränderlich betrachtet.

Im weiteren wird eine sich auf den Zeitabschnitt zwischen Wiederholungsmessungen beziehende Formel für Höhennetze und für den Fall eines einfachen linearen Bewegungsmodells angegeben. Die Formel wurde, ausgegangen aus einem Grundbegriff der mathematischen Statistik, mit Hilfe der Gütefunktion des Fisher-Tests abgeleitet [6, 7]. Das bedeutet zugleich, daß die zu ziehenden Schlußfolgerungen nur mit einem bestimmten Signifikanzniveau, mit einem gewissen, sich auf den Fisher-Test beziehenden Fehler zweiter Art und für die normalverteilten Meßergebnisse gelten. Die Formel hat für Fälle gerad- bzw. ungeradzahliger Wiederholungsmessungen mit Berücksichtigung der in der Praxis als reell zu betrachtenden und im weiteren noch zu behandelnden Voraussetzungen folgende Gestalt:

$$\tau_{\text{gerade}} = \frac{4\Phi(\alpha, \beta, q, f)}{g^2} \sqrt{\frac{(q+1) \cdot u_{\text{gerade}}}{Z}} \tag{1a}$$

$$\tau_{\text{ungerade}} = \frac{4\Phi(\alpha, \beta, q, f)}{(g-1)(g+3)} \sqrt{\frac{(q+1) \cdot u_{\text{ungerade}}}{Z}} \tag{1b}$$

Die Bezeichungen sind die folgenden:

$$\Phi(\alpha, \beta, q, f) = \delta(q+1)^{-\frac{1}{2}} \tag{2}$$

δ — der Nichtzentralitätsparameter der nichtzentralen Fisher-Verteilung;

q — die Anzahl der unabhängigen Elemente des Vektors der zu erwartenden absoluten Bewegungsgeschwindigkeiten der Höhenfestpunkte $\mathbf{V}$;

$$f = n\left[\sum_{k_i=1}^{g} (k_i - 1)\right]. \tag{3}$$

Der Wert $\Phi(\alpha, \beta, q, f)$ ist speziellen Diagrammen in Abhängigkeit vom Signifikanzniveau α und von der Testgüte β sowie von den Freiheitsgraden q und f zu entnehmen;

g — die Anzahl der Wiederholungsmessungen, inbegriffen die erste Durchmessung des Netzes;

k_i — die Anzahl der Hin- und Rückmessungen des i-ten Nivellements;

n — die Anzahl der Nivellementslinien;

$$u_{\text{gerade}} = \sum_{i=1}^{g} \frac{s_i^2}{k_i} \tag{4a}$$

$$u_{\text{ungerade}} = \sum_{i=1}^{g} \frac{s_i^2}{k_i} + \frac{s_g^2}{k_g} \tag{4b}$$

s_i — der zu erwartende mittlere km-Fehler des i-ten Nivellements;

$$Z = \underset{1,r}{\mathbf{V}'}\ \underset{r,n}{\mathbf{G}'}\ \underset{n,n}{\mathbf{Q}_l^{-1}}\ \underset{n,r}{\mathbf{G}}\ \underset{r,1}{\mathbf{V}}\ ; \tag{5}$$

$\mathbf{V}_{r,1}$ — der Vektor der zu erwartenden absoluten Bewegungsgeschwindigkeiten der Höhenfestpunkte;

$\mathbf{G}$ — die bei den benachbarten Punkten des Netzes die Elemente 1 und -1 enthaltende Matrix;

$\mathbf{Q}_l$ — die sich auf die beliebige Durchmessung des Netzes beziehende Kofaktor-Matrix;

r — die Anzahl der Höhenfestpunkte.

Der Wert τ bedeutet jenen Zeitabschnitt zwischen den einzelnen Wiederholungsnivellements, der minimalerweise notwendig ist, um die aus der Ausgleichung erhaltenen Unbekannten mit gewissem Signifikanzniveau und mit gegebener Testgüte als Geschwindigkeiten annehmen zu können, damit sie nicht die Wirkung zufälliger Messungsfehler widerspiegeln.

In den Formeln (1a) und (1b) wurden die folgenden Voraussetzungen angenommen:

a) Die Werte s_i und k_i im i-ten Nivellement sind gleich für das ganze Netz;

b) die geometrische Struktur des Netzes bleibt im Laufe der Zeit unverändert;

c) bei beliebiger Durchmessung des Netzes sind die Kovarianzverhältnisse gleichbleibend;

d) es gibt keine Korrelation zwischen dem i-ten und j-ten Wiederholungsnivellement;

e) die Meßfehler enthalten keinen systematischen Anteil (das ist zweifellos die strengste und am schwierigsten einhaltbare Voraussetzung); diese Voraussetzung hängt auch damit zusammen, daß zwischen den Meßwerten keine Korrelation bestehen darf;

f) die Zeitpunkte für Messungen einzelner Nivellementslinien weichen von Zentralepochen aller Nivellements ungefähr gleichmäßig ab.

Abgesehen von der praktischen Realität, idealisieren die erwähnten Voraussetzungen gewissermaßen die Schlußfolgerungen, deshalb bilden die Abweichungen der reellen Verhältnisse von den vorausgesetzten den Gegenstand spezieller Untersuchungen.

3. Die Formeln (1a) und (1b) können sinngemäß für ein beliebiges Bewegungsnetz verwendet werden, die Ordnung der zu erwartenden Bewegungsgeschwindigkeiten muß aber anhand vorläufiger geologischer oder anderer Informationen annähernd bekannt sein.

Im weiteren werden für das Präzisionsnivellementsnetz Ungarns einige Ergebnisse der experimentellen Prüfung bei $g = 2$ gezeigt [8]. Auf Grund der bisher durchgeführten Untersuchungen und Berechnungen stehen für dieses

Netz die zu erwartenden vertikalen Punktbewegungs-Geschwindigkeiten zur Verfügung. Diese sind von Größe 1 bis 2 mm pro Jahr. In Tabelle I werden die Zeitabschnitte zwischen dem ersten und dem Wiederholungsnivellement in Jahren für einige Wertepaare (s_1, s_2) bzw. (k_1, k_2) gezeigt. Die Tabellenwerte beziehen sich auf das Signifikanzniveau $\alpha = 0{,}99$ und die Testgüte $\beta = 0{,}9$.

Tabelle I

f	$1-\alpha = 0{,}99$ $1-\beta = 0{,}9$	$k_1; k_2$ \ $s_1; s_2$ mm/$\sqrt{\text{km}}$	0,8; 0,7	0,7; 0,6	0,6; 0,5	0,5; 0,4	0,4; 0,3
46	1,44	1; 2	16,0	13,9	11,8	9,8	7,7
92	1,32	1; 3	14,0	12,2	10,4	8,6	6,8
92	1,32	1; 4	13,6	11,9	10,1	8,4	6,7
138	1,27	2; 2	11,3	9,8	8,3	6,8	5,3
184	1,24	2; 3	10,2	8,8	7,5	6,2	4,9

Die zu erwartenden Geschwindigkeitswerte von Festpunkten wurden entsprechend der vorher gebildeten vertikalen Erdkrustenbewegungskarte Ungarns ausgewählt.

Aus den erhaltenen Ergebnissen können für das Präzisionsnivellementsnetz Ungarns folgende Schlußfolgerungen gezogen werden:

a) Der minimale Zeitabschnitt zwischen den Zentralepochen zweier Nivellements ist auch bei relativ kleiner Meßgenauigkeit und verhältnismäßig geringen Geschwindigkeitswerten nicht zu lang. So können in verhältnismäßig kurzer Zeit für die vertikalen Geschwindigkeiten mit großer Wahrscheinlichkeit zuverlässige Werte angegeben werden.

b) Die Erhöhung der Anzahl von Hin- und Rückmessungen über eine bestimmte Grenze hat keine große Bedeutung. Die Ergebnisse führen zur Schlußfolgerung, daß die zweifache Hin- und Rückmessung weitgehend ausreichend ist.

c) Die Meßgenauigkeit (der zu erwartende mittlere km-Fehler) spielt eine kleinere Rolle, als zu erwarten wäre. Die zur Zeit zur Verfügung stehenden Instrumente entsprechen den für die Genauigkeit des Netzes gestellten Forderungen.

Als eine sehr strenge Forderung muß noch einmal auf die Verminderung systematischer Meßfehler sowie auf die Untersuchung ihrer Natur bzw. auf die Kenntnis ihrer numerischen Werte eingegangen werden. In dieser Hinsicht ist diese Forderung wichtiger als die Erhöhung der Meßgenauigkeit.

SCHRIFTTUM

1. MORITZ, H.: The method of the least-squares collocation in geometrical geodesy, Pergamon Press Oxford, 1972.
2. MÉLYKUTI, G.: A legkisebb négyzetek módszere és a kollokáció (Die Methode der kleinsten Quadrate und die Kollokation). *Geodézia és Kartográfia*, 28(1976), 95—100.
3. ZÁVOTI, J.: Ideas on the practical application of collocation. *Acta Geod., Geoph. et Mont. Hung.* (im Druck).
4. BÁCSATYAI, L.: Некоторые теоретические аспекты нивелирный сетей с целью выявления вертикалных ь скоростей земной коры. Результаты научно сотрудничества между ЦЛВГ АН Болгарии в Софии и ГГНИ АН Венгрии в Шопроне, Sopron, 1976, 270—319.
5. BÁCSATYAI, L.: Függőleges földkéregmozgási sebességek statisztikai analízise és a szintezési hálózatok tervezése (Statistische Analyse der vertikalen Erdkrustenbewegungsgeschwindigkeiten und Planung der Nivellementsnetze). Dissertation, Sopron, 1977.
6. SCHEFFÉ, H.: The analysis of variance. John Wiley & Sons, inc. New York, 1959.
7. PELZER, H.: Zur Analyse geodätischer Deformationsmessungen. DGK, Reihe C, Heft 164, 1971.
8. BÁCSATYAI, L.: A kéregmozgásvizsgálati szintezési hálózatok tervezéséről (Über die Planung der Nivellementsnetze für Erdkrustenbewegungsuntersuchungen). *Geodézia és Kartográfia* (im Druck).

К ВОПРОСУ О ПРОЕКТИРОВАНИИ НИВЕЛИРНЫХ СЕТЕЙ, С ОСОБЫМ ВНИМАНИЕМ НА ИССЛЕДОВАНИЯ ДВИЖЕНИЙ ЗЕМНОЙ КОРЫ

Л. БАЧАТЯИ

РЕЗЮМЕ

Сделаны некоторые замечания к проектированию геодезических сетей в целях изучения движений земной коры. В дальнейшем для нивелирных сетей в случае линейной модели движения задается формула, определяющая минимальный интервал времени между повторными измерениями в зависимости от числа и точности измерений, а также от числа повторений. При этом величина ожидаемых абсолютных скоростей пунктов, а также размеры и конфигурация высотной сети считаются неизменными. Применение формулы показано на примере венгерской нивелирной сети высшего порядка. Из полученных результатов сделаны соответствующие выводы.

Acta Geodaet., Geophys. et Montanist. Acad. Sci. Hung. Tomus 14 (1—2), pp. 141—148 (1979)

ADJUSTMENT OF QUADRILATERALS COMPUTED FROM ELECTROMAGNETIC DISTANCE MEASUREMENTS ENCUMBERED BY TEMPERATURE AND OTHER METEOROLOGICAL EFFECTS

A. TÁRCZY-HORNOCH

ACADEMICIAN

M. VERŐ-HETÉNYI

GEODETIC AND GEOPHYSICAL RESEARCH INSTITUTE OF THE HUNGARIAN ACADEMY OF SCIENCES, SOPRON

[Manuscript received March 2, 1978]

It is proposed to use in the adjustment of trilateration networks instead of the length ratios an unknown parameter u_i in each point, which takes into account meteorological (temperature) effects in the form of $S(1 + u_i)$, where S is the measured distance. In such a form the scale factor is undetermined, and the normal matrix is singular. The additional condition to be introduced can be $\Sigma u = 0$ (the average scale factor is errorfree) or else one measured length is supposed to be errorfree.

The important problem described in the title is dealt with in many publications containing useful ideas, as shown by the references in CROSS and NORRIS [1]. Most of them introduce into the adjustment the length ratios of the distances measured in the same point at nearly the same time. These are also used by ROBERTSON [2] in a paper containing similarly many useful ideas.

It is worth while to quote ANGUS-LEPPAN about the length ratios: "Observational and meteorological evidence indicates that much of the uncertainty due to refraction will be eliminated by using the ratio of lengths measured from the same point with a short time interval between the measurements. This ratio will remain constant to a higher degree than actual lengths" [3; pp. 358—359]. We fully agree with him. A certain explanation is needed to the comparison of the ratios computed from the measured lengths (p. 363) with the ratios after the adjustment (p. 364). If the measured lengths are denoted by index 1, then — according to Fig. 1 (also on p. 361 of [3]) which has been supplemented

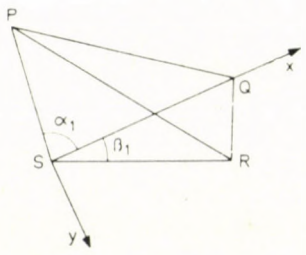


Fig. 1

according to our aims – the first length ratio is $A = \frac{PS_1}{PR_1}$, the second $B = \frac{PR_1}{PS_1}$, etc. As the distance PS_1 appears in both ratios A and B, these values are correlated (ANGUS-LEPPAN) and may not be used independent of each other in the adjustment. That is why the corrections are added in [4; pp. 202–205] to the measurements.

Let us proceed further, and introduce as unknowns into the adjustment instead of length ratios the regular errors of the length unit: u_P to all the three distances measured in P, u_Q for the distances measured from Q, u_R from R, u_S from S. The length corrections v are added to the distances already corrected for the regular errors.

In Fig. 1 an auxiliary system of coordinates $x-y$ has been introduced with the origin in S and the x-axis through Q in which x_S and y_S and y_Q respectively are zeros, and x_Q, x_P, y_P, x_R and y_R are to be determined together with the u values. The following equations can be deduced:

$$
\begin{aligned}
&x_Q = SQ_1(1 + u_S) + v_{SQ} = QS_1(1 + u_Q) + v_{QS}\\
&x_P^2 + y_P^2 = \left(SP_1(1 + u_S) + v_{SP}\right)^2 = \left(PS_1(1 + u_P) + v_{PS}\right)^2\\
&x_R^2 + y_R^2 = \left(SR_1(1 + u_S) + v_{SR}\right)^2 = \left(RS_1(1 + u_R) + v_{RS}\right)^2 \qquad (1)\\
&(x_R - x_P)^2 + (y_R - y_P)^2 = \left(RP_1(1 + u_R) + v_{RP}\right)^2 = \left(PR_1(1 + u_P) + v_{PR}\right)^2\\
&(x_Q - x_P)^2 + (-y_P)^2 = \left(QP_1(1 + u_Q) + v_{QP}\right)^2 = \left(PQ_1(1 + u_P) + v_{PQ}\right)^2\\
&(x_Q - x_R)^2 + (-y_R)^2 = \left(QR_1(1 + u_Q) + v_{QR}\right)^2 = \left(RQ_1(1 + u_R) + v_{RQ}\right)^2 .
\end{aligned}
$$

Equations 1 can be expressed in function of the length corrections. If the approximative values of the coordinates x_Q, x_P, y_P, x_R, y_R are denoted by $x_{Q,0}$, $x_{P,0}$, $y_{P,0}$, $x_{R,0}$, $y_{R,0}$ (their calculation will be treated later), their changes by δx_Q, δx_P, δy_P, δx_R, δy_R; in the following their squares and the products of v and u, as second-order small terms will be neglected, then the following correction equations result:

$$
\begin{aligned}
v_{SQ} &= \delta x_Q - SQ_1 \cdot u_S + x_{Q,0} - SQ_1 = 0\\
v_{QS} &= \delta x_Q - QS_1 \cdot u_Q + x_{Q,0} - QS_1 = 0\\
v_{SP} &= \frac{x_{P,0}}{SP_1}\,\delta x_P + \frac{y_{P,0}}{SP_1}\,\delta y_P - SP_1\,u_S + \frac{x_{P,0}^2 + y_{P,0}^2}{2SP_1} - \frac{SP_1}{2}\\
v_{PS} &= \frac{x_{P,0}}{PS_1}\,\delta x_P + \frac{y_{P,0}}{PS_1}\,\delta y_P - PS_1\,u_P + \frac{x_{P,0}^2 + y_{P,0}^2}{2PS_1} - \frac{PS_1}{2}\\
v_{SR} &= \frac{x_{R,0}}{SR_1}\,\delta x_R + \frac{y_{R,0}}{SR_1}\,\delta y_R - SR_1\,u_S + \frac{x_{R,0}^2 + y_{R,0}^2}{2SR_1} - \frac{SR_1}{2} \qquad (2)
\end{aligned}
$$

$$v_{RS} = \frac{x_{R,0}}{RS_1}\delta x_R + \frac{y_{R,0}}{RS_1}\delta y_R - RS_1\, u_R + \frac{x_{R,0}^2 + y_{R,0}^2}{2RS_1} - \frac{RS_1}{2}$$

$$v_{RP} = \frac{x_{R,0} - x_{P,0}}{RP_1}\delta x_R \frac{x_{R,0} - x_{P,0}}{RP_1}\delta x_P + \frac{y_{R,0} - y_{P,0}}{RP_1}\delta y_R -$$

$$- \frac{y_{R,0} - y_{P,0}}{RP_1}\delta y_P - RP_1\, u_R + \frac{(x_{R,0} - x_{P,0})^2}{2RP_1} + \frac{(y_{R,0} - y_{P,0})^2}{2RP_1} - \frac{RP_1}{2}$$

$$v_{PR} = \frac{x_{R,0} - x_{P,0}}{PR_1}\delta x_R - \frac{x_{R,0} - x_{P,0}}{PR_1}\delta x_P + \frac{y_{R,0} - y_{P,0}}{PR_1}\delta y_R -$$

$$- \frac{y_{R,0} - y_{P,0}}{PR_1}\delta y_P - PR_1 u_P + \frac{(x_{R,0} - x_{P,0})^2}{2PR_1} + \frac{(y_{R,0} - y_{P,0})^2}{2PR_1} - \frac{PR_1}{2}$$

$$v_{QP} = \frac{x_{Q,0} - x_{P,0}}{QP_1}\delta x_Q - \frac{x_{Q,0} - x_{P,0}}{QP_1}\delta x_P + \frac{y_{P,0}}{QP_1}\delta y_P -$$

$$- QP_1 u_Q + \frac{(x_{Q,0} - x_{P,0})^2}{2QP_1} + \frac{(-y_{P,0})^2}{2QP_1} - \frac{QP_1}{2}$$

$$v_{PQ} = \frac{x_{Q,0} - x_{P,0}}{PQ_1}\delta x_Q - \frac{x_{Q,0} - x_{P,0}}{PQ_1}\delta x_P + \frac{y_{P,0}}{PQ_1}\delta y_P -$$

$$- PQ_1 u_P + \frac{(x_{Q,0} - x_{P,0})^2}{2PQ_1} + \frac{(-y_{P,0})^2}{2PQ_1} - \frac{PQ_1}{2}$$

$$v_{QR} = \frac{x_{Q,0} - x_{R,0}}{QR_1}\delta x_Q - \frac{x_{Q,0} - x_{R,0}}{QR_1}\delta x_R + \frac{y_{R,0}}{QR_1}\delta y_R -$$

$$- QR_1 u_Q + \frac{(x_{Q,0} - x_{R,0})^2}{2QR_1} + \frac{(-y_{R,0})^2}{2QR_1} - \frac{QR_1}{2}$$

$$v_{RQ} = \frac{x_{Q,0} - x_{R,0}}{RQ_1}\delta x_Q - \frac{x_{Q,0} - x_{R,0}}{RQ_1}\delta x_R + \frac{y_{R,0}}{RQ_1}\delta y_R -$$

$$- RQ_1 u_R + \frac{(x_{Q,0} - x_{R,0})^2}{2RQ_1} + \frac{(-y_{R,0})^2}{2RQ_1} - \frac{RQ_1}{2}\,.$$

The 12 equations of Eq. 2 belong to the group of the adjustment of indirect observations, and they can be adjusted. The 9 unknowns are: δx_Q, δx_P, δy_P, δx_R, δy_R, u_P, u_Q, u_R, u_S. If the distance measurements are of different accuracy, different weights must be assigned to them. The adjustment yields the mean square errors of the adjusted distances, too.

The approximate coordinate $x_{Q,0}$ can easily be determined:

$$x_{Q,0} = SQ_1\,.$$

For the determination of the approximative coordinates of P and R, the angles α_1 and β_1 are needed. These can be computed from the formulas:

$$\cos\frac{\alpha_1}{2} = \sqrt{\frac{s_1(s_1 - PQ_1)}{SP_1 \cdot SQ_1}} \quad \text{and} \quad \cos\frac{\beta_1}{2} = \sqrt{\frac{s_2(s_2 - RQ_1)}{SR_1 \cdot SQ_1}} \tag{3}$$

where

$$s_1 = \frac{SP_1 + SQ_1 + PQ_1}{2} \quad \text{and} \quad s_2 = \frac{SR_1 + SQ_1 + RQ_1}{2} \tag{4}$$

with these one gets:

$$\begin{aligned} x_{P,0} &= SP_1 \cos\alpha_1 \\ y_{P,0} &= -SP_1 \sin\alpha_1 \end{aligned} \quad \text{and} \quad \begin{aligned} x_{R,0} &= SR_1 \cos\beta_1 \\ y_{R,0} &= SR_1 \sin\beta_1 . \end{aligned} \tag{5}$$

The advantage of this method is that the regular errors of the distances measured from the points can be compared. The necessity of the determination of a greater number of unknowns is no problem with computers.

As a numerical example we use the measured data of ANGUS-LEPPAN's quadrilateral [3; p. 363]:

$SQ_1 = 20253.9370$ m	$RP_1 = 25344.1465$ m
$QS_1 = 20253.9553$ m	$PR_1 = 25344.0896$ m
$SP_1 = 13845.2188$ m	$QP_1 = 22404.4287$ m
$PS_1 = 13845.2330$ m	$PQ_1 = 22404.5221$ m
$SR_1 = 18032.4872$ m	$QR_1 = 8508.8038$ m
$RS_1 = 18032.4516$ m	$RQ_1 = 8508.7624$ m

α_1 and β_1 can be computed:

$$\cos\frac{\alpha_1}{2} = 0.7675329 \quad \text{from this} \quad \alpha_1 = 79°44'03.40''$$

$$\cos\frac{\beta_1}{2} = 0.9766374 \quad \text{from this} \quad \beta_1 = 24°49'06.92''$$

and the approximative coordinates are:

$x_{P,0} = 2467.4063$ m	$x_{R,0} = 16367.0301$ m
$y_{P,0} = -13623.5818$ m	$y_{R,0} = 7569.0734$ m

With this values the correction equations according to Eq. 2 can be written in a matrix form:

$$\underset{12,1}{\bar{\mathbf{v}}} = \underset{12,9}{\mathbf{A}}\ \underset{9,1}{\bar{\mathbf{x}}} + \underset{12,1}{\bar{\mathbf{L}}} . \tag{6}$$

(the matrices with an upper line mean vectors). The vector **x** contains the nine unknowns mentioned earlier.

As the scale factor of the lengths is not uniquely determined in a lateration network, the normal matrix of the unknowns is singular and in such a form the inverse cannot be computed.

In order to enable the determination of the unknowns, an independent condition is introduced:

$$\Sigma u = 0 . \tag{7}$$

This condition states that the average length unit of the distance measurements should coincide with the theoretical length unit; that means it contains no regular error and the average meteorological conditions coincide with the long-term average. Such a hint has been already made by ANGUS-LEPPAN [3; p. 365] together with other possibilites.

This condition can also be taken as a supplementary correction equation which is added to the original ones. The zero valued correction can be assumed as the correction of a so-called pseudo-observation. In order to fulfil this supplementary correction equation, its weight receives very high values with respect to the weights of original observations (in the present case these weights are of unit value).

In computer experiments no problems occurred with weights $10^6 < p_{13} < 10^{12}$. The "high" value of this weight is in a certain sense influenced by the fact that the coefficients of the last four unknowns (u_P, u_Q, u_R, u_S) are very great in respect of the other five unknowns, and that this difference was partly eliminated by multiplying them by 10^{-4}.

Thus, the supplementary correction is added to the matrix of the equation system 2, and the following system of correction equations results:

$$\begin{bmatrix} \bar{\mathbf{v}} \\ 0 \end{bmatrix} = \begin{bmatrix} \mathbf{A} \\ \mathbf{b}^T \end{bmatrix} \bar{\mathbf{x}} + \begin{bmatrix} \bar{\mathbf{L}} \\ 0 \end{bmatrix}$$

where $\mathbf{b}^T = (0, 0, 0, 0, 0, 1, 1, 1, 1)$

If the following notations are introduced:

$$\bar{\mathbf{v}}' = \begin{bmatrix} \bar{\mathbf{v}} \\ 0 \end{bmatrix}, \quad \mathbf{A}' = \begin{bmatrix} \mathbf{A} \\ \mathbf{b}^T \end{bmatrix} \quad \text{and} \quad \bar{\mathbf{L}}' = \begin{bmatrix} \bar{\mathbf{L}} \\ 0 \end{bmatrix}$$

then $\underset{13,1}{\bar{\mathbf{v}}'} = \underset{13,9}{\mathbf{A}'} \underset{9,1}{\bar{\mathbf{x}}} + \underset{13,1}{\bar{\mathbf{L}}'}$

This form shows that the original system of correction equations is augmented by a row (the number of columns has remained the same). In the following the adjustment method coincides with the traditional method. The unknowns can be determined from the following:

$$\underset{9,1}{\bar{\mathbf{x}}} = (\underset{9,13}{\mathbf{A}'^T} \underset{13,13}{\mathbf{P}} \underset{13,9}{\mathbf{A}'})^{-1} \underset{9,13}{\mathbf{A}'^T} \underset{13,13}{\mathbf{P}} \underset{13,1}{\bar{\mathbf{L}}'} = \underset{9,9}{\mathbf{Q}} \cdot \underset{9,13}{\mathbf{A}'^T} \underset{13,13}{\mathbf{P}} \underset{13,1}{\bar{\mathbf{L}}'} . \tag{8}$$

Numerical data (unknowns and corrections) for the case with a weight of $p_{13} = 10^8$ of the supplementary correction will be now presented:

$$\begin{aligned}
\delta x_Q &= +0.0288 \text{ m} \\
\delta x_P &= +0.0808 \text{ m} \\
\delta y_P &= +0.0146 \text{ m} \\
\delta x_R &= -0.0321 \text{ m} \\
\delta y_R &= -0.0043 \text{ m} \\
u_Q &= +1.010 \cdot 10^{-6} \\
u_P &= -0.468 \cdot 10^{-6} \\
u_R &= -0.538 \cdot 10^{-6} \\
u_S &= -0.002 \cdot 10^{-6}
\end{aligned}$$

$$\begin{aligned}
v_{SQ} &= +0.0289 \text{ m} \\
v_{QS} &= -0.0099 \text{ m} \\
v_{SP} &= -0.0002 \text{ m} \\
v_{PS} &= -0.0080 \text{ m} \\
v_{SR} &= -0.0323 \text{ m} \\
v_{RS} &= +0.0130 \text{ m} \\
v_{RP} &= -0.0165 \text{ m} \\
v_{PR} &= +0.0385 \text{ m} \\
v_{QP} &= +0.0216 \text{ m} \\
v_{PQ} &= -0.0387 \text{ m} \\
v_{QR} &= -0.0331 \text{ m} \\
v_{RQ} &= +0.0214 \text{ m} \\
v_{\text{suppl.}} &= +0.000043 \cdot 10^{-6}
\end{aligned}$$

As it can be seen, the last supplementary correction is nearly zero. The approximative coordinates corrected by their changes are:

$$\begin{aligned}
x_P &= 2467.4871 \text{ m} \qquad & x_R &= 16366.9980 \text{ m} \\
y_P &= -13623.5672 \text{ m} \qquad & y_R &= 7569.0691 \text{ m}
\end{aligned}$$

$$\begin{aligned}
x_Q &= 20253.9658 \text{ m} \\
y_Q &= 0
\end{aligned}$$

A further possibility to resolve the indefiniteness due to the unknown scale factor is to suppose a measured distance errorless, as the measurements were distributed so that the average result is not influenced by the meteorological conditions [3; p. 365).

In the present case the errorfree distance should be the following:

$$\frac{(SQ + QS)}{2} = H = 20253.9461 \text{ m} .$$

In consequence, the length in direction of the axis x gets no correction in the course of the adjustment ($\delta x_Q = 0$), and the unknowns u_Q and u_S are also determined. Therefore one has:

$$\begin{aligned}
\frac{H}{(SQ)} = (1 + u_S) &= 1.000\,000\,449 \\
u_S &= +0.000\,000\,449 = -0.449 \cdot 10^{-6} \\
\frac{H}{(QS)} = (1 + u_Q) &= 0.999\,999\,546 \\
u_Q &= -0.000\,000\,454 = -0.454 \cdot 10^{-6} .
\end{aligned}$$

According to the adjustment of the indirect observations, the system of correction equations is in a matrix form the following:

$$\underset{10,1}{\bar{\mathbf{v}}} = \underset{10,6}{\mathbf{A}} \cdot \underset{6,1}{\bar{\mathbf{x}}} + \underset{10,1}{\bar{\mathbf{L}}} \ . \tag{6a}$$

In this equation, two rows (those of v_{SQ} and v_{QS}) are missing due to the errorfree distance, and also three rows corresponding to the unknowns δx_Q, u_S and u_Q. The unknowns can be computed in analogy of Eqs 8, supposing unit weights:

$$\underset{6,1}{\bar{\mathbf{x}}} = \underset{6,10}{(\mathbf{A}^T} \ \underset{10,10}{\mathbf{P}} \ \underset{10,6}{\mathbf{A})^{-1}} \underset{6,10}{\mathbf{A}^T} \cdot \underset{10,10}{\mathbf{P}} \cdot \underset{10,1}{\bar{\mathbf{L}}} = \underset{6,6}{\mathbf{Q}} \cdot \underset{6,10}{\mathbf{A}^T} \cdot \underset{10,10}{\mathbf{P}} \cdot \underset{10,1}{\bar{\mathbf{L}}} \ . \tag{8a}$$

The values of the corrections and unknowns are the following:

$$\begin{aligned}
\delta x_P &= +0.0836 \text{ m} \\
\delta y_P &= +0.0182 \text{ m} \\
\delta x_R &= -0.0361 \text{ m} \\
\delta y_R &= -0.0031 \text{ m} \\
u_P &= -1.064 \cdot 10^{-6} \\
u_R &= -0.814 \cdot 10^{-6}
\end{aligned}$$

$$\begin{aligned}
v_{SP} &= -0.0095 \text{ m} \\
v_{PS} &= -0.0027 \text{ m} \\
v_{SR} &= -0.0435 \text{ m} \\
v_{RS} &= +0.0149 \text{ m} \\
v_{RP} &= -0.0151 \text{ m} \\
v_{PR} &= +0.0480 \text{ m} \\
v_{QP} &= +0.0272 \text{ m} \\
v_{PQ} &= -0.0525 \text{ m} \\
v_{QR} &= -0.0309 \text{ m} \\
v_{RQ} &= +0.0135 \text{ m}.
\end{aligned}$$

The final coordinates are:

$$\begin{aligned}
x_P &= 2\,467.4899 \text{ m} \qquad & x_R &= 16\,366.9940 \text{ m} \\
y_P &= -13\,623.5636 \text{ m} \qquad & y_R &= 7\,569.0703 \text{ m}
\end{aligned}$$

We find as advantage of both methods presented here that corrections are added to measured lengths and that the scale factor can be easily included in any form into the adjustment.

Acknowledgement

The authors wish to express their thanks to Dr. T. VINCENTY of the US National Geodetic Survey for helpful comments about the method used here and about the numerical results.

REFERENCES

1. CROSS, P. A.—NORRIS, I. C.: The adjustment of length ratios. *Survey Review*, 23(1976), 336—341.
2. ROBERTSON, K. D.: The use of line pairs in trilateration and traverse. *Survey Review*, 21(1972), 290—306.
3. ANGUS-LEPPAN, P. V.: Adjustment of trilateration using length ratios. *Survey Review*, 21(1972), 358—368.
4. TÁRCZY-HORNOCH, A.: Refinement of trilateration adjustment using length ratios. *Acta Geod. Geoph. Mont. Hung.*, 8(1973), 197—206.
5. V. HETÉNYI, M.: Free-network adjustment with constraints. *Acta Geod. Geoph. Mont. Hung.*, 11(1976), 311—319.

УРАВНИВАНИЕ ТРИЛАТЕРАЦИОННЫХ СЕТЕЙ С ИЗМЕРЕННЫМИ ЭЛЕКТРОМАГНИТНЫМ ПУТЕМ СТОРОНАМИ, С УЧЕТОМ ТЕМПЕРАТУРЫ И ДВУХ МЕТЕОРОЛОГИЧЕСКИХ ВЛИЯНИЙ

А. ТАРЦИ-ХОРНОХ—М. ВЕРЁ ХЕТЕНИ

РЕЗЮМЕ

В статье предлагается при уравнивании трилатерационных сетей вместо отношения длин ввести для каждой точки новый неизвестный параметр u_i, учитывающий метеорологические (температурные) влияния ввиде $S_i(1 + u_i)$, где S_i — измеренная длина. В таком виде масштаб неопределен, нормальная матрица вырождена. В качестве дополнительного условия служит условие $\Sigma u = 0$ (средний масштаб безошибочный) или условие, что измеренная длина безошибочна.

Acta Geodaet., Geophys. et Montanist. Acad. Sci. Hung. Tomus 14 (1—2), pp. 149—154 (1979)

AMPLITUDE AND VELOCITY OF SEISMIC WAVES EXCITED BY WEIGHT DROPPING

GY. SZEIDOVITZ

GEODETIC AND GEOPHYSICAL RESEARCH INSTITUTE OF THE HUNGARIAN ACADEMY OF SCIENCES, DEPARTMENT OF SEISMOLOGY, BUDAPEST

[Manuscript received February 15, 1977]

Maximum amplitudes and propagation velocities of seismic waves have been investigated at 36 sites of different geological conditions (rock types). At distances of 5—30 m from the weight dropping, measurements were carried out enabling the determination of a linear connection between the velocity of the seismic waves and the value ln c computed from maximum amplitudes.

The demolishing effect of earthquakes depends on the condition, the structure and the dimension of buildings, on the elastic properties of the rocks in their environment, on the ground-water level, on the intensity of the quake and on the distance of its source.

According to MEDVEDYEV's study [1] it is the safest to build on granite which has the greatest seismic impedance. The intensity-amplifying effect of other rocks of smaller impedances are defined by the equation

$$n = 1.67 \log \frac{\varrho_g v_g}{\varrho_k v_k}, \tag{1}$$

where n is the increase of intensity in MKS degrees, ϱ_g; ϱ_k is the density of the granite and of the medium investigated, respectively, v_g; v_k the velocity of the wave propagation in the respective rocks.

As it is known, the damage of the objects is the greater, the greater the amplitude of the particle velocity and acceleration of earthquake waves. Thus, a connection must exist between the maximum amplitudes and the seismic impedances. In order to study this connection, we investigated the velocities and amplitudes of seismic waves excited by weight dropping in different rocks. In spite of difference of the amplitude, frequency and phase conditions of the elastic waves excited in this way from these earthquake waves, the intensity-increase computed from the greatest amplitudes reproduced in good approximation the values computed from seismic impedances [2].

After the first results we continued the investigation in 36 areas of different geological structure. At the beginning of the investigations some questions arose: as the damping of the amplitudes of the seismic waves is not the same in the different rocks, the ratio of amplitudes and so the intensity-increase computed from them gets a function of the distance between excitation and observation. It is possible to observe the maximum amplitudes of the seismic waves at the same distance from the source, in this case, however, we cannot get any information just about the absorption properties of the rocks.

The amplitudes of the seismic oscillations depend — beside the excitation distance, the elastic properties of rocks and the excitation energy — on a lot of factors very difficult to calculate with. The excitation energy did not change in our measurements, therefore, the maximum amplitudes of the seismic oscillations depend in the first place on the source distance, then on the elastic properties of the rock investigated. Consequently, it is reasonable to describe the dependence of the amplitude on distance by the following functions:

$$A = c_1 r^{-m_1} \qquad (2)$$
$$A = c_2 e^{-m_2 r} ,$$

where A is the maximum amplitude (mm), r the distance between observation and excitation in m. The parameters m_1, m_2, c_1, c_2 were computed by means of the least-squares method. About 30 data pairs (amplitudes-distances) were collected from each investigated area in order to have statistically great samples. It should be mentioned here that Eq. (2) cannot be used in the close vicinity of the exciting source. Our measurements were carried out in distances 5—30 m from the source, hence, for this interval all considerations are valid.

The values m_1 and c_1 for the different areas and the deterministic coefficient have been calculated. The latter expresses that part of the variance of the depending variable (A) which is supposed to be the effect of the independent variable (r). Except for some areas, the value of the deterministic coefficient lies near 1, hence the mathematical formulas applied for the approximation of the curves proved to be correct.

In Fig. 1 the logarithms of the values c_1 were plotted against the velocities of seismic waves propagating in the rocks investigated. The wave velocity

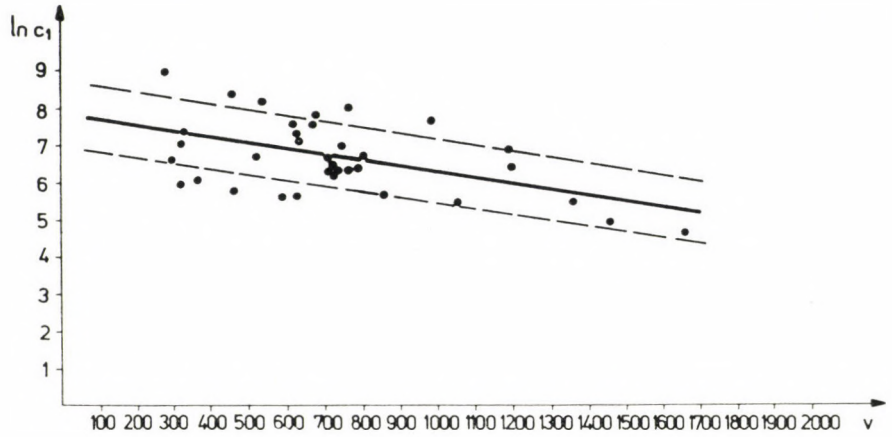


Fig. 1. Connection between the propagation velocity and the amplitude of seismic oscillations. Continuous line shows values of ln c_1 estimated from the linear regression, the dotted straight lines were received from the corrected scatter of the estimates

was determined from the data of the first arrivals. We suppose that the values $\ln c_1$ are somehow in connection with the elastic properties of the rocks. A straight line determined by the equation

$$\ln c_1 = -0.00166\, v + 7.84 \tag{3}$$

fits best the values $\ln c_1$. The correlation coefficient characterizing the connection between the two variables is 0.5, i.e. rather small. On the basis of our preliminary studies we assumed a closer connection between the velocity and the amplitude of the seismic waves.

Measuring errors cannot be the reason of the low correlation, since we have chosen very carefully the directly coupled system consisting of a galvanometer and of a geophon giving the minimum transient. We suppose that the low correlation is caused by the effect of one or more variables. Investigations were also extended into this direction, but they did not give appropriate results.

The following considerations have led to the determination of a closer connection existing between v and $\ln c_1$. The amplitudes plotted against the excitation distance yield — when approximated by Eq. (2) — for each investigated rock a parameter pair $\ln c_1 - m_1$. It can be expected that $\ln c_1$ is proportional to the amplitude of the seismic wave and m_1 gives information about the dependence of the waves on the excitation distance. The method of least squares determines the values of these parameters in accordance with a prescribed condition independently of the physical meaning. They have just opposite effects on the determination of the amplitudes, therefore, parameter pairs characterizing two data sets with only small differences can differ from each other in a high degree. Without supposing any causal relation between the two parameters, we represented $|\, m_1 \,|$ in function of $\ln c_1$ (Fig. 2). It can be seen that the points can be approximated by a straight line with the equation:

$$m_1 = 0.301 \ln c_1 - 0.519\,. \tag{4}$$

The correlation between the two parameters is close (deterministic coefficient: 0.72). This connection hinders a study of the correlation between v and $\ln c_1$. It is obvious that the connection between $\ln c_1$ and m_1 expressed by Eq. (4) has no physical meaning. It seems suitable to use instead of Eq. (2) an approximation where m_1 and $\ln c_1$ are independent of each other.

The values m_1 are only in few areas higher than -1, their average is -1.39. It seemed suitable to approximate the amplitude values instead of Eq. (2) by the equation:

$$A = \frac{c}{r} e^{-ar}\,, \tag{5}$$

where the parameters c and a can also be calculated by the method of least squares. It is obvious from those said above that only a very loose connection

is possible between the two parameters. In Fig. 3 the values a are represented in function of $\ln c$. According to the calculations the equation of this straight line has the form

$$a = -0.22 \ln c + 0.57 .$$

0.0036, i.e. a value near zero, has been received as deterministic coefficient. Since practically no connection was determined between the two parameters,

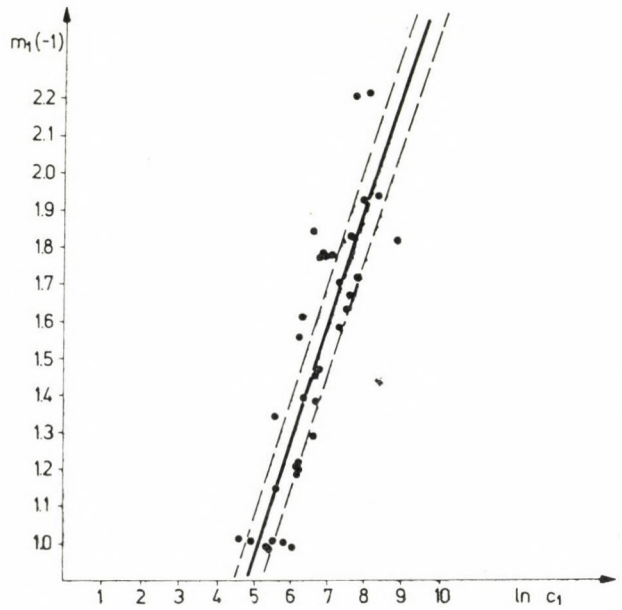


Fig. 2. Connection between the coefficients m_1 and $\ln c_1 \cdot m_1$ values estimated from the linear regression are denoted by continuous line, straight lines calculated from the estimated scatter of the estimate by dotted line

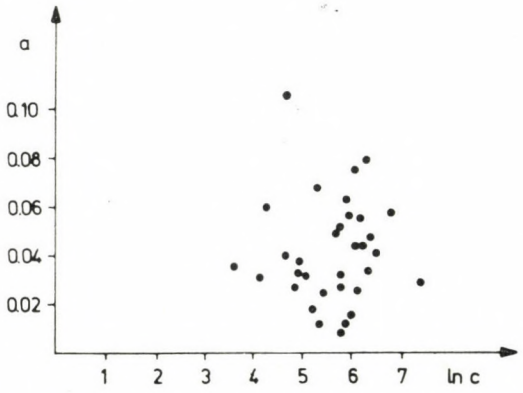


Fig. 3. Data of a and $\ln c$. No correlation could be defined between the values a and $\ln c$

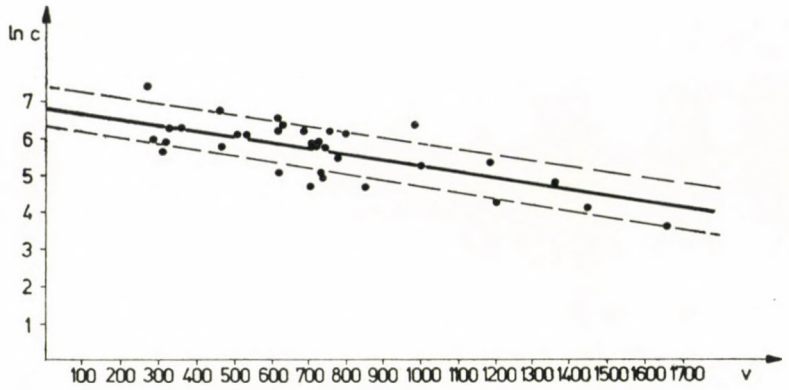


Fig. 4. Connection between the propagation velocity and the amplitude of seismic oscillations if m and $\ln c$ are independent of each other

we assumed that if the low correlation between v and $\ln c_1$ had really that reason, now we find a closer connection between the two variables. In Fig. 4 the values $\ln c$ are plotted vs. velocity. The points can be approximated by a straight line with the equation

$$\ln c = -0.00173\, v + 6.87\,. \tag{6}$$

In case of an approximation by Eq. 2 we received 0.3 for deterministic coefficient. Now this increased to 0.5 which corresponds to a correlation coefficient of 0.7, and indicates a definite connection between the two variables.

The connection between the velocity of seismic waves and the maximum amplitudes as revealed here illustrates how one variable can influence the other, even if this is hidden by other effects.

Let us assume the velocity of the longitudinal waves 500 m/sec in a loose ($\varrho = 1.5$) rock and 1760 m/sec in a more solid one ($\varrho = 2.4$). A value of $\ln c_1 = -0.00173 \cdot 500 + 6.87 = 6$ belongs to the velocity 500 m/sec and $\ln c_2 = -0.00173 \cdot 1760 + 6.87 = 3.82$ to the velocity 1760 m/sec. The ratio of the values c belonging to the two velocity values is 8.8. The increase of intensity with respect to the more solid rocks calculated from c_1/c_2 and from the seismic impedances are 1.63 and 1.3, respectively. MEDVEDYEV deduced the connection given in [1] on the basis of the study of a great number of damaging earthquakes. We determined Eq. (4) being valid for the upper loose layers independently of earthquakes. Departing from two entirely different bases, the values of intensity increases differ only by 0.3. Since our investigations have given informations only on the elastic properties of the near-surface layers — due to the conditions of excitation — the assumption seems to be reasonable that the damaging effect of the earthquakes is strongly influenced by the elastic properties of the upper, several meters deep loose layer.

REFERENCES

1. МЕДВЕДЕВ С. В.: Инженерная Сейсмология. Государственное Издательство литературы по строительству, архитектуре и строительным материалам. Москва, 1962.
2. SZEIDOVITZ, GY.: A földrengések romboló hatásának vizsgálata a földtani felépítés függvényében (Study of the damaging effect of earthquakes in dependence of the geological structure). *Geof. Közl.* 22(1974), 69—76.

ИЗУЧЕНИЕ СООТНОШЕНИЙ АМПЛИТУД И СКОРОСТЕЙ СЕЙСМИЧЕСКИХ ВОЛН ПРИ ВОЗБУЖДЕНИИ ПАДАЮЩИМ ВЕСОМ

ДЬ. СЕЙДОВИЦ

РЕЗЮМЕ

На породах с 36 различными геологическими структурами были исследованы максимальная амплитуда и скорость распространения сейсмических волн, возбужденных падающим весом. На основе измерений, проведенных на расстоянии 5—30 м от места возбуждения можно было выявить линейную зависимость между скоростью сейсмически колебаний и ln c, вычисляемого из максимальных амплитуд.

Acta Geodaet., Geophys. et Montanist. Acad. Sci. Hung. Tomus 14 (1—2), pp. 155—170 (1979)

VARIATIONS TELLURIQUES LENTES OBSERVÉES A M'BOUR (SÉNÉGAL)

J. METZGER

OFFICE DE LA RECHERCHE SCIENTIFIQUE ET TECHNIQUE OUTRE-MER, PARIS

[Manuscrit présenté le 30 Juin 1977]

Des enregistrements continus de courants telluriques ont été réalisés au Centre Géophysique de l'O.R.S.T.O.M. à M'Bour (Sénégal) à partir de mai 1965. La présente note décrit l'installation et son fonctionnement et analyse les phénomènes de dérive qui ont été constatés. Les variations diurnes moyennes des deux composantes Nord-Sud et Est-Ouest pour chacun des mois des années 1966 à 1968, ainsi que leurs moyennes saisonnières et annuelles, sont présentées sous forme de tableaux horaires et de graphiques; on y ajoute un certain nombre de diagrammes polaires illustrant ces variations et quelques résultats donnés par l'analyse harmonique.

Situation géographique et géologique

L'observatoire où ont été effectués les enregistrements a pour coordonnées 14°23′N et 16°57′W; il est situé sur la côte occidentale de l'Afrique, à 60 km à vol d'oiseau de la presqu'île du Cap-Vert et de Dakar et à environ 1 km de M'Bour, petite ville ne comportant pas d'installations industrielles gênantes. Le domaine de l'observatoire est en bordure immédiate de la mer; son altitude, de ce fait, est très faible: entre 3 et 4 m et l'électrode ouest, la plus proche du rivage, ne s'en trouve distante que de 80 m. La côte est sensiblement rectiligne et présente une orientation NW-SE.

Du point de vue géologique, cette région fait partie du vaste bassin sédimentaire du Sénégal, dont l'épaisseur, dans les environs de M'Bour, dépasse 4000 m; sur une grande étendue autour de l'observatoire, les terrains superficiels sont constitués de calcaires grossiers du paléocène, recouverts de sables argileux et d'alluvions éoliennes. Les résistivités électriques des couches de surface ont été mesurées par quelques sondages: les 10 ou 15 premiers mètres présentent des valeurs comprises entre 5 et 20 ohm · m; pour les profondeurs plus grandes on dispose d'une carte de résistivités apparentes en lignes de 6000 m, établie par la Compagnie Générale de Géophysique pour tout le Sénégal occidental (1): cette carte indique une résistivité de 10 à 12 ohm · m aux alentours de M'Bour et des valeurs généralement inférieures à 25 ohm · m dans toute la moitié ouest du bassin sédimentaire.

Le climat de la région, bien qu'adouci par la proximité de l'océan, est de type sahélien et se caractérise par une saison absolument sèche (octobre à juin), tempérée, puis chaude, suivie d'un été très pluvieux dont les précipitations, souvent orageuses, atteignent habituellement une hauteur totale de 800 à 1000 mm.

Installation et fonctionnement

Les deux lignes telluriques, d'une longueur de 500 m chacune, sont orientées selon les directions géographiques N-S et E-W; indiquons en passant que la déclinaison magnétique est d'environ 14 °W. Les électrodes sont constituées de plaques horizontales de plomb, de 1,50 m sur 1 m, enfouies à 2 m de profondeur et elles sont reliées au dispositif d'enregistrement par un gros câble, de bonne isolation et légèrement enterré.

On a utilisé des galvanomètres SEFRAM, du type 140/1, présentant les caractéristiques suivantes:

période: 2,5 sec.
résistance interne: 30 ohms
résistance externe critique: 450 ohms
sensibilité: $2{,}7 \cdot 10^{-9}$ A/mm à 1 m.

Chacun des circuits comprenait en outre une résistance en série de 70 000 ohms, destinée à réduire l'effet des fluctuations éventuelles des résistances des électrodes et des lignes, ainsi qu'un dispositif anti-foudre à éclateurs et fusibles, analogue à celui qui est utilisé à l'observatoire de Dourbes (2).

L'enregistrement des variations telluriques, de même que des tops horaires, s'effectuait sur papier photographique grâce à un enregistreur La Cour, assurant un déroulement de 15 mm/h; on obtenait en outre le tracé d'une ligne de base par l'inscription d'un spot fixe. L'ensemble des dispositifs de contrôle et d'enregistrement a été installé à la station sismique de l'observatoire, situé à proximité du croisement des deux lignes telluriques; non loin de là se trouvait enterrée une cinquième électrode, identique aux prises terminales et utilisée pour le contrôle des électrodes de mesure.

Les étalonnages consistaient à introduire dans le circuit une (ou plusieurs) force électromotrice connue, au moyen d'un dispositif potentiométrique. Durant deux ans et demi les valeurs d'échelle, pour les deux lignes, étaient les suivantes:

NS: 1,62 EW: 1,42 mV/km/mm,

valeurs qui se sont révélées stables à 2% près lors d'étalonnages répétés régulièrement. En mai 1968, le montage a été modifié afin d'augmenter les sensibilités; les valeurs d'échelle sont alors devenues:

1,02 et 1,06 mV/km/mm.

Il ét ait également possible, grâce à une dérivation sur les circuits, de mesurer directement les différences de potentiel entre les extrémités des lignes à l'aide d'un potentiomètre de prospection BRGM; ces mesures «absolues», effectuées de temps à autre, permettaient de vérifier les valeurs d'étalonnage et de contrôler les enregistrements.

Dérive des électrodes — Phénomènes parasites

Quelques indications ont été données plus haut sur le climat et le régime pluviométriques, qui peuvent influencer les enregistrements (3). Leur effet a pu être constaté au cours des essais préliminaires effectués en 1965 sur deux électrodes provisoires, constituées de quelques piquets d'acier plantés en surface. Leur différence de potentiel, restée stable en saison sèche, se mit à varier considérablement dès la première averse, puis présenta des fluctuations allant jusqu'à 100 mV durant toute la saison des pluies: c'était la manifestation de divers phénomènes parasites et complexes, tels qu'électrofiltration, modification de gradient thermique et de concentration ionique aux électrodes, ou encore variation importante de la résistance des prises de terre (peut-être insuffisamment amortie par la résistance en série).

Qu'en était-il des électrodes utilisées pour les enregistrements permanents et qui étaient enterrées? Elles aussi montraient chaque année une évolution irrégulière durant les mois de juillet à octobre ou novembre; les phénomènes parasites s'y manifestaient donc avec un retard d'environ un mois sur les pluies, ce qui pourrait être le temps mis par l'eau à atteindre la profondeur de 2 m. L'amplitude des fluctuations constatées demeurait en général inférieure à 25 mV, mais atteignit exceptionnellement 35 mV: elles restaient donc 3 à 4 fois plus faibles que celles qui avaient été observées avec les prises superficielles.

Outre les perturbations décrites ci-dessus, les dérives constatées sur les deux composantes présentèrent les caractères suivants: — la ligne NS accusa une variation importante mais uniforme durant les dix premiers mois de l'année 1966, puis resta stable pendant les deux années suivantes;

— une dérive saisonnière et régulière se manifesta sur la composante EW sous forme d'une ondulation s'étalant sur quelques mois et centrée sur la fin de décembre; la position de l'électrode ouest, proche du rivage, et le caractère bien tranché de la saison des pluies conduisent à penser qu'il peut s'agir de l'effet d'un flux et reflux annuels des infiltrations marines devant les nappes souterraines d'eau douce.

— sur la même composante apparaissaient parfois et en toute saison des oscillations d'amplitude et de période très variables (de 5 à 20 mV, de 4 à 15 jours); ne leur ayant trouvé aucune correspondance sur l'autre composante, ni dans le régime des marées, nous les considérons comme des fluctuations aléatoires, dues à une moindre qualité de l'une ou l'autre électrode de cette ligne.

On peut se demander dans quelle mesure ces phénomènes parasites affectent les résultats, lesquels ne portent dans la présente étude que sur des moyennes mensuelles; sauf exceptions — quelques jours à variation anormale ont été rejetés du calcul des moyennes —, il est justifié de considérer la dérive

comme approximativement linéaire sur une période de 24 h donnée. Elle se trouve donc éliminée, sans erreur résiduelle notable, par une correction linéaire qui sera décrite un peu plus loin.

Dépouillement

Les enregistrements sont semblables aux magnétogrammes La Cour, mais comportent une ligne de base commune aux deux composantes. Le dépouillement a consisté à lire, à l'aide d'une grille graduée en mV/km, les écarts moyens à la ligne de base par demi-heures successives; un tel intervalle, moitié de celui qui est habituellement utilisé en magnétisme lent, a été choisi en vue d'une analyse plus fine des variations telluriques (bien que les tableaux qui suivent ne donnent que des écarts horaires). Par sommation et division, il est alors aisé d'obtenir la variation diurne moyenne d'un mois ou d'une période donnés.

Un grand nombre de ces courbes moyennes reflétaient de façon plus ou moins prononcée l'effet de la dérive et accusaient une certaine pente moyenne, positive ou négative (par exemple de 3,8 mV/km sur 24 h pour le mois le plus perturbé). On les a donc corrigées linéairement, de manière à rendre égales les valeurs de 0 et 24 h, correction qui a été appliquée systématiquement pour tous les mois.

Résultats numériques et représentations graphiques

a) Tableaux des valeurs horaires; amplitude diurne

C'est en partant des nombres ainsi obtenus qu'ont été calculés, pour chaque mois, les écarts (semi-horaires) par rapport à leur moyenne, finalement

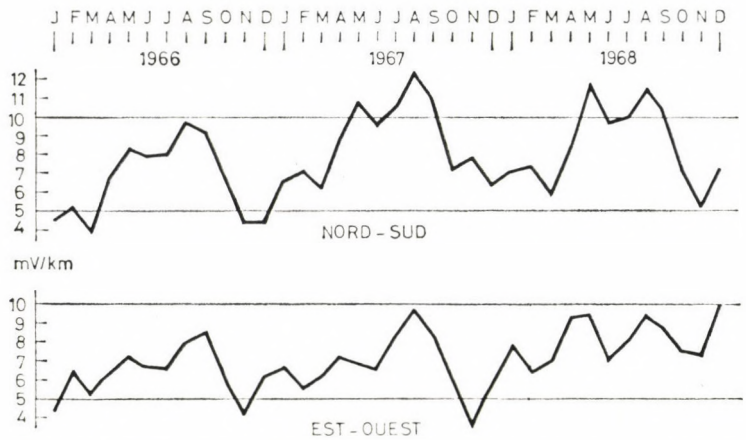


Fig. 1. Évolution annuelle de l'amplitude diurne des composantes telluriques NS et EW

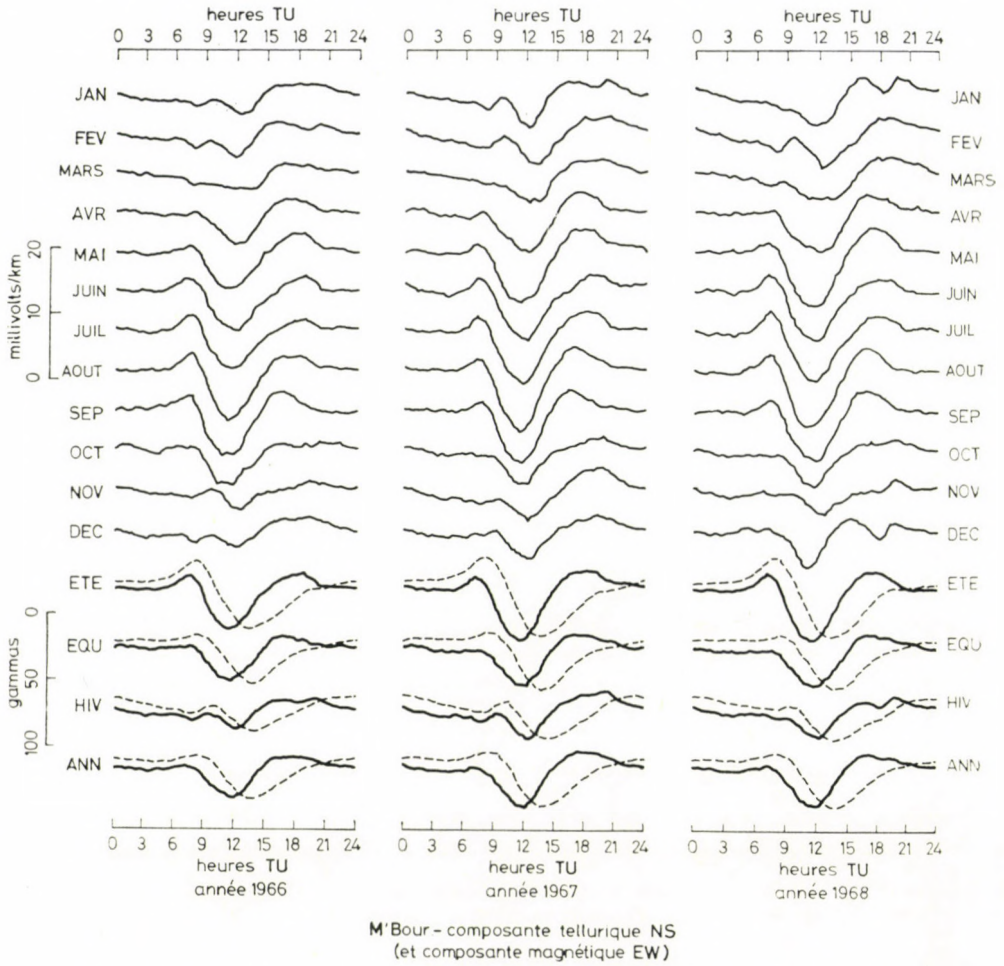


Fig. 2. Variations diurnes des composantes tellurique NS et magnétique EW

convertis en écarts horaires. Les tableaux I à VI donnent le résultat définitif des calculs, à raison d'un tableau par composante et par année (1966 à 1968); les valeurs y sont exprimées en 1/10 de mV/km et la convention de sens fait correspondre au signe + un courant tellurique dirigé vers le Nord ou vers l'Est. En plus des variations de chaque mois, les tableaux indiquent les variations moyennes saisonnières (été, équinoxe, hiver) et annuelles.

La dernière colonne donne l'amplitude diurne moyenne, dont l'évolution dans le temps est représentée par la figure 1. Malgré l'irrégularité de ces graphiques, on y discerne, pour chacune des composantes, une fluctuation annuelle, avec un minimum en hiver, ainsi qu'une lente croissance, certainement liée à la phase ascendante du cycle solaire consécutive au minimum de 1965.

b) Graphiques diurnes

Les figures 2 et 3 donnent une représentation graphique, avec un pas semi-horaire, des variations diurnes de chacune des moyennes mensuelles des deux composantes. Ce sont les courbes d'été qui illustrent le mieux les caractères essentiels de ces variations, qui peuvent se schématiser, pour les deux composantes, en un minimum très accusé vers midi, compris entre deux maxima, l'un vers 7—8 h, l'autre dans l'après-midi ou la soirée, les valeurs de nuit étant stables ou ne variant que faiblement. Minimum de midi et maximum du soir se produisent toujours sur l'élément E un peu plus tôt que sur l'élément N.

Outre une fluctuation annuelle de leur amplitude, signalée dans un paragraphe précédent, ces courbes subissent à partir de l'automne une évolu-

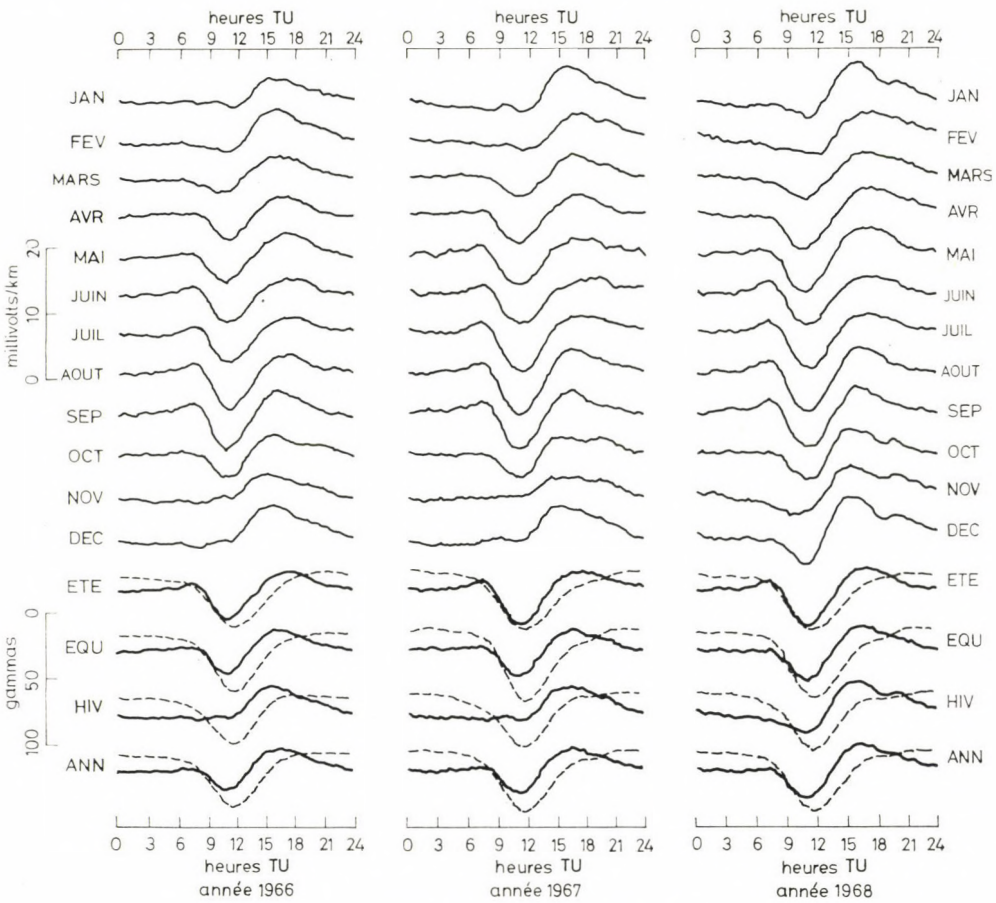


Fig. 3. Variations diurnes des composantes tellurique EW et magnétique NS

tion pouvant se décrire ainsi: atténuation, puis disparition du maximum matinal et même du minimum de midi, mais persistance du maximum du soir. D'autres déformations concernent surtout la composante N: un minimum secondaire apparaît vers 8 h sur la plupart des courbes d'hiver des trois années; à la même saison, un dernier minimum, moins fréquent, se situe vers 18 h. Ce minimum secondaire du soir est également visible, mais légèrement plus tard, sur quelques courbes d'hiver de la composante E.

Aux valeurs saisonnières et annuelles, figurées par un trait renforcé, on a superposé en pointillé les moyennes magnétiques correspondantes, moyennes tirées des enregistrements La Cour de l'observatoire et rapportées aux axes géographiques. Il convient de noter que ces variations (et leur échelle) sont orientées positivement vers la bas des figures; en effet, les composantes magnétiques, normalement orientées vers le Nord et, pour M'Bour où la déclinaison est occidentale, vers l'Ouest, doivent être inversées toutes les deux pour respecter les lois de l'èlectromagnétisme et illustrer ainsi un certain parallélisme des deux phénomènes, étant entendu qu'à chaque élément tellurique correspond l'élément magnétique perpendiculaire. Précisons en outre que le rapport d'échelle de ces tracés est de 5 gammas pour 1 mV/km.

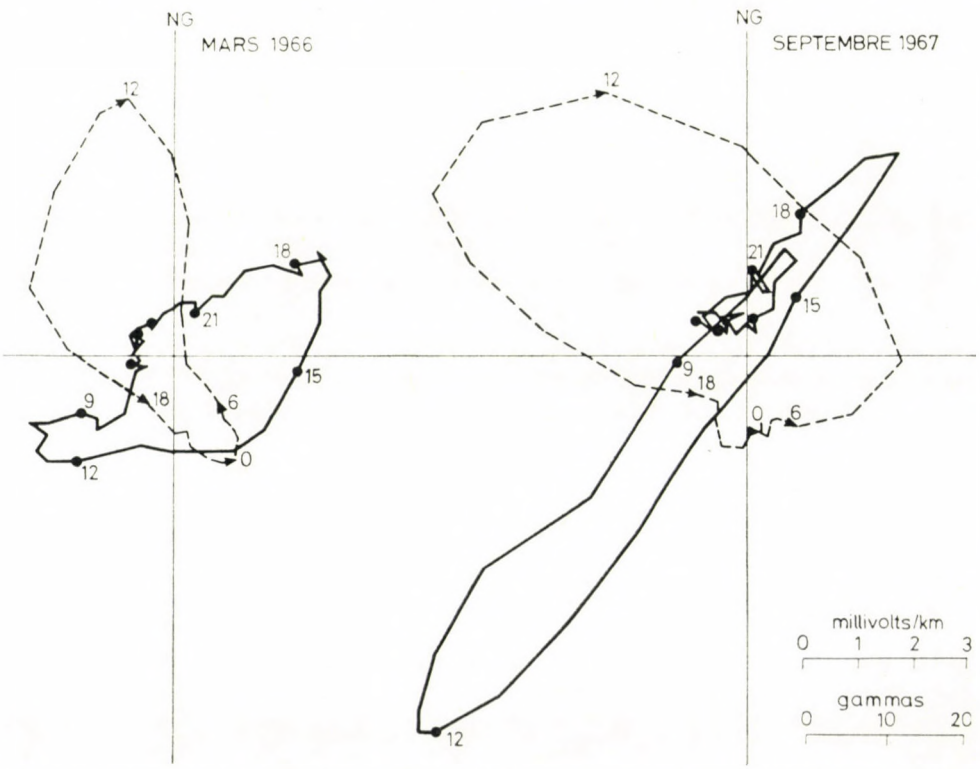


Fig. 4. Exemples de diagrammes polaires telluriques et magnétiques (moyennes mensuelles)

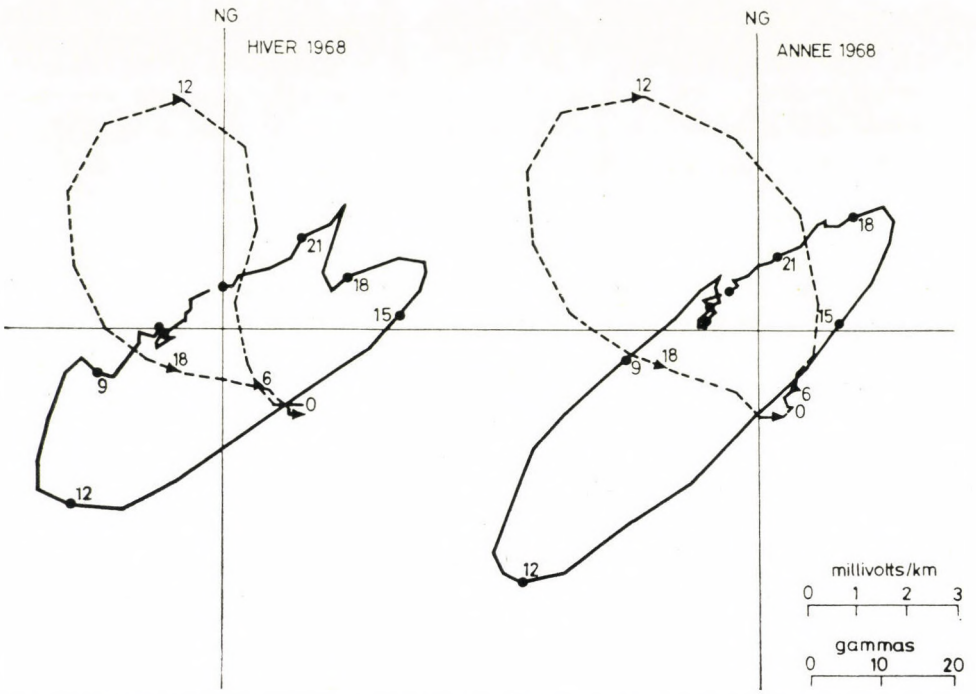


Fig. 5. Exemples de diagrammes polaires telluriques et magnétiques (moyennes saisonnière et annuelle)

c) Diagrammes polaires

Une illustration plus intéressante consiste à combiner les variations des deux composantes de chaque mois ou saison en diagrammes polaires (4); les figures 4 et 5 en montrent quelques exemples. Ces diagrammes sont tracés par intervalles semi-horaires et marqués toutes les 3 heures d'un point et de l'indication de l'heure (entre 9 et 21 h).

Leur forme générale s'apparente à celle d'une ellipse plus ou moins régulière et plus ou moins allongée, dont le grand axe est incliné de 40° en moyenne (avec des écarts de $\pm 10°$) sur l'axe N-S géographique. Ces courbes sont parcourues dans le sens contraire des aiguilles d'une montre et la vitesse de parcours est rien moins qu'uniforme: elle est élevée pendant les heures de jour, entre les maxima du matin et du soir et très réduite durant la nuit. Les variations minimes que montraient les graphiques diurnes, généralement entre 21 et 7 h, rendent parfois le tracé à ces heures-là fort enchevêtré.

L'évolution saisonnière reflète avant tout la variation annuelle d'amplitude, qui entraîne un allongement considérable des courbes en été et à l'équinoxe d'automne (voir fig. 4); l'aplatissement des «ellipses» pourrait également dépendre du décalage horaire des extrema sur les deux composantes, mais ce

décalage est relativement constant en cours d'année. Le minimum de 8 h, signalé précédemment sur la composante N, est généralement peu discernable sur ces diagrammes, vu qu'il se superpose au reste du tracé; par contre, le minimum secondaire du soir, quand il apparaît sur les deux composantes, se traduit par une encoche plus ou moins large à l'extrémité NE de la courbe (voir, par exemple, la courbe d'hiver 1968, figure 5).

Ici encore, on a ajouté en pointillé les courbes correspondantes des variations magnétiques; elles sont dessinées par intervalles horaires, avec indication de l'heure toutes les 6 h, la correspondance d'échelle étant cette fois de 7 gammas pour 1 mV/km. Ces courbes sont nettement plus arrondies que les précédentes et elles sont piriformes pour les mois d'hiver et de printemps; on peut aussi leur appliquer ce qui a été dit plus haut sur le sens et la vitesse de parcours. La différence essentielle entre les deux types de courbes réside dans l'orientation respective de leurs grands axes, qui sont le plus souvent sensiblement orthogonaux: leur écart est d'environ 80° en été, 100° aux mois d'équinoxe et plus élevé ou incertain en hiver.

d) Analyse harmonique

Toutes les moyennes mensuelles et saisonnières ont également été développées en série de Fourier. Nous donnons ci-après les principaux résultats (onde diurne et deux premiers harmoniques) concernant les variations saisonnières et annuelle de l'année 1968; les demi-amplitudes sont exprimées en mV/km, les phases en degrés.

		Demi-amplitudes			Phases		
Comp. N:	Été	2,36	2,82	1,67	109	−83	102
	Équinoxe	2,15	1,81	0,97	120	−88	88
	Hiver	1,70	0,95	0,56	125	−98	98
	ANNÉE	2,06	1,85	1,07	118	−87	97
Comp. E:	Été	1,82	2,29	1,25	134	−67	117
	Équinoxe	2,07	1,88	0,95	150	−60	123
	Hiver	2,66	1,34	0,83	170	−46	136
	ANNÉE	2,11	1,81	1,00	154	−60	123

On notera les comparaisons suivantes, qui se vérifient également les autres années: pour les deux composantes l'onde semi-diurne est presque égale à la diurne pour l'année et l'équinoxe, elle lui est même un peu supérieure en été, mais très inférieure (environ la moitié) en hiver; les phases varient relativement peu d'une saison à l'autre. Les amplitudes des harmoniques suivants décroissent très rapidement, tandis que leurs phases montrent, pour les différents mois, une dispersion de plus en plus grande.

Tableau I

M'BOUR (SÉNÉGAL)										VALEURS HORAIRES	
H.TU	1	2	3	4	5	6	7	8	9	10	11
Janvier	2	−2	−4	−6	−6	−5	−6	−11	−12	−5	−8
Fèvrier	2	−1	−2	−4	−5	−3	−5	−15	−14	−7	−16
Mars	6	5	2	1	0	−1	−3	−12	−12	−13	−17
Avril	6	7	4	2	1	1	0	3	1	−11	−26
Mai	4	4	1	1	3	5	9	14	0	−28	−46
Juin	7	6	6	5	6	11	21	25	12	−24	−42
Juillet	8	7	4	1	3	6	18	29	15	−23	−45
Août	5	4	5	7	6	8	18	31	14	−25	−56
Septembre	7	4	9	8	12	13	20	27	3	−37	−59
Octobre	11	12	6	1	3	8	10	8	4	−24	−47
Novembre	6	5	0	−4	−2	−3	−5	−9	−4	4	0
Décembre	0	−2	−8	−8	−7	−5	−5	−13	−13	−5	−9
Étè	6	5	4	3	4	8	16	25	10	−25	−47
Équinoxe	8	7	5	3	4	5	7	7	−1	−21	−37
Hiver	2	0	−4	−5	−5	−4	−5	−12	−11	−3	−8
Année	5	4	2	0	1	3	6	6	0	−16	−31

Tableau II

M'Bour (Sénégal)										Valeurs horaires en 1/10	
H. TU	1	2	3	4	5	6	7	8	9	10	11
Janvier	−8	−9	−10	−9	−8	−7	−6	−9	−10	−8	−10
Février	−11	−13	−13	−13	−11	−11	−10	−16	−18	−19	−25
Mars	−5	−7	−7	−7	−7	−7	−6	−12	−15	−24	−24
Avril	−2	0	−1	1	1	1	2	3	−5	−25	−36
Mai	−6	−3	−3	−3	−1	−1	3	1	−13	−32	−41
Juin	0	−1	1	2	3	4	10	11	−4	−28	−41
Juillet	0	−1	−3	−4	−1	1	7	11	1	−27	−41
Août	1	0	2	3	4	6	11	15	1	−29	−50
Septembre	−1	−3	2	2	5	6	12	15	−2	−36	−51
Octobre	−3	−2	−2	−2	−1	1	2	−1	−7	−24	−35
Novembre	−10	−10	−12	−15	−14	−13	−13	−15	−14	−9	−5
Décembre	−14	−17	−19	−18	−19	−18	−18	−23	−22	−16	−12
Été	−1	−1	−1	−1	1	3	8	10	−4	−29	−43
Équinoxe	−3	−3	−2	−1	−1	0	3	1	−7	−27	−37
Hiver	−11	−12	−13	−14	−13	−12	−12	−16	−16	−13	−13
Année	−5	−6	−5	−5	−4	−3	−1	−2	−9	−23	−31

en 1/10 mV/Km — Composante N—1966

12	13	14	15	16	17	18	19	20	21	22	23	24	Amp
—20	—25	—18	1	13	17	18	19	19	17	12	8	4	44
—30	—26	—7	12	21	21	17	9	13	18	12	6	4	51
—20	—17	—18	—9	9	17	18	16	13	10	10	8	6	38
—41	—42	—26	—5	12	24	26	22	14	7	8	7	5	68
—49	—41	—26	—4	9	22	32	33	24	11	10	9	5	82
—50	—48	—29	—14	—2	12	22	28	22	8	6	7	7	78
—50	—45	—27	—10	1	10	18	23	17	9	10	12	10	79
—66	—54	—33	—6	14	24	25	27	16	11	11	8	7	97
—59	—51	—25	2	27	33	28	16	9	5	3	2	2	92
—49	—32	—21	—5	10	15	12	12	12	18	14	15	8	67
—20	—26	—13	—3	1	3	6	12	17	13	10	7	5	43
—19	—21	—12	0	12	19	19	18	22	17	11	7	3	43
—54	—47	—29	—8	6	17	24	28	20	10	9	9	7	82
—42	—36	—23	—4	15	22	21	17	12	10	9	8	5	64
—22	—25	—12	2	12	15	15	14	18	16	11	7	4	43
—40	—36	—21	—3	11	18	20	20	17	12	10	8	5	60

mV/Km — Composante E — 1966

12	13	14	15	16	17	18	19	20	21	22	23	24	Amp
—16	—8	5	22	27	25	22	14	8	6	0	—2	—5	43
—22	—9	12	31	39	39	31	19	16	11	3	—4	—6	64
—20	—3	8	20	27	28	25	21	11	5	3	—1	—4	52
—35	—20	—3	10	22	28	27	22	11	2	1	—1	—2	64
—34	—20	—3	13	22	30	31	27	20	9	5	2	—3	72
—39	—29	—10	6	15	21	23	25	18	8	4	1	1	66
—41	—32	—12	4	16	22	24	24	18	11	8	7	6	65
—51	—37	—18	6	20	26	29	23	14	8	8	5	4	80
—46	—30	—8	14	29	34	28	19	12	5	—1	—1	—5	85
—35	—19	1	18	25	22	15	12	14	13	7	4	—2	60
—8	4	19	27	27	23	19	14	12	7	0	—6	—8	42
—11	2	21	35	39	37	30	20	17	12	4	—2	—9	62
—41	—29	—11	7	18	25	27	25	17	9	6	4	2	70
—34	—18	0	16	26	28	24	18	12	6	3	0	—3	65
—14	—3	14	29	33	31	25	17	13	9	2	—3	—7	49
—30	—17	1	17	26	28	25	20	14	8	4	0	—3	59

Tableau III

M'Bour (Sénégal)										Valeurs horaires en 1/10	
H. TU	1	2	3	4	5	6	7	8	9	10	11
Janvier	6	1	−1	−3	−5	−6	−6	−14	−15	−1	−16
Février	7	1	−3	−6	−6	−8	−12	−16	−13	0	−6
Mars	7	6	3	1	−1	−2	−5	−10	−10	−14	−22
Avril	9	11	5	1	1	−1	−1	7	−4	−25	−37
Mai	6	8	3	3	4	6	12	16	−5	−43	−64
Juin	14	8	6	2	1	6	17	26	9	−28	−50
Juillet	9	5	4	5	3	7	18	26	4	−34	−60
Août	9	7	7	6	5	8	18	24	2	−42	−72
Septembre	8	7	7	6	5	5	12	19	5	−33	−61
Octobre	10	8	3	−2	−2	1	1	−2	−3	−13	−33
Novembre	6	0	−3	−8	−9	−8	−11	−16	−11	−8	−19
Décembre	4	0	−4	−5	−5	−5	−5	−4	0	−1	−21
Été	10	7	5	4	3	7	16	23	2	−37	−61
Équinoxe	8	8	4	1	1	1	2	3	−3	−21	−38
Hiver	6	1	−3	−5	−6	−7	−8	−12	−10	−3	−15
Année	8	5	2	0	−1	0	3	5	−3	−20	−38

Tableau IV

M'Bour (Sénégal)										Valeurs horaires en 1/10	
H. TU	1	2	3	4	5	6	7	8	9	10	11
Janvier	−7	−10	−13	−16	−16	−17	−17	−22	−21	−13	−20
Février	−6	−9	−10	−11	−8	−10	−11	−16	−16	−13	−17
Mars	−3	−2	−3	−2	−1	1	−1	−4	−9	−23	−31
Avril	0	3	0	0	2	5	4	4	−11	−31	−42
Mai	−1	3	−3	1	6	6	11	10	−8	−33	−45
Juin	4	−3	1	0	2	4	10	11	−3	−30	−42
Juillet	5	2	2	2	1	6	13	14	−3	−34	−54
Août	−1	−1	0	3	3	6	12	13	−4	−41	−62
Septembre	0	2	4	3	6	8	12	15	0	−33	−52
Octobre	0	−3	−3	−5	−4	−2	−1	−2	−11	−27	−36
Novembre	−11	−14	−14	−13	−12	−9	−10	−11	−10	−8	−8
Décembre	−15	−18	−21	−20	−21	−20	−20	−15	−12	−11	−15
Été	2	0	0	1	3	6	12	12	−5	−34	−51
Équinoxe	−1	0	0	−1	1	3	3	3	−8	−29	−40
Hiver	−10	−13	−14	−15	−14	−14	−14	−16	−14	−11	−15
Année	−3	−4	−5	−5	−4	−2	0	0	−9	−25	−35

mV/Km — Composante N — 1967

12	13	14	15	16	17	18	19	20	21	22	23	24	Amp
−38	−43	−16	8	19	22	22	13	22	23	14	6	5	66
−24	−40	−37	−17	−1	15	28	26	31	29	23	18	11	71
−33	−36	−34	−11	8	20	24	26	26	22	16	11	6	62
−49	−51	−35	−8	17	33	37	32	20	11	10	9	8	88
−67	−61	−38	−6	18	37	39	40	27	21	17	14	13	107
−63	−62	−36	−12	−1	11	23	32	31	20	16	16	17	95
−69	−62	−33	−4	13	26	33	35	29	14	10	11	9	104
−83	−66	−29	3	25	40	38	29	21	14	12	13	10	123
−71	−59	−25	5	27	38	30	22	14	14	11	8	6	109
−45	−37	−18	−1	7	11	16	21	27	22	14	8	8	72
−33	−38	−29	−10	1	17	29	33	40	33	21	13	10	78
−33	−37	−21	−6	7	12	19	24	27	22	14	10	7	64
−71	−63	−34	−5	14	29	33	34	27	17	14	13	12	105
−49	−46	−28	−4	15	25	27	25	21	17	13	9	7	76
−32	−40	−26	−6	6	17	25	24	30	27	18	12	8	70
−51	−49	−29	−5	12	24	28	28	26	20	15	11	9	79

mV/Km — Composante E — 1967

12	13	14	15	16	17	18	19	20	21	22	23	24	Amp
−23	−14	13	33	43	41	33	21	17	12	4	−3	−6	66
−22	−18	−7	9	22	31	33	22	21	20	10	4	0	55
−31	−19	−6	13	25	31	25	18	16	11	3	−3	−3	62
−39	−26	−7	10	22	30	29	22	14	7	2	0	0	72
−42	−31	−11	8	16	24	22	24	14	12	8	5	4	69
−43	−34	−15	3	9	17	21	23	23	13	10	9	11	66
−57	−43	−17	6	19	25	26	25	20	14	11	10	8	83
−61	−42	−12	14	30	35	30	23	18	12	10	9	4	97
−53	−34	−8	13	27	31	21	14	10	9	5	0	−1	84
−36	−19	6	22	22	19	16	19	22	15	6	1	1	58
−8	0	12	21	22	22	20	14	17	11	3	−5	−8	36
−13	2	24	38	38	33	29	21	18	11	4	−7	−11	59
−51	−38	−14	8	19	25	25	24	19	13	10	8	7	76
−40	−25	−4	14	24	28	23	18	15	11	4	0	−1	68
−16	−7	10	25	31	32	29	20	18	13	5	−3	−6	48
−35	−23	−2	16	25	28	25	21	18	12	6	2	0	63

Tableau V

M'Bour (Sénégal)									Valeurs horaires en 1/10		
H. TU	1	2	3	4	5	6	7	8	9	10	11
Janvier	10	6	1	−3	−6	−5	−7	−9	−19	−18	−29
Février	11	5	4	−3	−6	−5	−9	−17	−17	0	−10
Mars	6	6	4	1	−2	−1	−9	−12	−7	−13	−27
Avril	7	5	4	3	3	6	5	9	−8	−27	−41
Mai	6	7	6	9	6	11	18	19	−3	−42	−68
Juin	6	9	9	4	8	11	24	32	10	−28	−57
Juillet	5	3	3	1	4	8	23	34	10	−26	−55
Août	6	5	4	3	5	14	23	30	5	−43	−71
Septembre	4	6	5	6	3	6	15	22	6	−31	−55
Octobre	8	4	0	−1	−1	0	1	0	0	−15	−36
Novembre	5	3	−2	−7	−2	1	5	0	0	1	−7
Décembre	2	0	−1	1	6	8	5	7	−1	−14	−43
Été	6	6	6	4	6	11	22	29	5	−35	−63
Équinoxe	7	5	3	2	1	2	3	5	−2	−22	−40
Hiver	7	4	0	−3	−2	0	−2	−5	−9	−8	−22
Année	6	5	3	1	2	4	8	10	−2	−21	−42

Tableau VI

M'Bour (Sénégal)									Valeurs horaires en 1/10		
H. TU	1	2	3	4	5	6	7	8	9	10	11
Janvier	−11	−11	−15	−15	−17	−15	−14	−14	−20	−24	−31
Février	0	−4	−7	−11	−12	−11	−14	−22	−22	−23	−27
Mars	−3	−3	−3	−4	−6	−6	−10	−13	−18	−31	−37
Avril	1	0	−2	−5	−5	−3	−5	−7	−25	−46	−55
Mai	−3	−1	0	2	1	4	7	0	−18	−49	−57
Juin	−1	2	1	0	3	7	16	15	−2	−31	−46
Juillet	2	0	2	1	3	6	14	16	−2	−32	−50
Août	−2	0	2	1	2	8	13	16	−4	−41	−57
Septembre	−4	−1	2	3	2	5	11	16	−4	−35	−51
Octobre	−1	−2	−2	0	0	−1	−3	−2	−10	−30	−41
Novembre	−5	−3	−7	−11	−14	−13	−17	−22	−29	−36	−33
Décembre	−6	−11	−12	−13	−12	−11	−16	−15	−21	−36	−51
Été	−1	0	1	1	2	6	12	12	−7	−38	−52
Équinoxe	−2	−2	−1	−1	−2	−1	−2	−1	−14	−35	−46
Hiver	−5	−7	−10	−12	−14	−13	−16	−18	−23	−30	−35
Année	−3	−3	−3	−4	−5	−3	−2	−3	−15	−34	−45

mV/Km — Composante N — 1968

12	13	14	15	16	17	18	19	20	21	22	23	24	Amp
−42	−37	−21	5	24	29	17	9	27	26	18	13	10	71
−27	−45	−31	−16	−6	11	25	28	29	25	21	17	15	74
−31	−30	−32	−21	−2	16	27	28	28	24	21	17	9	60
−48	−50	−37	−7	18	34	30	29	18	12	15	11	8	84
−75	−64	−35	−1	20	38	43	39	25	11	10	11	9	118
−65	−56	−26	−8	9	17	24	26	23	10	9	6	6	97
−66	−56	−31	−11	7	23	28	26	23	11	11	13	11	100
−75	−59	−30	2	27	40	37	25	14	11	8	9	9	115
−65	−61	−30	−1	29	37	34	25	13	10	10	7	6	102
−47	−35	−15	−1	11	15	18	16	24	22	17	10	8	71
−22	−30	−18	−9	0	3	5	7	22	19	9	9	9	52
−49	−23	−1	19	24	15	2	−5	16	12	9	6	2	73
−70	−59	−31	−5	16	29	33	29	21	11	9	10	8	103
−48	−44	−28	−8	14	25	27	24	21	17	16	11	7	75
−35	−34	−17	0	10	15	12	10	23	21	14	11	9	58
−51	−45	−25	−4	13	23	24	21	22	16	13	11	8	75

mV/Km — Composante E — 1968

12	13	14	15	16	17	18	19	20	21	22	23	24	Amp
−31	−12	15	37	47	45	29	19	21	16	7	−1	−6	78
−29	−27	−6	16	26	33	35	29	26	20	14	7	8	64
−32	−16	−2	13	28	33	31	26	22	18	12	3	0	70
−45	−30	−10	11	30	38	38	35	26	21	18	11	7	93
−51	−33	−6	19	32	38	38	33	20	10	6	3	4	95
−46	−32	−11	5	18	24	25	21	19	8	5	1	0	71
−54	−39	−12	6	21	27	27	23	17	9	5	6	6	81
−55	−38	−12	17	35	37	31	19	12	7	4	2	2	94
−51	−36	−7	14	36	35	26	17	11	6	3	1	−1	87
−43	−23	6	29	32	29	21	13	17	9	4	−1	−2	75
−28	−9	16	32	37	30	22	19	25	21	14	8	4	73
−44	−11	19	43	49	43	29	18	23	19	13	5	−1	100
−52	−35	−10	12	26	32	30	24	17	8	5	3	3	84
−43	−26	−3	17	31	34	29	23	19	14	9	4	1	80
−33	−15	11	32	40	38	29	21	24	19	12	5	1	75
−42	−25	−1	20	32	34	29	23	20	14	9	4	2	79

Remerciements

Je tiens à remercier MM. Taher Maiga et Ousseynon Sow, qui ont effectué avec un soin minutieux la plus grande partie du dépouillement des enregistrements.

RÉFÉRENCES

1. Direction Fédérale des Mines et de la Géologie de l'A.-O.F. Reconnaissances hydrologiques et structurales par sondages électriques au Sénégal et en Mauritanie, 1956—1957.
2. Communication personnelle.
3. CAGNIARD, L.: Electricité tellurique. Handbuch der Physik, Vol. XLVII (Geophysik I). Springer-Verlag, Berlin, 1956.
4. ROUGERIE, P.: Contribution à l'étude des courants telluriques. Ann. Inst. Phys. Globe Paris, 20, 1942.

SLOW TELLURIC VARIATIONS OBSERVED AT M'BOUR (SENEGAL)

SUMMARY

Continuous registrations of telluric currents have been effected at M'Bour from beginning of May 1965. The present article describes the installation and its functioning and analyses the phenomena of trend which have been noticed. The average daily variations of the North-South and East-West components for each month of the years 1966—68, as well as their seasonal and annual averages, are presented in the form of hourly tables and graphs. A certain number of polar diagrams are added, illustrating these variations, and some results given by the harmonic analysis.

МЕДЛЕННЫЕ ТЕЛЛУРИЧЕСКИЕ ВАРИАЦИИ НА ОСНОВЕ НАБЛЮДЕНИЙ В М'БУРЕ (СЕНЕГАЛ)

Ж. МЕЦГЕР

РЕЗЮМЕ

В М'Буре с мая 1965-го года непрерывно регистрируются теллурические токи. В настоящей статье излагается оборудование и его действие, а также наблюденные тренды. Для каждого месяца 1966—68 гг. задается средний суточный ход Северо-Южной и Востоко-Западной компонент. Задаются также и сезонные и годовые средние, в виде часовых таблиц и графиков. Вариации илюстрируются на полярных диаграммах. Сообщается об отдельных результатах гармонического анализа.

Acta Geodaet., Geophys. et Montanist. Acad. Sci. Hung. Tomus 14 (1—2), pp. 171—179 (1979)

DYNAMICS OF SEISMIC WAVES CAUSED BY BLASTINGS IN MINES

D. CSOMOR—Z. KISS

CANDIDATES OF TECHNICAL SCIENCES

GY. SZEIDOVITZ

SEISMOLOGICAL OBSERVATORY OF THE GEODETIC AND GEOPHYSICAL RESEARCH INSTITUTE OF THE HUNGARIAN ACADEMY OF SCIENCES, BUDAPEST

[Manuscript received September 8, 1977]

In the paper an attempt is made to determine the absorption coefficients of the *P*- and *L*-waves on the basis of measurements in mines. The propagation velocities of the waves in Permian sandstone have also been determined. The dependence of the maximum amplitude of the *P*-wave on the charge quantity is given.

1. Introduction

As a consequence of mining activity, the equilibrium of the rock formations will be disturbed and the accumulated tension causes impulse-like microquakes. The accumulated tension can, however, cause sometimes sudden rockbursts and so damages in the mine or at the surface. Thus, it would be of great importance to know the time of the rockbursts. There are opinions that a greater accumulation of the tension is only possible, if microquakes do not occur, i.e. a relative longer quiet period precedes the rockbursts. Hence, the study of the frequency and intensity of microquakes gives important information on the time of the rockbursts as well as on their size.

In mines the noise due to mining activities mostly hampers a recognition of microquakes. Investigations are easier, if the propagation velocity, the amplitude conditions and the absorption coefficients of the wave phases occurring in the given rock formation are known. Based on this reasoning, we investigated the dynamic characteristics of seismic waves excited by experimental blastings.

2. Instruments and measuring method

In a gangway being a few hundred meters below the surface, 1 m deep holes were bored into the Permian sandstone near to each other and different quantities of explosive were blasted in them. A general plan of the measurements is given in Fig. 1. The seismic waves were recorded in the mine in 6

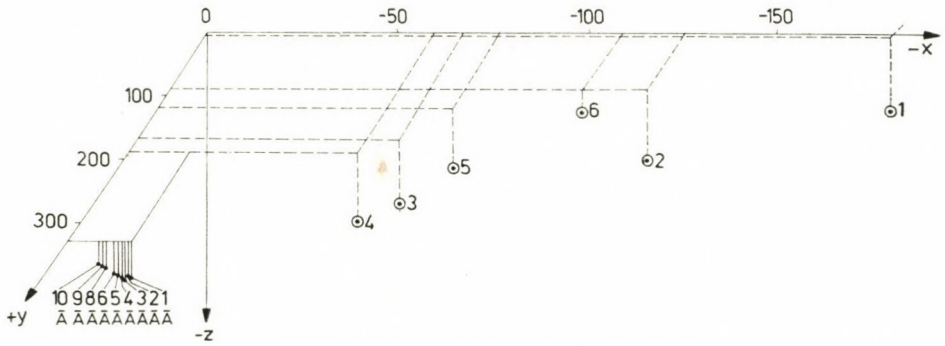


Fig. 1. Arrangement of the measurements: $\bar{A}$ blasting sites; ⊙ recording stations (1, 2, 3, 4, 5, 6)

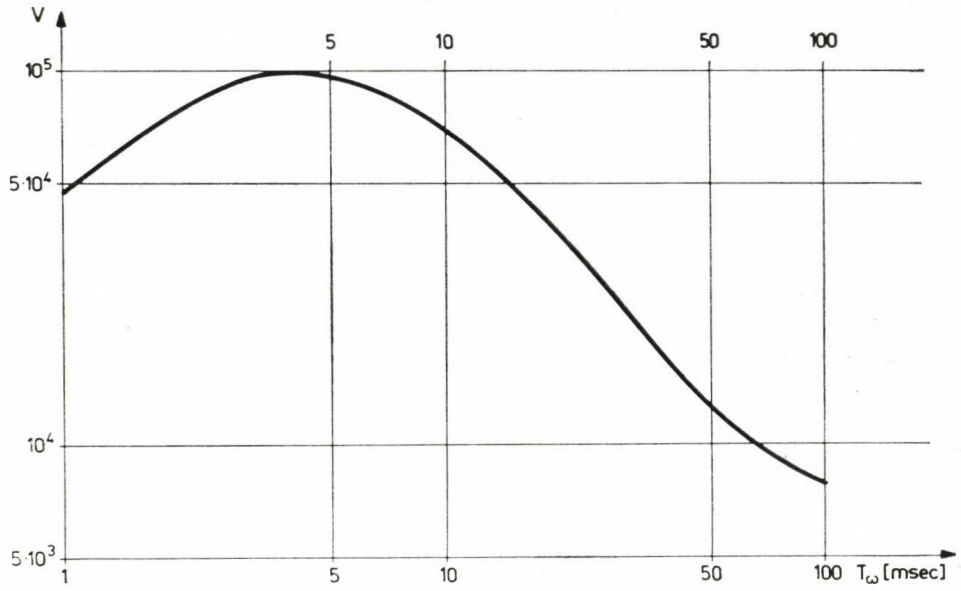


Fig. 2. Magnification curve of the seismographs: T_ω period of soil movements; V magnification of seismographs

measuring points lying at different distances from the excitation. Five vertical and one horizontal Vegik type seismometers were used. The measuring system consisted of a seismograph of 1 Hz natural frequency and a galvanometer of 250 Hz natural frequency. Records were made on photopaper with speed of 55 cm/sec. The magnification curve of the seismographs is shown in Fig. 2. Quantity of the explosives blasted in the holes, the distances between blasting and observation as well as the notations of the blasting points are compiled in Table I.

Table I

Blasting			Recording station					
Serial number	Notation of blasting site	Charge (kg)	1	2	3	4	5	6
			Δ(m)					
1	$6/\bar{A}$	2.0	366.83	268.09	169.59	148.25	221.47	332.50
2	$5/\bar{A}$	1.8	366.00	267.29	168.86	147.52	220.78	331.84
3	$4/\bar{A}$	1.4	365.22	266.54	168.17	146.83	220.13	331.22
4	$8/\bar{A}$	1.2	368.36	269.58	171.00	149.66	222.77	333.73
5	$3/\bar{A}$	1.0	364.52	265.86	167.54	146.22	219.55	330.67
6	$2/\bar{A}$	0.8	363.85	265.22	166.98	—	219.00	330.14
7	$9/\bar{A}$	0.6	369.07	270.28	171.64	—	223.38	334.30
8	$10/\bar{A}$	0.4	369.66	270.85	172.18	—	223.88	334.78
9	$1/\bar{A}$	0.2	363.27	264.67	166.47	—	218.52	329.68

Explosive material: NIDIN
Δ = observation distances

3. Processing of the observations

In this paper first arrivals (P-waves) and surface waves are mainly used. The travel time curves of the different phases are shown in Fig. 3. The first order regression line well characterizes the connection between arrival time and source distance. The equations of the linear approximation are:

$$t_P = 0.2144\Delta - 4.175$$
$$V_P = 4664 \text{ m/sec}$$
$$r_P^2 = 0.9821$$
$$t_x = 0.2460\Delta - 4.499$$
$$V_x = 4067 \text{ m/sec}$$
$$r_x^2 = 0.9966$$
$$t_L = 0.3072\Delta - 4.754$$
$$V_L = 3256 \text{ m/sec}$$
$$r_L^2 = 0.9918$$

where V is the propagation velocity of the different wave types, r^2 is the deterministic coefficient, index L means surface waves, x unidentifiable phases. The deterministic coefficients have a value near to 1 which means that the approximation is quite good.

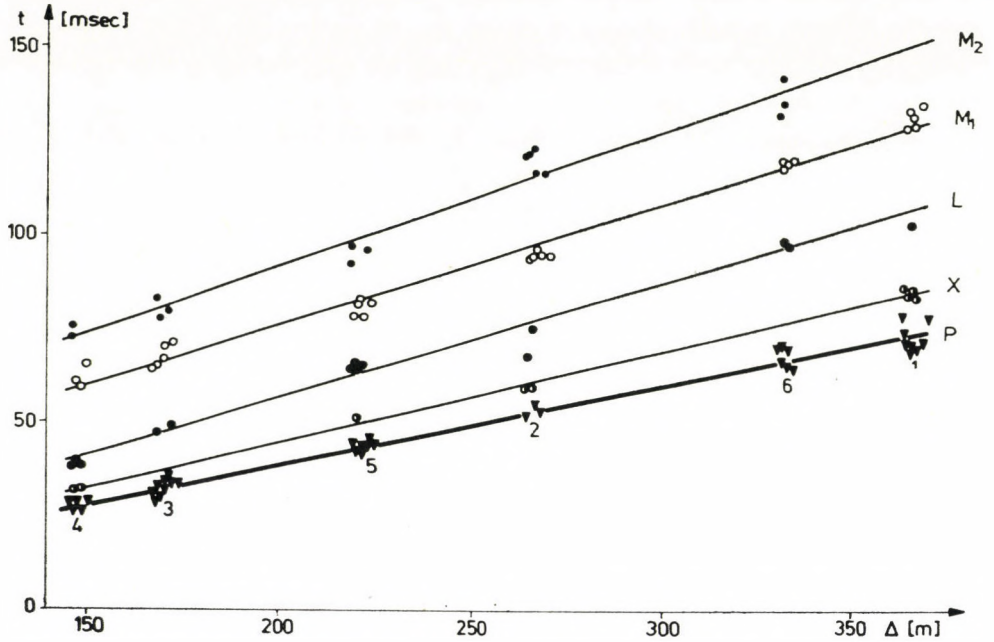


Fig. 3. Travel-time curves of the wave phases: t[msec] = propagation time; Δ [m] = distance from the blasting; 1, 2, 3, 4, 5, 6 = serial number of the stations

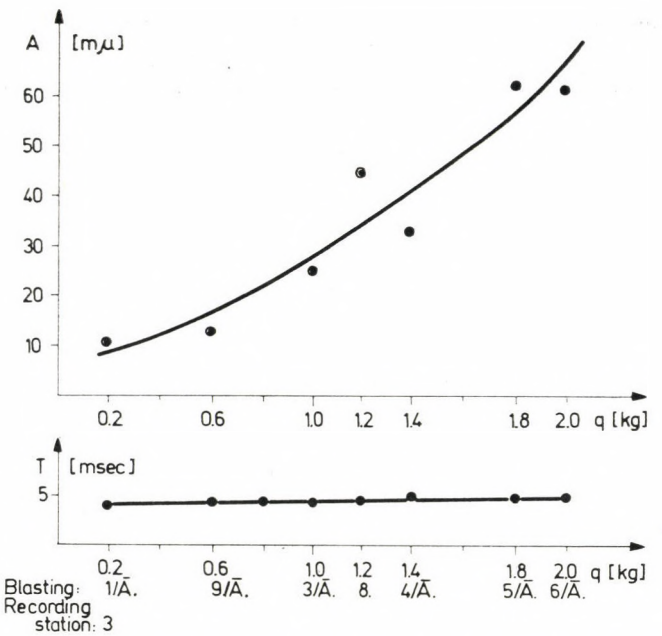


Fig. 4. The amplitude (A) decrease of the P-waves and the change of the corresponding periods (T) as a function of the charge quantity (q)

One or two amplitude maxima were found in the range of the surface waves (M_1; M_2). The arrival times of the latter are also shown in Fig. 3. Both series can be also well approximated by straight lines.

For the station No. 3 amplitudes (A) and periods (T) of the P-waves are plotted vs. the charge quantities (q) in Fig. 4. The distance from the source can be taken as constant due to the small distances between the blasting points. The following formula describes the connection between amplitude and charge:

$$A = 8.134\, e^{1.092\, q}\,.$$

This approximation fits well the measured data (deterministic coefficient 0.9226). There is only a small change in the period due to increasing charge ($T = 4.0-4.5$ msec). The third and fourth greatest amplitudes together with the corresponding periods are presented in Fig. 5 in function of distance. The dependence of the maximum amplitudes (M_1) of the surface waves on the distance at different charges can be seen in Fig. 6.

Seismic waves decay with distance more rapidly as it would follow from geometric considerations. Absorption plays also a role in the energy decrease of the waves.

The following formula describes the amplitude decrease of the seismic waves:

$$A = A_0\, \Delta^n\, e^{-\alpha \Delta} \qquad (1)$$

The absorption coefficient α depends on the wave period.

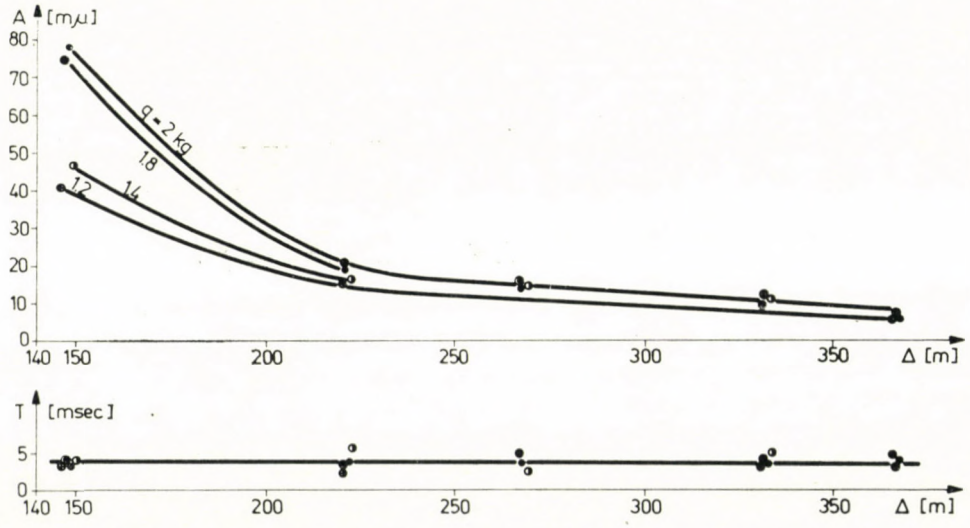


Fig. 5. The change of the amplitudes (A) and the periods (T) of the P-wave as function of the observation distance (Δ). (q is the charge quantity of the blastings)

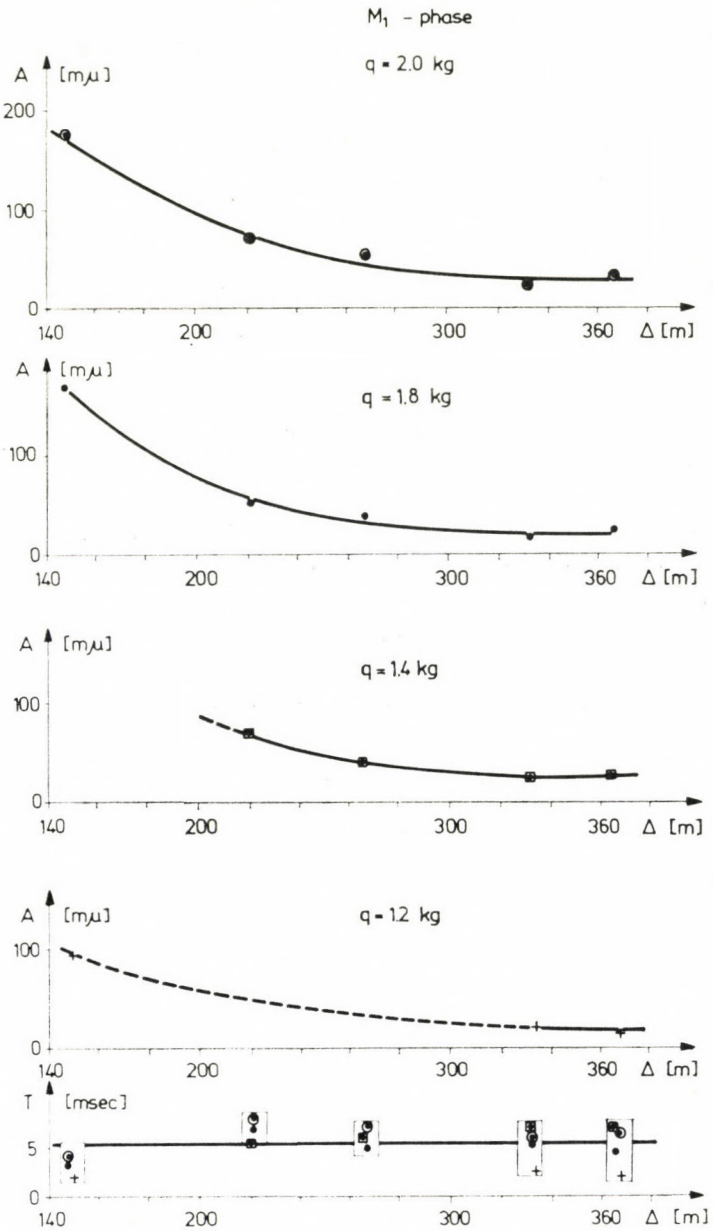


Fig. 6. **The changes of the maximum amplitudes (A) and the periods (T) of the surface waves as function of the observation distance Δ in case of different charge quantities (q) of the blasting**

According to investigations in [1], the following connection was found between the absorption coefficient and the period:

$$\alpha T^{-m} = \text{constant}, \tag{2}$$

where $m \geq 1$.

CALOI [2] received from theoretical considerations the formula:

$$\log \alpha = -2.0 \log T - 0.9 . \tag{3}$$

KIRILLOV and PUCHKOV [3], further KARUS and PASHECHNIK [4] investigated the change of the absorption coefficient in the short-period domain. A decrease of two orders in the period corresponds to one order increase of the absorption coefficient.

VADATI [5] investigated the amplitude changes of earthquake waves in the interval $200 < \Delta < 800$ km on the basis of data from Japan. He calculated the α values from the formula

$$A = A_0 \frac{e^{-\alpha \Delta}}{\sqrt{\Delta}} .$$

This connection is obtained from Eq. (1) with $n = -1/2$. According to his observations the connection

$$\alpha T = 0.015$$

is nearly valid.

Table II

P-wave

	$n = -1$			$n = -2$		
Charge (kg)	α	$\ln A_0$	r^2	n	$\ln A_0$	r^2
2	0.0072	10.22	0.91	0.0031	14.67	0.76
1.8	0.0053	9.87	0.83	0.0012	14.31	0.25
1.4	0.0040	9.21	0.78	0.0001	13.65	0.003
1.2	0.0025	0.03	0.46	0.0018	13.42	0.42

Table III

M_1-phase

	$n = -1$			$n = -\frac{1}{2}$		
Charge (kg)	α	$\ln A_0$	r^2	n	$\ln A_0$	r^2
2	0.0042	10.59	0.71	0.0069	8.57	0.85
1.8	0.0058	10.8	0.79	0.0078	8.58	0.86
1.4	0.0036	10.3	0.67	0.0054	7.98	0.81
1.2	0.0041	10.19	0.99	0.0062	7.99	0.99
1.0	0.0158	15.58	0.98	0.0178	10.34	0.98

One can see that different authors have no uniform opinion concerning the dependence of the absorption coefficient on period.

The absorption coefficient can be determined in the following way: The amplitudes of the seismic waves radiating from a source are measured at several points along a profile and the constants A_0, n and α are determined from Eq. (1) by means of the least-squares method. The parameter pairs α_i, T_i are determined for the waves of identical type but of different period. These are represented in a coordinate system and a smooth curve constructed for the data set.

In the practice the solution of the problem gets difficult due to problems which cannot be easily taken into account in course of the calculations (coupling between seismograph and rock, effect of loose layers, superposition of waves).

It can further occur that in cases when α and n are determined together, the values of these two quantities cannot be separated and consequently we get for A_0, n and α values lacking any physical sense.

In such cases it seems to be more suitable to determine at first the dependence of amplitudes on the distance, i.e. the exponent n on the basis of theoretical considerations.

From the first arrivals (P-wave) observed at the blasting of different charge-quantities we determined the values of α from Eq. (1) by supposing $n = -1$ and $n = -2$. For the surface waves, the absorption coefficients were calculated with the exponents $n = -1$ and $n = -1/2$. The results are compiled in Tables II and III.

4. Conclusions

a) On the basis of seismic measurements carried out in gangways, in the Permian sandstone of the investigated area the following propagation velocities have been determined for the longitudinal (P) and surface (L) waves:

$$V_P = 4664 \text{ m/sec}$$

$$V_L = 3256 \text{ m/sec} .$$

The observed surface waves are in a narrow sense Rayleigh waves.

b) The change of the amplitude of the P-waves versus charge quantity q can be described by the function:

$$A = 8.134\, e^{1.092\, q}$$

The corresponding periods change only a little in function of charge quantity.

c) An attempt was made to determine the absorption coefficients for the maxima of the P-waves and the Rayleigh waves (M_1 phase) by means of

blasting with different charge quantities. Supposing that the amplitude decrease of the M_1 phase is inversely proportional to the square root of the distance, the absorption coefficient has a scatter of less than 20 per cent (exception is the case of 1 kg charge). As a final result we got on the area investigated an absorption coefficient of $\alpha_{M_1} = 0.0065$ for the maxima of the Rayleigh waves.

The values of the absorption coefficients obtained for the *P*-waves are essentially smaller, but due to the great scatter they cannot be considered as reliable.

REFERENCES

1. Kárnik, V.: Magnitudenbestimmung europäischer Nahbeben. *Geofysikálni Sbornik*, No. 47(1956), 399—457.
2. Caloi, P.: Comportamento delle onde di Rayleigh in uno mezzo firmo-elastico indefinito. *Annali di Geofisica*, 1(1948), 551—567.
3. Kirillov, F. A.—Puchkov, S. V.: Raszprostzranenie kolebania *v* grunte ot isztocsnikov tipa impulsza. *Tr. Sejsm. inst. AN SSSR* No. 59(1953).
4. Karus, J. V.—Pashechnik, I. P.: O prirode uprugich voln, vozbuzsdaemich v realnich sredach garmonicseskim istocsnikom. *Izv. AN SSSR, ser. geofiz.* No. 2(1955), 89—100.
5. Vadati, K.: Shallow and deep earthquakes. *Geoph. Magazine*, No. 4, Vol. IV(1931), 231—284.

ДИНАМИЧЕСКОЕ ИССЛЕДОВАНИЕ ВЗРЫВОВ СЕЙСМИЧЕСКИХ ВОЛН, ПРОИЗВЕДЕННЫХ В ШАХТЕ

Д. ЧОМОР—З. КИШШ—ДЬ. СЕЙДОВИЦ

РЕЗЮМЕ

В статье, на основании измерений, проведенных в шахте, делаем попытку для определения абсорбционных коэффициентов волн *P* и *Л*; дальше определили скорость распространения волн в пермском песчанике. Задаем зависимость максимальной амплитуды волны P от величины заряда.

Acta Geodaet., Geophys. et Montanist. Acad. Sci. Hung. Tomus 14 (1—2), pp. 181—226 (1979)

УПРУГИЕ ХАРАКТЕРИСТИКИ МИНЕРАЛЬНОГО ВЕЩЕСТВА В ТЕРМОБАРИЧЕСКИХ УСЛОВИЯХ ЗЕМНЫХ НЕДР

Т. С. ЛЕБЕДЕВ—В. А. КОРЧИН

ИНСТИТУТ ГЕОФИЗИКИ АН УССР, КИЕВ

[Поступило 2 ноября 1977 г.]

На примерах экспериментального изучения минеральных образований Украинского щита показано, что породы кислого, среднего и основного составов дифференцируются по упругим свойствам в условиях атмосферного и высоких давлений. Кислым образованиям присущи относительно низкие значения V_p, V_s, E, G и большая сжимаемость. В условиях высоких давлений они характеризуются релаксационными явлениями в виде хрупко-пластических микронарушений структуры минерального вещества. Породы основного состава при росте давления склонны к плавному увеличению упругих параметров и пластифицируются без каких-либо аномальных явлений. Образованиям среднего состава свойственны промежуточные характеристики.

Упругие параметры минерального вещества в условиях высоких температур (при атмосферном давлении) изменяются в основном за счет его разуплотнения, обусловленного неравномерным и анизотропным расширением породообразующих минералов, а также изменением их упругих характеристик. Наиболее подвержены воздействию температуры крупнозернистые образования кислого состава и породы, обогащенные вторичными минералами.

Результаты опытов при одновременном воздействии высоких давлений и температур по различным региональным PT-программам позволяют считать, что в верхних горизонтах земной коры (до 3—6 км) величины упругих параметров пород (V_p, V_s, E, G и K) могут монотонно увеличиваться благодаря возрастающему с глубиной влиянию давления. Температура в этих условиях в основном лишь пластифицирует минеральное вещество.

Состояние пород при высоких лабораторых PT-режимах, соответствующих интервалу глубин порядка 5—30 км, характеризуется понижением значений их упругих параметров по сравнению с таковыми, полученными в опытах при высоких давлениях и комнатной температуре. Изменение упругих свойств на этих глубинах происходит по сложным законам с возникновением зон пониженных скоростей. Характер последних (местоположение по разрезу, протяженность и величина градиента) обусловлен особенностями распределения с глубиной давления, температуры и минерального состава пород.

Эти зоны можно разделить на толстослойные (порядка 10—20 км) и тонкослойные (около 3—7 км). Кислым образованиям свойственны тонкослойные зоны, расположенные преимущественно в верхних частях коры. Для пород основного и среднего составов чаще предполагается наличие толстослойных зон. Области с высокими температурными градиентами должны характеризоваться тонкослойными зонами. В условиях негидростатического распределения давления толстослойные зоны пониженных скоростей могут быть приурочены преимущественно к образованиям основного состава.

Высказано предположение о термодинамической природе некоторых зон пониженных скоростей, выделяемых методами взрывной сейсмологии на глубнах 10 ÷ 30 км в толще континентальной земной коры. К этим зонам приурочены породы среднего или основного составов, характеризующиеся пониженной упругостью, меньшей плотностью, повышенной хрупкостью вблизи их границ и более высокой пластичностью в центральных частях.

Результаты Лабораторных исследований упругих свойств горных пород и минералов при высоких термодинамических параметрах позволяют не только выяснять важные вопросы природы и закономерностей их изменения в недрах Земли, но и широко используются для теоретического и экспери-

ментального моделирования различных физико-механических, физико-химических, тектонофизических и других процессов и явлений, происходящих на больших глубинах. Данные опытов, наряду с материалами изучения различных геофизических полей, дают возможность более точно прогнозировать состояние и состав минерального вещества, а также строение глубоких частей земной коры [1, 5, 6, 8—11, 15, 18, 41, 42, 44, 45, 48, 57 и др.].

Однако, даже большого количества лабораторных данных об изменении упругих параметров пород только при воздействии одного давления явно недостаточно для комплексного анализа распределения минеральных масс в земных недрах. Необходимы сведения об их поведении при одновременном воздействии высоких давлений (P) и температур (T). Ввиду многих технических и методических трудностей проведения таких экспериментов в настоящее время во всем мире изучено (начиная с 1937 г.) всего лишь около 100 образцов горных пород и минералов [2—4, 7, 10, 15, 18, 27—29, 31, 33, 35, 47, 49, 50—57, 59, 62, 63 и др.].

В этой статье обобщены новые результаты экспериментальных исследований скоростей распространения продольных (V_p) и поперечных (V_s) волн, а также упругих параметров горных пород при различных режимах воздействия P и T. На основании информативности данных об изменениях упругих характеристик минерального вещества при высоких гидростатических и квазигидростатических давлениях, температурах, и, наконец, в модельных одновременно действующих P и T, представлено возможное состояние пород верхних частей земной коры, для которых были заданы различные конкретные варианты изменений давлений и температуры с глубиной.

Исследования выполнены в Отделе физических свойств вещества Земли Института геофизики АН УССР (Киев) на установках высокого гидростатического и квазигидростатического давлений (до 6 кбар) и температур (до 320—350°С) [18, 20, 28, 34, 36, 37 и др.]. В опытах использован метод программного моделирования в аппаратах высокого давления трех основных термодинамических режимов глубиных зон коры Украинского докембрийского щита [15, 38, 39, 61]. Упругие параметры горных пород были рассчитаны по материалам одновременных измерений V_p и V_s в соответствующих образцах [15, 19, 32, 33, 51, 57, 62, 63 и др.], а также данных об их плотности.

Знание модулей и коэффициентов упругости твердых тел весьма важно для понимания природы сил сцепления в них, так как эти параметры количественно отражают характер взаимодействия их микро- и макроструктурных единиц. Поэтому закономерности поведения упругих характеристик в соответствующих PT-условиях можно использовать при объяснении существенных изменений состояния вещества. Акустические методы, основанные на измерениях скорости распространения упругих волн, позволяют исследовать свойства твердого тела при низких и высоких температурах, в области высоких и сверхвысоких давлений, изучать динамику его различных физико-

химических превращений и т. д. Рассматривая вещество как сплошную среду в рамках теории упругости, для изотропных тел упругие характеристики можно выразить через скорости распространения упругих колебаний и плотность [14, 43]. Состояние твердого тела при различных видах упругой деформации может быть выражено модулями Юнга (E), сдвига (G) и сжатия (K), коэффициентом Пауссона (σ) и постоянными Ламэ (λ и μ).

При всестороннем сжатии многокомпонентного поликристаллического минерального вещества (каким является горная порода), в большинстве случаев лишь квазиизотропного, в исследуемом образце возникают внутренние напряжения сложного характера, которые вызывают изменения его объема и формы. Именно эти явления хорошо характеризуют модули соответственно объемного сжатия и сдвига. Одновременно при всестороннем давлении в горных породах под воздействием внутренних напряжений развиваются локальные продольные и поперечные деформации, которые неизбежно влекут за собой микроструктурные изменения. Величина продольной деформации образца минерального вещества зависит в основном от его непосредственного сопротивления воздействию главных сил гидростатического давления и характеризуется модулем Юнга. Коэффициент Пуассона, описывающий величину поперечной деформации, определяет возможность «передачи» породой действия внешних напряжений вдоль направлений, не совпадающих с силами гидростатического сжатия. Эта величина является источником информации о наличии и характере проявления внутренних напряжений в образцах и качественно определяет интенсивность развития процессов упругости и пластичности в деформируемых объектах. Принимая во внимание такую информативность упругих параметров горных пород, становится очевидной важность их экспериментального изучения в опытах при различных термобарических условиях.

Упругие свойства пород при гидростатических давлениях и комнатной температуре. Минеральный состав (в овъемных) и некоторые физические характеристики изученных нами образцов пород Украинского щита кислого, среднего и основного составов в условиях атмосфер довления и представлены в табл. I. Результаты изменений скоростей распространения продольных (V_p) и поперечных (V_s) упругих волн ультразвукового диапазона для всех трех групп при высоких гидростатических давлениях и комнатной температуре приведены на рис. 1—3. Не останавливаясь подробно на описании зависимостей $V_{p,s} = f(P)$ по отдельным образцам, отметим лишь общие закономерности для пород указанных групп. С повышением основности V_p и V_s возрастают. Наиболее низкие средние значения скоростей при атмосферном давлении присущи породам кислого состава ($V_{p_{001}} = 5{,}25 \div 6{,}0$ км/сек; $V_{s_{001}} = 3{,}15 \div 3{,}5$ км/сек) (рис. 1). Породы среднего состава характеризуются соответственно скоростями $5{,}5 \div 6{,}35$ и $3{,}10 \div 3{,}8$ км/сек (рис. 2). Основные имеют наиболее высокие значения: $V_{p001} = 6{,}0 \div 6{,}8$ и $V_{s001} = 3{,}15 \div 3{,}85$

Таблица I

Минеральный состав (в объмных процентох) и физические свойства образцов некоторых

№№ пп	Наименование породы и район отбора	Содержание SiO_2, весовые %	Pl	КПШ	Q	Px	Bi	Hb	Gr	Акц. и рудн.
	Кислого состава									
1.	Кварцит, Овруч	97,35	—	—	100	—	—	—	—	—
2.	Чарнокит I, Черневцы	72,85	34,3	21,8	38,3	3,4	—	—	—	0,8
3.	Гранит житомирский, Богуслав	72,84	35,0	23,0	23,0	—	—	9,6	—	2,0
4.	Гранит кировоградский, Кировоград	72,29	28,4	36,2	24,5	—	—	9,5	—	1,4
5.	Гранит порфировидный I, Пугачевка	71,89	35,2	27,3	29,4	—	—	5,2	—	2,9
6.	Гранит житомирский II, Житомир	72,62	47,4	23,0	23,3	—	—	6,3	—	—
7.	Чарнокит II, Хощеватое	71,24	52,1	—	27,9	16,1	—	—	—	3,9
8.	Гранит рапакиви I, Пенизевичи	71,24	6,1	60,7	17,8	—	3,9	1,7	—	3,3
9.	Гранит порфировидный II, Бехи	70,71	29,2	21,7	34,8	—	—	8,9	—	5,6
10.	Гранит рапакиви II, Корсунь-Шевченковский	70,13	16,0	63,8	11,5	—	4,6	2,8	—	1,2
11.	Гранит чудново-бердичевский, Жежелево	64,97	30,3	17,2	28,7	—	—	13,4	10,4	—
12.	Гранит клесовский, Клесово	64,65	56,0	7,0	12,6	—	6,8	8,0	—	4,4
	Среднего состава									
13.	Чарнокит III, Завалье	64,16	62,5	—	19,8	15,4	—	—	—	1,1
14.	Собит, Калинино	62,87	55,9	8,0	5,7	5,7	—	11,8	—	8,1
15.	Гранодиорит, Шепетовка	61,96	49,4	3,1	21,6	—	—	19,3	—	6,6
16.	Диорит I, Тригурье	61,95	45,7	11,4	14,1	—	9,6	16,0	—	3,2
17.	Гранит осницкий, Клесово	59,43	66,7	7,5	7,5	—	3,4	8,3	—	6,6
18.	Порфирит клесовский, Томашгород	54,12	49,7	2,3	10,8	—	18,1	11,6	—	7,5
19.	Диорит II, Ракитное	52,63	52,7	—	7,8	—	19,7	17,5	—	2,3
20.	Диорит III, Виры	52,80	41,5	3,8	5,1	—	16,1	14,0	—	4,1
	Основного состава									
21.	Лабрадорит I, Каменка	54,94	61,7	12,0	14,7	3,1	1,1	—	—	3,0
22.	Лабрадорит II, Слипчинцы	52,97	84,0	—	2,9	4,6	—	—	—	6,2
23.	Габбро-норит, Головино	52,27	67,7	—	—	29,3	—	—	—	3,0
24,	Диабаз, Класово	46,31	61,6	—	—	25,8	—	—	—	5,5
25.	Гнейс, Завалье	46,00	39,5	—	7,4	14,6	14,1	—	5,3	4,9
26.	Пироксенит, Фастов	44,18	—	—	—	43,5	—	—	—	12,4
27.	Эклогитоподобная порода I, Хощеватое	59,05	28,6	—	42,6	—	—	—	26,0	2,8
28.	Эклогитоподобная порода II, Завалье	46,60	26,6	—	3,4	28,8	12,1	—	22,6	4,1

пород украинского щита при атмосферном давлении и комнатной температуре

Вторичные	δ, г/см³	ϱ, г/см³	n, %	V_p, км/сек	V_s, км/сек	V_p/V_s	E, Мбар	G, Мбар	K, Мбар	β, Мбар$^{-1}$	σ	λ Мбар
—	2,650	2,652	≈0	6,18	4,04	1,50	0,90	0,41	0,38	2,63	0,10	0,11
1,4	2,689	2,649	1,5	5,86	3,52	1,66	0,80	0,33	0,47	2,12	0,22	0,25
—	2,669	2,643	1,4	5,39	3,17	1,70	0,66	0,26	0,41	2,42	0,23	0,25
—	2,644	2,645	≈0	5,44	3,21	1,69	0,67	0,27	0,42	2,38	0,23	0,24
—	2,660	2,629	1,0	5,76	3,50	1,65	0,77	0,32	0,41	2,43	0,19	0,20
—	2,655	2,639	0,6	5,53	3,30	1,67	0,70	0,28	0,42	2,35	0,22	0,23
—	2,770	2,756	0,5	6,35	3,82	1,66	0,98	0,40	0,58	1,74	0,22	0,31
6,5	2,695	2,660	1,3	6,04	3,40	1,78	0,78	0,30	0,56	1,82	0,27	0,35
—	2,675	2,647	1,1	5,69	3,21	1,77	0,69	0,27	0,49	2,03	0,27	0,31
—	2,645	2,636	0,3	5,24	3,35	1,56	0,68	0,30	0,33	3,04	0,15	0,13
—	2,799	2,777	0,8	5,56	3,28	1,70	0,74	0,30	0,46	2,22	0,23	0,26
5,2	2,738	2,737	≈0	6,03	3,28	1,84	0,76	0,29	0,60	1,66	0,29	0,41
1,2	2,911	2,865	1,6	6,24	3,51	1,78	0,90	0,35	0,64	1,55	0,27	0,41
3,8	2,770	2,733	1,4	5,63	3,30	1,71	0,74	0,30	0,47	2,13	0,24	0,27
—	2,754	2,756	≈0	5,58	3,38	1,65	0,76	0,31	0,44	2,28	0,21	0,23
—	2,752	2,744	0,3	5,53	3,22	1,72	0,71	0,28	0,46	2,17	0,24	0,27
—	2,752	2,719	1,3	5,69	3,07	1,85,	0,66	0,26	0,54	1,86	0,29	0,37
—	2,753	2,759	≈0	5,74	3,45	1,66	0,80	0,33	0,47	2,12	0,22	0,25
—	2,866	2,860	0,2	5,75	3,40	1,69	0,81	0,33	0,50	2,00	0,23	0,28
9,4	2,903	2,861	1,5	5,34	3,24	1,65	0,73	0,30	0,42	2,41	0,21	0,22
4,4	2,810	2,811	≈0	6,18	3,38	1,82	0,83	0,32	0,65	1,54	0,29	0,49
2,3	2,741	2,734	0,2	6,40	3,59	1,82	0,90	0,36	0,66	1,52	0,27	0,42
—	2,977	2,977	≈0	6,91	3,75	1,84	1,08	0,42	0,86	1,16	0,29	0,58
7,1	3,035	3,035	≈0	6,07	3,63	1,73	0,99	0,40	0,65	1,54	0,25	0,38
14,2	2,744	2,736	0,3	5,51	3,11	1,77	0,67	0,26	0,48	2,09	0,27	0,30
44,1	3,925	3,273	0,7	6,55	3,76	1,74	1,16	0,46	0,79	1,27	0,25	0,48
—	3,192	2,151	1,3	6,57	3,85	1,71	1,16	0,47	0,74	1,36	0,24	0,43
2,4	3,192	3,173	0,6	6,77	3,72	1,82	1,13	0,44	0,87	1,15	0,28	0,58

км/сек (рис. 3). При высоком гидростатическом давлении (5 кбар) распределение скоростей по группам основности пород существенно не отличается: например, в породах кислого состава $V_{p5} = 6{,}6 \div 6{,}8$ и $V_{s5} = 3{,}4 \div 3{,}7$; среднего — $V_{p5} = 6{,}2 \div 7{,}0$ и $V_{s5} = 3{,}65 \div 4{,}0$; основного — $V_{p5} = 6{,}75 \div 8{,}10$ и $V_{s5} = 3{,}7 \div 4{,}20$ км/сек.

Однако, судя по кривым, разброс значений скоростей велик даже для конкретной разновидности пород при атмосферном и высоком давлениях. Это объясняется их минеральным составом, текстурно-структурными особенностями и пористостью [15—18, 30, 57—59 и др.]. Среди кислых образований наибольшие значения скоростей при атмосферном давлении имеют крупнозернистые породы с невысокой пористостью (рис. 1, обр. 7, 8, 12) или с повышенным содержанием кварца (рис. 1, обр. 1). При росте давления до максимального в опыте самые высокие скорости наблюдаются у равномернозернистых гранитов и чарнокитов, а также пород с повышенным содержанием плагиоклаза (30 ÷ 40%) и кварца (20 ÷ 25%). У крупнозернистых гранитов с незначительной пористостью значения $V_{p,s} = f(P)$ увеличиваются с малыми градиентами.

Более высокие скорости в образованиях среднего состава связаны с наличием в них пироксена и роговой обманки. С увеличением давления максималь-

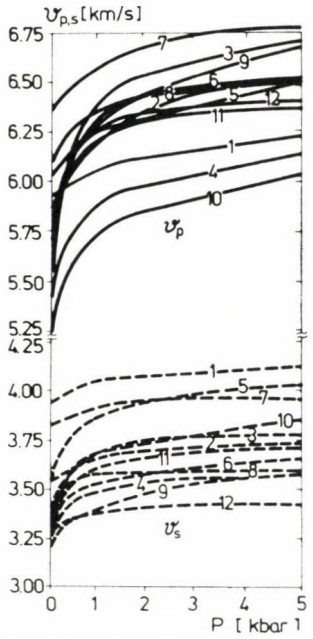


Рис. 1. Изменения скоростей продольных (V_p) и поперечных (V_s) волн в зависимости от гидростатического давления в образцах пород кислого состава. I — кварцит; 2, 7 — чарнокиты I, II; 3, 6 — граниты житомирские I, II; 4 — гранит кировоградский; 5, 9 — граниты порфировидные I, II; 8, 10 — граниты рапакиви I, II; 11 — гранит чудново-бердичевский; 12 — гранит клесовский

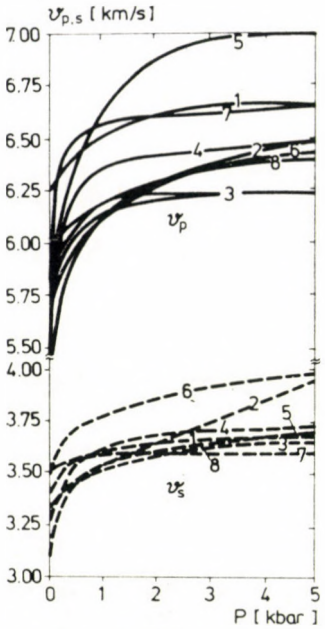


Рис. 2. Изменения скоростей продольных (V_p) и поперечных (V_s) волн в зависимости от гидростатического давления в образцах пород среднего состава. I — чарнокит III; 2 — собит; 3 — гранодиорит; 4, 7, 8 — диориты I, II, III; 5 — гранит осницкий; 6 — порфирит клесовский

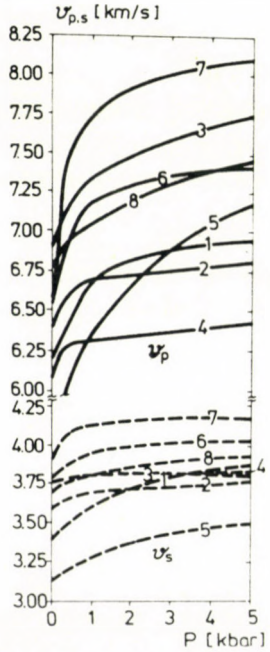


Рис. 3. Изменения скоростей продольных (V_p) и поперечных (V_s) волн в зависимости от гидростатического давления в образцах пород основного состава. 1, 2 — лабрадориты I, II; 3 — габбро-норит; 4 — диабаз; 5 — гнейс Amf—Px—Pl; 6 — пироксенит; 7, 8 — эклогитоподобные породы I, II

ные изменения сокростей оказались присущи породам с повышенным содержанием плагиоклаза и биотита (рис. 2, обр. 5). Прирост же скоростей в образцах, обогащенных кварцем наименьший (рис. 2, обр. 1, 3, 6). Изменения V_p и V_s в породах среднего состава в начальном диапазоне давлений происходят более плавно, а линейный участок $V_{p,s} = f(P)$ появляется несколько позже. Это связано с незначительным содержанием в них кварца и большим количеством плагиоклаза и биотита, которые в целом пластифицируют породу под давлением.

Породы основного состава отличаются высокими значениями V_p и V_s и их большим разбросом во всех диапазонах давлений (рис. 3). Указанные величины V_p и V_s обусловлены, прежде всего, присутствием в породах минералов (гранат, роговая обманка) с повышенными значениями скоростей. Различие же в минеральном составе объясняет широкий спектр наблюдаемых скоростей. Низкие значения $V_{p,s}$ в амфиболопироксено-плагиоклазовом гнейсе (рис. 3, обр. 5) обусловлены многокомпонентностью его минерального состава, повышенным содержанием вторичных минералов и незначительным плагиоклазов. Возможно, сказывается также слоистая структура породы. Высокий рост скорости продольных волн при воздействии давления также объясняется исходной «рыхлостью» породы (связанной со сложностью ее состава) и присутствием в ней способствующих интенсивному росту $V_{p,s}$ минералов (кварц, роговая обманка, пироксен, гранат). Приближение основных пород к мономинеральному составу влечет увеличение скоростей при атмосферном давлении (рис. 3, обр. 3,6). Однако, мономинеральные лабрадориты (рис. 3, обр. 1, 2) имеют невысокие скорости, поскольку, как показало изучение шлифов, они состоят из сильно разориентированных крупных зерен лабрадора со значительно измененными границами. Наибольшие скорости в условиях высокого давления зарегистрированы в наших опытах для образца эклогитоподобной породы, содержащей максимальное количество граната (26%), расположенного среди кварца (42,6%), являющегося упругим материалом, обеспечивающим высококачественный акустических контакт между минералами. Взаимодействие кварца и плагиоклаза (которыми заполнена остальная часть объема образца) объясняет плавное возрастание скоростей с увеличением давления.

На рис. 4—7 приведены изменения упругих параметров от давления. Представлены материалы по модулям Юнга и сдвига (рис. 4, 5), сжимаемости (рис 6) и коэффициенту Пуассона (рис. 7). С увеличением давления от атмосферного до 2 кбар модули продольной (E) и поперечной (G) деформаций увеличиваются по криволинейному закону с высокими градиентами, аналогично скоростям. Дальнейшее повышение давления вызывает изменения E и G по линейному закону, с меньшими градиентами. Как и значения скоростей, эти модули увеличиваются с повышением основности пород. Породы кислого состава характеризуются широкой областью значений E при ат-

мосферном давлении ($\Delta E_{001} = 0{,}90-0{,}45 = 0{,}45$ Мбар), которая при 5 кбар сужается до 0,20 Мбар. Аналогичным образом для средних пород ΔE_{001} составляет 0,35, а для ΔE_5 равно 0,15 Мбар. Для пород основного состава широкий спектр значений E_{001} сохраняется и при давлениях ($\Delta E_{001} = 0{,}5$;

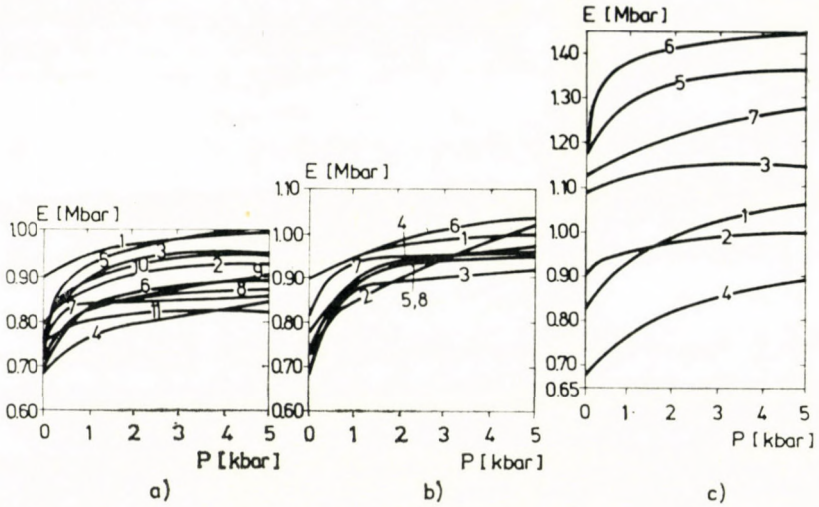


Рис. 4. Зависимости модуля Юнга от изменения гидростатического давления. *а)* образцы пород кислого состава: 1 — кварцит; 2 — чарнокит I; 3, 6 — граниты житомирские I, II; 4 — гранит кировоградский; 5, 8 — граниты порфировидные I, II; 7, 8 — граниты рапакиви I, II; 10 — гранит чудново-бердический; II — гранит клесовский. *б)* образцы пород среднего состава: обозначения те же, что и на рис. 2. *в)* образцы пород основного состава: 1, 2 — лабрадориты I, II; 3 — габбро-норит; 4 — гнейс Amf—Px—Pl; 5 — пироксенит; 6, 7 — эклогитоподобные породы I, II

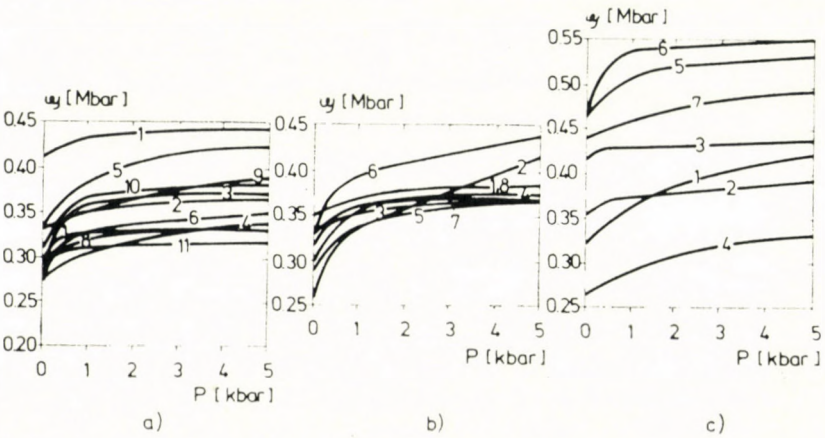


Рис. 5. Изменения модуля сдвига при воздействии гидростатического давления *а)* образцы пород кислого, *б)* среднего, *в)* основного составов. Обозначения те же, что, соответственно, и на рис. 4 *а, б, в*

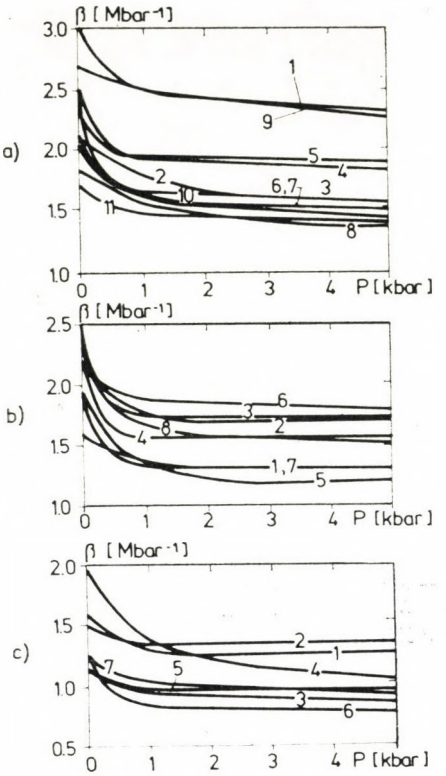


Рис. 6. Изменения сжимаемости в условиях гидростатического давления *а)* образцы пород кислого, *б)* среднего, *в)* основного составов. Обозначения те же, что соответственно и на рис. 4 *а, б, в*

$\Delta E_5 = 0{,}55$ Мбар). Модуль сдвига кислых пород менее чувствителен к воздействию давления ($\Delta G_{001} = 0{,}2$; $\Delta G_5 = 0{,}15$). Для средних ΔG_{001} и ΔG_5 — составляют соответственно 0,15 и 0,1, а основных — 0,2 и 0,22 Мбар.

Закономерности изменения сжимаемости (β) для изученных пород несколько иные (рис. 6). Если при атмосферном давлении наблюдается четкое разделение по сжимамости с повышением основности пород, то в условиях высоких давлений это различие почти отсутствует. Для пород кисого состава $\Delta\beta_{001} = 3{,}6-1{,}2 = 2{,}4$ и $\Delta\beta_5 = 2{,}3-1{,}1 = 1{,}2$; среднего — $\Delta\beta_{001} = 2{,}4-1{,}6 = 0{,}8$ и $\Delta\beta_5 = 1{,}8-1{,}2 = 0{,}6$; основного — $\Delta\beta_{001} = 2{,}0-1{,}2 = 0{,}8$; $\Delta\beta_5 = 1{,}3-0{,}7 = 0{,}6$ Мбар$^{-1}$. Как видно, породы основного состава имеют самые низкие значения сжимаемости, что можно объяснить их текстурно-структурными особенностями и минеральным соством. В наших опытах с минералами установлено, что наибольшей сжимаемостью обладает кварц. Это подтверждается и исследованиями кварцита (рис. 6а, обр. 1). Следовательно, увеличение количества кварца в породе повышает ее сжимаемость. Такую же

роль выполняет калиевый полевой шпат (КПШ). Например, обр. 4, 5, 9 (рис. 6а), содержащие наибольшее количество кварца и КПШ характеризуются максимальными значениями β. Большую сжимаемость имеют крупнозернистые породы, которые даже в гидростатических условиях давления склонны к некоторому разрушению, повышающему коэффициент объемного сжатия при дальнейшем увеличении давления. Присутствие плагиоклаза не способствует увеличению сжимаемости, так как этот минерал весьма пластичный, причем пластичность его с давлением растет. В условиях гидростатического сжатия зерна плагиоклаза стремятся изменить свою форму при том же объеме. Поэтому их влияние на значение β невелико, о чем свидетельствует сжимаемость пород среднего и основного составов.

При исследованиях в условиях высоких давлений особый интерес представляет выяснение особенностей изменения коэффициента Пуассона (σ) горных пород. Известно, что в естественных условиях σ больше у пластичных тел, чем у хрупких. Поэтому коэффициент Пуассона позволяет качественно характеризовать изменения пластичности и хрупкости породы при воздействии высокого давления. Поскольку σ характеризует способность твердого тела к взаимноортогональным деформациям, он может свидетельствовать и о перераспределении внутренних напряжений в объеме образца при высоких давлениях [13].

На основании этих положений проанализируем состояние пород различного состава в условиях гидростатического сжатия. Образованиям кислого состава присущ широкий спектр значений коэффициента Пуассона (от 0,10 до 0,35) (рис. 7а). Минимальные значения σ имеют разности, обогащенные кварцем (кварцит, гранит равномернозернистый и чарнокит); они наиболее хрупкие. Кроме того, низкие значения σ отмечены у образцов крупнозернистых гранитов рапакиви и чудново-бердичевского. Породам с повышенным содержанием плагиоклаза и КПШ присущи высокие значения σ. В условиях больших давлений коэффициент Пуассона кислых образований изменяется по-разному. Однако можно установить некоторые закономерности. Так, породы с большим содержанием кварца (например, кварциты) мало изменяют σ (рис. 7а, обр. 1); с ростом давления незначительно увеличивается их пластичность. Среднезернистые породы с умеренным содержанием кварца характеризуются экстремальными областями изменений σ. Чем больше кварца, тем более явно выражены максимальные значение σ (рис. 7а, обр. 4, 6, 8, 10). Это явление можно объяснить следующим образом. Как уже обсуждалось [21—25], даже в условиях высокого гидростатического давления образец породы находится в сложнонапряженном состоянии в связи с неоднородной деформацией породообразующих минералов. С увеличением содержания кварца — наиболее хрупкого, твердого и достаточно анизотропного минерала — неоднородность распределения напряжений возрастает. Зерна кварца выступают здесь в роли инденторов, стремящихся проникнуть в окружа-

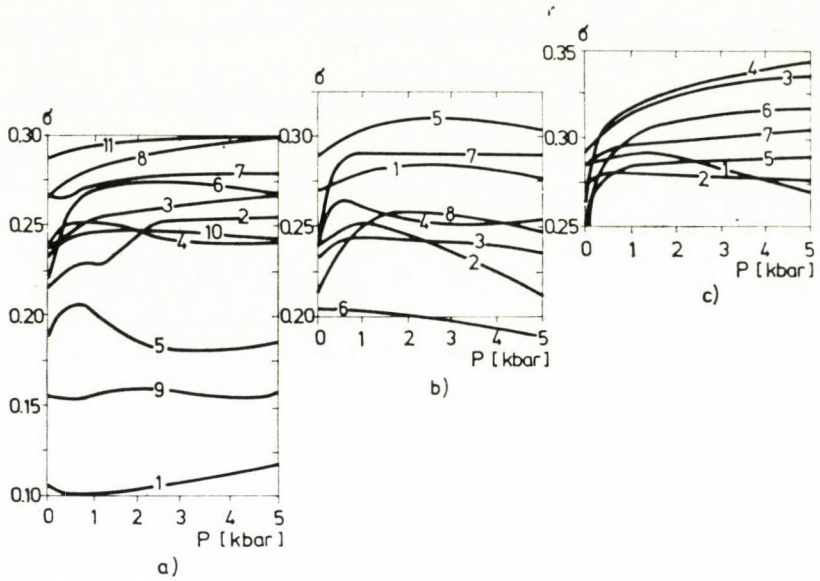


Рис. 7. Изменения коэффициента Пуассона при различном гидростатическом давлении *а)* образцы пород кислого, *б)* среднего, *в)* основного составов. Обозначения те же, что соответственно и на рис. 4 *а, б, в*

ющие их менее упругие минералы (КПШ) и более пластичные (плагиоклаз) или разрушить некоторые из них (пироксен, биотит) вдоль слоев. Это, в свою очередь, приводит к нарушению пропорциональности между продольной и поперечной деформациями $\left(\sigma = \frac{E}{2G} - 1\right)$. В таких условиях сдвиговые деформации увеличиваются, а, следовательно, значения коэффициента Пуассона уменьшаются, что приводит к понижению пластичности породы. С ростом давления вновь возможно увеличение пласличности с временным «залечиванием» вызванных структурных нарушений и, естественно, возрастание коэффициента Пуассона (рис. 7а, обр. 2). Увеличению σ от давления способствует обогащение породы пластичными минералами (плагиоклазом, пироксеном); при этом зависимости $\sigma = f(P)$ выражаются плавными линиями, аналогично кривым V_p и V_s (рис. 7а, обр. 3, 8, 11). Для пород среднего состава (рис. 7б) значения σ при атмосферном давлении и изменения $\sigma = f(P)$ схожи с данными для кислых образований. У пород с повышенным содержанием плагиоклаза значения σ растут во всем диапазоне давлений (рис. 7б, обр. 1, 5, 7). Увеличение в породе кварца и анизотропного биотита приводит к уменьшению с повышением давления значений коэффициента Пуассона (рис 7б, обр. 2,6).

Если породы кислого и среднего состава имеют в большинстве случаев почти одинаковые значения σ при атмосферном и при высоком давлениях ($\sigma_{001} = 0{,}22—0{,}26$ и $\sigma_5 = 0{,}22—0{,}32$), то коэффициент Пуассона образований

основного состава несколько выше ($\sigma_{001} = 0{,}25—0{,}30$; $\sigma_5 = 0{,}27—0{,}35$) (рис. 7в). Значения σ этих пород плавно увеличиваются с ростом давления. На преимущественном большинстве кривых $\sigma = f(P)$ отсутствуют какие-либо аномальные области. Прежде всего это объясняется структурными особенностями и минеральным составом пород. Все они мелкозернистые с повышенным содержанием пластичных минералов (плагиоклаз, пироксен). Ход изменения кривых $\sigma = f(P)$ основных пород позволяет считать, что с увеличением давления эти образования стремятся к более пластичному состоянию, чем кислые и средние.

Сравнение результатов опытов при квази- и гидростатических давлениях и комнатной температуре. Известно, что распределение давления в земных недрах не всегда является гидростатическим. На больших глубинах отклонения от гидростатического режима могут достигать 10 и более процентов. Это несомненно отражается на особенностях изменения упругих параметров горных пород с глубиной. Многие исследователи сопоставляют материалы экспериментального изучения упругих характеристик, полученных в опытах, осуществлявшихся при гидростатическом и квазигидростатическом давлениях. Однако, очень часто это делается без всяких оговорок. В то же время неоднородность распределения давления в квазигидростатических камерах может достигать 10—15%. Это несомненно изменяет упругие характеристики образцов исследуемого минерального вещества по сравнению с их значениями, полученными в гидростатических условиях.

В этой связи нами была выполнена серия опытов, с целью выяснения воздействия на упругие параметры пород неравномерности распределения напряжения в образцах при высоких давлениях. Для этого были изготовлены образцы, идентичные ранее исследованным при гидростатических давлениях до 5 кбар. На рис. 8—10 для сравнения представлены наиболее характерные результаты измерений $V_{p,s} = f(P)$ и $G = f(P)$ в гидростатических и квазигидростатических условиях. Там же указаны погрешности определения соответствующих пара метров. Ход кривых изменений скоростей при гидростатических ($P_г$) и квазигидростатических ($P_к$) давлениях различен и характеризуется определенными закономерностями. Наибольшие расхождения присущи крупнокристаллическим породам. Скорости в этом случае с увеличением давления изменяются плавно (рис. 8, 9). Причем при гидростатическом нагружении образцов они несколько выше, чем при квазигидростатическом. Это связано о увеличением неупругих деформаций, развивающихся в образце породы при дополнительных осевых нагрузках, имеющих место в камерах квазивсестороннего давления типа «цилиндрпоршень», особенно в начальном интервале давлений ($P < 2$ кбар), которые вызывают разрушение первоначальной структуры породы. Аналогичная картина свойственна и обогащенным кварцем среднезернистым разностям с пористостью более 1%. Однако, эти различия выражены менее четко (рис. 8, 9, обр. 3). Рассмотрим далее характер изменения

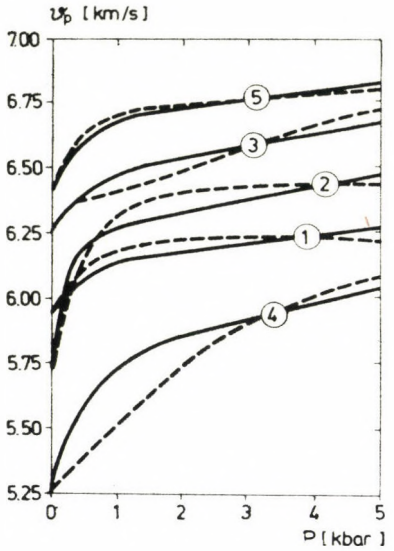


Рис. 8. Изменения V_p при гидростатическом (сплошние линии) и квазигидростатическом (пунктирные линии) давлениях в образцах различных пород 1 — кварцит; 2 — гранит порфировидный I; 3 — чарнокит II; 4 — гранит рапакиви II; 5 — лабрадорит II

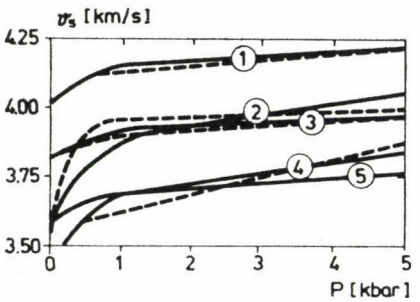


Рис. 9. Изменения V_s при гидростатическом (сплошные линии) и квазигидростатическом (пунктирные линии) давлениях в образцах различных пород. Обозначения те же, что соответственно и на рис. 8

коэффициента Пауссона при увеличении давления (рис. 10, обр. 3, 4). Для крупнозернистых и пористых пород в начальном интервале давлений σ резко уменьшается. Увеличивается осевое напряжение вдоль образующей образца, повышается его хрупкость. Напряжения, достигая предельной величины, релаксируют, вызывая различного вида структурные изменения в образце (хрупко-пластические микронарушения структуры породы). При дальнейшем повышении нагрузки преобладающее осевое давление уменьшается и образец приходит в состояние гидростатического сжатия. Но, поскольку предшест-

вующие разрушения способствуют последующему уплотнению породы, ее упругие параметры с увеличением давления могут быть выше, чем у подобных пород при тех же гидростатических давлениях.

Мелко- и среднезернистые малопористые породы характеризуются значительно меньшими различиями скоростей в условиях квази- и гидростатических давлений. Причем с увеличением давления скорости при квазигидростатическом давлении оказались несколько выше, чем в гидростатике (рис. 8, 9, обр. 1, 2). Это явление можно объяснить, рассмотрев данные об изменении коэффициента Пуассона (рис. 10, обр. 1, 2). Пластические деформации, возникающие в этих породах в результате неравномерного распределения напряжений в рабочем объеме камеры квазигидростатического давления ($P_к$), ослабляют эффект хрупкого разрушения породы. Коэффициент Пуассона в начальном интервале $P_к$ возрастает, указывая на повышение пластичности минерального вещества и его уплотнение. Повышение значений упругих параметров в квазигидростатике происходит значительно эффективнее, чем в гидростатике.

Крупнокристаллические мономинеральные образования и монокристаллы в начальном интервале (до 3 кбар) претерпевают дополнительные осевые напряжения в камере квазигидростатического давления, что способствует более резкому повышению упругих констант этих пород. При дости

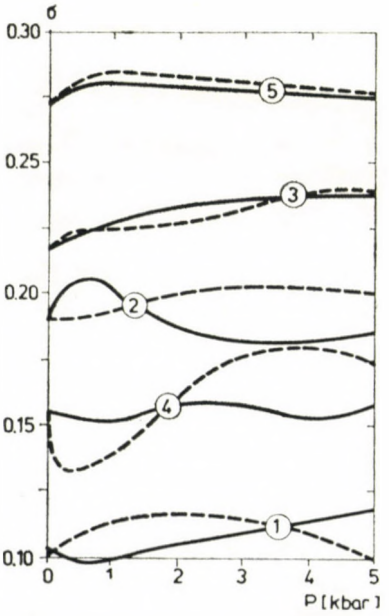


Рис. 10. Изменения коэффициента Пуассона при гидростатическом (сплошные линии) и квазигидростатическом (пунктирные линии) давлениях по образцам разных пород. Обозначения те же, что и на рис. 8

жении определенных значений P их упругие характеристики начинают уменьшаться (рис. 10, обр. 5) за счет разрушающего действия анизотропных внутренних напряжений в объемах монокристаллов.

Таким образом, дополнительные напряжение, возникающие в образцах горных пород как следствие нарушения при экспериментах гидростатических условий, могут увеличивать или уменьшать их упругие свойства. Эти явления связаны с текстурно-структурными особенностями, пористостью и минеральным составом проб, а также временем приложения давления в опыте. Крупнокристаллические обогащенные кварцем среднезернистые кислые породы при дополнительных напряжениях, возникающих в квазигидростатических условиях, в начальном интервале давлений ухудшают свои упругие параметры по сравнению с гидростатическим режимом. При дальнейшем повышении давления и уменьшении неоднородности распределения напряжений значения упругих постоянных приближаются к наблюдаемым в гидростатической обстановке. Мелкозернистые породы среднего и основного составов в условиях дополнительных напряжений улучшают, обычно, свои упругие характеристики. Однако, при повышении квазигидростатического давления и уменьшении неоднородности распределения напряжений этот эффект исчезает. При давлениях более 3 кбар различия между значениями упругих параметров одноименных горных пород разного состава, измеренных в аппаратах квази- и гидростатических давлений, уменьшаются и в большинстве случаев не превышают ошибок определений.

Влияние высоких температур при атмосферном давлении. Изменения упругих параметров минерального вещества в температурных полях на разных глубинах можно оценить лишь при тщательном их исследовании в условиях воздействия различных давлений, в том числе и при атмосферном [7, 12, 28, 29, 34, 46 и др.]. Влияние высоких температур на изменение V_p и V_s в атмосферных условиях изучено на образцах, аналогичных исследованным нами при высоких давлениях.

Результаты экспериментального изучения $V_{p,s}=f(T)$ представлены на рис. 11а, б, в. Средние значения уменьшения скоростей от в интервале 20—400°С в изученных породах кислого состава составляют (в %) $\frac{\Delta V_p}{V_p}=45$ и $\frac{\Delta V_s}{V_s}=40$; среднего — 40 и 35, основного — 30 и 25. В кварците (рис. 11а, обр. 1) скорости в указанном диапазоне температур измеяются лишь на 10%, аналогично стеклам и плавленному кварцу.

Различия изменений $V_{p,s}=f(T)$ в породах всех трех групп оказались не только количественными. В образованиях кислого состава при температурах до 100°С скорости уменьшаются с небольшими градиентами (порядка 0,002 для V_p и 0,001 км/сек. °С для V_s). Далее, до 300°С, можно выделить область наибольшего снижения скоростей $\left(\frac{dV_p}{dT}\approx 0{,}010,\ \frac{dV_s}{dT}\approx 0{,}005\ \text{км/сек}\cdot{}^\circ\text{С}\right)$.

Температура выше 300°С вызывает более плавное их уменьшение $\frac{dV_p}{dT} \approx$ $\approx 0{,}006$; $\frac{dV_s}{dT} \approx 0{,}002$ км/сек·°С). Для пород среднего состава четко выделяются лишь две области снижения V_p и V_s. Первая — в интервале от 20 до 250°С $\left(\frac{dV_p}{dT} \approx 0{,}008; \frac{dV_s}{dT} \approx 0{,}006 \text{ км/сек·°С}\right)$, вторая — 250 ÷ 400°С $\left(\frac{dV_p}{dT} \approx 0{,}006; \frac{dV_s}{dT} \approx 0{,}005 \text{ км/сек·°С}\right)$.

В основных породах скорости изменяются как и в кислых, но первая зона плавного уменьшения V_p и V_s иногда ограничивается 200°С $\left(\frac{dV_p}{dT} \approx\right.$ $\left. \approx 0{,}003; \frac{dV_s}{dT} \approx 0{,}002 \text{ км/сек·°С}\right)$. Значительные градиенты изменения скоростей обнаружены в интервале 170—250°С: $\frac{dV_p}{dT} \approx 0{,}020$ и $\frac{dV_s}{dT} \approx 0{,}008$ км/сек·°С. Затем они уменьшаются соответственно до 0,003 ÷ 0,010 и 0,002 ÷ ÷ 0,005 км/сек·°С.

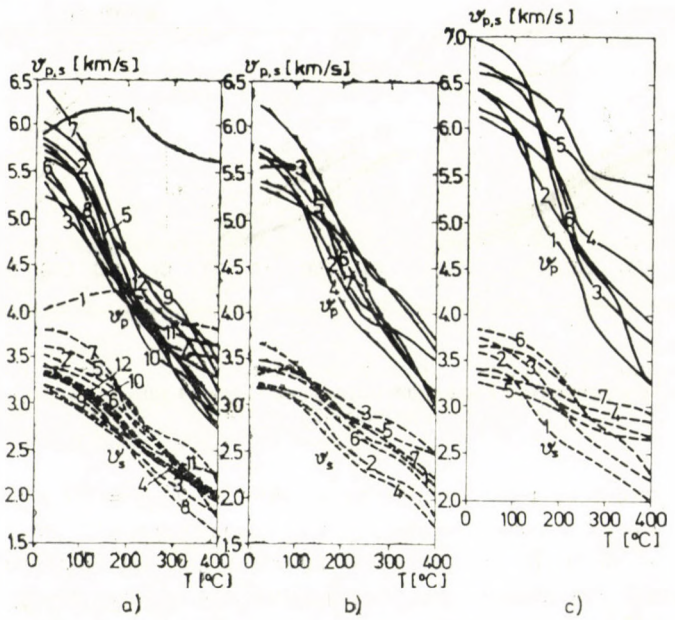


Рис. 11. Изменения V_p и V_s от температуры при атмосферном давлении *а)* в образцах пород кислого состава: 1 — кварцит; 2, 7 — чарнокиты I, II; 3, 6 — граниты житомирские I, II; 4 — гранит кировоградский; 5, 9 — граниты порфировидные I, II; 8, 10 граниты рапакиви I, II; 11 — гранит чудново-бердичевский; 12 — гранит клесовский *б)* в образцах пород среднего состава: 1 — чарнокит III, 2 — собит; 3 — гранодиорит; 4 — гранит осницкий; 5 — порфирит клесовский; 6, 7 — диориты II, III *в)* в образцах пород основного состава: 1, 2 — лабрадориты I, II; 3 — габбро-норит; 4 — даибаз; 5 — пироксенит; 6, 7 — эклогитоподобные породы I, II

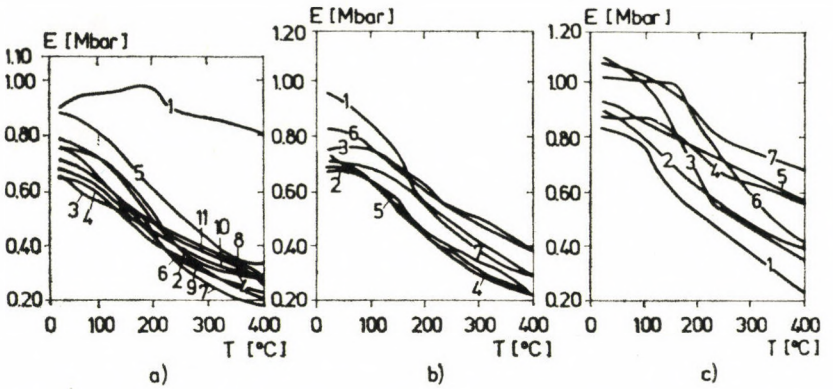


Рис. 12. Изменения модуля Юнга от температуры при атмосферном давлении *а)* образцы пород кислого состава: 1 — кварцит; 2 — чарнокит I; 3, 6 — граниты житомирские I, II; 4 — гранит кировоградский; 5, 8 — граниты порфировидные I, II; 7, 9 — граниты рапакиви I, II; 10 — гранит чудново-бердичский; 11— гранит клесовский *б)* образцы пород среднего состава: 1 — чарнокит III; 2 — собит; 3 — гранодиорит; 4, 7 — диориты I, III; 5 — гранит осницкий; 6 — порфирит клесовский *в)* образцы пород основного состава: обозначения те же, что и на рис. 11 в

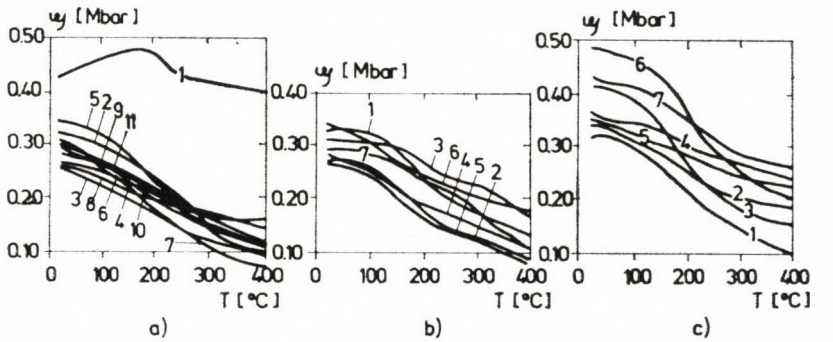


Рис. 13. Изменения модуля сдвига от температуры при атмосферном давлении *а)* образцы пород кислого, *б)* среднего, *в)* основного составов. Обозначения те же, что соответственно и на рис. 12а, б; IIв

Обнаруженные закономерности изменения $V_{p,s} = f(T)$ удобно обсуждать по материалам вычислений упругих характеристик минерального вещества, приведенных на рис. 12—15. Известно, что основным фактором, обусловливающим уменьшение упругих параметров горных пород при нагреве, является нарушение их природной структуры за счет неравномерного и анизотропного расширения породообразующих минералов в температурных полях. В этой связи полезно привести данные (рис. 16) о тепловом коэффициенте линейного расширения некоторых минералов [5,51]. Как видно, наибольшие значения $\Delta\alpha/\alpha$ присущи кварцу, наименьшие — плагиоклазу, а микроклин занимает промежуточное положение. Следовательно, обогащенным

кварцем породам будут присущи максимальные изменения упругих параметров, а плагиоклазом — минимальные. Очевидно, большие изменения характерны для многокомпонентных анизотропных образований. Это подтверждается результатами опытов. Например, кислые породы, содержащие большое количество кварца, отличаются наибольшими изменениями скорости ультразвука. Образования основного состава менее подвержены температурным изменениям, так как состоят в основном из плагиоклаза. Эти же породы, значительно обогащенные кварцем и гранатом (рис. 11в, обр. 7), характеризуются довольно значительными изменениями скорости от температуры.

Несмотря на то, что в образованиях различного состава V_p и V_s уменьшаются от температуры (в интервале 50—400°С) по-разному, изменение модулей Юнга (E) и сдвига (G) остаются для исследованных нами групп пород практически одинаковыми (соответственно —0,13 и —0,06 Мбар/°С).

Состояние породы при нагреве более четко может быть охарактеризовано изменениями сжимаемости и коэффициента Пауссона. Известно, что сжимаемость уменьшается с ростом основности пород и увеличивается с повышением содержания в них кварца. При высоких температурах ее изменения зависят также и от минерального состава, структурно-текстурных особенностей, пористости. В целом с увеличением температуры сжимаемость всех пород возрастает, наибольшие изменения β присущи кислым образова-

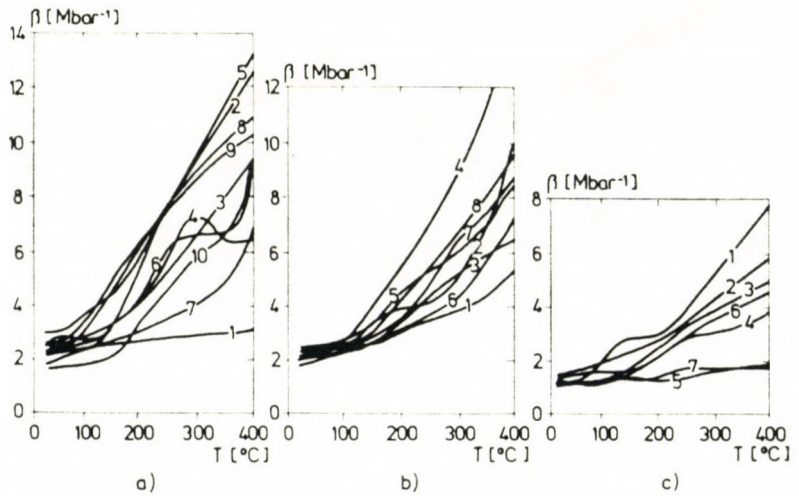


Рис. 14. Изменения сжимаемости от температуры при атмосферном давлении: *а)* образцы пород кислого состава: 1 — кварцит; 2 — чарнокит I; 3, 5 — граниты житомирские I, II; 4 — гранит кировоградский; 6, 8 — граниты рапакиви I, II; 7 — гранит порфировидный II; 9 — гранит чудново-бердичевский; 10 — гранит клесовский; *б)* образцы пород среднего состава: 1 — чарнокит III; 2 — собит; 3 — гранодиорит; 4, 7, 8 — диориты I, II, III; 5 — гранит осницкий; 6 — порфирит клесовский; *в)* образцы пород основного состава: обозначения те же, что и на рис. 11;в

ниям (рис. 14а), наименьшие — основным (рис. 14в). Для пород одного и того же состава характерна следующая закономерность: чем выше пористость и чем больше в породе вторичных минералов, тем значительнее увеличение сжимаемости. Это позволяет полагать, что при изменении температуры породы с низкими упругими характеристиками активнее ухудшают свою структуру и становятся более рыхлыми, чем породы не претерпевшие вторичных преобразований.

Такое явление вполне закономерно, так как измененные породы характеризуются несовершенными упругими связями на границах зерен породообразующих минералов. При увеличении температуры упругие свойства пород в зонах контактов ухудшаются более интенсивно. Можно поэтому предположить, что в тектонически активных зонах влияние температуры на изменение упругих параметров пород более значительно, чем в спокойных областях. Наблюдается также зависимость от зернистости породы: чем больше размеры зерен, тем значительнее изменяется сжимаемость. Характерна еще одна особенность: сжимаемость мономинеральных пород возрастает от температуры значительно меньше, чем многокомпонентных образований (рис. 14а, обр. 1).

Для оценки механизма изменения упругих характеристик пород при высоких температурах, обусловленного перераспределением внутренних микронапряжений в объеме образца, рассмотрим зависимости коэффициента Пуассона от температуры (рис. 15). Этот параметр изменяется по весьма сложным законам, отражая роль термонапряжений при нагреве. Образования кислого состава имеют широкий спектр значений σ в интервале температур от 20 до 400°С (рис. 15а). Средним присущ довольно узкий диапазон значений δ_0 (0,18 ÷ 0,27) при комнатной температуре, который значительно расширяется при 400°С ($\sigma_T = 0{,}02 \div 0{,}22$) (рис. 15б). При нагреве основных пород разброса знаений почти не изменяется (рис. 15в; $\Delta\sigma_0 = 0{,}08$; $\Delta\sigma_T = 0{,}09$). Характер изменений $\sigma = f(T)$ неоднозначен не только для пород различного состава, но и одноименных. Последнее обусловлено особенностями их структуры и вариациями содержания породообразующих минералов. В интервале 20—100°С происходит небольшое плавное изменение σ. В некоторых же случаях коэффициент Пуассона увеличивается в связи с термоупругим уплотнением породы (рис. 15а, обр. 4; рис. 15б, обр. 7; рис. 15в, обр. 3, 6). Иногда имеет место уменьшение σ, обусловленное низкотемпературной релаксацией термоупругих напряжений и, следовательно, разупрочнением минерального вещества. Эта область изменений $\sigma = f(T)$ характеризуется в основном некоторой термостойкостью минералов, а также водонасыщенностью породы. Изменение объема адсорбционной воды и переход ее в новое состояние приводит к активному перемещению последней в образце. Вода проникает через слаборазвитые микротрещины к поверхности образца или локализуется до определенной температуры в объеме

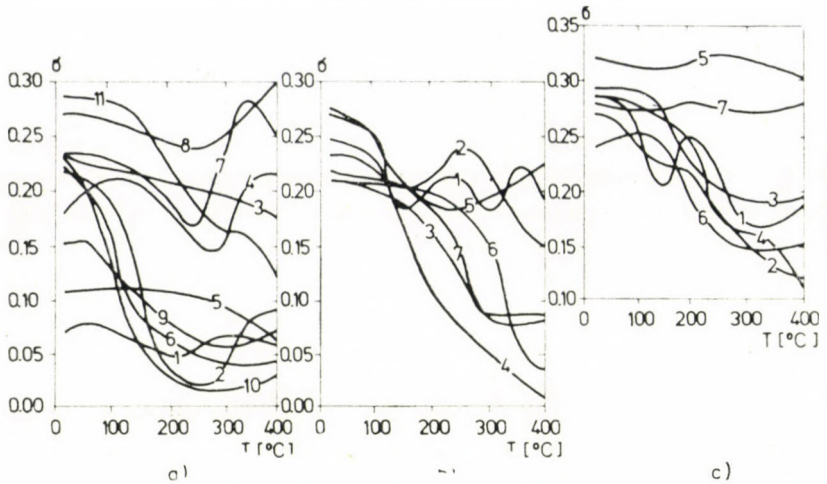


Рис. 15. Изменения коэффициента Пуассона от температуры при атмосферном давлении; *а)* образцы пород кислого, *б;* среднего, *в)* основного составов. Обозначения те же, что соответственно и на рис. 12 а, б; 11 в

пробы, производя расклинивающее действие, которое ослабляет межмолекулярные связи. Вода, перераспределяемая таким образом при температурах менее 100°С, в некоторых случаях может повышать пластичность породы (σ возрастает). Локализовавшаяся в замкнутом объеме (при температурах 100°С и выше), она увеличивает существующие термонапряжения. Это приводит к перенапряжениям отдельных частей образца. Порода становится более хрупкой (σ уменьшается).

Дальнейший нагрев до 250—280°С характеризуется, как правило, наибольшими изменениями упругих параметров (особенно для пород кислого и среднего составов). Объемное расширение породообразующих минералов приводит к уменьшению расстояния между плоскостями раздела отдельных минералов. Увеличиваются силы деформации последних за счет роста термоупругих напряжений. Прочность связей в этом случае улучшается. Возрастающие деформационные силы снижают пластичность породы и поэтому коэффициент Пуассона уменьшается.

При увеличении температуры происходит также анизотропное тепловое расширение минералов, имеющих по разным кристаллографическим направлениям различные значения коэффициента линейного теплового расширения (рис. 16). Это обусловливает постоянное развитие релаксационных явлений на границах зерен, которые проявляются в виде вязкого скольжения между минералами. Последнее приводит к деформационным изменениям отдельных минералов и всего образца. Неравномерно усиливаясь по мере увеличения температуры, эти явления на определенном этапе становятся основными и приводят зерна породообразующих минералов к хрупко-пластическим деформациям.

В некоторых случаях при негреве свыше 250°С пластифицирующее действие температуры может вызвать увеличение коэффициента Пуассона (рис. 15а, обр. 1, 2, 4, 8, 9; рис. 15б, обр. 1, 2, 5; рис. 15в, обр. 1, 5, 7). Рост температуры выше 300°С чаще всего способствует вторичному процессу накопления термоупругой энергии за счет усиления тепловых колебаний атомов кристаллической решетки минералов. Охлаждение образцов от 400 до 300—250°С подтверждает это предположение. То-есть, при уменьшении температуры изменения упругих параметров оказались такими же, как и при увеличении. Следовательно, в указанном интервале температур изменения упругих характеристик пород обусловлены в основном их минеральным составом, а не структурой и ее нарушениями во время нагрева.

Высказанные выше предположения о влиянии температуры (<400°С) на упругое состояние пород подтверждаются также тщательным изучением шлифов исследованных образцов до и после их нагрева. В отдельных минералах установлено появление микротрещиноватости (наиболее отчетливо в кварце и полевых шпатах). Наблюдается сильное волнистое (а иногда «блоковое») угасание кварца, указывающее на механические деформации последнего. Следует отметить, что более интенсивные изменения присущи крупным (свыше 0,3 мм в поперечнике) зернам кварца. Мелкие же почти не изменяют своей структуры. Кроме того, обнаружена деформация и миграция межзерновых границ, приобретающих при этом зубчатую и извилистую конфигурацию.

Одновременное воздействие высоких температур и квазигидростатических давлений. Исследованы скорости распространения продольных и поперечных волн и упругие параметры (E, G, β и σ) некоторых пород Украинского щита в опытах по трем типам программ термобарических режимов,

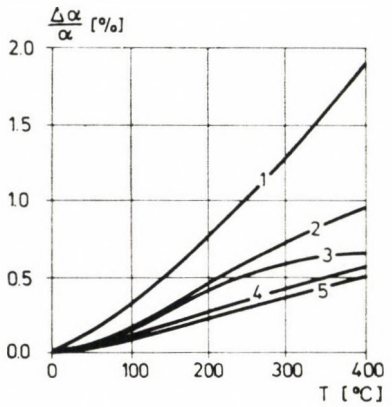


Рис. 16. Относительное изменение коэффициента объемного расширения минералов от температуры; 1 — кварц, 2 — гранит, 3 — микроклин, 4 — плагиоклаз (№ 44), 5 — плагиоклаз (№ 23)

соответствующих конкретным районам (рис. 17). Объектами изучения также являлись образцы пород кислого, среднего, и основного составов (см. таблицу).

Рассмотрим некоторые общие закономерности изменений скоростей в этих породах для глубинных термобарических условий второго типа (рис. 18). В начальных PT режимах опытов (интервал глубин 2—5 км) значения V_p и V_s

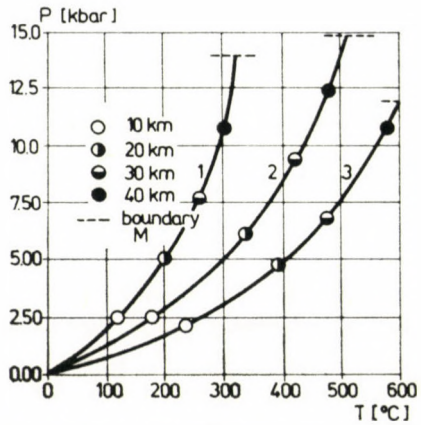


Рис. 17. Программы опытов, соответствующих распределению давлений и температур с глубиной в земной коре юго-западной (1 — первый тип), центральной (2 — второй тип) и юго-восточной (3 — третий тип)частей Украинского щита

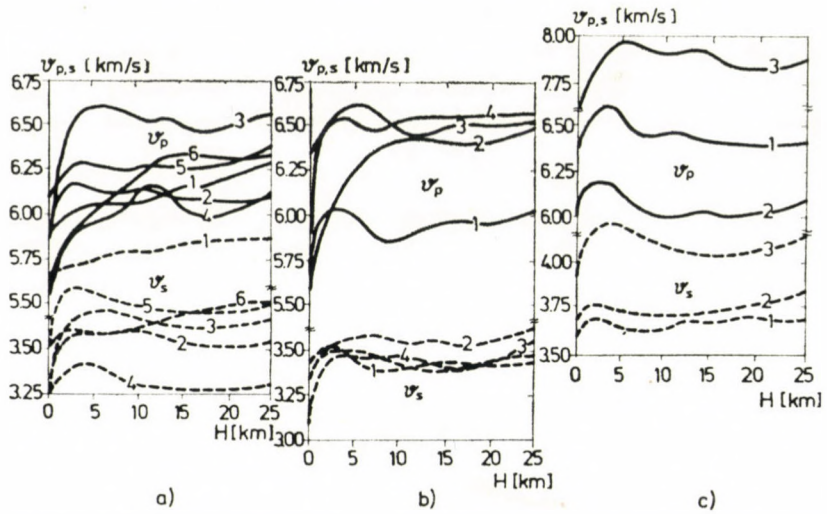


Рис. 18. Изменения V_p и V_s в зависимости от глубины; *а)* в образцах пород кислого состава: 1 — кварцит, 2 — чарнокит I; 3 — гранит житомирирский I; 4 — гранит кировоградский; 5 — гранит порфировидный I; 6 — гранит рапакиви II; *б)* в образцах пород среднего состава: 1 — собит; 2, 4 — диориты I, II; 3 — гранит осницкий; *в)* в образцах пород основного состава: I — лабрадорит II; 2 — диабаз; 3 — эклогитоподобная порода I

увеличиваются также, как при соответствующих давлениях и только комнатной температуре. Достигнув определенных величин они начинают уменьшаться. Снижение скоростей наблюдается, как правило, до глубин 7—10 км. Затем они в некоторых случаях вновь начинают возрастать. На кривых $V_p, V_s = f(PT) = f(H)$ выделяются зоны понижения скоростей. Особенно четко они проявляются для образцов пород среднего и основного составов (рис. 18 б, в). Дальнейший рост PT-параметров (то-есть, увеличение глубины) на изменение V_p и V_s действует по-разному. В ряде случаев на кривых скоростей характерно проявление новых экстремальных зон, вначале максимальных (на глубинах 12 ÷ 15 км), а затем минимальных (15 ÷ 20 км). Иногда же области таких вторичных экстремумов отсутствуют. Тогда после первого максимума (глубины 2—5 км) скорости плавно уменьшаются и, достигнув минимума (H = 14—18 км), вновь постепенно увеличиваются. Обнаруженные закономерности для V_s выражены менее четко.

Сопоставляя средние значения изменений V_p и V_s в породах кислого, среднего и основного составов при различных P, T и PT-режимах, можно отметить следующие особенности. Наибольшие изменения скоростей при P = 5 кбар и T = 20°C присущи породам среднего состава. Для этих же пород характерны максимальные изменения V_p и V_s от температуры при атмосферном давлении. Однако, в них же наблюдается самый интенсивный рост скоростей при одновременном воздействии P и T. Приложенное внешнее давление почти полностью компенсирует возможные механические изменения структуры указанных пород, вызываемые воздействием высоких температур. Поэтому различие между $V_p = f(P_5)$ и $V_p = f(P_5 T_{300}) = f(H)$ оказалось незначительным (0,26 км/сек). В породах основного состава наблюдаются наименьшие изменения скоростей от давления, в то время как от температуры они весьма значительны. При одновременном воздействии P и T на образцы пород основного состава влияние одновременно давления и температуры оказалось больше, чем самого давления: $V_p(P_{5кб}) - V_p(H_{20км}) = 0{,}50$ км/сек. Поэтому на глубинах порядка 20 км значения V_p и V_s могут соответствовать таковым в этих же породах на дневной поверхности. Изменения скоростей в кислых образованиях при различных термодинамических условиях характеризуются промежуточным положением между средними и основнюми.

Наблюдаемые закономерности изменения V_p и V_s в зависимости от P, T и PT связаны, прежде всего, с особенностями минерального состава и структуры образцов исследованных пород. Например, для среднезернистых разностей с наиболее многообразным содержанием минералов и сильно обогащенных плагиоклазом (породы среднего состава) при увеличении PT-параметров наблюдаются наибольшие увеличения скоростей за счет преобладания компенсирующего воздействия давления. Обогащенные кварцем кислые крупнозернистые породы и эклогитоподобные основные образования менее чувствительны к компенсирующему внешнему давлению. Это, как уже от-

мечалось, связано с неравномерным распределением напряжений, более четко выраженным у крупнозернистых мономинеральных пород при любых видах внешних воздействий. Подтверждением этого предположения служат данные о динамике изменений их E, G, β и σ в условиях одновременного воздействия P и T. На рис. 19—22 представлены зависимости от глубины указанных упругих параметров пород среднего, кислого и основного составов по PT-программе второго типа (см. рис. 17).

Сравним значения модулей Юнга (E), рассчитанные по данным изменений V_p и V_s при гидростатическом давлении и комнатной температуре, с результатами, полученными в опытах при одновременном воздействии квазигидростатического давления и высоких температур. Следует отметить, что если при увеличении только P модуль продольной деформации возрастает плавно для всех изученных нами разновидностей пород, то при одновременном воздействии P и T он, достигая какого-то максимального значения в интервале 3—4 км, в дальнейшем или не изменяется вообще, или уменьшается, образуя минимум $E = f(H)$ на глубинах 12—18 км. При PT, соответствующих глубинам более 20 км, чаще всего E вновь возрастает. Расположение минимумов $E = f(H)$ связано с особенностями минерального состава пород. Для кислых образований они наблюдаются на глубинах 17 ÷ 18 км, средних — 10 ÷ 15 и основных — 12 ÷ 16 км. При одновременном воздействии P и T значения модуля Юнга оказались меньшими, чем в условиях только гидростатического давления. Лишь в некоторых случаях (рис. 19а, обр. 1; рис. 19в, обр. 3) они несколько выше. Наиболее четко это наблюдается для сильно обогащенных кварцем эклогитоподобных пород. Таким образом, коэффициент пропорциональности между приложенными силами и величиной деформации вдоль

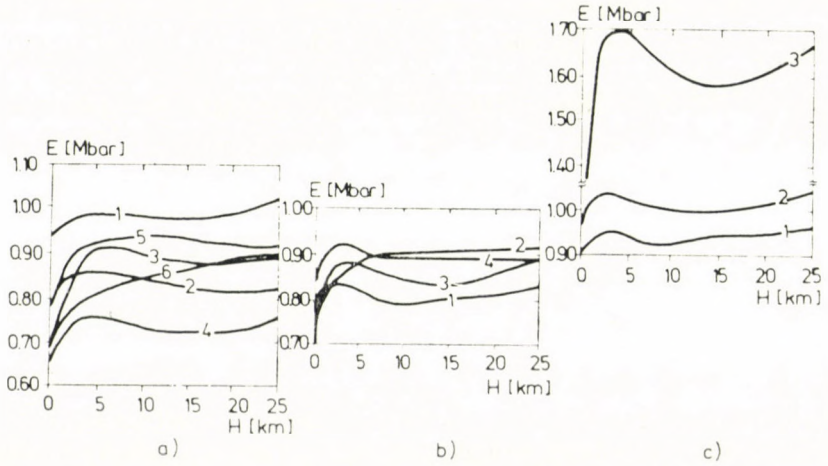


Рис. 19. Изменения модуля Юнга в зависимости от глубины *а)* образды пород кислого, *б)* среднего, *в)* основного составов. Обозначения те же, что соответственно и на рис. 18 а, б, в

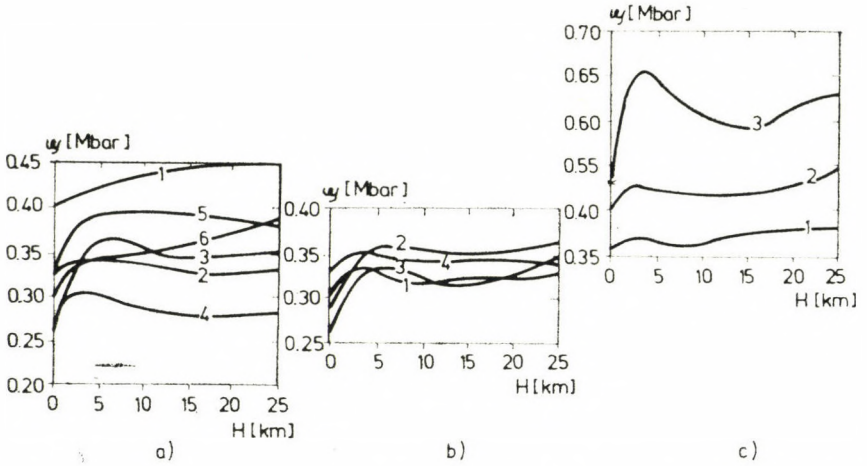


Рис. 20. Изменения модуля сдвига в зависимости от глубны. *а)* образцы пород кислого, *б)* среднего, *в)* основного составов. Обозначения те же, что и на рис. 18 а, б, в

оси действия главных напряжений, на больших глубинах, практически зависит от внешнего компенсирующего давления. Температура в этом случае играет роль пластифицирующего фактора, хотя с ее изменениями иногда связано появление зон пониженной упругости пород на глубинах от 5 до 30 км.

Закономерности изменения модуля сдвига (G) в PT условиях опытов, соответствующих различным глубинам (рис. 20), аналогичны изменениям модуля Юнга. Однако выражены они менее четко. Следовательно, модуль сдвига (подобно V_s) менее чувствителен к воздействиям P и T.

Интересно сопоставить данные о динамической сжимаемости (β) изученных пород для термобарического режима второго типа (рис. 21). Как известно, сжимаемость характеризует способность пород к всестороннему сжатию, а значит и к изменению плотности за счет внешнего всестороннего давления. При высокотемпературных ($T = 400°C$) исследованиях нами обнаружено увеличение β в 4—6 раз, что связано с термомеханическими изменениями пород. Гидростатическое же давление до 5 кбар уменьшает сжимаемость не более чем в два раза (увеличение плотности до 2%). В случае увеличения температуры при атмосферном давлении, а также роста давления в условиях комнатной температуры, сжимаемость изменяется плавно, экстремальных областей не наблюдается. При одновременном воздействии P и T сжимаемость изменяется по сложным законам, а иногда $\frac{d\beta}{dH}$ меняет свой знак на противоположный. На кривых $\beta = f(H)$ наблюдаются экстремальные области с аномалиями, достигающими на различных глубинах не более 0,3 Мбар$^{-1}$. В пересчете на плотность это соответствует ее уменьшению на 0,02—0,05%. Таким образом, разуплотнение пород, вызываемое влиянием температуры,

лишь частично компенсируется давлением. При одновременном воздействии P и T сжимамость остатся выше, чем в обстановке чисто гидростатического давления. Например, при 5 кбар и 300°С для пород кислого состава $\Delta\beta = \beta_H - \beta_p \approx 0{,}7$ Мбар$^{-1}$ (в пересчете на плотность $\frac{\Delta\varrho}{\varrho} \approx 0{,}1\%$). Для средних и основных пород $\Delta\beta$ соответственно уменьшается до $0{,}3 \div 0{,}5$ Мбар$^{-1}$.

Следовательно, поведение сжимаемости горных пород в условиях одновременного воздействия высоких P и T свидетельствует о весьма сложных процессах, происходящих при различных термодинамических режимах. PT-обстановки, соответствующие глубинам порядка 3—4 км, уплотняют породу. Этому иногда способствует и температура. При PT-параметрах, соответствующих 5—10 км, в некоторых случаях воздействие T разуплотняет породу (сжимаемость увеличивается). На кривых $\beta = f(H)$ в этом интервале глубин можно наблюдать зоны более высоких значений β (наиболее четко это проявляется у образований кислого состава, рис 21а). При дальнейшем повышении PT наблюдается вторая область уменьшения β. Следовательно, глубже $10 \div 18$ км порода вновь начинает уплотняться.

С целью более глубокого понимания природы изменений физико-механических свойств минерального вещества на больших глубинах рассмотрим закономерности изменения коэффициента Пуассона (σ) при высоких давлениях и температурах (рис. 22). Сопоставим данные $\sigma_\varrho = f(P)$, $\sigma_T = f(T)$ и $\sigma_H = f(PT) = f(H)$.

Полиминеральные образования при нагреве до 250°С теряют свою пластичность и приобретают значительную хрупкость за счет накопления в объемах изучаемых образцов анизотропных термонапряжений. При дальнейшем повышении температуры напряжения релаксируют в виде хрупко-пластических нарушений первоначальной структуры. Последняя становится более пластичной и, следовательно, восприимчивой к внешним воздействиям. В условиях комнатной температуры увеличение давления пластифицирует

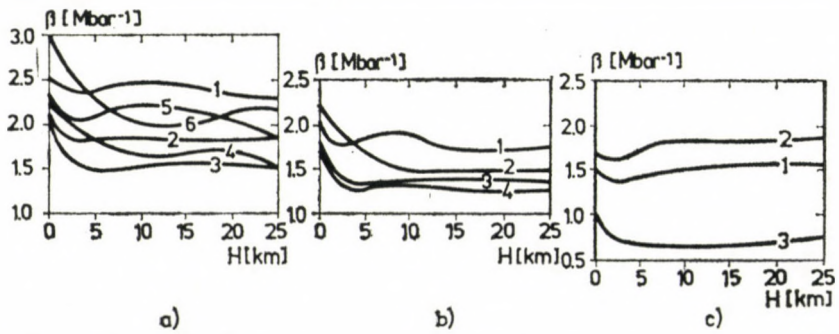


Рис. 21. Изменения сжимаемости в зависимости от глубины. *а)* образцы пород кислого, *б)* среднего, *в)* основного составов. Обозначения те же, что соответственно и на рис. 18 а, б, в

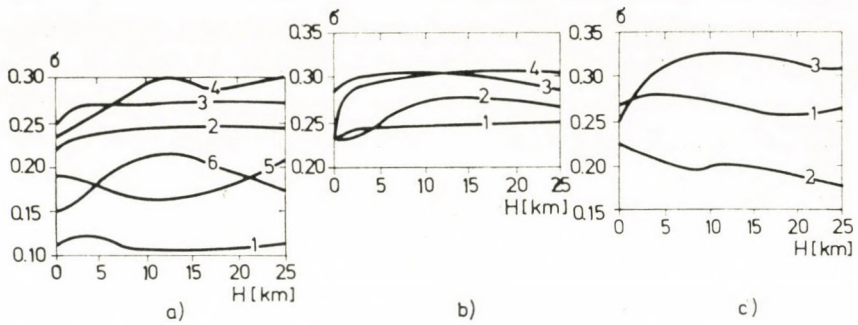


Рис. 22. Изменения коэффициента Пуассона в зависимости от глубины; *а)* образцы пород килого, *б)* среднего, *в)* основного составов. Обозначения те же, что соответственно и на рис. 18 а, б, в

породу, ее коэффициент Пуассона возрастает. Основываясь на приведенных фактах, можно качественно охарактеризовать изменения пород, как бы погружаемых на различные глубины. Например, в начальном интервале PT, соответствующем глубинам 5—10 км (1—2,5 кбар; 120—180°С), воздействие давления преобладает. Порода становится динамичной и, следовательно, более пластичной. Температура заметно способствует этому. Так, даже для гранитов рапакиви, которые менее пластичны ($\sigma_{001} = 0{,}15$), значения коэффициента Пуассона при одновременном воздействии P и T (соответствующих глубине 7 км) составляет около 0,20 (рис. 22а, обр. 6). В условиях гидростатического и квазигидростатического давлений (2 кбар) при температуре 20°С коэффициент Пуассона равен 0,16. При 150°С и атмосферном давлении величина σ уменьшается до 0,10.

Повышение пластичности с глубиной присуще образованиям любого состава. Однако, на глубинах 10 и более км не все они ведут себя одинаково. Для некоторых характерно уменьшение пластичности (σ_H с увеличением PT уменьшается). Одновременное воздействие давлений и темепратур не обеспечивает необходимой релаксации неоднородных напряжений, возникающих в образцах. Порода стремится к более упругому и одновременно более хрупкому состоянию. Это явление характерно для крупнозернистых и мономинеральных пород: порфировидные граниты, граниты рапакиви, лабрадориты (рис 22а, обр. 46,; рис. 22в, обр. 3). Равномернозернистые породы, обогащенные пластичными минералами (плагиоклазом и пироксеном), менее чувствительны к изменениям термодинамических условий больших глубин. Об этом свидетель ствуют данные $\sigma = f(H)$ для образований среднего состава.

Упругие характеристики образцов некоторых пород были исследованы нами по всем трем типам программ опытов при одновременном изменении давления и температуры, соответствующих их распределению в земной коре различных частей Украинского щита (рис. 17) [15, 38, 39, 61]. Аппаратура высоких квазигидростатических давлений и температур, созданная в Отделе

физических свойств вещества Земли Института геофизики АН УССР (Киев) [18, 28, 29] позволяет осуществлять моделирование термодина мических режимов до глубин порядка 30 км ($P \approx 7$ кбар, $T \approx 350°C$). Результаты опытов представлены на рис. 23—26. Не останавливаясь подробно на деталях изменений того или много параметра с глубиной при соответствующих PT-режимах, сопоставим материалы экспериментальных исследований идентичных пород по трем указанным программам. Прежде всего, следует отметить, что породы различного состава по-разному реагируют на изменения режимов опытов. Весьма чувствительными к вариациям PT-параметров оказались образования кислого состава.

Наибольшие градиенты увеличения скорости до глубины 2—3 км зафиксированы в опытах по программе высокотемпературного режима, наименьшие — низкотемпературного. Появление первых зон максимальных скоростей, если таковые выделяются на кривых $V_{p,s} = f(H)$, также связано с определенным режимом опытов. Эти значения $V_{p,s}$ выше при опытах по низкотемпературным программам, но соответствуют большим глубинам. При распределении с глубиной более высоких температур отмечаются усложненные зависимости $V_{p,s} = f(H)$. В этих случаях на кривых появляются дополнительные максимумы и минимумы. Наибольшие амплитуды отклонения скоростей от средних значений обнаружены в опытах по высокотемпературным программам. Для низкотемпературных программ зависимости $V_{p,s} = f(H)$ приближаются к закономерностям, наблюдаемым в условиях высоких гидростатических давлений и комнатной температуры. Причем, при увеличении отношения $\frac{dT}{dH}$ и усложнении минерального состава породы, значительнее усиливается различие между $V_{p,s} = f(H)$ и $V_{p,s} = f(P_z)$. Аналогичные зависимости, обусловленные режимами опытов, характерны также для изменений E, G, β и σ (рис. 25, 26). В качестве примера сопоставим данные по коэффициенту Пуассона идентичных образцов, полученные в опытах по различным PT-программам. Для пород кислого состава увеличение $\frac{dT}{dH}$ влечет за собой уменьшение хрупкости крупнозернистых и мономинеральных образований при тех же компенсирующих давлениях (рс. 22а, обр. 2, 3, 5; рис. 25г, обр. 1, 2; рис. 26г, обр. 1). Как уже отмечалось, породы среднего состава слабо реагируют на изменение PT-параметров. Следовательно, воздействие на них температуры легко компенсируется увеличением давления. Это же подтверждается в опытах по различным программам. Например, σ диорита и собита независимо от соотношений P и T с глубиной остается примерно одинаковым (табл. К, обр. 14, 19; рис. 22б, обр. 1, 4; рис 25г, обр. 3; рис. 26г, обр. 2). Пластичность основных пород увеличивается с ростом $\frac{dT}{dH}$ как и образований кислого состава (рис. 22, рис. 25г, обр. 4, 6, 7).

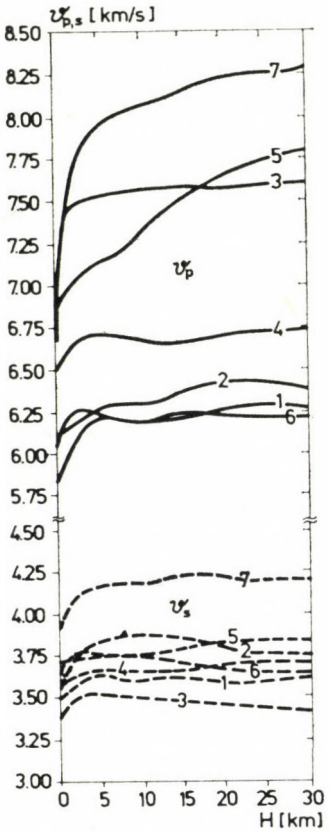


Рис. 23. Изменения скорости продольных (V_p) и поперечных (V_s) волн в образцах пород различного состава при термобарическом режиме первого типа. 1 — чарнокит I; 2 — гранит порфировидный I; 3 — диорит II; 4 — лабрадорит II; 5 — габбро-норит; 6 — диабаз; 7 — эклогитоподобная прода I

Сопоставление результатов опытов в условиях высоких гидростатических и квазигидростатических давлений и температур. На установке гидростатического давления при высоких температурах [20] было изучено четыре образца пород Украинского щита различного состава: кислого — гранит порфировидный (рис 27), среднего — гранит осницкий и чарнокит (рис. 28, 29), основного — диабаз (рис. 30). Опыты были выполнены по двум режимам *PT*-программы одного типа. Первый соответствовал средним значениям изменений давлений и температур с глубиной, характерных для центральной части Украинского щита ($H = 20$ км: $P = 5{,}3$ кбар; $T = 315°C$). Второму были заданы те же давления, но при минимальных температурных градиентах ($H = 20$;км: $P = 5{,}3$ кбар; $T = 290°C$). Скорости продольных и поперечных волн были изучены при *PT* режимах, соответствующих глубинам до 25 км. Оба образца гранитов исследованы при увеличении и уменьшении

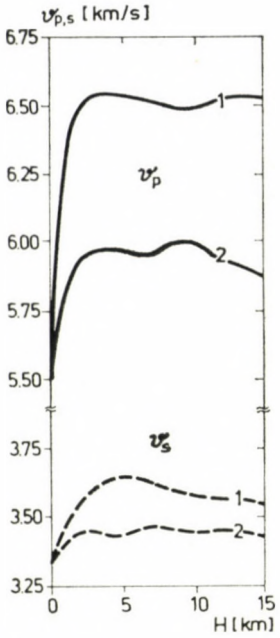


Рис. 24. Изменения V_p, $V_s = f(PT) = f(H)$ в образцах пород различного состава при термобарическом режиме третьего типа. 1 — гранит житомирский, 1,2 — собит

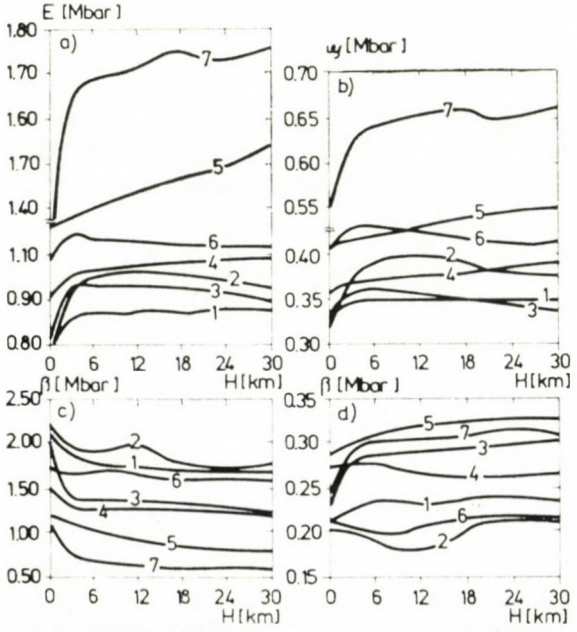


Рис. 25. Изменения модуля Юнга (а), модуля сдвига (б), сжимаемости (в) и коэффициента Пуассона (г) образцов пород различного состава при термобарическом режиме первого типа. Обозначения те же, что и на рис. 23.

PT-параметров. Результаты экспериментального изучения V_p и V_s представлены на рис 27—31, где для удобства анализа материалов приведены также зависимости $V_{p,s} = f(P_г)$ и $V_{p,s} = f(H) = f(P_к T)$, полученные для дубликатов этих образцов.

Скорости продольных и поперечных волн в опытах при высоких гидростатических давлениях и температурах, как и в условиях высоких квази-

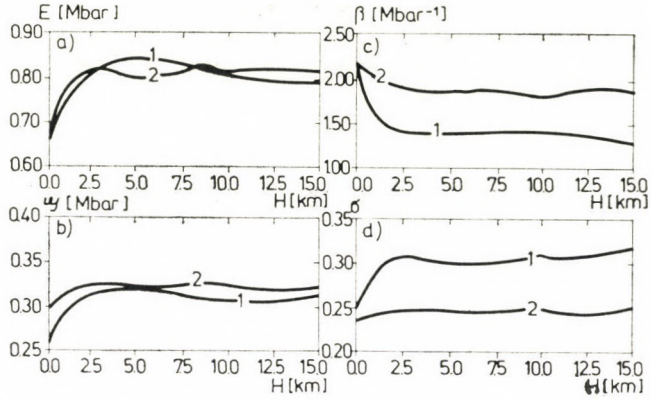


Рис. 26. Изменения модуля Юнга (а), модуля сдвига (б), сжимаемости (в) и коэффициента Пуассона (г) образцов пород различного состава при термобарическом режиме третьего типа. Обозначения те же, что и на рис. 24

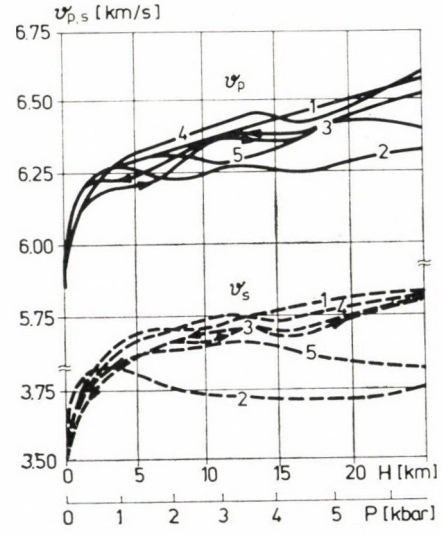


Рис. 27. Изменения V_p и V_s в граните порфировидном I при различных PT-условиях опытов. 1 — $V_p, V_s = f(P_г)$; 2 — $V_p, V_s = f(P_к T) = f(H)$, термобарический режим второго типа; 3 — $V_p, V_s = f(P_г T) = f(H)$, термоборический режим такой же, прямой и обратный ход кривой; 4 — $V_p, V_s = f(P_г T) = f(H)$, термобарический режим такой же, но при $\min dT/dH$; 5 — $V_p, V_s = f(P_к T) = f(H)$, термобарический режим первого типа

гидростатических давлений и температур, изменяются по сложному закону (рис. 27—30). На кривых $V_{p,s} = f(P_e T) = f(H)$ легко выделить несколько экстремумов. Наиболее четко они выражены у диабаза ($V_{p_{max}}$ на 2 и 12 км; $V_{p_{min}}$ на 16 и 18 км) и почти отсутствуют на кривых $V_{p,s} = f(H)$ для чарнокита

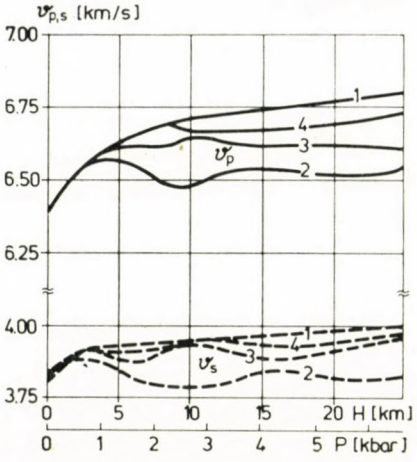


Рис. 28. Изменения V_p и V_s в рачноките II при различных PT-условиях опытов. Обозначения те же, что и на рис. 27 (1, 2, 3, 4)

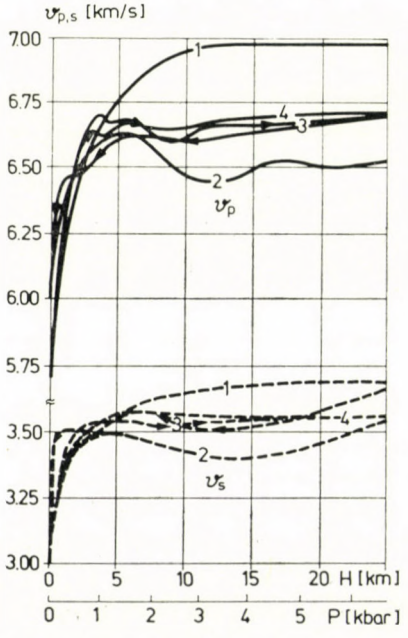


Рис. 29. Изменения V_p и V_s в граните осницком при различных PT-условиях опытов. Обозначения те же, что и на рис. 27 (1, 2, 3, 4)

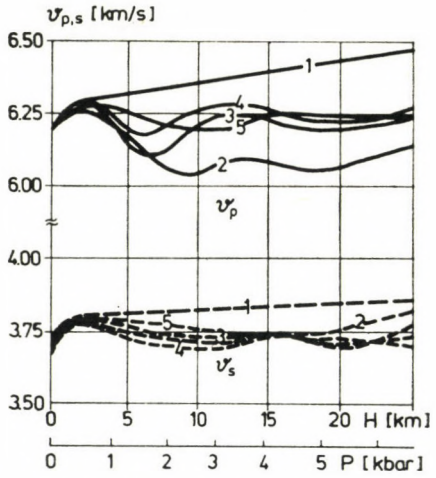


Рис. 30. Изменения V_p и V_s в диабазе при различных PT-условиях опытов. Обозначения те же, что и на рис. 27

и осницкого гранита. Очень важно отметить, что аномальные области изменения скоростей сохраняются и при обратном ходе опыта (уменьшение давления и температуры), хотя с несколько меньшими отклонениями. Это подтверждает наше предположение о том, что зоны пониженных и повышенных скоростей обусловлены перераспределением термоупругих и упругих напряжений, вызванных воздействием внешних давлений и температур в объеме многокомпонентной поликристаллической минеральной среды.

Возникающие внутренние напряжения вызывают обратимые изменения упругих параметров пород при гидростатическом распределении давления и небольших значениях $\frac{dT}{dH}$. Следовательно, горные породы на больших глубинах весьма чувствительны к вариациям термодинамических обстановок. Нарушение термодинамического равновесия на какой-либо глубине должно вызывать изменение упругих характеристик горных пород, о чем свидетельствует обратный ход кривых $V_{p,s} = f(H)$ (рис. 27, 29, кр. 3). Таким образом, приложеные по соответствующим программам внешние гидростатические давления целиком компенсируют возможные нарушения структуры пород в высокотемпературных полях.

Сложный закон изменения $V_{p,s} = f(H)$ в значительной степени обусловлен внутренними полями напряжений в объеме исследуемого образца, которые иногда вызывают полную обратимость изменений упругих параметров минерального вещества. При квазигидростатических давлениях (рис. 27, 30, кр. 2,5) задаваемые PT-режимы опытов в широких пределах изменяют значения $V_{p,s}$. Аналогичные явления наблюдаются и при гидростатических давлениях (рис. 27, 30, кр. 3, 4). В экспериментах по программе второго типа, но с

несколько заниженным тепловым режимом (всего лишь на 1,25°С/км), были зарегистрированы более высокие скорости. При этом наибольший рост V_p и V_s отмечался в интервале глубин 4—8 км и составлял: для кислых пород около 125, средних — порядка 80, основных — почти 100 м/сек. Еще раз подчеркнем, что породы среднего состава, обогащенные плагиоклазом и содержащие кварц в умеренных количествах, менее чувствительны к вариациям ***PT***-режимов. Интересные результаты были получены для порфировидного гранита в опытах по низкотемпературной программе. V_p и V_s в этом случае оказались выше, чем при гидростатических давлениях и комнатной температуре. Этот факт очевидно обусловлен интенсивным уплотнением многокомпонентной пористой ($n = 1\%$) породы при воздействии температуры до появления значительных термоупругих напряжений.

Как и при квазигидростатических давлениях, высокотемпературный режим опытов в гидростатике способствует повышению пластичности пород (σ возрастает), уменьшению значений упругих модулей (E и G) и увеличению сжимаемости (β) (рис. 32). Сравнивая абсолютные значения скоростей (рис. 27—30) и других упругих характеристик исследованных образцов при высоких квазигидростатических и гидростатических давлениях можно оценить влияние дополнительных (негидростатических) напряжений на изменения физико-механических свойств горных пород в ***PT*** обстановках, соответствующих большим глубинам. В квазигидростатических условиях при одинаковых температурных режимах снижаются значения скоростей, а также модулей Юнга и сдвига. Увеличивается сжимаемость и наблюдается более плавное изменение коэффициента Пуассона. Это связано с неупругими микродеформациями и разрушением исходной структуры изучаемых проб в неоднородных полях напряжений.

На кривых $V_{p,s} = f(P_к T)$ более четко прослеживаются зоны экстремальных изменений скоростей. Особенно выделяется первый максимум, ко-

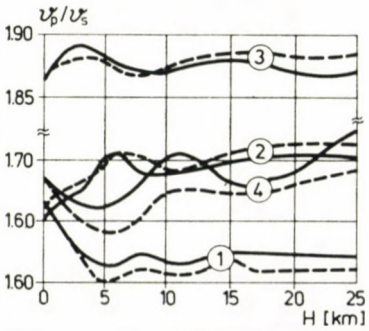


Рис. 31. Изменения $V_p/V_s = f(P_г T) = f(H)$ при термобарическом режиме второго типа. 1 — гранит порфировидный I; 2 — чарнокит II; 3 — гранит осницкий; 4 — диабаз. Пунктирные линии — термобарический режим при min dT/dH

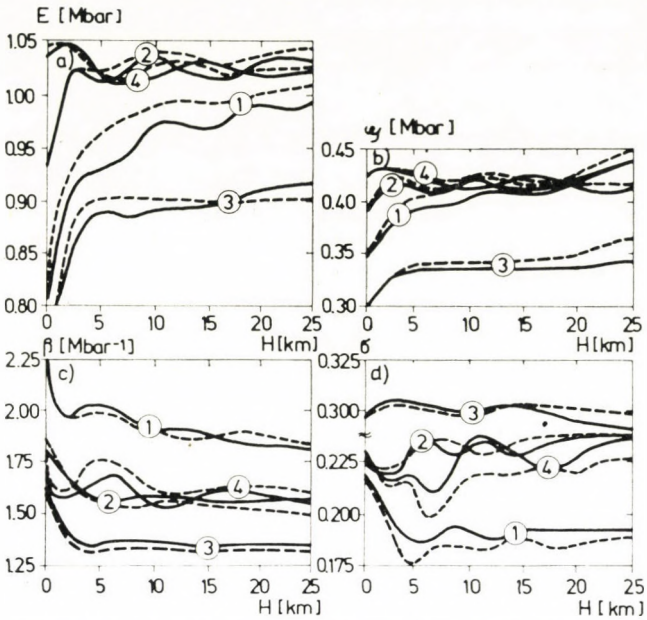


Рис. 32. Изменения модуля Юнга (а), модуля сдвига (б), сжимаемости (в) и коэффициента Пуассона (г) образцов пород различного состава при термобарическом режиме второго типа (давление гидростатическое). 1 — гранит порфировидный I; 2 — чарнокит II; 3 — гранит осницкий; 4 — диабаз. Пунктирные линии — термобарический режим при $\min \frac{dT}{dH}$

торый в опытах при гидростатическом давлении, как правило, не фиксируется. Однако, на кривых $V_{p,s} = f(P_e T)$ с увеличением давления выделяются максимумы скоростей, которые почти незаметны на кривых $V_{p,s} = f(P_к T)$ Эти максимумы являются следствием нарастающих в породе внутренних напряжений, возникающих за счет высоких температур и давлений. В квазигидростатических условиях при воздействии дополнительных напряжений внутренние значительно проще релаксируют в виде локальных хрупкопластичных микродеформаций минералов с последующим уплотнением продуктов разрушения. Поэтом ус увеличением РТ параметров (вплоть до соответствующих глубинам порядка 20—25 км) в условиях квазигидростатических давлений наблюдается более интенсивный рост скоростей, чем в гидростатических.

Некоторые обобщения. Результаты экспериментальных исследований динамики изменений упругих параметров минерального вещества в соответствующих условиях высоких квази- и гидростатических давлений, температур, в том числе при одновременном их воздействии, указывают на наличие сложных законов распределения физико-механических свойств горных пород и минералов в недрах земной коры.

Влияние гидростатического давления до 1—3 кбар (при комнатной температуре) обуславливает значительное возрастание упругих параметров горных пород за счет изменений типа, количества и объема макродефектов (поры, трещины, межзерновые границы и т. п.). Закрытие пор, трещин и улучшение межзерновых контактов связано с упругими и неупругими деформациями минерального вещества. Это влечет накопление и перераспределение в объеме образца остаточных и наведенных микронапряжений, неоднородность которых иногда будет увеличиваться с повышением давления. Указанные явления способствуют активизации подвижности микродефектов кристалла (точечные дефекты, дислокации, локализация примесных атомов). При наиболее благоприятных условиях значительное количество этих дефектов покидает основную часть минерала, улучшая тем самым упругие характеристики минеральной ассоциации в целом. С повышением давления изменения упругих характеристик в основном определяются атомно-молекулярными взаимодействиями собственно минеральных компонент и их упругой анизотропией. Если слагающие породу минералы достаточно анизотропны, то при дальнейшем росте давления возможно интенсивное накопление внутренних неоднородных микронапряжений, которые будут релаксировать в виде хрупких микроразрушений и пластичных течений. Последние замедляют увеличение упругих параметров минерального вещества с повышением гидростатического давления. Следует, однако, подчеркнуть, что все эти изменения во многом зависят от исходных характеристик образца горной породы (его минерального состава, величины и типа пористости, состояния отдельных минералов, крупности и ориентации зерен и т. п.) и, естественно, условий проведения опытов.

Наши исследования коллекции образцов некоторых минеральных образований кислого, среднего и основного составов Украинского щита позволили подтвердить закономерность: с повышением основности пород возрастают скорости продольных и поперечных волн, а также увеличиваются модули Юнга и сдвига. Эта зависимость сохраняется и при высоких гидростатических давлениях. Повышенные значения упругих характеристик пород среднего состава (по сравнению с кислыми образованиями) обусловлены появлением в их составе пироксена и роговой обманки. В связи с обогащением пород среднего состава плагиоклазами при незначительном содержании кварца, их упругие параметры возрастают с увеличением давления, характеризуясь большими градиентами, чем у кислых пород. Наиболее высокие значения упругих параметров у основных пород, обогащенных гранатом и роговой обманкой.

Воздействия высокого давления на изменения сжимаемости пород также связано с их составом. Наиболее сжимаемыми оказались породы кислого состава. Наименьшее стремление к увеличению плотности при росте давления наблюдается у основных образований. Коэффициент Пуассона, характери-

зующий способность твердого тела к взаимноортогональным деформациям и качественно отражающий его хрупкое или пластичное состояние, позволяет довольно детальное проанализировать динамику изменений упругих параметров горных пород различного состава в условиях высоких давлений. Более хрупкими являются проды со значительным содержанием кварца, пластичными — характеризующиеся повышенным количеством плагиоклаза. Поэтому породам кислого состава присущи более низкие значения σ, чем основного. В условиях высоких давлений кислые образования склонны к накоплению и последующей релаксации в объемах проб внутренних микронапряжений, на что указывают области максимумов и минимумов кривых $\sigma = f(P)$. Породы основного состава с увеличением давления стремятся к более пластичному состоянию. Следовательно, образования, обогащенные биотитом, плагиоклазом, пироксеном и роговой обманкой сильнее восприимчивы к изменениям внешних условий, причем без каких-либо релаксационных явлений.

Большим глубинам земной коры не всегда присущ гидростатический закон распределения давлений. Негидростатическое его воздействие на образцы пород в лабораторных опытах вызывает соответствующие изменения упругих параметров, которые связаны с текстурно-структурными особенностями пород, их пористостью и минеральным составом, а также скоростью нагружения образцов во время экспериментов. Крупнокристаллические и обогащенные кварцем среднезернистые кислые образования при дополнительных напряжениях в квазигидростатической обстановке в начальном интервале давлений характеризуются более низкими упругими параметрами, чем в гидростатике. Мелкозернистые же породы среднего и основного составов в квазигидростатике улучшают свои упругие характеристики. При давлениях выше 3 кбар различия между значениями упругих параметров, измеренными в гидростатических и квазигидростатических обстановках, становятся ничтожно малыми. На основании этого можно предположить, что обогащенные кварцем верхние слои вещества земной коры (до 10—15 км) в условиях квазигидростатического давления менее пластичны и склонны к хрупким деформациям. Породы же среднего и основного составов более глубоких горизонтов при наличии дополнительных напряжений увеличивают свою пластичность и становятся динамичнее и мобильнее.

Снижение упругих характеристик горных пород при нагреве в условиях атмосферного давления в основном обусловлено нарушением их природной структуры за счет неравномерного и анизотропного расширения породообразующих минералов в температурных полях. При этом обогащенным кварцем породам присущи максимальные изменения упругих параметров, а плагиоклазом — минимальные. Самые большие изменения наблюдаются у многокомпонентных анизотропных образований. Упругие параметры пород, обогащенных вторичными минералами, а также обладающих несовершенными

связями на границах зерен, с увеличением температуры интенсивно изменяются.

Разнообразие изменений физико-механических свойств горных пород, наблюдаемых при раздельном влиянии высоких P и T, обусловливает довольно сложное их распределение в условиях одновременного воздействия последних. В самых верхних слоях земной коры (до 3—6 км) упругие параметры (V_p, V_s, E, G и K) минерального вещества монотонно увеличиваются с градиентами, зависящими, в основном, от состава пород, их структурно-текстурных характеристик, особенностей изменения с глубиной давления и температуры, наличия неоднородных напряжений и т. д.

Если предположить постоянство состава минеральных образований до глубин 5—6 км., наибольшие градиенты увеличения V_p, V_s, E и G будут характерны для пород среднего состава, а наименьшие — для основного. Градиенты изменения с глубиной упругих параметров мелкозернистых основных образований выше, чем крупнозернистых, обогащенных кварцем. Для участков коры, состоящих из равномернозернистых пород кислого и среднего составов с большим содержанием кварца, характерны высокие градиенты увеличения упругих свойств при росте температурного градиента с глубиной. Аналогичным образом воздействуют на эти породы дополнительные напряжения. Подавляющее большинство средних и основных образований в указанном интервале глубин индеферентны к росту температурного градиента от 10 до 25°С/км. Однако, неоднородность распределения давления с глубиной (менее 10%) обуславливает увеличение изменения их упругих свойств.

Сжимаемость горных пород в верхних слоях коры изменяется наиболее интенсивно. Наиболее высокими ее значениями характеризуются образования кислого состава, самыми низкими — основного. Большая плотность присуща породам в областях с пониженным тепловым потоком при гидростатическом распределении давления. Наличие же дополнительных напряжений обуславливает разуплотнение минерального вещества. Наиболее эффективно это проявляется в кислых образованиях. Менее чувствительны к разуплотнению породы среднего состава.

Анализ данных изменения отношения между продольными и поперечными деформациями (коэффициент Пуассона) позволяет качественно охарактеризовать изменение пластичности пород с глубиной. До 5—6 км все они независимо от состава стремятся к пластическому состоянию. По нашим данным исключением являются крупнозернистые разности, обогащенные кварцем. В верхних слоях коры минеральное вещество среднего и основного составов можно считать довольно пластичным. В областях с повышенными температурными градиентами при квазигидростатическом распределении давлений породы характеризуются большей пластичностью. В случае гидростатического распределения давления их пластичность будет уменьшаться с глубиной весьма незначительно в связи с преобладанием термоупругих на-

пряжений. Таким образом, можно полагать, что преобладающее влияние на изменение упругих констант горных пород в указанном диапазоне глубин оказывает давление.

Предполагая постоянство минерального состава, земная кора на моделируемых глубинах (порядка 5—20 км) может в большинстве случаев характеризоваться наличием зон пониженных скоростей. Они вероятно имеют термодинамическую природу и являются результатом противоположного эффекта воздействия давления и температуры на состояние пород. Поскольку горным породам присуща сложная структура и многокомпонентность состава накопление упругой энергии и последующая релаксация внутренних напряжений могут повторяться с некоторой периодичностью, зависящей от состояния минерального вещества на соответствующих глубинах, а также во многом обусловленной величинами градиентов температуры и давления. Поэтому в некоторых случаях в земной коре могут существовать несколько зон пониженных скоростей различного характера.

По толщине зоны пониженных скоростей можно разделить на две группы: первая (толстослойные) — 10—20 км, вторая (тонкослойные) — 3—7 км. Второй группе свойственны более высокие градиенты скоростей, посравнению с первой. Зоны пониженных скоростей первой группы в основном характерны для образований основного и среднего составов и особенно при квазигидростатическом распределении давления. Указанные изменения скоростей в этих зонах очень зависят от величин температурных градиентов. В районах с низкими градиентами в квазигидростатических обстановках они выражены слабо. В областях высоких градиентов на фоне общего уменьшения скоростей указанные зоны также выделяются слабо. Более четко в этих условиях проявляются зоны второй группы, повторяющиеся на небольших глубинах. Они чаще свойственны образованиям кислого состава и некоторым средним породам, обогащенным кварцем. Следует подчеркнуть, что тонкослойные зоны могут осложнять области пониженных скоростей большой мощности, как бы являясь структурами более низкого порядка.

При гидростатическом распределении двваления тонкослойные зоны пониженных скоростей с периодичностью повторения 5—7 км (по расстоянию между максимумами значений $V_{p,s} = f(H)$) выражены довольно четко. В этом случае градиенты скоростей несколько выше, чем в квазигидростатических условиях (при аналогичных температурах).

Материалы экспериментального изучения упругих параметров горных пород в различных PT условиях позволяют охарактеризовать физико-механическое состояние минерального вещества выявленных зон пониженных скоростей. Ему присущи заниженные значения модулей Юнга и сдвига, меньшая плотность (повышенная сжимаемость). По изменениям коэффициента Пуассона можно полагать, что в большинстве случаев породы, ограничивающие зоны пониженных скоростей, находятся в более пластичном состоянии (по

сравнению с веществом их центральных частей), наибольшим изменениям V_p и V_s соответствуют максимальные значения $\sigma = f(PT)$. Эти предположения касаются модели земной коры однородной по составу. Если же допустить на глубинах 5—30 км наличие значительных вариаций минерального состава, то закономерности изменения физико-механического состояния пород будут несколько иными. В кислых породах (различного состава и структурно-текстурных особенностей) зоны пониженных скоростей не выделяются. С повышением основности пород эти зоны выявляются в минеральных ассоциациях, характеризующихся значительными вариациями состава. Предполагается, что в породах среднего состава зоны пониженных скоростей будут расположены в интервале глубин 7—15 км ($\Delta V_p < -0{,}15$ км/сек в районах, где $\frac{dT}{dH} \approx 15°$C/км). Мощность их менее 7 ÷ 8 км. Породам основного состава по данным $V_{p,s} = f(H)$ такие зоны могут быть присущи глубинам свыше 10 ÷ ÷ 20 км ($\Delta V_p - 0{,}2$ км/сек), при мощности более 15 км. Таким образом, зоны пониженных скоростей, имеющих термодинамическую природу, вероятно существуют и при наличии мощных толщ образований основного или среднего составов.

Очевидно на границах зон пониженных скоростей имеет место градиентное изменение акустической жесткости минерального вещества, что в определенных условиях может быть зафиксировано методами взрывной сейсмологии при определенных методах интерпретации. Действительно, в различных геологических регионах на глубинах порядка 10 ÷ 30 км в толще континентальной земной коры выявлены обширные зоны пониженных скоростей.

В заключение представим некоторые общие выводы по всему материалу.

1. На примере экспериментального изучения по различным PT-программам минеральных образований Украинского щита показано, что породы кислого, среднего и основного составов дифференцируются по упругим свойствам в условиях атмосферного и высокого давлений. Кислым породам присущи относительно низкие значения V_p, V_s E, G и большая их сжимаемость. В условиях высоких давлений они менее пластичны и характеризуются релаксационными явлениями в виде хрупко-пластических микронарушений структуры минерального вещества. При различных давлениях породы основного состава склонны к плавному увеличению упругих параметров и пластифицируются без каких-либо аномальных явлений.

2. Упругие характеристики горных пород при гидростатических и квазигидростатических давлениях изменяются по-разному. Наибольшие расхождения характерны для крупнозернистых кислых пород, наименьшие — для мелкозернистых образований основного состава. Последние весьма пластичны даже в условиях неоднородного распределения давления.

3. Упругие параметры минерального веществ в условиях высоких температур (при атмосферном давлении) изменяются в основном за счет его

разуплотнения, обусловленного неравномерным и анизотропным расширением породообразующих минералов, а также ухудшением их упругих характеристик. Наиболее подвержены изменениям крупнозернистые образования кислого состава и некоторые породы, обогащенные вторичными минералами.

4. Результаты опытов при одновременном воздействии высоких давлений и температур позволяют считать, что в верхних горизонтах земной коры (до 3—6 км) величины упругих параметров горных пород (V_p, V_s, E, G и K) могут монотонно увеличиваться благодаря возрастающему с глубиной влиянию давления. Температура в этих условиях в основном влияет на рост пластификации минерального вещества.

5. Состояние пород при высоких лабораторных PT-режимах, соответствующих интервалу глубин порядка 5—30 км, характеризуется понижением значений их упругих параметров по сравнению с таковыми в опытах при высоких давлениях и комнатной температуре. Изменение упругих свойств на этих глубинах происходит по сложным законам с возникновением зон пониженных скоростей. Характер последних (местоположение по разрезу, протяженность и величина градиента) обусловлен особенностями распределения с глубиной давления, температуры и минерального состава пород.

6. Эти зоны можно разделить на толстослойные (толщиной порядка 10—20 км) и тонкослойные (около 3—7 км). Кислым образованиям свойственны тонкослойные зоны, расположенные преимущественно в верхних частях коры. Для пород основного и среднего составов чаще предполагается наличие толстослойных зон. Областям с высокими температурными градиентами очевидно присущи тонкослойные зоны. В условиях негидростатического распределения давления протяженные зоны пониженных скоростей могут иметь место преимущественно в образованиях основного состава.

7. Наши экспериментальные данные позволяют также сделать предположение о термодинамической природе некоторых зон пониженных скоростей, выделяемых методами взрывной сейсмологии на глубинах $10 \div 30$ км в толще континентальной земной коры. К этим зонам приурочены породы среднего или основного составов, характеризующиеся пониженной упругостью, меньшей плотностью, повышенной хрупкостью вблизи их границ и более высокой пластичностью в центральных частях.

ЛИТЕРАТУРА

1. АФАНАСЬЕВ, Г. Д.: Строение и состав земной коры в связи с проблемами геологической петрологии. *Изв. АН СССР, сер. геолог.*, № 11 (1970), 3—26.
2. БАЮК, Е. И.: Упругие свойства минералов при высоких давлениях и температурах. *Геофиз. сб. АН УССР*, 51 (1973), 27—32.
3. БАЮК, Е. И.—ТЕДЕЕВ, Р. В.: Влияние температуры на скорость продольных волн в горных породах при высоких давлениях. В кн.: «Физические свойства горных пород при высоких термодинамических параметрах». Материалы III-го Всесоюзного совещания. «Наукова думка», Киев, 1971, 7—10.

4. БАЮК, Е. И.—ТЕДЕЕВ, Р. В.: Скорость продольных волн в образцах горных пород при одновременном воздействии высоких давлений и температур. *Изв. АН СССР, сер. физика Земли*, № 8 (1974), 63—70.
5. БЕЛИКОВ, Б. П.—АЛЕКСАНДРОВ, К. С.—РЫЖОВА, Т. В.: Упругие свойства породообразующих минералов и горных пород. «Наука», Москва, 1970.
6. БЕЛОУСОВ, В. В.: Земная кора и верхняя мантия материков. «Наука», Москва, 1966.
7. ВОЛАРОВИЧ, М. П.: Исследование упругих свойств горных пород при высоких давлениях в связи с изучением земной коры и верхней мантии. В кн.: «Физико-механические свойства горных пород верхней части земной коры.» «Наука», Москва, 1968, 30—36.
8. ВОЛАРОВИЧ, М. П.—ГУРЕВИЧ, А. С.: Исследование динамического модуля упругости горных пород в зависимости от температуры. *Изв. АН СССР, сер. геофиз.*, № 4 (1957), 417—425.
9. ВОЛАРОВИЧ, М. П.—БАЮК, Е. И.—ЕФИМОВА, Г. А.: Упругие свойства минералов при высоких давлениях. «Наука», Москва, 1975.
10. ВОЛАРОВИЧ, М. П.—БАЮК, Е. И.—ЛЕВЫКИН, А. И.—ТОМАШЕВСКАЯ, И. С.: Физико-механические свойства горных пород и минералов при высоких давлениях и температурах. «Наука», Москва, 1974.
11. ГЗОВСКИЙ, М. В.: Основы тектонофизики. «Наука», Москва, 1975.
12. ДМИТРИЕВ, А. П.: Физические свойства горных пород при высоких температурах. «Недра», Москва, 1969.
13. КУЗЬМЕНКО, В. А.: Новые схемы деформирования твердых тел. «Наукова думка» Киев, 1973.
14. ЛАНДАУ, Л. Д.—ЛИФШИЦ, Е. М.: Теория упругости. «Наука», Москва, 1965.
15. ЛЕБЕДЕВ, Т. С.: Физические свойства пород литосферы в условиях больших глубин. В кн.: «Проблемы физики Земли на Украине», «Наукова думка», Киев, 1975, 98—117.
16. ЛЕБЕДЕВ, Т. С.—БУРТНЫЙ, П. А.—КОРЧИН, В. А.: Связь порового пространства со скоростью упругих волн в горных породах при высоких давлениях. *Геофиз. сб. АН УССР*, 54 (1973), 7—17.
17. ЛЕБЕДЕВ, Т. С.—БУРТНЫЙ, П. А.—КОРЧИН, В. А.: Некоторые вопросы поведения порового пространства и его связь со скоростью упругих волн в горных породах при высоких давлениях. В кн.: «Геофизические исследования земной коры и мантии Украины», «Наукова думка», Киев, 1975, 46—51.
18. ЛЕБЕДЕВ, Т. С. и др.: Упругие свойства горных пород при высоких давлениях. «Наукова думка», Киев, 1972.
19. ЛЕБЕДЕВ, Т. С.—КОРЧИН, В. А.—ШАПОВАЛ, В. И.—ЛАХТАНОВ, В. Т.: Методика и аппаратура одновременных исследований скорости распространения поперечных и продольных волн в горных породах при высоких давлениях. *Геофиз. сб. АН УССР*, 58 (1974), 41—49.
20 ЛЕБЕДЕВ, Т. С.—КОРЧИН, В. А.—ВАСИЛЯКА, В. Т.: Исследования в гидростатических условиях упругих свойств минерального вещества при высоких термодинамических параметрах. *Геофиз. сб. АН УССР*, 69 (1976), 26—34.
21. ЛЕБЕДЕВ, Т. С.—ОРОВЕЦКИЙ, Ю. П.—ШАПОВАЛ, В. И.—КОРЧИН, В. А.: Полиморфные переходы в карбонатных породах и скорость ультразвука в них и некоторых изверженных и метаморфических образованиях при гидростатическом давлении до 15 кбар. *Геофиз. сб. АН УССР*, 62 (1974), 57—63.
22. ЛЕБЕДЕВ, Т. С.—ОРОВЕЦКИЙ, Ю. П.—КОРЧИН, В. А.: Изменение структуры кристаллов мориона при гидростатическом давлении до 15 кбар. В кн.: «Тезисы докладов У-ой Международной конференции по физике и технике высоких давлений». «Наука», Москва, 1975, 214.
23. ЛЕБЕДЕВ, Т. С.—ОРОВЕЦКИЙ, Ю. П.—КОРЧИН, В. А.: Исследования при высоких гидростатических давлениях изменений дислокационной структуры кварца и связь с ними физических свойств кварцсодержащих пород. *Геофиз. сб. АН УССР*, 70 (1976), 71—85.
24. ЛЕБЕДЕВ, Т. С.—ОРОВЕЦКИЙ, Ю. П.—ШАПОВАЛ, В. И.—КОРЧИН, В. А.: Скорости ультразвука и полиморфные переходы в карбонатных породах при гидростатических давлениях до 15 кбар. В кн.: «Физические свойства горных пород при высоких давлениях и температурах. Материалы IV-го Всесоюзного совещания. «Мецниереба», Тбилиси, 1974, 83—86.
25. ЛЕБЕДЕВ, Т. С.—ОРОВЕЦКИЙ, Ю. П.—КОРЧИН, В. А.: Динамика полиморфных преобразований и изменение скорости ультразвука в карбонатных породах и минералах состава $CaCO_3$ при различных термодинамических условиях. В кн.:

«Исследования физических свойств минерального вещества земли при высоких термодинамических параметрах», «Наукова думка», Киев, 1977.
26. ЛЕБЕДЕВ, Т. С.—ФОЛЬШТАДТ, Г.—КОРЧИН, В. А.—ЗАЙПОЛЬД, У.—ШАПОВАЛ, В. И.—ФРОЙНД, Д.: Сравнительные характеристики методик исследований некоторых физических параметров горных пород при различных PT режимах опытов в ГДР и УССР. В кн.: «Физические свойства горных пород при высоких давлениях и температурах». Материалы IV-го Всесоюзного совещания. «Мецниереба», Тбилиси, 1974, 42—45.
27. ЛЕБЕДЕВ, Т. С.—ШАПОВАЛ, В. И.—КОРЧИН, В. А.: Экспериментальные исследования воздействия высоких температур и давлений на изменение скорости в изверженных породах Украинского щита. В кн.: «Давление и механические напряжения в развитии состава, структуры и рельефа литосферы», «Недра», Ленинград, 1969, 216—218.
28. ЛЕБЕДЕВ, Т. С.—ШАПОВАЛ, В. И.—КОРЧИН, В А.: Исследования воздействия высоких температур и давлений на изменение скорости в изверженных и метаморфических горных породах. *Геофиз. сб. АН УССР*, 31 (1969), 75—93.
29. ЛЕБЕДЕВ, Т. С.—ШАПОВАЛ, В. И.—КОРЧИН, В. А.: Изучение влияния высоких давлений и температур на скорость упругих волн в некоторых породах Украинского щита. *Геофиз. сб. АН УССР*, 32 (1969), 5—17.
30. ЛЕБЕДЕВ, Т. С.—ШАПОВАЛ, В. И.—КОРЧИН, В. А.—БУРТНЫЙ, П. А.: Экспериментальные данные о некоторых физических свойствах кристаллических пород центральной части Украинского щита. *Геофиз. сб. АН УССР*, 34 (1970), 19—28.
31. ЛЕБЕДЕВ, Т. С.—ШАПОВАЛ, В. И.—КОРЧИН, В. А.: Физические параметры некоторых гранитоидов в экспериментальных условиях соответствующих верхним частям земной коры. В кн.: «физические свойства, состав и строение верйней мантии», Москва 1971, 32—33.
32. ЛЕБЕДЕВ, Т. С.—ШАПОВАЛ, В. И.—КОРЧИН, В. А.: Деформационные и плотностные характеристики магматических и метаморфических пород при высоких давлениях. В кн.: «Физические свойства горных пород при высоких термодинамических параметрах», Материалы III-го Всесоюзного совещания. «Наукова думка», Киев, 1971, 190—194.
33. ЛЕБЕДЕВ, Т. С.—ШАПОВАЛ, В. И.—КОРЧИН, В. А.: Изучение некоторых упругих параметров горных пород при высоких давлениях и температурах. Там же, стр. 33—36.
34. ЛЕБЕДЕВ, Т. С.—ШАПОВАЛ, В. И.—КОРЧИН, В. А.: Упругие свойства горных пород Украинского щита при высоких температурах (экспериментальные данные). Там же, стр. 128—131.
35. ЛЕБЕДЕВ, Т. С.—ШАПОВАЛ, В. И.—КОРЧИН, В. А.: Новые данные о скорости продольных волн в горных породах при высоких термодинамических параметрах. *Геофиз. сб. АН УССР*, 49 (1972), 9—27.
36. ЛЕБЕДЕВ, Т. С.—ШАПОВАЛ, В. И.—КОРЧИН, В. А.: Установка для исследований физических свойств горных пород при давлениях до 15 кбар и высоких температурах. *Геофиз. сб. АН УССР*, 59 (1974), 30—35.
37. ЛЕБЕДЕВ, Т. С.—ШАПОВАЛ, В. И.—КОРЧИН, В. А.: Изучение физических свойств горных пород и минералов при давлениях до 15 кбар и высоких температурах. В кн.: «Физические свойства горных пород при высоких давлениях и температурах», Материалы IV-го Всесоюзного совещания. «Мецниереба», Тбилиси, 1974, 87—89.
38. ЛЕБЕДЕВ, Т. С.—ШАПОВАЛ, В. И.—КОРЧИН, В. А.: Моделирование региональных глубинных термодинамических условий земной коры при изучении физических свойств минерального вещества. Там же, стр. 40—41.
39. ЛЕБЕДЕВ, Т. С.—ШАПОВАЛ, В. И.—КОРЧИН, В. А.: Сроггаммное моделирование глубинных термодинамических условий при экспериментальных исследованиях упругих свойств минерального вещества. В кн.: «Геофизические исследования земной коры и мантии Украины», «Наукова думка», Киев, 1975, 25—30.
40. ЛЯВ, А.: Математическая теория упругости. Изд-во АН СССР, Москва—Ленинград, 1955.
41. МАГНИЦКИЙ, В. А.: Внутреннее строение и физика Земли. «Недра», Москва, 1965.
42. УРАЗАЕВ, Б. М.—ВОЛАРОВИЧ, М. П.—КУРСКЕЕВ, А. К.: Физические свойства горных пород в глубинных термодинамических условиях. «Наука», Алма-Ата, 1973.
43. Физическая акустика (под ред. Мезона), т. I, «Мир», Москва, 1966.
44. Физические свойства горных пород при высоких термодинамических параметрах. Материалы III-го Всесоюзного совещания. «Наукова думка», Киев, 1971.

45. Физические свойства горных пород при высоких давлениях и температурах. Материалы IV-го Всесоюзного совещания. «Медниереба», Тбилиси, 1974.
46. ЯМЩИКОВ, В. С.: Исследование зависимости модуля упругости горных пород от температуры. *Изв. АН СССР, сер. Физика Земли*, № 10, 1965, 83—87.
47. BIRCH, F.: Elasticity of igneous rocks at high temperatures and pressures. *Bull. Geol. Soc. Amer.*, 54(1943), 263—275.
48. BIRCH, F.: Interpretation of the seismic structure of the crust in the light of experimental studies of wave velocities in rocks. Contributions in Geophysics in Honor of Beno Gutenberg, Pergamon Press, New York, 1958.
49. BIRCH, F.—BANCROFT, D.: The elasticity of glass at high temperatures and the vitreous basaltic substratum. *Amer. J. Sci.*, 240(1942), 457—490.
50. FIELITZ, K.: Elastic wave velocities in different rocks of high pressure and temperatures up to 750 °C. *Zeitschrift für Geophysik*, 37(1971), 943—956.
51. S. P. CLARK, JR. (ed.): Handbook of Physical Constants. Yale University, New Haven, Connecticut 1966.
52. HUGHES, D. S.—CROSS, J. H.: Elastic wave velocities in rocks at high pressure and temperature. *Geophysics*, 16(1951), 577—593.
53. HUGHES, D. S.—JONES, H. J.: Variation of elastic moduli of igneous rocks with pressures and temperatures. *Bull. Geol. Soc. Amer.*, 61(1950), 843—856.
54. HUGHES, D. S.—MAURETTE, C.: Variation of elastic wave velocities in granites with pressures and temperatures. *Geophysics*, 21(1956), 277—287.
55. HUGHES, D. S.—MAURETTE, C.: Variation of elastic wave velocities in basic igneous rocks with pressure and temperature. *Geophysics*, 22(1957), 23—31.
56. HUGHES, D. S.—MAURETTE, C.: Détermination des vitesses d'onde élastique dans diverses roches en fonction de la pression et de la température. *Rev. Inst. Franc. Petrole et Ann. combustible, liquide*, No 12(1957), 730—752.
57. LEBEDEV, T. S.: Investigations of some physical properties of mineral matter under thermodynamic conditions of the Earth's interior. *Z. geol. Wiss.*, 3(1957), 717—739.
58. LEBEDEV, T. S.—BURTNY, P. A.—KORCHIN, V. A.: Behaviour of the pore space in granites and its relationship with elastic wave velocities at high pressure and temperature. *Gerlands Beitr Geophysik*, 83(1974), 170—180.
59. LEBEDEV, T. S.—SHAPOVAL, V. I.—KORCHIN, V. A.: Effect of high temperatures and pressures on changes in ultrasonic velocities in some igneous and metamorphic rocks of the Ukrainian Shield. *Gerlands Beitr Geophys.*, 79(1970), 108—116.
60. LEBEDEV, T. S.—SHAPOVAL, V. I.—KORCHIN, V. A.: A Study of Some Elastic Parameters of Rocks at High Pressures and Temperatures. Report to the XVth General Assembly of the International Geodesy and Geophysics Union (Moscow, 30 July—14 August, 1971). "Naukova dumka", Kiev, 1971, 38—41.
61. LEBEDEV, T. S.—SHAPOVAL, V. I.—KORCHIN, V. A.: Programmed modelling of deep thermodynamic conditions in experimental studies of elastic properties of mineral matter. *Gerlands Beitr Geophys.*, 83(1974), 340—346.
62. LEBEDEV, T. S.—SHAPOVAL, V. I.—KORCHIN, V. A.: Elastic velocities in rocks at high values of thermodynamic parameters. *Z. geol. Wiss.*, 4(1973), 431—450.
63. LEBEDEV, T. S.—SHAPOVAL, V. I.—KORCHIN, V. A.: Untersuchungen der Geschwindigkeit von elastischen Wellen in Gesteinen unter den thermodynamischen Bedingungen der Erdkruste. *Veröffentl. Zentralinst. Physik. Erde.* No. 22(1974), 17—54, Potsdam

ELASTIC CHARACTERISTICS OF THE MINERAL MATTER IN THE THERMOBARIC CONDITIONS OF THE EARTH'S INTERIOR

T. S. LEBEDEV—V. A. KORCHIN

SUMMARY

It has been proved by experimental investigations on minerals of the Ukrainian Shield that the rocks of acidic, neutral and basic composition can be separated on the basis of their elastic properties in cases of atmospheric conditions and under high pressure. Acidic formations are characterized by relatively low V_p, V_s, E and G values and high compressibility. Under high pressure they are characterized by relaxation phenomena in the form of plastic microchanges with ruptures in the mineral structure. Rocks of basic composition show the tendency

that their elastic parameters increase with increasing pressure. These rocks become plastic without any anomalous behaviour. Formations of natural composition have transitional characteristics.

The elastic parameters of the minerals change at high temperature (and atmospheric pressure) mainly due to the discordant and anisotropic expansion of the minerals as well as due to the rarefaction caused by the changes of the elastic characteristics of the minerals. Rocks of acidic composition with a structure of great grains and those rich in secondary minerals are mostly affected by high temperature.

The experimental results received at simultaneous effects of high temperature and pressure seem to prove according to the different PT programs that in the upper levels of the earth crust (till 3—6 km depth) the elastic parameters of the rocks (V_p, V_s, E, G and K) can increase monotonously due to the pressure increasing with depth. Within such conditions the minerals will only be plasticized by the temperature. At high pressure and temperature corresponding to depths of 5—30 km the state of rocks is characterized by the decrease of the values of the elastic parameters in comparison with experiments carried out at high pressure and room-temperature. In these depths the change of the elastic properties follows complicated laws, whereby low-velocity layers come into being. The characteristics of the latter position in the profile, extension and gradient value are determined in function of pressure, temperature and the mineral composition of the rocks by the distribution characteristics.

These zones can be divided into thick-layer (10—20 km) and thin-layer (4—7 km) zones. Acidic formations are primarily characterized by the thin-layer zones in the upper part of the crust. The presence of rocks of basic and neutral composition in the thick-layer zones is more frequently supposed. Areas of great temperature gradient are characterized by thin-layer zones. At non-hydrostatic pressure the low-velocity thick-layer zones can be chiefly produced by formations of neutral composition.

In this paper a thermodynamic nature of certain low-velocity zones is supposed. These velocities have been revealed by explosion-seismic methods in the continental earth crust in depths of 10—30 km. These zones are characterized by rocks of neutral and basic composition, having low elasticity, smaller density, higher fragility at their borders and higher plasticity in the inner part.

Acta Geodaet., Geophys. et Montanist. Acad. Sci. Hung. Tomus 14 (1—2), pp. 227—236 (1979)

QUASI-PERIODIC VARIATIONS OF IONOSPHERIC ABSORPTION WITH CHARACTERISTIC CHANGES DURING A SOLAR CYCLE

F. MÄRCZ

GEODETIC AND GEOPHYSICAL RESEARCH INSTITUTE OF THE HUNGARIAN ACADEMY OF SCIENCES, SOPRON

[Manuscript received December 15, 1977]

Ionospheric absorption measured at mid-latitude stations in Europe shows quasi-periodic variations as revealed by power-spectra. Peaks in the spectra (between 3 and 30 days) frequently occur around 4—6, 8—9 and 12—14 days. Similar quasi-periodic variations can be found in some parameters of the lower atmosphere (troposphere, stratosphere), but only those of ionospheric absorption have been analysed in detail. The dominant periods of the ionospheric night absorption selected on the basis of prominent peaks in spectra for individual years of a solar cycle (1964—1974) have shown characteristic changes. Dominant periods around solar activity maximum seem to be shorter than in the remaining part of the cycle investigated. A comparable tendency is also present in parameters of solar activity. The quasi-periodic variations of ionospheric absorption may partly be attributed to a solar source on the basis of co-spectra determined from solar X-ray flux data and different ionospheric absorption data.

1. Introduction

Preliminary results derived from power spectra of daily data of radio wave absorption in the LF-range indicated quasi-periodic variations in a parameter of the lower ionosphere [1]. The prominent peaks in the spectra were generally found around 5—6, 8—9 and 11—12 days in that study. LAUTER [2] also reported periods partly similar to the mentioned ones in LF and HF absorption data, and GRASNICK and ENTZIAN [3] have shown periods between 4 and 8 days both for absorption and ozone data. SCHWENTEK [4] found wave-like structures in the day-to-day variation of ionospheric absorption during the winter 1971/1972. The most frequent periods were around 7 days and they also occurred in the variation of atmospheric pressure measured at ground as presented by SCHWENTEK [4]. Several other papers have confirmed the earlier findings and provided further examples of supposed links between parameters of lower and upper atmospheric regions in respect to quasi-periodic variations.

Radio wave absorption in the LF-range is a parameter of the lower ionosphere and can strongly be affected by magnetospheric and solar influences (e.g. [5, 6]). BOSSOLASCO and ELENA [7] have convincingly shown the correlation between ionospheric absorption and major stratospheric warmings in winter. Certain enhancements of the ionospheric absorption can be followed by an increase of atmospheric electric potential gradient measured at ground [8], that hints at a temporary and indirect link between these parameters due to extraterrestrial influences.

Thus, the quasi-periodic variations of ionospheric absorption can be connected both with processes of the lower atmosphere and those of the different spheres up to the Sun, or even originate from them. The planetary scale fluctuations in the troposphere have frequently been considered as sources of quasi-periodic variations found in different parameters of higher atmospheric levels. Since CHARNEY and DRAZIN [9] have shown difficulties for a vertical propagation of planetary waves on a theoretical basis, the possible explanations of couplings between quasi-periodic variations detected both in tropospheric and ionospheric parameters are restrained.

The present study is mainly aimed at the analysis of quasi-periodic variations in absorption data during a solar cycle. Tropospheric, stratospheric, geomagnetic and solar parameters are additionally included into the analysis; however, the emphasis should be on solar ones for investigating their role in quasi-periodic variations of ionospheric absorption.

2. Data and method of analyses

First of all an 11-year series of ionospheric absorption determined at 245 kHz by the A3 method in Kühlungsborn (GDR, $\varphi_{\text{geogr.}} = 54°07'$ N, $\lambda = 11°46'$ E) has been investigated by power-spectrum analysis. The aim was to detect quasi-periodic variations in the spectrum with periods between 3 and 30 days. The lower limit is set by the method of computation, the upper one just allows to check the presence or lack of a 27-day period or so. In the short period part of the spectrum, between 3 and 10 days, the computations were carried out for periods of whole days, in the remaining part only periods with even numbers of days were analysed. In order to check the role of solar activity variation, data of individual years between 1964 and 1974 were treated separately.

Some non-ionospheric parameters measured in the same interval, or during a part of it were additionally included into the spectral analysis. These parameters are the following:

- daily sums of three-hourly Kp-indices (1964—1974),
- daily means of atmospheric electric potential gradient measured both at Swider (Poland) and Nagycenk (Hungary) (1964—1973),
- air pressures observed at Vienna near the ground, as well as in 10 and 20 km altitudes at midnight (GMT) (1967—1973).

The geomagnetic and atmospheric electric parameters have shown associations with ionospheric absorption [5, 8]. This is the reason why these parameters have been included into the present investigations, too. Air-pressure data were chosen for analysing also neutral (i.e. non-electric) parameters from several atmospheric altitudes concerning quasi-periodic vari-

ations. Furthermore, the investigations have especially been extended to ionospheric absorption measured at different frequencies.

The peaks in spectra were characterized according to their relative importance. An arbitrarily chosen scale including three steps was used. A maximum rising most definitely from the adjacent parts of the spectrum was characterized by index 3 and the corresponding period was considered as dominant. Index 2 indicated important, but not dominant peaks and index 1 the small peaks. This treatment made a proper comparison of spectra of different parameters of the same year (e.g. 1968 in Table I) and the tracing of changes in spectra during a solar cycle, or a part of it possible.

3. Results

3.1 *Spectrum characterics of different parameters for 1968*

Table I presents the indices of peaks in the spectra for 1968 according to the scale mentioned. Indices 3 are additionally encircled. Here, the characterization hints at the existence of several groups of quasi-periodic variations. In six parameters out of seven the dominant periods occurred between 8 and 14 days. For 1968, the dominant periods are shorter in geomagnetic activity, ionospheric absorption and atmospheric electric potential gradient than in air pressure data. In addition to the period groups around 8—9 days and 12—16

Table I

Characterization of peaks in power-spectra of different parameters for 1968 (index 3: dominant peaks; index 2: important peaks; index 1: small peaks)

Year	Parameter	Periods (days)																
		3	4	4	6	7	8	9	10	12	14	16	18	20	22	24	26	28	30
1968	ΣKp Göttingen				1			③				2						1	
	Absorption 245 kHz Kühlungsborn		1				③				1				1				
	Potential gradient Swider			③				1				1							
	Potential gradient Nagycenk		1					③			2								
	Air pressure (0.2 km) Vienna			2			1			③					1		2		
	Air pressure (10 km) Vienna			1				2		③					1				
	Air pressure (20 km) Vienna							2			③		1		1				

days, a rather stable group seems to exist in the period band between 4 and 6 days, though it only includes a dominant period of a single parameter. There are some indications for variations with periods of 22 days. The 27-day variation occurs in two parameters only.

Investigations of data taken from several other years have also revealed quasi-periodic variations with similar periods in the different parameters. Direct connections between these parameters should not be considered merely on the basis of occasional similarity of periods. Nevertheless, the simultaneous or shifted occurrence of these quasi-periodic variations can help in detecting processes and relationships being important in the investigated altitudes of the atmosphere.

3.2 *Dominant periods depending on solar activity*

In this section quasi-periodic variations of ionospheric absorption are analysed in detail. Results derived from other parameters are presented only occasionally.

Figure 1 shows the distribution of spectral maxima during the interval from 1964 to 1974 for the night absorption measured at 245 kHz in Kühlungsborn. Small maxima (index 1) are signed by crosses, important peaks (index 2) by circles; heavy dots indicate dominant periods (index 3). The dots lie between the two curves in the figure, that hints at a peculiar tendency. The dominant periods of the ionospheric night absorption are shorter during solar activity maximum than during lower solar activity. The 27-day period of solar rotation and its first two harmonics are also marked. The dominant periods are around the second harmonic (13.5 days) in six years out of eleven.

The occurrence of shorter dominant periods during solar activity maximum and longer ones in the remaining part of the cycle could be confirmed by night absorption data determined at another frequency (185 kHz) in the LF-range at Kühlungsborn. The results are given in the lower part of Fig. 2,

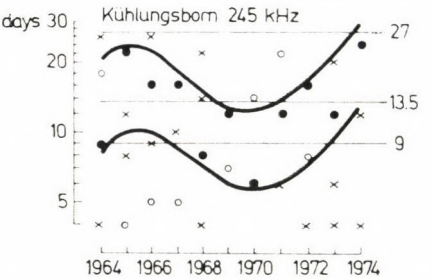


Fig. 1. Characteristic peaks in power-spectra of ionospheric night absorption measured at 245 kHz (Kühlungsborn) between 1964 and 1974. (Heavy dots: dominant peaks; Circles: important peaks; Crosses: small peaks. The curves emphasize the changes of dominant periods)

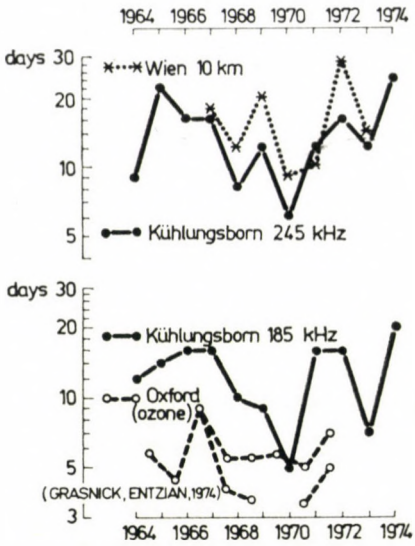


Fig. 2. Upper part: Changes in dominant periods for ionospheric night absorption at 245 kHz (Kühlungsborn) between 1964 and 1974 and for air pressure at 10 km altitude (Vienna) between 1967 and 1973, respectively. *Lower part:* Changes in dominant periods of ionospheric night absorption at 185 kHz (Kühlungsborn) between 1964 and 1974, as well as in characteristic periods of total ozone content (Oxford) for winters from 1964 to 1972 as published by GRASNICK and ENTZIAN [3]

which also shows the characteristic periods of total ozone content measured in Oxford during winter months from 1964 to 1972, as published by GRASNICK and ENTZIAN [3]. These results hint at shorter characteristic periods around solar activity maximum also in case of this stratospheric parameter. For comparison, the tendency found for night absorption at 245 kHz is once more drawn in the upper part of Fig. 2 where the changes of dominant periods for air pressure in the troposphere (10 km height) are plotted, too. The latter results cover only the interval from 1967 to 1973.

The connecting lines between yearly values in Fig. 2 do not want to suggest an exact year-by-year change of the length of dominant periods. This presentation should indicate the tendency change in dominant periods along with solar activity variations for appropriate parameters. In addition, it cannot be excluded that peaks in spectra applied as indicators of dominant periods sometimes have a random character. However, in this case even the random noise has more energy in the shorter period part of the spectrum during solar maximum conditions.

Figure 3 shows the results for the night absorption measured at a higher frequency (1178 kHz) in Kühlungsborn during the same interval (1964—74). Here, the dominant periods are shortest in a later phase of the solar cycle (i.e. in 1970—71) in comparison with those of Fig. 2 at two lower frequencies (in 1968—70), excepting the rather short period in 1964. (This latter peculiarity

has also been shown in Fig. 2, especially for 245 kHz.) The dominant periods of the atmospheric pressure at 10 km are again presented in Fig. 3.

A rather long data series of ionospheric night absorption was at our disposal from a further station. In Průhonice (Czechoslovakia, $\varphi_{\text{geogr.}} = 49°59'$ N, $\lambda = 14°33'$ E) the measurements have been carried out at 272 kHz and the data covered the interval from 1965 to 1974. In spite of the rather long dominant period in 1970 as well as the quite short ones in 1973 and 1974, the dominant periods shown in Fig. 4 for Průhonice night absorption generally reveal a tendency which is similar to that found for Kühlungsborn. Besides, an asymmetry appears between longer periods preceding and following the maximum of solar activity. Air pressure data from 20 km altitude over Vienna have also been analysed and the results are given for years between 1967 and 1973 in Fig. 4. In case of this parameter, the relatively shorter dominant periods can be traced again during the time of solar activity maximum.

Finally, noon data of ionospheric absorption measured at three different frequencies were also investigated. A reverse tendency has occasionally been found, especially at higher frequencies. (The results are not shown here.)

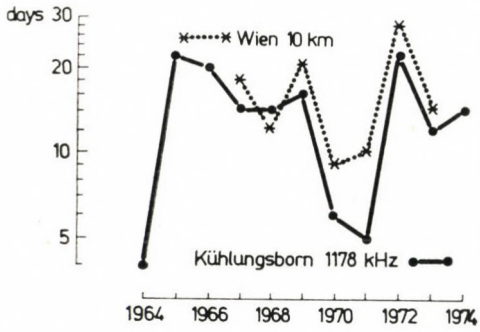


Fig. 3. The same as in the upper part of Fig. 2, but for 1178 kHz in case of ionospheric night absorption

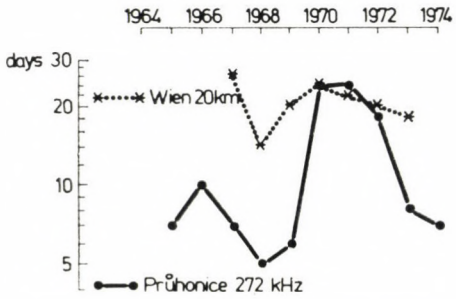


Fig. 4. Changes in dominant periods for ionospheric night absorption at 272 kHz (Průhonice) between 1965 and 1974 and for air pressure at 20 km altitude (Vienna) between 1967 and 1973, respectively

4. Discussion

As shown by several analyses, quasi-periodic variations can be present both in ionospheric absorption and in parameters characterizing the lower atmospheric levels. These results of statistical nature can indicate interrelations between processes at different altitudes, e.g. due to planetary waves, however, an exact interpretation is still lacking. In case of ionospheric absorption, it should be supposed that processes controlled or caused by solar phenomena may influence, or partly generate the quasi-periodic variations. Periodic oscillations in ionizing components of the solar radiation (ultra-violet, X-rays and particles) can likely contribute (at least occasionally) to the development of quasi-periodic variations in ionospheric parameters.

In the lower ionosphere, X-ray radiation (mainly below 10 Å) is an important ionizator of oxygen and nitrogen (O_2 and N_2). For 1971, we have determined co-spectra of daily means of solar X-ray flux data measured in the intervals of 1—8 Å and 8—20 Å by SOLRAD—9 and EXPLORER—37 satellites and absorption data measured at mid-latitude stations (*Kühlungsborn:* 128, 185, 245 and 1178 kHz for night; *Průhonice:* 272 kHz for night and *Neustrelitz:* 2614 and 2775 kHz for noon). Results given in Table II show that the maximum coherence between these solar and ionospheric parameters occurred mainly around 9—10 and/or 20—22 days (sometimes also at 26 days) in the interval investigated. (Maximum values are underlined in Table II in case of ≥ 0.40.) Apostolov and Letfus [10] have also analysed solar X-ray flux data in the intervals of 1—8 and 8—20 Å (between 1969 and 1972). In the corresponding domain their spectra revealed periods around 12, 20 and 22 days in addition to a fundamental 27-day variation.

It cannot be excluded that quasi-periodic variations of ionospheric absorption partly originate from fluctuations with similar periods in solar X-ray flux, being a quite important ionizing factor in the lower ionosphere. Naturally, further ionizing factors, or other influences of extraterrestrial origin may also be considered as possible sources of quasi-periodic variations in ionospheric absorption. There are some recent results [11] showing a correlation between ionospheric absorption and interplanetary magnetic field polarity changes. It is not the purpose of this paper but it should be investigated in the future whether a relationship could be found between these two parameters concerning the quasi-periodic variations, too.

Two further parameters generally used as indicators of solar activity were analysed similarly to ionospheric absorption (in Section 3). The analyses were especially aimed at tracing changes in dominant periods. Results are shown for the interval between 1964 and 1974 in Fig. 5. The dominant periods found in solar radio emission at 2800 MHz (Ottawa) and in sunspot relative numbers (Zürich) are indicated by heavy dots. (Circles and crosses have the

Table II

Maximum values in co-spectra of ionospheric absorption

Absorption at frequency (kHz) Station	Periods							
	3	4	5	6	7	8	9	10
Night 128							*.45*	
Kühlungsborn			.11				*.43*	
Night 185			.25		.12			
Kühlungsborn		.22						.12
Night 245				.30				*.45*
Kühlungsborn				.22				*.43*
Night 272		.30				*.40*		
Průhonice		.26			*.41*			
Night 1178				.37				
Kühlungsborn				.35				.32
Noon 2614				.13			*.40*	
Neustrelitz			.12				*.40*	
Noon 2775		.23						*.52*
Neustrelitz		.16						*.50*

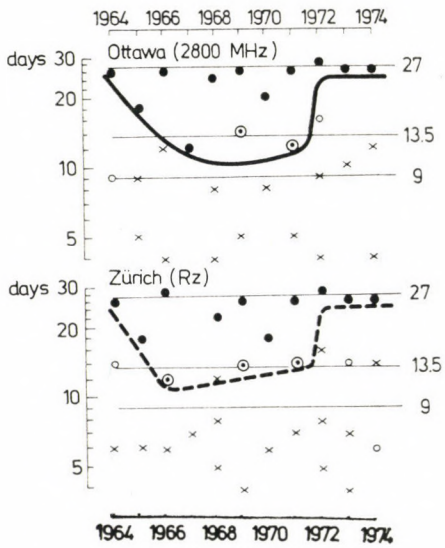


Fig. 5. Characteristic peaks in power-spectra of solar radio emission at 2800 MHz (upper part) and sunspot relative numbers (lower part) between 1964 and 1974. (Encircled dots stand for dominant-like peaks, other notations are the same as in Fig. 1)

and solar X-ray flux data for 1971

(days)										X-ray flux interval (Å)
12	14	16	18	20	22	24	26	28	30	
							.61			1— 8
.35							*.69*			8—20
.14					*.45*					1— 8
					.36					8—20
	.32			*.52*						1— 8
	.25			*.48*						8—20
			.59				*.71*			1— 8
			.48				*.67*			8—20
.29				*.62*						1— 8
				.57						8—20
		.38			.14					1— 8
		.40								8—20
					.48					1— 8
					.44					8—20

same denotation as given in connection with Fig. 1.) Encircled dots in Fig. 5 stand for "dominant-like" periods, i.e. peaks almost as large as those indicating the dominant periods. As could be expected, periods around 27 days were dominating during the greater part of the investigated interval. Nevertheless, among the dominant periods, there are shorter ones, too. The dominant-like periods occur next to the line indicating the second harmonic of the 27-day variation. Curves drawn into the figure show that in spite of some exceptions the shorter periods are dominant, or dominant-like mainly towards solar activity maximum, but this tendency is completely over (from 1972) following the maximum. Consequently, the occurrence of shorter dominant periods of ionospheric night absorption in and around years of maximum solar activity can really be attributed to solar influences, however, the clearing up of the mechanism and processes involved needs further investigations.

The present study wanted to hint at the importance of quasi-periodic variations in ionospheric absorption. Namely, parameters of the lower ionosphere seem to be useful for tracing variations which are connected on the one hand with processes of the lower and upper atmosphere and on the other with extraterrestrial effects. Because of the complexity of the influences, we certainly need continuous and simultaneous informations about several parameters in appropriately chosen altitudes of the atmosphere in addition to the steady monitoring of solar phenomena.

Data used in analyses were taken from the following material

Aerologische Berichte, Zentralanstalt für Meteorologie und Geodynamik, Wien (1967—1973),
Annuaire météorologique et de l'électricité atmosphérique, Warszawa (1964—1965),
Geomagnetic Planetary Indices, Göttingen (1964—1974),
Geophysikalische Beobachtungsergebnisse H.H.I., Berlin (1968—1974),
Geophysikalische Messreihen, Kühlungsborn (1964—1967),
Geophysical Observatory Reports, Observatory of Nagycenk, Sopron (1967—1973),
Ionospheric Data, Observatories Průhonice and Panska Ves (1965—1974),
Materialy i Prace 23, 28, 38, 44, 53, 63, 77, 80, Warszawa (1966—1973),
Observatoriumsberichte, Sopron (1964—1966),
Solar Geophysical Data, NOAA, Boulder (1971—1972).

REFERENCES

1. MÄRCZ, F.: Preliminary report on the power spectra of ionospheric absorption. *Acta Geod. Geoph. Mont. Hung.*, 7(1972), 197—206.
2. LAUTER, E. A.: Evidence and characteristics of internal and planetary waves within the D-region plasma. Proc. COSPAR Symp. Methods of Measurements and Results of Lower Ionosphere Structure (Ed. by K. RAWER), 1974, 377.
3. GRASNICK, K. H.—ENTZIAN, G.: On the variation of the total amount of ozone and the behaviour of some ionospheric parameters in the winter-time upper atmosphere. *Geod. Geoph. Veröffl. NKGG, DDR*, Reihe II, Heft 18 (1974), 21—35.
4. SCHWENTEK, H.: Wave-like structures in the variation of ionospheric absorption. *J. atmos. terr. Phys.*, 36(1974), 1173—1178.
5. MÄRCZ, F.: Further studies on ionospheric absorption and geomagnetic activity. *Acta Geod. Geoph. Mont. Hung.*, 8(1973), 297—312.
6. MÄRCZ, F.—VERŐ, J.: Ionospheric absorption and Pcl-type micropulsations following enhanced geomagnetic activity. *J. atmos. terr. Phys.*, 39(1977), 295—302.
7. BOSSOLASCO, M.—ELENA, A.: Absorption de la couche D et température de la mésosphère. *Compt. Rend. Acad. Sci. Paris*, 256(1963), 4491.
8. MÄRCZ, F.: Links between atmospheric electricity and ionospheric absorption due to extraterrestrial influences. *J. geophys. Res.*, 81(1976), 4566—4570.
9. CHARNEY, J. G.—DRAZIN, P. G.: Propagation of planetary-scale disturbances from lower into the upper atmosphere. *J. geophys. Res.*, 66(1961), 83—109.
10. APOSTOLOV, E. M.—LETFUS, V.: Spectral analysis of the time variations of solar X-rays in the 1—8 Å and 8—20 Å regions. *Bull. Astr. Inst. Czech.*, 26(1975), 193—198.
11. SCHLEGEL, K.—ROSE, G.—WIDDEL, H. U.: Interplanetary magnetic field polarity changes and D-region radio wave absorption. *J. atmos. terr. Phys.*, 39(1977), 101—103.

КВАЗИПЕРИОДИЧЕСКИЕ ВАРИАЦИИ ИОНОСФЕРНОГО ПОГЛАЩЕНИН И ИХ ХАРАКТЕРНЫЕ ИЗМЕНЕНИЯ В ТЕЧЕНИЕ ЦИКЛА СОЛНЕЧНОЙ АКТИВНОСТИ

Ф. МЕРЦ

РЕЗЮМЕ

При помощи спектрального анализа могут быть обнаружены квазипериодические вариации в ионосферном поглащении, измеренном на станциях Европы на средних широтах. В рассмотренном диапазоне спектров (от 3 до 30 дней) часто появляются пики около 4—6, 8—9 и 12—14 дней. В некоторых параметрах можно найти подобные квазипериодические вариации, но подробный анализ был проведен только относительно ионосферного поглащения. На основе чётких пиков в спектрах, определенных для отдельных годов цикла солнечной активности (1964—74) были выбраны доминирующие периоды ночного поглащения, которые показывают характерные изменения. По-видимому, доминирующие периоды короче около максимума солнечной активности, чем в другие промежутки исследованного цикла. Подобная тенденция может быть обнаружена и в параметрах солнечной активности. Квазипериодические вариации ионосферного поглащения частью могут быть происходящими от солнца. К этому можно прийти на основе данных о потоке рентгеновского излучения и результатов анализов коспектров, проведенных данными поглащения.

Acta Geodaet., Geophys. et Montanist. Acad. Sci. Hung. Tomus 14 (1—2), pp. 237—245 (1979)

DEUTUNG DER REFRAKTIONSSEISMISCHEN MESSUNGEN AUF DEM ÖSTLICHEN ABSCHNITT DES ALPENLÄNGSPROFILES

K. ARIC—R. GUTDEUTSCH

INSTITUT FÜR METEOROLOGIE UND GEOPHYSIK, WIEN

I. ALBU—E. MITUCH—K. POSGAY

GEOPHYSIKALISCHES INSTITUT ROLAND EÖTVÖS, BUDAPEST

[Eingegangen am 14. April, 1978]

Die Auswertung des Alpenlängsprofiles (ALP) zwischen Judenburg (Österreich) und Hosszúpereszteg (Ungarn) mit ebenen geneigten Grenzflächen zeigt, daß die M-Diskontinuität von Westen nach Osten um 9 km ansteigt. In Anbetracht der starken lateralen Inhomogenitäten der Wellengeschwindigkeiten werden 2 P-Geschwindigkeit-Tiefen-Modelle vorgeschlagen, von denen das eine bei Verwendung von SP E und das andere bei Verwendung von SP F des ALP gültig ist. Beide Modelle enthalten eine Geschwindigkeitsinversion in der Oberkruste und eine weitere in der Unterkruste. Die in der Unterkruste ist nur durch schwache, undeutliche Signale objektiv belegt und kann noch nicht als gesichert angesehen werden. Dagegen sind die Einsätze, die von der M-Diskontinuität herrühren, sehr deutlich. Die Modelle stellen wegen dem äußerst komplizierten geologischen Aufbau dieses Gebietes nur erste Näherungen dar.

Einleitung

Die vorliegende Untersuchung betrifft den östlichsten Teil des Alpenlängsprofiles (ALP) zwischen Judenburg (SP E) und Hosszúpereszteg (SP F). Das Profilabstandszeichen: 05. Über die technische Durchführung des Projektes ist bereits berichtet worden (Alpine Explosion Seismology Group 1976). Das ausgewertete Profilstück hat eine Länge von 210 km und verläuft in ost-westlicher Richtung (Abb. 1). Ganz im Westen schließt es das Altkristallin der Niederen Tauern auf, überschreitet westlich von Graz den Alpenostrand und verläuft sodann im Bereich tertiärer und quartärer Sedimente des Grazer Beckens, das gebietsweise von tertiärem Vulkanismus durchsetzt ist. Dieser Vulkanismus zeigt den Rand des östlich anschließenden pannonischen Beckens an. Das Profilende bei SP F befindet sich bereits im Pannonikum mit mächtigen tertiären Sedimenten. Das Meßgebiet schließt damit den interessanten Grenzbereich zwischen den Ostalpen und dem pannonischen Becken auf, dessen tieferer Krustenaufbau bisher noch wenig geophysikalisch erforscht ist.

Seismogrammontagen

Die Abb. 2 und 3 stellen Seismogrammontagen der Schüsse SP E nach Osten und SP F nach Westen dar. Die ersten Einsätze der Signale von SP E bilden eine zunächst stark und in größeren Distanzen schwächer gekrümmte

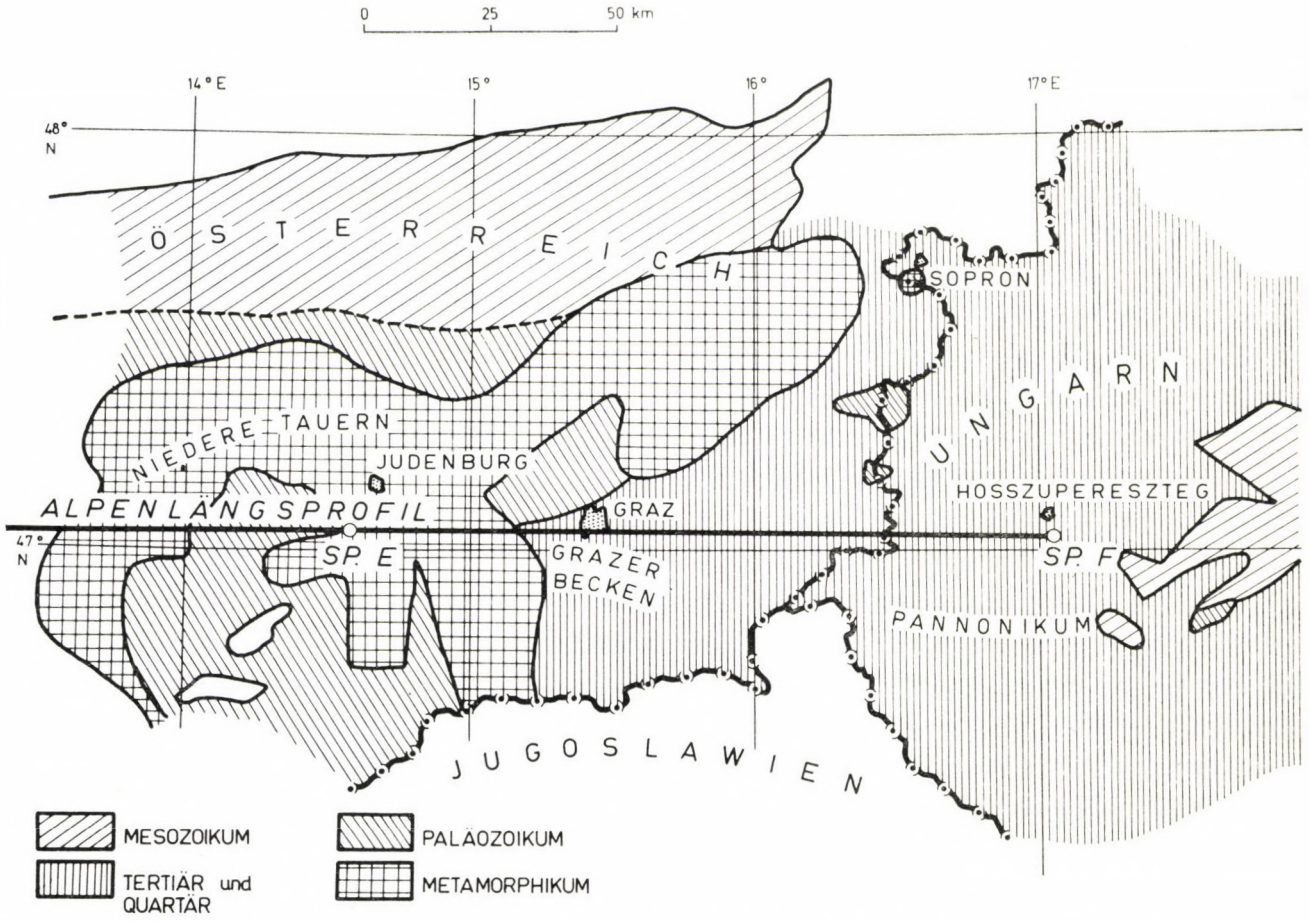


Abb. 1. Schematische geologische Karte des österreich-ungarischen Grenzgebietes und die Lage des Alpenlängsprofiles

Laufzeitkurve (1). Bei 70 km kommt es zu einer Laufzeitanomalie. Hier beginnen die Signale hinter der erwarteten Laufzeit zurückzubleiben. Die Verzögerung erreicht 0.3 sec bei 85 km. Nach diesem Signal folgen mindestens 2 weitere in Abständen von 0,3—0,4 sec, die diese Verzögerung zeitlich versetzt mitmachen. Es entsteht der Eindruck, als ob diese späteren Einsätze nicht an

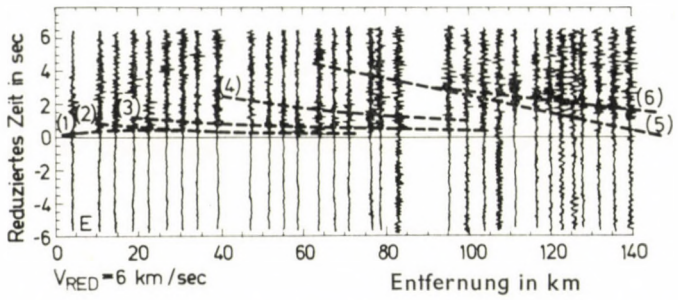


Abb. 2a. Seismogrammontage der Schüsse SP E nach Osten

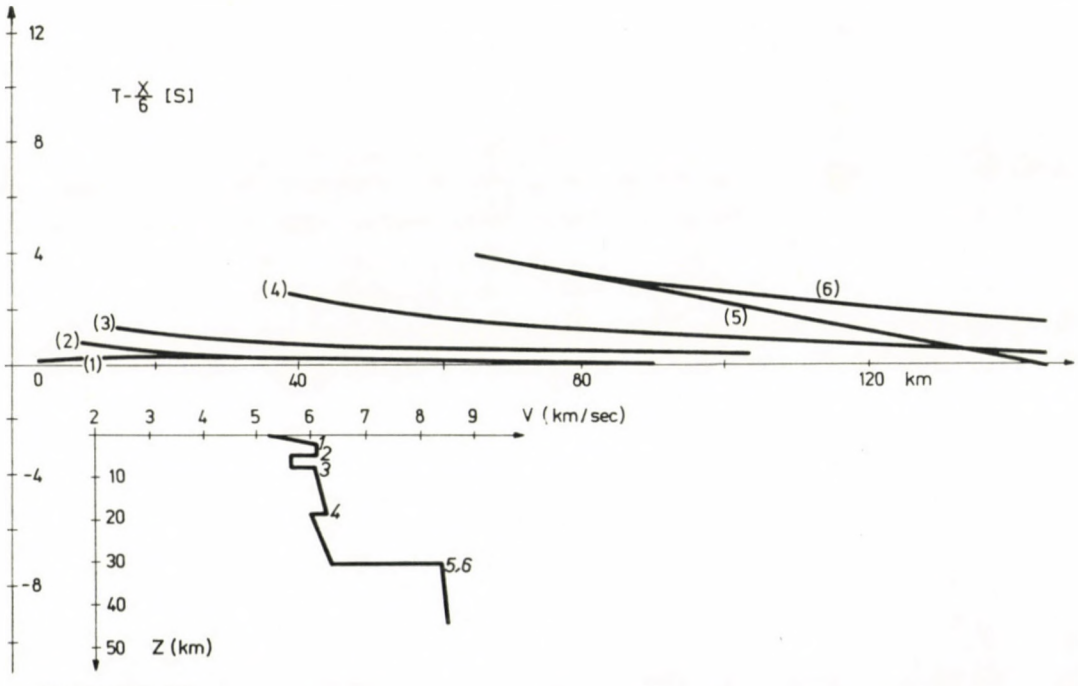


Abb. 2b. **Das Modell für SP E mit horizontaler Schichtung und die dazugehörige synthetische Laufzeitkurve**

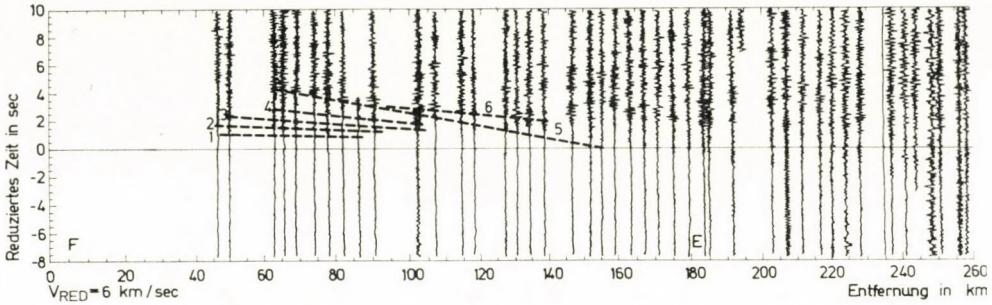


Abb. 3a. Seismogrammontage der Schüsse SP F nach Westen

die Ersteinsätze tangieren, sondern parallel zu diesen verlaufen. Wichtig ist die Beobachtung, daß der Störpegel ab 80 km sehr stark ansteigt. Das dürfte einerseits damit zusammenhängen, daß das Gebiet hier stärker besiedelt ist (Nähe von großen Städten, Industrie), andererseits aber befindet sich bei 80 km etwa der Alpenostrand und die Grazer Bucht mit N-S-streichenden tertiären Brüchen, die das Profil kreuzen [10]. Diese können leicht eine stärkere Extinktion der Wellen bewirken. Wegen des hohen Störpegels kann jedenfalls nicht entschieden werden, ob die P_G-Welle (Abb. 2; (2)) ab einer bestimmten Entfernung verschwindet, was als Indiz für eine Geschwindigkeitsinversion zu deuten wäre. Ab etwa 65 km tritt bei der reduzierten Laufzeit von 4,3 sec ein energiereiches Signal mit sehr hoher Scheingeschwindigkeit auf. Es bildet langanhaltende Schwingungszüge infolge der Interferenz verschiedener Wellen und legt die Deutung als P_M P-Reflexion nahe.

Die Seismogramme von SP F (Abb. 3) beginnen mit einer Informationslücke bis ca. 40 km. Darum sind die Anfangsäste und ihre Geschwindigkeit nicht festlegbar. Im Vergleich zu Abb. 2 jedoch kann man erkennen, daß die ersten Signale von SP F um etwa 0,7 sec später eintreffen als die mit vergleichbarer Entfernung von SP E. Diese Verspätung ist leicht durch die Sedimentbedeckung im Bereich des SP F und auch durch die Topographie entlang des Profiles zu erklären. Abgesehen hiervon besteht eine gewisse Ähnlichkeit dieser Seismogrammontage mit Abb. 2. Die dort erkennbaren späteren Einsätze — siehe Laufzeitkurven (2) und (3) in der Abb. 2 — sind auch hier vorhanden. Innerhalb des vermessenen Beobachtungsintervalles von ca. 220 km ist ein Verschwinden der P_G-Einsätze nicht nachzuweisen. Darum fehlt auch auf diesem Profil das sichere Zeichen für eine Geschwindigkeitsinversion.

Im erwarteten Zeitbereich der P_M P-Reflexion zeigen die Seismogramme kräftige Signale (6). Weil der Störpegel verhältnismäßig klein ist, kann man auch das energieschwache Signal der P_n-Welle klar identifizieren (5).

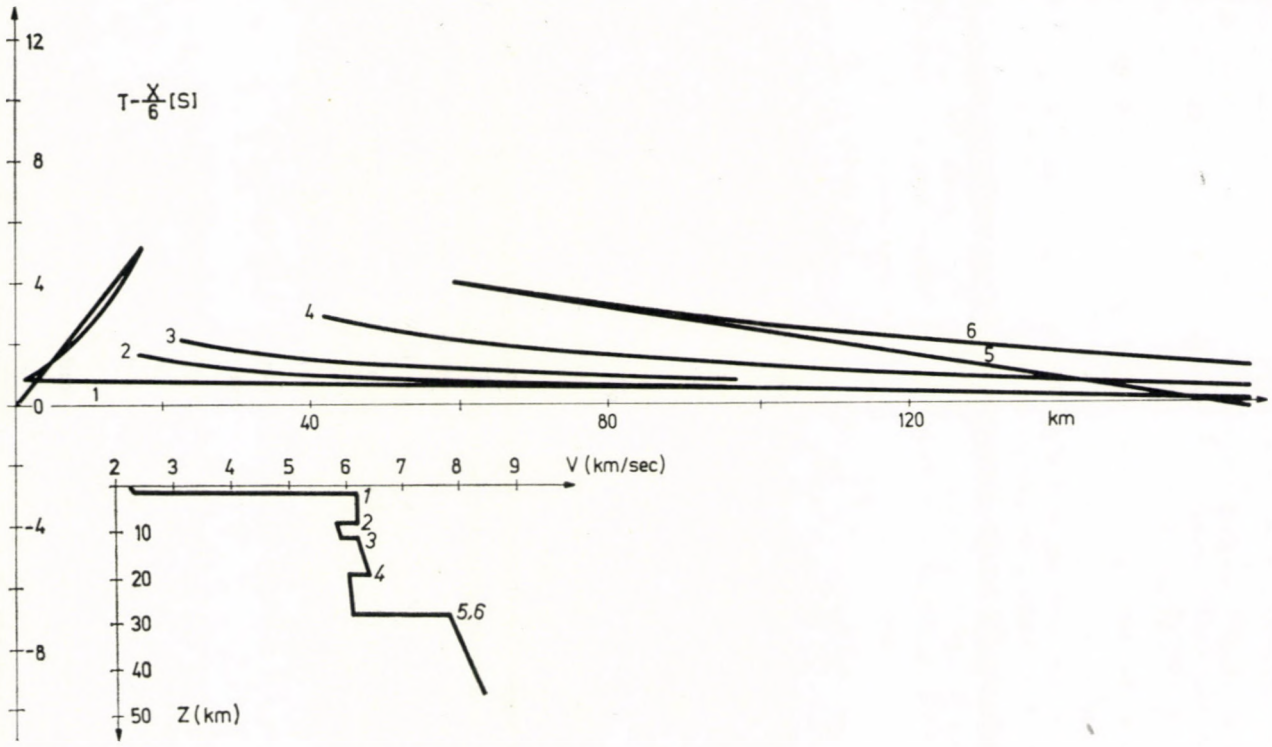


Abb. 3b. Das Modell für SP F mit horizontaler Schichtung und die dazugehörige synthetische Laufzeitkurve

Deutungsversuche

Die Deutung ist aus zwei Gründen schwierig, erstens weil entlang dem Profil extrem starke Veränderungen der Gesteinsbeschaffenheit vorliegen, insbesondere am Alpenostrand, und zweitens weil es unmöglich ist, das Abreißen einer Laufzeitkurve und damit eine Geschwindigkeitsinversion sicher nachzuweisen. In Anbetracht dieser Situation ist es naheliegend, zunächst von einem einfachen Modell des Untergrundes auszugehen. Dieses einfache Modell setzt voraus, daß die M-Diskontinuität eine ebene geneigte Grenzfläche ist, an der die P-Geschwindigkeit eine Unstetigkeit aufweist (Abb. 4). Als weitere Information wird die Kenntnis des Krustenaufbaues im Bereich der Schußpunkte E und F verwendet. So dient die von H. MILLER et al. [6] erhaltene Geschwindigkeitsverteilung für den weiter westlich anschließenden Abschnitt des Alpenlängsprofiles bis zur M-Diskontinuität als Modell für den Bereich um SP E bis 105 km Entfernung. Weiter östlich davon wird jene Geschwindigkeitsverteilung verwendet, die auf dem ungarischen Refraktionsprofil (NP-1) nächst SP F gemessen wurde [8]. Unter dieser Voraussetzung erhält man das Modell einer nach Osten um ca. 9 km ansteigenden M-Diskontinuität (Abb. 4). Sie wird unter SP E in 36 km und unter SP F in 27 km Tiefe angetroffen.

Als alternative Deutung werdem im folgenden 2 Modelle mit horizontaler Schichtung, eines für Abb. 2 (SP E) und eines für Abb. 3 (SP F) gültig, vorgeschlagen. Die oben besprochene Laufzeitverzögerung (in Abb. 2 bei 70 km) wird nicht als die Folge einer „Schattenzone", wie die durch Geschwindigkeitsinversionen hervorgerufen werden, gedeutet, sondern als Folge der plötzlichen Mächtigkeitsänderung oberflächennaher Sedimente mit kleiner Wellengeschwindigkeit. Die weitgehende Parallelität der späteren Einsätze zum Ertseinsatz (Abb. 2; (2), (3)) könnte durch Wechselwellen vom Typ PS oder SP oder auch durch multiple Reflexionen einer Welle innerhalb einer Schicht eine Erklärung finden. Neben diesen ist aber auch die Deutung als P-Reflexion von der Unterfläche einer eingelagerten Schicht kleiner Wellengeschwindigkeit, also einer Inversionszone, denkbar. Wir halten die zweite Möglichkeit aus Gründen, die unten erläutert werden, für die wahrscheinlichere, sind uns aber bewußt, daß diese Modelle wegen der besonderen Situation lateraler Ungleichförmigkeit nicht mehr als das gemittelte Verhalten der Erdkruste in dem von den Wellen durchlaufenen Gebiet wiedergeben.

Abb. 2a zeigt das Modell für Abb. 2 (SP E) und die dazugehörige synthetische Laufzeitkurve. Das Modell zeigt nahe der Erdoberfläche zunächst eine rasche und dann eine langsamere Zunahme der P-Geschwindigkeit mit der Tiefe. Diesem Tiefenbereich ist der Laufzeitast (1) zuzuordnen. Die Gründe, die für die von 8 bis 12 km Tiefe ausgedehnte Inversionszone sprechen, sind folgende:

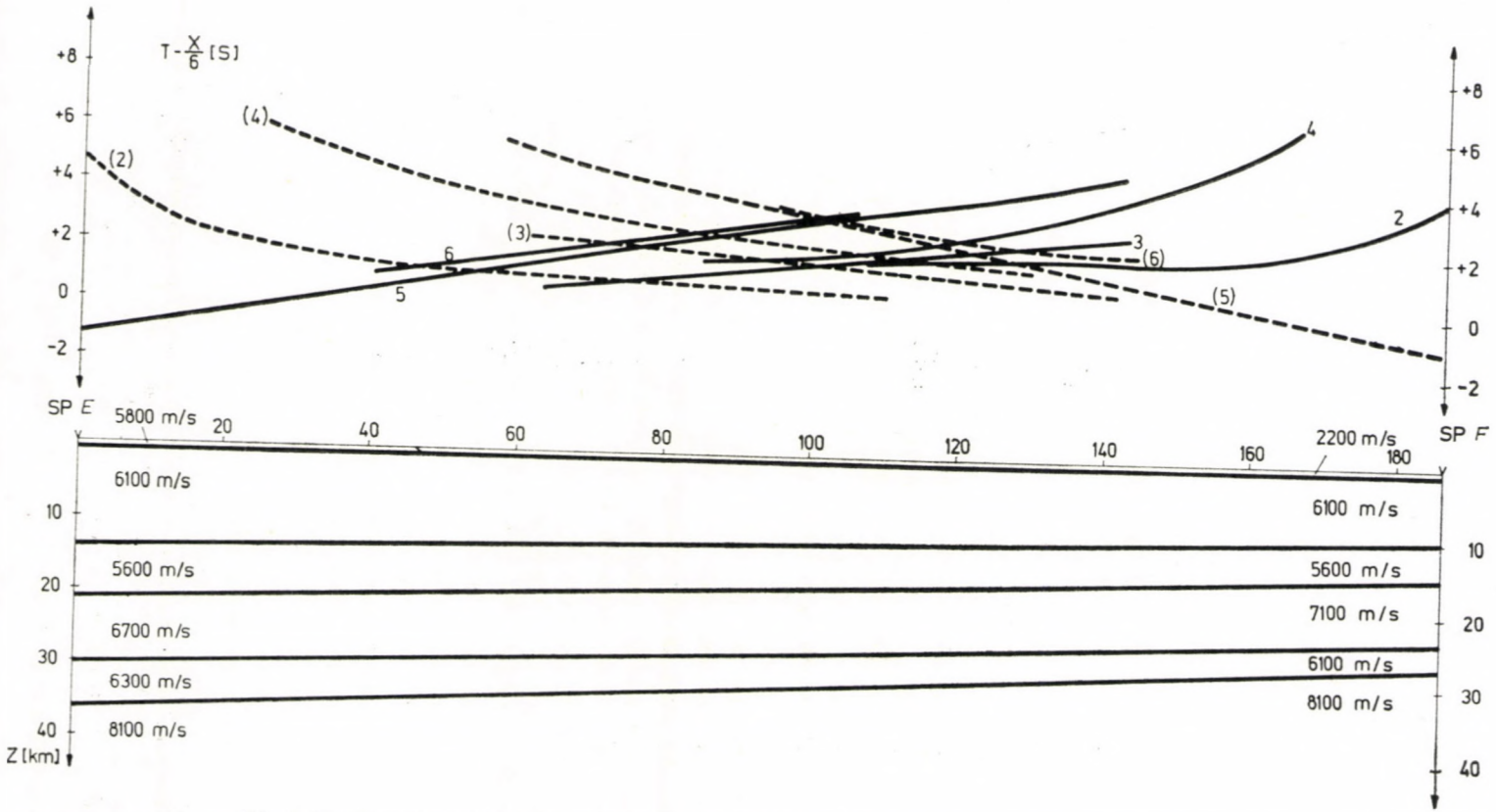


Abb. 4. Das Modell mit Voraussetzung, daß die M-Diskontinuität eine ebene geneigte Grenzfläche ist

1. Labormessungen an Granit aus den Hohen Tauern bei hohem Druck und hoher Temperatur zeigen, daß eine P-Geschwindigkeitsinversion ab 8 km Tiefe wahrscheinlich ist. In diesem Falle wäre der Wiederanstieg der P-Geschwindigkeit bei 12 km leicht durch die Phasenumwandlung des Quarzes im Granit von der α- in die β-Modifikation erklärlich [4, 5]. Die Tatsache, daß der Wellenleiter in dieser Tiefe wahrscheinlich aus vorwiegend granitischem Material besteht, erhärtet diese Deutung.

2. Der gut belegte Laufzeitast (2) tangiert den Ersteinsatz und kann als Reflexion der „Kanal"-Oberfläche interpretiert werden.

3. Der sehr gut belegte Laufzeitast (3) bildet eine Parallele zum Ersteinsatz. Er wird als Reflexion von der „Kanal"-Unterfläche gedeutet.

4. Steilwinkelreflexionen, beobachtet am SP E, zeigen mehrere Einsätze.

Die zweite Inversionszone zwischen 18 und 29 km ist nur schwach belegt. Es gibt schwache Argumente für ihre Existenz. MILLER et al. haben für das westlich anschließende Profilstück SP D des Alpenlängsprofiles in diesem Tiefenbereich eine Inversionszone gefunden. Viel weiter östlich, nämlich im östlichen Teil Ungarns, stellte POSGAY [9] mit Hilfe eines reflexionsseismischen Experimentes mit Mehrfachüberdeckung eine Inversion in entsprechender Tiefe fest. Wir nehmen an, daß man zwischen den beiden Gebieten interpolieren kann, daß also die Inversionszone auch zwischen den Schußpunkten SP E und SP F vorhanden sein muß. Über die Tiefenstruktur unseres Meßgebietes ist sehr wenig bekannt, insbesondere liegen aber auch keine physikalischen Informationen vor, die dieser Annahme widersprechen. Der Laufzeitast (4) würde dann eine Reflexion von der unteren „Kanal"-Oberfläche bedeuten. In dem entsprechenden Zeitbereich findet man undeutliche und schwache Einsätze, die man schwerlich als Argument für die untere Inversionszone ins Feld führen kann. Die P_M P-Laufzeitkurve (6) ist gut belegt.

Das für SP F gültige Modell (Abb. 3a) ist bis zu M-Diskontinuität aus den Durchschnittsgeschwindigkeiten der ungarischen Explorationsseismik [8] in Anlehnung an Abb. 2a abgeleitet worden. Es enthält jedoch die beiden Geschwindigkeitsinversionen in der Ober- und Unterkruste. Die Anpassung ist so erfolgt, daß kein Widerspruch zu der Tiefenangabe der M-Diskontinuität von 27 km Tiefe auf dem ungarischen Profil NP-1 entsteht. Die Zuordnung der einzelnen Laufzeitäste ist die gleiche wie in Abb. 2a (SP E). Im Gegensatz zu dieser ist die P_n-Welle (5) gut gesichert.

Danksagung

Dem ungarischen Geologischen Zentralamt und dem Nationalkomitee des Österreichischen Geodynamischen Projektes sei für ihre finanzielle Unterstützung und dem ungarischen Erdöltrust für die Mitarbeit gedankt. Diese Arbeit stellt einen Beitrag zu dem von den Österreichischen und Ungarischen Akademien der Wissenschaften geförderten Forschungsschwerpunkt „Das Übergangsgebiet zwischen Ost-Alpen und Pannonikum" dar.

SCHRIFTTUM

1. Alpine Explosion Seismology Group (Reporter: H. Miller): A Lithospheric Seismic Profile along the Axis of the Alps — First Results PAGEOPH 1976.
2. Aric, K.: Seismische Großsprengungen im Lavant- und Tor-See zur Vermessung des Alpenkörpers. Informationstag für Sprengtechnik, WIFI, Linz 1975.
3. Aric, K.—Gutdeutsch, R.: Erste Ergebnisse des Alpenlängsprofiles (Schußpunkte *E*, *F* und *I*) Vortrag DGG, Braunschweig 1977.
4. Fielitz, K.: Untersuchungen zur Temperaturabhängigkeit von Kompressions- und Scherwellengeschwindigkeiten in Gesteinen unter erhöhtem Druck. Diss. Technische Universität Clausthal, 1971.
5. Fielitz, K.: Compressional and Shear Wave Velocities as a Function of Temperature in Rocks at High Pressure. Explosion Seismology in Central Europe, Springer Verlag, Berlin 1976, 40—44.
6. Miller, H.—Gebrande, H.—Schmedes, E.: Ein verbessertes Strukturmodell für die Ostalpen, abgeleitet aus refraktions-seismischen Daten unter Berücksichtigung des Alpenlängsprofiles. *Geolog. Rundschau*, 66(1977), 289—308.
7. Miller, H.—Ansorge, J.—Aric, K.—Perrier, G.: Preliminary Results of the Alpine Longitudinal Profile, 1975, from France to Hungary, in Geodynamic Vol.: Alps, Apennines, Hellenides, Geodynamic Investigations along Geotraverses by an International Group of Geoscientists. Editors: H. Closs, D. Roeder, Kl. Schmidt (in press).
8. Mituch, E.—Posgay, K.: The Crustal Structure of Central and Southeastern Europe Based on the Results of Explosion Seismology, 28 Hungary. Geophysical Transactions, Hungarian Geophysical Institute Roland Eötvös, 1972, 118—129.
9. Posgay, K.: Mit Reflexionsmessungen bestimmte Horizonte und Geschwindigkeitsverteilung in der Erdkruste und im Erdmantel. Geophysical Transactions, Hungarian Geophysical Institute Roland Eötvös, 1975, 13—17.
10. Tollmann, A.: Ostalpentektonik I. Die bruchtektonische Zyklenordnung im Orogen am Beispiel der Ostalpen. *Geotektonische Forschungen*, Heft No. 34, 1970.

ЗНАЧЕНИЕ РЕФРАКЦИОННО-СЕЙСМИЧЕСКИХ ИЗМЕРЕНИЙ НА ВОСТОЧНОЙ ЧАСТИ ПРОДОЛЬНОГО ПРОФИЛЯ АЛЬП

И. АЛЬБУ—К. АРИК—Р. ГУТДОЙЧ—Е. МИТУК—К. ПОШГАИ

РЕЗЮМЕ

Обработка продольного профиля Альп (ALP) между Юденбургом (Австрия) и Хоссуперестег (Венгрия) с плоскими наклонными граничными поверхностями показывает, что М-разрывность увеличивается с запада на восток на 9 км. Учитывая сильные боковые неоднородности скорости волн предлагаются 2 Р-скоростные глубинные модели, из которых одна пригодна при применении SPE, а другая при SPF ALP. Обе модели содержат одну инверсию скорости в верхней коре и одну в нижней. Инверсия в нижней коре заметна только через слабые, незначительные сигналы, поэтому ее пока нельзя рассматривать как надежную. Напротив, сигналы, происходящие от М-разрывности, очень ясны. Модели представляют пока из-за чрезвычайно сложного геологического строения этой территории только первые приближения.

Acta Geodaet., Geophys. et Montanist. Acad. Sci. Hung. Tomus 14 (1—2), pp. 247—256 (1979)

INVESTIGATION OF CAPILLARY-GRAVITY WAVES IN A THIN NON-NEWTONIAN FILM FLOW BY POTENTIAL-THEORY METHOD

E. BOBOK

CANDIDATE OF TECHNICAL SCIENCES

STUDY-GROUP FOR MINING RESEARCH,
TECHNICAL UNIVERSITY OF HEAVY INDUSTRY, MISKOLC

[Manuscript received November 30, 1976]

Capillary-gravity waves are investigated in a thin, non-Newtonian fluid flow. The flow is unsteady, periodic, non-decaying. The velocity field is determined as the second boundary problem of the potential theory. The boundary condition is the velocity distribution of an arbitrarily viscous fluid flow at a suitably chosen cross-section. The results show the dependence of the velocity profiles on the behaviour-index, the shape of the waves, and the stability depending on the Reynolds and the Froude number.

The turning of science into the forces of production is the characteristic feature of the scientific-technical revolution started in modern industrial society. Technological processes are rooted increasingly in the result of such basic research works which have been placed by the practicists among the sphere of pure science not without malice. Development in the investigation of the environmental protection in the last decade is a case in point: what happens if both scientific knowledge and technical facilities are suitable and the requirements of society are established? This tendency is reflected in the interest with which the specialists of the environmental protection turn to the research of capillary-gravity waves occurring on the film flow.

GRIMLEY's work was the first systematic experimental investigation in this field [1].

The conditions of the occurrence of the laminar turbulent and the transition regions were investigated for a long time only experimentally [2, 3, 4, 5].

The first analytical method was made by JEFFREYS [6]. The capillary effects were neglected, and only Newtonian-type viscous forces were considered.

LANDAU and LEVITCH have taken into consideration the effect of the capillary forces too, in investigating the film flow on the surface of a rigid body taken out of a stratified static fluid [7].

In KAPITSA's analysis the computed and experimental results are in agreement, due to an approximate solution of the Navier—Stokes equation [8].

In the author's former work KAPITSA's analysis was extended to purely viscous non-Newtonian fluids [9]. The equation of motion was averaged across the film thickness; after some simplifications the mean velocity, the phase velocity of the waves, the mean thickness of the film and the wave-number

were obtained. At last a very simple, approximate expression for the stability of the waves was found.

In the foregoing works there are one-dimensional relationships between averaged parameters, which are acceptable for today's practice, but cannot be considered as the base of further development.

This paper presents the determination of the velocity field developing in the capillary-gravity wave motion, as the second boundary value; or NEUMANN's problem of the potential theory. The mathematical apparatus seems to be rather unusual, but it is a very flexible procedure, well fitting into the feasibility of the digital computer.

The two basic equations of the problem are based upon a pure kinematic thought. Nevertheless, the boundary conditions are originated from the solution of the equation of motion referring to the arbitrarily viscous fluid, so they are suitable to represent any general relationship between stress and deformation.

The iteration procedure is one of the most applicable numerical methods for the solution of partial differential equations.

As it is shown in Fig. 1, a thin viscous fluid layer flows downward on a great flat plate, due to the gravitational force. The flow is laminar, the viscous forces cannot be neglected because of the small thickness of the layer. On the surface of the film capillary-gravity waves occur due to the capillary tension and are moving in the direction of the flow at a wave speed greater than the fluid velocity. The potential energy of the gravitational field keeps balance with the mechanical energy dissipation, therefore the waves are non-decaying, their wave-speed, amplitude and wavelength are constant.

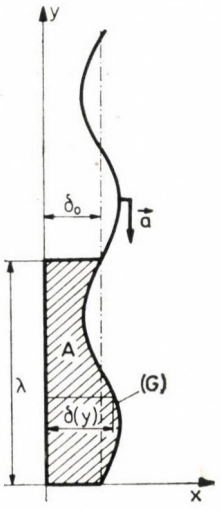


Fig. 1

The fluid is considered incompressible. Let x and y be rectangular coordinates. The Cartesian coordinate system $Oxyz$ is chosen with its origin in the plate, and the x axis is perpendicular to the latter. The y axis is in a direction opposite the motion. In the direction z there is no change of the flow pattern, so the flow is two-dimensional. The coordinate system moves with the wave velocity a in the $-y$ direction. Therefore, the unsteady flow in the absolute coordinate system will be steady in the moving, relative coordinate system. The relative flow is rotational due to the viscous forces. The two basic equations representing incompressibility and vorticity are the following:

$$\frac{\partial w_x}{\partial x} + \frac{\partial w_y}{\partial y} = 0 \tag{1}$$

and

$$\frac{\partial w_y}{\partial x} - \frac{\partial w_x}{\partial y} = \Omega(x, y)\,, \tag{2}$$

where w_x and w_y are the relative velocity components in the moving coordinate system. The relationship between the absolute and the relative velocities is

$$\vec{c} = \vec{a} + \vec{w}\,. \tag{3}$$

The $\Omega(x, y)$ function, yet unknown, is the only z-direction component of the vorticity vector. Eq. (1) will become identity, if

$$w_x = \frac{\partial \psi}{\partial y}\,, \quad w_y = -\frac{\partial \psi}{\partial x}\,, \tag{4}$$

so that knowledge of the $\psi(x, y)$ function determines the complete velocity field. Moreover, it is evident that the curves $\psi = \text{const}$ are the streamlines of the field. ψ is called the stream function. The derivatives (4) substituted to Eq. (2) lead to the following Poisson-equation

$$\frac{\partial^2 \psi}{\partial x^2} + \frac{\partial^2 \psi}{\partial y^2} = -\Omega(x, y)\,. \tag{5}$$

To obtain the solution we use GREEN's formula referring to two-dimensional scalar functions. This (as it is known) is valid for any arbitrary simply connected region in an inner point:

$$2\pi\psi = \iint_A \Delta\psi \ln t\, dA + \oint_G \frac{\partial \psi}{\partial n} \ln t\, ds - \oint_G \psi \frac{\partial}{\partial n} (\ln t)\, ds \tag{6}$$

and for an outer point:

$$0 = \iint_A \Delta\psi \ln t \, dA + \oint_G \frac{\partial \psi}{\partial n} \ln t \, ds - \oint_G \psi \frac{\partial}{\partial n} (\ln t) \, ds , \tag{6a}$$

where

A — is the surface area of the region
Δ — is the Laplace operator
t — is the distance between the reference point (where we are looking for the value of ψ) and the run point of the integration
G — is the control circuit at the boundary of the domain
$\partial\psi/\partial n$ — is the normal derivative at the boundary of the domain in inward direction.

The flat plate is much larger than the film thickness or the wavelength. Like pipe-flow, the length of the plate can be considered infinite, so the film in the state of wave motion can be considered a congruent flow-pattern series, which is periodic in y of wavelength, from $-\infty$ to $+\infty$.

One of them containing the reference point is "inner", all the others are "outer" point domains (Fig. 2). Since these regions and flow patterns are congruent, it is sufficient to determine the velocity field in one domain only. After summation we obtain:

$$2\pi\psi = \sum_{\mu=-\infty}^{\infty} \left\{ \oint_{G_\mu} \left[\frac{\partial \psi}{\partial n} \ln t_\mu - \psi \frac{\partial}{\partial n} (\ln t_\mu) \right] ds + \iint_{A_\mu} \Delta\psi \ln t_\mu \, dA \right\} . \tag{7}$$

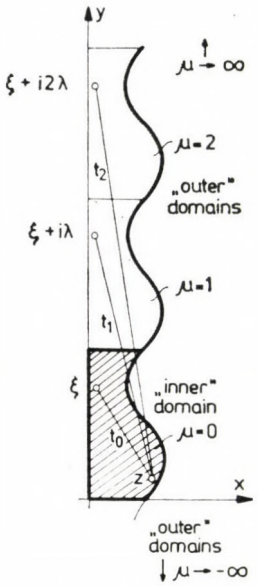


Fig. 2

In the case of plane flow the apparatus applied can be simplified, involving complex variable functions. Then the conjugate velocity is:

$$\overline{w} = w_x - iw_y = \frac{\partial \psi}{\partial y} - i\frac{\partial \psi}{\partial x} . \tag{8}$$

Let the complex coordinate be

$$z = x + iy , \tag{9}$$

and the run point of integration:

$$\zeta_\mu = \xi_\mu + i\eta_\mu . \tag{10}$$

The distance between the "outer" reference point and the run point is

$$t_\mu = \sqrt{(x - \xi_\mu)^2 + (y - \eta_\mu)^2} . \tag{11}$$

The derivative of its logarithm, which can be found in GREEN's formula:

$$\frac{\partial}{\partial y}(\ln t_\mu) + i\frac{\partial}{\partial x}(\ln t_\mu) = \frac{y - \eta_\mu + i(x - \xi_\mu)}{(y - \eta_\mu)^2 + (x - \xi_\mu)^2} = \frac{i}{z - \xi_\mu} . \tag{12}$$

Using formulas (7), (8) and (12) we get the conjugate of the relative velocity w, at the reference point z:

$$2\pi w = i \sum_{\mu=-\infty}^{\infty} \left\{ \oint_{G_\mu} \left[\frac{\partial \psi}{\partial n} \frac{ds}{z - \zeta_\mu} - \psi \frac{\partial}{\partial n} \frac{ds}{z - \zeta_\mu} \right] + \iint_{A_\mu} \Delta\psi \frac{dA}{z - \zeta_\mu} \right\} . \tag{13}$$

The last line integral in this formula will be rearranged. In the coordinate system determined by the orthogonal unit vectors, since the normal vector of the G curve takes an inward direction, the following differential rule is valid:

$$\frac{\partial}{\partial s} = \frac{1}{i}\frac{\partial}{\partial n} = -i\frac{\partial}{\partial n} . \tag{14}$$

Therefore:

$$\frac{\partial}{\partial s}\left(\frac{1}{z - \zeta_\mu}\right) = -i\frac{\partial}{\partial n}\left(\frac{1}{z - \zeta_\mu}\right) = \frac{i}{(z - \zeta_\mu)^2}\frac{d\zeta_\mu}{ds} . \tag{15}$$

After these, the integral can be conversed in a way that it contains the derivative of the function wanted, instead of itself

$$\oint_{G_\mu} \psi \frac{\partial}{\partial n}\left(\frac{1}{z - \zeta_\mu}\right) ds = i \oint_{G_\mu} \psi \frac{d\zeta_\mu}{ds}\frac{ds}{(z - \zeta_\mu)^2} =$$

$$= i\left[\frac{\psi}{z - \zeta_\mu}\right]_{s=0}^{0} - i \oint_{G_\mu} \frac{\partial \psi}{\partial s}\frac{ds}{z - \zeta_\mu} .$$

The quantity in the bracket will disappear, since it will be integrated over a closed circuit, where the stream function is single-valued. Thus we get the following expression:

$$\oint_{G_\mu} \frac{\partial}{\partial \boldsymbol{n}} \left(\frac{1}{z - \zeta_\mu} \right) d\boldsymbol{s} = -i \oint_{G_\mu} \frac{\partial \psi}{\partial \boldsymbol{s}} \frac{d\boldsymbol{s}}{z - \zeta_\mu} . \tag{16}$$

Substituted into Eq. (13) we obtain

$$2\pi \overline{\boldsymbol{w}} = i \sum_{\mu=-\infty}^{\infty} \left\{ \oint_{G_\mu} \left(\frac{\partial \psi}{\partial \boldsymbol{n}} + i \frac{\partial \psi}{\partial \boldsymbol{s}} \right) \frac{d\boldsymbol{s}}{z - \zeta_\mu} + \iint_{A_\mu} \frac{\Delta \psi}{z - \zeta_\mu} dA \right\} . \tag{17}$$

Summing the circuit integrals taking over the G_μ curves, the line integrals over the internal boundaries cancel, since each is traversed twice, but in opposite directions, leaving only the circuit integral over the external boundary: on the wall, and on the free surface. In this respect, because of the congruent flow patterns, the $\Delta\psi$ and $(\partial\psi/\partial \boldsymbol{n} + \boldsymbol{i}\, \partial\psi/\partial \boldsymbol{s})$ quantities are invariant, thus they may be taken out before the Σ symbol. The summation must be completed only for the $1/(z - \zeta_\mu)$ values, from which we get, since

$$\zeta_\mu = \zeta_0 + i\mu\lambda ,$$

$$\sum_{\mu=-\infty}^{\infty} \frac{1}{z - \zeta - i\mu\lambda} = \frac{\pi}{\lambda} \coth \frac{\pi}{\lambda} (z - \zeta) . \tag{18}$$

We must consider that the velocity at the wall (over the $x = 0$ line) is constant, it is equal to the translation velocity of the coordinate system, but in opposite direction.

Thus the line integral over this section is

$$\oint_{\Sigma(\overline{AD})_\mu} \left(\frac{\partial \psi}{\partial \boldsymbol{n}} + \boldsymbol{i} \frac{\partial \psi}{\partial \boldsymbol{s}} \right) \frac{d\boldsymbol{s}}{z - \zeta_\mu} = -\boldsymbol{a} \oint_{\Sigma(\overline{AD})_\mu} \frac{d\boldsymbol{s}}{z - \zeta_\mu} = -\boldsymbol{a}\pi . \tag{19}$$

On the free surface the velocity has no component perpendicular to it. Consequently, the following boundary condition is obtained:

$$\left. \frac{\partial \psi}{\partial \boldsymbol{s}} \right|_{x=\delta} = 0 . \tag{20}$$

The tangential velocity component so far is an unknown function:

$$\left. \frac{\partial \psi}{\partial \boldsymbol{n}} \right|_{x=\delta} = \boldsymbol{w}_{t\delta}(y) . \tag{21}$$

The surface distributed vortex function is also unknown, but it needs to be computed in order to obtain the surface integral. We will carry out an iterative solution: let both functions be approximately determined by any physically permissible, mathematically advantageous simplifying assumption.

At first, we will determine both functions approximately; afterwards the conjugate velocity field will be determined iteratively step by step, more precisely.

From the point of view of numerical process, iteration is a series of great blocks, while the feasibility of the computer can be exploited advantageously. It is necessary for the convergence of the iteration to choose the data of the zeroth step very cautiously.

The problem is to answer simultaneously two unseparable questions: we must determine both the velocity field of the film flow and the shape of the region of integration, which is bounded by a streamline of the relative velocity field on the free surface. At the same time, the shape of the free surface must be such that the integrals referring to this domain supply the velocity field connecting to the prescribed boundary conditions.

Before the iteration procedure we assume the following.

We will discuss laminar flow. The method introduced is suitable to determine turbulent velocity field too, but experiments show there are no capillary waves in the turbulent region [5] and it is not necessary to consider it.

The constitutive equation of the fluid can be arbitrary. Now we consider pure viscous (power law type) non-Newtonian fluids. The Newtonian fluids are included as a special case.

The wavelength is much greater than the mean thickness of the film

$$\lambda \gg \delta_0 .$$

Thus the following conditions are valid as a consequence of the boundary-layer theory:

$$c_y \gg c_x; \quad c_y \frac{\partial c_y}{\partial y} = O\left(c_x \frac{\partial c_y}{\partial x}\right) \; ; \quad \frac{\partial p}{\partial x} = 0 .$$

Let us assume that the distribution of $C_y(x)$ equals the velocity distribution of a laminar, parallel stratified flow, which has the same thickness as the wave-surface film at a given place [9]

$$c_y = \frac{2n+1}{n+1}\left[1 - \left(1 - \frac{x}{\delta}\right)^{\frac{n+1}{n}}\right] c_0 , \tag{22}$$

where n is the behaviour index, c_0 is the cross-sectional averaged velocity

$$c_0 = \frac{1}{\delta}\int_0^{\delta} c_y(x)\, dx . \tag{23}$$

Assuming sinusoidal free surface,

$$\delta = \delta_0[1 + A \sin(ky - \omega t)] . \tag{24}$$

It is evident that

$$\frac{\partial c_y}{\partial y} \ll \frac{\partial c_y}{\partial x} .$$

Since the coordinate transformation gives no change in the rotation, the Ω_z component in the relative coordinate system will be identical with the absolute vorticity component, originated from the derivation of the absolute velocity field

$$\Omega = -\frac{\partial c_y}{\partial x} = -\frac{g_y}{\nu}\left[\delta_0 - x + A \sin (ky - \omega t)\right] . \tag{25}$$

Replacing $\Delta\psi$ by this in Eq. (17), further substituting $w_{\delta y}$ instead of w_δ we will get:

$$\overline{w}(z) = i\frac{a}{2} + \frac{i}{2\lambda}\iint_A \frac{g_y}{\nu}\left[\delta_0 - x + A \sin (ky - \omega t)\right] \cdot$$

$$\cdot \operatorname{cth}\frac{\pi}{\lambda}(z - \zeta)\, dA + \frac{i}{2\lambda}\int_\delta w_{\delta y} \coth\frac{\pi}{\lambda}(z - \zeta_\delta)\, ds , \tag{26}$$

where ζ is the run point of integration in the A region, ζ_δ is the same at the free surface. The velocity at the surface is

$$w_\delta \cong w_{\delta y} = a - \frac{2n + 1}{n + 1} c_0 . \tag{27}$$

Now we can compute the velocity field of the film flow, while capillary waves occur. During the computation some useful alterations must be made. For example, we separated the real and the imaginary parts of the complex

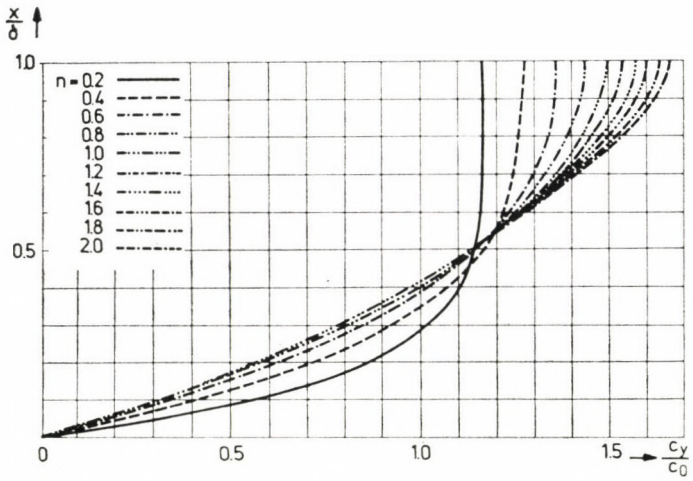


Fig. 3

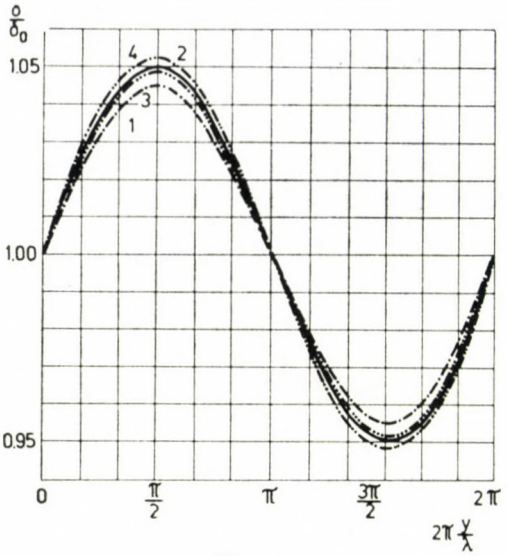


Fig. 4

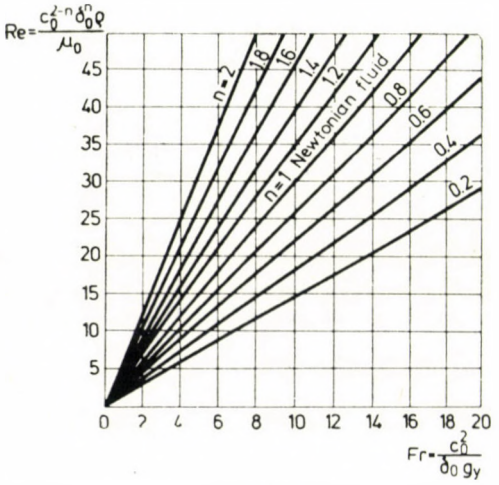


Fig. 5

variable coth function, the integrals were computed in numerical form, etc. This part of the work left the hydrodynamical apparatus intact and it contains no such mathematical elements which will be worth publishing the details of this lengthy procedure. The results of computation are summarized in the diagrams.

In Fig. 3 are given the dimensionless velocity profiles of the non-Newtonian fluids having different behaviour indexes depending on the distance from the wall. For pseudoplastic fluids, where $n < 1$, the velocity distribution is more equalized than with the Newtonian ones. For dilatant fluids, for ex-

ample clay suspensions, where $n > 1$, the velocity profile is "peaky", with a greater value of maximum velocity.

In Fig. 4 is shown the change of the shape of the free surface during the iteration procedure step by step.

Fig. 5 shows the threshold value of the occurrence of the waves, depending on the Reynolds and the Froude numbers, defined by the mean film thickness. The boundary of the stability is a straight line, which depends on the behaviour index. The pseudoplastic and the dilatant behaviour differ markedly from the Newtonian type.

The present paper shows that the potential theory methods in a suitably chosen coordinate system are convenient to describe the unsteady, periodic flow of arbitrary structural-viscous fluids, and the results give us a more accurate knowledge of this phenomenon.

REFERENCES

1. GRIMLEY, H.: *Transaction Inst. Chem. Eng.*, 23(1945), 228.
2. BINNIE, A. M.: *Journal of Fluid Mechanics*, 2(1957), 555.
3. KIRKBRIDGE, C. G.: *Trans. Am. Inst. Chem. Eng.*, 30(1933), 170.
4. FRIEDMANN, S. J.—MILLER, C. O.: Liquid films in the viscous flow region. *Ind. Chem.*, 33(1941), 885.
5. COLBURN, A. P.: Note on the calculation of condensation when a portion of the condensate layer is in turbulent motion. *Trans. Am. Inst. Chem. Eng.*, 30(1933), 197.
6. JEFFREYS, H.—JEFFREYS, B. S.: Methods of Mathematical Physics. Cambridge 1946, 266.
7. LANDAU, L. N.—LEVICH, V. G.: *Acta Physicochimica USSR* 17(1942), 42.
8. KAPITSA, P. L.: Wave motion of a thin layer of a viscous liquid. *Journal of Experimental and Theoretical Physics*, USSR 1(1948).
9. BOBOK, E.: Capillary-gravity waves in a thin non-Newtonian film on a flat plate. *Periodica Polytechnica*, 17(1973), 211.
10. FRANK, PH.—MISES, R.: A mechanika és fizika differenciál- és integrálegyenletei (Differential and integral equations of mechanics and physics). Műszaki Könyvkiadó, Budapest 1966.
11. OBÁDOVICS, GY.: Gyakorlati számítási eljárások (Practical computation methods). Műszaki Könyvkiadó, Budapest 1973.
12. BRONSTEJN, I. N.—SZEMENGYAJEV, K. A.: Matematikai zsebkönyv, 3. kiadás (Handbook of Mathematics). Műszaki Könyvkiadó, Budapest 1974.

ИССЛЕДОВАНИЕ КАПИЛЯРНОГО ВОЛНОВОГО ДВИЖЕНИЯ ТОНКОЙ, НЕНЬЮТОНИАНСКОЙ ЖИДКОСТНОЙ ПЛЕНКИ

Э. БОБОК

РЕЗЮМЕ

Были исследованы капилярные волны, возникающие при течении жидкостной пленки с нелинейным материальным уравнением. Течение нестационарное, преиодическое и незатухающее. Определение поля скоростей проводилось как вторая краевая задача теории потенциалов. Как краевое условие было выбрано распределение скоростей среды с произвольной вязкостью на выгодно выбранном месте поля. Результаты показывают зависимость индекса поведения, вид волн и зависимость стабильности от чисел Рейнолдса и Фроуда.

Acta Geodaet., Geophys. et Montanist. Acad. Sci. Hung. Tomus 14 (1—2), pp. 257—266 (1979)

ОПРЕДЕЛЕНИЕ ОСНОВНЫХ ПАРАМЕТРОВ ЭКСПЛУАТАЦИИ СКВАЖИНАМИ ЛИНЗ БОКСИТА В СЛУЧАЕ КОНКУРЕНЦИИ РАЗНОСНЫМ КАРЬЕРОМ

Й. ПАТВАРОШ

КАФЕДРА ГОРНОВЕДЕНИЯ ПОЛИТЕХНИЧЕСКОГО УНИВЕРСИТЕТА ТЯЖЕЛОЙ ПРОМЫШЛЕННОСТИ, МИШКОЛЬЦ

[Поступило 10 февраля 1977 г.]

Для добычи карстого-бокситных тел с рассеянным залеганием и малого основания, но с большой толщиной гидравлическая скважинная эксплуатация может успешно конкурировать с традиционной разработкой карьером. Статьей определяются технико-экономическими расчетами оптимальные параметры разработки скважиной (дальность разработки и предельная глубина) или то, когда является целесообразным перейти с одной горной технологической системы на другую.

Введение

Для эксплуатации линз боксита, помещающихся вблизи от поверхности, если они залегали между легко извлекаемыми боковыми породами, одним из наиболее эффективных решений является разносная эксплуатация карьером. Однако ниже некоторой глубины расходы на разработку карьера значительно повышаются из-за большого количества безрудной породы, сносимой с поверхности минерального вещества. Особенно быстрым является возрастание расходов тогда, если лишь меньшая доля вынимаемой массы пород может быть извлечена беспрерывно высокомощными подвижными машинами, а большая часть — лишь поступательно взрывной технологией.

Экономичность заложения разработки карьером значительно ухудшается в том случае, если тело минерала заполняет систему трещин, т. е. развивается в качестве горна. В таком случае разработка карьера производится лишь на утолщающейся части тела минерала, находящейся вблизи от поверхности, в то время как более нижняя его часть, заполняющая трещины и имеющая большую мощность, но малое горизонтальное распространение, остается в качестве потери на месте.

Упомянутые трудности горного дела в случае разработки карьера, по нашему, большей частью могут быть устранены, применяя гидравлическую технологию эксплуатации скважинами. Эксплуатация скважинами в случае применения буровых и транспортных оборудований соответствующей мощности более гибко может быть заложена для эксплуатации минеральных тел с неправильным развитием в пространстве, чем эксплуатация карьером.

На рис. 1 показывается такой случай залегания, когда одинаково может идти речь как о скважинной, так и о разносной эксплуатации минерального тела. В выборе между этими двумя системами эксплуатации месторож-

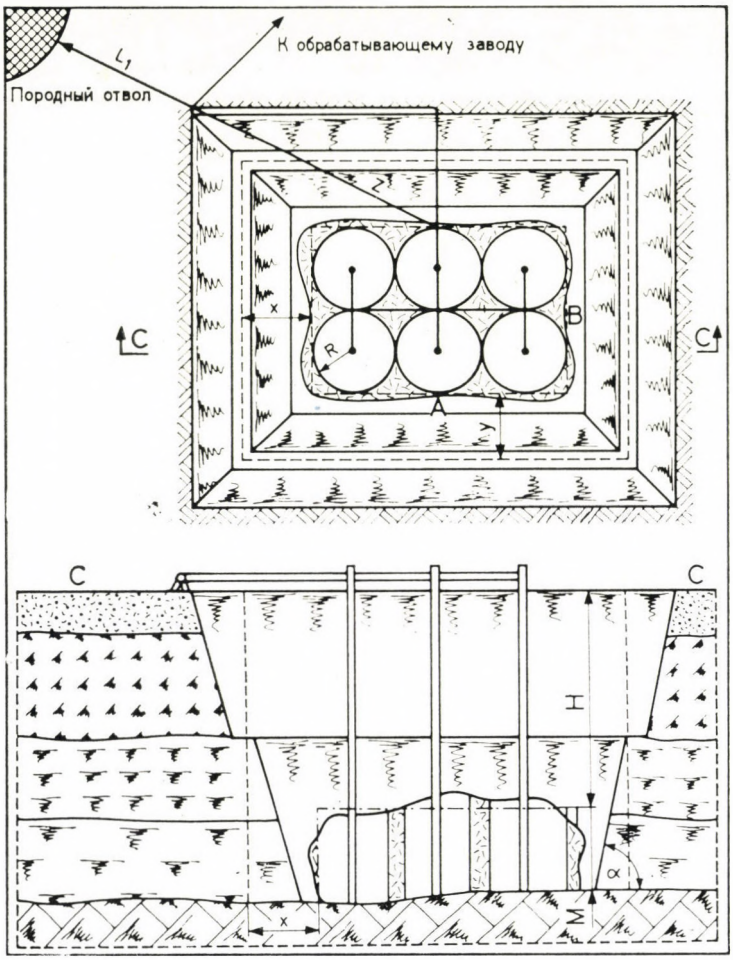


Рис. 1. Схема для эксплуатации скважинами и карьера минерального тела

дений в этом случае может играть решающую роль сопоставление полной суммы расходов [1, 2, 3].

В дальнейшем для упрощения вычислений и выявления различий в порядках при написании всех расходов метода эксплуатации месторождения разносом вводятся допустимые и на практике два приближения:

1. извлекаемая масса безрудной породы и полезное минеральное вещество заменяется правильной призмой четырехугольной формы;

2. наклон уступов учитывается генеральным углом откоса.

Расходы на эксплуатацию скважинами

Все расходы на эксплуатацию скважинами сложенно можно написать на основе *рис. 1* в следующей форме: [1, 2,3].

$$\Sigma K_f = \frac{A \cdot B \cdot (H + M)}{4R^2} \cdot k_f + \frac{A \cdot B \delta_f \cdot k_{mf}}{4} \cdot \left(H + \frac{M}{2}\right) +$$

$$+ A \cdot B \cdot \delta_f \cdot \left(\frac{B}{2} + Z\right) \cdot k_{mo} \quad (Ft_m)$$

где

A, B — геометрические размеры минерального тела (линзы боксита) в горизонтальной проекции (м)

H — глубина покрывающей линии минерального тела от поверхности (м)

M — толщина минерального тела (м)

k_f — удельные расходы по прохождению скважины эксплуатации (⌀80—100) (форинт/м)

δ_f — производительность залежи в случае эксплуатации скважинами (т/м²)

k_{mf} — расходы вертикального перемещения в эксплуатационной скважине (Фт/тм)

$B/2 + Z$ — длина трассы гидравлического транспорта внутри области разработки карьера в случае эксплуатация скважинами (м)

k_{mo} — удельные расходы гидравлического транспорта (Фт/тм).

В интересах простого подчеркивания различий между скважинным и карьерным методами предполагалось, что расходы на перемещение от области эксплуатации до установки обработки практически являются сходными. В действительности при эксплуатации скважинами транспорт к установке обработки может быть осуществлен гидравлически, т. е. постепенно, в то время как в случае применения разносной разработки карьера транспорт производится обычно циклично грузовиком. Исходя из их двух видов эксплуатационного метода транспорта, на практике могут возникать существенные различия по расходам между упомянутыми методами эксплуатации и их следует применять во внимание и при расчетах [1, 2, 3].

Расходы по разносной разработке карьера

Расходы по расносной разработке карьера определяются в решающей мере количеством безрудной породы, удаляемым с полезного тела минерала.

Объем перемещаемой безрудной породы для случая рис. 1 вычисляем следующим соотношением:

$$V_m = H \cdot [A \cdot B + 2B \cdot X + A \cdot y + 4x \cdot y] + M \cdot [2B \cdot X + 2A \cdot y + 4x \cdot y] \quad (m^3)$$

Для упрощения дальнейших вычислений предполагается и то, что

$$x = y = H \cdot \operatorname{ctg} \alpha ,$$

где

α — генеральный скос (градус).

С учетом выше сказанного все расходы, связанные с разработкой карьера можно подробно написать следующими формами:

а) расходы по разносу покрывающих слоев

$$K_a = V_m \cdot k_m \quad (Ft) ,$$

где

k_m — удельные расходы по разносу (Фт/м^3)

б) непосредственные эксплуатационные расходы полезного минерального вещества

$$K_b = A \cdot B \cdot \delta_k \cdot k_b \quad (Ft) ,$$

где

δ_k — производительность месторождения в случае разработки карьером (т/м^2)

k_b — непосредственная себестоимость эксплуатации полезного минерального вещества (Фт/тм)

в) расходы по перемещению в горизонтальном направлении внутри карьера

$$K_c = A \cdot B \cdot \delta_k \left(\frac{B}{2} + y \right) \cdot k_{mb} + A \cdot B \cdot \delta_k \cdot \left(\frac{A}{2} + x \right) \cdot$$

$$\cdot k_{mb} + V_m \cdot \gamma_m \cdot \left(\frac{B}{2} + y \right) \cdot k_{ma} + V_m \cdot \gamma_m \cdot \left(\frac{A}{2} + x \right) \cdot$$

$$\cdot k_{m.a} \quad (Ft/тм) ,$$

где

$k_{mb}; k_{ma}$ — удельные расходы по перемещению полезного минерального вещества и безрудной породы внутри карьера (Фт/тм).

г) расходы по перемещению в вертикальном направлении внутри карьера

$$K_d = V_m \cdot \gamma_m \cdot \frac{H}{2} \cdot k_{mv} + A \cdot B \cdot \delta_k \cdot \left(H + \frac{M}{2} \right) \cdot k_{mv} \quad (Ft) ,$$

где

γ_m — средний объемный вес очищаемой безрудной породы (т/м^3)

k_{mv} — удельные расходы по перемещению в вертикальном направлении внутри карьера (Фт/тм)

д) расходы по перемещению безрудной породы от карьера до места образования отвала:

$$K_e = V_m \cdot \gamma_m \cdot L_1 \cdot k_{mh} \quad (Ft),$$

где

L_1 — расстояние центра тяжести породного отвала от карьера (м)
k_{mh} — удельные расходы по перемещению породного отвала до места образования отвала (Фт/тм)

е) расходы по образованию породного отвала

$$K_f = V_m \cdot k_{mhk} \quad (Ft),$$

где

k_{mhk} — удельные расходы по образованию породного отвала (Фт/м³)

ж) расходы по мелиоризации и обратной насыпи безрудной породы

$$K_g = V_m \cdot \gamma_m \cdot L_1 + \left(\frac{A}{2} + x\right) + \left(\frac{B}{2} + y\right) k_{mh},$$

где

k_{mhk} — удельные расходы по образованию породного отвала и мелиорации (Фт/тм³).

Таким образом, все расходы, связанные с эксплуатацией карьером могут быть написаны следующим выражением:

$$\Sigma K_k = K_a + K_b + K_c + K_d + K_e + K_f + K_g \quad (Ft).$$

Определение основных параметров эксплуатации скважинами

Из равенства эксплуатации скважинами и каръером минерально экономная дальность эксплуатации скважинами может быть вычислена следующим отношением: [1, 2, 3]

$$R_{\text{mjn}} = \sqrt{\frac{A \cdot B \cdot (H + M) \cdot k_f}{4 \cdot \Sigma K_k - \left[A \cdot B \cdot \delta_f \cdot k_{mf} \cdot \left(H + \frac{M}{2}\right) + 4 \cdot A \cdot B \cdot \delta_f \left(\frac{B}{2} + Z\right) \cdot k_{mo}\right]}}$$

Горная работа с эксплуатацией скважинами является во всех отношениях экономнее, если эксьлуатация полезного минерального вещества может быть осуществлена на технически большей вычисленного таким образом значения дальности.

Предельная глубина эксплуатации скважинами определяется следующим образом:

$$H_{\max} = \frac{4R^2 \cdot \Sigma K_k - \left[A \cdot B \cdot M \cdot k_f + A \cdot B \cdot \frac{M}{2} \cdot R^2 \cdot \delta_f \cdot k_{mf} + 4A \cdot B \cdot \delta_f \left(\frac{B}{2} + Z \right) k_{mo} \right]}{A \cdot B \cdot k_f + A \cdot B \cdot R^2 \cdot \delta_f \cdot k_{mf} + 2R^2 \cdot V_m \cdot \gamma_m \cdot k_{mf}} (M).$$

Из этого соотношения можно установить, что предельная глубина эксплуатации скважинами определяется лишь итерацией, так как и объем очищаемой безрудной породы зависит от глубины (1, 2, 3).

Пример

Пусть будут определены основные параметры эксплуатации скважинами в случае конкуренции карьером со следующими основными данными для случая *рис. 1:*

$A = 90$ м; $B = 60$ м; $M = 20$ м; $H = 100$ м

$\delta_f = 198{,}76$ т/м²; $\delta_k = 54$ т/м²; $Z = 86$ м; $\alpha = 60°$

$k_{mf} = 0{,}015$ Фт/тм; $k_{mo} = 0{,}010$ Фт/тм

$k_m = 10$ Фт/м³; $k_b = 30$ Фт/т; $k_{mo} = 0{,}010$ Фт/тм

$k_{mb} = 0{,}012$ Фт/тм; $\gamma_m = 2{,}0$ т/м³; $L_1 = 500$ м

$k_{mh} = 0{,}008$ Фт/тм; $k_{mhk} = 1{,}0$ Фт/м³; $k_f = 30000$ Фт/м.

Подстановкой основных данных для минеральных дальностей эксплуатации скважинами получаем следующий результат:

$$R = \sqrt{\frac{90 \cdot 60 \cdot (100 + 20) \cdot 30000}{4 \cdot 88 \cdot 920320 - 90 \cdot 60 \cdot 198{,}76 \cdot 0{,}015 + 110 \cdot 0{,}015 + 4 \cdot 160 \cdot 0{,}010}}$$

$$= 7{,}46 \simeq 7{,}5 \text{ м}.$$

Результат показывает, что расходы по эксплуатации скважинами, заложенными в сети 15×15 являются практически идентичными с расходами карьера. И так, эксплуатация скважинами, заложенными в сети 20×20 м является во всех отношениях экономичнее карьера.

На рис. 2 показаны экономии, достигнутые эксплуатацией скважинами по отношению к карьеру, в зависимости от эксплуатационной дальности. Хорошо видно, что относительно незначительное увеличение дальности эксплуатации скважинами к какой экономии может привести по сравнению с минимально экономной стоимостью. Из рисунка ясно и то, что дальность эксплуатации скваживаами практически целесообразно увеличитьлишь до $R = 20$ м, так как достигаемые после этого экономии малы, а техническая и безопасная исполнимость эксплуатации быстро ухудшается.

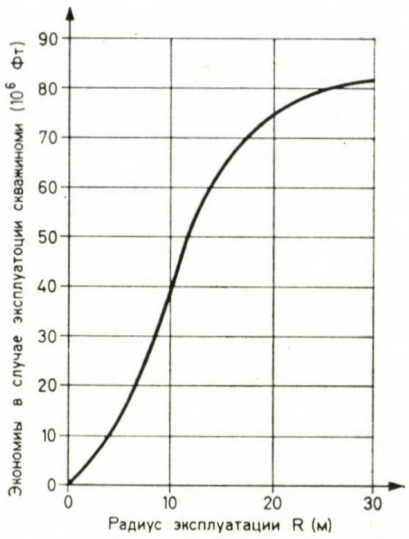


Рис. 2. Экономия (в милл. Форинтов), достигаемая благодаря эксплуатации скважинами по сравнению с карьером — в зависимости от радиуса эксплуатации

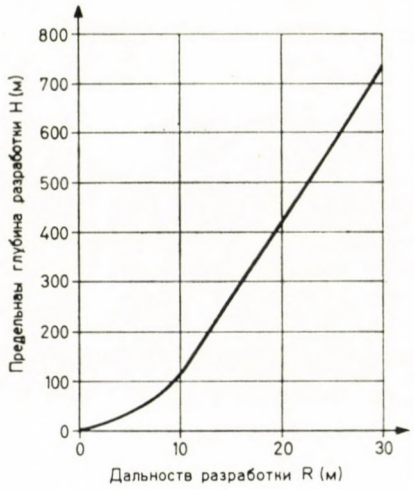


Рис. 3. Изменение предельной глубины разработки скважинами в зависимости от радиуса эксплуатации в случае конкуренции с карьером

На рис. 3 показывается изменение предельной глубины эксплуатации скважинами в зависимости от дальности эксплуатации скважинами. Этим рисунком собственно говоря выражается то, что расходам карьера с отношением очистки 1 : 5 соответствуют расходы по эксплуатации скважинами примерно такой глубины в зависимости от дальности эксплуатации.

Возможности применения комбинированной разработки месторождения

Комбинированное применение разработки карьером и эксплуатации скважинами может быть произведено при разработке минеральных месторождений с трещиноватой забуткой, лежащих вблизи от поверхности. В таком случае, напр., — соответственно схеме на рис. 4 — верхняя выпучивающаяся часть минерального тела может быть разработана разносной разработкой карьером. Нижняя, более тонкая, но в смысле глубины большая часть минерального тела, наоборот, эксплуатируема с помощью скважин. Для эксплуатации части нижнего минерального тела скважины могут быть начаты, например, управленным скосом с подошвы карьера. Упомнутое решение имеет с одной стороны такое преимущество, что количество компактного известняка, очищаемого для эксплуатации трещиноватого минерального тела, значительно меньше, с другой стороны эксплуатация осуществляется гораздо более короткой скважиной.

На рис. 5 показывается случай, когда в среде большего минерального тела, заслуживающего эксплуатации разработкой карьером, находится расчлененно в пространстве больше меньших линз. Эксплуатацию меньши минеральных тел разработкой карьером делает технически и экономно невозможной, с одной стороны, их более скромное в отдельности богатство

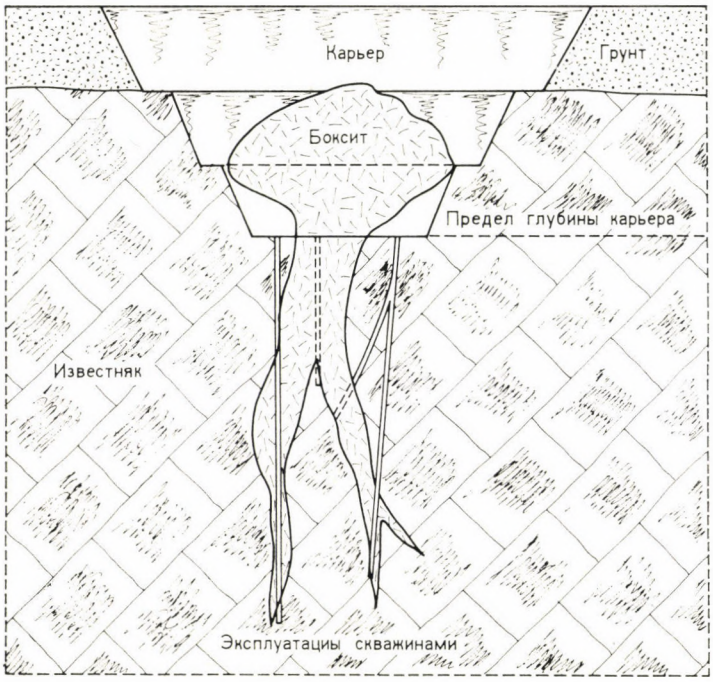


Рис. 4. Схема комбинированной разработки горнообразно развитого минерального тела

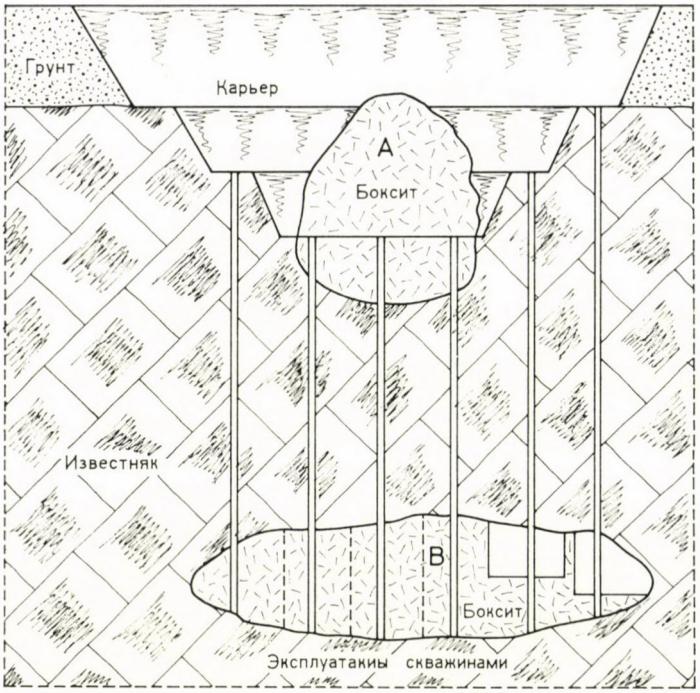


Рис. 5. Схеме возможностей эксплуатации горизонтально и вертикально расчлененных линз боксита разработкой карьером и скважинным комбинированным способом

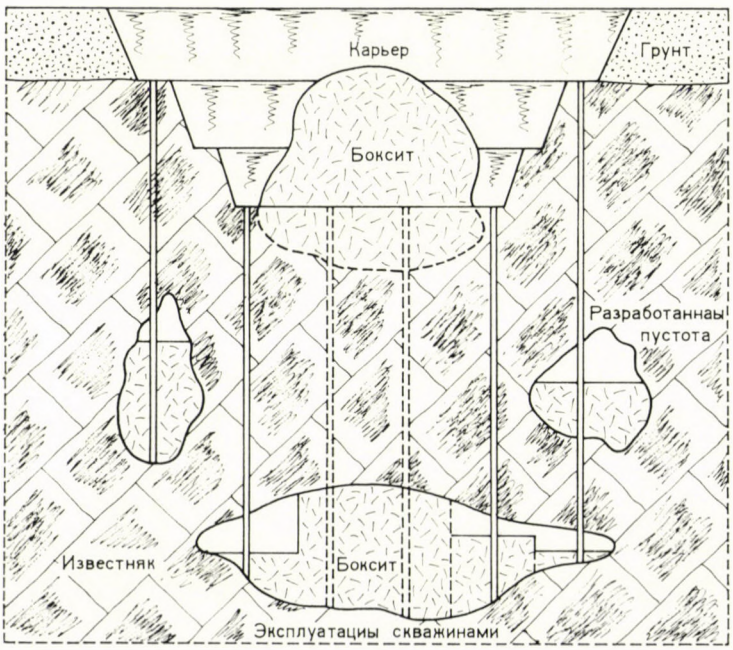


Рис. 6. Схема эксплуатации месторождения боксита с этажным развитием разработкой карьером и скважинным комбинированным способами

минералов, с другой стороны, находящийся в большом количестве компактный известняк, очищаемый для их добывания. Однако есть возможность для разработки минерального богатства этих меньших линзообразных минеральных тел скваживаами, начинающимися с подошвы эксплуатируемой ямы минерального тела, разрабатываемого карьером с берм. Таким комбинированными решением значительно могут быть уменьшены необоснованные потери минерала для народного хозяйства.

На рис. 6 показывается возможность комбинированной эксплуатации месторождения боксита с поэтажным развитием. Здесь, например, вблизи от поверхности в большей глубине под минеральным телом *A* помещается линза боксита *R*, имеющая также значительное минеральное богатство. Из-за большого количества очищаемого покрывающего известняка нельзя и подумать о разработке карьером линзы *Б*. Экономная эксплуатация может быть осуществлена наоборот, с помощью скважин, начинающихся в яме карьера линзы *A*. Выгодным является и то, что на заполнение пустот, возникающих при разработке минерального тела *Б* через скважины возвращаема безрудная порода, очищенная для обработки линзы *A* (1, 2, 3).

ЛИТЕРАТУРА

1. Patvaros, J.: Új típusú bányászati-technológiai rendszer alkalmazási lehetőségei hazai bauxit-előfordulásaink kitermelésében (Возможности применения горно-технологической системы нового типа при эксплуатации отечественных месторождений боксита). *Nehézipari Műszaki Egyetem Közleményei, Bányászat*, 22(1976), 237—251.
2. Patvaros, J.: Fúrólyukas bányaművelési rendszer alkalmazási lehetőségei hazai ásványelőfordulásaink kitermelésében (Возможности применения системы эксплуатации скважинами в разработке отечественных месторождений полезных ископаемых). Конкурс Академии по исследованию, 1973, п. 73.
3. Patvaros, J.: Fúrólyukas hidraulikus bauxit kitermelés (Гидравлическая эксплуатация боксита скважинами), 1976.

DETERMINATION OF THE BASIC PARAMETERS OF HEWING BAUXITE LENSES THROUGH BORE-HOLES IN CASE OF OPEN-CUT MINING

J. PATVAROS

SUMMARY

For the exploitation of karstic bauxite bodies of small extension but great thickness the hydraulic hewing through bore-holes can successfully compete with traditional open-cut methods. The optimum parameters of the bore-hole hewing (hewing distance and depth limit) as well as when to pass over from one technology to the other are determined by technical-economical calculations.

Acta Geodaet., Geophys. et Montanist. Acad. Sci. Hung. Tomus 14 (1—2), pp. 267—287 (1979)

ON THE WEIGHTED LINEARIZATION

L. BALLA—T. MEGGYES

TECHNICAL UNIVERSITY OF HEAVY INDUSTRY, MISKOLC

[Manuscript received June 9, 1977]

The study deals with a new method for linearizing polynomials of the second order used as approximate functions for measurement data. Information within a given interval has to be weighted according to its importance or frequency. For this reason, while determining the approximate line by means of the least squares method a known or prescribed weight function has to be taken account of. The points of intersection of the polynomial of the second order and of the approximate line are determined in the study for a weight function of Gaussian character. If the values of the independent variable can be adjusted, it is advantageous to perform measurements at the points of intersection only, but to repeat them several times. The auxiliary functions needed to determine the abscissa of the points of intersection are given in tables. The method can be generalized for more variables. The linearization method used until now can be considered as a special case of the weighted approximation, having a constant weight function.

Symbols

a, c	coefficients
b	intercept on the y-axis
D	pipe diameter (m)
D^2	variance
f, g	symbols denoting function
g	acceleration due to gravity (9.80666 ms^{-2})
F, G, H	symbols denoting function
H	well bottom depth (m)
l	distance (m)
L	pipe length (m)
m	slope
M	expected value
M_L	air molecular weight (28.966 kg/kmol)
n	number of measurement points
p	pressure (bar)
p_w	well head pressure (bar)
p_{wf}	well bottom pressure (bar)
q_g	standard volumetric flow rate of gas (m^3/d)
q_m	mass flow rate of gas ($kg\ s^{-1}$)
R	universal molar gas constant (8314.6 J/kmol°K)
$s(x)$	weight function
T	temperature (°K)
z, u	transformed independent variables
Z	compressibility factor of real gases
x	independent variable
y	measured value, dependent variable
α	semi-width of range
γ_r	gas relative density
ε	squared mean of deviations
σ	parameter of weight function
σ_m^2	variance

φ	symbol of function
ξ	middle of range
λ	pipe friction factor (four times Fanning factor)

Subscripts

abs	absolute
all	allowable
c	calculated
i, j, k	index of serial number
l	lower
m	number of variables; measured
max	maximum
p	point of intersection
t	transformed
u	upper

While evaluating measurement results, deriving simplified formulae or solving control and automation problems, one often has to replace (approximate) a polynomial of the second order or another which can be approximated closely with it, by a line within a given (part) interval. Analogue modelling of flow phenomena in drift networks of mines or in water and gas pipe networks can be mentioned as examples. Simpler and less expensive elements can be used for constructing the electrical model if the second order characteristics of the sections in the network have been approximated by straight lines. Two basic cases can be distinguished: the information within a given interval is not of equal importance or the independent variable cannot be influenced (it is a natural variable). In the first case, different weights can be attributed to the points of the curve by using a prescribed weight function — provided that the importance of the different parts of the interval does not vary to an extent which would justify the neglection of some parts and the choice of a smaller (inner) interval. If we intend to approximate measurement results dependent on a (natural) variable which cannot be influenced, the values will follow a random distribution within the physically possible range of the natural variable. For this reason, the correct procedure is now to apply a weight function characterizing the distribution, for the samples (measurement results) of finite number.

Both cases can be treated in a similar way: the parameters of the approximate line are calculated from the data of the polynomial of the second order, using the least-squares principle. Since a curve has to be replaced by a straight line, the parameters of the approximate line have to meet the requirement of minimizing the weighted integral of the squared deviations between the line and the curve to be approximated. As different importance can be attributed to different points within the interval in question or they occur with different frequency, the ordinate deviations between the line and the curve to be approximated have to be weighted by a weight function characterizing that phenomenon. This view enables us to evaluate the information according

to its actual importance. The procedure applied hitherto can be considered as a special case of the method to be described in this paper: the same weight, i.e. identical importance was attributed to all information without any specified consideration.

Our task can be formulated mathematically as follows: a given function $g(x)$ has to be approximated by a function $f(x; \{a_i\})$ in the closed interval $(x_l; x_u)$ so as to minimize the value of the integral

$$\varepsilon^2(\{a_i\}) = \int_{x_l}^{x_u} s(x) \left[g(x) - f(x; \{a_i\})\right]^2 dx, \quad i = 0, 1, 2, \ldots n . \tag{1}$$

In Eq. (1) $s(x)$ is a known non-negative weight function.

If the function $f(x)$ is of the form

$$f(x; \{a_i\}) = a_0\varphi_0(x) + a_1\varphi_1(x) + \ldots + a_n\varphi_n(x) \tag{2}$$

and functions $\varphi_i(x)$ are real ones forming an orthogonal system with respect to function $s(x)$, i.e.

$$\int_{x_l}^{x_u} s(x)\, \varphi_i(x)\, \varphi_j(x)\, dx = 0 , \quad i \neq j \tag{3}$$

then the coefficients looked for are [1]:

$$a_i = \frac{\int_{x_l}^{x_u} s(x)\, g(x)\, \varphi_i(x)\, dx}{\int_{x_l}^{x_u} s(x)\, \varphi_i^2(x)\, dx} . \tag{4}$$

In the following a special case will be investigated. Let our functions be

$$g(x) = c_2x^2 + c_1x + c_0 \tag{5}$$

and

$$f(x; \{a_i\}) = a_1x + a_0 . \tag{6}$$

Let the weight function $s(x - \xi)$ be a symmetrical one about the axis $x = \xi$, where

$$\xi = \frac{x_l + x_u}{2} .$$

It holds for function $s(x - \xi)$:

$$\int_{x_l}^{x_u} s(x - \xi)\, dx = 1 . \tag{7}$$

On substituting Eqs (5) and (6) into Eq. (1):

$$\varepsilon^2(a_1; a_0) = \int_{x_l}^{x_u} s(x - \xi) \left[c_2x^2 + c_1x + c_0 - (a_1x + a_0)\right]^2 dx . \tag{8}$$

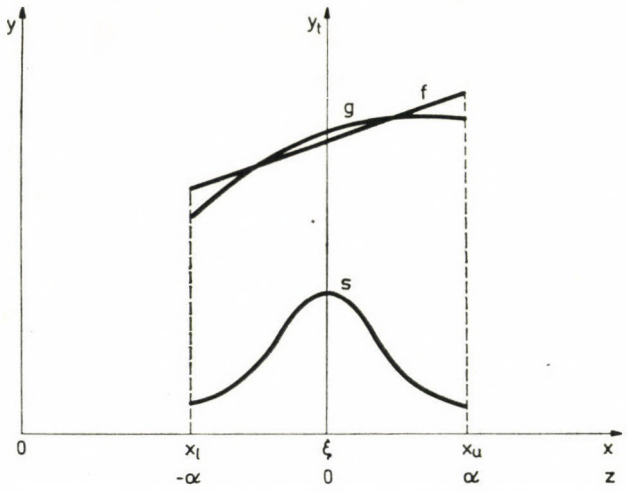


Fig. 1. Coordinate transformation

Let us introduce the transformation $z = x - \xi$, then $dz = dx$. The transformation does not change the value of $\varepsilon^2(a_1; a_0)$ since the relative position of functions (5) and (6) remains the same (Fig. 1):

$$\varepsilon^2(a_1; a_0) = \varepsilon^2(a_{1t}; a_{0t}) \,, \tag{9}$$

where index t refers to the transformation. Thus:

$$\varepsilon^2(a_{1t}; a_{0t}) = \int_{-\alpha}^{\alpha} s(z) \, [c_{2t}z^2 + c_{1t}z + c_{0t} - (a_{1t}z + a_{0t})]^2 \, dz \,, \tag{10}$$

where

$$\alpha = \frac{x_u - x_l}{2} \,.$$

Since function $a_{1t}z + a_{0t}$ has the form of (2), with

$$\varphi_0(z) = 1 \quad \text{and} \quad \varphi_1(z) = z \,,$$

conditon (3) holds for:

$$\int_{-\alpha}^{\alpha} s(z) \, z dz = 0 \,,$$

because $s(z)$ is an even function. Thus, the coefficients a_{1t} and a_{0t} looked for can be obtained from Eq. (4) in the following way:

$$a_{1t} = \frac{\int_{-\alpha}^{\alpha} s(z) \, (c_{2t}z^2 + c_{1t}z + c_{0t}) \, z \, dz}{\int_{-\alpha}^{\alpha} s(z) \, z^2 dz} \tag{11}$$

and

$$a_{0t} = \frac{\int_{-\alpha}^{\alpha} s(z)\,(c_{2t}z^2 + c_{1t}z + c_{0t})\,dz}{\int_{-\alpha}^{\alpha} s(z)\,dz} \,. \tag{12}$$

If n is a positive odd integer, it holds:

$$\int_{-\alpha}^{\alpha} s(z)\,z^n\,dz = 0 \tag{13}$$

since $s(z)$ is an even function, and in case of an odd n, the function z^n is also odd, consequently

$$\int_{-\alpha}^{0} s(z)\,z^n\,dz = -\int_{0}^{\alpha} s(z)\,z^n\,dz \tag{14}$$

which proves the correctness of Eq. (13). Using Eq. (13) and the formulae of integration we obtain:

$$a_{1t} = c_{1t} \,. \tag{15}$$

In order to determine a_{0t}, one has to use the relation

$$\int_{-\alpha}^{\alpha} s(z)\,dz = 1 \,. \tag{16}$$

Using this, coefficient a_{0t} can be expressed as

$$a_{0t} = c_{0t} + c_{2t}\int_{-\alpha}^{\alpha} s(z)\,z^2\,dz \,. \tag{17}$$

The points of intersection of functions $g_t(z)$ and $f_t\big(z;\,\{a_{1t};\,a_{0t}\}\big)$ can be determined from the condition

$$g_t(z) = f_t\big(z;\;\{a_{1t}\,a_{0t}\}\big) \,. \tag{18}$$

Substituting:

$$c_{2t}z_p^2 + c_{1t}z_p + c_{0t} = c_{1t}z_p + c_{0t} + c_{2t}\int_{-\alpha}^{\alpha} s(z)z^2dz \,.$$

The abscissae of the points of intersection are as follows:

$$z_p = \pm\sqrt{\left\{\int_{-\alpha}^{\alpha} s(z)\,z^2\,dz\right\}} \,. \tag{19}$$

Let us now investigate which parameters the ratio z_p/α depends on, if the weight function is of the following form:

$$s(z) = \frac{e^{-z^2/2\sigma^2}}{\int_{-\alpha}^{\alpha} e^{-z^2/2\sigma^2}\,dz} \,, \tag{20}$$

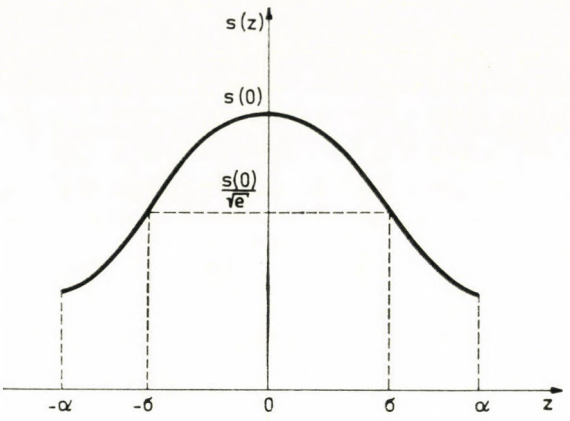


Fig. 2. Weight function $s(z)$

where σ is defined in the following way: the substitution value of the weight function at $\pm\sigma$ equals the ratio of its value at 0, and $\sqrt{e}$:

$$s(\pm\sigma) = \frac{s(0)}{\sqrt{e}} .$$

A typical weight function is illustrated in Fig. 2. We now introduce the new variable $u = z/\sigma$ whereby Eq. (19) becomes:

$$\frac{z_p}{\alpha} = \pm \sqrt{\left\{ \frac{\int_{-\alpha/\sigma}^{\alpha/\sigma} e^{-u^2/2}\, u^2\, du}{\left(\frac{\alpha}{\sigma}\right)^2 \int_{-\alpha/\sigma}^{\alpha/\sigma} e^{-u^2/2}\, du} \right\}} . \tag{21}$$

From Eq. (21) it can be seen that

$$\frac{z_p}{\alpha} = \pm F\left(\frac{\alpha}{\sigma}\right) . \tag{22}$$

Using Eq. (22) and the transformation formula $z = x - \xi$, the abscissa values of the points of intersection of functions $g(x)$ and $f(x; \{a_1; a_0\})$ can be expressed as follows:

$$x_p = \xi \pm \alpha F\left(\frac{\alpha}{\sigma}\right) . \tag{23}$$

In consequence, the abscissae of the points of intersection depend on α, σ and ξ only; they are independent of the values c_i and a_i, thus the points of intersection can be determined if the interval and the weight function are known.

In the following we shall determine the function $F(\alpha/\sigma)$. Since functions $e^{-u^2/2}$ and $e^{-u^2/2}u^2$ are even, the limits of integrals in Eq. (21) can be changed without changing the value of the expression:

$$F\left(\frac{\alpha}{\sigma}\right) = \sqrt{\left\{\frac{\int_0^{\alpha/\sigma} e^{-u^2/2}\, u^2\, du}{\left(\frac{\alpha}{\sigma}\right)^2 \int_0^{\alpha/\sigma} e^{-u^2/2}\, du}\right\}} . \tag{24}$$

We introduce the notation

$$G\left(\frac{\alpha}{\sigma}\right) = \int_0^{\alpha/\sigma} e^{-u^2/2}\, du . \tag{25}$$

Integrating by parts:

$$\int_0^{\alpha/\sigma} e^{-u^2/2}\, u^2\, du = G\left(\frac{\alpha}{\sigma}\right) - \left(\frac{\alpha}{\sigma}\right) e^{-\alpha^2/2\sigma^2} . \tag{26}$$

On substituting Eq. (26) into Eq. (24) we obtain:

$$F\left(\frac{\alpha}{\sigma}\right) = \sqrt{\left\{\frac{G\left(\frac{\alpha}{\sigma}\right) - \left(\frac{\alpha}{\sigma}\right) e^{-\alpha^2/2\sigma^2}}{\left(\frac{\alpha}{\sigma}\right)^2 G\left(\frac{\alpha}{\sigma}\right)}\right\}} . \tag{27}$$

The values of $G(\alpha/\sigma)$ can be determined from tables [1] or by means of Taylor series. Using tables, the values have to be multiplied by $\sqrt{2\pi}$ in order to obtain $G(\alpha/\sigma)$. The character of function $F(\alpha/\sigma)$ is shown in Fig. 3. Using l'Hospital's rule:

$$\underset{\alpha/\sigma \to 0}{\text{Limit}}\ F\left(\frac{\alpha}{\sigma}\right) = \frac{1}{\sqrt{3}} .$$

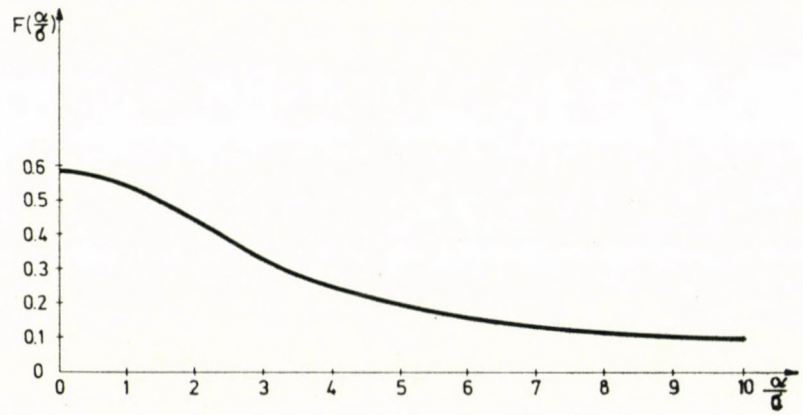


Fig. 3. $F(\alpha/\sigma)$ vs. α/σ

If α/σ tends to infinity, the limit of $F(\alpha/\sigma)$ becomes:

$$\underset{\alpha/\sigma\to\infty}{\text{Limit}}\ F\left(\frac{\alpha}{\sigma}\right) = 0\ ,$$

since

$$\underset{\alpha/\sigma\to\infty}{\text{Limit}}\ G\left(\frac{\alpha}{\sigma}\right) = \sqrt{\frac{\pi}{2}}\ ,$$

as shown in [1]. When

$$\underset{\sigma\to\infty}{\text{Limit}}\ s(z) = \frac{1}{2\alpha}\ ,$$

the case of uniformly weighted approximation is obtained. The abscissae of the points of intersection are now:

$$x_p = \xi \pm \frac{\alpha}{\sqrt{3}}\ ,$$

which results also from applying the least-squares method with a weight function $s(x) \equiv 1$. The values of $F(\alpha/\sigma)$ have been calculated by a Hewlett–Packard HP-65 calculator and are displayed in Table I.

The squared mean ε of the deviations can be calculated from the following formula:

$$\varepsilon = |c_2|\ a^2 \sqrt{\left\{\frac{3F^2\left(\frac{\alpha}{\sigma}\right)}{\left(\frac{\alpha}{\sigma}\right)^2} - \frac{e^{-\alpha^2/2\sigma^2}}{\frac{\alpha}{\sigma}G\left(\frac{\alpha}{\sigma}\right)} - F^4\left(\frac{\alpha}{\sigma}\right)\right\}} \tag{28}$$

which has been obtained by integrating Eq. (10) and substituting Eq. (15) for a_{1t}, Eq. (17) for a_{0t} and $c_{2t} = c_2$. In the special case of $\alpha/\sigma = 0$, ε becomes:

$$\varepsilon = \frac{2}{3\sqrt{5}}\ |c_2|\ \alpha^2\ .$$

The mean of the absolute values of the deviations can be formulated as follows:

$$\varepsilon_{\text{abs}} = \int_{-\alpha}^{\alpha} s(z)\ |c_{2t}z^2 + c_{1t}z + c_{0t} - (a_{1t}z + a_{0t})|\ dz\ . \tag{29}$$

Since the mean of the deviations equals zero, the integrals of the positive and negative deviations are equal in absolute value, consequently:

$$\varepsilon_{\text{abs}} = 2\left|\int_{-\alpha F(\alpha/\sigma)}^{\alpha F(\alpha/\sigma)} s(z)\ [c_{2t}z^2 + c_{1t}z + c_{0t} - (a_{1t}z + a_{0t})]\ dz\right|, \tag{30}$$

because the function $c_{2t}z^2 + c_{1t}z + c_{0t}$ is of second order and the function $a_{1t}z + a_{0t}$ has two points of intersection inside the closed interval $(-\alpha;\ \alpha)$.

Table I

Function $F(\alpha/\sigma)$ vs. α/σ

$\frac{\alpha}{\sigma}$	0.00	0.01	0.02	0.03	0.04	0.05	0.06	0.07	0.08	0.09
0.0	0.577350	577346	577335	577315	577289	577254	577212	577162	577104	577039
0.1	57697	57688	57680	57670	57660	57648	57636	57624	57610	57596
0.2	57581	57566	57549	57532	57514	57495	57475	57455	57434	57412
0.3	57389	57366	57341	57317	57291	57264	57237	57209	57180	57151
0.4	57121	57090	57058	57025	56992	56958	56923	56888	56851	56814
0.5	56776	56738	56699	56659	56618	56576	56534	56491	56447	56403
0.6	56357	56311	56265	56217	56169	56120	56070	56020	55969	55917
0.7	55864	55811	55757	55702	55647	55590	55533	55476	55417	55358
0.8	55299	55238	55177	55115	55052	54989	54925	54860	54795	54729
0.9	54662	54595	54525	54456	54387	54316	54246	54175	54103	54029
1.0	53955	53881	53808	53732	53655	53577	53501	53423	53344	53264
1.1	53184	53104	53022	52940	52858	52775	52692	52607	52522	52437
1.2	52350	52263	52176	52088	51999	51510	51821	51731	51640	51548
1.3	51456	51364	51271	51177	51084	50989	50893	50798	50702	50605
1.4	50508	50410	50312	50213	50115	50015	49915	49814	49713	49612
1.5	49510	49408	49304	49201	49098	48994	48889	48784	48679	48573
1.6	48467	48361	48254	48147	48039	47931	47823	47714	47605	47496
1.7	47386	47277	47166	47057	46945	46834	46722	46611	46499	46386
1.8	46274	46161	46048	45935	45822	45708	45594	45480	45366	45251
1.9	45136	45022	44907	44792	44676	44561	44445	44329	44213	44097
2.0	43981	43865	43749	43632	43516	43399	43283	43166	43049	42932
2.1	42815	42699	42582	42465	42348	42231	42114	41997	41880	41763
2.2	41646	41529	41412	41296	41179	41062	40946	40829	40713	40596
2.3	40480	40364	40248	40132	40016	39900	39785	39669	39554	39439
2.4	39324	39209	39095	38980	38866	38751	38638	38524	38410	38297
2.5	38184	38071	37958	37846	37734	37622	37510	37398	37287	37176
2.6	37065	36955	36844	36734	36625	36515	36406	36297	36189	36080
2.7	35972	35865	35757	35650	35543	35437	35331	35225	35120	35014
2.8	34910	34805	34701	34597	34494	34391	34288	34185	34083	33981
2.9	33880	33779	33678	33578	33478	33378	33279	33180	33082	32984
3.0	32886									
3.5	28484									
4.0	24987									
4.5	22221									
5.0	20000									

This follows from Eq. (22) since, as seen, $F(\alpha/\sigma) < 1/\sqrt{3}$. On substituting a_{1t} and a_{0t}:

$$\varepsilon_{\text{abs}} = 2 \left| \int_{-\alpha F(\alpha/\sigma)}^{\alpha F(\alpha/\sigma)} s(z) \left[c_{2t} z^2 - c_{2t}\, \alpha^2\, F^2 \left(\frac{\alpha}{\sigma} \right) \right] dz \right| . \tag{31}$$

By integrating Eq. (31):

$$\varepsilon_{\text{abs}} = 2|c_2|\, \alpha^2 F^2 \left(\frac{\alpha}{\sigma} \right) \frac{G\left(\frac{\alpha}{\sigma} F\left(\frac{\alpha}{\sigma} \right) \right)}{G\left(\frac{\alpha}{\sigma} \right)} \left[1 - F^2 \left(\frac{\alpha}{\sigma} F\left(\frac{\alpha}{\sigma} \right) \right) \right] . \tag{32}$$

It can be proved that the deviation is maximum if $z = \pm\alpha$, for this reason

$$\varepsilon_{\max} = |c_2|\, \alpha^2 \left[1 - F^2 \left(\frac{\alpha}{\sigma} \right) \right] . \tag{33}$$

The ratio of the mean of the absolute values of the deviations and of the maximum deviation characterizes the uniformity of the approximation:

$$\frac{\varepsilon_{\text{abs}}}{\varepsilon_{\max}} = \frac{2F^2\left(\frac{\alpha}{\sigma} \right)}{1 - F^2\left(\frac{\alpha}{\sigma} \right)} \frac{G\left(\frac{\alpha}{\sigma} F\left(\frac{\alpha}{\sigma} \right) \right)}{G\left(\frac{\alpha}{\sigma} \right)} \left[1 - F^2 \left(\frac{\alpha}{\sigma} F\left(\frac{\alpha}{\sigma} \right) \right) \right] . \tag{34}$$

In the case of a uniformly weighted approximation:

$$\operatorname*{Limit}_{\alpha/\sigma \to 0} \frac{\varepsilon_{\text{abs}}}{\varepsilon_{\max}} = \frac{2}{3\sqrt{3}}$$

The error formulae of the approximation have always to be formulated so as to characterize the actual situation.

The method discussed above can be applied also for m independent variables. Having performed the transformation $z_i = x_i - \xi_i$, the minimum of the following function is looked for:

$$\varepsilon^2(\{a_i\};\ \{a_{ij}\};\ a_0) = \int_{-\alpha_1}^{\alpha_1} \dots \int_{-\alpha_i}^{\alpha_i} \dots \int_{-\alpha_m}^{\alpha_m} s(\{z_i\}) \left[(\Sigma c_{2i} z_i^2 + \right. \tag{35}$$

$$\left. + \sum_{i \neq j} \sum c_{ij}\, z_i\, z_j + \Sigma c_i z_i + c_0 - (\Sigma a_i z_i + \sum_{i \neq j} \sum a_{ij}\, z_i z_j + a_0) \right]^2 dz_1 \dots dz_i \dots dz_m ,$$

where

$$s(\{z_i\}) = \prod_{i=1}^{m} s(z_i) = \frac{e^{-\Sigma z_i^2/2\sigma_i^2}}{\prod_{i=1}^{m} \int_{-\alpha_i}^{\alpha_i} e^{-z_i^2/2\sigma_i^2} dz_i} \tag{36}$$

for which the following holds

$$\int_{-\alpha_1}^{\alpha_1} \dots \int_{-\alpha_i}^{\alpha_i} \dots \int_{-\alpha_m}^{\alpha_m} s(\{z_i\})\, dz_1 \dots dz_i \dots dz_m = 1 \,. \tag{37}$$

Similarly to the method discussed previously, the points of intersection create a space of m dimensions whose equation is:

$$\sum_{i=1}^{m} c_{2i}\left[z_i^2 - \alpha_i^2 F^2\left(\frac{\alpha_i}{\sigma_i}\right)\right] = 0 \,. \tag{38}$$

The solutions of Eq. (38) being independent of c_{2i} are:

$$z_{ip} = \pm\alpha_i F\left(\frac{\alpha_i}{\sigma_i}\right) \quad . \tag{39}$$

Next, we apply the transformation

$$x_{ip} = \xi_i \pm \alpha_i F\left(\frac{\alpha_i}{\sigma_i}\right) \,. \tag{40}$$

This means that choosing $\binom{m}{0} + \binom{m}{1} + \binom{m}{2}$ different points from set $\{x_{ip}\}$ and determining the values of $g(\{x_i\})$ in these points, the approximate space of $m + 1$ dimensions is obtained as the solution of simultaneous linear equations. The squared mean of the deviations can be written:

$$\varepsilon = \left\{ \Sigma c_i^2 \alpha_i^4 \left[\frac{3F^2\left(\frac{\alpha_i}{\sigma_i}\right)}{\left(\frac{\alpha_i}{\sigma_i}\right)^2} - \frac{e^{-\alpha_i^2/2\sigma_i^2}}{\frac{\alpha_i}{\sigma_i} G\left(\frac{\alpha_i}{\sigma^1}\right)} - F^4\left(\frac{\alpha_i}{\sigma_i}\right) \right] + \right. \tag{41}$$

$$\left. + 4 \sum_{i \neq j} \sum c_i c_j \alpha_i^2 \alpha_j^2 F^2\left(\frac{\alpha_i}{\sigma_i}\right) F^2\left(\frac{\alpha_j}{\sigma_j}\right) \right\}^{1/2} .$$

The linearization method can be used for approximating not only functions of the second order but also those which can be approximated with functions of the second order. The functions to be treated in practice can be identified by the criterion that the second derivative should not change its sign over the interval investigated.

The functions to be approximated are in many cases not known analytically, instead points furnished by measurements are available. The measured values are subject to measurement error, in consequence they do not lie on the theoretical curve of the second order or on that which can be approximated with a curve of the second order. If the function is known on the basis of the physical character of the phenomenon to be of second order or near to it,

and we intend to linearize the function, the approximate line can be determined from the measurement points directly. According to the method applied hitherto, measurements were carried out using a more or less uniform pitch in the possible interval or that of interest (Fig. 4). The measurement results were linearized, using the least-squares method and thus the parameters of the approximate line were determined. However, the approximate line determined in this way differs from the line ensuring best fit to the theoretical curve. The greater the errors of the measurement points are, the greater the deviation is.

Using the method outlined here, the parameters of the approximate line can be determined with a high probability so as to ensure greater accuracy. Since the abscissae are known where the approximate line intersects

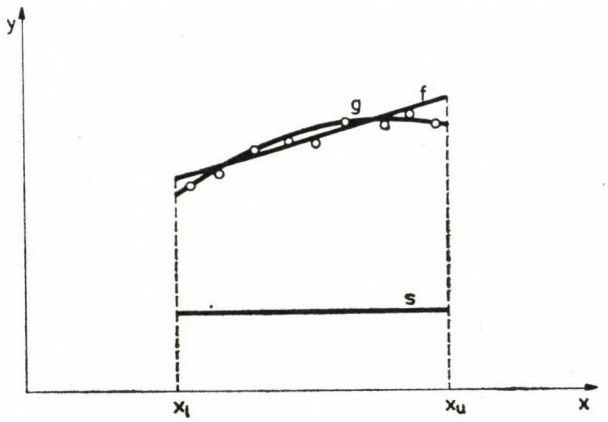


Fig. 4. Linearization based on many points having uniform weight

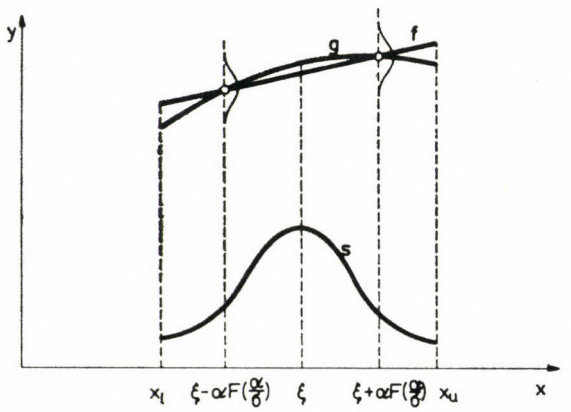


Fig. 5. Linearization using weighting, based on two points

the theoretically accurate curve of the second order, it is sufficient to determine the values of the dependent variable in these two points by means of measurements. Having carried out more measurements in each of these points, the arithmetic mean is considered as the most probable value of the dependent variable (Fig. 5).

Let us now investigate which one of the approximating methods gives more accurate result when a curve of the second order is to be approximated. Let the origin of the coordinate system be at the centre of the domain $(-\alpha; \alpha)$. Inside the domain, every point is supposed to have equal importance, i.e. the approximation is uniformly weighted. One measurement shall be performed in each point z_i yielding the results y_i. The measurement errors are in each point independent of each other, they have a random character and their variances are identical. Let the expected value of the measurement be equal to the value of substitution of the function in point z_i:

$$M(y_i) = c_{2i} z_i^2 + c_{1i} z_i + c_{0i} .$$

The variance of the measured values becomes:

$$D^2(y_i) = \sigma_m^2 .$$

The approximation will be carried out for the sake of comparison with the help of *a)* the least-squares method and *b)* the method outlined in this paper.

a) Let n_1 points be considered in the interval $(-\alpha; \alpha)$ including the endpoints, which are placed as to have uniform pitch. Here n_1 means a positive integer greater than unity. The abscissa of the i-th point is

$$z_i = -\alpha + i \frac{2\alpha}{n_1 - 1}, \qquad i = 0, 1, \ldots, n_1 - 1$$

Determining the approximate line by the least-squares method, the equation of the approximate line becomes:

$$y = \frac{\Sigma y_i z_i}{\Sigma z_i^2} z + \frac{\Sigma y_i}{n_1},$$

with the slope

$$m_1 = \frac{\Sigma y_i z_i}{\Sigma z_i^2},$$

and the intercept

$$b_1 = \frac{\Sigma y_i}{n_1} .$$

It can be easily proved that

$$\Sigma z_i = 0$$

$$\Sigma z_i^2 = n_1 \frac{\alpha^2 (n_1 + 1)}{3(n_1 - 1)}$$

and $$\Sigma z_i^3 = 0 .$$

The expected value of the slope can be calculated as

$$M(m_1) = M\left(\frac{\Sigma y_i z_i}{\Sigma z_i^2}\right) = \frac{1}{\Sigma z_i^2} M(\Sigma y_i z_i) = \frac{1}{\Sigma z_i^2} \Sigma M(y_i z_i) =$$

$$= \frac{1}{\Sigma z_i^2} \Sigma z_i M(y_i) = \frac{1}{\Sigma z_i^2} \Sigma (c_{2t} z_i^3 + c_{1t} z_i^2 + c_{0t} z_i)$$

i.e.

$$M(m_1) = c_{1t} ,$$

the variance of the slope becomes

$$D^2(m_1) = D^2\left(\frac{\Sigma y_i z_i}{\Sigma z_i^2}\right) = \frac{1}{(\Sigma z_i^2)^2} D^2(\Sigma y_i z_i) = \frac{1}{(\Sigma z_i^2)^2} \Sigma D^2(y_i z_i) =$$

$$= \frac{1}{(\Sigma z_i^2)^2} \Sigma z_i^2 D^2(y_i) = \frac{\sigma_m^2}{\Sigma z_i^2}$$

i.e.

$$D^2(m_1) = \frac{3\sigma_m^2 (n_1 - 1)}{\alpha^2 n_1 (n_1 + 1)} .$$

Similarly, the expected value of the intercept is

$$M(b_1) = c_{0t} + c_{2t} \frac{\alpha^2 (n_1 + 1)}{3(n_1 - 1)}$$

and its variance

$$D^2(b_1) = \frac{\sigma_m^2}{n_1} .$$

It can be stated that, using this pattern of the measurements and this method of approximation, the expected value of the slope is equal to the theoretical value, the expected value of the intercept, however, differs from the theoretical one by $c_{0t} + c_{2t}\, \alpha^2/3$. The greater n_1 is, the better the expected value of the intercept approaches the theoretical value.

b) Following the suggestions of the method outlined in this paper, let us consider $n_2/2$ measurement points at $-\alpha/\sqrt{3}$ and $n_2/2$ ones at $\alpha/\sqrt{3}$. Here n_2 is a positive even number. The equation of the approximate line can now be written as follows:

$$y = \frac{\Sigma y_i \left(\frac{\alpha}{\sqrt{3}}\right) - \Sigma y_i \left(-\frac{\alpha}{\sqrt{3}}\right)}{\frac{\alpha n_2}{\sqrt{3}}} z + \frac{\Sigma y_i \left(-\frac{\alpha}{\sqrt{3}}\right) + \Sigma y_i \left(\frac{\alpha}{\sqrt{3}}\right)}{n_2}$$

with the slope

$$m_2 = \frac{\Sigma y_i \left(\frac{\alpha}{\sqrt{3}}\right) - \Sigma y_i \left(-\frac{\alpha}{\sqrt{3}}\right)}{\frac{\alpha n_2}{\sqrt{3}}}$$

and the intercept

$$b_2 = \frac{\Sigma y_i \left(-\frac{\alpha}{\sqrt{3}}\right) + \Sigma y_i \left(\frac{\alpha}{\sqrt{3}}\right)}{n_2} .$$

Similarly to the deduction made for the previous method, the expected value of the slope becomes

$$M(m_2) = c_{1l}$$

and its variance is

$$D^2(m_2) = \frac{3\sigma_m^2}{\alpha^2 n_2} .$$

The expected value of the intercept can be written as

$$M(b_2) = c_{0l} + c_{2l} \frac{\alpha^2}{3} ,$$

and its variance

$$D^2(b_2) = \frac{\sigma_m^2}{n_2} .$$

It is clear that, using this method of measurement and approximation, the expected values of the slope and intercept are identical with the theoretical values.

If, using method *a)*, the points have non-uniform pitch, there is a high probability that the expected values of the slope and intercept of the approximate line will differ from the theoretical values. This means that, using this method of approximation, the best result can be obtained if the measurement points follow a uniform pitch pattern. Comparing the corresponding variances of both methods, the following statements can be formulated:

$$D^2(b_1) \lessgtr D^2(b_2) , \qquad \text{if} \qquad n_1 \lessgtr n_2$$

$$D^2(m_1) \lessgtr D^2(m_2) , \qquad \text{if} \qquad n_1 \lessgtr n_2 - 3 .$$

If the measurements are not subject to random errors, i.e. $\sigma_m^2 = 0$, all the variances equal zero. In this case, the approximate line determined according to the method outlined in this paper, is definitely more accurate and $n_2 = 2$ measurements are now sufficient.

If the measurements are subject to random errors, the variances of the slope and of the intercept of the approximate line determined according to

the present method, can be greater than those of method *a)*, depending on the ratio of n_1 to n_2. These variances are, however, not characteristic of the accuracy of the approximation on their own.

Summing up our considerations as regards the accuracy of the approximation methods: using the method proposed in this paper, the expected values of both the slope and the intercept of the approximate line are equal to the theoretical values. Following the other method, the expected value of only the slope will be equal to the theoretical value. Relying upon this finding, the probability is great that the new method proposed in this paper is the more accurate one.

In order to determine the approximate line, a knowledge of α/σ being the independent variable of function $F(\alpha/\sigma)$, is required. A minimum of information about the weight function is sufficient for the calculation of α/σ. Using the transformed weight function (being symmetrical about the y_t-axis), the values of substitution at $z = 0$ and $z = \pm\alpha$ are as follows:

$$s(0) = -\frac{1}{\int_{-\alpha}^{\alpha} e^{-z^2/2\sigma^2}\, dz}$$

and

$$s(\alpha) = \frac{e^{-\alpha^2/2\sigma^2}}{\int_{-\alpha}^{\alpha} e^{-z^2/2\sigma^2}\, dz} \,.$$

Dividing one equation by the other:

$$e^{\alpha^2/2\sigma^2} = \frac{s(0)}{s(\alpha)} \,,$$

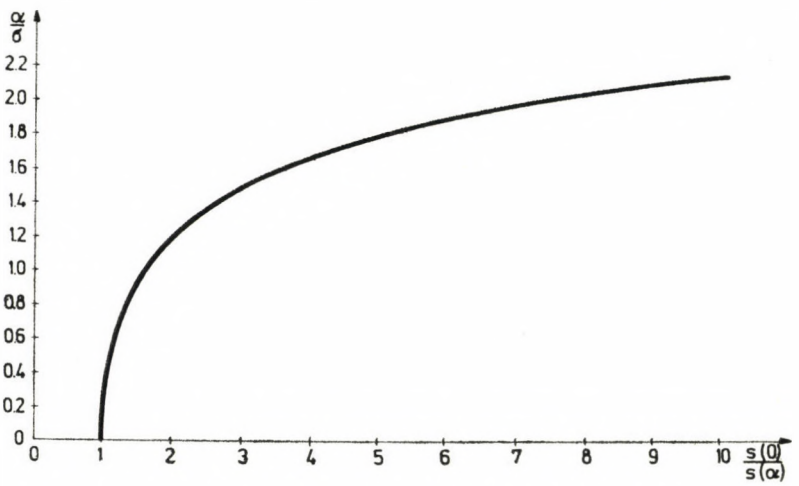


Fig. 6. α/σ *vs.* $s(0)/s(\alpha)$

Table II

α/σ *vs.* $s(0)/s(\alpha)$

$\frac{s(0)}{s(\alpha)}$	0.0	0.1	0.2	0.3	0.4	0.5	0.6	0.7	0.8	0.9
1	0.000	0.437	0.604	0.724	0.820	0.901	0.970	1.030	1.084	1.133
2	1.177	1.218	1.256	1.291	1.323	1.354	1.382	1.409	1.435	1.459
3	1.482	1.504	1.525	1.545	1.564	1.583	1.601	1.618	1.634	1.650
4	1.665	1.680	1.694	1.708	1.721	1.734	1.747	1.759	1.771	1.783
5	1.794	1.805	1.816	1.826	1.837	1.846	1.856	1.866	1.875	1.884
6	1.893	1.902	1.910	1.919	1.927	1.935	1.943	1.950	1.958	1.965
7	1.973	1.980	1.987	1.994	2.001	2.007	2.014	2.021	2.027	2.033
8	2.039	2.045	2.051	2.057	2.063	2.069	2.074	2.080	2.086	2.091
9	2.096	2.102	2.107	2.112	2.117	2.122	2.127	2.132	2.137	2.141
10	2.146									

hence

$$\frac{\alpha}{\sigma} = \sqrt{\left\{2 \ln \frac{s(0)}{s(\alpha)}\right\}} \ .$$

This shows that only the ratio of the values of substitution of the weight function at zero and α is required to determine α/σ. The values α/σ *vs.* $s(0)/s(\alpha)$ are illustrated in Table II for the interval of practical importance. The character of the curve of the same function is shown in Fig. 6. If the problem investigated is connected with sampling from an infinite population or the variable depends on a natural parameter, the weight function is given. On the other hand, if the information is not equally important over the whole interval, the weight function can be prescribed. Having, e.g. a value of substitution of the weight function at zero twice the value of substitution at α, i.e.

$$\frac{s(0)}{s(\alpha)} = 2 \ ,$$

the ratio α/σ (see Table II or Fig. 6) becomes

$$\frac{\alpha}{\sigma} = \sqrt{(2 \ln 2)} \approx 1.177 \ .$$

And if

$$s(0) = s(\alpha) \ ,$$

then

$$\frac{\alpha}{\sigma} = 0 \ ,$$

which holds if $\sigma \to \infty$ since α is not infinite. I.e. the special case $s(0) = s(\alpha)$ means the uniformly weighted approximation.

The approximation task can also be formulated in a way that the interval is not known where the function has to be linearized but the error caused

by the linearization is limited. Consequently, the closed interval $(-\alpha, \alpha)$ has now to be determined which surrounds the known ξ symmetrically and where the error of approximation does not exceed the allowed value. Depending on the character of the problem, one of the equations (28), (32) or (33) can be used to determine α. Whichever type of deviation is regarded as criterion, expressing α from equations (28), (32) or (33) a formula of the type

$$\alpha = H\left(|c_2|, \frac{\alpha}{\sigma}, \varepsilon_{\text{all}}\right) \tag{42}$$

is obtained. If the weight function or σ is known (the two are equivalent), α can be determined from Eq. (42) by iteration:

$$\alpha_{k+1} = H\left(|c_2|, \frac{\alpha_k}{\sigma}, \varepsilon_{\text{all}}\right). \tag{43}$$

As zeroth approximation

$$\alpha_1 = H(|c_2|, 0, \varepsilon_{\text{all}}) \tag{44}$$

is used where $\alpha_0/\sigma = 0$ results from the assumption $\sigma \to \infty$, i.e. while determining α, we start from the uniformly weighted approximation. The iteration is continued until the condition

$$|\alpha_{k+1} - \alpha_k| \leqq \delta, \tag{45}$$

is met where δ is an arbitrarily small number.

The maximum error can be specified when linearizing over a given interval. This means that α, σ and ε_{all} are fixed. While solving this type of problem, two cases can occur:

$$\alpha_c \geqq \alpha \tag{46a}$$

or

$$\alpha_c < \alpha. \tag{46b}$$

In equations (46) α_c means a calculated value to distinguish it from α being a datum. Equation (46a) expresses the relation that ε does not exceed the allowed value over an interval greater than $(-\alpha; \alpha)$, consequently, if the approximation is made only for the range $(-\alpha; \alpha)$, then

$$\varepsilon \leqq \varepsilon_{\text{all}}$$

which is suitable. If inequality (46b) holds, the approximation cannot be carried out for the whole interval $(-\alpha; \alpha)$ so as to meet the requirement $\varepsilon \leqq \varepsilon_{\text{all}}$. A polygonial linearization can solve the problem: the whole interval is separated into subintervals and the linearization is carried out in each of these subintervals separately. Finding the optimum method of the polygonial linearization needs further investigation.

In order to illustrate the use of the method discussed, let us solve a practical example. A common problem in planning and optimizing gas networks in oil and gas fields is to predict the steady head loss of gas wells. Using computer techniques, the task is generally solved by iteration. The number of the iterational steps influences considerably the running time which determines the computation costs. Since the computation costs can be rather high when solving major planning tasks, it is useful to reduce the running time.

The variation of pressure in the tubing is described by the following differential equation:

$$\frac{dp}{dl} = \frac{1}{1 - c_v \dfrac{ZT}{p^2}} \left(- c_v \frac{Z}{p} \frac{dT}{dl} - c_v \frac{T}{p} \frac{dZ}{dl} + c_\lambda \frac{\lambda ZT}{p} + c_l \frac{p}{TZ} \right)$$

where

$$c_v = \frac{16 q_m^2 R}{D^4 \pi^2 M_L \gamma_r}$$

$$c_\lambda = \frac{8 q_m^2 R}{D^5 \pi^2 M_L \gamma_r}$$

$$c_l = \frac{g H M_L \gamma_r}{RL} \quad .$$

The head loss between well bottom and well head can be determined in various ways. Table III shows that the accuracy of the different methods is approximately the same, while the running times differ widely. When calculating the errors, the deviations from the measured values have been taken into account. Table III also shows that a second-order approximation is allowed.

The linearization can be carried out using measurement data or the differential equation describing the phenomenon. When linearizing with the help of the differential equation, the values calculated from the differential equation are considered as measurement points.

Table III

Comparison of various calculation methods

Method	Mean of absolute values of deviations %	Relative running time
Numerical differentiation	12.92	100
Second-order approximation	13.50	10
Linearization	12.62	1

Let us now calculate the well bottom pressure as a function of well head pressure, standard gas volumetric flow rate and well bottom depth. The range limits are as follows:

well head pressure:	50 bar—80 bar
gas volumetric flow rate:	80 000 m^3/d—23 000 m^3/d
well bottom depth:	875 m—975 m

Let the tubing diameter be 75.99 mm, the relative gas density vary between 0.586 and 0.607, the well head temperature between 20 °C and 57 °C. The correlation

$$p_{wf} = -11.435 + 1.158\, p_w + 0.109 \cdot 10^{-3}\, q_g + \\ + 5.68 \cdot 10^{-3}\, H - 1.48 \cdot 10^{-6}\, p_w q_g$$

has been determined from measurements in the Hajdúszoboszló gas field. When linearizing the solution of the differential equation of the phenomenon at uniform distances, the correlation becomes:

$$p_{wf} = -10.718 + 1.107\, p_w + 0.591 \cdot 10^{-4}\, q_g + \\ + 7.33 \cdot 10^{-3}\, H - 5.33 \cdot 10^{-7}\, p_w q_g .$$

By linearizing the solution of the differential equation with the help of the method discussed in this paper, one gets the following result:

$$p_{wf} = -9.931 + 1.107\, p_w + 0.55 \cdot 10^{-4}\, q_g + \\ + 6.48 \cdot 10^{-3}\, H - 4.977 \cdot 10^{-7}\, p_w q_g .$$

Table IV displays values characterizing the accuracy of various linearization methods. A comparison of these values shows that the correlation determined from measurements proves to be the most accurate one. Since the linearization has to be carried out in various ranges, the method based on measurements

Table IV

Accuracy of various linearization methods

Method	Mean of deviations %	Mean of absolute values of deviations %	Number of points
Non-equal pitch, practical measurements	—1.01	8.43	16
Equal pitch, differential equation	—2.31	13.08	27
Present new method, based on differential equation	1.49	12.62	8

proves to be unnecessarily expensive. The accuracy of the linearization method using the differential equation is satisfactory, for this reason there is no need for carrying out expensive measurements.

When linearizing the solution of the differential equation at uniform distances or with the help of the method discussed in the paper, nearly equal accuracy can be obtained, consequently, the new method can be suggested.

REFERENCE

1. Korn, G. A.—Korn, T. M.: Matematikai kézikönyv műszakiaknak (Mathematical handbook for scientists and engineers). Műszaki Könyvkiadó, Budapest, 1975.

О ВЕСОВОЙ ЛИНЕАРИЗАЦИИ

Л. БАЛЛА—Т. МЕДДЕШ

РЕЗЮМЕ

В статье разрабатывается новый метод для линеаризации уравнивающих полиномов второй степени. В заданном интервале информации по их важности или частоте должны быть взвешены. Поэтому для вычисления уравнивающей прямой метод наименьших квадратов нужно применять с учетом известной или предписанной весовой функции. Определяются точки пересечения полинома второй степени с уравнивающей прямой. Если етсь возможность для утановки значения независимой переменной, то целесообразно измерения провести только в точках пересечения. Вспомогательные функции, необходимые для определения значений абсцисс точек пересечения, приводятся в таблицах. Метод можно обобщить для случая нескольких переменным. Примененный до сих пор метод является специальным случаем показанного теперь весового уравнивания, когда функция плотности постоянна.

Acta Geodaet., Geophys. et Montanist. Acad. Sci. Hung. Tomus 14 (1—2), pp. 289—297 (1979)

NON-ELECTRIC USE OF GEOTHERMAL ENERGY IN HUNGARY

T. BOLDIZSÁR

TECHNICAL UNIVERSITY, MISKOLC

[Manuscript received November 2, 1977]

The most accessible geothermal energy reserves are nearer to the surface and are an easy target of energy exploitation. The medium and low temperature resources (50—150 °C) can be used for space heating very economically since their dissolved salt content is low and direct heat consumption is widespread all over the world where the climate is moderate or cold. The efficiency of energy conversion is about 5 times higher than for production of electricity and the stored heat is more than hundred times as much as that of high temperature resources, consequently, in the future non-electric use will progress over electric use. The most extensive and successful use for district heating is practised in Iceland, and for agriculture in Hungary.

The Pannonian basin is a conduction dominated territory with high regional heat flow between 2.0—3.0 HFU. At present, the Upper-Pannonian sediment reservoir is used between 1000—2400 m in depth for geothermal energy production with outflow temperatures of 60—100 °C. Immense heat is stored in this reservoir, from which more than 350 wells produce about 360 m^3/min hot water. The brutto thermal output is 1200 MW, yearly actual heat consumption is 2500 million kWh.

Introduction

The most accessible geothermal energy reserves, which contain a relatively low amount of dissolved solids and are nearer to the surface, consequently of moderate temperature, are an easy and economical target of energy exploitation. These medium or low temperature resources can be used for communal heating, in industry and agriculture. From the overall energy consumption of the US 15% and 20% can be supplied with hot water of 100 °C resp. 150 °C temperature, that is why the market for low and medium temperature thermal water is broad and in space heating valuable amount of oil and natural gas is spared by using geothermal energy.

The search for geothermal resources for non-electrical applications is essentially the same as the search for geothermal resources for production of electricity. However, temperatures which are acceptable in order that the resource be usable for non-electrical applications are lower, a temperature range of 40 °C to 150 °C is required. Such relatively low temperatures clearly imply a lower energy density. An immediate reaction might be to conclude that relatively lower energy densities preclude for economic reasons drilling to depths perhaps greater than 3000 metres in order to exploit the resource. However, the 3—6 times greater efficiency of recovery of energy in non-electrical applications weighs against this conclusion.

Geothermal waters with temperatures of 50 to 160 °C are apparently widespread over all continents. There appears to be no technical impediment to drilling into geothermal reservoirs in the temperature range of 50 °C to 160 °C.

Techniques for extracting geothermal liquid vary according to the temperature of the liquid and the requirement to keep the fluid in liquid phase at the surface of the earth. Geothermal water with outflow temperatures greater than 100 °C, and at greater than the appropriate, corresponding saturation pressure *in situ* will move to the surface under its own "power" if the head within the well is reduced below hydrostatic, owing to flashing. If flashing is undesirable for the application being considered, pumping to maintain greater than saturation pressures is required. The most common type of pump used for completing geothermal wells for non-electrical applications is a shaft-driven deep well pump. Shaft driven pumps play a key role in the space heating.

The Reykjavik District Heating System uses natural heat resources, found in the city and its vicinity, to heat 11,000 houses, serving some 88,000 inhabitants. The hot water is obtained by drilling fractured basalts in geothermal areas down to a depth of 2000 metres. The temperature of the water in the areas already utilized varies between 80 and 130 °C. The water is pumped out of the boreholes with deep well pumps located at depths of 100—120 m.

Collecting mains connect the boreholes to main pumping plants which pump the water to the distributing pumping plants. From these plants the water is distributed throughout the town in street mains at a supply temperature of 80 °C.

The water used is chemically clean, directly potable and contains only a small amount of dissolved solids; it is also non-corrosive to steel, and ordinary black steel pipes are used throughout in the system. Load density in the city is low, the average being 20 MW/km^2 and 1.9 MW/km of distribution mains. The maximum heating load is 350 MW and the available energy 370 MW including a 35 MW oil fired heat peak power plant.

The climate in Southern Iceland is mild considering latitude, the mean temperature in July being 11 °C, and in January —0.4 °C, and the consumption in January is only 2.3 times that of July; thus, due to the relatively cold summers and warm winters, the equivalent hours at peak power for natural heat alone are 4500 per year (load factor 51 per cent). Water-meters are used for billing and the cost of heating averages 30 per cent of the cost of individual fuel oil boiler heating.

Geothermal energy resources of Hungary

The Hungarian basin within the Carpathian arc filled up mainly by Tertiary sediments is characterized by extreme high heat flow amounting to 2.0—3.4 μcal/cm^2 sec (84—138 mW/m^2). The temperature gradient is 50—60 °C/km, roughly twice as much as the normal global value.

The Pannonian basin under Hungarian territory is filled up with about 120 000 km^3 Tertiary sediments under 500 m depth. The upper 500 m is not considered owing to low formation temperature. The main geothermal reservoir in the Upper-Pliocene contains 38 000 km^3 sediments of which round 20% is sand or sandstone. 3470 km^3 water in the pores of the permeable rocks can be mobilised by lowering the pressure around the geothermal wells. The geothermal formation extends outside the boundaries of Hungary into Czechoslovakia, Romania, Yugoslavia and Austria. Outside Hungary no systematic geothermal explorations have been made, but from petroleum exploration data we estimate the geothermal potential around Hungary, within the Carpathian basin, about 60% of the Hungarian value.

Putting down wells, the Pannonian reservoir supplies geothermal energy by means of overflowing hot water of 60—100°C temperature without pumping, but owing to decreasing reservoir pressure the production decreases in time and after 4—8 years pumping is necessary to lower the water level in the wells. 10 per cent pressure reduction at 2000 m depth means 20 kg/cm^2 depression. The energy of pumping required is moderate (less than 100 kW compared to the heat output of 5000 kW of an average geothermal well) and if we calculate 20 kg/cm^2 depression, we are on the safe side, as far as economics of geothermal energy production is concerned.

The Pannonian basin is a conduction dominated territory with high regional heat flow. The heat production of convection systems is negligible compared to the vast amount of heat stored in the sediments. There are no hot igneous systems within the Carpathian arc. According to heat flow measurements, taking in account the rock conductivities, the following amounts of stored heat referred to 15 °C can be computed (Table I).

Table I

Interval km	Stored heat 10^{18} cal
0— 3	12 600
3—10	119 700
	132 300

From the economical point of view at present, only the upper 3 km can be utilised for production of geothermal energy. The heat content of this part is detailed in Table II.

Table II

Sediment unit	Volume km³	Stored heat 10^{18} cal	Remarks
Tertiary	160 000	10 560	Chiefly Miocene and Pliocene
Upper-Pannonian	38 000	1 938	Permeable, low salinity
Upper-Pannonian under 1000 m	17 490	768	Reservoir temperature 70—140 °C

Deeper than 3500—4000 m there are about 600 km³ mostly Miocene geopressurised sediments of 200—300 °C reservoir temperature. The hot water contains dissolved natural gas. Production of geothermal energy is contemplated in the future. Preliminary estimates indicate about $600 \cdot 10^{18}$ cal heat content in geopressurised zones.

The recoverable part of the geothermal resources depends on reservoir characteristics, production methods and conversion processes in utilization plants. In Hungary at present the great geothermal reservoir in the Upper-

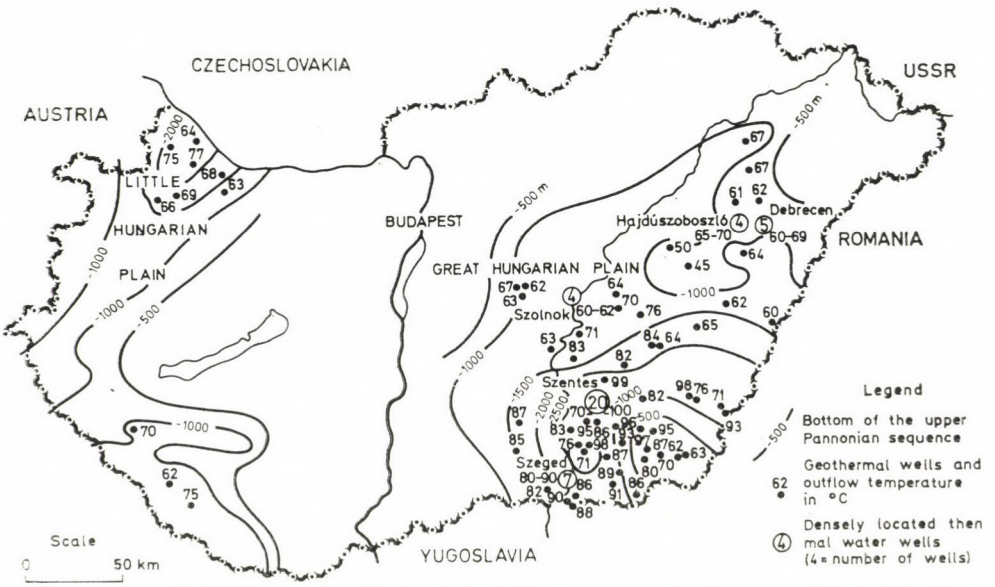


Fig. 1. Bottom isobath lines of the Upper Pannonian geothermal reservoir

Table III

(see references)

Country	Recoverable		Remarks
	heat 10^{18} cal	electricity MWcent	
U.S.A.	150.0	10 000	estimated
U.S.S.R.	26.2	165	for 100 years
Italy	13.6	130 – 660	estimated
Iceland	100.0	200	estimated
New Zealand	13.0	1 560	for 100 years
Hungary	15.0	—	50 per cent identified

Pannonian under 1000 m is used and wells produce hot water with temperatures between 50 and 100 °C. This hot water body with low salinity can be economically used only as a heating agent for heating, drying, cooling plants and supply of warm water for agriculture, industry, flats, spas and swimming pools. The conversion to electricity is not of economical interest.

The recoverable part of the 17 490 km² Upper-Pannonian geothermal reservoir, storing $768 \cdot 10^{18}$ cal heat considering the elastic dilatation, with formation compressibility

$$c_f = 5.70 \cdot 10^{-5} \text{ cm}^2/\text{kg}$$

is 0.99 km³/at. Contemplating 100 at pressure reduction

$$99 \text{ km}^2$$

hot water can be produced with average temperature of 90 °C. The produced amount of heat referred to 15 °C is

$$7.42 \cdot 10^{18} \text{ cal}$$

i.e. round 10 000 MWcentury. Considering the deep karst water in Mesozoic basement rocks and other reservoirs, the overall recoverable energy in Hungary is about $15 \cdot 10^{18}$ cal. Geothermal energy is available on 40 000 km².

At present, all over the world the Pannonian geothermal reservoir stores the greatest amount of identified heat which can be mobilised and used.

According to geothermal resource assessments published at the UN Symposium of San Francisco in May 1975, the estimated figures of the most important geothermal energy-producing countries are compiled in Table III.

Geothermal energy production

At the end of 1976 Hungary uses 496 geothermal wells of more than 35 °C outflow temperature chiefly for space heating and balneology. 52 wells are used in water works, where near surface water is scarce. Now the Hungarian

Government intensifies the use of geothermal energy for residential and commercial purposes. 40 per cent of the territory of Hungary is suitable for economic hot water production aiming space heating, and in the future in these geothermal regions new developments will not receive allocation of oil or natural gas for space heating.

Table IV lists the nominal heat capacity of geothermal wells of more than 60 °C outflow temperature. Heat production is given in million kilocalories per hour and thermal megawatts.

Table V presents the nominal heat capacity of wells and the actual consumption of geothermal energy according to the type of usage. In Table V

Table IV

Hungarian geothermal energy wells with outflow temperatures more than 60 °C in 1976

Application	Number of wells	Flow rate m^3/min	Heat production referred to +15 °C	
			10^6 kcal/h	MW
Agriculture	62	100.5	423.57	492.53
District heating	7	11.4	49.47	57.51
Industry	2	3.2	8.54	9.94
Balneology and swimming pools	49	51.7	166.17	193.18
Water works	2	2.1	5.74	6.68
Recharge wells	4	4.1	12.18	14.16
Not yet used	21	17.1	61.68	71.69
Total	147	190.1	727.35	845.69
Average	—	1.293	4.95	5.75

Table V

Geothermal energy production and use in Hungary in 1976

Application	Number of wells	Flow rate m^3/min	Nominal power* MW	Yearly actual heat consumption	
				MW year	10^6kWh
Agriculture**	77	117.0	535.44	105	919.8
District heating	8	11.7	58.39	30	262.8
Industry	13	14.0	24.50	15	131.4
Balneology and swimming pools	194	165.3	439.47	140	12.664
Not yet used	51	34.3	108.27	—	—
Total	343	342.3	1166.34	290	2540.4

* Referred to +15 °C
** Greenhouses, animal husbandry, drying, etc.

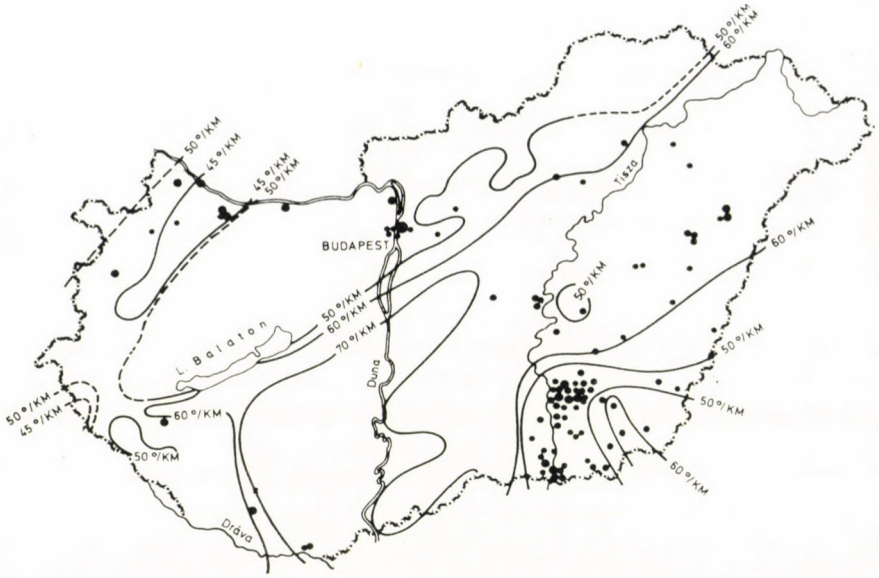


Fig. 2. Temperature gradient chart with most important hot water wells

196 wells of less than 60 °C outflow temperature are also included, most of them produce hot water between 40—60 °C temperature.

At the end of 1975 1.7 million m^2 greenhouse is heated by geothermal energy, this sector is the main consumer, producing tomato, paprika, cucumber and other vegetables, further carnation, roses and hortensia. Cow stalls, pigsties and chicken houses come next. Five geothermal drying and one cooling plant are used for conservation of grains, fruits and vegetables. Low temperature water of about 35—40 °C is used for soil heating, with or without dilution for irrigation and in farm swimming pools. There is one fish pond heated by thermal well.

Eight district heating plants provided space heating and warm water supply for 3500 flats with 710 000 m^3 heated space.

In Hungary 134 swimming pools and spas are based on thermal water from 194 wells.

51 wells are shut down temporarily, awaiting construction of heating units, mainly in agriculture and balneology.

Industrial use of geothermal energy is less developed. It is used for food procession, and in textile and paper industry.

Plans are being made for increasing the use of geothermal energy. Chief prospective market is the district heating of those areas where geothermal energy is available with up to 100 °C temperature. Since most houses are being built by state funds it is easy to force state building companies to heat geothermally, simply by not supplying them fossil fuel, which is also produced and distributed by the state.

Research activities are increasing not only by home research units but also by international cooperation. There is already a geothermal technical-scientific agreement between Hungary and Italy. Talks are being made between the National Science Foundation, the Ford Foundation and the Hungarian government for making common geothermal projects on the non-electric use of geothermal energy.

Plans for the future

The Government's advisory bodies presented the following plans for exploiting geothermal energy resources more intensively (Table VI).

Table VI

	At the end of 1980	Between 1981—1990
District heating, number of flats	6 800	80 000
Warm water supply, number of flats	58 000	200 000
Greenhouses, m^2	2 400 000	9 000 000

At the end of 1990 yearly about 600 000 tons of fuel-oil are expected to be substituted by geothermal space heating. Up to now no elaboration of the development of industrial and other agricultural application is available.

REFERENCES

BARELLI et al.: Geothermal Potential of Central-Southern Italy. Sec. U.N. Geothermal Symp. I—13. Berkeley, 1975.

BODVARSSON: Geothermal Resources of Iceland. Sec. U.N. Geothermal Symp. I—4. Berkeley, 1975.

BOLDIZSÁR, T.: Measurement of Terrestrial Heat Flow in the Coal Mining District Komló. *Acta Technica Acad. Sci. Hung., XV* (1956), 219—228.

BOLDIZSÁR, T.: Geothermic Investigations in the Hungarian Plain. *Acta Geologica Acad. Sci. Hung., V* (1958a) 245—254.

BOLTON: Geothermal in New Zealand. Sec. U.N. Geothermal Symp. I—5. Berkeley, 1975.

DVOROV: Study and Use of the Earth's Deep Heat in the USSR. Klamath-Falls Symp. of Non-electric Use of Geoth. Energy 1974.

FOMIN—MAVRITSKY: Geothermal Resources of the USSR. Sec. U.N. Geothermal Symp. I—13. Berkeley, 1975.

KORIM: Geological Aspects of Thermal Water Occurrences in Hungary. *Geothermics 1*, (1972), 96—102.

WHITE—WILLIAMS: Assessment of Geothermal Resources of the U.S. 1975. Geological Survey Circ. 726.

НЕЭЛЕКТРИЧЕСКОЕ ИСПОЛЬЗОВАНИЕ ГЕОТЕРМИЧЕСКОЙ ЭНЕРГИИ В ВЕНГРИИ

Т. БОЛДИЖАР

РЕЗЮМЕ

Наиболее легко добываемые запады геотермической энергии лежат близко к поверхности и их эксплуатация не трудна. Средне — и низкотемпературные запасы (50—150°) очень экономично можно использовать для пространственного отопления, ибо содержание соли в них невелико. Непосредственное использование тепла широко распространено везде в мире при умеренном и холодном климате. Эффективность преобразования энергии примерно в 5 раз больше, чем в случае производства электрической энергии, и храненное тепло больше чем в сто раз превышает тепло высокотемпературных запасов, следовательно, в будущем неэлектрическое использование будет быстрее развиваться, чем электрическое. Самое распространенное и результативное использование претворено в жизнь в Исландии в провинциальном отоплении, а также в Венгрии в сельском хозяйстве.

Паннонский бассейн может быть характеризован кондукцией, с региональным тепловым потоком 2,0—3,0 HFV (единица теплового потока). Ныне используется верхне-паннонский осадочный бассейна из глубины 1000—2400 м с целью производства геотермальной энергии, с температурой на выходе 60—100°C. В этом резервуаре хранится огромное количество тепла. Отсюда больше чем из 350 колодцев производится примерно 360 м³/мин горячей воды. Валовое производство тепла составляет 1200 MB, а ежегодное реальное использование тепла 2500 миллионов Квч.

Acta Geodaet., Geophys. et Montanist. Acad. Sci. Hung. Tomus 14 (1—2), pp. 299—310 (1979)

ÜBER DIE THEORETISCHEN GRUNDLAGEN DER WEGSTRECKENTRASSIERUNG

J. ZAMBÓ

MITGLIED DER UNGARISCHEN AKADEMIE DER WISSENSCHAFTEN
UNIVERSITÄT FÜR SCHWERINDUSTRIE, MISKOLC

[Eingegangen am 2. Februar 1978]

In einem als eben betrachteten Gelände sollen zwischen zwei oder mehrere Punkte Wegtrassen gelegt werden, wobei die Isohypsen $[y_i = y_i(x_i)]$ der gewichteten Fläche $Q = Q(x, y)$ gegeben sind und das Gewicht der Streifen bzw. Gebiete zwischen den Isohypsen als konstant betrachtet wird. Zu suchen ist das Minimum von $\Sigma Q_i s_i$, worin Q_i das zum Streifen gehörige Gewicht, s_i aber die Länge des den Streifen durchquerenden Wegabschnittes bedeuen. Es werden jene Bedingungsgleichungssysteme abgeleitet, deren Erfüllung durch Iterationen zu der Lösung führt. Es hat sich herausgestellt, daß man zu einem wesentlich einfacheren Verfahren gelangt, als mit dem umständlichen Entwürf mit Hilfe dynamischer Programmierung. Die Gewichte können sich in verschiedener Weise melden; sie können z. B. von der Zeit herrühren, in welcher man an das Ende der Wegstrecke gelangt, ferner von den Baukosten usw.

In einem orthogonalen Koordinatensystem seien zwei Punkte (A und B) und eine Kurvenschar $y_1 = y_1(x_1)$; $y_2 = y_2(x_2)$; . . . ; $y_i = y_i(x_i)$; . . . ; $y_n = y_n(x_n)$ gegeben. Diese Kurven sind die Isohypsen einer gegebenen Fläche $Q = Q(x, y)$, worin Q das Gewicht bedeutet. Zwischen die beiden Punkte sei ein Polygonzug gelegt, dessen Seiten s_A, s_1, s_2, . . . , s_i, . . . , s_{n-1}, s_B, die Eckpunkte aber A, 1, 2, . . . , i, . . . , n, B sind (Abb. 1). Die zu den einzelnen Seiten gehörigen Gewichte seien: Q_A, Q_1, Q_2, . . . , Q_i, . . . , Q_{n-1}, Q_B, wobei die Gewichte für jene Felder gelten, die sich jeweils zwischen zwei Kurven ergeben. So bezieht sich z. B. das Gewicht Q_1 auf das Feld zwischen den Kurven $y_1 = y_1(x_1)$ und $y_2 = y_2(x_2)$. Demnach wird in dem von einer oder zwei Isohypsen begrenzten Gebiet das Gewicht als konstant betrachtet.

Die Gleichung für die gewichtete Summe des Polygonzuges lautet also:

$$S_{AB} = Q_A s_A + \sum_{i=1}^{i=n-1} Q_i s_i + Q_B s_B .$$

Geprüft sei nun, welcher der unendlich vielen Polygonzüge das Minimum von S_{AB} ergibt.

Als Ausdruck der Seiten s kann folgendes geschrieben werden:

$$S_{AA} = Q_A \sqrt{(x_1 - x_A)^2 + [y_1(x_1) - y_A]^2} + \\ + \sum_{i=1}^{i=n-1} Q_i \sqrt{(x_{i+1} - x_i)^2 + [y_{i+1}(x_{i+1}) - y_i(x_i)]^2} + \\ + Q_B \sqrt{(x_B - x_n)^2 + [y_B - y_n(x_n)]^2} .$$

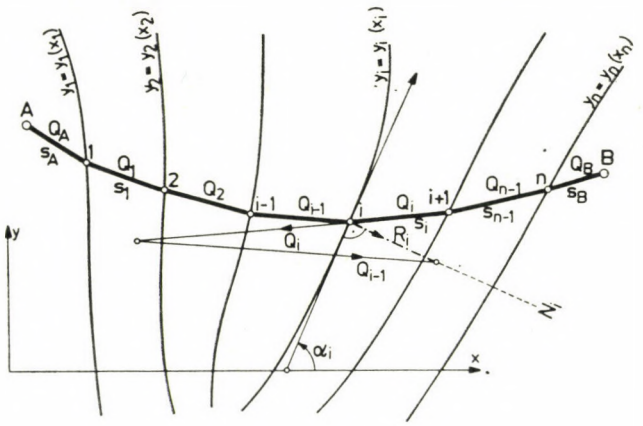


Abb. 1

Werden nun die Differentialquotienten nach $x_1, x_2, \ldots, x_i, \ldots, x_n$ gebildet und diese gleich Null gesetzt, so ist:

$$Q_A(\cos\varphi_A + \sin\varphi_A \operatorname{tg}\alpha_1) - Q_1(\cos\varphi_1 + \sin\varphi_1 \operatorname{tg}\alpha_1) = 0$$

$$Q_1(\cos\varphi_1 + \sin\varphi_1 \operatorname{tg}\alpha_2) - Q_2(\cos\varphi_2 + \sin\varphi_2 \operatorname{tg}\alpha_2) = 0$$

$$\vdots$$

$$Q_{i-1}(\cos\varphi_{i-1} + \sin\varphi_{i-1} \operatorname{tg}\alpha_i) - Q_i(\cos\varphi_i + \sin\varphi_i \operatorname{tg}\alpha_i) = 0$$

$$\vdots$$

$$Q_{n-2}(\cos\varphi_{n-2} + \sin\varphi_{n-2} \operatorname{tg}\alpha_{n-1}) - Q_{n-1}(\cos\varphi_{n-1} + \sin\varphi_{n-1} \operatorname{tg}\alpha_{n-1}) = 0$$

$$Q_{n-1}(\cos\varphi_{n-1} + \sin\varphi_{n-1} \operatorname{tg}\alpha_n) - Q_B(\cos\varphi_B + \sin\varphi_B \operatorname{tg}\alpha_B) = 0\,.$$

Hierin sind:

$$\cos\varphi_A = \frac{x_1 - x_A}{s_A}$$

$$\cos\varphi_B = \frac{x_B - x_n}{s_B}$$

$$\cos\varphi_i = \frac{x_{i+1} - x_i}{s_i}$$

$$\sin\varphi_A = \frac{y_1(x_1) - y_A}{s_A}$$

$$\sin\varphi_B = \frac{y_B - y_x(x_n)}{s_B}$$

$$\sin\varphi_i = \frac{y_{i+1}(x_{i+1}) - y_i(x_i)}{s_i}\,.$$

α_i aber ist der Richtungswinkel der im Punkt i der Kurve $y_i = y_i(x_i)$ gezogenen Tangente.

Nach den entsprechenden goniometrischen Umformungen kann geschrieben werden:

$$Q_A \cos(\varphi_A - \alpha_1) - Q_1 \cos(\varphi_1 - \alpha_1) = 0$$

$$Q_1 \cos(\varphi_1 - \alpha_2) - Q_2 \cos(\varphi_2 - \alpha_2) = 0$$

$$\vdots$$

$$Q_{i-1} \cos(\varphi_{i-1} - \alpha_i) - Q_i \cos(\varphi_i - \alpha_i) = 0$$

$$\vdots$$

$$Q_{n-2} \cos(\varphi_{n-2} - \alpha_{n-1}) - Q_{n-1} \cos(\varphi_{n-1} - \alpha_{n-1}) = 0$$

$$Q_{n-1} \cos(\varphi_{n-1} - \alpha_n) - Q_B \cos(\varphi_B - \alpha_n) = 0\,.$$

Das Gleichungssystem kann durch jeden beliebigen Wert Q, z.B. durch Q_i dividiert werden; man erhält dann:

$$\lambda_A \cos(\varphi_A - \alpha_1) - \lambda_1 \cos(\varphi_1 - \alpha_1) = 0$$

$$\vdots$$

$$\lambda_{i-1} \cos(\varphi_{i-1} - \alpha_i) - \cos(\varphi_i - \alpha_i) = 0$$

$$\vdots$$

$$\lambda_{n-1} \cos(\varphi_{n-1} - \alpha_n) - \lambda_B \cos(\varphi_B - \alpha_n) = 0\,.$$

Dieses Gleichungssystem besagt, daß der Polygonzug zwischen den Punkten A und B dann den Extremwert von S_{AB} ergibt, wenn die Resultierende von zwei in irgendeinem Punkt des Polygonzuges angreifenden Vektoren auf die zum Eckpunkt gehörige Normale der durch den Eckpunkt verlaufenden Isohypse $y = y(x)$ entfällt. So entfällt die Resultierende R_i der beiden im Eckpunkt i angreifenden Vektoren auf die zum Punkt i gehörige Normale (N_i). Der Skalarwert der beiden Vektoren ist Q_i oder 1, bzw. Q_{i-1} oder λ_{i-1}; ihre Richtung aber ist durch die Punkte i und $i + 1$, bzw. i und $i - 1$ gegeben, wobei der Sinn der Vektoren zu Punkt i hinweist.

Die Einführung der relativen Gewichte λ ist nicht unbedingt notwendig, doch kann dies in der Praxis der Einfachheit halber begründet sein, besonders wenn auf diese Weise das Verhältnis der Gewichte leichter angegeben werden kann.

Die Extremfälle (z.B. $\alpha_r = 90°$) werden nicht geprüft, teils weil mit ihnen praktisch nicht zu rechnen ist, teils aber weil das Koordinatensystem beliebig gewählt werden kann.

Es ist völlig klar, daß jener Polygonzug, der das obige Gleichungssystem erfüllt, nur angenähert durch Iteration bestimmt werden kann.

In Abb. 2 sind zeichnerisch die beiden Punkte A und B, ferner die Isohypsen der Gewichtfläche, also die Kurven $y = y(x)$ gegeben. Das Gewicht des Streifens zwischen zwei Isohypsen betrachtet man als Mittelwert der Gewichte der beiden Isohypsen. Bei dieser verhältnismäßig einfachen Gewichtsfläche ist leicht einzusehen, daß der von Punkt A ausgehende Flügel des gesuchten Polygonzuges zwischen dem normalen Polygonzug (A, 1_n, 2_n, . . .) und dem die beiden Punkte verbindenden Geradenabschnitt verläuft. Der erste Schritt bezeichne den Polygonzug A, 1_0, 2_0, . . ., 5_0, B. Wie man sieht, entfällt die Resultierende R_5 nicht auf die dem Punkt 5_0 zugeordnete Normale (N_5), sondern weicht von dieser um den Winkel β ab. Es muß also der Polygonzug in der auf der Zeichnung angedeuteten Richtung, eventuell in mehreren Schritten solange verschwenkt werden, bis man zu dem Polygonzug A, 1, 2, 3, 4, 5, B gelangt, der den Extremwert für die Summe der gewichteten Seiten ergibt. Im vorliegenden Fall kann eindeutig festgestellt werden, daß der Extremwert ein absolutes Minimum bezeichnet. In jedem Fall der Praxis muß diese Prüfung durchgeführt werden.

Es kann nämlich prinzipiell vorkommen, daß das Bedingungsgleichungssystem auch von mehreren Polygonzügen erfüllt wird. Zwar gehört ein solcher Fall — praktisch genommen — zu den Seltenheiten; kommt er aber doch vor, so ist die Bezeichnung des absoluten Minimums ziemlich einfach.

Als Sonderfall kann jener zählen, wenn die Isohypsen parallel, und auf den Geradenabschnitt $A\ B$ normal verlaufen. In diesem Fall ergibt der Geradenabschnitt $A\ B$ das absolute Minimum. Doch das kommt in der Praxis nicht vor.

Werden die Isohypsen verdichtet, dann erhöht sich die Anzahl der Polygonseiten und nähert sich einer zwischen die Punkte A und B legbaren Kurve.

Abb. 3 stellt eine relativ einfache Gewichtfläche dar. Da die Isohypsen von der auf den geraden Abschnitt A normalen Richtung nicht allzusehr abweichen, weicht auch der Polygonzug, der das Minimum sicherstellt, nicht sehr vom geraden Abschnitt $A\ B$ ab.

In Abb. 4 ist ein Fall aus der Praxis zu sehen. Sie stellt für ein Kupfererzvorkommen das Sohlenfeld des Bergwerksbetriebes dar. Die beiden Punkte A und B bezeichnen zwei Seigerschächte. Die beiden Schächte sollen mit einer Sohlenstrecke verbunden werden. Da die Vererzung nicht gleichmäßig ist und in der Feldesmitte reichere Erze anstehen, schwanken auch die spezifischen Kosten der Sohlenstrecke und der Verlust je Meter. In den von den Isohypsen begrenzten Gebieten sei der Cu-Gehalt der Reihe nach: 4, 2, 1, 0, 5, 0,25%. Dementsprechend sei der kalkulierte Verlust der Reihe nach: 100, 200, 400, 800, 1600 \$/m. Zu suchen ist jener Polygonzug, bei dem der Verlust der Sohlenstrecke einen Mindestwert beträgt.

Nach einem entsprechenden Iterationsverfahren sichert der Polygonzug A, a, b, c, d, e, f, g, h, B das Verlustminimum. Die nichtgewichtete Länge dieses

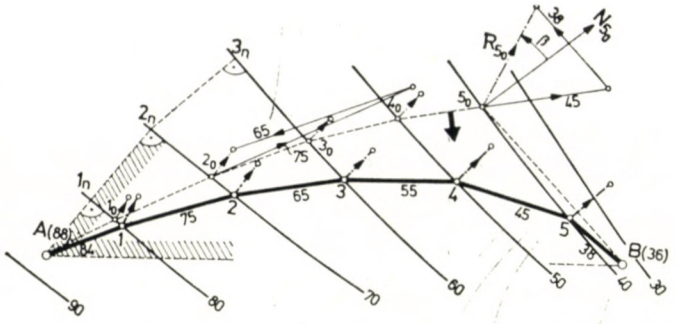


Abb. 2

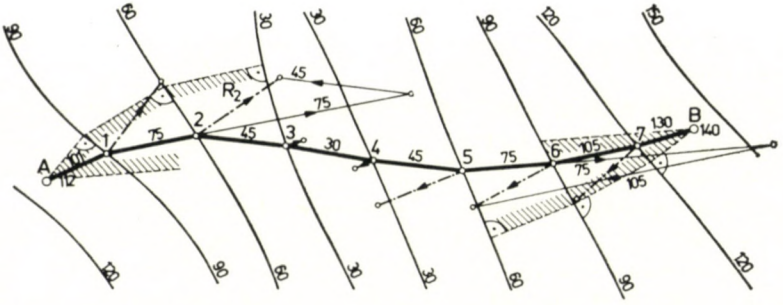


Abb. 3

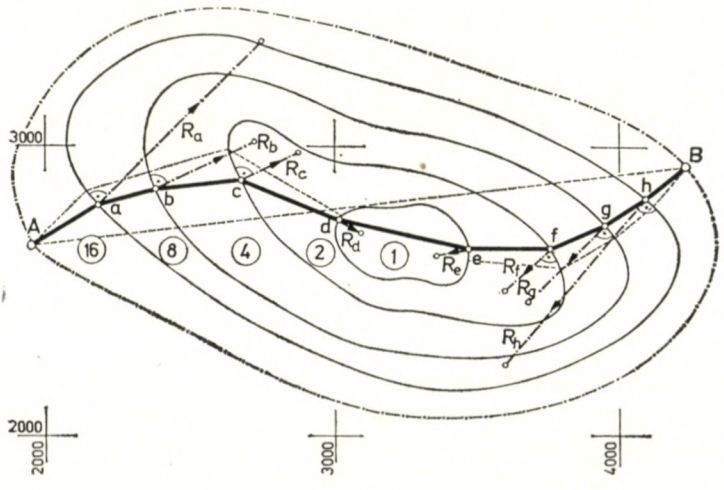


Abb. 4

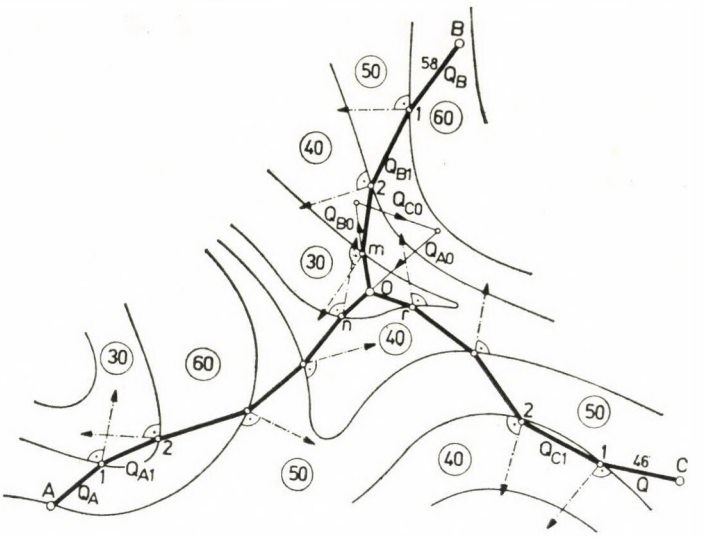


Abb. 5

Polygonzuges beträgt 2420 m, die des geraden Abschnittes $A\ B$ aber 2300 m. Demgegenüber beträgt der Wert des gewichteten Polygonzuges $138 \cdot 10^4$ \$, der des geraden Abschnittes aber $164 \cdot 10^4$ \$, die Differenz ist also $26 \cdot 10^4$ \$. Als weiterer Vorteil ist zu verbuchen, daß sich der Polygonzug besser als der Geradenabschnitt $A\ B$ der Vererzungsdichte anschmiegt.

Nach dem Fall eines gewichteten Polygonzuges zwischen zwei Punkten sei nun jener Fall erörtert, bei dem mehrere Punkte gegeben sind. Der besseren Übersicht halber seien nur drei Punkte gegeben (Abb. 5). Zu suchen ist jener Punkt O, der mit den drei Punkten (A, B, C) durch gewichtete Polygonzüge so verbunden werden soll, daß die Summe der gewichteten Seiten der drei Polygonzüge ein Minimum beträgt.

Auf Grund des Vorherigen kann folgendes Bedingungsgleichungssystem aufgeschrieben werden:

$$
\begin{aligned}
&Q_A \cos(\varphi_A - \alpha_{A1}) - Q_{A1} \cos(\varphi_{A1} - \alpha_{A1}) = 0\\
&Q_{A1} \cos(\varphi_{A1} - \alpha_{A2}) - Q_{A2} \cos(\varphi_{A2} - \alpha_{A2}) = 0\\
&\vdots\\
&Q_{A(n-1)} \cos(\varphi_{A(n-1)} - \alpha_{An}) - Q_{AO} \cos \varphi_A - \alpha_{AO}) = 0\\
&Q_B \cos(\varphi_B - \alpha_{B1}) - Q_{B1} \cos(\varphi_{B1} - \alpha_{B1}) = 0\\
&Q_{B1} \cos(\varphi_{B1} - \alpha_{B2}) - Q_{B2} \cos(\varphi_{B2} - \alpha_{B2}) = 0\\
&\vdots\\
&Q_{B(m-1)} \cos(\varphi_{B(m-1)} - \alpha_{Bm}) - Q_{BO} \cos(\varphi_{BO} - \alpha_{Bm}) = 0
\end{aligned}
$$

$$
\begin{aligned}
&Q_C \cos(\varphi_C - \alpha_{C1}) - Q_{C1} \cos(\varphi_{C1} - \alpha_{C1}) = 0\\
&Q_{C1} \cos(\varphi_{C1} - \alpha_{C2}) - Q_{C2} \cos(\varphi_{C2} - \alpha_{C2}) = 0\\
&\vdots\\
&Q_{C(r-1} \cos(\varphi_{C(r-1)} - \alpha_{Cr}) - Q_{CO} \cos(\varphi_{CO} - \alpha_{Cr}) = 0\\
&Q_{AO} \cos \varphi_{AO} + Q_{BO} \cos \varphi_{BO} + Q_{BO} \cos \varphi_{CO} = 0\\
&Q_{AO} \sin \varphi_{AO} + Q_{BO} \sin \varphi_{BO} + Q_{CO} \sin \varphi_{CO} = 0\,.
\end{aligned}
$$

Die letzteren zwei Bedingungsgleichungen nahmen deshalb diese Form an, da der gesuchte Punkt O an keine bestimmte Isohypse gebunden wurde.

Aus dem Bedingungsgleichungssystem folgt: Zum Punkt O gehört dann ein Extremwert, wenn die Resultierende der den Punkt O direkt angreifenden Vektoren einen Wert gleich Null hat, ferner wenn die Resultierende der in den Eckpunkten des Polygonzuges $(1, 2, \ldots, n; 1, 2, \ldots, m; 1, 2, \ldots, r)$ angreifenden zwei Vektoren auf die dem Punkt der Isohypse zugeordnete Normale zu liegen kommt, wobei die Skalarwerte der Vektoren entsprechend dem Vorherigen der Reihe nach durch die Gewichte, ihre Richtung aber durch je zwei Eckpunkte gegeben sind, während ihr Drehsinn zum Punkt hinweist.

Die Bezeichnung des gesuchten Punktes O ist auch hier nur in aufeinander folgenden Schritten durch Iteration möglich. Wird akzeptiert, daß innerhalb eines von ein oder zwei Isohypsen begrenzten Gebietes das Gewicht konstant ist, dann können die vom Punkt O ausgehenden drei Polygonseiten $(O - n; O - m; O - r)$ miteinander einen Winkel von 120° einschließen, jedoch nur dann, wenn der gesuchte Punkt O nicht auf einen der gegebenen Punkte entfällt.

Um die Genauigkeit zu erhöhen ist es zweckmäßig, nach entsprechender Informierung die in der Zeichnung dargestellten Isohypsen in der Umgebung des voraussichtlichen Ortes von Punkt O zu verdichten, damit die letzten Seiten der Polygone (s_{AO}, s_{BO}, s_{CO}) je kürzer werden. Man kann sogar so verfahren, daß man bei der Iteration die durch die Punkte O der einzelnen Schritte verlaufenden Isohypsen entwirft. Hierüber sei weiter unten berichtet.

Sind mehr als drei Punkte gegeben, dann müssen die obigen Beziehungen sinngemäß angewendet werden.

Abb. 6 führt zur Lösung einer weiteren Aufgabe. Gegeben seien der Einfachheit halber drei Punkte (A, B, C), ferner die Isohypsen $y_i = y_i(x_i)$. In der Ebene der gewichteten Polygonzüge sei ferner eine Kurve (nicht eine Isohypse) gegeben, deren Gleichung $y_0 = y_0(x_0)$ lauten soll. Zu suchen ist jener Punkt O der Kurve $y_0 = y_0(x_0)$, welchen die mit den Punkten A, B und C gewichteten Polygonzüge so verbinden, daß die gewichteten Werte der Polygonzüge $(A, 1, \ldots, n, O; B, 1, \ldots, m, O; C, 1, \ldots, r, O)$ einen Mindestwert ergeben.

Es ist leicht einzusehen, daß die Bedingungsgleichungen bis zu den Punkten n, m und r dieselben sind wie jene, die sich bei freier Wahl des Punktes O

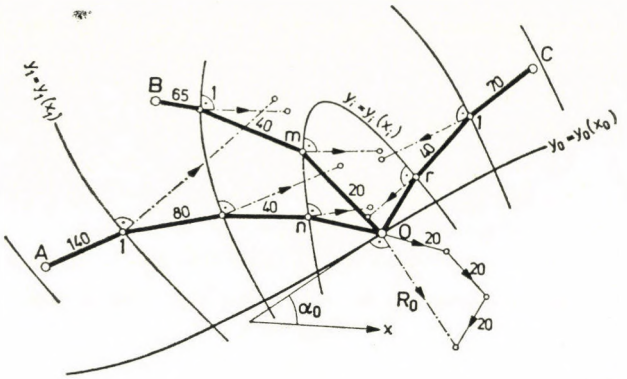


Abb. 6

ergeben. Wo nun der Punkt O nur ein Punkt der Gleichung $y_0 = y_0(x_0)$ sein kann, lautet die letzte Bedingungsgleichung

$$Q_{AO} \cos(\varphi_{AO} - \alpha_0) + Q_{BO} \cos(\varphi_{BO} - \alpha_0) + Q_{CO} \cos(\varphi_{CO} - \alpha_0) = 0 .$$

Dies besagt: Die Resultierende des den Punkt O direkt angreifenden Vektorsystems entfällt auf die dem Punkt O zugeordnete Normale der Kurve $y_0 = y_q(x_0)$.

Kehren wir nun zu Abb. 5 zurück. Bei dem Suchen nach dem endgültigen Punkt O wird im ersten Schritt des Iterationsverfahrens ein Punkt O_1 angenommen, für den dann die ihn durchlaufende Isohypse $y_{01} = y_{01}(x_{01})$ entworfen werden kann. Der Punkt O_1 wurde dann richtig angenommen, wenn an Stelle der dort angegebenen zwei letzten Bedingungsgleichungen folgende Bedingungsgleichung tritt:

$$Q_{AO_1} \cos(\varphi_{AO_1} - \alpha_{01}) + Q_{PO_1} \cos(\varphi_{BO_1} - \alpha_{01}) + Q_{CO_1} \cos(\varphi_{CO_1} - \alpha_{01}) = 0 ,$$

d. h. die Resultierende der den Punkt O_1 direkt angreifenden drei Vektoren entfällt auf die dem Punkt O_1 der Isohypsenlinie $y_{01} = y_{01}(x_{01})$ zugeordnete Normale. Natürlich erfolgt dies im allgemeinen nicht schon beim ersten Schritt. Im folgenden bzw. in den folgenden Schritten muß dieses Verfahren solange wiederholt werden, bis man zu dem die praktischen Ansprüche erfüllenden Punkt O gelangt. Diese Methode führt zu einer genaueren Lösung als jene, bei welcher in der Umgebung des gesuchten Punktes O die Isohypsen nicht verdichtet wurden. Doch welche Methode auch immer befolgt wird, erfordert das Iterationsverfahren immer viel Umsicht und die nötige Übung. Glücklicherweise hat in der Praxis eine übertriebene Genauigkeit hier keinen Sinn, da sich der gewichtete Wert (S) kaum ändert, wenn statt dem wirklichen Punkt O ein Punkt O' bezeichnet wird, vorausgesetzt, daß der Abstand OO' nicht groß ist .

In Abb. 7 wird ein Fall aus der Praxis vorgestellt. Dieser ähnelt der in Abb. 4 dargestellten Aufgabe. Es soll — ausgehend vom gegebenen Punkt A —

eine Strecke so aufgefahren werden, daß deren anderer Endpunkt ein Punkt der durch den gegebenen Punkt B verlaufenden Geraden E sei, wobei der Kostenverlust der Auffahrung ein Minimum betragen soll. Die Kosten der im Tauben aufgefahrenen Strecke seien 1600 \$/m. Mit zunehmendem Vererzungsgrad sinkt der spezifische Kostenverlust der Streckenauffahrung. Es können demnach die Isohypsen entworfen werden, bzw. sie sind gleichfalls gegeben. Im vorliegenden Fall wurden nur die den Verlust halbierenden Isohypsen bzw. Streifen dargestellt. Es besagt z. B. der mit 4 bezeichnete Streifen, daß in dem diesen Streifen durchörternden Streckenabschnitt der Verlust im Durchschnitt 400 \$ beträgt.

In Kenntnis der theoretischen Zusammenhänge konnte festgestellt werden, daß die gesuchte Kurve G normal auf die Gerade E eintrifft. Wird von detailliertem Entwerfen und Wiederholungen hier abgesehen, so ist das Endresultat, daß die Kurve G die Gerade E im Punkt E_0 erreicht. Die Kurve G konnte durch Verdichten der Isohypsen angenähert erzielt werden.

Selbstredend kann auch der volle Wert des Verlustes errechnet werden. Dieser beträgt im Fall der Kurve G rund $80 \cdot 10^4$ \$. Werden aber die Punkte A und B durch eine Gerade verbunden, dann beläuft sich der Verlust auf $230 \cdot 10^4$ \$; die Differenz beträgt also $150 \cdot 10^4$ \$.

Wie bei Abb. 4, so kann auch hier gesagt werden, daß die Kurve G noch den weiteren Vorteil hat, sich der Vererzung gut anzupassen.

Natürlich kann, wenn es die Zweckmäßigkeit erfordert, die Kurve abschnittsweise ausgerichtet werden.

Noch eine grundlegende Aufgabe sei hier dargelegt (Abb. 8). Gegeben seien in der Zeichnung für eine gewichtete Fläche deren Isohypsen: $y_{A1} = y_{A1}(x_{A1})$; $y_{A2} = y_{A2}(x_2)$; $y_{B1} = y_{B1}(x_{B1})$; $y_{B2} = y_{B2}(x_{B2})$; . . .; ferner seien in

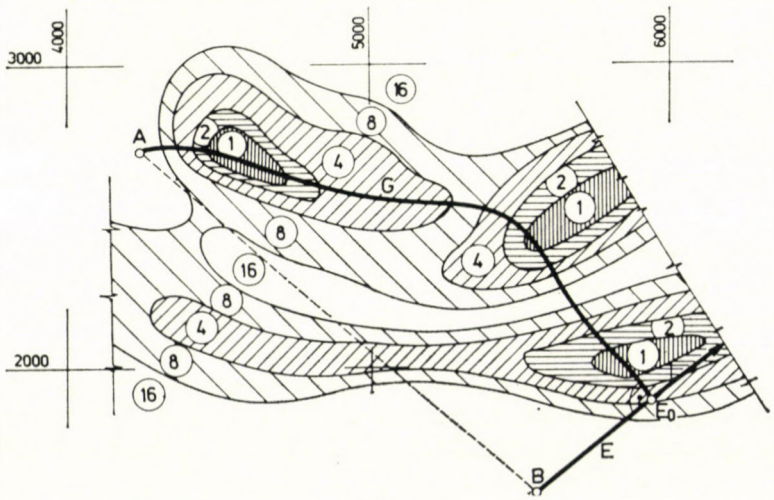


Abb. 7

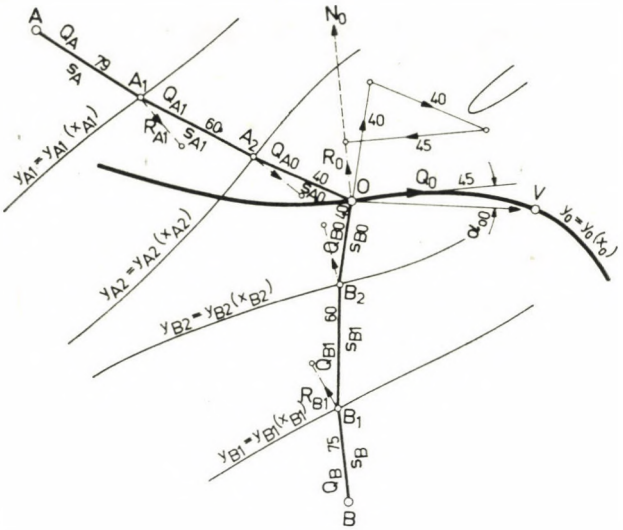


Abb. 8

der Bildebene eine Kurve $y_0 = y_0(x_0)$, auf dieser ein Punkt V, sodann der Einfachheit halber nur die beiden Punkte A und B gegeben. Schließlich sei noch das der Kurve $y_0 = y_q(x_0)$ zugeordnete Gewicht Q_0 gegeben.

Zu suchen ist auf der Kurve $y_0 = y_0(x_0)$ ein solcher Punkt O, daß die Beziehung

$$S = Q_A s_A + Q_{A1} s_{A1} + \ldots + Q_{AO} s_{AO} + \\ + Q_B s_B + Q_{B1} s_{B1} + \ldots + Q_{BO} s_{BO} + \\ + Q_0 \cdot \widehat{OV}$$

ein Minimum ergebe.

Als Ausdruck für den Kurvenabschnitt $\widehat{OV}$ kann geschrieben werden:

$$\widehat{OV} = \int_{x_{0O}}^{x_{0V}} \sqrt{1 + y_0'^2}\, dx_0 .$$

Die geraden Abschnitte s_A, s_{A1}, . . ., s_{AO}, s_B, s_{B1}, . . ., s_{BO} können in der vorhergehend dargelegten Weise ausgedrückt werden.

Werden nun die Differentialquotienten nach x_{A1}, x_{A2}, . . ., x_{AO}; x_{B1}, x_{B2}, . . ., x_{BO} und x_0 aufgeschrieben, so lauten nach entsprechenden goniometrischen Transformationen unsere Bedingungsgleichungen:

$$Q_A \cos(\varphi_A - \alpha_{A1}) - Q_{A1} \cos(\varphi_{A1} - \alpha_{A1}) = 0$$
$$Q_{A1} \cos(\varphi_{A1} - \alpha_{A2}) - Q_{A2} \cos(\varphi_{A2} - \alpha_{A2}) = 0$$
$$\vdots$$
$$Q_B \cos(\varphi_B - \alpha_{B1}) - Q_{B1} \cos(\varphi_{B1} - \alpha_{B1}) = 0$$

$$Q_{B1} \cos (\varphi_{B1} - \alpha_{B2}) - Q_{B2} \cos (\varphi_{B2} - \alpha_{B2}) = 0$$
$$\vdots$$
$$Q_{AO} \cos (\varphi_{AO} - \alpha_{0O}) + Q_{BO} \cos (\varphi_{BO} - \alpha_{0O}) + Q_0 = 0 .$$

Auf Grund des Vorherigen kann nun dieses Bedingungsgleichungssystem leicht interpretiert werden. Besondere Beachtung verdient nur die letzte Gleichung: Die Resultierende der in Punkt O direkt angreifenden drei Vektoren entfällt auf die dem Punkt O der gegebenen Kurve $y_0 = y_0(x_0)$ zugeordnete Normale (N_0), wobei Q_{AO}, Q_{BO}, und Q_O die Skalarwerte sind. Richtung und Sinn der ersten zwei Vektoren sind als bekannt gegeben, während die Richtung des der Kurve $y_0 = y_0(x_0)$ zugeordneten Vektors die zum Punkt O gehörige Tangente ist, sein Drehsinn aber von Punkt V zu Punkt O hinweist. Die Lage des Punktes V bestimmt demnach nur den Drehsinn des Vektors mit Skalarwert Q_0, was besagt, daß der Punkt V wo immer auf der von Punkt O ausgehenden Halbkurve liegen kann.

Die Abb. 8 stellt zugleich auch ein Zahlenbeispiel vor.

Wenn außer der Kurve $y_0 = y_0(x_0)$ auch andere Punkte $(A, B, C, D, \ldots)$ gegeben sind, dann muß das Verfahren sinngemäß angewendet werden.

Abb. 9 stellt ein einfaches Beispiel aus dem Themenkreis des Anlegens von Bergwerken dar. Hier soll man aus dem gegebenen Punkt A mit einer untertätigen Richtstrecke bis zur Isohypse $y_{A1} = y_{A1}(x_{A1})$ gelangen, wonach dann ein Schleppschacht bis zur Isohypse $y_{A2} = y_{A2}(x_{A2})$ folgt, an den sich

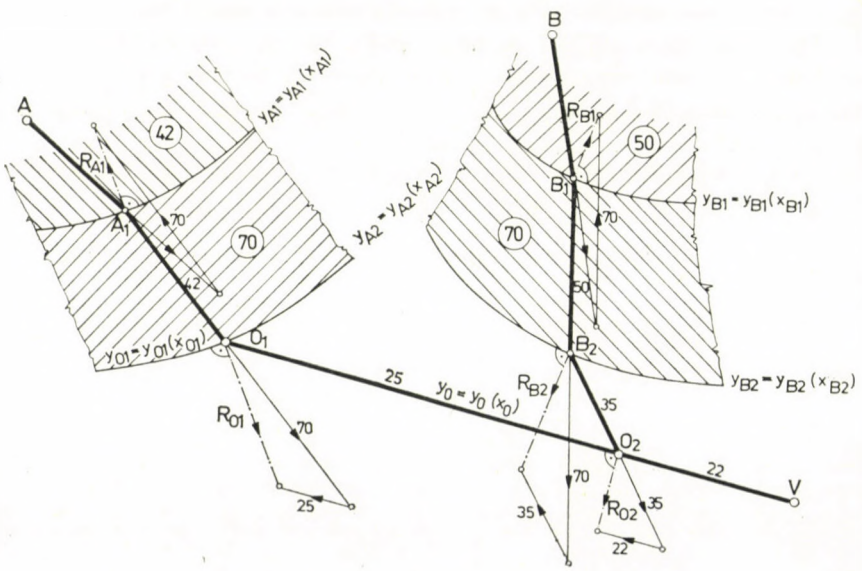


Abb. 9

dann über Tage ein gerader Abschnitt $y_0 = y_0(x_0)$ anschließt, auf dem ein Bandförderer zu dem gegebenen Punkt V hinführt. Von dem gegebenen Punkt aus gelangt man gleichfalls über eine untertägige Richtstrecke zur Isohypse $y_{B1} = y_{B1}(x_{B1})$, danach mit einem Schleppschacht bis zur Isohypse $y_{B2} = y_{B2}(x_{B2})$, während über Tage ein Bandförderer zur Geraden $y_0 = y_0(x_0)$ anschließt.

Der Aufgabe gemäß ist $y_{A2} = y_{A2}(x_{A2})$ nicht nur eine Isohypse, sondern auch eine gegebene Zwangsbahn, d. h. zugleich auch $y_{01} = y_{01}(x_{01})$. Zu suchen ist demnach der Punkt O_1, als der Schnittpunkt der Geraden $y_0 = y_0(x_0)$ mit der Kurve $y_{01} = y_{01}(x_{01})$. Mit anderen Worten: Die Richtung der Geraden $y_0 = y_0(x_0)$ ist nicht im voraus festgelegt. Ebenso ist nun auf dem nach Vorherigem schon festgelegten geraden Abschnitt der Punkt O_2 zu suchen. Die Gewichte lauten der Reihe nach: Das Gewicht von $AA_1 = 42$, von $A_1O_1 = 70$, von $O_1O_2 = 25$, von $O_2V = 22$, von $BB_1 = 50$, von $B_1B_2 = 70$, von $B_2O_2 = 35$. Die Gewichte sind relative Gewichte.

Lösung: R_{A1} entfällt auf die dem Punkt A_1 der Isohypse $y_{A1} = y_{A1}(x_{A1})$ zugeordnete Normale, R_0 auf die dem Punkt O_1 der Isohypse $y_{O1} = y_{O1}(x_{O1})$ zugeordnete Normale; R_{B1} auf die dem Punkt B_1 der Isohypse $y_{B1} = y_{B1}(x_{B1})$ zugeordnete Normale; R_{B2} auf die dem Punkt B_2 der Isohypse $y_{B2} = y_{B2}(x_{B2})$ zugeordnete Normale und schließlich R_{O2} auf die dem Punkt O_2 des geraden Abschnittes $y_0 = y_0(x_0)$ zugeordnete Normale.

Selbstredend ist die in Abb. 9 zu sehende Lösung das Endergebnis eines Iterationsverfahrens.

Wählt man in der Praxis anstatt der das Minimum sichernden Lösung eine andere, so kann die prozentuelle Erhöhung leicht angegeben werden, woraus sich natürlich auch der Kostenzuwachs errechnen läßt.

Die Erörterung einiger grundlegender theoretischer Zusammenhänge der Streckentrassierung kann nicht nur zur Lösung von bergbaulichen Aufgaben benützt werden, sondern auch überall, wo Straßentrassen, Leitungstrassen u. dgl. projektiert werden sollen.

О ТЕОРЕТИЧЕСКИХ ОСНОВАХ ПРОЕКТИРОВАНИЯ ТРАСС

Й. ЗАМБО

РЕЗЮМЕ

На местности, принятой за плоскую, надо проложить трассу между двумя или большими пунктами, когда на местности заданы изолинии весовой поверхности $Q = Q(x, y)$ и вес полос, площадей между изолиниями принимается постоянным. Требуется найти минимум выражения $\Sigma Q_i S_i$, где Q_i означет вес полосы, а S_i длину участка трассы, пересекающей полосу. Автор выводит системы условных уравнений, удовлетворение которым приводит к решению итерационным путем. Становится ясным, что получается способ, значительно проще, чем сконструирование динамическим программированием. Веса могут быть различного происхождения, например, могут произойти из времени для прохода трассы, затрат на постройку и т. д.

RECENSIO

G. Atanasiu: Opere alese (Selected works)

Editura Academiei Republicii Socialiste Romania, 1977

The author, former professor of physics and geophysics at the University Bucharest, was versatile in his scientific activity. The present volume contains a selection of his papers published between 1922 and 1974. Twenty papers are written in French, one in English and nine in Roumanian.

The papers are grouped into three main chapters. In the first (Photoconductive semiconductors) we find six papers dealing with problems in electro-chemistry, photoelectricity and optics. Experimental data on the photoelectrical effect of different semiconductive crystals are listed.

For the geophysicist the second and third chapters are of much more interest. Chapter "Geomagnetism" reviews the activity in Roumania in the last three decades. The results of the observation of the elements of the geomagnetic field and their secular variation are summed up and interpreted. A great amount of numerical data and a collection of iso-maps of the whole country as well as for several selected areas (Transylvania, Moldavia, etc.) are surely of great interest.

The third chapter "Georadioactivity" mainly deals with the radioactive investigation of the mineral waters in Roumania, first of all in Transylvania. Here again, the great amount of data must be emphasized which hardly can be found elsewhere in such a collected form.

It is a very interesting book in many respects, as a cross-section of the author's scientific work as well as a source of a great data amount. We only regret that the biography of the author — who made pioneer work in geophysics in his country — has not been translated into French.

Á. Wallner

INDEX

Halmos, F.: Geodynamical evaluation of Doppler satellite observations 3
Rinner, K.: Geodetic work and projects at the observatory of Graz-Lustbühel 17
Groten, E.: On variations of geocentric positions with time 31
Hein, G.—Groten, E.: On the use of bandwidth and profile reduction in combination solutions of satellite altimetry 59
Schaab, H.: Investigation of the geoid in Europe by the collocation method 71
Мозжухин, О. А.: Учет рефракции в нивелировании на основе метеорологических измерений 81
Ferencz, Cs.: A possibility of using quasi-single-frequency Doppler—Faraday measurements — A proposal 93
Mentes, Gy.: Development of horizontal pendulum recordings 101
Závoti, J.: Ideas on the practical application of collocation 111
Lichtenegger, H.: Formelsysteme zur Berechnung der Sonnenephemeriden 125
Bácsatyai, L.: Zur Frage der Planung der Höhennetze, mit Rücksicht auf die Erdkrustenbewegungs-Untersuchungen 135
Tárczy-Hornoch, A.—Verő-Heténvi, M.: Adjustment of quadrilaterals computed from electromagnetic distance measurements encumbered by temperature and other meteorological effects 141
Szeidovitz, Gy.: Amplitude and velocity of seismic waves excited by weight dropping 149
Metzger, J.: Variations telluriques lentes observées a M'Bour (Sénégal) 155
Csomor, D.—Kiss, Z.—Szeidovitz, Gy.: Dynamics of seismic waves caused by blastings in mines 171
Лебедев, Т. С.—Корчин, В. А.: Упругие характеристики минерального вещества в термобарических условиях земнях недр 181
Märcz, F.: Quasi-periodic variations of ionospheric absorption with characteristic changes during a solar cycle 227
Albu, I.—Mituch, E.—Posgay, K.—Aric, K.—Gutdeutsch, R.: Deutung der refraktionsseismischen Messungen auf dem östlichen Abschnitt des Alpenlängsprofiles 237
Bobok, E.: Investigation of capillary-gravity waves in a thin non-Newtonian film flow by potential-theory method 247
Патварош, Й.: Определение основых параметров эксплуатации скважинами линз боксита в случае конкуренции разносным карьером 257
Balla, L.—Meggyes, T.: On the weighted linearization 267
Boldizsár, T.: Non-electric use of geothermal energy in Hungary 289
Zambó, J.: Über die theoretischen Grundlagen der Wegstreckentrassierung 299

Recensio

Atanasiu, G.: Opere alese (Selected works) — *Á. Wallner* 311

Printed in Hungary

A kiadásért felel az Akadémiai Kiadó igazgatója — Műszaki szerkesztő: Zacsik Annamária

A kézirat nyomdába érkezett: 1978. VII. 3. — Terjedelem: 27,65 (A/5) ív, 153 ábra 4 melléklet

79.6053 Akadémiai Nyomda, Budapest — Felelős vezető: Bernát György

Acta Geodaetica, Geophysica et Montanistica, eine Halbjahresschrift der Ungarischen Akademie der Wissenschaften, veröffentlicht Originalbeiträge aus dem Bereich der Geodäsie, Geophysik und des Bergbaus in deutscher, englischer, französischer oder russischer Sprache.

Redaktion: H-9400 Sopron, Múzeum u. 6.

Jahresabonnementspreis: $ 36.00.

Bestellbar bei »Kultura« Außenhandelsunternehmen (1389 Budapest 62, P.O.B. 149) oder seinen Auslandsvertretungen.

Acta Geodaetica, Geophysica et Montanistica est une revue biannuelle de l'Académie Hongroise des Sciences publiant des essais originaux du domaine de la géodésie, géophysique et des sciences minières en français, anglais, allemand ou russe.

Rédaction: H-9400 Sopron, Múzeum u. 6.

Le prix de l'abonnement: $ 36.00 par an.

On peut s'abonner à l'Entreprise du Commerce Extérieur « Kultura » (1389 Budapest 62, P.O.B. 149) ou chez représentants à l'étranger.

Acta Geodaetica, Geophysica et Montanistica выходят два раза в год в издании Академии наук Венгрии. В журнале публикуются оргнгинальные исследования по проблемам геодезии, геофизики и горного дела на русскдм, английском, немецком и французском языках.

Адрес редакции: **H-9466 Sopron, Múzeum u 6.**

Подписная цена на год: $ 36,00.

Заказать журнал через Внешнеторговое предприятие
62, P. O. B. 149) или через его заграничные представительства.

Reviews of the Hungarian Academy of Sciences are obtainable at the following addresses:

AUSTRALIA
C.B.D. LIBRARY AND SUBSCRIPTION SERVICE, Box 4886, G.P.O., *Sydney N.S.W. 2001*
COSMOS BOOKSHOP, 145 Ackland Street, *St. Kilda (Melbourne), Victoria 3182*

AUSTRIA
GLOBUS, Höchstädtplatz 3, *1200 Wien XX*

BELGIUM
OFFICE INTERNATIONAL DE LIBRAIRIE, 30 Avenue Marnix, *1050 Bruxelles*
LIBRAIRIE DU MONDE ENTIER, 162 Rue du Midi, *1000 Bruxelles*

BULGARIA
HEMUS, Bulvar Ruszki 6, *Sofia*

CANADA
PANNONIA BOOKS, P.O. Box 1017, Postal Station "B", *Toronto, Ontario M5T 2T8*

CHINA
CNPICOR, Periodical Department, P. O. Box 50 *Peking*

CZECHOSLOVAKIA
MAD'ARSKÁ KULTURA, Národní třida 22, *115 66 Praha*
PNS DOVOZ TISKU, Vinohradská 46, *Praha 2*
PNS DOVOZ TLAČE, *Bratislava 2*

DENMARK
EJNAR MUNKSGAARD, Norregade 6, *1165 Copenhagen*

FINLAND
AKATEEMINEN KIRJAKAUPPA, P. O.Box 128, *SF-00101 Helsinki 10*

FRANCE
EUROPÉRIODIQUES S. A., 31 Avenue de Versailles, *78170 La Celle St. Cloud*
LIBRAIRIE LAVOISIER, 11 rue Lavoisier, *75008 Paris*
OFFICE INTERNATIONAL DE DOCUMENTATION ET LIBRAIRIE, 48 rue Gay-Lussac, *75240 Paris Cedex 05*

GERMAN DEMOCRATIC REPUBLIC
HAUS DER UNGARISCHEN KULTUR, Karl-Liebknecht-Strasse 9, *DDR-102 Berlin*
DEUTSCHE POST ZEITUNGSVERTRIEBSAMT, Strasse der Pariser Kommüne 3—4, *DDR-104 Berlin*

GERMAN FEDERAL REPUBLIC
KUNST UND WISSEN ERICH BIEBER, Postfach 46, *7000 Stuttgart 1*

GREAT BRITAIN
BLACKWELL'S PERIODICALS DIVISION, Hythe Bridge Street, *Oxford OX1 2ET*
BUMPUS, HALDANE AND MAXWELL LTD., Cowper Works, *Olney, Bucks MK46 4BN*
COLLET'S HOLDINGS LTD., Deningston Estate, *Wellingborough, Northants NN8 2QT*
WM. DAWSON AND SONS LTD., Cannon House, *Folkestone, Kent CT19 5EE*
H. K. LEWIS AND CO., 136 Gower Street, *London WC1E 6BS*

GREECE
KOSTARAKIS BROTHERS, International Booksellers, 2 Hippokratous Street, *Athens-143*

HOLLAND
MEULENHOFF-BRUNA B.V., Beulingstraat 2, *Amsterdam*
MARTINUS NIJHOFF B.V., Lange Voorhout 9—11, *Den Haag*
SWETS SUBSCRIPTION SERVICE, 347b Heereweg, *Lisse*

INDIA
ALLIED PUBLISHING PRIVATE LTD., 13/14 Asaf Ali Road, *New Delhi 110001*
150 B-6 Mount Road, *Madras 600002*
INTERNATIONAL BOOK HOUSE PVT. LTD., Madame Cama Road, *Bombay 400039*
THE STATE TRADING CORPORATION OF INDIA LTS., Books Import Division, Chandralok, 36 Janpath, *New Delhi 110001*

ITALY
EUGENIO CARLUCCI, P.O. Box 252, *70100 Bari*
INTERSCIENTIA, Via Mazzé 28, *10149 Torino*
LIBRERIA COMMISSIONARIA SANSONI, Via Lamarmora 45, *50121 Firenze*
SANTO VANASIA, Via M. Macchi 58, *20124 Milano*
D. E. A., Via Lima 28, *00198 Roma*

JAPAN
KINOKUNIYA BOOK-STORE CO. LTD., 17-7 Shinjuku-ku 3 chome, Shinjuku-ku, *Tokyo 160-91*
MARUZEN COMPANY LTD., Book Department, P.O. Box 5050 Tokyo International, *Tokyo 100-31*
NAUKA LTD. IMPORT DEPARTMENT, 2-30-19 Minami Ikebukuro, Toshima-ku, *Tokyo 171*

KOREA
CHULPANMUL, *Phenjan*

NORWAY
TANUM-CAMMERMEYER, Karl Johansgatan 41—43, *1000 Oslo*

POLAND
WĘGIERSKI INSTYTUT KULTURY, Marszałkowska 80, *Warszawa*
CKP I V ul. Towarowa 28 *00-958 Warszawa*

ROUMANIA
D. E. P., *Bucureşti*
ROMLIBRI, Str. Biserica Amzei 7, *Bucureşti*

SOVIET UNION
SOJUZPETCHATJ — IMPORT, *Moscow*
and the post offices in each town
MEZHDUNARODNAYA KNIGA, *Moscow G-200*

SPAIN
DIAZ DE SANTOS, Lagasca 95, *Madrid 6*

SWEDEN
ALMQVIST AND WIKSELL, Gamla Brogatan 26, *101 20 Stockholm*
GUMPERTS UNIVERSITETSBOKHANDEL AB, Box 346, *401 25 Göteborg 1*

SWITZERLAND
KARGER LIBRI AG, Petersgraben 31, *4011 Basel*

USA
EBSCO SUBSCRIPTION SERVICES, P. O. Box 1943, *Birmingham*, Alabama *35201*
F. W. FAXON COMPANY, INC., 15 Southwest Park, *Westwood, Mass. 02090*
THE MOORE-COTTRELL SUBSCRIPTION AGENCIES, *North Cohocton, N. Y. 14868*
READ-MORE PUBLICATIONS, INC., 140 Cedar Street, *New York, N. Y. 10006*
STECHERT-MACMILLAN, INC., 7250 Westfield Avenue, *Pennsauken N. J. 080110*

VIETNAM
XUNHASABA, 32, Hai Ba Trung, *Hanoi*

YUGOSLAVIA
JUGOSLAVENSKA KNJIGA, Terazije 27, *Beograd*
FORUM, Vojvode Mišica 1, *21000 Novi Sad*

12. VI. 1979 HU ISSN 0374—1842 Index: 26.031

Acta GEODAETICA, GEOPHYSICA et MONTANISTICA

ACADEMIAE SCIENTIARUM HUNGARICAE

ADIUVANTIBUS
G. BARTA
J. VERŐ
J. ZAMBÓ
REDIGIT
A. TÁRCZY-HORNOCH

AKADÉMIAI KIADÓ, BUDAPEST

TOMUS 14
FASCICULUS 3
1979

ACTA GEODAETICA, GEOPHYSICA et MONTANISTICA

Academiae Scientiarum Hungaricae

A Magyar Tudományos Akadémia Föld- és Bányászati Tudományok Osztályának folyóirata

Szerkesztőség: H-9400 Sopron, Múzeum u. 6.
Kiadja az Akadémiai Kiadó, 1054 Budapest, Alkotmány utca 21.

Az *Acta Geodaetica, Geophysica et Montanistica* eredeti tanulmányokat közöl a geodézia, geofizika és a bányászati tudományok tárgyköréből, angol, német, francia vagy orosz nyelven. Félévenként jelenik meg, évi egy, kb. 400—500 oldalas kötetet alkotva.

Megrendelhető az Akadémiai Kiadónál (1363 Budapest Pf. 24.), a külföld részére pedig a „Kultura" Külkereskedelmi Vállalatnál (1389 Budapest 62, P.O.B. 149).

Acta Geodaetica, Geophysica et Montanistica is a semiannual review of the Hungarian Academy of Sciences, publishing papers on geodesy, geophysics and mining in English German, French or Russian.

Editorial Office: H-9400 Sopron, Múzeum u. 6.

Subscription: $ 36.00 per year.

Orders may be placed with "Kultura" Foreign Trading Company (1389 Budapest 62, P.O.B. 149) or its representatives abroad.

Acta Geodaet., Geophys. et Montanist. Acad. Sci. Hung. Tomus 14 (3), pp. 313—340 (1979)

LABORATORY DETERMINATION OF ROCK CHARACTERISTICS
I. UNIAXIAL COMPRESSION TESTS

CS. ASSZONYI

HUNGARIAN COAL BOARD, TATABÁNYA

L. KAPOLYI

MINISTRY OF HEAVY INDUSTRY, BUDAPEST

R. RICHTER

TECHNICAL UNIVERSITY OF HEAVY INDUSTRY, MISKOLC

[Manuscript received February 24, 1977]

The study deals with the determination of a rheological model most suitable for characterizing mechanical rock properties, and with the prediction of the actual values of material properties. It analyses the ways of determining rock characteristics by means of laboratory uniaxial compression tests and gives a simple method for test evaluation.

1. Introduction

It has been proved by Cs. ASSZONYI [3] that the law of material for continua is represented by the correlation between the stress tensor (i.e. conductive current intensity of momentum) and the non-homogeneity of the displacement field. This correlation can be expressed mathematically in the following form:

$$\boldsymbol{F} = \boldsymbol{L} \nabla \circ \mathbf{u}, \tag{1}$$

where $\boldsymbol{F}$ is the stress tensor, $\mathbf{u}$ the displacement vector, $\boldsymbol{L}$ the so-called momentum conductivity tensor of the fourth order and ∇ is HAMILTON's linear differential operator.

Equation (1) expresses the fact that a system exposed to mechanical interaction tends towards being homogenized and equalized.

The matrix of the stress tensor $\boldsymbol{F}$ is a symmetric, as it follows from the law of the conservation of moment of momentum, thus the general form of the material equation ([2] p. 351) leads to

$$\boldsymbol{F} = \boldsymbol{L}\boldsymbol{D}, \tag{2}$$

or writing it in scalar equations:

$$\sigma_x = L_{11}\,\varepsilon_x + L_{12}\,\varepsilon_y + L_{13}\,\varepsilon_z + L_{14}\,\gamma_{xy} + L_{15}\,\gamma_{yz} + L_{16}\,\gamma_{zx},$$

$$\sigma_y = L_{21}\,\varepsilon_x + L_{22}\,\varepsilon_y + L_{23}\,\varepsilon_z + L_{24}\,\gamma_{xy} + L_{25}\,\gamma_{yz} + L_{26}\,\gamma_{zx},$$

$$\sigma_z = L_{31}\,\varepsilon_x + L_{32}\,\varepsilon_y + L_{33}\,\varepsilon_z + L_{34}\,\gamma_{xy} + L_{35}\,\gamma_{yz} + L_{36}\,\gamma_{zx},$$

$$\tau_{xy} = L_{41}\,\varepsilon_x + L_{42}\,\varepsilon_y + L_{43}\,\varepsilon_z + L_{44}\,\gamma_{xy} + L_{45}\,\gamma_{yz} + L_{46}\,\gamma_{zx},$$

$$\tau_{yz} = L_{51}\,\varepsilon_x + L_{52}\,\varepsilon_y + L_{53}\,\varepsilon_z + L_{54}\,\gamma_{xy} + L_{55}\,\gamma_{yz} + L_{56}\,\gamma_{zx},$$

$$\tau_{zx} = L_{61}\,\varepsilon_x + L_{62}\,\varepsilon_y + L_{63}\,\varepsilon_z + L_{64}\,\gamma_{xy} + L_{65}\,\gamma_{yz} + L_{66}\,\gamma_{zx},$$

where

$$\boldsymbol{D} = \frac{1}{2}\,[\nabla \circ \mathbf{u} + \mathbf{u} \circ \nabla],$$

which will be called for sake of simplicity's sake the deformation tensor.

Equation (2) is an exact law of material for both *small* and *great* deformations. In Eq. (2) $\boldsymbol{D}$ is in reality only a simplifying notation, which can be considered, in the range of small deformations with a good approximation, as CAUCHY's number of deformation (specific extension and angular distortion).

The stress and deformation tensor can be written in a form more commonly used in rheological studies by using the expressions

$$\sigma_0 = \frac{1}{3}\,(\sigma_x + \sigma_y + \sigma_z) = \frac{1}{3}\ \mathrm{inv}_1\,\boldsymbol{F} = \frac{1}{3}\,S,$$

$$\varepsilon_0 = \frac{1}{3}\,(\varepsilon_x + \varepsilon_y + \varepsilon_z) = \frac{1}{3}\ \mathrm{inv}_1\,\boldsymbol{D} = \frac{1}{3}\,\Theta,$$

for medium or average stress and deformation:

$$\boldsymbol{F} = (\boldsymbol{F} - \sigma_0\,\boldsymbol{I}) + \sigma_0\,\boldsymbol{I} = \boldsymbol{T} + \boldsymbol{T}_0,$$

$$\boldsymbol{D} = (\boldsymbol{D} - \varepsilon_0\,\boldsymbol{I}) + \varepsilon_0\,\boldsymbol{I} = \boldsymbol{E} + \boldsymbol{E}_0,$$

where

$$\boldsymbol{T} = \begin{Vmatrix} \sigma_x - \sigma_0 & \tau_{xy} & \tau_{xz} \\ \tau_{yx} & \sigma_y - \sigma_0 & \tau_{yz} \\ \tau_{zx} & \tau_{zy} & \sigma_z - \sigma_0 \end{Vmatrix}$$

is the so-called *stress deviation tensor* representing the deviation of the actual state of stress from the hydrostatic one,

$$\boldsymbol{T}_0 = \begin{Vmatrix} \sigma_0 & 0 & 0 \\ 0 & \sigma_0 & 0 \\ 0 & 0 & \sigma_0 \end{Vmatrix} = \sigma_0 \begin{Vmatrix} 1 & 0 & 0 \\ 0 & 1 & 0 \\ 0 & 0 & 1 \end{Vmatrix}$$

is the *stress spherical tensor* describing the hydrostatic state of average stress,

$$\boldsymbol{E} = \begin{Vmatrix} \varepsilon_x - \varepsilon_0 & \frac{1}{2}\gamma_{xy} & \frac{1}{2}\gamma_{xz} \\ \frac{1}{2}\gamma_{yx} & \varepsilon_y - \varepsilon_0 & \frac{1}{2}\gamma_{yz} \\ \frac{1}{2}\gamma_{zx} & \frac{1}{2}\gamma_{zy} & \varepsilon_z - \varepsilon_0 \end{Vmatrix}$$

is the *deviation tensor of deformations* expressing the distortion deformation without any change in volume and

$$\boldsymbol{E}_0 = \begin{Vmatrix} \varepsilon_0 & 0 & 0 \\ 0 & \varepsilon_0 & 0 \\ 0 & 0 & \varepsilon_0 \end{Vmatrix} = \varepsilon_0 \begin{Vmatrix} 1 & 0 & 0 \\ 0 & 1 & 0 \\ 0 & 0 & 1 \end{Vmatrix}$$

is the *spherical tensor of deformations* describing the so-called *change-in-volume* or *isotropic* deformation.

2. Isotropism and approximative assumptions

It has been shown [2] that in the case of perfect anisotropism 21 momentum conduction functions should be determined for the law material. To simplify the following investigations the isotropism of rock continuum will be assumed thus the task will be reduced to the determination of 2 functions. Although the importance of isotropism is not negligible in rock mechanics, this will be done, however, not as if the rocks were considered as isotropic, but because

— on the one hand, by assuming the materials to be isotropic the material equation would be significantly simplified which in turn enables the used a simple mathematical apparatus. In this way qualitative conclusions can be drawn, ensuring good orientation in choosing the right type of support in developing the technique of construction, etc. without knowing exactly the actual values of material constants and *in-situ* parameters.

— On the other hand, the majority of rocks do not behave perfectly anisotropicaly but have some special characteristics correlated with different directions, i.e. the material and strength properties are different in parallel or perpendicular directions with regard to stratification. This phenomenon is called *orthotropism*. Although the investigations have assumed isotropic continuum, they are still important, since the results about isotropic materials illustrate that correlations of rheologically orthotropic materials can be as easily derived, as the physical aquations of linear elastic orthotropic materials on the basis of HOOKE's law.

In the investigations what follow the material equation of isotropic continus will be determined. This requires to define the actual form of the equations

$$\boldsymbol{T} = \boldsymbol{f}(\boldsymbol{E}),$$

$$\boldsymbol{T}_0 = \boldsymbol{f}_0(\boldsymbol{E}).$$

The general law of material for isotropic continua has been formulated in [2] p. 353 Eq. (46) as

$$\boldsymbol{F} = \lambda \boldsymbol{D} + \mu \Theta \boldsymbol{I} = \lambda \boldsymbol{D} + 3\mu \boldsymbol{E}_0, \tag{3}$$

where

$$\boldsymbol{T} = \lambda \boldsymbol{E},$$

$$\boldsymbol{T}_0 = (\lambda + 3\mu)\boldsymbol{E}_0$$

can be written according to our previous discussions. In these equations λ and μ are general functions depending on thermodynamical variables and time.

While formulating the material equation an approximation should be used to compromise two contrary requirements:

Requirement 1: the equation should reflect the physical mechanical properties of the rock as adequately as possible,

Requirement 2: a model should be found enabling an as simple mathematical formulation as possible for the practical calculations.

In compromising these requirements it should be kapt in mind that the quality of the approximation and the order of the error be known with a satisfactory accuracy.

In the derivation of the law of material the following assumptions can be made:

1. The mechanical state of the rocks does not depend directly (implicitly) on time because this would mean that the physical equation expressing material properties were not invariant with respect the choice of the beginning of the time of measurements.

Consequently, the well-known important role of time can be taken into account by including the time-derivatives of the stress and deformation tensors, i.e. the physical equation can take the form

$$\boldsymbol{f}(\boldsymbol{T}, \boldsymbol{E}, \dot{\boldsymbol{T}}, \dot{\boldsymbol{E}}, \ddot{\boldsymbol{T}}, \ddot{\boldsymbol{E}}, \dots) = \boldsymbol{O},$$

$$\boldsymbol{f}_0(\boldsymbol{T}_0, \boldsymbol{E}_0) = \boldsymbol{O}.$$

2. It can also be assumed that the effect of higher order derivatives (stress change or deformation change acceleration, etc.) can be neglected, and thus the material equation will be simplified to the form:

$$\boldsymbol{f}(\boldsymbol{T}, \boldsymbol{E}, \dot{\boldsymbol{T}}, \dot{\boldsymbol{E}}) = \boldsymbol{O},$$

$$\boldsymbol{f}_0(\boldsymbol{T}_0, \boldsymbol{E}_0) = \boldsymbol{O}. \tag{4}$$

3. After these considerations we now have to determine the actual type of the function (4). This can not be done in a theoretical way since there is no physical (mechanical) basis to give further hints as to the actual form of function (4). The only way to proceed further is to assume different types of functions, to carry out specially designed laboratory tests, and to try to find that particular functional form which best fits the measured results. Nevertheless, this can not be considered as safe method either. Obviously it would be incorrect to determine a function precisely fitting all measured results, as e.g. in case of $(n + 1)$ measurements to formulate the material equation as a polynomial of n-th order, since the observation results may be burdened with smaller or bigger measurement errors. For this reason, one needs a type of function eliminating the measurement errors to a large extent, thus giving a better description of the phenomenon investigated than the observation data would do. Accordingly, the function approximating the measurement data should be such that any deviation should reflect errors in the observations.

A polynomial of-the n-th order perfectly fitting to $(n + 1)$ measurements would not reflect a *material law*. On the contrary, it would merely be a description of the experiment combined with measurement errors. One needs a type of function which closely, fits the measurement results satisfies the justified assumption 1 and 2, and emphasizes these characteristic mechanical properties which have already been recognized in past experience.

On the basis of these considerations the most general linear law of material can be considered as the best approximation describing the physical properties of rock continua. This can be determined in the form

$$\begin{aligned} \boldsymbol{f} &\equiv \boldsymbol{C}_0 + C_1\boldsymbol{T} + C_2\dot{\boldsymbol{T}} + C_3\boldsymbol{E} + C_4\dot{\boldsymbol{E}} = \boldsymbol{O}, \\ \boldsymbol{f}_0 &\equiv C_5'\boldsymbol{T} + C_6\boldsymbol{E} = \boldsymbol{T}_0 + C_5\boldsymbol{E}_0 = \boldsymbol{O}. \end{aligned} \tag{5}$$

The equation of state (5) can be rewritten by introducing the so-called rheological constants in a form more commonly used in literature:

$$\begin{aligned} \boldsymbol{T} &= 2G\boldsymbol{E} + 2\eta\dot{\boldsymbol{E}} - \tau\dot{\boldsymbol{T}} + \boldsymbol{C}_0, \\ \boldsymbol{T}_0 &= 3K\boldsymbol{E}_0,\ \dot{\boldsymbol{T}}_0 = 3K\dot{\boldsymbol{E}}_0. \end{aligned} \tag{6}$$

This model is due to HOHENEMSER and PRAGER in Eq. (6) G is the shear (or rigidity) modulus (kp/cm^2), η is the viscosity coefficient (kp, day/cm^2), (kp, h/cm^2), τ time of relaxation (day), (h), $\boldsymbol{C}_0$ a constant (plasticity) tensor (kp/cm^2), K is the compressibility or bulk modulus (kp/cm^2).

The rheological model (6) is a general equation of state which applies to all the simple linear rheological bodies, as special cases:

a) $\boldsymbol{T} = \boldsymbol{O}$ [PASCALian (fluid) body]

b) $\boldsymbol{T} = 2G\boldsymbol{E}$ [HOOKEian (elastic) body]

c) $\boldsymbol{T} = 2\eta\dot{\boldsymbol{E}}$ [NEWTONian (fluid) body]

d) $\boldsymbol{T} = \boldsymbol{C}_0$ [SAINT-VENANTian (brittle-plastic) body]

e) $\boldsymbol{T} = 2G\boldsymbol{E} + 2\eta\dot{\boldsymbol{E}}$ [KELVINian (elastic-viscous) body]

f) $\boldsymbol{T} = 2G\boldsymbol{E} - \tau\dot{\boldsymbol{T}}$ [Elastic body with relaxation]

g) $\boldsymbol{T} = 2\eta\dot{\boldsymbol{E}} - \tau\dot{\boldsymbol{T}}$ [MAXWELLian (fluid) body]

h) $\boldsymbol{T} = 2G\boldsymbol{E} + \boldsymbol{C}_0$ [Elastic-plastic body]

i) $\boldsymbol{T} = 2\eta\dot{\boldsymbol{E}} + \boldsymbol{C}_0$ [BINGHAMian (viscoplastic) body]

j) $\boldsymbol{T} = 2G\boldsymbol{E} + 2\eta\dot{\boldsymbol{E}} - \tau\dot{\boldsymbol{T}}$ [POYNTING—THOMSONian body]

k) $\boldsymbol{T} = 2G\boldsymbol{E} + 2\eta\dot{\boldsymbol{E}} + \boldsymbol{C}_0$ [Elastic-viscous-plastic body]

l) $\boldsymbol{T} = 2\eta\dot{\boldsymbol{E}} - \tau\dot{\boldsymbol{T}} + \boldsymbol{C}_0$ [PRANDTL—REUSSian (elastoplastic) body]

3. The standard model

In rock mechanical investigations it is in many cases a justified method to consider the physical equation as a *homogeneous linear* one in order to gain simpler solutions, i.e. in course of the calculations and theoretical studies one can rely on POYNTING—THOMSON's so-called "standard" model. This idealized model describes, with a fair approximation a great part of rock properties presently known.

This general homogeneous linear material model takes account only implicitly of the effect of time, and is thus independent (invariant) of the beginning of time of the measurement. This formulation is represented by the POYNTING—THOMSON's model. This model explicitly neglects the effect of the derivatives of higher than first order. Consequently, its mathematical form simple enough to be used in approaching the solutions of practical tasks. The model itself can be written as follows:

$$a) \qquad \boldsymbol{T} = 2G\boldsymbol{E} + 2\eta\dot{\boldsymbol{E}} - \tau\dot{\boldsymbol{T}},$$

$$b) \qquad \boldsymbol{T}_0 = 3K\boldsymbol{E}_0. \tag{7}$$

This relation describes the connection between stress and deformation tensor in the form of a differential equation. That this material law is a justifiable one can be proved by comparing it with the equations

$$\boldsymbol{T} = \lambda\boldsymbol{E},$$

$$\boldsymbol{T}_0 = (\lambda + 3\mu)\,\boldsymbol{E}_0.$$

Although the actual forms of the functions λ and μ can not be determined, it will be clear from the following analysis of properties that

$$\lambda > 0$$

i.e. a positive $\boldsymbol{T}$ belongs to positive $\boldsymbol{E}$. Furthermore from the equation

$$3K = \lambda + 3\mu$$

follows:

$$\mu = K - \frac{\lambda}{3},$$

and because K is positive

$$\mu > -\frac{\lambda}{3}$$

consequently the standard body satisfies ONSAGER's conditions of positive definiteness [2].

In the following section the properties of the standard model will be briefly discussed.

3.1 *Uniaxial state of stress*

Let us formulate the materials equation for an uniaxial state of stress in order to derive evaluation methods of laboratory tests and to throw light upon the inner correlations with material constants well-known in the field of elasticity.

Let σ denote the axial stress, ε the axial strain and ε_ν the transverse one. With these symbols the stress and deformation tensors and their deviation tensors become:

$$\boldsymbol{F} = \begin{Vmatrix} \sigma & 0 & 0 \\ 0 & 0 & 0 \\ 0 & 0 & 0 \end{Vmatrix} \quad \boldsymbol{T} = \begin{Vmatrix} \sigma - \sigma_0 & 0 & 0 \\ 0 & -\sigma_0 & 0 \\ 0 & 0 & -\sigma_0 \end{Vmatrix},$$

$$\boldsymbol{D} = \begin{Vmatrix} \varepsilon & 0 & 0 \\ 0 & \varepsilon_\nu & 0 \\ 0 & 0 & \varepsilon_\nu \end{Vmatrix} \quad \boldsymbol{E} = \begin{Vmatrix} \varepsilon - \varepsilon_0 & 0 & 0 \\ 0 & \varepsilon_\nu - \varepsilon_0 & 0 \\ 0 & 0 & \varepsilon_\nu - \varepsilon_0 \end{Vmatrix}$$

and

$$\sigma_0 = \frac{1}{3}\sigma, \quad \dot{\sigma}_0 = \frac{1}{3}\dot{\sigma}_0, \quad \varepsilon_0 = \frac{1}{3}(\varepsilon + 2\varepsilon_\nu), \quad \dot{\varepsilon}_0 = \frac{1}{3}(\dot{\varepsilon} + 2\dot{\varepsilon}_\nu).$$

We can now write the equation for the σ component of the tensor equation (7a):

$$\sigma - \sigma_0 = 2G(\varepsilon - \varepsilon_0) + 2\eta(\dot{\varepsilon} - \dot{\varepsilon}_0) - \tau(\dot{\sigma} - \dot{\sigma}_0)$$

which can be converted into

$$\sigma - \sigma_0 = 2G\left(\varepsilon - \frac{\sigma_0}{3K}\right) + 2\eta\left(\dot{\varepsilon} - \frac{\dot{\sigma}_0}{3K}\right) - \tau(\dot{\sigma} - \dot{\sigma}_0) \tag{8}$$

by means of (7b). The relations

$$\sigma_0 = \frac{1}{3}\sigma \quad \text{and} \quad \dot{\sigma}_0 = \frac{1}{3}\dot{\sigma}$$

can be used in transforming equation (8):

$$\frac{2}{3}\left[1 + \frac{G}{3K}\right]\sigma = 2G\varepsilon + 2\eta\dot{\varepsilon} - \frac{2}{3}\left[\tau + \frac{\eta}{3K}\right]\dot{\sigma},$$

$$\sigma = \frac{9GK}{3K+G}\varepsilon + \frac{9\eta K}{3K+G}\dot{\varepsilon} - \frac{3K\tau + \eta}{3K+G}\dot{\sigma}. \tag{9}$$

Introducing the notations

$$E = \frac{9GK}{3K+G},$$

$$\lambda = \frac{9\eta K}{3K+G},$$

$$\vartheta = \frac{3K\tau + \eta}{3K+G},$$

equation (9) can be written in the simple form

$$\sigma = E\varepsilon + \lambda\dot{\varepsilon} - \vartheta\dot{\sigma}, \tag{10}$$

where E is YOUNG's modulus [kp/cm^2],

λ linear viscosity coefficient or creep coefficient [kp, day/cm^2], [kp, h/cm^2], [MPad], [MPah]

ϑ constant of relaxation [day], [h].

For HOOKE's linearly elastic body, the relation between YOUNG's modulus E and the shear modulus G can also be expressed with the help of POISSON's ratio m. Using this well-known relation, the following equations can be obtained:

$$E = 2G\frac{m+1}{m} = 3K\frac{m-2}{m} = \frac{9KG}{3K+G},$$

$$G = \frac{1}{2}E\frac{m}{m+1} = \frac{3}{2}K\frac{m-2}{m+1} = \frac{3EK}{9K-E},$$

$$K = \frac{1}{3}E\frac{m}{m-2} = \frac{2}{3}G\frac{m+1}{m-2} = \frac{EG}{9G-3E},$$

$$m = \frac{2G}{E-2G} = \frac{6K}{3K-E} = \frac{6K+2G}{3K-2G}.$$

$$\lambda = 2\eta\frac{m+1}{m} = \eta\frac{E}{G} = \eta\frac{9K-E}{3K} = \eta\frac{9K}{3K+G},$$

$$\eta = \frac{1}{2}\lambda\frac{m}{m+1} = \lambda\frac{G}{E} = \lambda\frac{3K}{9K-E} = \lambda\frac{3K+G}{9K},$$

$$\tau = \frac{(3K+G)-\eta}{3K} = \frac{1}{2}\vartheta\frac{3m}{m+1} - \frac{1}{2}\frac{\eta}{G}\frac{m-2}{m+1} =$$

$$= \frac{1}{2}\vartheta\frac{3m}{m+1} - \frac{\eta}{3K},$$

$$\vartheta = \frac{3K\tau+\eta}{3K+G} = 2\tau\frac{m+1}{3m} + \frac{\eta}{G}\frac{m-2}{3m} =$$

$$= \frac{m+1}{3m}\left[2\tau + \frac{2\eta}{3K}\right] = \frac{9K-E}{9K}\left[\tau + \frac{\eta}{3K}\right] =$$

$$= \frac{E\tau}{3G} + \frac{3G-E}{3G}\cdot\frac{\eta}{G}.$$

3.2 *Mechanical model of the standard body*

The mechanical model of POYNTING—THOMSON's body is shown in Fig. 1. This model consists of a spring of spring constant $C_1 = E$ representing HOOKE's body and another spring (of spring constant C_2) arranged in parallel, as well as a cylinder filled with a fluid of viscosity μ_2 with a perforated piston moving inside it. If x denotes the displacement of the acting point of the force F, x_1 and x_2 the displacements of the left and right hand branches, and F_1, F_2 the forces in the branches, then the equation describing the operation of the mechanical model can be obtained from the following assumptions:

assumption of equilibrium: $F = F_1 + F_2$,

assumption of equal displacements: $x_1 = x_2 = x$.

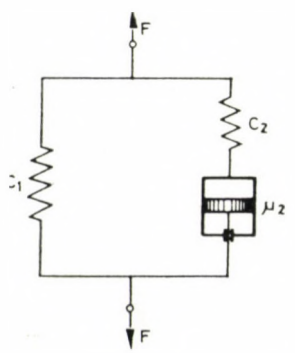


Fig. 1. Mechanical model of POYNTING—THOMSON's body

Taking into account that

$$x = x_1 = \frac{F_1}{C_1}, \quad \dot{x} = \dot{x}_1 = \frac{\dot{F}_1}{C_1}, \quad \dot{x} = \dot{x}_2 = \frac{\dot{F}_2}{\mu_2} + \frac{F_2}{C_2},$$

we arrive at the equation:

$$F = C_1 x + \left(1 + \frac{C_1}{C_2}\right) \mu_2 \dot{x} - \frac{\mu_2}{C_2} \dot{F},$$

the identity of which with equation (15) will be obvious by introducing the notations

$$F \equiv \sigma, \quad \dot{F} \equiv \dot{\sigma}, \quad \varepsilon \equiv x, \quad \dot{\varepsilon} \equiv \dot{x},$$

$$C_1 \equiv E, \quad \left(1 + \frac{C_1}{C_2}\right) \mu_2 \equiv \lambda, \quad \frac{\mu_2}{C_2} \equiv \vartheta.$$

This shows that the mechanical model in Fig. 1 corresponds to POYNTING—THOMSON's rheological medium.

3.3 *The physical equation implying the stress and deformation tensors*

While solving rock mechanical tasks one often needs the physical equation containing stress and deformation tensors in a unique expression instead of deviation and spherical tensors.

Using relation (7) one can write

$$\begin{aligned} \boldsymbol{F} &= \boldsymbol{T} + \boldsymbol{T}_0 = 2G\boldsymbol{E} + 3K\boldsymbol{E}_0 + 2\eta\dot{\boldsymbol{E}} - \tau\dot{\boldsymbol{T}} = \\ &= 2G(\boldsymbol{D} - \boldsymbol{E}_0) + 3K\boldsymbol{E}_0 + 2\eta(\dot{\boldsymbol{D}} - \dot{\boldsymbol{E}}_0) - \tau(\dot{\boldsymbol{F}} - \dot{\boldsymbol{T}}_0) = \\ &= 2G\boldsymbol{D} + (3K - 2G)\boldsymbol{E}_0 + 2\eta\dot{\boldsymbol{D}} + (3K\tau - 2\eta)\dot{\boldsymbol{E}}_0 - \tau\dot{\boldsymbol{F}} = \\ &= 2G\left[\boldsymbol{D} + \left(\frac{3K}{2G} - 1\right)\boldsymbol{E}_0\right] + 2\eta\left[\dot{\boldsymbol{D}} + \left(\frac{3K\tau}{2\eta} - 1\right)\dot{\boldsymbol{E}}_0\right] - \tau\dot{\boldsymbol{F}}. \end{aligned}$$

Since

$$\frac{3K}{2G} - 1 = \frac{\dfrac{Em}{m-2}}{\dfrac{Em}{m+1}} - 1 = \frac{3}{m-2},$$

$$\frac{3K}{2\eta}\tau - 1 = \frac{\dfrac{Em}{m-2}\tau}{\dfrac{\lambda m}{m+1}} - 1 = \frac{E}{\lambda} \cdot \frac{m+1}{m-2}\tau - 1,$$

$$\boldsymbol{E}_0 = \varepsilon_0 \boldsymbol{I} = \frac{1}{3}(\varepsilon_x + \varepsilon_y + \varepsilon_z)\boldsymbol{I} = \frac{1}{3}\Theta \boldsymbol{I},$$

formula (11) can be converted into

$$\boldsymbol{F} = 2G\left[\boldsymbol{D} + \frac{\Theta}{m-2}\boldsymbol{I}\right] + 2\eta\left[\dot{\boldsymbol{D}} + \mu\frac{\dot{\Theta}}{m-2}\boldsymbol{I}\right] - \tau\dot{\boldsymbol{F}}, \tag{12}$$

which is the physical equation of the standard body solved as to express stress. Writing out equations (12) in scalar components:

$$\sigma_x + \tau\dot{\sigma}_x = 2G\left[\varepsilon_x + \frac{1}{m-2}(\varepsilon_x + \varepsilon_y + \varepsilon_z)\right] + 2\eta\left[\dot{\varepsilon}_x + \frac{\mu}{m-2}(\dot{\varepsilon}_x + \dot{\varepsilon}_y + \dot{\varepsilon}_z)\right],$$

$$\sigma_y + \tau\dot{\sigma}_y = 2G\left[\varepsilon_y + \frac{1}{m-2}(\varepsilon_x + \varepsilon_y + \varepsilon_z)\right] + 2\eta\left[\dot{\varepsilon}_y + \frac{\mu}{m-2}(\dot{\varepsilon}_x + \dot{\varepsilon}_y + \dot{\varepsilon}_z)\right],$$

$$\sigma_z + \tau\dot{\sigma}_z = 2G\left[\varepsilon_z + \frac{1}{m-2}(\varepsilon_x + \varepsilon_y + \varepsilon_z)\right] + 2\eta\left[\dot{\varepsilon}_z + \frac{\mu}{m-2}(\dot{\varepsilon}_z + \dot{\varepsilon}_y + \dot{\varepsilon}_z)\right],$$

$$\tau_{xy} + \tau\dot{\tau}_{xy} = G\gamma_{xy} + \eta\dot{\gamma}_{xy},$$

$$\tau_{yz} + \tau\dot{\tau}_{yz} = G\gamma_{yz} + \eta\dot{\gamma}_{yz},$$

$$\tau_{zx} + \tau\dot{\tau}_{zx} = G\gamma_{zx} + \eta\dot{\gamma}_{zx},$$

with

$$\mu = \frac{1}{3}\left[(m+1)\frac{E}{\lambda}\tau - (m-2)\right] = \frac{1}{3}\left[(m+1)\frac{G}{\eta}\tau - (m-2)\right].$$

The physical equation can be similarly solved so as to express deformation. From the relation

$$\boldsymbol{T} = 2G(\boldsymbol{D} - \boldsymbol{E}_0) + 2\eta(\dot{\boldsymbol{D}} - \dot{\boldsymbol{E}}_0) - \tau\dot{\boldsymbol{T}}$$

follows that

$$2G\boldsymbol{D} + 2\eta\dot{\boldsymbol{D}} = \boldsymbol{T} + 2G\dot{\boldsymbol{E}}_0 + \tau\dot{\boldsymbol{T}} + 2\eta\dot{\boldsymbol{E}}_0 =$$

$$= \boldsymbol{F} - \boldsymbol{T}_0 + \frac{2G}{3K}\boldsymbol{T}_0 + \tau(\dot{\boldsymbol{F}} - \dot{\boldsymbol{T}}_0) + \frac{2\eta}{3K}\dot{\boldsymbol{T}}_0 = \tag{13}$$

$$= \boldsymbol{F} + \left(\frac{2G}{3K} - 1\right)\boldsymbol{T}_0 + \tau\dot{\boldsymbol{F}} + \left(\frac{2\eta}{3K} - \tau\right)\dot{\boldsymbol{T}}_0,$$

and since

$$\frac{2G}{3K} - 1 = -\frac{3}{m+1},$$

$$\frac{2\eta}{3K} - \tau = \frac{\lambda}{E}\frac{m-2}{m+1} - \tau,$$

$$\boldsymbol{T}_0 = \sigma_0 \boldsymbol{I} = \frac{1}{3}(\sigma_x + \sigma_y + \sigma_z)\boldsymbol{I} = \frac{1}{3}\boldsymbol{S}\boldsymbol{I},$$

instead of (13) can we obtain:

$$2G\boldsymbol{D} + 2\eta\dot{\boldsymbol{D}} = \left[\boldsymbol{F} - \frac{S}{m+1}\boldsymbol{I}\right] + \tau\left[\dot{\boldsymbol{F}} - \frac{\dot{v}S}{m+1}\boldsymbol{I}\right] \tag{14}$$

or, in scalar components:

$$E\varepsilon_x + \lambda\dot{\varepsilon}_x = \left[\sigma_x - \frac{1}{m}(\sigma_y + \sigma_z)\right] + \vartheta\left[\dot{\sigma}_x - \frac{\varkappa}{m}(\dot{\sigma}_y + \dot{\sigma}_z)\right],$$

$$E\varepsilon_y + \lambda\dot{\varepsilon}_y = \left[\sigma_y - \frac{1}{m}(\sigma_z + \sigma_x)\right] + \vartheta\left[\dot{\sigma}_y - \frac{\varkappa}{m}(\dot{\sigma}_z + \dot{\sigma}_x)\right],$$

$$E\varepsilon_z + \lambda\dot{\varepsilon}_z = \left[\sigma_z - \frac{1}{m}(\sigma_x + \sigma_y)\right] + \vartheta\left[\dot{\sigma}_z - \frac{\varkappa}{m}(\dot{\sigma}_x + \dot{\sigma}_y)\right],$$

$$G\gamma_{xy} + \eta\dot{\gamma}_{xy} = \tau_{xy} + \tau\dot{\tau}_{xy},$$

$$G\gamma_{yz} + \eta\dot{\gamma}_{yz} = \tau_{yz} + \tau\dot{\tau}_{yz},$$

$$G\gamma_{zx} + \eta\dot{\gamma}_{zx} = \tau_{zx} + \tau\dot{\tau}_{zx},$$

with

$$v = \frac{\lambda\mu}{E\tau} = \frac{1}{3}\left[(m+1) - \frac{\lambda}{E\tau}(m-2)\right],$$

$$\varkappa = \frac{\tau v}{\vartheta} = \frac{\lambda\mu}{E\vartheta} = \frac{\eta\mu}{G\vartheta}.$$

Equation (14) represents the physical equation of the standard body solved as to express deformation.

3.4 *Properties of the standard model*

In case of a constant rate of stress change, i.e., where $\dot{\sigma} = \dot{\sigma}_a =$ **constant**, the equation of state (10) can be written in the form

$$\dot{\varepsilon} + \frac{E}{\lambda}\varepsilon = \frac{\dot{\sigma}_a}{\lambda}t + \frac{\dot{\sigma}_a}{\lambda}\vartheta.$$

The solution of the homogeneous differential equation

$$\dot{\varepsilon} + \frac{E}{\lambda}\varepsilon = 0$$

is, as already:

$$\varepsilon = Ce^{-\frac{E}{\lambda}t}.$$

Substituting this solution into the inhomogeneous differential equation the function $C = C(t)$ can be determined by integrating the equation

$$\frac{dC}{dt}e^{-\frac{E}{\lambda}t} = \frac{\dot{\sigma}_a}{\lambda}(\vartheta + t).$$

Thus:

$$C = \int dC = \frac{\dot{\sigma}_a}{\lambda}\int (\vartheta + t)e^{\frac{E}{\lambda}t}\,dt = \frac{\dot{\sigma}_a}{E}\vartheta e^{\frac{E}{\lambda}t} + \frac{\dot{\sigma}_a}{\lambda}\int te^{\frac{E}{\lambda}t}\,dt =$$

$$= \frac{\dot{\sigma}_a}{E}\vartheta e^{\frac{E}{\lambda}t} + \frac{\dot{\sigma}_a}{E}te^{\frac{E}{\lambda}t} - \frac{\dot{\sigma}_a}{E}\frac{\lambda}{E}e^{\frac{E}{\lambda}t} + A,$$

and

$$\varepsilon = \frac{\dot{\sigma}_a}{E}\left[t - \left(\frac{\lambda}{E} - \vartheta\right) + A'e^{-\frac{E}{\lambda}t}\right],$$

where the integration constant A' can be written on the basis of the initial condition

$$\varepsilon|_{t=0} = \frac{\dot{\sigma}_a}{E}\left[\vartheta - \frac{\lambda}{E} + A'\right] = 0$$

as follows:

$$A' = \frac{\lambda}{E} - \vartheta.$$

Correspondingly, the change of deformation with time can be presented by the formula

$$\varepsilon = \frac{\dot{\sigma}_a}{E}\left[t - \left(\frac{\lambda}{E} - \vartheta\right)\left(1 - e^{-\frac{E}{\lambda}t}\right)\right],$$

which is illustrated in Fig. 2 for various rates of stress change.

The relationship between deformation and stress is given by:

$$\varepsilon = \frac{1}{E}\left[\sigma - \dot{\sigma}_a\left(\frac{\lambda}{E} - \vartheta\right)\left(1 - e^{-\frac{E}{\lambda}\frac{\sigma}{\dot{\sigma}_a}}\right)\right].$$

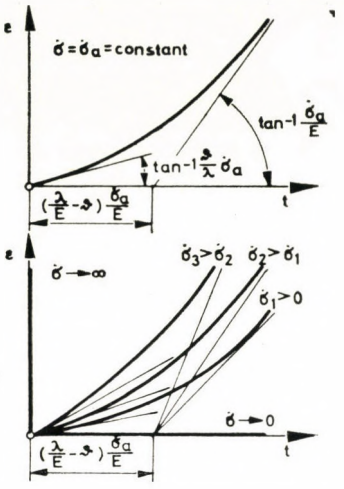


Fig. 2. Deformation plotted against time at a constant rate of stress variation for the standard model

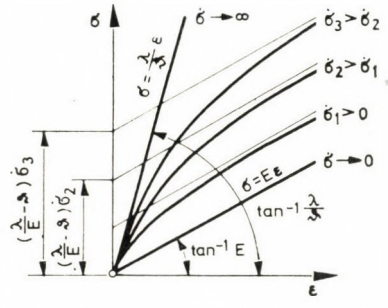


Fig. 3. Stress vs. deformation for the standard model at a constant rate of stress variation

From Fig. 3 it can be seen that the model behaves like HOOKE's linearly elastic body in the case of very slow changes of load ($\dot{\sigma} = 0$) and in the case

$$\frac{\lambda}{E} = \vartheta,$$

when the delay time of the deformations equals the time of relaxation.

Constant rate of deformation. For $\dot{\varepsilon} = \dot{\varepsilon}_a = \text{constant}$ and the initial conditions the correlation

$$\sigma = E\left[\varepsilon + \dot{\varepsilon}_a \frac{\lambda}{E} - \vartheta\right)\left(1 - \mathrm{e}^{-\frac{1}{\vartheta}\frac{\varepsilon}{\dot{\varepsilon}_a}}\right)\Big]$$

is valid (Fig. 4).

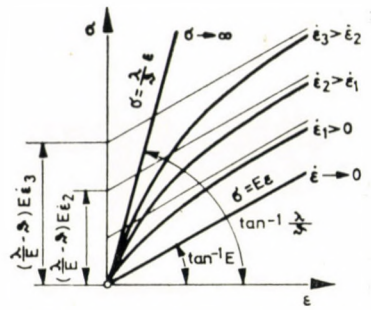


Fig. 4. Stress vs. deformation for the standard model at a constant rate of deformation

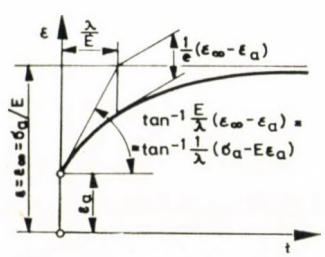


Fig. 5. Creep curve of POYNTING—THOMSON's model

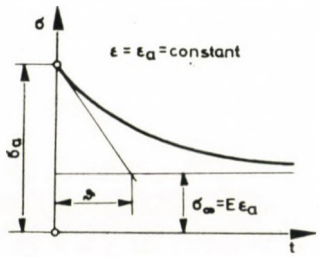


Fig. 6. Stress reduction (relaxation) diagram of POYNTING—THOMSON's model at a fixed deformation

Constant stress. The creep curve of POYNTING—THOMSON's standard model is:

$$\varepsilon = \frac{\sigma_a}{E} - \left(\frac{\sigma_a}{E} - \varepsilon_a\right) e^{-\frac{E}{\lambda}t} = \varepsilon_\infty - (\varepsilon_\infty - \varepsilon_a)\, e^{-\frac{E}{\lambda}t}.$$

This is shown in Fig. 5.

Constant deformation. The stress relaxation is for the standard body at fixed deformation (Fig. 6):

$$\sigma = E\varepsilon_a + (\sigma_a - E\varepsilon_a)\, e^{-\frac{t}{\vartheta}} = \sigma_\infty + (\sigma_a - \sigma_\infty)\, e^{-\frac{t}{\vartheta}}.$$

Uniaxial experiment. Fig. 7 displays one out of a great number of laboratory test results carried out on core samples of drilling No. 38 in the Mány area. The sample used for the experiment was a cylindrical limestone body of diameter 18 mm and length 30 mm — extracted from a depth of 394.40—400.70 m. This sample contained Miliola and Alveola fossils. The left hand side of Fig. 7 shows the so-called creep test. The right hand side displays the results of the relaxation test (where F is the load and λ the compression of the sample). The experiment shows significantly the delay of the deformations (the phe-

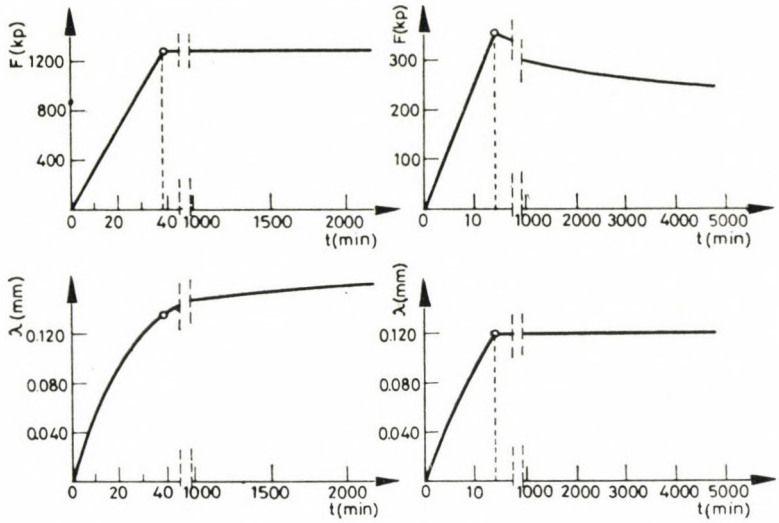


Fig. 7

nomenon of creep) and the reduction of stresses to a given level. All the rock samples of the basins of Tatabánya and Mány showed

— elastic behaviour,
— creep and
— relaxation.

Conlcusion. The comparison of the results of theoretical model investigations with known properties of the rocks has proved the standard model (with homogeneous linear equation of state) to be suitable to reproduce the most important rock characteristics.

As a result of our investigations, the materials equation reproducing rock properties has been arrived at.

4. Notes on laboratory experiments

In the previous chapter the characteristics of uniaxial deformation have been investigated with the help of idealized rheological models exposed to stress. Depending on the material equation chosen, there are many kinds of the deformation curves and all of them have proved that the basic deformation constants (E and m) cannet be calculated from the corresponding values of stress and deformation elements but in media free of rheological phenomena, or in extreme cases only.

The majority of results of rock material tests on the load-deformation behaviour indicate that changes with time can be observed even, in short periods and their effects on the measured data "disturb" the ideal (linearly elastic) characteristics and throw doubt upon the reliability of the measured values of the mechanical parameters (constants) of the rocks.

Two questions arise:

a) Which idealized (speculative) model would approach the amount of data, whose load-deformation correlation can be characterized by the corresponding measured pairs of values?

b) Knowing the measured data, how can the rheological parameters of the data and that of the best fitting idealized model be determined?

In the present study the answers to questions (*a*) and (*b*) will be looked for by using the already interpreted idealized model.

To predict the behaviour of rock blocks and the effect of rocks on support structures and to gain information about stress variations and deformations in these structures, we should know the rheological parameters of the rocks (YOUNG's modulus, POISSON's ratio, viscosity coefficient, time of relaxation). These parameters can be measured on rock blocks (*in situ* measurements in mines) or on laboratory specimens.

The measurements carried out at given points of rock blocks furnish data representing an integrated effect of the surroundings and a natural co-operation between the measurement area and the surrounding as fixed by the measurement points. For this reason *in situ* measurements can be considered more reliable than observation results achieved by experiments on specimens, since in this case the effect of the sorroundings is believed to be replaced by that of the load equipment while the measurement area is restricted to the specimen.

The present study is concerned with analysing and evaluating load-experiments on laboratory specimens. In this case it is possible to choose initial and boundary conditions freely within a wider range of stress and in this way to simply read off one or another of the material constants from the load-tension diagrams without any special evaluation.

5. Uniaxial compression experiments

We start out from the assumption that rocks can be characterized by an homogeneous linear equation of state, i.e. that there is an *homogeneous linear* correlation between stress and deformation deviation tensors as well as the spherical tensors marked with indices$_0$. This means that from among the following idealized rheological models that giving the best approach should be fitted to the rock material investigated resp. to the measured data, — taking into account the rock's behaviour as a solid:

$\boldsymbol{T} = 2G\boldsymbol{E}$	$\boldsymbol{T}_0 = 3K\boldsymbol{E}_0$	[HOOKEian body]
$\boldsymbol{T} = 2\eta\dot{\boldsymbol{E}}$	$\boldsymbol{T}_0 = 3K'\boldsymbol{E}_0$	[NEWTONian body]
$\boldsymbol{T} = 2G\dot{\boldsymbol{E}} + 2\eta\boldsymbol{E}$	$\boldsymbol{T}_0 = 3K\boldsymbol{E}_0$	[KELVINian body]
$\boldsymbol{T} = 2\eta\dot{\boldsymbol{E}} - \tau\dot{\boldsymbol{T}}$	$\boldsymbol{T}_0 = 3K\boldsymbol{E}_0$	[MAXWELLian body]
$\boldsymbol{T} = 2G\boldsymbol{E} + 2\eta\dot{\boldsymbol{E}} - \tau\boldsymbol{T}$	$\boldsymbol{T}_0 = 3K\boldsymbol{E}_0$	[Standard body]

The following are the simplest experiments to be carried out in laboratory:

$\dot{\sigma} =$ constant (proportional load test)
$\sigma =$ constant (creep test)
$\varepsilon =$ constant (relaxation test).

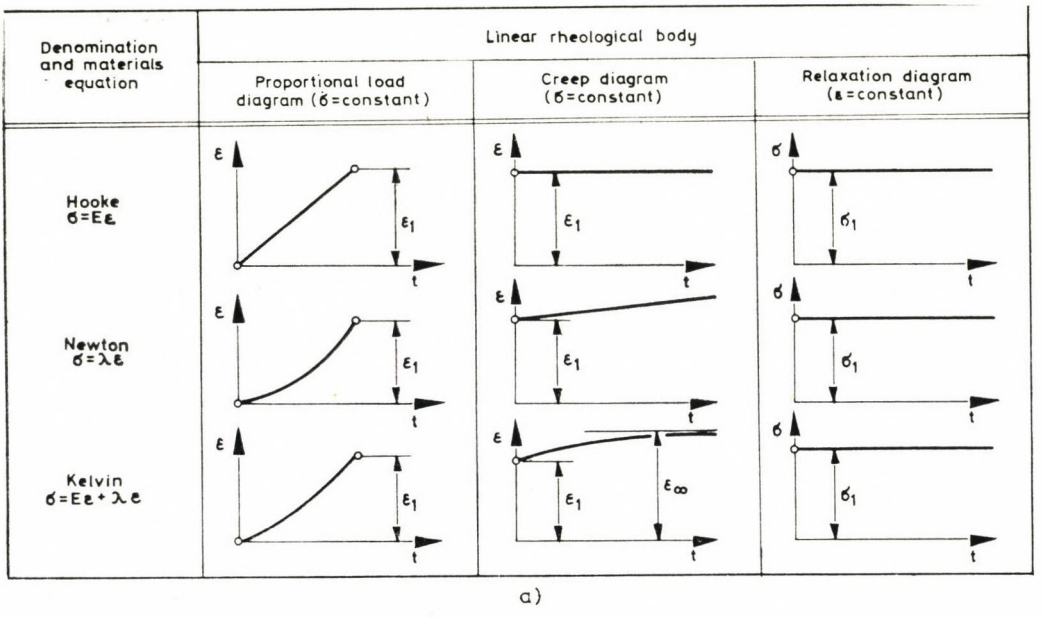


Fig. 8a. Proportional load, creep and relaxation curves of various simple homogeneous linear rheological models

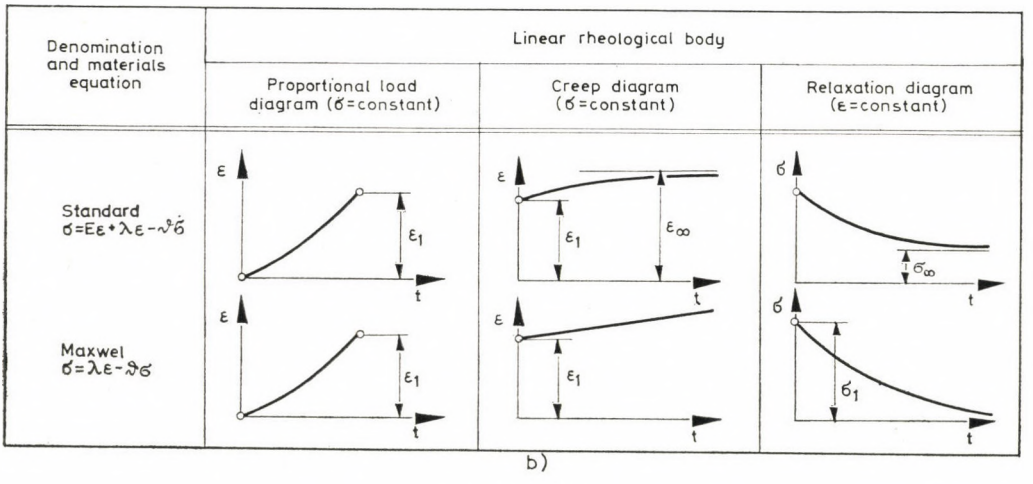


Fig. 8b

From the above primary tests the types of behaviour can be made clear. This enables us to decide which of the rheological models should be applied to the material investigated. Relying upon these findings our next investigations will be limited to the primary tests only.

Figure 8 displays test results related to various theoretical models. This enables us to choose unambiguously on the basis of the *creep* and *relaxation* curves, that particular idealized model which would gives the best approach for the rock investigated from among the homogeneous linear bodies.

6. Carrying out the experiments

The following sections will give a brief review of the load equipment necessary to perform the various tests.

6.1 *Proportional load test*

The specimens can be loaded with a constant rate of increasing load by any common compression testing machine, which is supplied with facilities

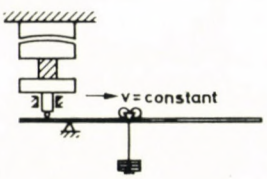


Fig. 9

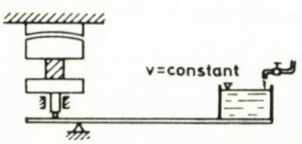


Fig. 10

for increasing the load continuously instead of step-wise (e.g. by putting equal weights on a load disc at equal time intervals). The widest variety of methods can serve for this purpose. The sketch in Fig. 9 demonstrates a method of stress variation with a constant rate, by moving a given weight with constant velocity. Figure 10 shows how the required load can be produced by a fluid flowing with constant velocity into a reservoir.

6.2 *Creep test*

A stabilized load of given intensity can be produced by commonly used equipment. This requirement can be fulfilled by a constant weight in the case of a weight load, by constant amplitude of pendulum in the case of a pendulum load, and by stabilised fluid pressure in case of a hydraulic load. The only problem arising at this point that the experiment demands a high degree of accuracy of the control unit.

6.3 *Relaxation test*

In this type of experiment any further deformation will be prevented after having achieved a given strain ε_1 and the load will be decreased while recording the variation of

$$\sigma = f(t) \qquad [f(t_1) > f(t_2), \text{ if } t_1 < t_2],$$

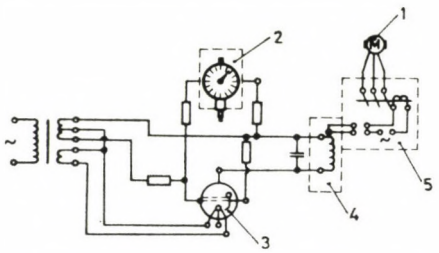


Fig. 11. Electronical transducer stabilising deformation. 1. Electric motor moving load; 2. geometrical amplifier; 3. electronic tube; 4. relay; 5. switch

with time and keeping the value of the deformation at the value

$$\varepsilon = \varepsilon_1 = \text{constant}.$$

KŁECZEK's electronic control device can be used for the purpose of this experiment (Fig. 11). Having attained the initial value of deformation the switches of the geometrical amplifier 2 will be short-circuited. If the deformation differs from the required value (the distance between both jaws changes by the order of 0.0002 . . . 0.0005 mm) the switches open and the electromechanical system of the transducer receives a signal from amplifier 2 and closes the circuit of the electronic tube 3. Relay 4 in the anode circuit of the electronic tube close the switches which cause the excitation of switch 5. This starts motor 1 which reduces the load. Having attained the value required, the system stops again. The continuous uninterrupted operation of the relaxometer is guaranteed by feeding it from two automatically controlled and independent transformers.

7. Determining the materials equation

If equipment is available which enables both creep and relaxation tests to be performed on rock samples, then — in turn — two kinds of investigations can be carried out.

Case A: The specimen is loaded with a constant rate of stress variation until the required value of load σ_1 is achieved (time t_1) and meanwhile the deformations will be stabilized at that particular value and the decrease of

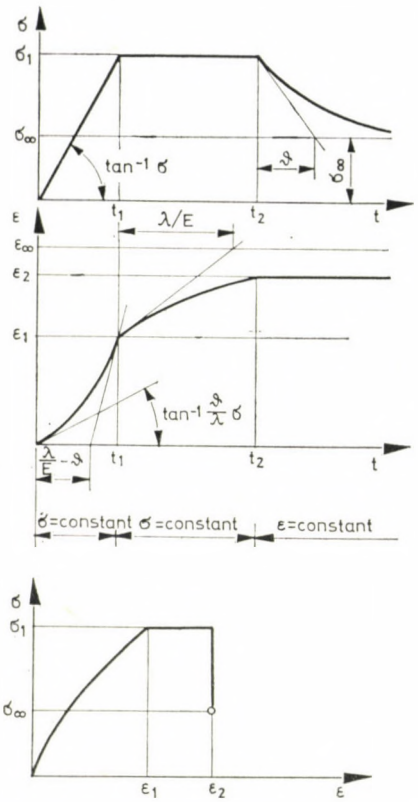


Fig. 12. Proportional load, creep and relaxation test

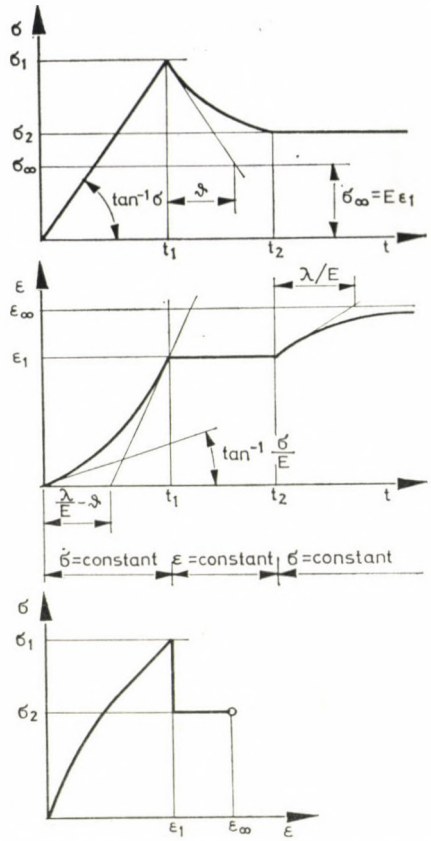


Fig. 13. Proportional load, relaxation and creep test

stress is recorded. The theoretical performance of the experiment is displayed in Fig. 12.

Case B: Contrary to the previous case, after having achieved the values σ_1 and ε_1, first the deformation is stabilized and then the load at time t_2 (Fig. 13).

The theoretical curves related to these two experiments are displayed in Figs 14 and 15 for various rheological models. The diagrams $\sigma - \varepsilon$ prove that the material equation can be determined since the representing model can be selected.

Figures 14 and 15 show that in given cases the actual type of the materials equation (KELVIN's, MAXWELL's, etc.) can be directly determined from the records without too much special calculation and evaluation.

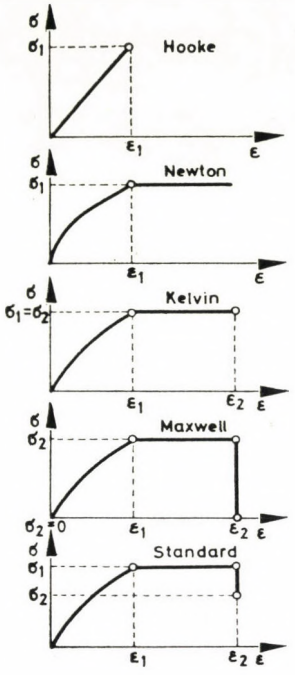


Fig. 14. Proportional load, creep and relaxation test for various rheological models

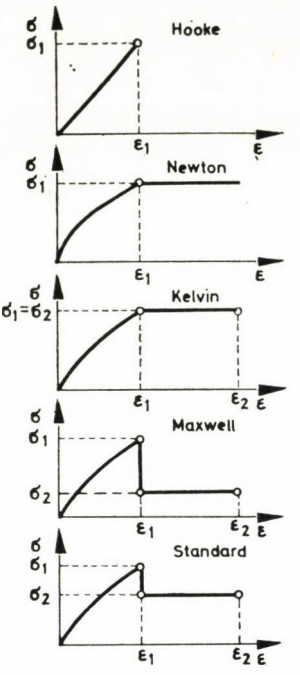


Fig. 15. Proportional load, relaxation and creep test for various rheological models

8. Direct determination of the materials constants

In the following investigations an experiment schedule will be outlined which enables a direct determination of the values of the rheological constants. The demonstration will only be carried out for the standard model since the results for the simple (NEWTON's, KELVIN's, etc.) models can be easily obtained by replacing the respective constants by zero.

Let σ denote the axial stress of the specimen and ε the corresponding specific compression. The tensile strains in a plane perpendicular to the load are equal which results from the uniaxial state of stress. These strains are denoted by ε_ν.

The tensor equation

$$\boldsymbol{T} = 2G\boldsymbol{E} + 2\eta\dot{\boldsymbol{E}} - \tau\dot{\boldsymbol{T}} \quad \text{and} \quad \boldsymbol{T}_0 = 3K\boldsymbol{E}_0$$

can be reduced in the case of uniaxial state of stress to the following two scalar equations:

$$\sigma = E\varepsilon + \lambda\dot{\varepsilon} - \vartheta\dot{\sigma}, \tag{15}$$

$$\sigma = \frac{Em}{m-2}(\varepsilon + 2\varepsilon_\nu). \tag{16}$$

8.1 *Proportional load test*

At $\dot{\sigma} = \dot{p} = \text{constant}$

rate of stress variation the correlation

$$\varepsilon = \frac{1}{E}\left[\sigma - \dot{p}\left(\frac{\lambda}{E} - \vartheta\right)\left(1 - \mathrm{e}^{-\frac{E}{\lambda}\frac{\sigma}{\dot{p}}}\right)\right] \tag{17}$$

holds between deformation and stress. Hence, it can be seen that in the case of very slow loading, i.e. if

$$\dot{p} \to 0,$$

the model behaves as HOOKE's linearly elastic body. Figure 16 displays the relations between stress and deformation to be explected at very slow loading for various simple theoretical rheological models.

If a very quick loading process

$$\dot{p} \to \infty$$

could be carried out the results to be expected would be as illustrated in Fig. 17. By comparing both diagrams the theoretical rheological model giving the best approach could be selected and the respectively values

$$E \text{ and } \frac{\lambda}{\vartheta}$$

would have been read directly.

The rates of loading "very slow" and "very quick" which may rise to infinitiy, depend on the material tested. For this reason, previous experiments with various rates of loading can indicate whether the extreme rates of loading, $\dot{p} \to 0$ and $\dot{p} \to \infty$ resp., necessary for a given material can be produced by the equipment available or that these rates have no reality at all.

If during the experiment the transverse strains (in a plane perpendicular to the load) are also registered, one can gain further information about the material equation and material constants.

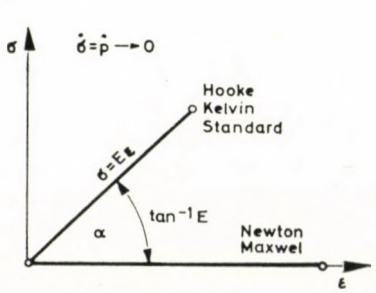


Fig. 16

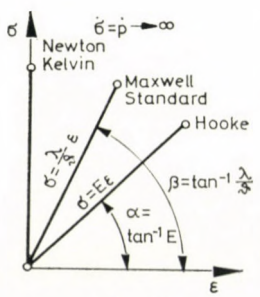


Fig. 17

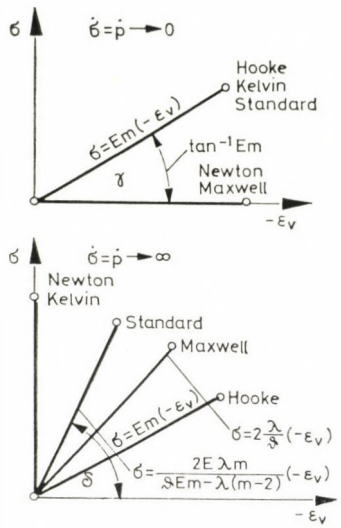


Fig. 18

Using equation (16) we obtain:

$$\varepsilon_v = \frac{1}{2}\varepsilon - \frac{m-2}{2Em}\sigma = \frac{1}{E}\left[\frac{\sigma}{m} - \frac{1}{2}\dot{p}\left(\frac{\lambda}{E} - \vartheta\right)\left(1 - e^{-\frac{E}{\lambda}\frac{\sigma}{\dot{p}}}\right)\right]. \qquad (18)$$

The relations related to both extreme cases of load are shown in Fig. 18. By measuring the values ε and ε_v, from the slopes

$$\tan\alpha = A; \quad \tan\beta = B; \quad \tan\gamma = C; \quad \tan\delta = D$$

of the straight lines, the constants

$$E = A$$

$$m = \frac{C}{A}$$

$$\frac{\lambda}{\vartheta} = B$$

can be determined. The equation

$$D = \frac{2E\lambda m}{\vartheta Em - \lambda(m-2)} = \frac{2BC}{C - B\left(\frac{C}{A} - 2\right)}$$

makes it possible to check the measurements and compensate for errors. The four equations resulting from the four slopes are, however, not independent of

each other thus the values λ and ϑ can not be calculated separately from the equations, only their quotient.

8.2 *Creep test*

The loading of the specimen will be stopped and stabilised at time $t = t_0$. At time t_0 we have:

$$\varepsilon|_{t=t_0} = \varepsilon_0 \text{ and } \sigma|_{t=t_0} = \sigma_0.$$

By recording the further variation of strain, we obtain the creep curve which can be described in the case of the standard model by the following equation:

$$\varepsilon = \frac{\sigma_0}{E} - \left(\frac{\sigma_0}{E} - \varepsilon_0\right) e^{-\frac{E}{\lambda}(t-t_0)} = \varepsilon_\infty - (\varepsilon_\infty - \sigma\varepsilon_0)\, e^{-\frac{E}{\lambda}(t-t_0)}. \qquad (19)$$

Figure 19 displays the creep curves of various idealized rheological models.

Using the results of the investigation in Section 8.1 all the rheological constants can be determined.

8.3 *Relaxation test*

The relaxation curve of the stress variation at fixed deformation is shown in Fig. 20.

9. Simple experiment schedule

Relying upon our findings we can state that at least two experiments (load-types) have to be carried out on the same specimen in order to determine the values of the rock constants. Since the relaxation test is technically the

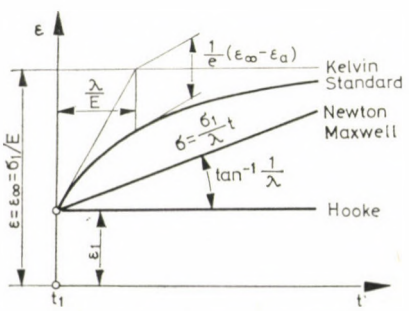


Fig. 19. Creep diagrams of homogeneous linear rheological models

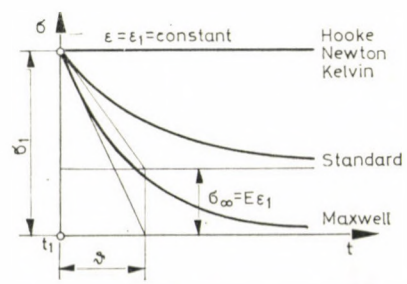


Fig. 20. Relaxation diagrams of homogeneous linear rheological models

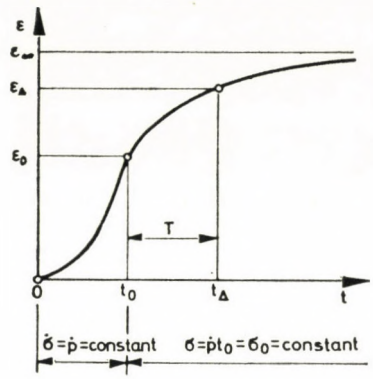


Fig. 21

most difficult to perform, the experiment can be conducted in two steps, as follows:

$$\text{Step (i):} \quad \dot{\sigma} = \dot{p} = \text{constant}, \quad 0 \leqq t \leqq t_0,$$

$$\text{Step (ii):} \quad \sigma = \sigma_0 = \text{constant}, \quad t_0 \leqq t < \infty.$$

To determine directly the rheological rock constants one has to follow the schedule, as outlined below:

In step (i) the specimen is loaded with a constant rate of stress variation. At time t_0, when the load is fixed the corresponding values

$$t_0, \sigma_0, \varepsilon_0 \tag{20a}$$

are recorded (see Fig. 21). Afterwards the specimen is allowed to creep at constant load and at an arbitrary time to the corresponding values

$$t_\Delta, \sigma_0, \varepsilon_\Delta \tag{20b}$$

are recorded. At the end of the experiment, when the specimen does not suffer any further deformation, the reading of

$$\varepsilon_\infty \tag{20c}$$

can be taken. If POISSON's ratio m is to be determined as well, the transverse strain

$$\varepsilon_{v0} \tag{20d}$$

has to be measured additionally at time t_0.

Making use of measurement data (20a)—(20d) the material constants can be calculated from the equations

$$\varepsilon_0 = \frac{1}{E}\left[\sigma_0 - \dot{p}\left(\frac{\lambda}{E} - \vartheta\right)\left(1 - \exp\left\{-\frac{E\sigma_0}{\lambda\dot{p}}\right\}\right)\right],$$

$$\varepsilon_{\Delta} = \varepsilon_{\infty} - (\varepsilon_{\infty} - \varepsilon_0) \exp\left\{-\frac{E}{\lambda} T\right\},$$

$$\frac{\sigma_0}{E} = \varepsilon_{\infty}$$

$$\sigma_0 = \frac{Em}{m-2}(\varepsilon_0 + 2\varepsilon_{\vartheta 0})$$

in the following form:

$$E = \frac{\sigma_0}{\varepsilon_{\infty}},$$

$$\lambda = \frac{\sigma_0}{\varepsilon_{\infty}} \frac{T}{\ln a}, \tag{21}$$

$$\vartheta = \frac{T}{\ln a} - \frac{\varepsilon_{\infty} - \varepsilon_0}{\dot{p}b} \frac{\sigma_0}{\varepsilon_{\infty}},$$

$$m = \frac{2\varepsilon_{\infty}}{\varepsilon_{\infty} - \varepsilon_0 - 2\varepsilon_{\nu 0}},$$

where

$$a = \frac{\varepsilon_{\infty} - \varepsilon_0}{\varepsilon_{\infty} - \varepsilon_{\Delta}},$$

$$b = 1 - \exp\left\{-\frac{\sigma_0}{\dot{p}} \cdot \frac{\ln a}{T}\right\},$$

$$T = t_{\Delta} - t_0.$$

The advantage of the proposed experiment schedule is that the material constants can be determined by means of a series of experiments on a unique specimen while measuring various functions of the same materials constants. The results may be made even more reliable by taking into account some more corresponding triads of measurement values. The material constants according to Eq. (21) can be regarded now as approximate values and they can be included in the adjusting calculation in the form of $(E + \Delta E)$, $(\lambda + \Delta\lambda)$, $(\vartheta + \Delta\vartheta)$ and $(m + \Delta m)$ respectively.

The scattering of the materials constants can be calculated by evaluating series of experiment equally weighted and carried out on specimens of the actual material.

REFERENCES

1. ASSZONYI, Cs.: On a rheological theory of rock continua. Doctor's Thesis. Hungarian Academy of Sciences. Budapest 1975.
2. ASSZONYI, Cs.: On a new theory of rock mechanics. *Acta Geod. Geoph. Mont. Hung.*, 8 (1974), 313—322.
3. ASSZONYI, Cs.: Mechanical theory of continua. *Acta Geod. Geoph. Mont. Hung.*, 8 (1974), 323—360.
4. ASSZONYI, Cs.: Determination by *in-situ* measurements of the characteristic parameters of the field of primary stresses and deformations. Publications of Technical University of Heavy Industry, Miskolc 31 (1970), 39—60.
5. ASSZONYI, Cs.: Laboratory determination of the physical equations and rheological materials constants of rocks. Research Report. Technical University of Heavy Industry, Miskolc 1972, 1—52.
6. ASSZONYI, Cs.—KAPOLYI, L.: Determination of mechanical parameters of rocks. Papers of the Veszprém Committee of the Hungarian Academy of Sciences, Veszprém 1976, 1—192.
7. ASSZONYI, Cs.—KAPOLYI, L.—HUSZÁR, I.: Laboratory determination of rock constants using creep tests. *Tatabányai Szénbányák Műszaki Közgazdasági Közleményei*, No. 4, 1971, 177—182.
8. KAPOLYI, L.: Some problems on the rock mechanics of future underground mining. SESSA Spring Meeting, Los Angeles, California 1973, 1—34.
9. FILCEK, H.: Laboratory compression experiments and rheological properties of rocks. Przeglad Naukowo-Techniczny AGH (Scientific Technical Review of the Mining and Metallurgical University), Cracow, Serie G/1, 1959.
10. KŁECZEK, Z.: Experimental criteria for choosing a rheological model of rocks. Prace Komisje Nauk Technicznych Górnictwo (Publications of the Mining Technical Science Committee), 5 (1967), 33—50.
11. RICHTER, R.: Measurement of rock-pressure "in-situ" in elastic rocks. Publications of the Technical University of Heavy Industry, Miskolc 21 (1960), 25—27.

ЛАБОРАТОРНОЕ ОПРЕДЕЛЕНИЕ ХАРАКТЕРИСТИК ГОРНЫХ ПОРОД

I. ЭКСПЕРИМЕНТЫ С ОДНООСНЫМ СЖАТИЕМ

Ч. АССОНИ—Л. КАПОЙИ—Р. РИХТЕР

РЕЗЮМЕ

В статье рассматриваются определение наивыгоднейшей реологической модели для описания механических свойств данных горных пород и установление конкретных значений вещественных постоянных. Для лабораторных экспериментов с одноосным сжатием анализируются виды определения характеристик горных пород. Задается один простой метод для разработки эксперимента.

Acta Geodaet., Geophys. et Montanist. Acad. Sci. Hung. Tomus 14 (3), pp. 341—359 (1979)

II. DETERMINATION OF ROCK CHARACTERISTICS USING RHEOLOGICAL CREEP INVESTIGATION

CS. ASSZONYI

HUNGARIAN COAL BOARD, TATABÁNYA

L. KAPOLYI

MINISTRY OF HEAVY INDUSTRY, BUDAPEST

I. HUSZÁR

UNIVERSITY OF AGRICULTURE, GÖDÖLLŐ

[Manuscript received February 24, 1977]

The study deals with the determination of rheological material characteristics of rocks by means of creep investigation. It describes the equipment designed and manufactured for the laboratory experiments, the principle and procedure of the measurements, and the method of evaluation of the results obtained. Measured values of the material constants obtained from core samples of drillings in the Nagyegyháza coal basin ara also presented.

1. Introduction

Mining industry creates underground excavations to exploit useful minerals from the earth's crust. In this way the primary (or quasi primary) state in the earth's crust is disturbed, and secondary and tertiary fields of stress and deformation are produced which tend to eliminate the inhomogeneity caused by the excavation, to re-establish the original state, and to produce a state with the same characteristics, respectively. The support of the excavations is necessary for the miners benefit and is against the natural tendency for the excavations to collapse. These supports provide the mining activity with a new, necessary and possibly safe state of equilibrium, which is at least quasi steady.

Since the upper layers of the earth's crust have been exhausted, mining industry has been forced to work in ever deeper layers. Thus new circumstances have come into the foreground. While mining near the earth surface, the supports of the excavations were able to carry the excess load due to the change in the state of stress. In deeper layers there is no support which could resist the total excess load, the so-called stress of deformation being the differential between primary and tertiary states.

This situation has led to new conclusions in rock mechanics and has resulted in the development of new support structures. In these structures, the support and the surrounding rock create a dual system working together and one part of the excess load is carried by the surrounding rock. Consequently, the excess load is not carried totally by the support. In case of a well-

designed support, both co-operating elements of the system, i.e. the surrounding rock and the very support, carry and balance a proportional part of the excess load, according to their carrying capacity.

As well-known, supports play an important role among the cost factors of mining. For this reason, more economical and efficient methods of using supports should be investigated. Therefore, a better knowledge of rock mechanics and pressure conditions in mines is required for designing these supports.

Furthermore, the knowledge of the mechanical material characteristics and that of the state of stress of the surrounding rock can lead to the development of new support techniques and equipment. These types of support have a new feature: as one of the elements of the dual rock-support system they form the *in situ* pressure conditions within the range of possibilities so as to make them the most advantageous for mining operations. They produce a load level, which can be carried by the rock and the support in a combined action without any deterioration. Using this technique the load to be carried by the support can be predicted. It amounts only to that level which can be balanced with simple and in-expansive supports, taking into account their endurance as well. For example the pressurized steel arch supports and the gunite concrete walls (both of which are particularly suitable for productive construction and show the elastic characteristics of shell structures) are ideally suited to drift supporting. For supporting working places, frame, shield and combined type hydraulic supports have been developed, the construction principle of which ensures an automatic closed circuit control of the dual system rock-support. The control prevents the support from being overloaded. The excess load beyond the designed value is carried by the surrounding rock. However, if this is not possible, because of the strength properties of the rock, directed convergence can be regulated by the hydraulic control unit such that the rock load becomes less than its strength limit. The size and distribution of the reaction forces transferred from the support to the surrounding rock should help in the roof maintenance, and the control of the diversion and reduction of the elastic energy stored in the surrounding rocks should produce ambient conditions enabling safe operation (e.g. by preventing face bumping). It is more simple and economical to prevent face bumping by controlling ground pressure in the surrounding rocks than by using special mechanical equipment which hinders operations in the working place.

To design support techniques properly, to manufacture support systems and to develop their technology of *in situ* construction one needs to know

— the physical-mechanical properties of the surrounding rocks, and
— the characteristics and the requirements of the supports.

In the present study it is intended to deal with only one facet of this complex problem, namely wilt the determination of the mechanical properties and material constants of the surrounding rocks.

In engineering the question often arises as to whether rocks can be considered as leastic bodies obeying HOOKE's law similarly to metals or building material. Obviously, this would imply a certain approximation. The elastic model is, however, independent of time i.e. it is not sensitive to changes of time. At the same time observations in mining industry have proved that the time factor plays an important role in developing the state of stress and deformation of the surrounding rocks. For this reason the simple elastic model can not be considered as a good approximation.

Ground pressure and time-dependent change of deformations due to pressure can be attributed to two principal features:

— the time-dependent process of creating and ceasing excavation (i.e. mining operations),
— some material characteristics of the rocks being represented by their creep, relaxation, etc.

From a consideration of these factors it is obvious that the rocks surrounding mine excavations should be considered in most cases as a time-dependent "rheological" medium. The physical equation of the material should be formulated according to this principle.

In [8] if has been shown comparing the properties of rheological bodies obeing various simple material equations with real rock properties that rocks can be characterized by means of the POYNTING—THOMSON's standard body having the homogeneous linear materials equation

$$\sigma = E\varepsilon + \lambda\dot{\varepsilon} - \vartheta\dot{\sigma}.$$

Consequently, in the further investigations it will be assumed that the rock satisfies this material equation. With this in mind, in what follows it will be shown how to determine the material constants with uniaxial compression experiments.

2. Uniaxial compression experiments

Apart from determining the breaking strength of rock samples, the laboratory compression test can be aimed at

— determining the relationship between uniaxial stress and deformation (i.e. material equation) of the rock,
— finding the actual values of material constants.

Unfortunately, the uniaxial compression test is unable to answer two important questions, *a)* what the materials equation of the rocks is like and *b)* with what degree of approximation can the physical equation chosen be applied. There are two main reasons for this:

a) before designing an experimental procedure and determining the range of parameters to be measured we have to have an assumption on the

correlation between the mechanical variables — stress and deformation. Accordingly, assuming the physical equation to be formulated by neaus of the physical equation to be formulated known functions f_1, f_2 and f_3 e.g. in the form

$$\sigma = f_1(\varepsilon) + f_2(\dot{\varepsilon}) + f_3(\dot{\sigma})$$

i.e. as a sum of additive functions of the variables, then the unknown ones can be determined from the results of properly designed experiments using the method of least squares. It cannot be taken for granted, however, that another consideration would not lead to another material law being closer to reality, e.g. in the form

$$\sigma = F_1(\varepsilon) + F_2(\dot{\varepsilon}, \dot{\sigma}).$$

b) The actual correlation and material constants determined from the experiment are characteristic of the rock only in case of uniaxial state of stress. As well-known, material constants themselves are more or less dependent on the state of stress. It has been proved that they depend on the depth, within certain limits, and a deviation can be observed between rock characteristics obtained from uniaxial and triaxial experiments, respectively, in the case of the same materials.

In spite of the above difficulties the results of uniaxial experiments are very useful for mining practice and design work since they provide a fair approximation of the strength properties to be made, depending also on time, at least for uniaxial state of stress. This widens our previous knowledge by providing us with the actual values of constants of some rocks material. However the main reason for using uniaxial tests is that is not always possible to carry out *in situ* measurements.

The following experiments are suitable above all for creating time-dependent variation in stress and deformation:

a) $\dot{\sigma} =$ constant (proportional load test)
b) $\dot{\varepsilon} =$ constant (proportional deformation test)
c) $\sigma =$ constant (creep test)
d) $\varepsilon =$ constant (relaxation test)

Combining these tests, the following uniaxial compression experiments can be carried out to determine the rock constants:

a) Gradual loading of the specimen starting from zero up to a given value σ_a at a constant rate of stress variation, afterwards recording the creep of the material at the fixed value σ_a of stress (Fig. 1).

b) Loading of the specimen up to the value σ_a at a constant rate of stress variation, at time t_0 fixing the deformation at the value ε_a which corresponds to σ_a and then recording the relaxation of the stress (Fig. 2).

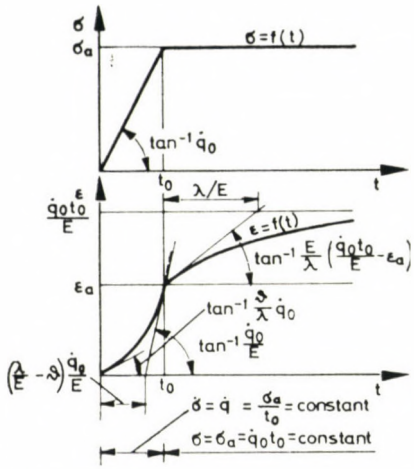


Fig. 1. Loading at a constant rate of stress variation followed by creep

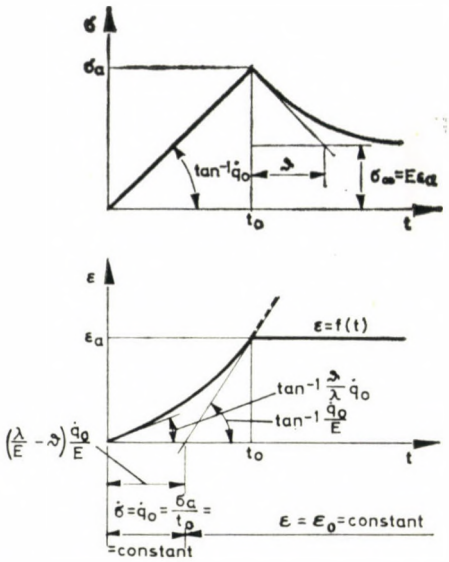


Fig. 2. Loading at a constant rate of stress variation followed by relaxation

c) Loading of the specimen at a constant rate of deformation, having achieved the value ε_a and fixing of the load at the value σ_a which corresponds to the deformation ε_a (Fig. 3).

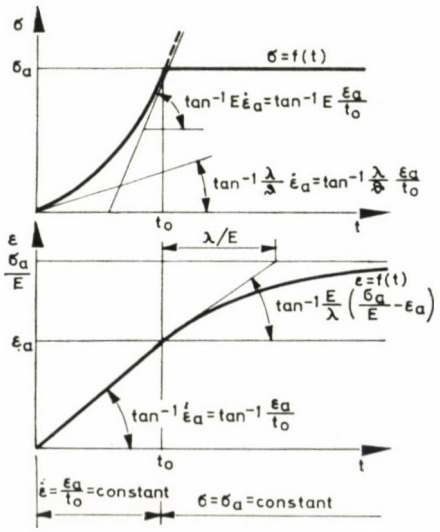


Fig. 3. Loading at a constant rate of change of deformation followed by creep

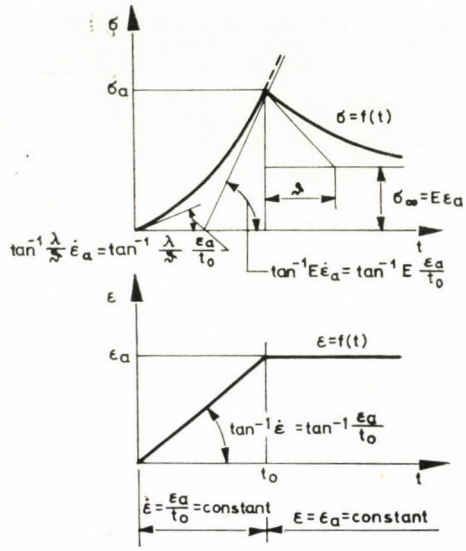


Fig. 4. Loading at a constant rate of change of deformation followed by relaxation

d) Loading of the specimen at a constant rate of deformation. Having achieved the value ε_a of deformation all further strain is prevented and the relaxation of stress is recorded (Fig. 4).

The following describes the creep investigation as outlined under *a)*.

3. Experimental device

The compressive force necessary for the investigation was produced by the device illustrated in Fig. 5.

The specimen is placed between compression plates on the rigid frame 1. The loading force is transferred by compression cylinder 3 being guided by

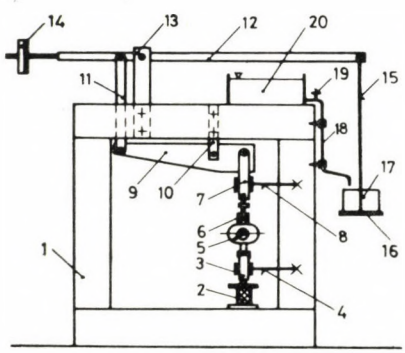


Fig. 5. Experimental device enabling laboratory creep investigation of rock samples

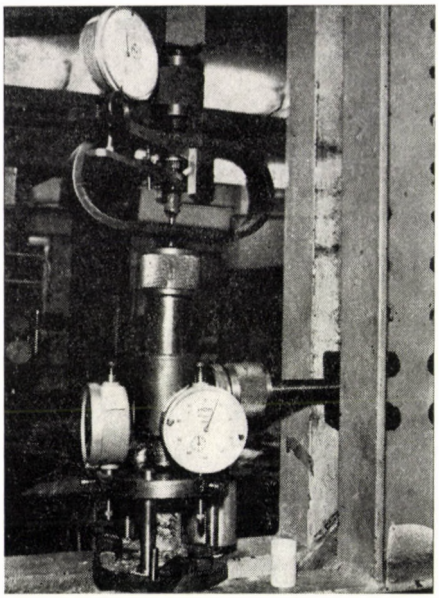


Fig. 6. Experimental device for uniaxial compression experiments. The device enables force and displacement measurements for creep tests. A fractured specimen can be seen in the device and an intact one beside it

sleeve 4. The calibrated dynamometer 5 is connected directly to this point and is represented by an elastic arch provided with a dial gauge. Loading head 6 is connected to its upper end. This can be adjusted by a thread to which the force is transferred through loading rod 7 itself being supported from the side by sleeve 8. The force is supplied by double-armed lever 9 which is pivoted at support 10. Its other end is connected through rod 11 to double-armed lever 12. This is, however, pivoted at support 13. On its left hand end tare 14 is to be found which also can be adjusted by a screw. Balance rod 15 is connected to the right hand end of the lever. Balance pan 16 supports calibrated glass vessel 17. To this vessel flows the water from reservoir 20 through pipe 18 and adjustable tap 19.

Figure 6 illustrates the experimental device used in the laboratory of the Department of Mechanics at the University of Agriculture, Gödöllő.

Figure 7 illustrates, in greater detail, the position of the specimen. Base plate 1 is fixed rigidly to the frame. The specimen 2 is located centrally. This is made possible by a co-ordinate system which has been scratched into the base plate. Loading plate 3 is in connection with the upper surface of the specimen, which is always returned to the same position relative to the base plate with the help of locating pins 4. In this way parallellism and centrality are ensured. A ball socket is located centrally on the upper surface of the loading plate. The ball 5 transferring the load touches the loading plate at this ball socket.

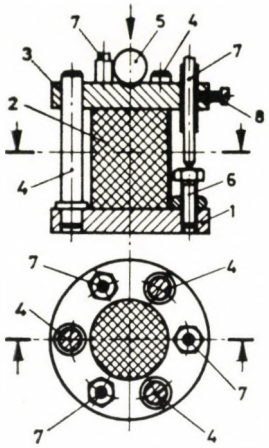


Fig. 7

The central loading of the specimen is ensured with a high accuracy in this arrangement. The dial gauges 7 touch the measurement basis surfaces which can be adjusted vertically by threads 6. The dial gauges are fixed to the loading plate by screws 8 in a pitch of 120°.

Because of the double leverage (10×10) a relatively small weight can create a satisfactory high compression load of the specimen. The possible friction on the moving arms and any error in the leverage can be ignored since the dynamometer is located directly at the place of load transferring.

The loading process is carried out using the assumption $\dot{\sigma} = \text{constant}$ by allowing water of flow into glass vessel 17 thorugh tap 19. Having achieved the desired weight, the tap is closed. While the water level in reservoir 20 is constant the discharge velocity is also constant. Therefore a constant rate of stress variation is ensured by the device. By the adjustment of tap 19 various velocities can be reached.

Having achieved the prescribed initial load corresponding to σ_a the load is not changed further. The constant weight also produces a constant load on the specimen. By choosing arbitrary values of the fluid volume, the value of load can be varied.

The actual measurement is accomplished by measurement of length and can be carried out by taking readings from the dial gauges from time to time.

The use of three dial gauges enables us to check whether the displacement of the loading plates is in parallel or not. This gives an indication of whether the deformation is uniform with respect to the direction of the compressive force. Moreover, this arrangement ensures a good check on the readings as three measurement data are available in each case.

Readings should be taken very often (if necessary at every 10—30 seconds) in the initial period, before achieving the constant value of load. Greater time

intervals can be chosen between the readings in the period of greater deformation rates (usually 2—5 minutes). In the flat section of the curve it is satisfactory to take readings less frequently, depending on the material, e.g. every 1/4—1 hour.

Five measuring devices are in operation simultaneously because of the very great number of measurements.

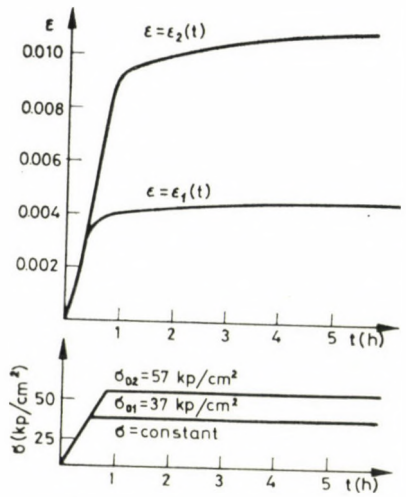


Fig. 8. Creep tests with two load levels. Specimen material: calcareous clay (Tatabánya State Coal Mines, Mine VI). Specimen dimensions: diameter 18 mm, length 30 mm. Rate of stress variation: 70 kp/cm² h.

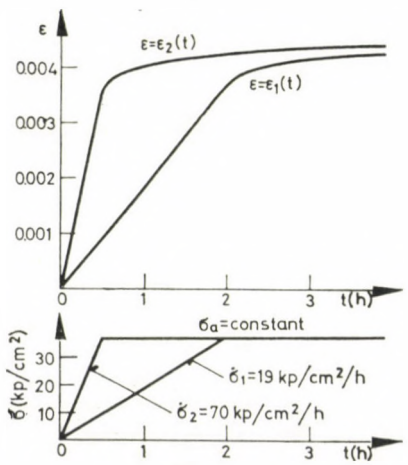


Fig. 9. Creep tests at two rates of stress variation. Specimen material: calcareous clay (Tatabánya State Coal Mines, Mine VI). Specimen dimensions: diameter 18 mm, length 30 mm. Maximum load: 37 kp/cm²

In Fig. 8 some measurement curves are displayed. In these cases the load has been increased at a constant rate. The two curves, however, belong to different base loads σ_a.

The curves of Fig. 9 correspond to the same base load σ_a but they have been determined at different rates of stress variation.



Fig. 10

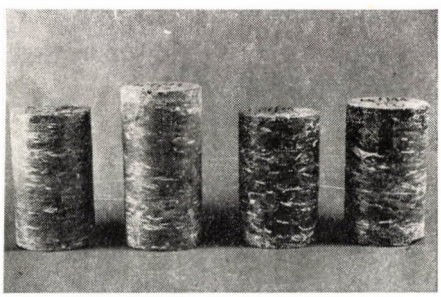


Fig. 11. Shallow-water calcareous clay specimens shaped by hand (first and second from left) and by machine (third and fourth from left). Place of origin: Nagyegyháza

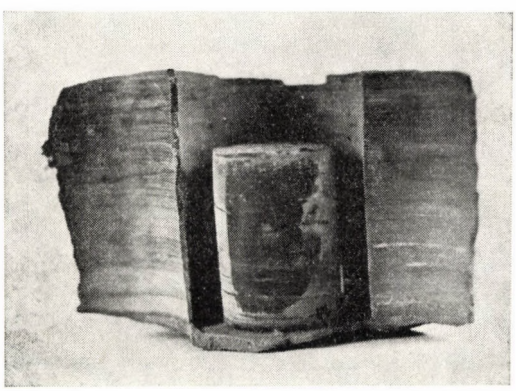


Fig. 12

Figure 10 illustrates the method of shaping the rock specimen by hand Specimens shaped by hand and by machine are compared in Fig. 11. A specimen cut out from a core sample using a crown bit is shown in Fig. 12.

4. Evaluation

The values of material constants being looked for can be determined from the corresponding values of deformation and time

$$\varepsilon_i, t_i \qquad i = 0, 1, \ldots, a-1$$

$$\varepsilon_a, t_a$$

$$\varepsilon_j, t_j \qquad j = a+1, \ldots, n$$

obtained from the experiments of Figs 8 and 9 at discrete points of time. In case of the standard model,

if $\dot{\sigma} = \dot{q}_0 = \text{constant}$

$$\varepsilon = \frac{\dot{q}_0}{E}\left[t - \left(\frac{\lambda}{E} - \vartheta\right)\left(1 - e^{-\frac{E}{\lambda}t}\right)\right],$$

if $\sigma = \sigma_a = \dot{q}_0 t_0 = \text{constant}$

$$\varepsilon = \frac{\dot{q}_0}{E} t_0 - \left(\frac{\dot{q}_0 t_0}{E} - \varepsilon_a\right) e^{-\frac{E}{\lambda}(t-t_0)} =$$

$$= \frac{\dot{q}_0}{E}\left[t_0 - \left(\frac{\lambda}{E} - \vartheta\right)\left(1 - e^{-\frac{E}{\lambda}t_0}\right) e^{-\frac{E}{\lambda}(t-t_0)}\right].$$

The function representing the sum of the squares of deviations can be written as follows:

$$\Delta \equiv \sum_i \left\{\varepsilon_i - \frac{\dot{q}_0}{E}\left[t_i - \left(\frac{\lambda}{E} - \vartheta\right)\left(1 - e^{-\frac{E}{\lambda}t_i}\right)\right]\right\}^2 +$$

$$+ \sum_i \left\{\varepsilon_j - \frac{q_0}{E}\left[t_0 - \left(\frac{\lambda}{E} - \vartheta\right)\left(1 - e^{-\frac{E}{\lambda}t_0} e^{-\frac{E}{\lambda}(t_j - t_0)}\right)\right]\right\}^2.$$

The rock constants can be calculated from the equations

$$\frac{\partial \Delta}{\partial E} = 0, \quad \frac{\partial \Delta}{\partial \lambda} = 0, \quad \frac{\partial \Delta}{\partial \vartheta} = 0$$

using the calculus of maxima and minima by iteration with the help of a computer.

5. Some characteristic experiments

The following series of figures illustrates the experiments carried out on specimens made from core samples. The core samples originate from the drillings Me 105, Me 114 and N 60 in the Nagyegyháza basin.

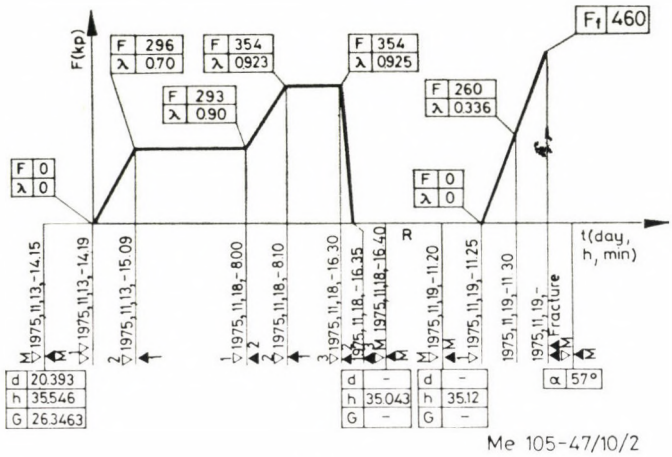


Fig. 13

Figure 13 displays the experiment on a shallow-water calcareous clay specimen (H = 288.10—288.40 m). The experiment consisted of a sequence of uniform load increase followed by creep, then further load increase, followed again by creep and load decrease to zero. Finally a gradually increasing loading period took place up to deterioration. The following symbols are used in this figure:

F — loading force [kp],
G — weight of specimen [p],
d — specimen diameter [mm],
h — specimen height [mm],
λ — compression, height reduction of the specimen [mm].

The other symbols used in the load diagrams are as follows:

▽▽ — experiment starts,
1 — load increase period,
2 — fixed load (creep) period,
3 — load decrease period,
M — measurement, checking the dimensions of the specimen,
R — removing the specimen from the device,
▽ — loading starts,
▼ — end of loading period,
▼▼ — end of the experiment.

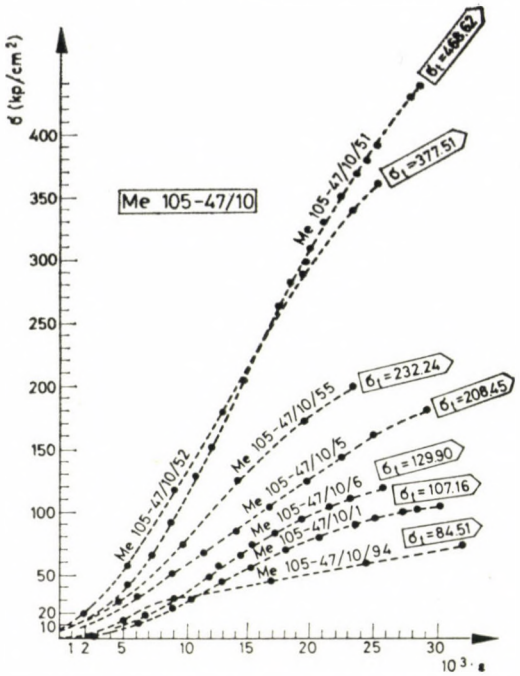


Fig. 14. Curves stress vs. deformation

Figure 14 displays the curves stress *vs.* deformation for the specimens made from core samples of the drilling Me 105 ⟨at a depth $H = 286.30$—289.80 m⟩ in the Nagyegyháza basin. The specimens have been loaded at a constant rate until they have fractured as can also be seen from Fig. 13. Figure 15 shows the broken specimen.

The section of a shallow-water clay specimen taken from a depth $H =$ $= 303.90$—305.30 m of the same drilling is displayed in Fig. 16. Its broken surface can be seen in Fig. 17. The stress *vs.* deformation curves obtained

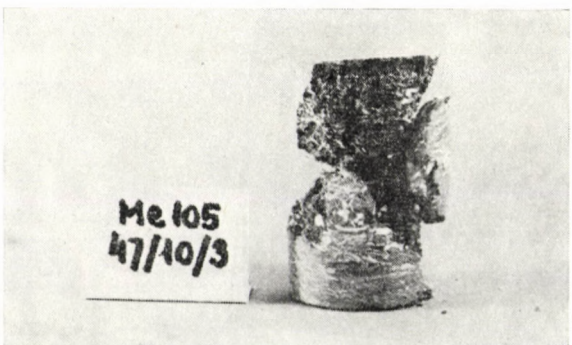


Fig. 15. Shallow-water calcareous clay specimen after fracture in a uniaxial compression test



Fig. 16. Shallow-water clay with little inclusion. The fracture of the core sample

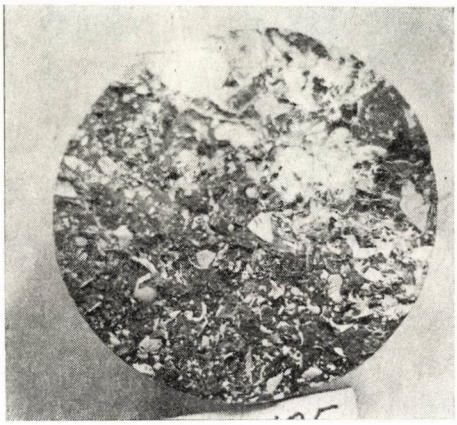


Fig. 17. Shallow-water clay with plenty of fossils. The section of the core sample

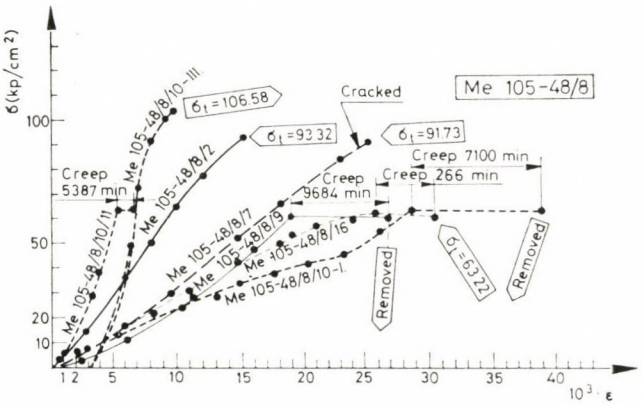


Fig. 18. Curves stress vs. deformation obtained from the experiments

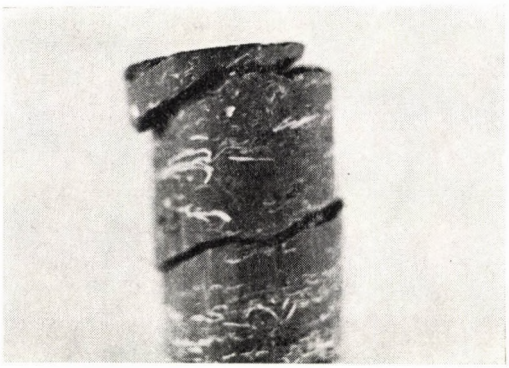


Fig. 19. Specimen broken into pieces along stratification while kept in hand after having been removed from the device

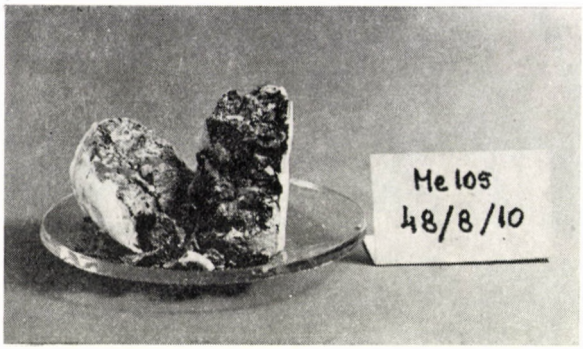


Fig. 20. Specimen of the experiment Me 105—48/810 broken by increasing the load several times

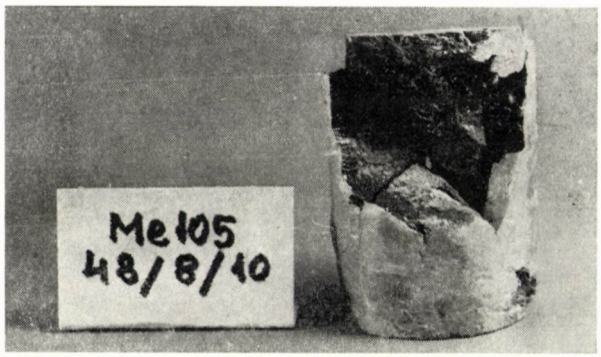


Fig. 21. The specimen of Fig. 20, removed from the device

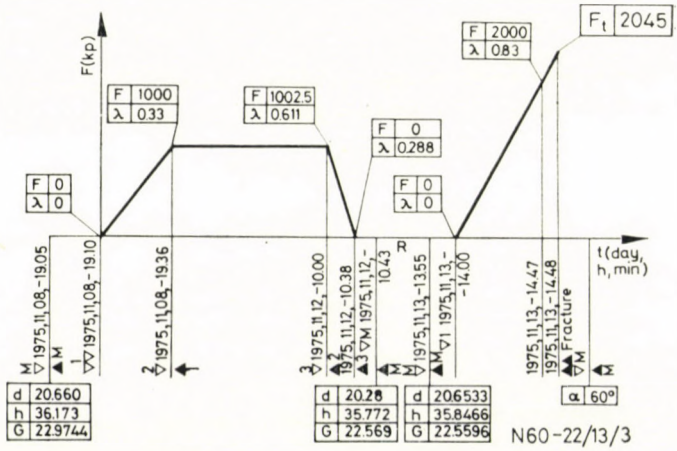


Fig. 22. Load against time in the case of a creep and fracture experiment

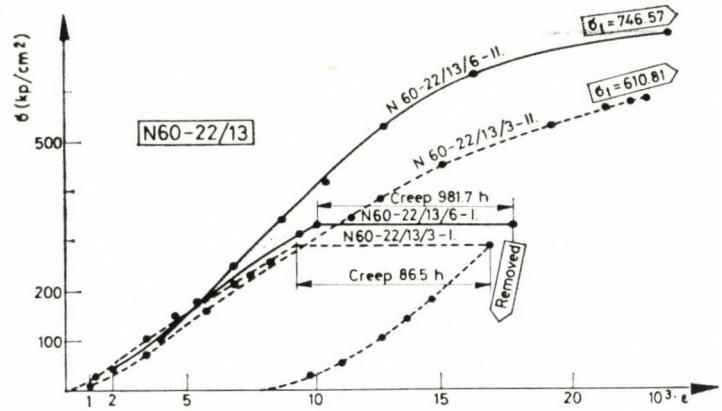


Fig. 23. Curves stress vs. deformation for fresh-water limestone specimens

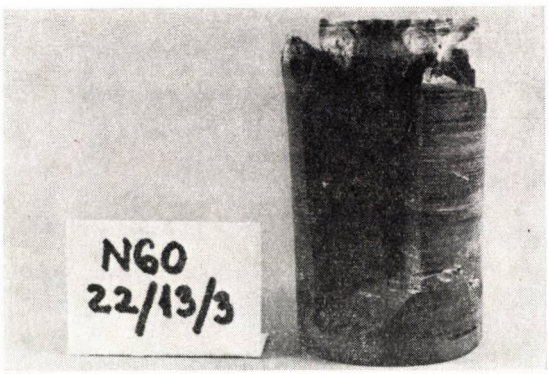


Fig. 24. Fractured fresh-water limestone specimen after creep



Fig. 25. The specimen of Fig. 24 before the experiment

Table I

Materials contants obtained by creep test

Specimen denomination	Material	E [kp/cm²]	λ [kp h/cm²]	ϑ[h]
Me 105—47/10/2	Shallow-water calcareous clay	36 856	72 266	17.108
Me 105—47/10/3		29 668	4 578	1.100
Me 105—47/10/10		31 963	4 932	1.061
Me 105—47/11/3		43 391	85 080	15.190
Me 105—48/8/9	Shallow-water clay	23 026	23 985	7.869
Me 105—48/8/10		17 017	17 725	8.276
N 60—22/13/2	Fresh-water limestone	20 153	395 150	14.990
N 60—22/13/3		18 280	358 430	11.947
Me 114—86/6/2	Fresh-water limestone	25 450	39 275	11.891

from the experiments are plotted in Fig. 18. Figures 19—21 illustrate the broken specimen.

Figures 22—25 show a fresh-water limestone specimen taken from a depth $H = 419.70$—420.10 m and the corresponding experiments, Figures 26—28 illustrate another specimen taken from a depth $H = 450.30$—450.90 m.

The Table I below contains the values of the material constants obtained from creep experiments carried out at the Department of Mechanics of the University of Agriculture at Gödöllő.

The table shows that the great structural and strength non-homogeneity of the specimens and of the core samples, respectively, results in a wide scattering of the measurement data, even through special care has been taken in shaping and storing the specimens and in carrying out the experiments. The limestone specimens e.g. having high breaking strength are prone to be split

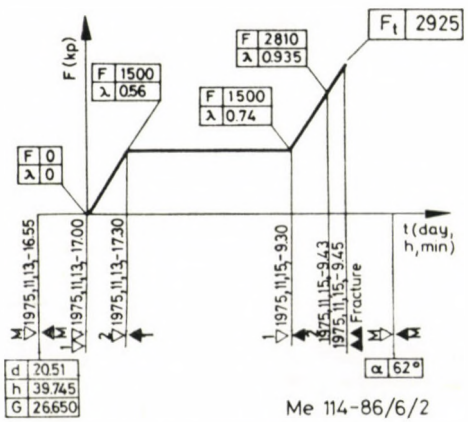


Fig. 26. Variation of load with time

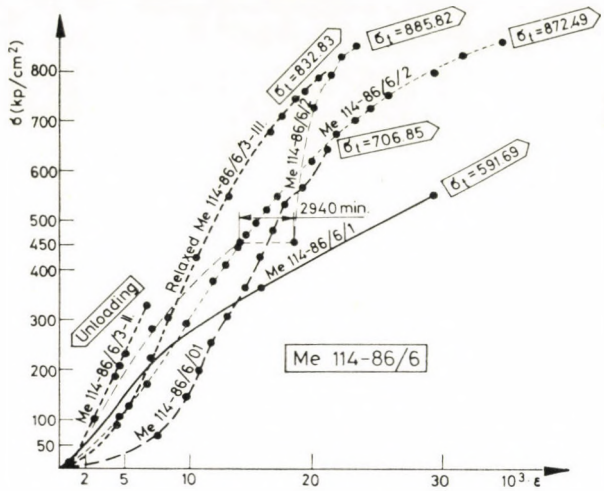


Fig. 27. Curves stress vs. deformation obtained from the experiments



Fig. 28. The specimen fractured during the experiments shown in Fig. 26

along specified directions, due to their anisotropism. In the specified directions slippings have occurred, which have led to the deterioration of the specimen. However in other cases splits have occurred immediately and the strength of the specimen has only slightly decreased, fracture having been occurred only after a further increase in load. On the contrary, the fresh-water limestone specimens N 60—22/13 furnished evidence of a remarkably high storage capacity of elastic energy. In these specimens the stored potential energy virtually blasted the specimen along more split surfaces after the breaking process had started.

The experiments thus for show that a great number of meanserements are required to accumulate data of a satisfactory confidence level from the observed results.

REFERENCES

1. Asszonyi, Cs.: On a rheological theory of rock continua. Doctor's Thesis. Hungarian Academy of Sciences. Budapest 1975.
2. Asszonyi, Cs.: On a new theory of rock mechanics. *Acta Geod. Geoph. Mont. Hung.*, 8 (1974), 313—322.
3. Asszonyi, Cs.: Mechanical theory of continua. *Acta Geod. Geoph. Mont. Hung.*, 8 (1974), 323—360.
4. Asszonyi, Cs.: Determination by *in-situ* measurements of the characteristic parameters of the field of primary stresses and deformations. Publications of Technical University of Heavy Industry, Miskolc 1970, 39—60.
5. Asszonyi, Cs.: Laboratory determination of the physical equations and rheological materials constants of rocks. Research Report. Technical University of Heavy Industry, Miskolc 1972, 1—52.
6. Asszonyi, Cs.—Kapolyi, L.: Determination of mechanical parameters of rocks. Papers of the Veszprém Committee of the Hungarian Academy of Sciences. Veszprém 1976, 1—192.
7. Asszonyi, Cs.—Kapolyi, L.—Huszár, I.: Laboratory determination of rock constants using creep tests. *Tatabányai Szénbányák Műszaki Közgazdasági Közleményei*, No. 4, 1971, 1977—1982.
8. Asszonyi, Cs.—Kapolyi, L.—Richter, R.: Laboratory determination of rock characteristics. I. Uniaxial compression tests. *Acta Geod. Geoph. Mont. Hung.* 14 (1979), 313—340.
9. Kapolyi, L.: Some problems on the rock mechanics of future underground mining. SESSA Spring Meeting Los Angeles, California 1973, 1—34.
10. Filcek, H.: Laboratory compression experiments and rheological properties of rocks. Przeglad Naukowo-Techniczny AGH (Scientific Technical Review of the Mining and Metallurgical University), Cracow, Serie G/1 1959.
11. Huszár, I.: Strength and rheological measurements on some core samples of drillings in the Nagyegyháza basin. Research Report. University of Agriculture, Gödöllő 1975, 1—259.
12. Kleczek, Z.: Experimental criteria for choosing a rheological model of rocks. Prace Komisje Nauk Technicznych Górnictwo (Publications of the Mining Technical Science Committee), 5 (1967), 33—50.

II. ОПРЕДЕЛЕНИЕ ПОСТОЯННЫХ ГОРНЫХ ПОРОД РЕОЛОГИЧЕСКИМ ИССЛЕДОВАНИЕМ ПОЛЗАНИЯ

Ч. АССОНИ—Л. КАПОЙИ—И. ХУСАР

РЕЗЮМЕ

В статье рассматривается определение вещественных характеристик горных пород реологическим исследованием ползания. Представляется оборудование, сконструированное и построенное для проведения лабораторных экспериментов, излагаются проведение и принцип изменений, а также метод обработки полученных результатов. Сообщается о значениях вещественных постоянных, определенных на пробных телах, изготовленных из стержневого образца исследовательских скважин, пробуренных в угольном бассейне Надьэдьхаза.

Acta Geodaet., Geophys. et Montanist. Acad. Sci. Hung. Tomus 14 (3), pp. 361—377 (1979)

III. DETERMINATION OF ROCK CHARACTERISTICS USING RELAXATION TESTS

CS. ASSZONYI
HUNGARIAN COAL BOARD, TATABÁNYA

I. HUSZÁR
UNIVERSITY OF AGRICULTURE, GÖDÖLLŐ

R. RICHTER
TECHNICAL UNIVERSITY OF HEAVY INDUSTRY, MISKOLC

[Manuscript received February 24, 1977]

The study deals with laboratory uniaxial experiments carried out on rock samples in order to determine their rheological constants. The authors believe that rocks can be characterized by the POYNTING—THOMSON's homogeneous linear rheological model with a good approximation below the yield stress. The paper describes the device manufactured to perform relaxation tests. Some ways of measurement evaluation are also presented.

1. Introductory remarks

It has been shown previously [1—4] that the material law suitable to characterise the principal properties of the rocks, can be found among those relating to the rheological bodies. A rather long way has been necessary to realise that.

Many simple compression tests have been carried out on Hungarian rock samples. The deviation of the curve stress *vs.* deformation from a linear one indicates that HOOKE's law does not provide us with a reliable approximation. Since the non-linear behaviour of the specimens has been observed also below the yields stress, it seemed reasonable to rely upon the correlations of non-linear mechanics. This would have meant fitting a curve of higher order (power, exponential, etc.) to the experimental data. This, however, could not have been accepted because of two reasons.

First, widely different functional types would give the best fit to results of different experiments. Thus the most different material equations ought to be included in rock mechanical investigations which would make the results over complicated and difficult to interpret. However, an unnecessarily high degree of complicacy indicates in the case of natural phenomena that the experiment, intended to discover the essence of a phenomenon, had not been successful enough. Otherwise the knowledge of the essential features of the phenomenon would make it possible to formulate the inner physical laws almost spontaneously.

On the other hand, using a function of higher order, the material law would not be the result of a physical consideration but rather some adjusting function of the data representing also inferent measurement errors. However,

in the nature, general and (for the actual mechanical system valid) specific physical laws must exist which determine the law of material of the rocks.

Experiences in mining indicate that the rocks surrounding excavations have to be considered as time-dependent "rheological" materials. A model analysis helped in choosing the proper model from among the rheological bodies, which could be taken into consideration. At first, the field of the laws which determine the choise of the model has been limited on the basis of mathematical-physical principles. After that the rock characteristics to be reflected by the model have been formulated as it seemed necessary according to mining experiences. Having performed the model analysis compromising D both requirements (cf. [2]), and having fixed the extent of the approximations, we decided to apply POYNTING—THOMSON's standard model. This model could be characterized by simple mathematical expressions being linear functions of time and containing no higher order terms. At the same time, POYNTING—THOMSON's model seemed to describe rock properties as perfectly as possible.

Our previous two studies [3, 4] described some laboratory experiments based on the standard model. The following sections describe the relaxation test and its evaluation, and the experimental device used to perform it.

The experiment consists of two steps, i.e. the corresponding curve of two respetive sections:

Section 1: loading with a constant rate of stress variation up to a given value of deformation $\varepsilon = \varepsilon_a$.

Section 2: keeping the deformation at a constant value ε_a.

The aim of the experiment is to determine the material constants of the rock from the values of load and deformation measured during the experiment.

2. The experimental device

The experimental device has to be able to load the specimens, to keep them at a fixed value of deformation and to record the whole process.

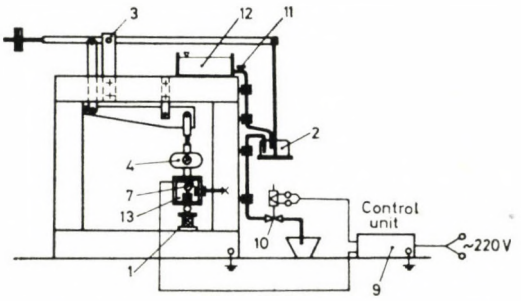


Fig. 1. Outline of the relaxation compression device

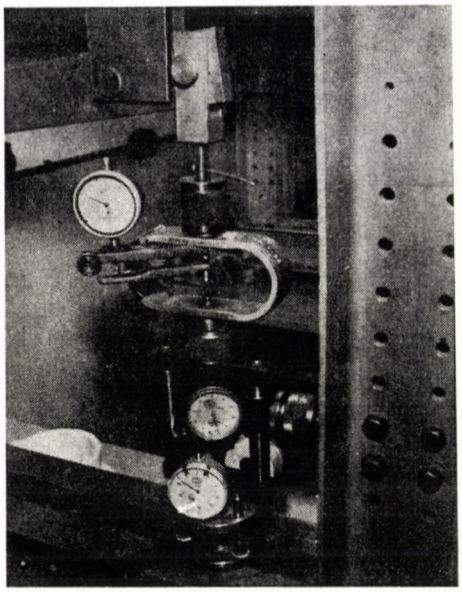


Fig. 2. Relaxation measuring device. Bottom: three dial gauges measuring deformation, top: dial gauge of the dynamometer, middle: dial gauge controlling load

The compressive load of the specimen is produced by the water allowed to flow into tank *2* of the device as illustrated in Fig. 1. Double lever *3* transfers the load towards the specimen. The variation of the load is controlled by the alteration of the water flow rate. The magnitude of the force acting on specimen *1* is indicated by the dial gauge of dynamometer *4* and is registered by a recorder connected electrically to the strain gauges which were glued on the arch of the dynamometer.

The picture of the device is shown in Fig. 2.

Figure 3 illustrates, in greater detail, the position of the specimen. The central loading of the specimen is ensured by ball *5* and locating pins *6*. Dial gauge *7* is applied with two aims. It indicates the deformation of the specimen continuously and operates magnet valve *10* (Fig. 1) with the help of adjustable switches *8* and control unit *9*. The magnet valve controls the flow rate of the water. Contacts *8* of dial gauge *7* have been manufactured of silver in order to ensure a safe connection. Dial gauge *7* has been placed to the axis of frame *13*. This axis coincides with that of the specimen. The outlined arrangement of the device ensures that dial gauge *7* measures the real change of length of the specimen. Three more dial gauges are located on compression plate *14* fitted to the pitch circle of locating pins *6*. The average of the readings of these dial gauges is equal to the reading of dial gauge *7* which gives a possibility of checking dial gauge *7*.

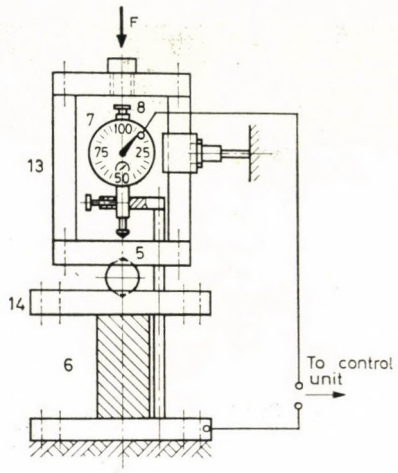


Fig. 3

During the relaxation test a 24 V relay switches magnet valve *10* to the 220 V main. Magnet valve *10* controls the load by adjusting the water flow rate. Contacts *8* do not close the circuit of the 24 V relay directly. A transistor amplifier is attached to it and this operates the relay. The diagram of control unit *9* containing the transistor amplifier is shown in Fig. 4. The transistor amplifier reduces the sparking on contacts *8*. On the other hand, it ensures the relay and the magnet valve to work even in the case of greater transition resistance. The resistors R_1, R_2 and R_3 adjust the operating point resistances of transistors *Tr 1* and *Tr 2*. Resistors R_1 and R_2 are connected in series with switches *8* of dial gauge *7*. If the contacts are open, the relay is pulled in and cuts off the circuit of the magnet valve. In this state, the current pulling in the relay flows through transistor *Tr. 2*. Consequently the inner resistance of the transistor is small. If contacts *8* close the circuit the current of transistor *Tr. 1* increases and its inner resistance decreases. This displaces the operating point of transistor *Tr. 2* to such extent that its inner resistance increases and the current carried by it and the relay, reduces to a minimum. As a result of this, the relay closes the circuit of the magnet valve. Diode *D* protects tran-

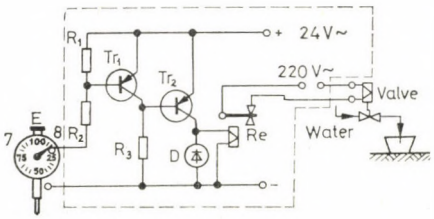


Fig. 4

sistor *Tr. 2* from an eventual overvoltage induced in the coil by a prompt current decrease. The transistor control circuit has proved to work reliably even in the case of a transition resistance of 3—4 MΩ.

The variation of the force acting on the specimen has been registered by a recorder. The sensor (transducer) was the dynamometer provided with four

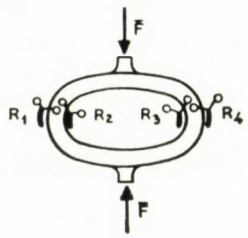


Fig. 5

strain gauges as outlined in Fig. 5. The strain gauges have been connected as to create a full Wheatstone bridge and this was connected to the all-purpose meter UM 111 (manufactured in the German Democratic Republic). The indicating instrument and the recorder of the all-purpose meter (the latter connected to the loop output) have been calibrated with the help of the dial gauge of the dynamometer. Since the dynamometer measures the actual force acting on the specimen by frame *13* directly, the friction force in the mechanism does not cause any measurement error. The full bridge built from the strain gauges ensured a good zero stability and an independence of temperature changes. This made possible to record reliably the cariation of load with time.

3. Description of the measurement

The load of the specimen was increased linearly with time, i.e. at a constant rate. The linear increase of load was produced by allowing water to flow with a constant flow rate into tank *2* (Fig. 1). The velocity and the flow rate of the water were kept constant by maintaining a steady water level in reservoir *12*. Changeable nozzles were inserted into the end section of the pipe connected to tap *11*. The actual value of the flow rate, required by the experiment, could be adjusted by inserting the corresponding nozzle into the pipe before starting the measurement. While loading the specimen the deformation was measured by the three dial gauges placed on compression plate *14* and by dial gauge *7* in frame *13*. Readings were taken at the dial gauges in every 10—30 seconds. The variation of the loading force was registered by a recorder. But in order to check the measurements, readings were taken and put down

also from the dial gauge of the standard dynamometer at given time intervals. The time of the linear loading of the specimens was 10—20 minutes, depending on the type of rock. For the purposes of the relaxation measurement, contacts *8* of dial gauge *7* have been adjusted according to the deformation value required, before starting the measurement. When the deformation of the specimen was as high as the adjusted value during the linear load increase, contacts *8* closed the circuit and the control unit operated magnet valve *10*. At this very instant, the flow rate of the water was reduced as to achieve a very slow rate of dripping. It should be noted here that the flow rate of the outflowing water is much higher than that of the inflowing one during the loading. Consequently, having achieved the deformation value adjusted, the increase of the load of the specimen is stopped instantaneously by opening the magnet valve and the load starts to decrease. This load decrease continues until contacts *8* of dial gauge *7* separate again. If the length of the specimen decreases due to the loading, contacts *8* close the circuit again and the whole process starts from the beginning. The water dripping into tank *2* compensates for losses due to evaporation during the measurement of several days. Readings were taken from the dial gauges (three of which were placed on the compression plate and one fitted in frame *13*) also during the relaxation process to check the deformation of the specimen.

During the relaxation measurement, the dial gauge of the dynamometer was also checked several times and the roadings with the corresponding time instants were noted.

The relaxation test device has also been checked from the point of view of sensitivity. The length tolerance was measured within which the specimen tested could be kept at a constant pre-stressed length. Since even dial gauges with a measurement accuracy of 1/1000 mm are unable to measure as little changes of length as that, an indirect measurement method had to be applied. For this reason the rock specimen had been removed from the device and was replaced by a steel specimen of known YOUNG's modulus. Having adjusted contacts *8* water was allowed to flow at a constant flow rate into tank *2*. Having achieved the adjusted value of strain, the contacts closed the circuit. When the magnet valve had allowed a certain amount of water to flow out, the contacts separated again. The inflowing water continued to flow thus the whole procedure was repeated. This caused a fluctuation not only in the length of the steel specimen, but also in the force which could be measured by the dynamometer. Since the force can be measured with a high accuracy, the length fluctuation was measured through a force measurement. The measurements repeated several times yielded a value always less than $\pm 2 \cdot 10^{-5}$ mm for the length variation of the steel specimen. This means that the experimental device was able to keep the specimen at a given pre-stressed value within the above tolerance in course of the relaxation test. The force fluctuation which

corresponded to this change of length was observable in the records in the form of a small saw-teeth. The measurements taken on the saw-teeth fluctuations of the records have proved that the stress fluctuations in the specimens due to fluctuations of the control did not exceed ± 1.5 kp/cm^2. Comparing this value with the maximum stress measured on the specimens during the experiments, the stress fluctuation represents $\pm 1\%$ of the quantities measured. The device turned out to have a very reliable zero stability since the measurement of the length variation of the specimen is performed fully mechanically. Relying upon these statements, the experimental device can be considered as to meet the requirements of the measurement accuracy.

A further essential feature of the experiments is to keep the ambient temperature constant, since the length variation of the specimen due to a temperature change of 1 °C exceeds the accuracy of the control. Having a specimen of length $l_0 = 30$ mm and a coefficient of thermal expansion $\alpha_t = 6 \cdot 10^{-6}/°C$, one gets a specific change in length $l_0/\Delta t = \alpha_t l_0 = 18 \cdot 10^{-5}$ mm/°C. In the case of a temperature change of 1 °C the actual change in length is by one order of magnitude greater than $\pm 2 \cdot 10^{-5}$ mm ensured by the control.

4. Evaluation

The values of the material constants of the material equation can be determined from the corresponding values

$$t_i,\ \varepsilon_i \qquad i = 0, 1, \ldots, a-1 \quad \text{(Section 1)}$$

$$t_a,\ \varepsilon_a,\ \sigma_a$$

$$t_i,\ \sigma_i \qquad i = a+1, \ldots, n \quad \text{(Section 2)}$$

measured at given instants of time.

The solution of POYNTING—THOMSON's model for section 1 ($\dot{\sigma} = \dot{\sigma}_* = $ constant) is:

$$\varepsilon = \frac{\dot{\sigma}_*}{E}\left[t + \left(\vartheta - \frac{\lambda}{E}\right)\left(1 - \mathrm{e}^{-\frac{E}{\lambda}t}\right)\right], \tag{1}$$

the solution for section 2 is as follows ($\varepsilon = \varepsilon_a = $ constant):

$$\sigma = E\varepsilon_a + (\sigma_a - E\varepsilon_a)\,\mathrm{e}^{-\frac{t-t_a}{\vartheta}}. \tag{2}$$

4.1 *Direct method*

The investigation is aimed at determining the materials constants of equations (1) and (2). Their approximate values can be determined from the data of three measurements.

In Eq. (2) the second member can be neglected in the case $t \to \infty$, in comparison with the first one. If t_n of the last measurement point is great enough, then

$$\sigma_n \approx E\varepsilon_a,$$

and

$$E_0 = \frac{\sigma_n}{\varepsilon_a} \tag{3}$$

respectively. E_0 represents here an approximate value of YOUNG's modulus E.

Substituting $E = E_0$ and the measured data t_k and σ_k into Eq. (2) we get the correlation

$$\sigma_k = E_0 \varepsilon_a + (\sigma_a - E_0 \varepsilon_a) \, \mathrm{e}^{-\frac{t_k - t_0}{\vartheta_0}} \tag{4}$$

from which the approximate value of the relaxation coefficient ϑ_0 can be calculated:

$$\vartheta_0 = \frac{T}{\ln f},$$

where

$$T = t_k - t_a, \quad f = \frac{\sigma_a - \sigma_n}{\sigma_k - \sigma_n}. \tag{5}$$

Substituting the corresponding values

$$t_a = \sigma_a / \dot{\sigma}_*, \quad E = E_0, \quad \vartheta = \vartheta_0$$

into Eq. (1):

$$\varepsilon_a = \frac{1}{E}\left[\sigma_a + \dot{\sigma}_* \left(\vartheta_0 - \frac{\lambda_0}{E_0}\right)\left(1 - \mathrm{e}^{-\frac{E_0 \sigma_a}{\lambda_0 \dot{\sigma}_*}}\right)\right].$$

Substituting relations (3) and (5) and rearranging:

$$1 - \frac{\sigma_a - \sigma_n}{\dot{\sigma}_* \left(\frac{\varepsilon_a}{\sigma_n} \lambda_0 - \frac{T}{\ln f}\right)} = \mathrm{e}^{-\frac{\sigma_n \sigma_a}{\varepsilon_a \dot{\sigma}_* \lambda_0}}. \tag{6}$$

From Eq. (6) the approximate value of the creep coefficient λ_0 can be calculated by succesive approximation of both sides of the equation.

4.2 *Improved method*

The value of the materials constants calculated from the data of three measurements can be made more correct by taking into account more measurement points.

We assume the relaxation coefficient ϑ to be determined with a higher degree of accuracy using data of section 2 than of section 1. From Eqs. (3) and (4) we obtain the simultaneous equations

$$\vartheta \ln \left[\frac{\sigma_a - \sigma_n}{\sigma_k - \sigma_n} \right] = t_k - t_a,$$

where $k = a + 1, \ldots, n$.

Summing and rearranging these equations we have the expression

$$\vartheta = \frac{\sum_{k=a+1}^{n} (t_k - t_a)}{\sum_{k=a+1}^{n} \ln \frac{\sigma_a - \sigma_n}{\sigma_k - \sigma_n}}$$

for the improved value of the relaxation coefficient.

The improved values E_0 and λ_0 can be obtained by fitting a curve on the basis of the least squares and by using Eq. (1). Because of the difficulties in the computation, function (1) is linearised: the materials constants are corrected by δE and $\delta\lambda$, i.e. YOUNG's modulus is written in the form $E = E_0 + + \delta E$ and the creep coefficient as $\lambda = \lambda_0 + \delta\lambda$. Having done that we obtain a sequence of the materials constants. Substituting these values into Eq. (1) and expanding it in terms of powers of δE and $\delta\lambda$, the deformation can be calculated to any given time t_i (members of higher than first order are neglected):

$$\varepsilon_{ik} = \varepsilon(t_i, E_0, \lambda_0, \vartheta) + a_i \delta E + b_i \delta\lambda,$$

$$(i = 1, 2, \ldots, a)$$

where

$$a_i = \left. \frac{\partial \varepsilon}{\partial E} \right|_{\substack{t_i \\ E_0, \vartheta_0, \lambda}} \quad \text{and} \quad b_i = \left. \frac{\partial \varepsilon}{\partial \lambda} \right|_{\substack{t_i \\ E_0, \lambda_0, \vartheta}}.$$

Let us now calculate the sum of the squares of the deviations of the values calculated this way from the measured ones:

$$\Delta \equiv \sum_{i=1}^{a} (\varepsilon_{ik} - \varepsilon_i)^2.$$

The quantities δE and $\delta\lambda$ can be determined by minimising Δ subject to the conditions

$$\frac{\partial \Delta}{\partial(\delta E)} = 0 \quad \text{and} \quad \frac{\partial \Delta}{\partial(\delta\lambda)} = 0.$$

The roots δE and $\delta\lambda$ obtained from the simultaneous linear equations represent the necessary corrections. With these corrections the quantities

$$E_1 = E_0 + \delta E,$$

$$\lambda_1 = \lambda_0 + \delta\lambda$$

determine the parameters of the theoretical curve giving the best fit with the measured points. The precision of this fit can be characterised by the quantities

$$H^{\mathrm{I}} = \sum_{i=1}^{a} \frac{1}{n_a} (\varepsilon_{ik} - \varepsilon_i)^2$$

and

$$H^{\mathrm{II}} = \sum_{i=a+1}^{n} \frac{1}{n_r} (\sigma_{ik} - \sigma_i)^2.$$

Here n_a is the number of the experiments while increasing the load ($n_a = a$),
n_r = is the number of the experiments during the relaxation ($n_r = n - n_a = n - a$),
σ_{ik} = stress as calculated from Eq. (2).

H^{I} and H^{II} make it possible to judge about how far is the model chosen it suitable to describe the mechanical properties of the material.

The computation outlined above is rather cumbersome. For this reason a computer was used to calculate numerically the materials constants.

The relaxation represents a process lasting for a theoretically infinite time. Consequently, it is essential to know in how long finite time span can a result be obtained with the required accuracy. Let us denote the stress σ corresponding to $t \to \infty$ by σ_∞. If the last measurement datum σ_n is required to deviate from σ_∞ by 2%, then on substituting $\sigma_\infty = E\varepsilon_a$ and $\sigma_n = 1.02\,\sigma_\infty$ into Eq. (2), the length of the measurement time is obtained as follows:

$$t_n = \vartheta \left[\ln 50 \left(\frac{\sigma_a}{\sigma_\infty} - 1 \right) \right] + t_a.$$

Apart from ϑ, the time of the measurement depends also on the ratio σ_a/σ_∞. According to our measurements, this ratio is between $1.5 \sim 2$. If we take $\sigma_a/\sigma_\infty = 2$, then $t_n \sim 4\,\vartheta$.

There are other methods, as well, to determine the materials constants. One more will be described here.

Since the data of section 2 of the curve are more reliable, let us start from the correlations

$$\sigma = E\varepsilon_a + (\sigma_a - E\varepsilon_a)\, \mathrm{e}^{-\frac{t-t_a}{\vartheta}},$$

which originate from

$$\sigma_i + v_i = (E_0 + \delta E)\,\varepsilon_a + [\sigma_a - (E_0 + \delta E)\,\varepsilon_a]\,\mathrm{e}^{-\frac{t_i - t_a}{\vartheta_0 + \delta\vartheta}}$$
$$(i = a + 1, \ldots, n)$$

modified with the error members v_i. Having n—a equations, δE and $\delta\vartheta$ can be calculated using the condition

$$\Sigma\, v_i^2 \to \text{Min !}$$

Knowing the values of E and ϑ, only λ characterising the physical phenomenon of section 1, has to be calculated from this somewhat uncertain section. Since no discontinuity can take place between the two sections, λ can be calculated from equation

$$\varepsilon_a = \frac{\dot{\sigma}_*}{E}\left[t_a + \left(\vartheta - \frac{\lambda}{E}\right)\left(1 - \mathrm{e}^{-\frac{E}{\lambda} t_a}\right)\right].$$

4.3 *Stochastic method*

In order to determine the materials constants E, λ and ϑ the following correlations can be derived from Eqs (1) and (2):

$$\varepsilon(t_i) = \frac{\dot{\sigma}_*}{E}\left[t_i + \left(\vartheta - \frac{\lambda}{E}\right)\left(1 - \mathrm{e}^{-\frac{E}{\lambda} t_i}\right)\right], \qquad (i = 1, 2, \ldots, a) \tag{7}$$

$$\sigma(t_i) = \sigma_n + (\sigma_a - \sigma_n)\,\mathrm{e}^{-\frac{t_i - t_a}{\vartheta}}. \qquad (i = a + 1, \ldots, n) \tag{8}$$

Equations (7) and (8) are of different dimensions, for this reason they can not be combined into a single function for the purpose of the adjusting calculation. Consequently, the solution is sought for by successive approximations. One of the possible ways is as follows:

(i) An initial triad of the values E_0, λ_0 and ϑ_0 is determined using the direct method as outlined in section 4.1.

(ii) A triad of the values. E_1, λ_1 and ϑ_1 is then determined on the basis of the condition

$$\Delta_I(E, \lambda, \vartheta) \equiv \sum_{i=1}^{n} [\varepsilon_i - \varepsilon(t_i)]^2 \to \text{Min !} \tag{9}$$

using the observation data of section 1. Because of the complicacy of function $\varepsilon(t_i)$ it is useful to expand it linearly and to use, in Eq. (9), instead of $\varepsilon(t_i)$ the following expression:

$$\tilde{\varepsilon}_i = \varepsilon(t_i, E_0, \lambda_0, \vartheta_0) + a_i\,\delta E + b_i\,\delta\lambda + C_i\,\delta\vartheta$$
$$(i = 1, 2, \ldots, a).$$

(iii) The values E_2, λ_2 and ϑ_2 can be determined on the basis of the condition

$$\Delta_{II} \equiv \sum_{i=a+1}^{n} [\sigma_i - \sigma_i(t_i)]^2 \to \text{Min !} \tag{10}$$

and of its approximation, respectively, using the observation data of section 2. A linear expansion of the function

$$\sigma(t_i) = E\varepsilon_a + (\sigma_a - E\sigma_a)\, e^{-\frac{t_i - t_a}{\vartheta}} =$$

$$= \dot{\sigma}_* \left[t_a + \left(\vartheta - \frac{\lambda}{E} \right) \left(1 - e^{-\frac{E}{\lambda} t_a} \right) \right] +$$

$$+ \left\{ \sigma_a - \dot{\sigma}_* \left[t_a + \left(\vartheta - \frac{\lambda}{E} \right) \left(1 - e^{-\frac{E}{\lambda} t_a} \right) \right] \right\} e^{-\frac{t_i - t_a}{\vartheta}}$$

at the values E_1, λ_1 and ϑ_1 is useful also in this case as well.

Steps (ii) and (iii) are repeated until the changes in E, λ and ϑ will be less than a required value.

The advantage of this method as compared with that outlined in section 4.2 that is both sections of the curve, obtained by the proportional loading and relaxation test, can be used to determine the material constants of the rocks.

A *combined* evaluation of the data of both sections can be performed by converting Eqs (7) and (8) such as to have identical dimensions. This can be done e.g. by presuming a preliminary value E_* for E. Then the actual values of E, λ and ϑ can be determined from the equations

$$E_* \varepsilon_i + \vartheta_i = \dot{\sigma}_* \left[t_i + \left(\vartheta - \frac{\lambda}{E} \right) \left(1 - e^{-\frac{E}{\lambda} t_i} \right) \right], \qquad (i = 1, 2, \ldots, a)$$

$$\sigma_j + v_j = \sigma_n + (\sigma_a - \sigma_n)\, e^{-\frac{t_j - t_a}{\vartheta}} \qquad (j = a + 1, \ldots, n)$$

on the basis of the condition

$$\Delta \equiv \sum_{i=1}^{a} v_i^2 + \sum_{j=a+1}^{n} v_j^2 \to \text{Min !} \tag{11}$$

by linearising Eq. (11). By taking into account E_*, the calculation will be repeated using E obtained in this way.

5. Remarks

Summing up the results of papers [3, 4] and those of the present study, it is clear that we have possibilities at hand all to carry out the uniaxial compression tests required. The equipment necessary for performing the widest

variety of experiments are available, the evaluation principles and formulae have been determined, and the computer programs are ready. All these make possible to investigate the rock mechanics problems of any given area which seems to be interesting from the point of view of rock mechanics or support technique. At the same time, the area itself or the surrounding rocks can be characterized rheologically.

6. Some laboratory experiments

Figure 6 shows the relaxation curve of a shallow-water calcareous clay specimen extracted from a depth $H = 289.50—289.80$ m of the drilling Me 105 at Nagyegyháza. Having completed the relaxation measurement, the specimen was further loaded at a constant rate of increase. The specimen got deteriorated at a load of 1065 kp (Fig. 7).

Figure 8 shows the load diagram, and Fig. 9 illustrates the relaxation diagram, for the specimen N 60—6/5/11, a calcareous clay containing Globularia, extracted from a depth $H = 372.20—382.90$ m.

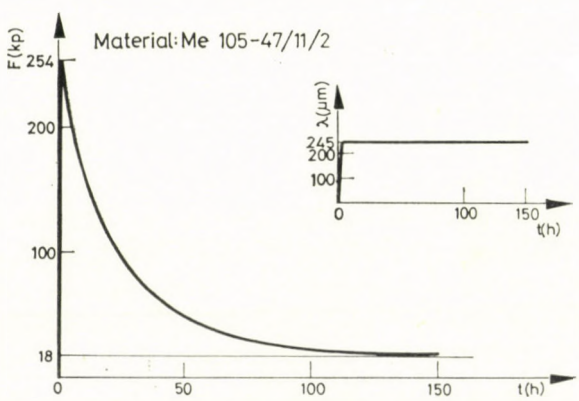


Fig. 6. Strain and relaxation plotted against time at a shallow-water calcareous clay specimen

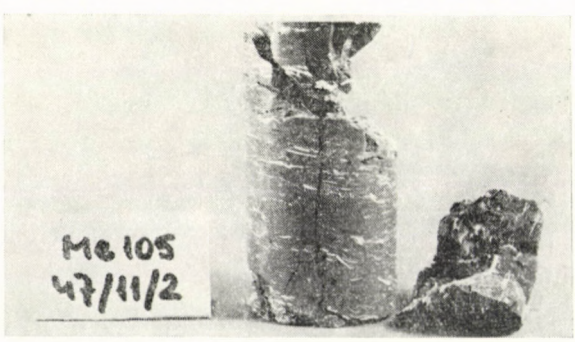


Fig. 7. Fractured specimen (shallow-water calcareous clay)

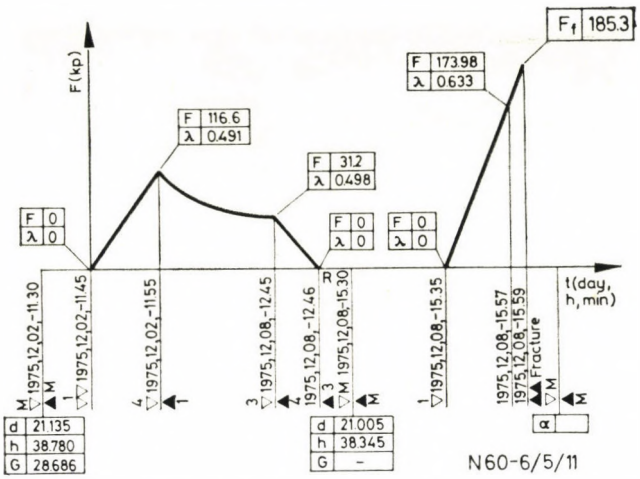


Fig. 8. Load plotted against time at a relaxation experiment on a calcareous clay specimen containing Globularia

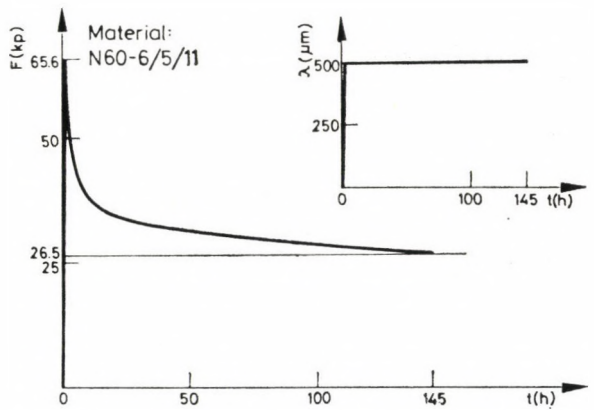


Fig. 9. Strain and relaxation of a calcareous clay specimen containing Globularia

The symbols used in Fig. 8 are as follows:

F = loading force [kp],
G = weight of the specimen [p],
d = specimen diameter [mm],
h = specimen height [mm],
λ = compression of the specimen, decrease of height [mm],

other symbols:

▽▽ — start of experiment,
1 — load increase period (constant rate of stress increase),

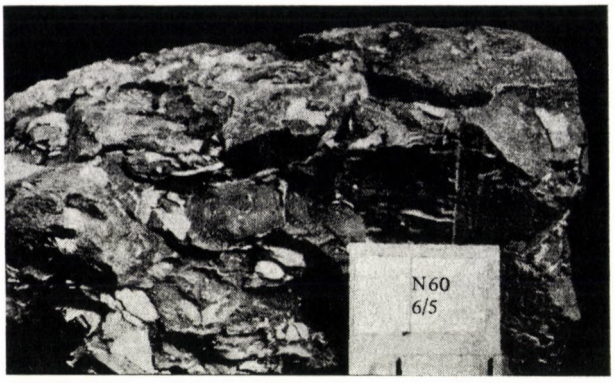


Fig. 10. Calcareous clay sample containing Globularia, magnified 1.8 times

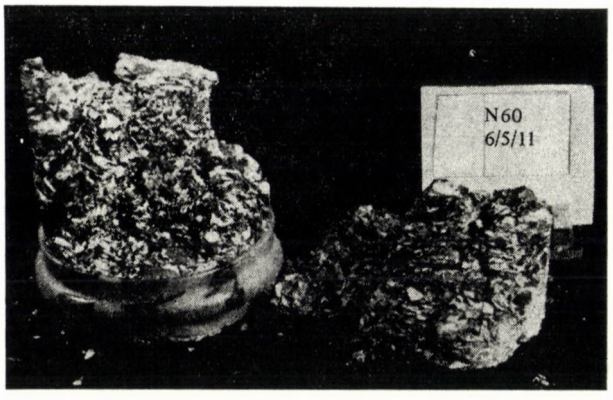


Fig. 11. Deteriorated specimen cut out of the sample shown in Fig. 10

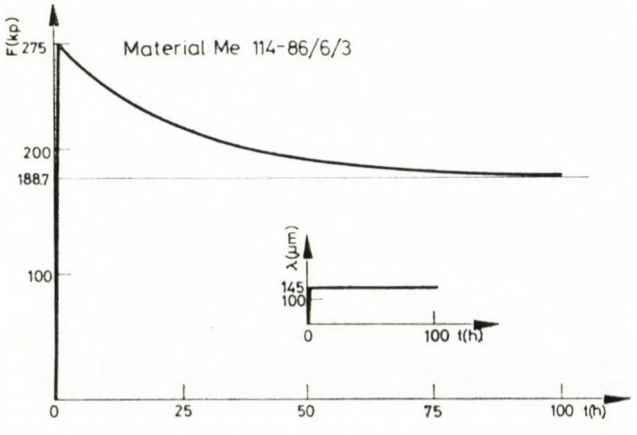


Fig. 12. Strain and relaxation curves of a fresh-water limestone specimen

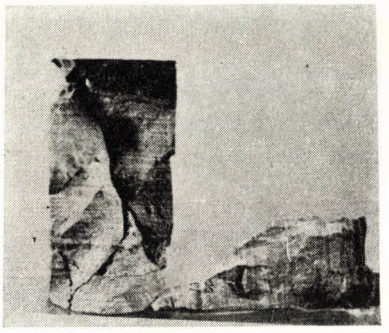


Fig. 13. Fractured fresh-water limestone specimen

3 — fixed deformation (relaxation period),
4 — unloading period,
M — measurement, checking the dimensions of the specimen,
R — removing the specimen from the device,
▽ — start of loading,
▼ — end of loading period,
▼▼ — end of the experiment.

Figure 10 shows the sample material 1.8 times magnified. Having been loaded up to fracture the specimen fell into morsels (Fig. 11).

Figure 12 illustrates the relaxation curve measured on a fresh-water limestone specimen. The specimen material originates from the drilling Me 114, and has been extracted from a depth $H = 450.30—450.90$ m. The picture of the specimen after fracture is shown in Fig. 13.

Table I displays some rheological constants determined by relaxation experiments.

Table I

Values of rock constants determined by relaxation tests

Specimen denomination	Material	E (kp/cm²)	λ (kp h/cm²)	ϑ (h)
Me 105—47/11/2	Shallow-water calcareous clay	7 472	421 330	32.194
Me 104—48/8/15	Shallow-water clay	16 095	92 999	29.964
N 60—6/5/11	Calcareous clay containing Globularia	6 495	8 205	5.611
Me 114—86/6/3	Fresh-water limestone	150 242	545 728	23.618

REFERENCES

1. Asszonyi, Cs.: Laboratory determination of the physical equations and rheological paterials constants of rocks. Research Report. Technical University of Heavy Industry, Miskolc 1972, 1—52.
2. Asszonyi, Cs.: On a rheological theory of rock continua. Doctor's Thesis. Hungarian Academy of Sciences. Budapest 1975.
3. Asszonyi, Cs.—Kapolyi, L.—Richter, R.: Laboratory determination of rock characteristics. I. Uniaxial compression tests. *Acta Geod. Geoph. Mont. Hung.* 14 (1979), 313—340.
4. Asszonyi, Cs.—Huszár, I.—Kapolyi, L.: Laboratory determination of rock characteristics. II. Determination of rock characteristics using rheological creep investigation. *Acta Geod. Geoph. Mont. Hung.* 14 (1979), 341—359.
5. Asszonyi, Cs.—Kapolyi, L.: Determination of mechanical parameters of rocks. Papers of the Veszprém Committee of the Hungarian Academy of Sciences. Veszprém 1976, 1—192.
6. Asszonyi, Cs.—Csorba, L.—Huszár, I.—Müller, Z.—Kapolyi, L.—Richter, R.: Determination of rock constants using relaxation tests. *Tatabányai Szénbányák Műszaki Közgazdasági Közleményei*, No. 4, 1974, 163—169.
7. Huszár, I.: Strength and rheological measurements on some core samples of drillings in the Nagyegyháza basin. Research Report. University of Agriculture, Gödöllő 1975, 1—259.

III. ОПРЕДЕЛЕНИЕ ПОСТОЯННЫХ ГОРНЫХ ПОРОД МЕТОДОМ РЕЛАКСАЦИИ

Ч. АССОНИ—И. ХУСАР—Р. РИХТЕР

РЕЗЮМЕ

Б статье сообщается об односных лабораторных экспериментах проведенных на пробных телах из горных пород, для определения реологических постоянных. Авторы считают, что горная порожа ниже границы пластичности хорошо описывается однородно-линейной реологической моделью Поинтинга-Томсона. Представляются оборудование, сконструированное для проведения релаксационной пробы и некоторые возможности для обработки измерений.

Acta Geodaet., Geophys. et Montanist. Acad. Sci. Hung. Tomus 14 (3), pp. 379—402 (1979)

IV. TRIAXIAL FRACTURE TESTS

CS. ASSZONYI

HUNGARIAN COAL BOARD, TATABÁNYA

I. HUSZÁR

UNIVERSITY OF AGRICULTURE, GÖDÖLLŐ

L. KAPOLYI

MINISTRY OF THE HEAVY INDUSTRIES, BUDAPEST

[Manuscript received February 24, 1977]

The study sums up briefly the major aspects of triaxial fracture of cylindrical specimens under fluid pressure and refers to recent applications of the method in rock investigations. A member of a family of devices, developed for the purposes of the experiments, and the triaxial fracture test carried out with the aid of this device, are described.

1. Introduction

The earth's crust consists of materials having different composition, state and structure and is characterised by sudden changes in composition, lamination, fractures, faults. It can be generally considered as to be in equilibrium. However, this state of equilibrium is disturbed when underground caverns, excavations are created or solid, liquid and gaseous materials are extracted. In the state of non-equilibrium, material motion is generated until the set-in of a new state of equilibrium. Due to this motion, a part of the energy accumulated in the crust, e.g. stored in form of elastic deformation, is released and can generate further motions. The mass displacements caused by these motions represent a danger to the stability of buildings and other structures. In order to estimate this danger, certain parameters have to be known.

The mechanical characteristics of the crust are usually determined by indirect measurements. One of these measurements is the triaxial investigation of specimens extracted from the crust. In the following the triaxial investigation of specimens cut out from rock samples will be dealt with, not touching upon the problem, how to predict the behaviour of rock masses of great extension on the basis of data measured on specimens.

As is well-known, the reliability of measurement data obtained from laboratory experiments cannot be compared with that of in situ results. Since time-dependent media have now to be investigated, it is not always possible to carry out the rheological measurements, especially near working places, on account of their being time-consuming (in connection with changes of the quasi-primary state during measurement). Thus, data necessary for designing roof supports and developing advantageous support technology are furnished, in many cases, by laboratory measurements only.

It is believed and, perhaps, the majority of researchers will agree that the data of triaxial compression tests furnish more reliable rock parameters than those of uniaxial compression tests. Not, because the laboratory tests and their evaluation are in this case more complicated but that the principle of this method approaches the triaxial *in situ* state of stress, dominating underground, more closely.

While performing triaxial compression tests, the specimen is subjected to a known external mechanical effect and the deformation caused by the known load is determined. Such circumstances are produced that enable us to describe mathematically the correlation between the measured mechanical parameters with sufficient accuracy and to explore deeper the phenomenon.

In the triaxial compression test the load produces a triaxial state of stress in the specimen. Similarly, a triaxial state of stress dominates the rock masses of great extension in nature. It can be assumed that the correlations and their constants determined by triaxial tests on rock specimens, can be extrapolated with a certain accuracy to the rock masses of great extension.

The laboratory test of rock samples can be aimed at various goals:

(i) Determination of the physical equation of the rock, i.e. the correlation between the mechanical variables: the stress and the produced deformation.

(ii) Measurement of the actual values of the material constants.

(iii) Determination of the plasticity limit of the rock materials.

(iv) Determination of the deterioration limit and deterioration conditions of rocks.

The triaxial tests, too, can be performed according to these aims. In this study only fracture tests are dealt with from among these experiments. In the fracture test the load on the specimen is increased until it breaks. The aim of this experiment is to throw light upon the circumstances which cause fracture.

2. The phenomenon of fracture

The fracture is called a *local* one, if at any point P of the specimen the interaction of the material particles is basically changed, e.g. continuity ceases and splitting sets in, due to deformation around this point. If the local fractures extend over such a great part of the body as to deteriorate it from the strength's point of view and it becomes unable to resist the load any longer, the fracture is called a *total* one.

If the material equation is supposed to be known, then the local fracture can be connected with the state of stress. Thus, in this case, the state of stress causing fracture can be considered as one of the strength characteristics of the body, corresponding to a fixed rate of deformation.

On the other hand, it follows from the laws of irreversible thermodynamics [3, 4] that the fracture depends on the deformation work of the system and, in particular, on a part of this work: the dissipative energy.

Local fractures can occur at various states of stress corresponding to the same rate of stress variation or same rate of deformation. The totality of all the possible states of stress causing fracture can be used as basic strength characteristics.

If the totality of the states of stress causing fracture, corresponding to given rates of stress variation or rates of deformation, is known, deductions can be made about the deterioration of the body. For this reason, the totality of the states of stress is investigated in various points of the body. If such state of stress can be found in any of the points which lies near a member of the measured totality of the states of stress, then a local fracture can be expected in this particular point of the body.

Uniaxial tests can furnish only one member of the totality of the states of stress causing fracture. However, using a series of triaxial tests which produce various states of stress, the totality of the states of stress causing fracture, related to the material of the specimen can be recognized. It is known from the investigations of ASSZONYI [3, 4] that the state of stress is not the cause of the fracture, it can be used only for describing the phenomenon under certain special circumstances — constant rate of stress variation or constant rate of deformation. The expression "state of stress causing fracture" has to be interpreted as to take account of this finding.

3. Triaxial investigation

Triaxial tests are carried out on suitable specimens. The state of stress in the investigated point P of the specimen can, generally, not be determined by direct measurement because of the finite dimensions of the experimental devices. It is, however, possible to carry out the measurement, if a homogeneous state of stress dominates a sufficient great part of the specimen. A homogeneous triaxial state of stress is produced e.g. in a rectangular, prismatic, homogeneous, isotropic and continuous body loaded by a uniformly distributed system of forces perpendicular to the planes. The principal axes of stress coincide with the normals of the planes. The principal stresses at any point of the body can be determined from the resultant F_i of the system of forces distributed on the planes and from the surface A_i of the plane (Fig. 1):

$$\sigma_1 = F_1/A_1, \quad \sigma_2 = F_2/A_2, \quad \sigma_3 = F_3/A_3.$$

Loading a specimen of this type as outlined above, a state of stress (σ_1, σ_2, σ_3) causing fracture can be recognized. Repeating the experiment under

various circumstances, a series of states of stress being characteristic of fracture can be determined. Having measurements closely enough to each other, intermediate values can be obtained by interpolation with a good approximation. This method of measurement is, however, very difficult, the device is compli-

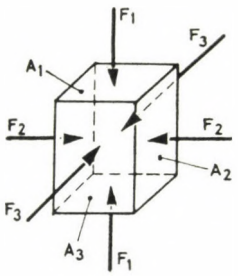


Fig. 1

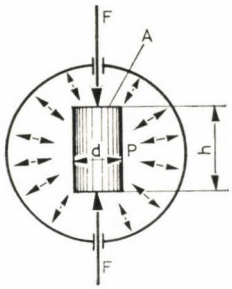


Fig. 2

cated, the loading process is circumstantial and the accuracy of the results is not satisfactory.

In practice, the measurements are carried out in the majority of the cases on straight-cylindrical solid or tubular specimens. The specimens are placed into a fluid space of pressure p and their end planes are loaded with a uniformly distributed axial force F (Fig. 2). During the experiment, pressure p is kept steady and force F is gradually increased until the specimen fractures. In a specimen of this type a homogeneous state of stress is generated, if the body is homogeneous, isotropic and continuous, and the uniformly distributed force F has only axial components in every point of the end plane. The axis and the radii are now principal axes of stress. The stress can be easily computed in every point of the body:

$$\sigma_1 = p + F/A, \quad \sigma_2 = \sigma_3 = p.$$

Consequently, the state of stress can be adjusted by regulating pressure p and axial force F. Measuring force F_f which caused fracture, at various pressures, a part of the totality of the states of stress causing fracture can be determined.

The state of stress is represented in the coordinate system (σ, τ) by a circle of diameter $(\sigma_1 - \sigma_2)$ having its centre on the σ-axis. If MOHR's circles of diameter $(\sigma_f - \sigma_p)$ representing the states of stress causing fracture, have been drawn, the interpolation can easily be done with the aid of the envelope of these circles. The $\tau(\sigma)$ envelope of MOHR's circles of the states of stress causing fracture is called the *fracture boundary curve* and can be used to characterise the totality of the states of stress causing fracture. If MOHR's circle representing a given state of stress approaches touches or intersects the fracture bound-

ary curve, then in this point of the body a fracture can be expected. The fracture boundary curve is, in general, a curve but with certain materials it is a straight line. Even in the previous case it can be considered a straight line. Thus, the boundary curve is described by the function

$$\tau = \sigma \cdot \tan \Phi + c.$$

Angle Φ in this function is called the *angle of inner friction* and the constant c is the *cohesion* (Fig. 3).

When fracture occurs, in the points where local fractures start, the shear stress

$$\tau_f = \sigma_f \cdot \tan \Phi + c$$

dominates, according to Coulomb's assumption. It is clear from this condition that fracture occurs in a plane (slipping plane) inclined to the end plane, for which

$$2\alpha = \Phi + 90°.$$

According to the energetical concept, the state of stress alone cannot be a fracture or strength characteristics unless combined with the state of deformation. At the same time, the correlation of both of these characteristics is a function of the rate of deformation. This means that a point of the fracture boundary curve represents this correlation at a given rate of deformation. Furthermore, the fracture boundary curve can be interpreted as a combined totality of the states of fracture stress and deformation corresponding to a given constant rate of deformation or stress variation. For various but constant

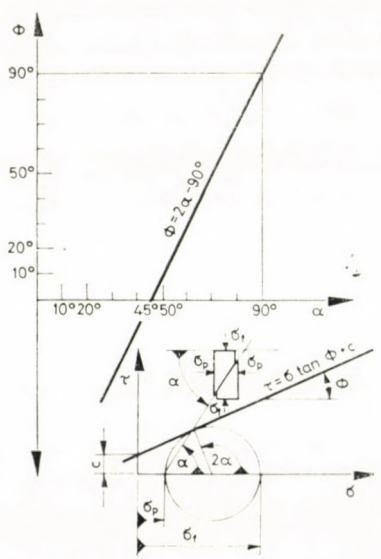


Fig. 3. Coulomb's fracture boundary condition and correlation between the angles

rates of deformation or rates of load, plotting yields a set of curves. According to the above-mentioned, the curves of this set can often be approximated quite well with straight lines which are easy to handle.

It follows from a form of ONSAGER's phenomenological relation (law of conduction) referring to mechanical systems [2, 3] that the stress tensor space and deformation tensor space are coaxial in isotropic media. This means that isotropism is a *sufficient condition* for coaxiality. The energetical concept does not fix the form of the material law either; thus coaxiality and proportionality of the state of stress and state of deformation hold for all isotropic bodies — not only for HOOKE's one.

4. Possibility of the determination of deformation characteristics using triaxial investigation

Let the cylindrical specimen be placed into a fluid space of pressure p and compressed axially by uniformly distributed force F. Assuming that the material of the specimen is isotropic, both the stress tensor space and the deformation tensor space in it are homogeneous. Furthermore both tensor spaces are coaxial and proportional to each other — according to our previous discussions. The correlation between both tensor spaces is determined, of course, by the material law. Proportionality in this case does not mean necessarily a linear correlation. However, the homogeneity of the tensor spaces makes it possible to determine both the stress characteristics and the deformation characteristics by measuring finite quantities. The axial strain and change of dimension, respectively, is now:

$$\varepsilon_z = \lim_{l_0 \to 0} \frac{\Delta l}{l_0} \approx \frac{\Delta l}{l_0} .$$

The radial strain becomes:

$$\varepsilon_y = \varepsilon_x = \lim_{d_0 \to 0} \frac{\Delta d}{d_0} \approx \frac{\Delta d}{d_0}$$

and the angular displacements:

$$\gamma_{xy} = \gamma_{yz} = \gamma_{zx} = 0.$$

Here l_0 is the original length of the cylindral specimen, Δl the change of length, d_0 the original diameter of the specimen and Δd the change of diameter. The specific change of volume can be similarly determined by measuring the original volume V_0 and the change of volume ΔV.

Difficulties arise, however, from the barrelling of the real specimen in measuring the transverse strains $\varepsilon_x = \varepsilon_y$. The problem can be eliminated by measuring specific change of volume

$$\Theta = \frac{\Delta V}{V_0} .$$

Since $$\Theta = \varepsilon_x + \varepsilon_y + \varepsilon_z,$$

the specific change of volume becomes:

$$\Theta = \frac{\Delta l}{l_0} + 2\,\frac{\Delta d}{d_0}.$$

Hence the radial strain:

$$\varepsilon_x = \frac{\Theta - \varepsilon_z}{2},$$

i.e. it can be calculated from the specific change of volume and axial strain of the specimen.

If the material law is known, further characteristics can be determined from the data obtained by this method. For example, if the material of the specimen behaves as HOOKE's body, using HOOKE's general law, the definition

$$m = \left| \frac{\varepsilon_z}{\varepsilon_x} \right|$$

of POISSON's ratio and the correlations

$$\sigma_1 = p + \frac{F}{A_0} = \sigma_z$$

and

$$\sigma_2 = \sigma_3 = p = \sigma_x = \sigma_y.$$

Resulting from the experiment conditions, POISSON's ratio becomes:

$$m = \left| \frac{d_0 \Delta l}{l_0 \Delta d} \right|;$$

and YOUNG's modulus:

$$E = \frac{\dfrac{F}{A_0} + (1 - 2m)p}{\varepsilon_z}.$$

5. Triaxial device

In order to perform triaxial fracture and deformation experiments, several triaxial compression devices have been designed and constructed in the last years at the Department of Mechanics of the Faculty of Mechanical Engineering of the University of Agriculture, Gödöllő, Hungary.

Device B-1 (Fig. 4) has been designed for specimens of average dimensions $\Phi\, 20 \cdot 33$ mm. The specimen and the cartridge containing it can be loaded up to 2000 kp, the highest cell pressure is 150 kp/cm². Pressure cell *l*

is a pressure-tight cylinder of inner diameter Φ 33 mm, closed at one end by anvil 2 and at the other by cap 3. Compression rod 5 is led through the cap with the help of low-friction, no-contact slit seal 4. Compression rod is loaded by force F from the outside. Cylindrical specimen 6 is first put into cartridge 7, which can be assembled outside the device. The assembled cartridge is then placed into the pressure cell which is finally closed by the cap. Dynamometer 8 is connected directly to the outer end of the compression rod (Fig. 5). The supporter of the dial gauge is affixed by a clamp to the free section of the compression rod between the cap and the dynamometer. The clamp limits

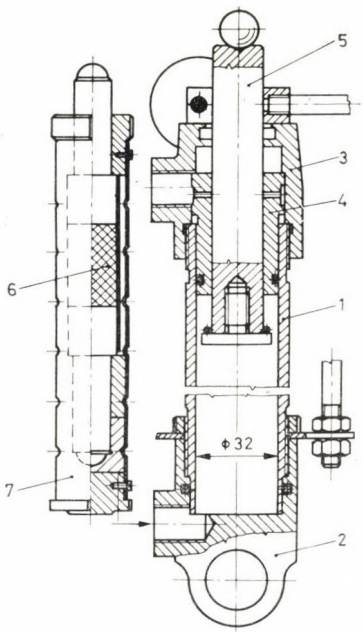


Fig. 4. Compression device with cartridge for triaxial testing samples of diameter 20 mm

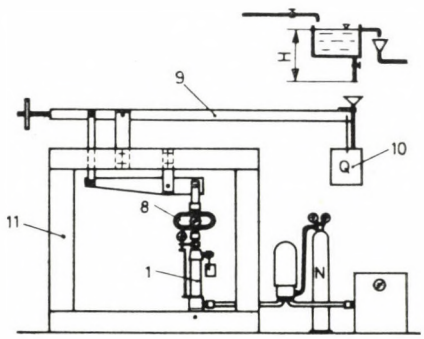


Fig. 5. Outline of the loading equipment of triaxial device B-1

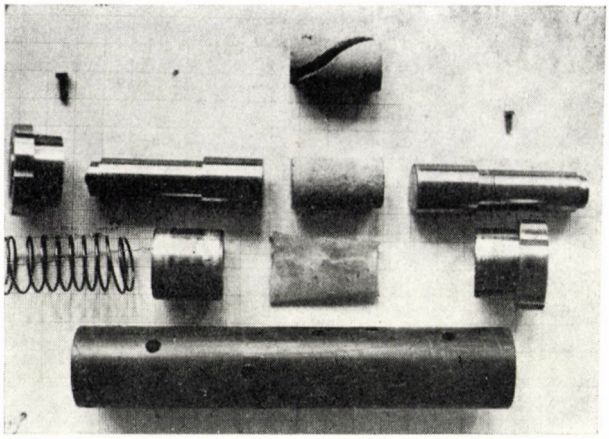


Fig. 6. Dismounted cartridge of the triaxial device. The specimen is placed between the compression plates. Top: fractured specimen

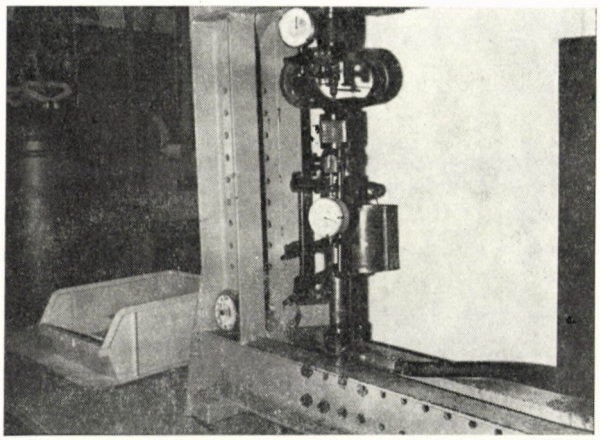


Fig. 7. Triaxial compression device ensuring measurement of force and displacement

the displacement of the compression rod, as well. The fluid filling the cell is oil. Pressure is produced by a supply unit fitted with a hydraulic battery and a pressure maintaining control unit. The axial loading force is produced by weight load 10 acting on dynamometer 7 through double lever mechanism 9. The loading mass was that of water whose volume could be adjusted. The whole device has been installed to angle-steel frame 11. In this arrangement, the deformation of the frame had practically no affect on the measurement accuracy. Fig. 6 illustrates the disassembled cartridge of device B-1.

The deformation of the dynamometer is indicated by the dial gauge, this enables us to determine the values of force with the help of a calibration dia-

gram. Strain gauges are glued on the surface of the arch of the dial gauge and inductive displacement transducers are connected to the compression rod. They make it possible to measure or record electrically the axial force and the displacement of the compression rod. This dynamometer was used while adjusting the cell pressure. The adjusted pressure was kept constant automatically by the control unit which enabled manual control, too.

The specimens are contained in cartridges also in the improved devices. Force and displacement are measured directly at the compression rod and loading occurs with the and of water through the lever mechanism. However, these devices ensure the measurement of pore pressure and the determination of the change of volume. The accuracy and comfort of the measurement procedure are also improved and specimens of greater dimensions can be used (Fig. 7).

6. Measurement procedure

The triaxial experiments were performed on specimens of average dimensions Φ 20 · 33 mm without tapping pore pressure. The measurement was first of all a fracture experiment in order to determine the fracture boundary curves. Axial deformation also were measured at the compression rod of the device. The measurement of the deformation was useful above all while observing fracture. The procedure, as outlined below, was performed at various pressures, on specimens cut out from the same sample material, according to the schedule, as follows:

1. The specimen was identified, its mark checked. The diameter, height and mass of the specimen were measured, the data were entered on record.

2. The specimen was covered with a film which protected it from the pressurised oil penetrating into it. (The film was made of a fluid of the type BAYPREN MKB 526, which can be painted by brush, has a milk-like consistence and after drying creates a rubber-like film.)

3. The specimen was covered with an isolating rubber diaphragm and installed into the cartridge.

4. The cartridge was placed into the pressure cell and the cell was closed.

5. The force and displacement measuring instruments were put into position, the loading mechanism was adjusted. The dynamometer was zeroed.

6. The loading lever mechanism was lifted and fixed, the cell was filled up with oil and the pressure increased up to the required value $\sigma_2 = p$. This value was determined with the help of the correlation

$$P_p = (d_r^2 \pi p)/4,$$

using the diameter d_r ($\varnothing$ 20 mm) of the compression rod and reading off the values on the dynamometer. Adjustment occurred by regulating manually the hydraulic supply unit and observing its manometer.

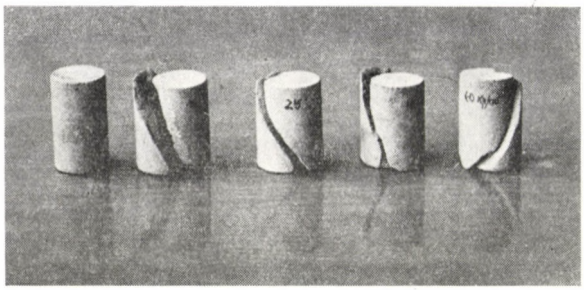


Fig. 8. Specimens fractured at various cell pressures. Left: intact specimen

7. The lever mechanism was balanced by increasing carefully the water load and was set on the specimen. At this stage the axial force F acting on the specimen was zero, and the dynamometer indicated the value corresponding to P_p. The displacement meter was now zeroed.

8. The axial loading force F was increased by adjusting the water load with a prescribed rate until the specimen fractured. Meanwhile the dynamometer force $D = P_p + F$ and the displacement ΔL of the compression rod was read off and recorded. The corresponding readings and time data were entered on record.

9. After fracture had occurred, the lever mechanism was lifted and fixed. The pressure was ceased, the oil drained and the cartridge removed from the cell.

10. The cartridge was cleaned from the oil and the fractured specimen removed from it.

11. The angle α between the slipping plane and the end plane was measured on the fractured specimen. The parts of the specimen were replaced, glued together and a picture was taken of it. The specimens were stored till the end of the measurement series (Fig. 8).

7. Analysis of fracture experiments

1. The initial mean diameter d_0 and initial mean height h_0 of the specimen were calculated from the measured and recorded values. The initial average cross-section A_0, the initial average volume V_0, the initial average mass m_0 and the initial average bulk density ϱ_0 were also calculated.

2. The axial force F_f causing fracture was calculated as follows:

$$F_f = D_f - P_p,$$

hence the average axial breaking stress:

$$\sigma_f = p + \frac{F_f}{A_0} = p + \frac{D_f - P_p}{A}$$

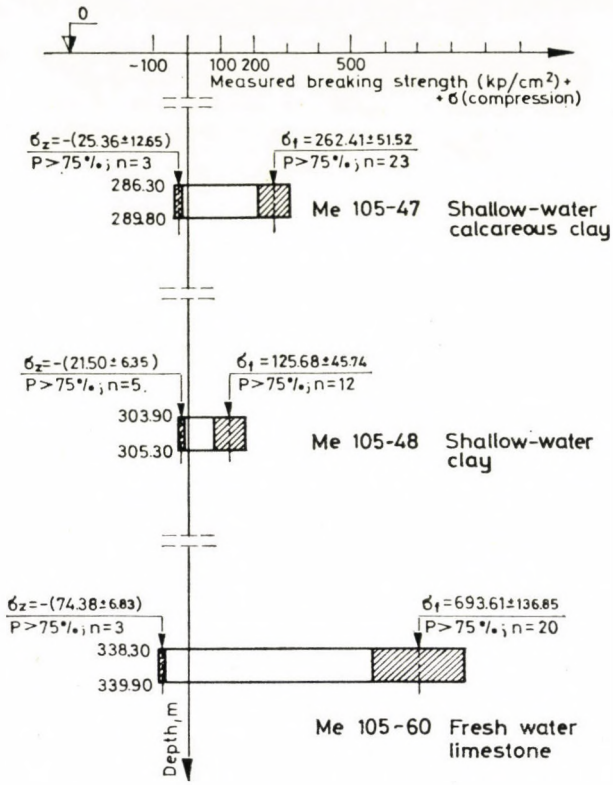


Fig. 9. Scattering bands of compressive and tensile strength values corresponding to $P > 75\%$. The data originate from uniaxial compression fracture tests performed axially and along the edges of specimens cut out from core samples of the drilling Me 105

with

$$p = \frac{P_p}{A_r} = \frac{P_p}{\frac{d_r^2 \pi}{4}} .$$

3. MOHR's circle with values $\sigma_1 \approx \sigma_f$ and $\sigma_2 \approx p$ was drawn in the (σ, τ) co-ordinate system (using suitable scale) in order to illustrate the state of fracture stress (σ_1, σ_2).

4. The above procedure was applied to all measurements of the series and an envelope was fitted to the series of Mohr's circles, thus the fracture boundary curve $\tau(\sigma)$ was obtained. If this curve does not deviate too strong from a straight line, it can be replaced by the latter.

5. The constants Φ and c were determined according to the equation of the fracture boundary curve. In practice, the sizes of Mohr's circles scatter because of the scattering of the strength values of the specimens. For this reason, while drawing the envelope, one has to face certain difficulties. Only

a band can be determined in which the envelop lies with a high probability. In estimating the slope Φ of the boundary curve, the angle α of the slipping plane measured on the specimen, has been used for checking. Their correlation is:

$$\Phi \approx 2\sigma - 90°.$$

If the specimens were under tension, it is not advisable to extrapolate the straight line.

6. The values obtained as outlined above, have been considered as strength characteristics furnished by quick triaxial fracture experiments on non-dehydrated specimens.

Figures 9—11 illustrate strength values determined by uniaxial fracture experiments on core samples extracted from drillings in the Nagyegyháza basin.

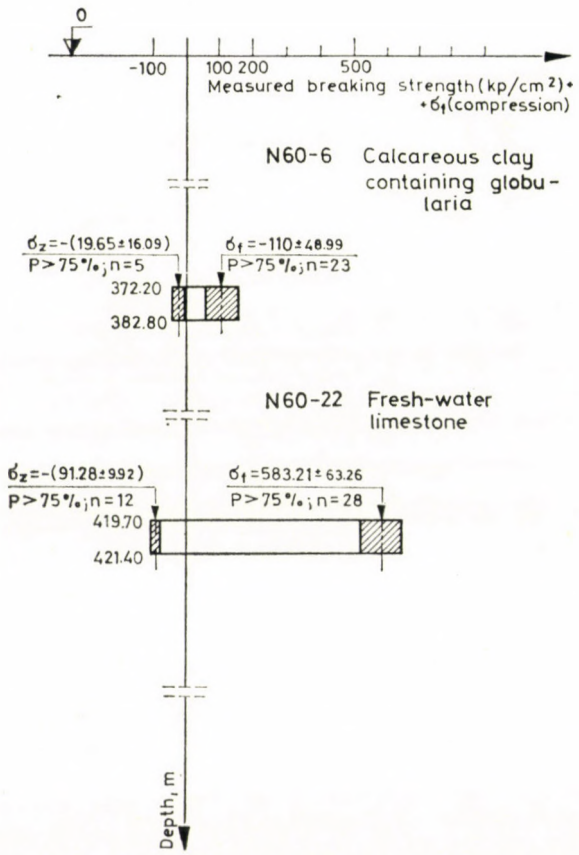


Fig. 10. Scattering bands of compressive and tensile strength values corresponding to $P > 75\%$. The data originate from uniaxial compression fracture tests performed axially and along the edges of specimens cut out from core samples of the drilling N 60

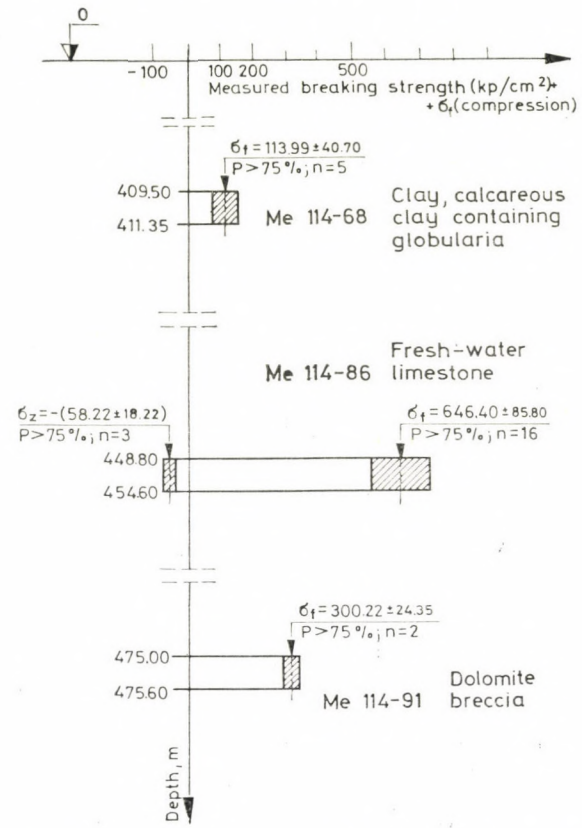


Fig. 11. Scattering bands of compressive and tensile strength values corresponding to $P > 75\%$ The data originate from uniaxial compression fracture tests performed axially and along the edges of specimens cut out from core samples of the drilling Me 114

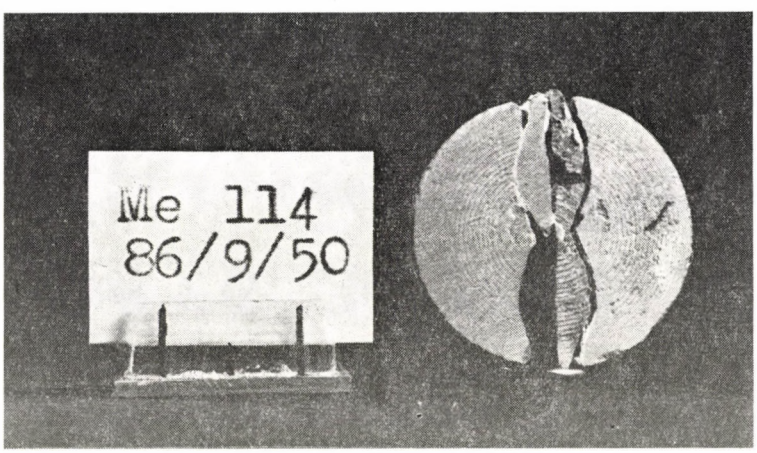


Fig. 12. Fractured fresh-water limestone specimen (Breaking force $F = 525$ kp)

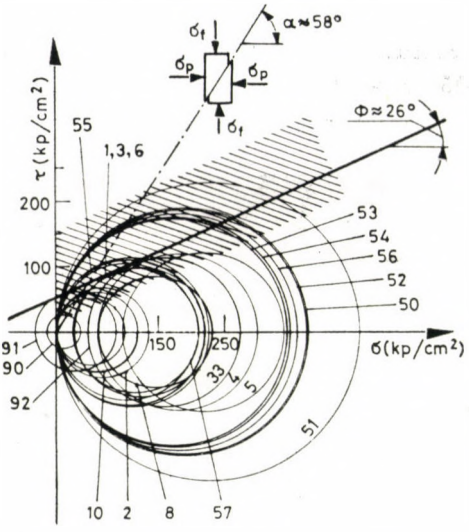


Fig. 13. Shallow-water calcareous clay



Fig. 14. Fractured shallow-water calcareous clay specimen

The values of the tensile strength were determined by the so-called fracture test along an edge. This means that the specimen had been loaded by loads perpendicular to two opposite generatrices. From the force F causing the fracturing of the specimen, values of stress

$$\sigma_{fA} = 3\frac{2F}{d\pi h}$$

and

$$\sigma_h = -\frac{2F}{d\pi h}$$

were calculated (Table II). A fresh-water limestone specimen is shown in Fig. 12 after having been fractured along an edge.

Figures 13—15 show shallow-water calcareous clay specimens and the deterioration boundary curve determined by triaxial experiments.

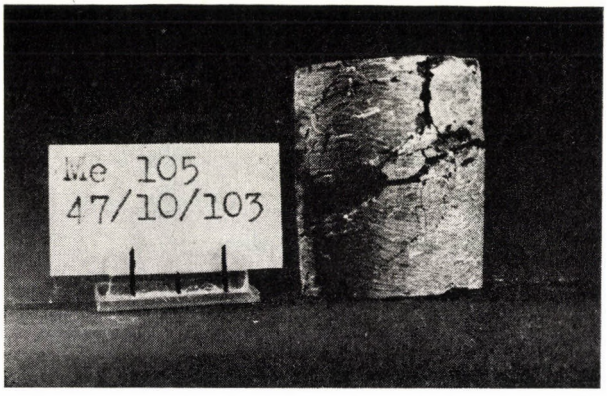


Fig. 15. Barrelling of the fractured specimen

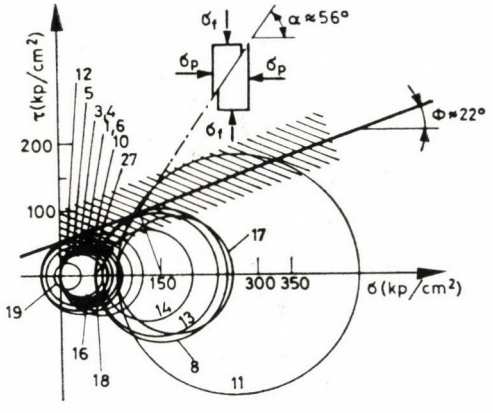


Fig. 16. Measurement results: shallow-water clay (Nagyegyháza, Me 105)

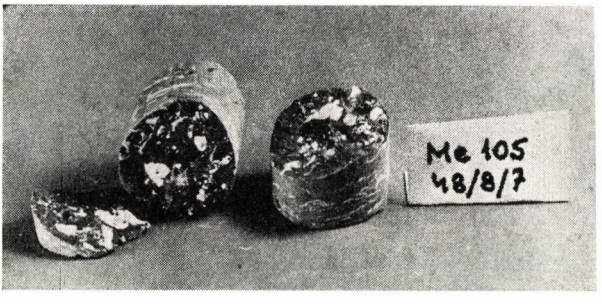


Fig. 17. Specimen split into two along lamination

Figure 16 illustrates Coulomb's straight line of shallow-water clay. Figure 17 shows a specimen of this series of experiments which was split into two along lamination. General deterioration can be seen in Figure 18. Figures 19—24 illustrate some results and broken specimens of the Nagyegyháza experiments.



Fig. 18. General deterioration

Table I displays the estimated values of the parameters of Coulomb's fracture boundary condition.

The specimens used in the experiments were of various length diameter ratios. They had practically the same diameter $d \approx 20$ mm and various heights. The diameters of the specimens did not scatter very much after having been cut by a crown bit, but their length was affected by the ambition to have plane and smooth end surfaces. The effect of the various ratios was ignored in calculating the values of the breaking strength.

The effect of the stumpiness of the specimens on the breaking strength was investigated by plotting the measured and calculated values of the breaking strength σ_f *vs.* the ratio d/h. Then the straight line was determined which could be fitted to this series of points. The equation of this straight line is in the $(\sigma_f, d/h)$ co-ordinate system:

$$\sigma_f = \sigma_{f\infty} + A \frac{d_0}{h_0},$$

where d_0 and h_0 are the mean diameter and height of the specimen "before experiment". In the case of combined measurements, when the dimensions of the specimen were determined before several measurement periods, the values refer to the last measurement before fracture. The value $\sigma_{f\infty}$ is the breaking strength extrapolated to the infinite long specimen.

Table I

	Specimen	Material	$\alpha°$	$\Phi°$	tan Φ	c_{min}	c_{max}
Me	105—47/9	Shallow-water	48	6	0.10	60	170
Me	105—47/10	calcareous clay	58	26	0.48	10	150
Me	105—47/11		59	28	0.53	50	120
Me	150—48/8	Shallow-water	56	22	0.40	15	100
Me	105—48/9	clay	47	4	0.07	5	50
Me	105—48/10		47	4	0.07	75	140
Me	105—60/14	Fresh-water	60	30	0.57	40	220
Me	150—60/15	limestone	63	36	0.72	50	300
Me	105—60/16		55	20	0.36	50	300
N	60—6/4	Calcareous clay	55	20	0.36	25	100
N	60—6/5	containing	50	10	0.17	10	300
N	60—6/6	Globularia	50	10	0.17	30	110
N	60—6/14		54	18	0.32	10	30
N	60—22/13	Fresh-water	60	30	0.57	80	250
N	60—22/14	limestone	60	30	0.57	70	230
N	60—22/15		65	40	0.83	50	120
Me	114—68	Clay, calcareous clay containing Globularia	53	16	0.28	10	60
Me	114—86/5	Fresh-water	50	10	0.17	100	300
Me	114—86/6	limestone	60	30	0.57	100	300
Me	114—86/9		60	30	0.57	100	230
Me	114—91/3	Dolomite breccia	65	40	0.83	25	100

Table II

Seam	Material	Seam strength σ_{fA} (kp/cm²)	P (%)	n (pc.)	Breaking strength σ_f (kp/cm²)	n (pc.)
Me 105—47	Shallow-water calcareous clay	262.41 ± 51.52	75	23	$105 + 162 \frac{d}{h}$	28
Me 105—48	Shallow-water clay	125.68 ± 45.74	75	12	$1.86 + 186 \frac{d}{h}$	18
Me 105—60	Fresh-water limestone	693.51 ± 136.85	75	20	$729 - 3.16 \frac{d}{h}$	20
N 60—6	Calcareous clay containing Globularia	110 ± 48.99	75	23	$1.44 + 141 \frac{d}{h}$	27
N 60—22	Fresh-water limestone	583.21 ± 63.26	75	28	$585 + 15.6 \frac{d}{h}$	29
Me 114—86	Fresh-water limestone	646.40 ± 85.80	75	16	$644 + 9.6 \frac{d}{h}$	18

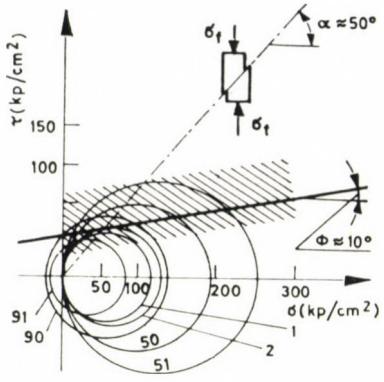


Fig. 19. Measurement results: calcareous clay containing Globularia (Nagyegyháza, N 60)

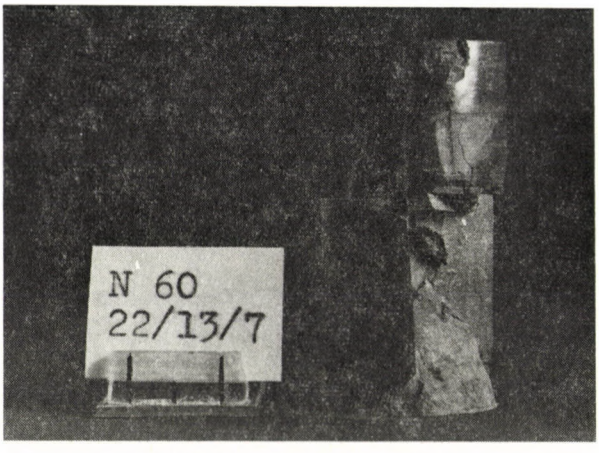


Fig. 20. Deteriorated specimen

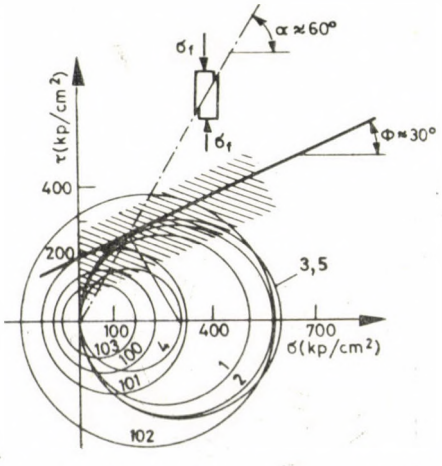


Fig. 21. Measurement results: fresh-water limestone (Nagyegyháza, N 60)

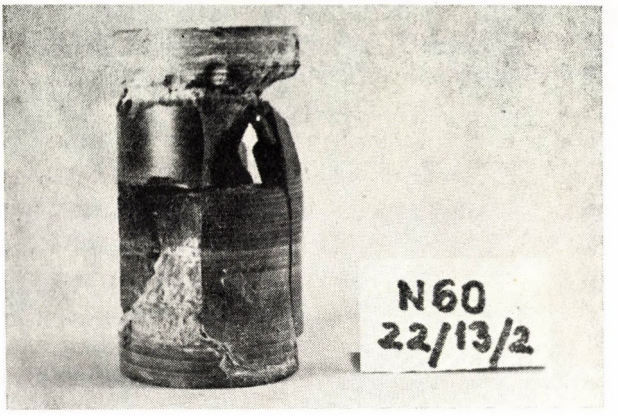


Fig. 22

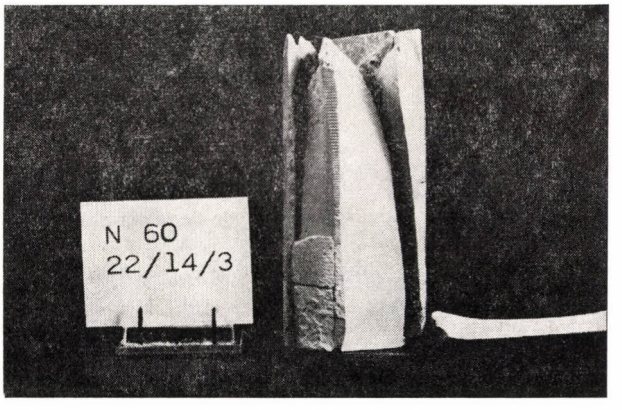


Fig. 23. Curved splits

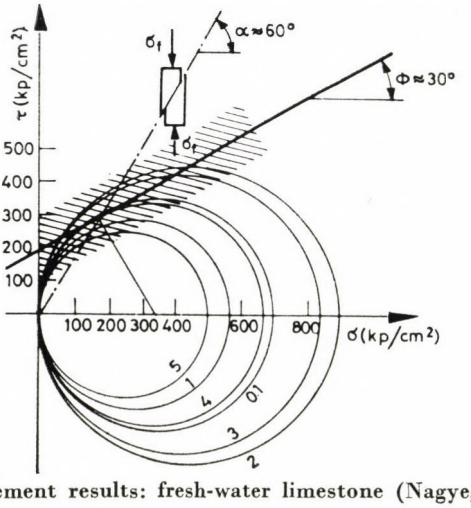


Fig. 24. **Measurement results: fresh-water limestone (Nagyegyháza Me 114)**

Further, the regression straight line R was determined, i.e. having exchanged the variables, a straight line was fitted to the points. The correlation coefficient, too, was calculated. The number n of the points taken account of in the calculation, was slightly different from the number of points used in calculating σ_{fA}. In the case of fresh-water limestones there was only a weak correlation between the breaking strength σ_f and the ratio d/h of the specimen. However, the measurable breaking strength of clay and calcareous clay was strongly affected by the ratio d/h of the specimen. This problem needs further investigation so much the more as the correlation was investigated only on specimens of diameters around Φ 20 mm. The results are displayed in Table II. Here P means the confidence level (%) and n is the number of measurements.

8. The number of experiments needed

Measuring a given parameter, e.g. σ_f, several times, the results obtained scatter, i.e. the individual values σ_{fi} usually differ from each other. The actual value of σ_f can be determined with a probability P from the measurement results σ_{fi} of number n as follows. The fact that the actual value of σ_f lies between the limits $(\overline{\sigma}_f + U_{\sigma f})$ and $(\sigma_f - U_{\sigma f})$ with a probability P, will be written:

$$\begin{cases} \sigma_f = \overline{\sigma}_f \pm U_{\sigma f} \\ P = P(|\overline{\sigma}_f - \sigma_{fi}| < U_{\sigma f}) > \left(1 - \dfrac{1}{t^2}\right), \\ n \end{cases}$$

Here $\overline{\sigma}_f$ means the expected value of the values σ_{fi} of number n:

$$\overline{\sigma}_f = \frac{\sum_{i=1}^{m} \sigma_{fi}}{n}$$

and

$$U_{\sigma f} = \frac{t \cdot D^*(\sigma_{fi})}{\sqrt{n}}$$

is the confidence limit, where t is an arbitrary number greater than one. $D^*(\sigma_{fi})$ is the sample standard deviation:

$$D^*(\sigma_{fi}) = \sqrt{\frac{\sum_{i=1}^{m} (\overline{\sigma}_f - \sigma_{fi})^2}{n - 1}}.$$

The value of probability P was calculated by CHEBISHEV's inequality, because the exact characteristics of the scattering are not well-known. This expresses

the following: the probability that the absolute value of the deviation between σ_{fi} and the average value σ_f is less than $U_{\sigma f}$ is greater than $1-(1/t^2)$. If t, called confidence coefficient, is chosen for 2, a probability higher than 75% is obtained. From the expression of P it can be written that

$$n > \left[\frac{t \cdot D^*(\sigma_{fi})}{\overline{\sigma}_f - \sigma_{fi}}\right]^2,$$

$$P > \left(1 - \frac{1}{t^2}\right).$$

This means, that if the number n of the measurements is greater than the expression on the R.H.S., the probability that the error

$$e = |\overline{\sigma}_f - \sigma_{fi}|$$

is less than a value having been put into the denominator, is greater than $1-(1/t^2)$.

9. Parameters influencing the measurement results

In fact, the specimen is a real body, not exactly homogeneous and isotropic, thus the values σ_x, σ_y and σ_z are not exact principal between the face plane of the specimen and the plate pressing upon the latter (anvil and compression rod, respectively). This hinders the face plane to deform freely, it becomes practically "clamped". This causes a barrel-like shape of the specimen (this is the reason of the problems in evaluating the measurement results of the transverse deformation). The other problem caused by the friction is that the specimen seems to have a higher strength than in reality. Because of these circumstances, the value of σ_f calculated with the above method, depends on the geometrical relations, further on the absolute dimensions of the specimen.

In consequence, none of the requirements of the evaluation assumed while planning the experiments, are fully met. However, the results obtained by the above experiments and calculation method give, in many cases, good approximate values, well usable in practice. While using these values, criticism is needed in taking account of the differences between ideal and real circumstances. If necessary, the results obtained have to be subjected to correction procedures in order to bring them closer to the real circumstances.

Porous materials e.g. do not meet the assumption of homogeneity. The pores are filled with gases and liquid. These phases start to flow in the more or less interconnected pore system, due to the pressure differentials caused by the deformation of the body. This influences the strength of the body considerably. The rocks are always porous; their porosity lies between 1 and 20%. The pore pressure u of the phase filling the pores contributes to carrying the load. However, this contribution changes if the pore pressure is altered because

of material flow or departure from the pores. Triaxial experiments have to be performed even in such cases, but the pore pressure u also has to be measured and MOHR's circle has to be corrected by setting its diameter to $(\sigma_f - u) - (\sigma_p - u)$. High porosity influences strongly the measurable breaking strength of the body, since the major part of the total volumetric deformation of the body is due to the deformation of the pore structure. At the same time the volume of the solid phase changes only slightly. Thus the porosity characteristic can change considerably during loading. To avoid this problem, new tendencies can be recognized (Roscoe) in trying to characterize the breaking strength by a boundary surface $\psi(\tau, \sigma, e)$ instead of $\tau(\sigma)$ boundary curve. Here e means one of prosity characteristics, e.g. pore number, i.e. the reciprocal of porosity. The procedure represents an approximation of the theory applied to Hooke's body, towards the real test results.

The parameters characterizing the fracture of rock samples scatter rather widely. The statistical evaluation can be done properly, only if relying upon a satisfactorily great number of experiments. If the material available for shaping specimens is not in abundance, e.g. in the case of core samples, it is more advantageous to prepare several but smaller specimens instead of fewer but bigger ones.

Nevertheless, in order to ensure the comparability of the results, it is necessary to establish the relation between the breaking strength of specimens prepared by the method outlined above, resp. their dimensions and height-diameter ratio.

It is our intention to carry out triaxial tests more accurately in future experiments. The measurement of transverse deformation is satisfactorily accurate only in the case of rigid materials but even here it is rather complicated. Accordingly to bibliography, measurement of the change of volume may give more accurate results. However, established methods are available only for specimens which can be saturated. The determination of deformation characteristics e.g. YOUNG's modulus and POISSON's ratio in this way is cumbersome.

Long-period triaxial experiments (creep, relaxation) seem to be more promising for the determination of the deformation characteristics. In this type of experiments, the greatest problem is to maintain the experimental conditions, first of all pressure and temperature for a long period and to ensure the stability of the recording instrument. Nevertheless, the time-dependent character of strength properties force us to carry out such experiments. In quick experiments, the correlation between the breaking strength and the rate of loading has to be cleared. A similar problem is the dependence on some main material properties, e.g. humidity, etc. Of course, a great number of measurement data is required to ensure a reliable analysis of the complex experiments.

REFERENCES

1. Asszonyi, Cs.: On a new theory of rock mechanics. *Acta Geod. Geoph. Mont. Hung.*, 8 (1974), 313–322.
2. Asszonyi, Cs.: Mechanical theory of continua. *Acta Geod. Geoph. Mont. Hung.*, 8 (1974), 323–360.
3. Asszonyi, Cs.: On a rheological theory of rock continua. Doctor's Thesis. Hungarian Academy of Sciences. Budapest 1975.
4. Asszonyi, Cs.: Plastic state and deterioration of rocks. III. Boundary conditions of rock deterioration. *Acta Geod. Geoph. Mont. Hung.*, 13 (1978), 25–42.
5. Asszonyi, Cs.: Laboratory determination of the physical equation and rheological materials constants of rocks. Research Report. Technical University of Heavy Industry, Miskolc 1972, 1–52.
6. Asszonyi, Cs.–Csorba, L.–Huszár, I.–Müller, Z.–Kapolyi, L.–Richter R.: Laboratory determination of rock constants using relaxation tests. *Tatabányai Szénbányák Műszaki Közgazdasági Közleményei*, No. 4, 1974, 163–169.
7. Asszonyi, Cs.–Huszár, I.–Kapolyi, L.: Laboratory determination of rock constants using creep tests. *Tatabányai Szénbányák Műszaki Közgazdasági Közleményei*, No. 4, 1971, 177–182.
8. Asszonyi, Cs.–Balássy, Z.–Huszár, I.–Kapolyi, L.: Laboratory determination of rock characteristics using triaxial tests. *Bányászati és Kohászati Lapok — Bányászat*, 10 (1977), 651–659.
9. Asszonyi, Cs.–Kapolyi, L.–Richter, R.: Laboratory determination of mechanical characteristics of rocks. *Tatabányai Szénbányák Műszaki Közgazdasági Közleményei*, No. 1, 1972, 16–23.
10. Huszár, I.: Strength and rheological measurements on some core samples of drillings in the Nagyegyháza basin. Research Report, University of Agriculture, Gödöllő 1975, 1–259.

IV. ЭКСПЕРИМЕНТЫ С ТРЕХОСНЫМ РАЗЛОМОМ

Ч. АССОНИ–И. ХУСАР–Л. КАПОЙИ

РЕЗЮМЕ

В статье кратко резюмируются главные точки зрения трёхосного разлома цилиндрических пробных тел в пространстве с жидкостным давлением и указывается на сегодняшнее использование метода при изучении горных пород. Показывается представитель семьи оборудования, разработанного для экспериментов и описываются эксперименты с трёхосным разломом на нем.

RECENSIO

ENERGETICS OF GEOLOGICAL PROCESSES
Hans Ramberg on his 60th birthday
Editors: *Saxena, S. K., Bhattacharji, S.*
Associate Editors: *Annersten, H., Stephansson, O.*
Berlin—Heidelberg—New York: Springer Verlag
ISBN 3-540-08119-4
148 figs., 31 tables. XVIII, 473 pages. 1977.
Cloth DM 64.70; USA $ 28.50

With this book the friends of Prof. H. Ramberg congratulate him, the famous Norvegian geoscientist on his sixtieth birthday. Prof. Ramberg's scientific work has centered around the application of basic physics (in his case thermodynamics and mechanics) to the problems of petrology and tectonics. One of the main result of his researches is the book:

"The Origin of Metamorphic and Metasomatic Rocks", which treated many problems in mineral chemistry related to the structures and assemblages of metamorphic rocks and what the petrogenetic significance of these are.

About this jubilee volume the editors write in the Preface: "The title and division of this volume into broad categories, geodynamics and geochemistry, illustrate the important fields in which the influence of Professor Ramberg as a pioneering researcher and teacher has had its greatest scientific impact". Original researches, reviews and ideas of the contributors have been compiled in the fields of geodynamics, structural geology, geochemistry and petrology without any logical order beyond the broad subdivisions. The Part I, Energetics of Geodynamic Processes consists of 10 contributions and the Part II, Energetics of Geochemical Processes consists of 8 contributions. Most of them are in connection of the scientific research work of Prof. Ramberg. For the sake of a short information about the contents we mention here some key words from the most interesting papers without claim of the fullness: gravitational instability and the structure of continents, geometric patterns of active strike-slip faults; metamorphic rocks in orogenic belts; subduction-zone ophiolites and island-arc ophiolites; disproportion equilibrium in ironbearing systems; thermodynamic control of metamorphic rocks; from crucibles through subduction to batholites, etc. These topics represent a wide area of the geoscience catalyzed by Prof. Ramberg for his active 30 years.

The book is worthy of Professor Ramberg's jubilee.

A. Ádám

INDEX

Asszonyi, Cs.—Kapolyi, L.—Richter, R.: Laboratory determination of rock characteristics. I. Uniaxial compression tests 313

Asszonyi, Cs.—Kapolyi, L.—Huszár, I.: II. Determination of rock characteristics using rheological creep investigation 341

Asszonyi, Cs.—Huszár, I.—Richter, R.: III. Determination of rock characteristics using relaxation tests 361

Asszonyi, Cs.—Huszár, I.—Kapolyi, L.: IV. Triaxial facture tests 379

Recensio 403

Printed in Hungary

A kiadásért felel az Akadémiai Kiadó igazgatója — Műszaki szerkesztő: Zacsik Annamária

A kézirat nyomdába érkezett: 1978. VIII. 28. — Terjedelem: 8,4 (A/5) ív, 87 ábra

79.6247 Akadémiai Nyomda, Budapest — Felelős vezető: Bernát György

Acta Geodaetica, Geophysica et Montanistica ist eine Halbjahresschrift der Ungarischen Akademie der Wissenschaften. Sie veröffentlicht Originalbeiträge aus dem Bereich der Geodäsie, Geophysik und des Bergbaus in deutscher, englischer, französischer oder russischer Sprache.

Redaktion: H-9400 Sopron, Múzeum u. 6.

Jahresabonnementspreis: $ 36.00.

Bestellbar bei »Kultura« Außenhandelsunternehmen (1389 Budapest 62, P.O.B. 149) oder seinen Auslandsvertretungen.

Acta Geodaetica, Geophysica et Montanistica est une revue semestrielle de l'Académie des Sciences de Hongrie publiant des essais originaux du domaine de la géodésie, géophysique et des sciences minières en français, anglais, allemand et russe.

Rédaction: H-9400 Sopron, Múzeum u. 6.

Prix de l'abonnement: $ 36.00 par an.

On peut s'abonner à l'Entreprise du Commerce Extérieur «Kultura» (1389 Budapest 62, P.O.B. 149) ou chez ses représentants à l'étranger.

Acta Geodaetica, Geophysica et Montanistica выходят два раза в год в издании Академии наук Венгрии. В журнале публикуются оргнгинальные исследования по проблемам геодезии, геофизики и горного дела на русском, английском, немецком и французском языках.

Адрес редакции: **H-9400 Sopron, Múzeum u. 6.**

Подписная цена на год: $ 36,00.

Заказать журнал через Внешнеторговое предприятие «Kultura» (1389 Budapest 62, P. O. B. 149) или через его заераничные представительства.

Reviews of the Hungarian Academy of Sciences are obtainable at the following addresses:

AUSTRALIA
C.B.D. LIBRARY AND SUBSCRIPTION SERVICE, Box 4886, G.P.O., *Sydney N.S.W. 2001*
COSMOS BOOKSHOP, 145 Ackland Street, *St. Kilda (Melbourne), Victoria 3182*

AUSTRIA
GLOBUS, Höchstädtplatz 3, *1200 Wien XX*

BELGIUM
OFFICE INTERNATIONAL DE LIBRAIRIE, 30 Avenue Marnix, *1050 Bruxelles*
LIBRAIRIE DU MONDE ENTIER, 162 Rue du Midi, *1000 Bruxelles*

BULGARIA
HEMUS, Bulvar Ruszki 6, *Sofia*

CANADA
PANNONIA BOOKS, P.O. Box 1017, Postal Station "B", *Toronto, Ontario M5T 2T8*

CHINA
CNPICOR, Periodical Department, P. O. Box 50 *Peking*

CZECHOSLOVAKIA
MAD'ARSKÁ KULTURA, Národní třida 22, *115 66 Praha*
PNS DOVOZ TISKU, Vinohradská 46, *Praha 2*
PNS DOVOZ TLAČE, *Bratislava 2*

DENMARK
EJNAR MUNKSGAARD, Norregade 6, *1165 Copenhagen*

FINLAND
AKATEEMINEN KIRJAKAUPPA, P. O.Box 128, *SF-00101 Helsinki 10*

FRANCE
EUROPÉRIODIQUES S. A., 31 Avenue de Versailles, *78170 La Celle St. Cloud*
LIBRAIRIE LAVOISIER, 11 rue Lavoisier, *75008 Paris*
OFFICE INTERNATIONAL DE DOCUMENTATION ET LIBRAIRIE, 48 rue Gay-Lussac, *75240 Paris Cedex 05*

GERMAN DEMOCRATIC REPUBLIC
HAUS DER UNGARISCHEN KULTUR, Karl-Liebknecht-Strasse 9, *DDR-102 Berlin*
DEUTSCHE POST ZEITUNGSVERTRIEBSAMT, Strasse der Pariser Kommüne 3—4, *DDR-104 Berlin*

GERMAN FEDERAL REPUBLIC
KUNST UND WISSEN ERICH BIEBER, Postfach 46, *7000 Stuttgart 1*

GREAT BRITAIN
BLACKWELL'S PERIODICALS DIVISION, Hythe Bridge Street, *Oxford OX1 2ET*
BUMPUS, HALDANE AND MAXWELL LTD., Cowper Works, *Olney, Bucks MK46 4BN*
COLLET'S HOLDINGS LTD., Deningston Estate, *Wellingborough, Northants NN8 2QT*
WM. DAWSON AND SONS LTD., Cannon House, *Folkestone, Kent CT19 5EE*
H. K. LEWIS AND CO., 136 Gower Street, *London WC1E 6BS*

GREECE
KOSTARAKIS BROTHERS, International Booksellers, 2 Hippokratous Street, *Athens-143*

HOLLAND
MEULENHOFF-BRUNA B.V., Beulingstraat 2, *Amsterdam*
MARTINUS NIJHOFF B.V., Lange Voorhout 9—11, *Den Haag*
SWETS SUBSCRIPTION SERVICE, 347b Heereweg, *Lisse*

INDIA
ALLIED PUBLISHING PRIVATE LTD., 13/14 Asaf Ali Road, *New Delhi 110001*
150 B-6 Mount Road, *Madras 600002*
INTERNATIONAL BOOK HOUSE PVT. LTD., Madame Cama Road, *Bombay 400039*
THE STATE TRADING CORPORATION OF INDIA LTS., Books Import Division, Chandralok, 36 Janpath, *New Delhi 110001*

ITALY
EUGENIO CARLUCCI, P.O. Box 252, *70100 Bari*
INTERSCIENTIA, Via Mazzé 28, *10149 Torino*
LIBRERIA COMMISSIONARIA SANSONI, Via Lamarmora 45, *50121 Firenze*
SANTO VANASIA, Via M. Macchi 58, *20124 Milano*
D. E. A., Via Lima 28, *00198 Roma*

JAPAN
KINOKUNIYA BOOK-STORE CO. LTD., 17-7 Shinjuku-ku 3 chome, Shinjuku-ku, *Tokyo 160-91*
MARUZEN COMPANY LTD., Book Department, P.O. Box 5050 Tokyo International, *Tokyo 100-31*
NAUKA LTD. IMPORT DEPARTMENT, 2-30-19 Minami Ikebukuro, Toshima-ku, *Tokyo 171*

KOREA
CHULPANMUL, *Phenjan*

NORWAY
TANUM-CAMMERMEYER, Karl Johansgatan 41—43, *1000 Oslo*

POLAND
WĘGIERSKI INSTYTUT KULTURY, Marszałkowska 80, *Warszawa*
CKP I V ul. Towarowa 28 *00-958 Warszawa*

ROUMANIA
D. E. P., *Bucureşti*
ROMLIBRI, Str. Biserica Amzei 7, *Bucureşti*

SOVIET UNION
SOJUZPETCHATJ — IMPORT, *Moscow*
and the post offices in each town
MEZHDUNARODNAYA KNIGA, *Moscow G-200*

SPAIN
DIAZ DE SANTOS, Lagasca 95, *Madrid 6*

SWEDEN
ALMQVIST AND WIKSELL, Gamla Brogatan 26, *101 20 Stockholm*
GUMPERTS UNIVERSITETSBOKHANDEL AB, Box 346, *401 25 Göteborg 1*

SWITZERLAND
KARGER LIBRI AG, Petersgraben 31, *4011 Basel*

USA
EBSCO SUBSCRIPTION SERVICES, P. O. Box 1943, *Birmingham*, Alabama *35201*
F. W. FAXON COMPANY, INC., 15 Southwest Park, *Westwood, Mass. 02090*
THE MOORE-COTTRELL SUBSCRIPTION AGENCIES, *North Cohocton, N. Y. 14868*
READ-MORE PUBLICATIONS, INC., 140 Cedar Street, *New York, N. Y. 10006*
STECHERT-MACMILLAN, INC., 7250 Westfield Avenue, *Pennsauken N. J. 080110*

VIETNAM
XUNHASABA, 32, Hai Ba Trung, *Hanoi*

YUGOSLAVIA
JUGOSLAVENSKA KNJIGA, Terazije 27, *Beograd*
FORUM, Vojvode Mišica 1, *21000 Novi Sad*

22. VI. 1979 HU ISSN 0374—1842 **Index: 26.031**

Acta GEODAETICA, GEOPHYSICA et MONTANISTICA

ACADEMIAE SCIENTIARUM HUNGARICAE

ADIUVANTIBUS
G. BARTA
J. VERŐ
J. ZAMBÓ
REDIGIT
A. TÁRCZY-HORNOCH

AKADÉMIAI KIADÓ, BUDAPEST

TOMUS 14
FASCICULUS 4
1979

ACTA GEODAETICA, GEOPHYSICA et MONTANISTICA

Academiae Scientiarum Hungaricae

A Magyar Tudományos Akadémia Föld- és Bányászati Tudományok Osztályának folyóirata

Szerkesztőség: H-9400 Sopron, Múzeum u. 6.
Kiadja az Akadémiai Kiadó, 1054 Budapest, Alkotmány utca 21.

Az *Acta Geodaetica, Geophysica et Montanistica* eredeti tanulmányokat közöl a geodézia, geofizika és a bányászati tudományok tárgyköréből, angol, német, francia vagy orosz nyelven Félévenként jelenik meg, évi egy, kb. 400—500 oldalas kötetet alkotva.

Megrendelhető az Akadémiai Kiadónál (1363 Budapest Pf. 24.), a külföld részére pedig a „Kultura" Külkereskedelmi Vállalatnál (1389 Budapest 62, P.O.B. 149).

Acta Geodaetica, Geophysica et Montanistica is a semiannual review of the Hungarian Academy of Sciences, publishing papers on geodesy, geophysics and minings in English, German, French or Russian.

Editorial Office: H-9400 Sopron, Múzeum u. 6.

Subscription: $ 36.00 per year.

Orders may be placed with "Kultura" Foreign Trading Company (1389 Budapest 62, P.O.B. 149) or its representatives abroad.

Acta Geodaet., Geophys. et Montanist. Acad. Sci. Hung. Tomus 14 (4), pp. 405—416 (1979)

SOME PROBLEMS OF THE CONNECTION OF NETWORKS DEDUCED FROM SATELLITE OBSERVATIONS AND OF TERRESTRIAL NETWORKS

F. HALMOS
DOCTOR OF TECHNICAL SCIENCES
GEODETIC AND GEOPHYSICAL RESEARCH INSTITUTE OF THE HUNGARIAN ACADEMY OF SCIENCES, SOPRON

[Manuscript received December 19, 1977]

The author deals with the problem of stiffening when connecting satellite and terrestrial geodetic networks. In addition to the accuracy analysis of the measurement methods, the effect of regular errors in geodetic networks of great extension are discussed, and possibilities are shown to moderate their effect in combined networks and in stiffenings, respectively. An analysis of the optimum distribution of stiffening measurements is also presented.

1. Introduction

The quality and stiffness of geodetic networks depend very much on the form of the network, on the density of its points and on the accuracy of angular, distance and height measurements. They depend further on the density and accuracy of certain control measurements and deductions, such as astronomical azimuth determinations, distance measurements with distance meters of exceptionally great range, astrogeodetic position determinations, azimuths deduced from satellite observations (photographic observations), distances (laser satellite observations) and point coordinates (e.g. from Doppler satellite observations), respectively.

In spite of the high accuracy which can be reached by the angular, and even more by the distance measurements ($1 \cdot 10^{-6}$), it should not be forgotten that when crossing huge areas, the errors can reach considerable values due to the error accumulation. If, e.g. the accuracy of the distance measurement is $0.5—1 \cdot 10^{-6}$, the *random error* reaches a value of 0.5—1 m at a distance of 1000 km. The effect of *systematical errors* is even more dangerous. Up to now, the accuracy analysis of geodetic networks has been based on the propagation of random errors. However small the systematical errors are in networks of great extension, their accumulation can yield very high values in certain measurement elements. Taking into account that the lowest possible mean square error of angular measurements is $\pm 0.5—0.6''$, the pure effect of random errors causes a mean square error of the point coordinates of ± 0.5 m at distances of 200—250 km in case of side lengths of 30 km. In contrast, if individual errors occur, only about its one tenth one twentieth part appears in the computed coordinates. Thus, e.g. in case of a bug of 0.5 m is made in a distance measurement, the

error is distributed between the coordinates and it causes only coordinate errors of 3—4 cm. A systematical error of 1 mm/km, however, causes in case of distances of 1000 km-s a coordinates error similar to a random error of ± 20 cm of the distance measurements on 30 km long sides, i.e. an error of about 1.0—1.1 m.

In national networks of very great extension, such as the Soviet triangular network, the mean square error of the coordinates reaches a value of ± 1.0—1.2 m in a distance of 1000 km from the origine of the coordinates [18]. In an up-to-date network lying inside of a circle with a radius of 250 km, the coordinate errors in respect to the origine in the centre are about ± 0.5—0.7 m.

2. Stiffening of the networks

The stiffening of triangular networks has been carried out up to now by azimuths (orientations), distances (scale) and measurements of the geographical longitude and latitude. It is interesting to note that the basic form of the networks has remained the triangle in spite of the considerable advantages offered by the *diagonal quadrangle* from the point of view of error propagation. This is supposedly partly due to difficulties in the construction of the network (higher demands in visibility), but it is more likely that it remained so due to the older adjustment method according to conditional observations. The adjustment is at present already everywhere made according to the observation equations

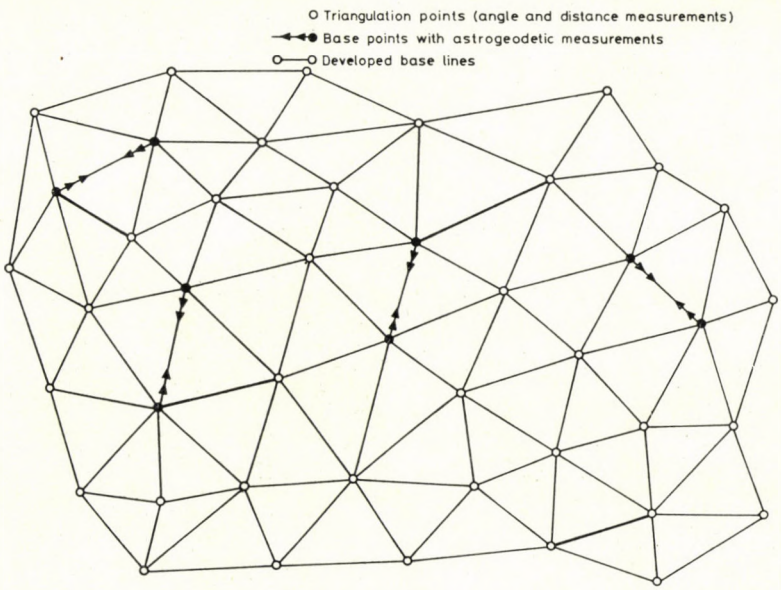


Fig. 1

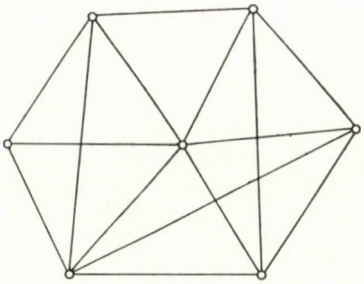


Fig. 2

using computers, and that means that all discomforts of the computations are avoided, and the method of the observation equations is uniform, be the measurement results of any kind (Figs 1 and 2).

With the development of the up-to-date technique of Doppler satellite observations and their increasing accuracy, an economical and advantageous possibility is being offered, for the connection of terrestrial networks (which themselves can be enough stiff). It should be remarked that by distributing the Doppler satellite points on the surface of the network parts to be connected, 7 parameters (6 translation parameters and the scale factor) can be determined. The deviation between the parameters will be less. In such a manner, Doppler points ensure an indirect stiffening of the network anyway. The point error which can be reached at present with Doppler satellite measurements is about ± 0.5 m [1, 4, 6]. Theoretical investigations were published in [7, 13] (Fig. 3).

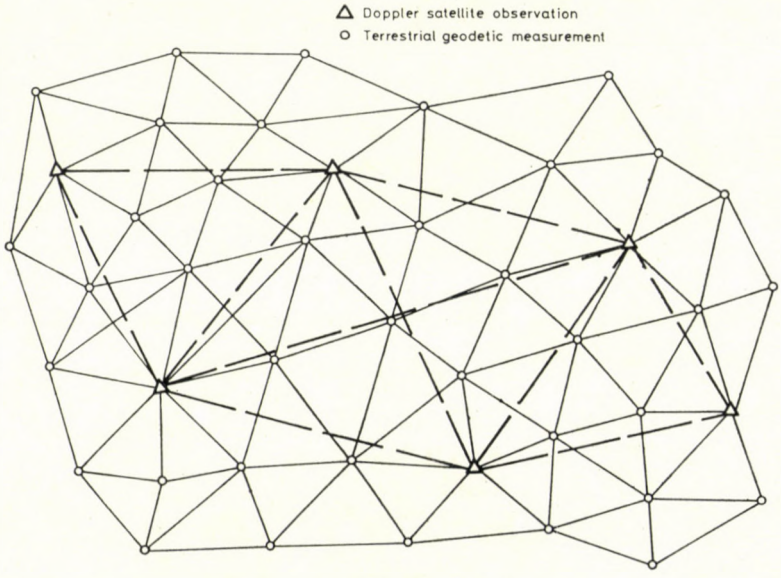


Fig. 3

The problem is what a density of the Doppler points is necessary to ensure a reliable connection and stiffening of terrestrial networks. According to WOLF's investigations [20], in a common adjustment of a terrestrial network and of Doppler points, the values of the coefficients of the reduced normal equation show the importance for the common adjustment of the data received with different measurement methods. If the reduced normal coefficient of a Doppler satellite observation is denoted by $\overline{N}_S$, the mean square error for unit weight by μ_S, those from terrestrial observations by $\overline{N}_T$ and by μ_T, respectively, the free terms by L_S and by L_T, then the following reduced normal equation results with the common unknown y:

$$\left(\frac{\overline{N}_S}{\mu_S^2} + \frac{\overline{N}_T}{\mu_T^2}\right) y + \left(\frac{L_S}{\mu_S^2} + \frac{L_T}{\mu_T^2}\right) = 0 \tag{1}$$

If

$$\frac{\overline{N}_S}{\mu_S^2} \to 0, \text{ then } Y = -\overline{N}_T^{-1}\,\overline{N}\,L_T \tag{2}$$

and

$$\frac{\overline{N}_T}{\mu_T^2} \to 0, \text{ then } y = -\overline{N}_S^{-1}\,L_S \tag{3}$$

respectively.

From the difference of the normal coefficients and the difference of the free terms it can be seen what is the neglection in the two cases. If the coefficient resulting from the Doppler satellite observation is much greater than that from the terrestrial observations, the latter can be even neglected and vice versa. However, the advantages from the connection of several networks in respect of the Doppler satellite observations should also be taken into account.

According to some preliminary error analyses made hitherto and taking into account the known accuracy data of both measurement methods, the following conclusions can be drawn considering also the problems of the stiffening of networks:

If the distance between Doppler satellite measurements is less than 100 km, then the data from terrestrial measurements are more accurate [6, 7] (the transition from the two-dimensional terrestrial network to the three-dimensional satellite network will be omitted here), at least in a relative sense, if one takes into account the present accuracy of Doppler satellite measurements.

If the Doppler satellite points are at distances of 150—250 km from each other, then both network types can be taken as of equal accuracy, i.e. the adjustment should be made together.

If the distance between the Doppler satellite points is more than 400 km, then the accuracy of these points influences so much the accuracy that it is unadvantageous to take into account results of terrestrial measurements

(the deviation of the plumb line and the problems of the reduction to the geoid-ellipsoid are naturally to be taken into account). That means that the Doppler satellite network is to be adjusted independently, then when computing the terrestrial network, the Doppler points are considered as predetermined, fixed. According to our computations, if a point error of ± 0.5 m is supposed in the Doppler observations, a direction error of 3″ (an accuracy of about $14 \cdot 10^{-6}$) results in case of 50 km long sides, 0.35″ in case of 400 km long sides, and 0.15″ in case of 1000 km long sides.

The problems of the accuracy and error analysis of terrestrial networks should not be dealt with in further details. Detailed analyses have been published in several papers [2, 11, 22, 8, 17]. It should be only mentioned that random measurement errors increase — independently of the geometrical form of the network, and of the measurement methods — approximately in proportion with the number of the measurements carried out. In consequence, advantageous (acceptable) point errors result even in case of greater random errors depending on the given geometric formation. On the contrary, systematical errors which seem to be insignificant, can be many times (in certain cases ten or hundred times) greater than the accumulated sum of random errors. Therefore, the *stiffening* of the networks with other measurement methods is of great importance as the regular errors of the different stiffening types differ in sign and in value, therefore their effect appears in a significantly decreased measure in the final results. Different-type regular errors are transformed in their sum into random errors if several measurement methods are combined.

There are no data at disposal about the regular errors of spatial three-dimensional networks deduced from Doppler satellite observations. Therefore it is difficult to determine in function of both the systematical and random errors the maximum value of the distance between the frame points determined by Doppler satellite points. For the random errors, the earlier mentioned data are valid.

The problems of the orientation and scale factor can be problematic in Doppler measurements. According to experiences hitherto there can be such an error in the scale factor that in addition to the random point error of ± 0.5 m, a systematical error of 1—5 m appears also. In spite of the information about directions and distances is included into the coordinate determination, it is insufficient, as on the one hand it refers to a given system with its errors, and on the other both are burdened with systematical errors. Therefore, in the future it is adviseable to combine the Doppler network with direction (azimuth) and distance determinations when national geodetic networks will be joined together in to great geodetic networks, in order to achieve a better stiffness in them. The directions are to be deduced from photographic observations or from the more accurate radio observations of quasars, the distances with long terrestrial bases and/or laser satellite observations. If the scale factor

and the orientation are controlled in Doppler observations, then the connection and the stiffening can be carried out purely by Doppler measurements.

It is well known that satellite geodetic networks can be computed without presuppositions. The measurement data of terrestrial geodetic networks, however, are to be transformed with *certain suppositions* in order to be able to use them in a spatial three-dimensional system. Thus, in addition to the accuracy of the measurements and of the geometric formation, the accuracy of the final results of the terrestrial triangulation and levelling depend, when reducing points on the surface of the Earth to the ellipsoid on the reality of the mathematical and physical hypotheses in the projection system used, on the accuracy of the reduction of the measurement results to the ellipsoid, on the density and accuracy of the known data about the gravity field of the Earth. One of the most important point in the reduction is the error of the geoid heights (at present $\pm 0.5-2.0$ m), further the error in the determination of the deviation of the plumb line. Due to these uncertainties, it is dubious whether the transformed terrestrial triangulation and levelling data should contribute significantly to the increase of the accuracy of the network from Doppler satellite observations. This refers mainly to high-precision levellings where the transformation is very questionable due to the inaccuracies in the determination of the ellipsoidic heights, and its accuracy is considerably less than the measurement accuracy. Similar, but from the point of view of the transformation considerably smaller errors are caused by the transformation of the other two coordinates, i.e. the ellipsoidic longitude and latitude of the points.

Due to the systematical errors in both measurement methods, it is not advisable to entour the network by a frame of Doppler points, it is better if the Doppler points cover the area of the whole network in a uniform surface distribution.

3. Computation of networks and error analysis

In case of the adjustment of the networks of great countries, the common network of several countries (e.g. that of the socialist countries), of continental or global networks, the number of the unknowns to be determined increases from 1000 to several millions. The inversion of matrices with so many unknowns includes significant errors due to rounding [12]. A common adjustment, even with present computers is impracticable. Therefore it is adviseable to use the decomposition method with band-structured matrices. For the single partitioned matrices which can be simultaneously solved, the Helmert—Wolf bloqueadjustment method can be advantageously used.

In order to enable an error analysis after the adjustment, the determination of the variance-covariance matrix is also needed. In simulated networks,

together with the azimuths, distances and Doppler-determined points, their optimum arrangement can also be studied in knowledge of the variance-covariance matrices. Such investigations have great importance, as it can be tried by them to diminish the effect of the systematical errors, too, in addition of the random errors, if such are also included. Anyway, the quadrangular form is more advantageous from an optimization point of view than the triangular form.

The supposition that the measurements in the network and the satellite observations are burdened only by random errors, is not adaptable in a network analysis. Even in case of terrestrial geodetic measurements, the systematical errors of the reduction to the ellipsoid or spheroid are to be added. In such a sense all theories on error propagation based exclusively on random errors give a too optimistic idea about the accuracy of the network. It should be once more emphasized that the detection and decrease of systematical errors can be reached only using different methods of determination and other observation data.

For the determination of the inner and outer accuracies of networks the so-called free adjustment can be used [10, 14, 3, 20, 16, 19]. The result of the free, i.e. without constraints, adjustment of networks coincides with the result of an adjustment when the origine of the coordinates is the gravity centre of the preliminary coordinates of all points and the orientation is also a weighted average. Such an adjustment yields the minimum valued variance-covariance matrix in function of the accuracy of the measurements between the network points and the configuration of the network. Let the original normal matrix be denoted by **N**, the coordinate changes by δ, the free terms of the equations by **L**. There are 6 further conditions to be added to these with the coefficient matrix **K** and with the orientation and translation unknowns $\bar{\delta}$ (if the scale is also to be determined, the number of the unknowns is 7):

$$\begin{bmatrix} \mathbf{N} & \mathbf{K} \\ (3n,\,3n) & (3n,\,6) \\ \mathbf{K} & \mathbf{0} \\ (6,3n) & (6,6) \end{bmatrix} \begin{bmatrix} \delta \\ \bar{\delta} \end{bmatrix} = \begin{bmatrix} \mathbf{L} \\ (3n,\,1) \\ \mathbf{0} \\ (6,1) \end{bmatrix}, \tag{4}$$

where n is the number of points. The following equation is valid for the matrix **K**:

$$\underset{(6,3n)}{\mathbf{K}} = \left[\begin{array}{ccc:ccc:c:ccc} 1 & 0 & 0 & 1 & 0 & 0 & & 1 & 0 & 0 \\ 0 & 1 & 0 & 0 & 1 & 0 & & 0 & 1 & 0 \\ 0 & 0 & 1 & 0 & 0 & 1 & \dots & 0 & 0 & 1 \\ 0 & Z_1 & -Y_1 & 0 & Z_2 & -Y_2 & & 0 & X_n & -Y_n \\ -Z_1 & 0 & X_1 & -Z_2 & 0 & X_2 & & -Z_n & 0 & X_n \\ Y_1 & -X_1 & 0 & Y_2 & -X_2 & 0 & & Y_n & -X_n & 0 \end{array}\right], \tag{5}$$

where X, Y, Z mean good approximative values of the coordinates of the points. The variance-covariance matrix of the adjusted $\bar{\mathbf{x}}$ coordinate values is:

$$\underset{(3n,\,3n)}{\mathbf{Q}_{\bar{x}}} = \underset{(3n,\,3n)}{(\mathbf{N}} + \underset{(3n,\,6)}{\mathbf{K}^T} \underset{(6,3n)}{(\mathbf{K}} \underset{(3n,\,6)}{\mathbf{K}^T)^{-1}} \underset{(6,3n)}{\mathbf{K}^{-1})} \underset{(3n,3n)}{(\mathbf{E}} - \underset{(3n,\,6)}{\mathbf{K}^T} \underset{(6,3n)}{(\mathbf{K}} \underset{(3,n6)}{\mathbf{K}^T)^{-1}} \underset{(6,3n)}{\mathbf{K})} . \tag{6}$$

That means that the results are in a system of coordinates where no points or directions are preferred. The normal matrix $\mathbf{N}$ is found as a function of the given orientation, scale factor and origine. The normal matrix $\mathbf{N}$ is found as a function of the given orientation, scale factor and origine. The first adjustment is generally made for this. The problem is, how to determine the values $\bar{\delta} = \bar{\mathbf{x}}$ and the corresponding $\mathbf{Q}_{\bar{X}}$, if $\mathbf{N}^{-1} = \mathbf{Q}_X$ is known. The transformation equation between the two systems is:

$$\bar{\mathbf{x}} = \mathbf{x} + \mathbf{K}\mathbf{t}, \tag{7}$$

where t symbolizes the transformation parameters. The conditions $\bar{\mathbf{x}}^T\bar{\mathbf{x}} = \min$ [21] and good approximative values yield:

$$\mathbf{t} = -(\mathbf{K}^T\mathbf{K})^{-1}\mathbf{K}^T\mathbf{x}. \tag{8}$$

From Eq. 7 one gets:

$$\bar{\mathbf{x}} = \mathbf{x} - \mathbf{K}(\mathbf{K}^T\mathbf{K})^{-1}\mathbf{K}^T\mathbf{x} = (\mathbf{E} - \mathbf{K}(\mathbf{K}^T\mathbf{K})^{-1}\mathbf{K}^T)\mathbf{x} = (\mathbf{E} - \mathbf{G})\mathbf{x}, \tag{9}$$

where

$$\mathbf{G} = \mathbf{K}(\mathbf{K}^T\mathbf{K})^{-1}\mathbf{K}^T. \tag{10}$$

Using simply the law of error propagation:

$$\mathbf{Q}_{\bar{x}} = (\mathbf{E} - \mathbf{G})\mathbf{Q}_x(\mathbf{E} - \mathbf{G})^T = \mathbf{Q}_x - (\mathbf{G}\mathbf{Q}_x + \mathbf{Q}_x\mathbf{G}^T - \mathbf{G}\mathbf{Q}_x\mathbf{G}^T). \tag{11}$$

Thus we got a simple method for the quick determination of the inner accuracy, in addition to the outer accuracy. The result of the free adjustment of networks depends on the number of points appearing in it. Therefore, it yields a qualitatively good information on the inner accuracy of the network, even if the numerical data are quantitatively not absolutely reliable.

The next question is what a system the observed Doppler data refer to. The used geodetic systems are the following:

a) Broadcast Ephemeris, based on WGS (World Geodetic System) 72,

b) Precise Ephemeris NWL 9-D (US Navy Navigation Satellites).

If an independent adjustment of the orbit is made (without taking into account the previously given ephemerides), or the origine and the orientation of the three axes of the coordinate system are previously given (6 data), or they are used as free parameters and a free adjustment is made, the aim can also be reached. If the ephemerides of the Navy Navigation Satellite System (NNSS) are used, the system given by them is also accepted. For orientation the Doppler observations must be combined with optical satellite observations, or with the much more accurate Very Long Base Interferometry (VLBI).

4. The connection of networks deduced from Doppler satellite observations and terrestrial geodetic measurements

If the Doppler network is independently adjusted and the same is made with the terrestrial network, and then the two networks are to be combined, 7 unknowns are to be used in the transformation. It can be supposed that the data computed from Doppler measurements are in a coordinate system which is rather near to that of the terrestrial measurements. In such a case the seven parameters include the effects of the regular errors due to the three components of the translation of the origines of the three-dimensional coordinate system in respect to each other (dX, dY, dZ), the three axial rotations (ε_X, ε_Y, ε_Z) and the scale factor ($\varkappa$). The computational basic surface (reference ellipsoid) has a major axis a and a flattening f, meaning two further parameters. It is further usual to distinguish the momentaneous geodetic system and the absolute geodetic system [9]. This results in the introduction of four or seven further transformation parameters. The latter is hardly possible, as for it no immediate data and information are available. The theoretical possibility is hampered in many cases by practical difficulties.

The best solution is received if the values X, Y, Z (or Φ, λ, h) from Doppler observations, the values X, Y (or Φ, λ) from triangulation and the heights from levellings ($H + N$, where H is the deviation of the ellipsoid from the geoid) are computed in a common three-dimensional model. The variance-covariance values of all measured or computed values are naturally taken into account. The necessary translation-rotation parameters, further the scale factor can be introduced as unknowns (Fig. 4). The system outlined here can be adapted for the interpretation of all kinds of measurements in the framework of a common adjustment model.

If the vectors of the point P are denoted by $\vec{\mathbf{r}}_P$ and $\vec{\varrho}_P$ in the Doppler-coordinate system (D and in the terrestrial geodetic coordinate system (TG)) respectively, which are relatively little translated and rotated in respect to each other, then the following connection holds between them [5]:

$$(\vec{\mathbf{r}}_0)_D + (1 + \varkappa)\, \mathbf{R}_X(\varepsilon_X)\, \mathbf{R}_Y(\varepsilon_Y)\, \mathbf{R}_Z(\varepsilon_Z)\, (\vec{\mathbf{r}}_P)_{FG} - (\vec{\varrho}_P)_D = 0\,, \qquad (12)$$

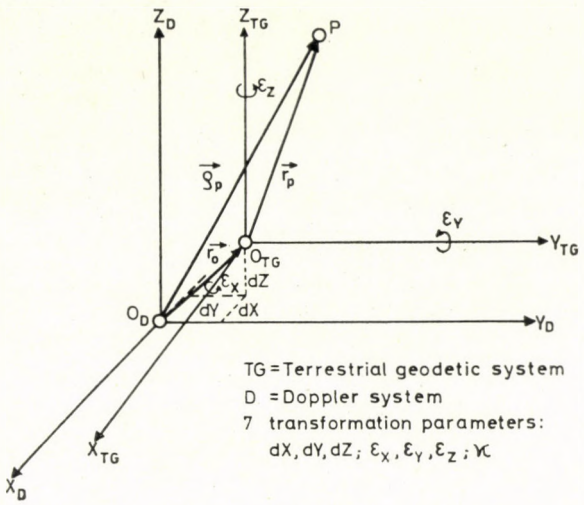


Fig. 4

where $\mathbf{R}_X$, $\mathbf{R}_Y$, $\mathbf{R}_Z$ are the transformation parameters:

$$\mathbf{R}_X = \begin{bmatrix} 1 & 0 & 0 \\ 0 & \cos\varepsilon_X & \sin\varepsilon_X \\ 0 & -\sin\varepsilon_X & \cos\varepsilon_X \end{bmatrix} \quad \mathbf{R}_Y = \begin{bmatrix} \cos\varepsilon_Y & 0 & -\sin\varepsilon_Y \\ 0 & 1 & 0 \\ \sin\varepsilon_Y & 0 & \cos\varepsilon_Y \end{bmatrix},$$

$$\mathbf{R}_Z = \begin{bmatrix} \cos\varepsilon_Z & \sin\varepsilon_Z & 0 \\ -\sin\varepsilon_Z & \cos\varepsilon_Z & 0 \\ 0 & 0 & 1 \end{bmatrix}. \tag{13}$$

MOLODENSKY's and his co-workers' model is based on the same principles with the difference that it yields a translational and scale factor solution only between terrestrial points.

Using the solution mentioned previously, one gets information about the systematical errors of terrestrial geodetic measurements. One can control the accuracy of the coordinates deduced from Doppler observations. A common adjustment of the Doppler observation and of the terrestrial geodetic measurements yields a rigid network, the optimum connection of the networks is ensured. Previous estimations have shown that the positional error of the origine is less than ± 1 m, the orientation has an error of about $\pm 0.1''$ for all the three axis, and the scale factor can be determined with an accuracy of $\pm 0.1 \cdot 10^{-6}$.

5. Conclusions

The inner and outer accuracies of geodetic networks can be significantly increased if the results of the terrestrial geodetic measurements and of the satellite observations are connected. A decrease of the systematical and random

errors can be reached in geodetic networks in addition to that by the Doppler satellite observations also by a combination of azimuth and distance measurements. If the average side length of the terrestrial geodetic network is 30 km, then it is advisable to use in each 200—250 km a Doppler point for the connection and stiffening of the network parts. It is further advisable to determine azimuth by optical satellite observations or by VLBI and distances by laser measurement at each tenth point. In terrestrial networks azimuths and distances, further Laplace points should be determined at each 100 km. In spite of the inclusion of the orientation and scale factor information into the coordinates of the points deduced from Doppler observations, a combination of the different type measurements is necessary in order to moderate the effect of the regular errors. The orientation can be also made by very-long-base line radio interferometry, as they are significantly superior in their accuracy to all traditional measurements.

REFERENCES

1. ANDERLE, R. I.: Transformation of terrestrial survey data of Doppler satellite datum. *Geophys. Res.*, 79 (1974), 5319—5331.
2. BAARDA, W.: Difficulties in establishing a model for testing crustal movements. In: Progress in Geodynamics. Elsevier Publ. (1975), Amsterdam.
3. BLAHA, G.: Inner adjustment contraints with emphasis on range observations. Rep. Dep. Geodetic Sc. of the Ohio State Univ. Columbus No. 148, 1971.
4. BROWN, D. C.: Doppler surveying with the JMR-1 receiver. *Bull. Géod.*, 50 (1976), 9—25.
5. BURŠA, M.: The theory of the determination of the non-parallelism of the minor axis of the reference ellipsoid. *Studia Geophysica et Geodaetica*, 6 (1962), 209—214.
6. DRACUP, J. F.: Updating survey networks. A practical application of satellite Doppler positioning. Int. Geodetic Symp. on Satellite Doppler Positioning, Las Cruces, 1977.
7. HALMOS, F.: Metodische Fragen der geodätischen Anwendung von Dopplerschen Satelliten-Beobachtungen. Paper presented at the Symposium on Satellite Geodesy, Sopron, May 6, 1976. *Acta Geodaet. Geophys et Mont.* 13 (1978).
8. HALMOS, F.—KÁDÁR, I.: An attempt to interpret physically the notion-system of geodetic information. *Bull. Géod.*, 51 (1977), 1—16.
9. KRAKIWSKY, E. I.—THOMSON, D. B.: Mathematical models for the combination of terrestrial and satellite networks. *Canadian Surveyor*, 28 (1974), 606—615.
10. MEISSL, P.: Die innere Genauigkeit eines Punkthaufens. *Öst. Z. f. Vermessungswesen*, 50 (1962), 186—194.
11. MEISSL, P.: Strength analysis of two-dimensional angular anblock networks. *Manuscripta geodaetica*, 1 (1976), 293—333.
12. MEISSL, P.—BARTELME, N.: Theoretical analysis of rounding error propagation during the direct solution of geodetic normal equations of the leveling type. International Association of Geodesy XVI. Generale Assemblee, Grenoble, 1975.
13. MIHÁLY, Sz.: Geodéziai alaphálózatok korszerűsítése a kozmikus geodézia segítségével (Improving classical networks by satellite geodesy). *Geodézia és Kartográfia*, 29 (1977), 174—182.
14. MITTERMAYER, E.: Eine Verallgemeinerung der Methode der kleinsten Quadrate zu Ausgleichung freier Netze. *Z. f. Vermessungswesen*, 96 (1971), 401—411.
15. MOLODENSKY, M. V.—YEREMEJEV, V.—JURKINA, M.: Methods for Study of the external field and figure of the Earth. Israel Scientific Translation, Jerusalem, 1962.
16. MUELLER, I. I.—GELDER, W.—KUMAR, K.: Error analyses for the proposed close grid geodynamic satellite measurement system (CLOGEOS). Ohio State Univ. Dep. of Geodetic Science Report No. 230, 1975.
17. RINNER, K.: The Importance of Geodetic Nets for Science, Economy and Engineering. Optimization of Design and Computation of Control Networks. Sopron, 3—9 July, 1977.

18. SAZANOV, A. Z.: Astro-geodetic networks of the USSR. Lay-out and adjustment principles. Actual accuracy. XV. Assembly of the IUGG. Moscow, 1971.
19. VERŐNÉ, HETÉNYI M.: Az önálló háromszöghálózatok kiegyenlítéséről (On the adjustment of independent triangulation networks). *Geodézia és Kartográfia*, 25 (1973), 248—253.
20. WOLF, H.: Supporting terrestrial triangulation work by satellite triangulation. Int. Symposium on satellite and terrestrial triangulation, Graz, 1972.
21. WOLF, H.: Freie Ausgleichungen in klassischer Sicht. Vortrag im Geodätischen und Geophysikalischen Forschungsinstitut, Sopron, 1976.
22. WOLF, H.: Das europäische Dreiecksnetz: Ursprung, Entwicklung und künftige Möglichkeiten, Geodätische Woche, Köln, 1975.

НЕКОТОРЫЕ ПРОБЛЕМЫ ПРИВЯЗКИ СЕТЕЙ, ВЫВЕДЕННЫХ ИЗ СПУТНИКОВЫХ И НАЗЕМНЫХ НАБЛЮДЕНИЙ

Ф. ХАЛМОШ

РЕЗЮМЕ

Автор рассматривает проблемы, влияющие на жёсткость привязки спутниковых и наземных геодезических сетей. Помимо анализа точности методов измерений рассматривается влияние систематических ошибок в геодезических сетях большой протяженности, а также возможности их ослабления в комбинированных сетях. Приводится также и анализ оптимального распределения измерений, повышающих жесткость сетей.

Acta Geodaet., Geophys. et Montanist. Acad. Sci. Hung. Tomus 14 (4), pp. 417—419 (1979)

AUSGLEICHUNG EINER MEHRMALS BEOBACHTETEN NIVELLIERUNGSSTRECKE NACH BEDINGUNGEN

W. K. HRISTOV†

MITGLIED DER BULGARISCHEN AKADEMIE DER WISSENSCHAFTEN, SOFIA
EHRENMITGLIED DER UNGARISCHEN AKADEMIE DER WISSENSCHAFTEN, BUDAPEST

[Eingegangen am 10. August 1978]

Es sei eine Nivellierungsstrecke mehrmals gemessen und es seien die Höhenunterschiede unter der Voraussetzung konstanter Vertikalgeschwindigkeiten nach Bedigungen ausgeglichen.

Eine Nivellierungsstrecke AB ist mehrmals gemessen worden, d.h. wir haben mehrere Höhenunterschiede $h_1, h_2, h_3, \ldots$ zu den Zeiten $t_1, t_2, t_3 \ldots$ gemessen. Es wird dabei angenommen, daß die Vertikalgeschwindigkeiten konstant sind. Es ist klar, daß wir nur die relative Höhe und die relative Vertikalgeschwindigkeit des einen Punktes, etwa B, in bezug auf den anderen Punkt, etwa A errechnen können. Um die absolute Höhe und die absolute Vertikalgeschwindigkeit des Punktes B zu erhalten, muß die absolute Höhe und die absolute Vertikalgeschwindigkeit des Punktes A bekannt sein. Der Punkt A habe zur Epoche T_0 eine absolute Höhe H_A und eine absolute Vertikalgeschwindigkeit V_A. Aus *zwei* Höhenunterschieden h_{AB} können wir den Höhenwert H_B und die Vertikalgeschwindigkeit V_B berechnen. Demzufolge gibt eine jede *weitere* Beobachtung h_{AB} je eine Bedingung. Also wenn wir n beobachtete Höhenunterschiede h_{AB} haben, so haben wir demnach n-2 Bedingungen.

Es sei $n = 3$. Wir haben 3 gemessene Höhenunterschiede und demnach 3 relative Geschwindigkeiten V_{AB}

$$V_{AB} = \frac{h_2 - h_1}{t_2 - t_1} + \frac{v_2 - v_1}{t_2 - t_1} \tag{1}$$

$$V_{AB} = \frac{h_3 - h_2}{t_3 - t_2} + \frac{v_3 - v_2}{t_3 - t_2} \tag{2}$$

$$V_{AB} = \frac{h_3 - h_1}{t_3 - t_1} + \frac{v_3 - v_1}{t_3 - t_1}, \tag{3}$$

die einander gleich sein müssen. Also bekommen wir durch Gleichsetzen scheinbar 3 Bedingungen: aus (1), (2); aus (1), (3) und aus (2), (3):

$$\frac{v_2 - v_1}{t_2 - t_1} + \frac{h_2 - h_1}{t_2 - t_1} = \frac{v_3 - v_2}{t_3 - t_2} + \frac{h_3 - h_2}{t_3 - t_2} \tag{4}$$

$$\frac{v_2 - v_1}{t_2 - t_1} + \frac{h_2 - h_1}{t_2 - t_1} = \frac{v_3 - v_1}{t_3 - t_1} + \frac{h_3 - h_1}{t_3 - t_1} \tag{5}$$

$$\frac{v_3 - v_2}{t_3 - t_2} + \frac{h_3 - h_2}{t_3 - t_2} = \frac{v_3 - v_1}{t_3 - t_1} + \frac{h_3 - h_1}{t_3 - t_1}\,. \tag{6}$$

In Wirklichkeit muß es nur eine Bedingung sein. Wenn wir (4) mit $(t_2-t_1)(t_3-t_2)$, (5) mit $(t_2-t_1)(t_3-t_1)$ und (6) mit $(t_3-t_2)(t_3-t_1)$ multiplizieren, ergeben sich:

$$(t_3-t_2)(v_2-v_1) + (t_3-t_2)(h_2-h_1) = (t_2-t_1)(v_3-v_2) + (t_2-t_1)(h_3-h_2), \tag{7}$$

$$(t_3-t_1)(v_2-v_1) + (t_3-t_1)(h_2-h_1) = (t_2-t_1)(v_3-v_1) + (t_2-t_1)(h_3-h_1), \tag{8}$$

$$(t_3-t_1)(v_3-v_2) + (t_3-t_1)(h_3-h_2) = (t_3-t_2)(v_3-v_1) + (t_3-t_2)(h_3-h_1). \tag{9}$$

Weiter, wenn wir in Gln. (7), (8), (9) die Multiplikationen und Abkürzungen durchführen, sehen wir, daß nur *eine* Bedingungsgleichung übrigbleibt

$$\begin{aligned} -(t_3-t_2)\cdot v_1 + (t_3-t_1)\cdot v_2 - (t_2-t_1)\cdot v_3 - (t_3-t_2)\cdot h_1 + \\ + (t_3-t_1)\cdot h_2 - (t_2-t_1)\cdot h_3 = 0, \end{aligned} \tag{10}$$

wie es auch sein soll.

Es sei $n = 4$. Wir haben 4 gemessene Höhenunterschiede und demnach $\binom{4}{2} = 6$ relative Geschwindigkeiten. Also erhalten wir durch Gleichsetzen scheinbar $\binom{6}{2} = 15$ Bedingungsgleichungen:

A) $\big((2\ 3), (2\ 4)\big), \big((2\ 3), (3\ 4)\big), \big((2\ 4), (3\ 4)\big)$, es fehlt h_1, v_1

B) $\big((1\ 3), (3\ 4)\big), \big((1\ 4), (1\ 3)\big), \big((1\ 4), (3\ 4)\big)$, es fehlt h_2, v_2

C) $\big((1\ 2), (1\ 4)\big), \big((1\ 2), (2\ 4)\big), \big((1\ 4), (2\ 4)\big)$, es fehlt h_3, v_3

D) $\big((1\ 2), (1\ 3)\big), \big((1\ 2), (1\ 3)\big), \big((1\ 3), (2\ 3)\big)$, es fehlt h_4, v_4

E) $\big((1\ 2), (3\ 4)\big), \big((1\ 3), (2\ 4)\big), \big((1\ 4), (2\ 3)\big)$.

Darin ist angegeben, aus welchen Messungen die Geschwindigkeiten bestimmt und welche Geschwindigkeiten miteinander verglichen werden. Es sind jedoch zwei wirkliche Bedingungsgleichungen: eine Gleichung aus *A)* und eine Gleichung aus *B)*; in der gleichen Weise sind *A), C)*; *A), D)*; *A),*

E); *B)*, *C)*; *B)*, *D)*; *D)*, *D)*; *C)*, *E)*; *D)*, *E)* zu bilden; also insgesamt $4 \cdot 9 + 3 \cdot 9 + 2 \cdot 9 + 1 \cdot 9 = 90$ Kombinationen.

Im allgemeinen Falle haben wir $\binom{n}{2} = \frac{n^2 - n}{2}$ Geschwindigkeiten, also

$$\left(\binom{\frac{n}{2}}{2}\right) = \frac{n^4 - 2n^3 - n^2 + 2n}{8}$$

scheinbare Bedingungsgleichungen. Aus diesen sind $n - 2$ unabhängige Bedingungsgleichungen nach dem Vorbild $n = 4$ zu nehmen.

Wenn wir aber nach vermittelnden Beobachtungen ausgleichen wollten, so hätten wir nur 2 Unbekannte, dH_B und dV_B, also 2 Normalgleichungen, gegenüber $n - 2$ bei der Ausgleichung nach Bedingungen. Man fragt sich dann, warum schlägt man die Ausgleichung nach Bedingungen vor? Die Nivellierungsstrecke AB ist im allgemeinen Bestandteil eines Nivellierungsnetzes, das man sehr oft nach *Bedingungen* ausgleicht. Deshalb muß man die mehrmals beobachteten Nivellierungsstrecken *auch* nach Bedingungen ausgleichen, d.h. zu den gewöhnlichen Netzbedingungen noch unsere Streckenbedingungen $n_1 - 2$, $n_2 - 2$, ... hinzufügen.

SCHRIFTTUM

1. Hristov, W. K.: Allgemeiner Fall der gemeinsamen Ausgleichung der Höhenwerte und Geschwindigkeiten eines Nivellements. *Acta Geod. Geoph. Mont. Hung.*, 13 (1978), 337—346.
2. ТРЕНКОВ, И.: Уравнивание по условным уравнениям многократно нивелированного замкнутого полигона при наличии вертикальных скоростей. Булгарска академия на науките, Висша геодезия 2, София, 1976.

УРАВНИВАНИЕ ПО МЕТОДУ УСЛОВИЙ НИВЕЛИРНОГО ХОДА, ИЗМЕРЕННОГО НЕСКОЛЬКО РАЗ

В. К. ХРИСТОВ

РЕЗЮМЕ

Пусть будет измерен нивелирный ход несколько раз, и пусть будут уравнены превышения, предполагая постоянную вертикальную скорость, по методу условий.

Acta Geodaet., Geophys. et Montanist. Acad. Sci. Hung. Tomus 14 (4), pp. 421—435 (1979)

MECHANICAL EROSION IN FLOW CHANNELS OF ROCKS

E. BOBOK—ZS. SOMOSVÁRI

TECHNICAL UNIVERSITY OF HEAVY INDUSTRIES, MISKOLC

[Manuscript received April 25, 1977]

Mechanical erosion in flow channels of rocks is characterized both by strength and rheological parameters of the rock and by the hydrodynamical parameters of the flowing water. It is shown that in the erosion process cavitation plays a more important role than shear stresses.

Introduction

The increased productivity and the security requirements necessitate the protection against water in mines of unfavourable hydrogeological conditions [1]. The measure of water danger depends on the natural isolation between the mining excavation and the aquifier. This so-called protecting layer suffices if it protects the excavation in spite of deformations, displacements and smaller fractures of the rock, caused by drifting [2]. In the protecting layer the interrelation between water flow and rock movements has great importance. This problem has been investigated by a complex analysis of rock mechanics and hydrodynamics in some recent works [1, 2, 3]. In the present paper we shall deal with a problem wich has been ousted to the periphery in former studies. We shall look for relationships between the parameters of mechanical erosion in flow channels of rocks. The process of mechanical erosion will be shown to have greater importance in water inrushes as realized today.

1. Shear stresses in turbulent flow

As it is presently accepted, the cause of mechanical erosion in flow channels of rocks is the shear stress, which begins to erode the surfaces of the voids exceeding a treshold value on the walls [2]. This shear stress can be determined as follows.

The pore structure of rocks is a stochastically distributed, tortuous, interwoven channel system. The flow channels in such a medium vary continuously in direction, size and shape. In these channels the flow can be reduced to a turbulent pipe-flow by introducing of the hydraulic radius and the equivalent pipe-length as shown in Fig. 1.

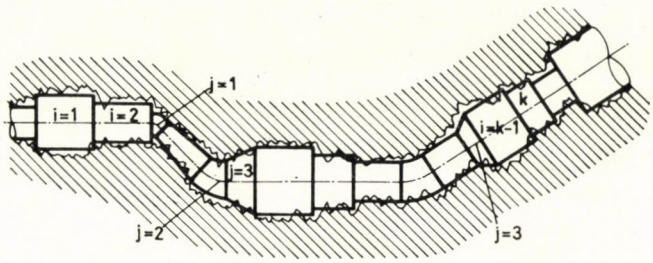


Fig. 1. Pipe-model of the flow channel-system

The flow channel of arbitrarily varying shape and cross section can be deduced to a pipe system consisting of straight pipe sections of different sizes and various sorts of elbows, diffusers and other fittings in series connection.

The effect of bends, fittings, enlargements and contractions in the pipe system is estimated by using the well-known equivalent length concept. The pipe length is increased for purposes of the head loss calculation by the sum of the equivalent lengths of fittings in the system. Thus, the relationship between head loss and mean velocity is described by the equation

$$h' = \sum_{i=1}^{k} \lambda_i \frac{L_i}{D_i} \frac{c_i^2}{2g} + \sum_{j=1}^{m} \zeta_j \frac{c_j^2}{2g} ,$$

where λ_i is the friction factor, L_i the length and D_i the inner diameter of the i-th pipe section; ζ_j is the loss-coefficient of the j-th fitting, c_i and c_j are the cross-sectional average velocities in those places. The same head loss can be produced by a straight cylindrical pipe of length L_e, diameter D_e and friction factor λ_e, as follows:

$$h' = \lambda_e \frac{L_e}{D_e} \frac{c_e^2}{2g} .$$

Thus, the pipe system can be replaced by the equivalent length pipe from the point of view of hydrodynamics.

Next, expressions will be deduced for the substitutive fictitious flow. The turbulent flow in the irregularly shaped flow channels will be equivalent to a "fully rough"-type turbulent flow in the pipe model.

The differential equation describing turbulent flow in a straight, circular pipe is:

$$\frac{\gamma J r}{2} + \mu \frac{dv}{dr} - \varrho l^2 \left(\frac{dv}{dr}\right)^2 = 0 .$$

In this equation

r — is radial coordinate
J — hydraulic gradient

v — velocity
μ — dynamic viscosity of the fluid
ϱ — density of the fluid
γ — specific gravity
l — mixing length, which is a characteristic parameter describeing the intensity of turbulence.

The first term of the equation is the accelerative force, the second the resistance due the viscous shear stress, the third the resistance due the additional virtual stress, caused by momentum flux due to turbulent movements.

It is necessary to distinguish two regimes during the solution of the above differential equation, in accordance with experimental data. First, in every turbulent flow there exists a very thin layer near the wall which behaves in essence like one in laminar motion. This is known as the laminar sublayer. In this layer all turbulent components must vanish at the walls so that they are very small in their immediate neighborhood. Thus the differential equation has the simple form:

$$\frac{\gamma J r}{2} + \mu \frac{dv}{dr} = 0 .$$

The shear stress on the pipe wall ($r = R$) is:

$$\tau_R = \frac{\gamma J R}{2} .$$

Dimensional considerations show that

$$v^* = \sqrt{\frac{\tau_R}{\varrho}}$$

has the dimension of velocity, it will be called *friction velocity*. In the laminar sublayer an additional assumption may be accepted: that the shear stress τ is constant throughout the range of the velocity, that is $\tau = \tau_R$. This leads to a linear velocity distribution:

$$\frac{v}{v_*} = \frac{v_*}{\nu} (R - r) ,$$

where $\nu = \mu/\varrho$ is the kinematic viscosity.

Outside the laminar sublayer viscous shear stresses are negligible, thus the differential equation becomes:

$$\frac{\gamma J r}{2} - \varrho l^2 \left(\frac{dv}{dr}\right)^2 = 0 .$$

In order to determine the turbulent flow it is necessary to find an expression for the turbulent shear stress which would relate it to the velocity components. As an extension of the mixing length hypothesis of PRANDTL [5] and on the basis of the experimental results of NIKURADSE [6], KÁRMÁN [7] proposed the following expression for mixing length in turbulent flows:

$$\tau = \varrho \varkappa^2 \left(\frac{dv}{dr}\right)^4 \left(\frac{d^2 v}{dr^2}\right)^{-2},$$

where the constant $\varkappa$ has a value of about 0.40—0.42.

Substituting into the differential equation, we get the expression:

$$\frac{\gamma J r}{2} + \varrho \varkappa^2 \left(\frac{dv}{dr}\right)^4 \left(\frac{d^2 v}{dr^2}\right)^{-2} = 0 .$$

The solution to the differential equation is the dimensionless velocity distribution

$$\frac{v_{\max} - v}{v^*} = \frac{1}{\varkappa}\left[\sqrt{\frac{r}{R}} + \ln\left(1 - \sqrt{\frac{r}{R}}\right)\right].$$

The cross-sectional average velocity in the pipe is:

$$c = \frac{v_*}{\varkappa} \ln \frac{v_* R}{\nu} + K,$$

where K is an integration constant.

The well-known expression of the head loss is:

$$h' = JL = \frac{2L}{\gamma R} \tau_R .$$

On the other hand, applying the Darcy—Weisbach resistance law:

$$h' = \lambda \frac{L}{2R} \frac{c^2}{2g} .$$

The stress on the wall is obtained

$$\tau_R = \frac{\gamma \lambda}{8g} c^2 .$$

and the friction velocity can be expressed as

$$v_* = c \sqrt{\frac{\lambda}{8}} .$$

The resistance coefficient depends on the ratio of the thickness of the laminar sublayer δ, and the size of roughnesses k. One has to distinguish three regimes depending on the value of the ratio δ/k. In each regime the hydrodynamical behaviour is different.

If $\delta/k \gg 1$, the laminar sublayer covers the roughness of the wall, the highest protrusions being contained within the sublayer. Vortices generated by the protrusions quickly dissipate in the laminar sublayer, thus the resistance coefficient only depends on the Reynolds-number.

If $\delta/k \cong 1$, the protrusions extend partly outside the laminar sublayer. In this transition regime the resistance coefficient depends on the Reynolds-number as well as on the relative roughness.

If $\delta/k < 1$, all protrusions reach outside the laminar sublayer, and non-decay perturbations are generated by them, the damping effect of the viscous forces is not appeared. The resistance coefficient only depends on the relative roughness.

The latter regime is the most important, in practice, since in super-capillary flow channels there are very rough wall-surfaces. We have to find the correlation between the friction velocity and the relative roughness. In the "totally rough" regime the resistance coefficient was determined by the accurate and systematic tests of NIKURADSE [6], in accordance with PRANDTL's and KÁRMÁN's theory:

$$\lambda = \left[2 \lg \left(3.715 \frac{D}{k}\right)\right]^{-2}.$$

Thus, the friction velocity is:

$$v_* = \frac{c}{2\sqrt{8}} \frac{1}{\lg \left(3.715 \frac{D}{k}\right)}.$$

Substituting this into the appropriate equation, we get the shear stress on the wall:

$$\tau_R = \frac{\varrho c^2}{32 \left[\lg \left(3.715 \frac{D}{k}\right)^2\right]}.$$

The shear stress depends quadratically on the cross-sectional average velocity, increases with the roughness, and decreases with the mean hydraulic diameter.

Since there are relatively few informations about the size of roughnesses in super-capillary flow channels, the reader may at first be skeptical of the value of this contribution. However, it should be noted that very wide varia-

tions in the roughness cause considerably smaller changes of the shear stress τ_R. This approach, therefore, allows to make fairly accurate predictions of τ_R from probable estimates of the roughness size.

The relative roughness values for reveted steal pipes are between 10 and 1000.

For breakstone-covered channels it seems reasonable to consider the $1 < D/k < 100$ interval. The cross-sectional average velocity c is certainly smaller than 50 m/s. The possible values of shear stress τ_R are given in the following Table:

c $\left[\frac{m}{s}\right]$	$\tau_R[Mp/m^2]$		
	$\frac{D}{k} = 1$	10	100
1	0.010	0.001	0.000
5	0.245	0.032	0.012
10	0.981	0.129	0.048
15	2.206	0.291	0.109
20	3.922	0.517	0.193
25	6.129	0.808	0.301
30	8.825	1.163	0.434
40	15.690	2.068	0.772
50	24.515	3.231	1.206

The Table shows that a considerable wall shear stress $\tau_R > 1$ Mp/m^2 only exists at high velocities and at very low relative roughnesses. The question is whether shear stresses of this range could induce mechanical erosion at all.

Let us observe that in the transition regime, where $\delta/k = 1$, the shear stress is $(\tau_R)_{\text{trans}}$.

Since $(\tau_R)_{\text{rough}} > (\tau_R)_{\text{trans}}$, we can restrict ourselves to the wholly rough region.

2. Effect of shear stress on the surface of holes

Investigation of stresses in the rock will be deduced to the regular-shaped case as above. First, we consider a vertical flow channel of circular cross-section. The stress components will be considered on the surface of the hole without the presence of water. The principal stress in radial direction is

$$\sigma_r = 0.$$

The tangential component is also principal:

$$\sigma_\gamma = \frac{2\, z\bar{\gamma}}{m-1}\,.$$

The third principal stress in axial direction is

$$\sigma_z = z\bar{\gamma},$$

where z is depth, $\bar{\gamma}$ the bulk specific gravity of the rock, m is the Poisson-number.

If water is flowing in the hole, shear stress τ_R appears on its surface, therefore, σ_z' and σ_r are no longer principal stresses.

The Mohr-circle modifies as shown in Fig. 2. The principal stresses in the region $< 2 < m < 3$ will be:

$$\sigma_1 = \sigma_9 = \frac{2z\bar{\gamma}}{m-1}$$

$$\sigma_2 = \frac{\sigma_z}{2} + \sqrt{\tau_R^2 + \left(\frac{\sigma_z}{2}\right)^2} = \frac{z\bar{\gamma}}{2} + \sqrt{\tau_R^2 + \left(\frac{z\bar{\gamma}}{2}\right)^2}$$

$$\sigma_3 = \frac{\sigma_z}{2} - \sqrt{\tau_R^2 + \left(\frac{\sigma_z}{2}\right)^2} = \frac{z\bar{\gamma}}{2} \sqrt{\tau_R^2 + \left(\frac{z\bar{\gamma}}{1}\right)^2}\,.$$

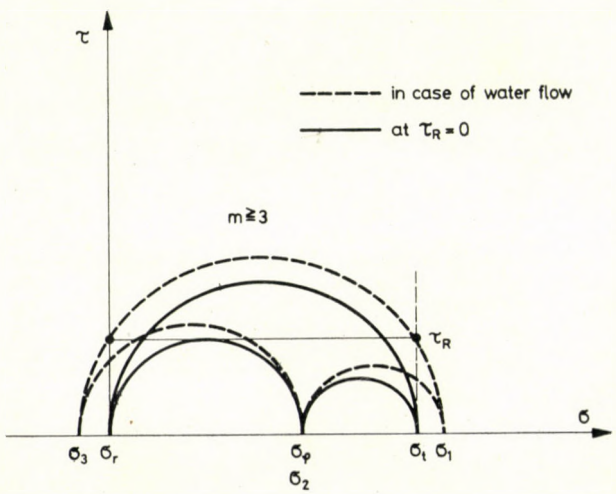


Fig. 2. Mohr-circles of stresses in the channel wall

While in the $m \geq 3$ domain:

$$\sigma_1 = \frac{\sigma_z}{2} + \sqrt{\tau_R^2 + \left(\frac{\sigma_z}{2}\right)^2} = \frac{z\bar{\gamma}}{2} + \sqrt{\tau_R^2 + \left(\frac{z\bar{\gamma}}{2}\right)^2}$$

$$\sigma_2 = \sigma_\varphi = \frac{2z\bar{\gamma}}{m-1}$$

$$\sigma_3 = \frac{\sigma_z}{2} - \sqrt{\tau_R^2 + \left(\frac{\sigma_z}{2}\right)^2} = \frac{z\bar{\gamma}}{2} - \sqrt{\tau_R^2 + \left(\frac{z\bar{\gamma}}{2}\right)^2} .$$

In this case the radial and axial directions are not principal directions.

Neglecting the pressure of water, we consider the most suitable conditions and locations for erosion. As it is known, the Coulomb-criterion is equivalent to the assumption of a linear Mohr-envelope:

$$\tau = \frac{1}{2\sqrt{B}} [\sigma(B-1) + \sigma_D] .$$

Accepting this criterion, fracture will occur on the surface of the hole, if

$$\sigma_3 = \frac{\sigma_1}{B} + \sigma_t = \frac{1}{B}(\sigma_1 - \sigma_D),$$

where

σ_D is the uniaxial compressive strength,
σ_t the tensile strength,
$B = -\sigma_D/\sigma z$ the Brinke-number $(B > 1)$
σ_1 the greatest principal stress,
σ_3 the lowest principal stress.

As shown in Fig. 2, the governing Mohr-circle extends to the domain of tensile loading if τ_R is existing. This state is very unfavourable, for rocks, because the resistance of rocks is weak opposite to the tensile loading. In the region $2 < m < 3$ the shear stress necessary to cause fracture is:

$$(\tau_R)^* = \left\{ \frac{1}{B^2} \left[\frac{2z\bar{\gamma}}{m-1} - \sigma_D \right]^2 - \frac{z\bar{\gamma}}{B} \left[\frac{2z\bar{\gamma}}{m-1} - \sigma_D \right] \right\}^{1/2} .$$

The corresponding expression in the $m > 3$ domain is

$$(\tau_R)^* = \left\{ \frac{1}{4} \left[\frac{z\bar{\gamma}}{2}(B-1) + \sigma_D \right]^2 - \left(\frac{z\bar{\gamma}}{2} \right)^2 \right\}^{1/2} .$$

Next, we consider a horizontal flow channel of circular cross-section. From the point of view of fracture we should investigate the stresses at the roof and at the floor of the hole. Without the presence of water the radial, tangential and axial stress components are all principal:

$$\sigma_r = 0$$

$$\sigma_\varphi = z\bar{\gamma}\frac{4-m}{m-1}$$

$$\sigma_z = z\bar{\gamma}\frac{4-m}{m(m-1)}\,.$$

In the case $m > 4$, both the tangential and axial stresses are tensile stresses.

If water flows in the channel, and moreover, $2 < m < 4$, the principal stresses are

$$\sigma_1 = \sigma_\varphi = z\bar{\gamma}\frac{4-m}{m-1}$$

$$\sigma_2 = \frac{\sigma_z}{2} + \sqrt{\tau_R^2 + \left(\frac{\sigma_z}{2}\right)^2} =$$

$$= \frac{z\bar{\gamma}}{2}\frac{4-m}{m(m-1)} + \sqrt{\tau_R^2 + \left[\frac{z\bar{\gamma}}{2}\frac{4-m}{m(m-1)}\right]^2}$$

$$\sigma_3 = \frac{\sigma_z}{2} - \sqrt{\tau_R^2 + \left(\frac{\sigma_z}{2}\right)} =$$

$$= \frac{z\bar{\gamma}}{2}\frac{4-m}{m(m-1)} - \sqrt{\tau_R^2 + \left[\frac{z\bar{\gamma}}{2}\frac{4-m}{m(m-1)}\right]^2}$$

In the $m > 4$ region:

$$\sigma_1 = \frac{\sigma_z}{2} + \sqrt{\tau_R^2 + \left(\frac{\sigma_z}{2}\right)^2}$$

$$\sigma_2 = \frac{\sigma_z}{2} - \sqrt{\tau_R^2 + \left(\frac{\sigma_z}{2}\right)^2}$$

$$\sigma_3 = \sigma_\varphi\,.$$

In the case $m = 4$ the loading is pure shear, that is

$$\sigma_1 = \tau_R$$

$$\sigma_2 = \tau_\varphi = 0$$

$$\sigma_3 = -\tau_R\,.$$

The shear stress necessary to fracture in the region $2 < m < 4$ is:

$$(\sigma_R)_* = \left\{ \frac{1}{B^2} \left[z\bar{\gamma} \frac{4-m}{m(m-1)} - \sigma_D \right]^2 - \frac{z\bar{\gamma}}{B} \frac{4-m}{m(m-1)} \times \right.$$
$$\left. \times \left[z\bar{\gamma} \frac{4-m}{m(m-1)} - \sigma_D \right] \right\}^{1/2}.$$

In the case $m > 4$ we get a simpler formula:

$$(\tau_R)^* = z\bar{\gamma} \frac{m-4}{m(m-1)} \sqrt{B(B-1)}.$$

Finally, in the case $m = 4$,

$$(\tau_R)^* = \frac{\sigma_D}{B+1}.$$

Some typical parameters of coherent rocks are, approximately:

$$\sigma_D = 10^3 \sim 10^4 \frac{Mp}{m^2}$$
$$B = 5 \sim 15$$
$$m = 3 \sim 5.$$

The practically important values of $z\bar{\gamma}$ are in the range of 10^2—10^3 Mp/m^2. It is obvious that τ_R cannot lead to erosion, since for weakly coherent rocks the shear stress necessary to the fracture of a vertical hole is $\tau_R^* > 330$ Mp/m^2. Erosion may be possible for incoherent rocks if their state of stress is near to the fracture due to lithostatic forces. In horizontal holes $\tau_R^* > 200$ Mp/m^2 for coherent materials. The result is the same as for vertical flow channels. [The shear stress of the flowing fluid cannot cause a considerable mechanical erosion in the flow channels.] In our opinion the main reason of the erosion is the cavitation occurring in the flow of the water.

3. Mechanical effects in cavitating flow

As it is known, the mechanical energy of the flowing fluid is constant along a streamline:

$$\frac{c^2}{2g} + \frac{p}{\gamma} + z + \lambda \frac{L_e}{D} \frac{c^2}{2g} = \text{const.}$$

This is the Bernoulli-equation for real fluids, its last term represents the energy loss due to viscosity. The kinetic energy $c^2/2g$ of the flowing fluid varies with the cross-sectional area of the channel:

$$\frac{c^2}{2g} = \frac{8}{g} \frac{Q^2}{(D^2 \pi)^2} .$$

where Q is the flow rate (m^3/sec).

Decrease of the cross-sectional area leads to the increase of kinetic energy and reduction of pressure. This depression can reach the saturation pressure of the vapor p_G belonging to the given temperature of the water.

At the saturation pressure of water vapor phase occurs and bubbles are formed which then are carried off by the flow. The two-phase flow composed of water and of its vapor is called cavitating flow. Cavitation bubbles grow in the low-pressure region, sometimes oscillate and eventually collapse and disappear where the pressure rises again.

Capillary pressure is inversely proportional to the radius of the bubbles. Thus, the rise of pressure to its maximum occurs in a time of about a microsecond and over a very small area. This pressure peak was determined as at least 12 000 atm in Jones' direct measurements. The peak pressures developed during collapse can be certainly high enough to cause mechanical damage to the rocks. This pin-prick-like loading over a very small area, and of high frequency, leads to surface damage of the flow channels.

From the point of view of fracture besides the high pressure peak, the high-frequency loading is also important. The rock, considered as a Poynting—Thomson-body, shows very different behaviour under different loading or shear rates. At uniaxial state of stress

$$\sigma = E\,\varepsilon + \lambda_0 \frac{d\varepsilon}{dt} - d \frac{d\sigma}{dt},$$

where

E is the Young's modulus,
λ_0 coefficient of linear viscosity,
ϑ constant of relaxation,
t time.

At constant speed of loading

$$\frac{d\sigma}{dt} = a$$

that is

$$\sigma = E\varepsilon + a\left(\frac{\lambda_0}{E} - \vartheta\right)\left(1 - e^{-\frac{E\sigma}{\lambda_0 a}}\right).$$

At quasi-static loading $a = 0$, thus

$$\sigma = E\varepsilon$$

finally, for $a = \infty$

$$\sigma = \frac{\lambda_0 \varepsilon}{\vartheta} .$$

For high-strength rocks

$$\frac{\lambda_0}{\sigma} \gg E$$

Thus, at high-speed loading, the behaviour of rock is brittle. For this reason cavitation erosion of even the highest-strength rocks is possible. Thus, mechanical erosion begins with cavitation, the damaged rock surface cannot withstand the shear stresses on the wall.

Because of the extreme complexity of the behaviour of cavitation bubbles and particularly because of the impossibility of describing in detail the hydrodynamical, thermodynamical and electrochemical aspects of this phenomenon, experimental studies seem more appropriate than analytical methods. A lot of important questions have arisen in the course of the investigation. Where does cavitation flow occur in the flow channel? To answer, using the known hydrodynamical equations, we have to know the geometry of the channel-system and the temperature.

The latter is necessary to determine saturation vapor pressure. The saturation pressure of water, as depending on temperature, is shown in Fig. 3.

Another important task is to determine the inception of cavitation. Altough in most engineering applications it has been assumed that cavitation would occur when the pressure drops to vapor pressure, it should be clear that this is an oversimplification. Surface tension, the varying air content, the structure of the flow pattern can all modify the occurrence of cavitation.

Materials exposed to cavitation are subject to severe damage, especially in regions of cavity collapse. The pressure peaks are certainly high enough to account for brittle or fatigue failure of most materials. Generally, ductile materials at first exhibit little or no loss in weight, brittle materials may exhibit weight loss early in the process. The resistance to cavitation damage is an important property of the different materials.

Figure 4 shows an experimental apparatus which is suitable to investigate this property. It consists of a closed-loop pipe system, in which the pressure level of the flow can be controlled by the vacuum pump joined to the tank. Bubbles are generated in the throat of the Venturi-like specimen, and they collapse in the diffuser-section.

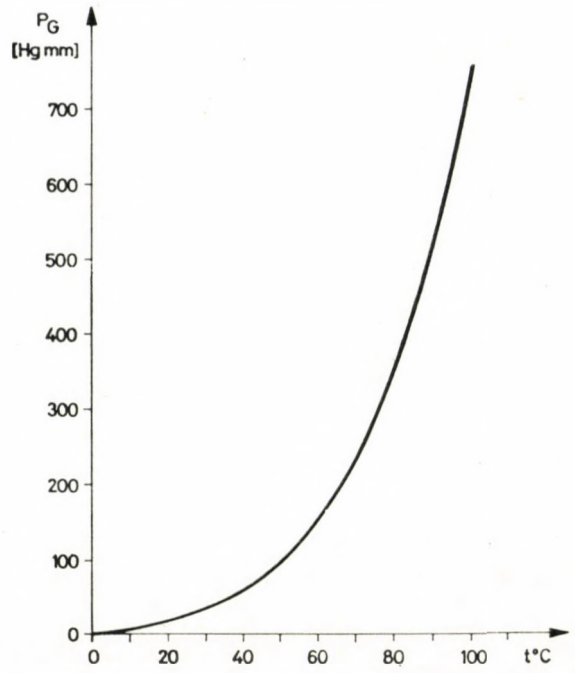


Fig. 3. Dependence of the vapor pressure of water on temperature

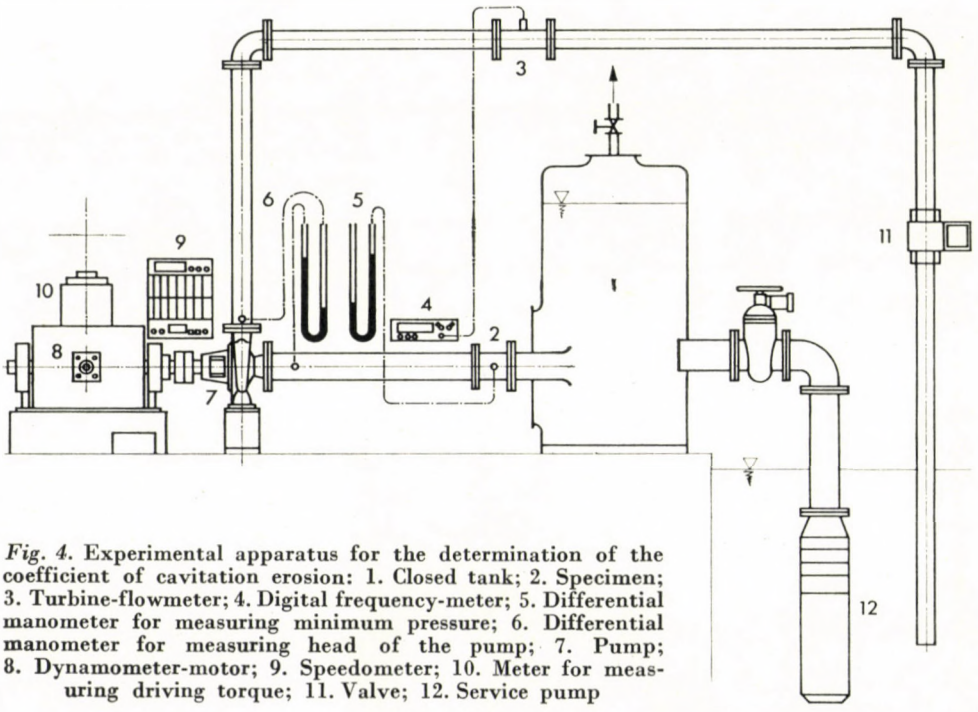


Fig. 4. Experimental apparatus for the determination of the coefficient of cavitation erosion: 1. Closed tank; 2. Specimen; 3. Turbine-flowmeter; 4. Digital frequency-meter; 5. Differential manometer for measuring minimum pressure; 6. Differential manometer for measuring head of the pump; 7. Pump; 8. Dynamometer-motor; 9. Speedometer; 10. Meter for measuring driving torque; 11. Valve; 12. Service pump

Specimens of the same shape but of different material can be exposed on cavitation erosion during a given time. The weight loss of the specimens characterizes the resistance of the rocks against cavitation damage.

$$B = \frac{\Delta G}{\Delta t} [g/\text{hours}] .$$

If the shape of the specimen and the experimental conditions are strictly standardized, this parameter can be very valuable for engineering applications.

4. Summary

The system of flow channels can be deduced to a straight, cylindrical pipe by introducting the equivalent length and the mean hydraulic radius. In this hydraulically equivalent pipe-flow shear stresses can be determined as function of the mean velocity and of the relative roughness of the walls.

The predicted shear stresses are not sufficient to cause fracture of any coherent rock. The cause of erosion is the process of cavitation. The high-frequency loading with high-pressure peaks can lead to the fracture of high strength rocks, as it follows from the Poynting—Thomson rheological model.

The rheological properties of the rocks *together* with the hydrodynamical parameters characterize the process of erosion. This extremely complex phenomenon can be investigated only experimentally. The resistance to cavitation damage of the rocks is a characteristic property of the materials. For experimental investigations a test apparatus has been designed and a measure of the resistance introduced.

REFERENCES

1. KAPOLYI, L.: New Trends of Research in Protection Against Mine Water. 7th. Conf. on Protection Against Mine Water, Budapest (1976).
2. SCHMIEDER, A.—KESSERÜ, Zs.—JUHÁSZ, J.—WILLEMS, T.—MARTOS, F.: Water Danger and Economy in Mining (In Hungarian). Műszaki Könyvkiadó, Budapest (1975).
3. SOMOSVÁRI, Zs.: Berechnung der Bodensenkungen und Formänderungen durch Wasserspiegelabsenkungen. 7th. Conf. on Protection Against Mine Water, Budapest (1976).
4. BOBOK, E.—SZABÓ, I.: Hidravlicheskoie issledovaniije karakteristik gyebita proriva vodi imeyuschikhmaksimum. 7th. Conf. on Prot. Ag. Mine Water, Budapest (1976).
5. PRANDTL, L.: The Essentials of Fluid Dynamics. Blackie, Glasgow (1952).
6. NIKURADSE, M.: Gesetzmäßigkeit der turbulenten Strömung in glatten Rohren. VDI. *Forschungsheft*, 356 (1932).
7. KÁRMÁN, T.: Turbulence and Skin Friction. *J. Aeronat. Sci.*, 1 (1936).
8. VARGA, J.: Handbook of Hydraulic and Pneumetic Mechanics (in Hungarian). Műszaki Könyvkiadó, Budapest, 1974.
9. ASSZONYI, Cs.—RICHTER, R.: An Introduction to the Rheological Theory of Rock Mechanics. NIM TK, 1974.

МЕХАНИЧЕСКАЯ ЭРОЗИЯ ВОДОНОСНЫХ ЗАХОДОК ГОРНЫХ ПОРОД

Э. БОБОК—Ж. ШОМОШВАРИ

РЕЗЮМЕ

Механическую эрозию водоносных заходок горных пород совместно характеризуют жесткостные и геологические свойства горной породы, а также гидродинамические параметры протечной воды.

В статье показывается, что в процессе эрозии определяющую роль играют не столько жапряжения на сдвиг, как кавитация.

Acta Geodaet., Geophys. et Montanist. Acad. Sci. Hung. Tomus 14 (4), pp. 437—448 (1979)

FEASIBILITY OF COMBINED MINING TECHNOLOGICAL SYSTEMS IN PRODUCTION OF MINERAL MASSIFS

J. PATVAROS
TECHNICAL UNIVERSITY OF THE HEAVY INDUSTRIES, MISKOLC

[Manuscript received May 19, 1977]

The study gives an analysis of the economy of combined application of various mining technological systems (underground, open-pit, sub-water and borehole mining) in exploitation of mineral massifs. An actual example illustrates the ways how to combine various mining technological systems in space and time so as to achieve an optimum.

Introduction

Complex production and use of minerals are feasible in many deposits both in Hungary and abroad instead of using conventional mining techniques. Utilising conventional mining methods, usually only one mining system (e.g., underground mining or open-pit mining) is adopted in the same mine. However, various technological systems could be applied to produce several useful components from mineral deposits all over the world. In this way a higher degree of economic efficiency can be achieved in exploiting the mineral massif of a mine as compared to mono-seam-production. Further increase can be achieved in the total profit by applying multi-step mineral processing for each of the useful minerals (sand, coal, bauxite, water etc.).

The study does not intend to analyse in details the natural (geologic, hydrogeologic etc.), technological and technical (mechanical) and economical parameters (investition demand, labour consumption etc.) affecting the economy of mining technological systems (open-pit mining — O, underground mining — U, sub-water-production — W, borehole-production — H). Their global evaluation is believed to be sufficient to ensure a comparison being correct in order of magnitude.

To the author's mind, this view and analysis are satisfactory to prove that various mining technological systems benefit from their being combined in space and time while exploiting a mineral massif. This combination enables us to utilize the natural possibilities in a complex way and to protect them [1, 2, 3, 4, 5, 6, 7].

Analysis of combined mining technological systems

Figure 1 shows the mining technological systems which can be used in producing solid minerals. The figure illustrates also the interconnection graphs of these technological systems.

As regards the applicability of mining technological systems, the mineral deposits can contain one useful component (coal or bauxite), only or several of them, respectively (sand, clay, coal, bauxite, water etc.). Mineral deposits containing one useful component only can be extracted, using one or more mining technological systems.

Dealing with production problems of an actual mineral deposit, a very careful technical-economical analysis can only determine that particular combination of mining technological systems which gives the best result.

The field of application of any mining technological system is limited by technical, economical and safety regulations. This field of application can be enlarged to a great extent by combining various mining technologies. Major groups of possible combinations can be outlined as follows:

i) Using various mining technological systems distributed in space and time in different seams of the same massif.

ii) Successive application of various systems in the same or different seams.

iii) Systems supported by each other.

Fig. 2 illustrates the exploitation of a productive mineral massif by combined mining technologies distributed in space and time. In this case, e.g. sand or clay is extracted by open-pit technology from the upper part of the

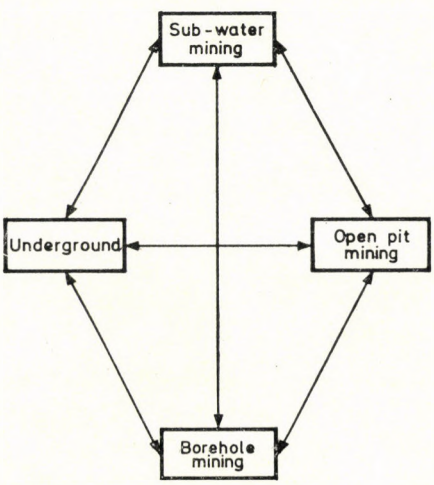


Fig. 1. Interconnection graph of mining technological systems

mineral massif of a district. The coal seam can be extracted from the middle of the field or from medium depth by underground mining. The material of the bauxite lenses bedded on the basement rock is extracted from the deepest level by borehole mining [5, 6 and 7].

The application of mining technological systems is considered as of successive type if (in the example of Fig. 2) the coal pillars remained in place after exploitation of the coal seam, or bauxite lenses in deeper layers are produced by borehole method.

Distributed or successive combined technological systems adopted to a mineral massif can ensure a higher degree of integration of the production processes than conventional mining technologies. Thus, in the example of Fig. 2, water produced by open-pit, underground and borehole mining can be used for winning, transporting, mineral processing, industrial and social water supply, for stowing cavities and disposal of waste. The combination of these technological systems brings about the technical advantage that in almost all of the working processes outlined here, more or less the same equip-

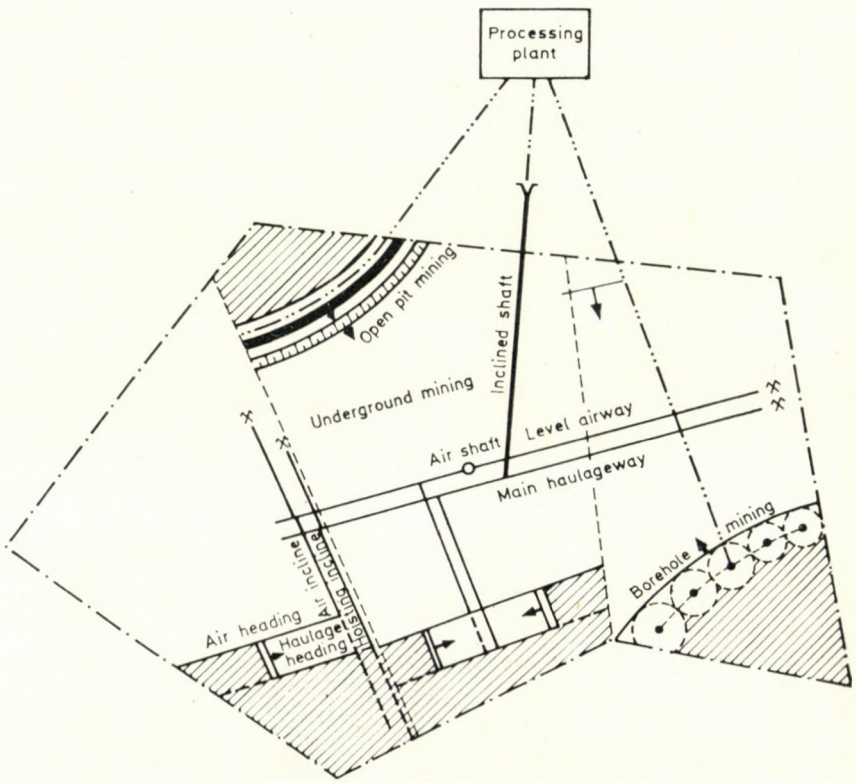


Fig. 2. Producing various mineral materials by combined mining technologies from a productive massif

ment and machinery can be used. This fact is of extraordinary importance from the point of view of reliability and maintenance of the technological systems.

Figure 3 illustrates a possible application of combinedmining technological systems supported by each other. Using this type of application, not only complex hydromechanisation of the working processes can be achieved, but the different products of these technologies (sand, coal, bauxite etc.) can be transported through a single underground main haulage road and hoisting shaft to the integrated mineral processing plant on the surface. The mining technological systems supported by each other can successfully overcome disadvanta-

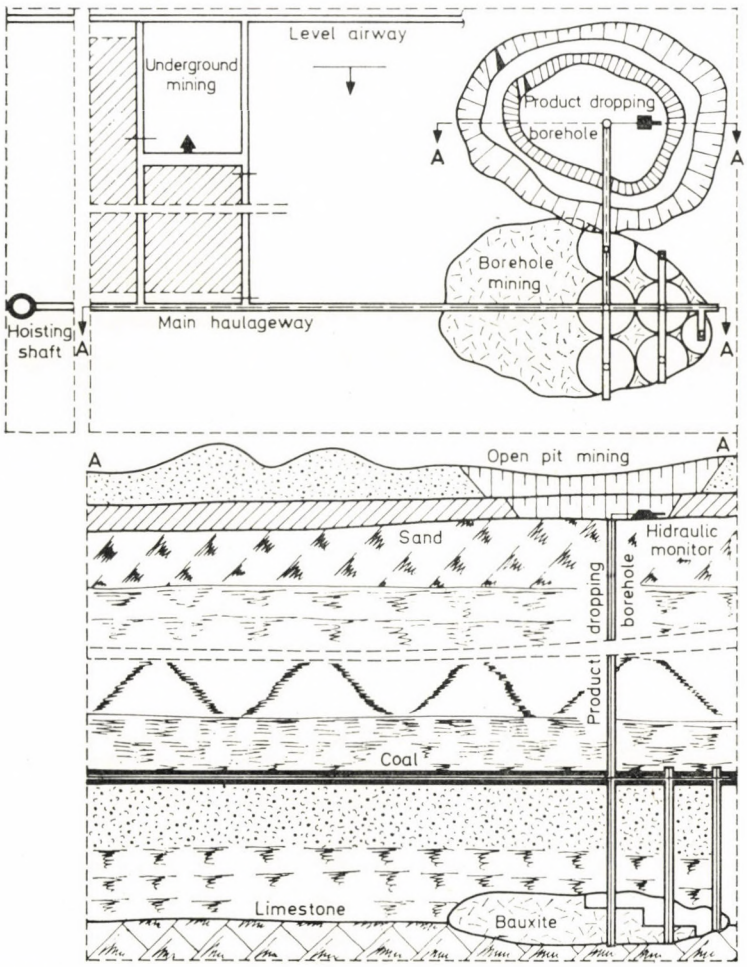


Fig. 3. Ways of joining various mining technological systems to a single main haulageway while extracting a mineral massif

geous surrounding conditions affecting the production and they can avoid damage to the natural environment caused by mining activities [5, 6 and 7].

According to Fig. 3, e.g. the underground production of the coal seam can solve the water drainage problems of the open-pit sand mining, thus lowering the production costs of sand mining. This example shows further that extracting bauxite through boreholes, water hoisting costs and danger due to water are essentially decreased. It is clear at the same time that damage and pollution caused to the environment are much less if the waste of open-pit mining can find its disposal in the mined-out areas of underground and borehole mining technological systems.

Figure 4 shows the variation of estimated production costs with increasing mining depth — the only parameter taken account of in this investigation. The curves compare the successive type of application and the system of technologies supported by each other. It can be clearly seen that the application of mining technological systems supported by each other, may essentially reduce the costs [3].

The profits to be gained by various mining technological systems can be analysed as illustrated in Table I. The subjects of the analysis are major blocks of the mineral deposit (coal, bauxite etc.) determined tectonically or by technical-economical calculations. Here Q_{ij} means the fraction in tons which can be extracted from the mineral reserves Q_i using mining technological system j (open-pit mining — O, underground mining — U, sub-water-production — W, borehole-production — H). The profit to be gained by producing unity amount

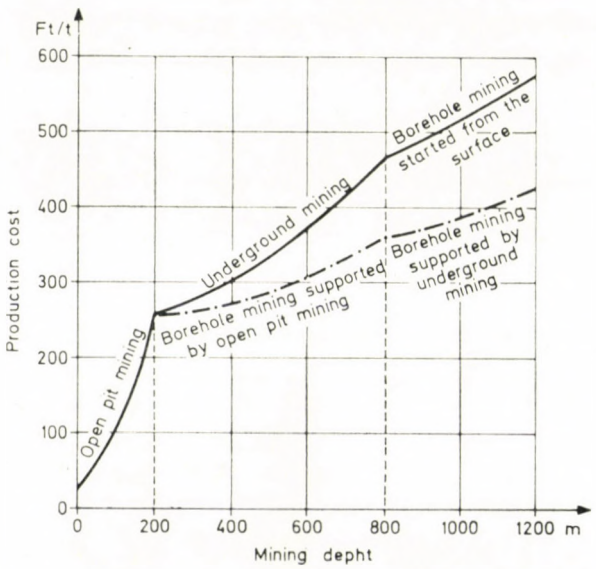


Fig. 4. Variation of production cost per ton with increasing mining depth, utilizing various mining technological systems

Table I

Fraction of mineral reserves	Mining technological system				Total profit
Q_i t	O	U	W	H	Ft
Q_1	$Q_{1O}\, e_{1O}$	—	$Q_{1W}\, e_{1W}$	—	$\sum_1^e Q_{1j}\, e_{1j}$
Q_2	$Q_{2O}\, e_{2O}$	—	$Q_{2W} e_{2W}$	—	$\sum_1^j Q_{2j}\, e_{2j}$
.	.	.	.	.	.
Q_i	—	$Q_{iU}\, e_{iU}$	—	$Q_{iH}\, e_{iH}$	$\sum_1^j Q_{ij}\, e_{ij}$
.	.	.	.	.	.
Q_n	—	$Q_{nU}\, e_{nU}$	—	$Q_{nH}\, e_{nH}$	$\sum_1^j Q_{nj}\, e_{nj}$
Total amount of mineral reserves $\sum_1^n Q_i = Q$	$\sum_1^n Q_{iO}\, e_{iO}$	$\sum_1^n Q_{iU}\, e_{iU}$	$\sum_1^n Q_{iW}\, e_{iW}$	$\sum_1^n Q_{iH}\, e_{iH}$	$\sum_1^n \sum_1^j Q_{ij}\, e_{ij}$

of mineral reserves Q_i using mining technological system j, is denoted by e_{ij} and expressed in Ft/t.

Using the data given in Table I, the mining technological systems should be applied to the units of the mineral deposit so as to ensure maximum total profit, i.e. to meet the demand $\sum_1^n \sum_1^j Q_{ij}\, e_{ij} \rightarrow \max$.

However, the task outlined here seems only at a first glance simple. This is the case if the technological systems are supposed to work with fixed structure, working method and machinery. If these parameters change, the determination of the optimum pattern of mining technological systems may require a considerable amount of calculation. The analysis aimed at to ensure optimum conditions, is further complicated if also the time factor is taken into account, i.e. that fact that the mining technological systems start or may start to work in different moments of time and they are in operation for various periods.

When dealing with production problems of any given mineral massif, the most advantageous mining technological system has to be determined separately for each useful component and area. A possible pattern of the technological system is shown in Table II for a massif with four minerals. Here Q_{ij} means the fraction of mineral i which can be extracted by mining

Table II

Mineral material		Mining technological system				Total profit
Denomination	Amount 10^6 t	O	U	W	H	Ft
Sand	Q_S	$Q_{SO}\, e_{SO}$	—	$Q_{SW}\, e_{SW}$	—	$\Sigma\, Q_{Sj}\, e_{Sj}$
Coal	Q_C	—	$Q_{CU}\, e_{CU}$	—	$Q_{CH}\, e_{CH}$	$\Sigma\, Q_{Cj}\, e_{Cj}$
Bauxite	Q_B	—	$Q_{BU}\, e_{BU}$	—	$Q_{BH}\, e_{BH}$	$\Sigma\, Q_{Bj}\, e_{Bj}$
Water	Q_W	—	$Q_{WU}\, e_{WU}$	—	$W_{WH}\, e_{WH}$	$\Sigma\, W_{Wj}\, e_{Wj}$
	$\Sigma\, Q_{\text{mineral}}$	$\Sigma\, Q_{iO}\, e_{iO}$	$\Sigma\, Q_{iU}\, e_{iU}$	$\Sigma\, Q_{iW}\, e_{iW}$	$\Sigma\, Q_{iH}\, e_{iH}$	$\sum_{1}^{i}\sum_{1}^{j} Q_{ij}\, e_{ij}$

technological system j (sand — S, coal — C, bauxite — B, water — W) and e_{ij} is the profit to be gained. The selection of the mineral materials according to mining methods on the basis of the profit e_{ij} to be gained is extremely difficult. One of the biggest problems is that e_{ij} is a multivariable-function depending on natural, technical and economical parameters even in the case of a given mining technological system.

Broadly outlined, e_{ij} characterizing any technological system can be generally formulated as follows:

$$e_{ij} = f_{ij}\,(H; q; Q; t; R; E; M; b) \quad [\text{Ft/t}]$$

with

- H average mining depth [m]
- q average annual output [10^6 t/a]
- Q amount of mineral to be extracted by a given mining technological system [10^6 t]
- t time of production increase including the time demand for prospecting and mine constructing [year]
- R average reliability index of a given mining technological system
- E specific energy consumption [kWh/t]
- M labour consumption [man, shift/t]
- b specific investition demand [Ft/t, a]

Table II represents the graph of a technological system. Here various ways and various interconnections of technological systems, respectively, can be determined for producing various mineral materials. The optimum combination of mining technological systems can be chosen for a given massif and a time horizon meeting the demand $\Sigma\, K_{Ti} \rightarrow \max$. This can be done from the possible combinations of Table III.

Table III

Combinations of mining technological systems	Producible useful mineral material				Total profit ΣK_{ij}
	S	C	B	W	
T_1	O	U	U	U	ΣK_{T1}
T_2	O	U	H	U	ΣK_{T2}
T_3	O	U	H	H	ΣK_{T3}
T_4	O	H	H	H	ΣK_{T4}
T_5	W	U	U	U	ΣK_{T5}
T_6	W	U	H	U	ΣK_{T6}
T_7	W	U	H	H	ΣK_{T7}
T_8	W	H	H	H	ΣK_{T8}

While choosing the technically and economically possible combinations, one has, of course, to take account of the scientific and technical progress which can cause the field of application of any mining technological system to widen essentially. It can be imagined, e.g. that in the future the same or nearly the same producing equipment will be used in the open-pit and underground mining technological systems, regardless of the development method.

The selection of the combinations of the mining technological systems is affected by the fact that the open-pit, underground and sub-water mining are in possession of well established structures and machine types which are under continous development. However, the majority of the winning and transporting machines of the borehole production method are to be developed and experimented in future only, except the drilling equipment.

Borehole production of solid minerals is usually connected with change of state (leaching, melting, gasification etc.) which is far more difficult to control than the conventional types of mining methods. On the other hand, it has to be taken into account that the borehole production as shown in Fig. 5, can be adopted in the widest variety of spatial arrangement and very flexibly connected to any other mining technological system [1, 2, 3, 4, 5, 6 and 7].

Using the borehole mining method, the production, transport and, perhaps, processing methods of oil production may be adopted to the mining of solid mineral deposits. Thus, the mining technological systems of solid and fluid minerals may be joined from scientific and technical point of view. The joint mining technological systems may ensure economic production of such mineral deposits which would be by far out of consideration if using only a conventional type of mining [1, 2 and 3].

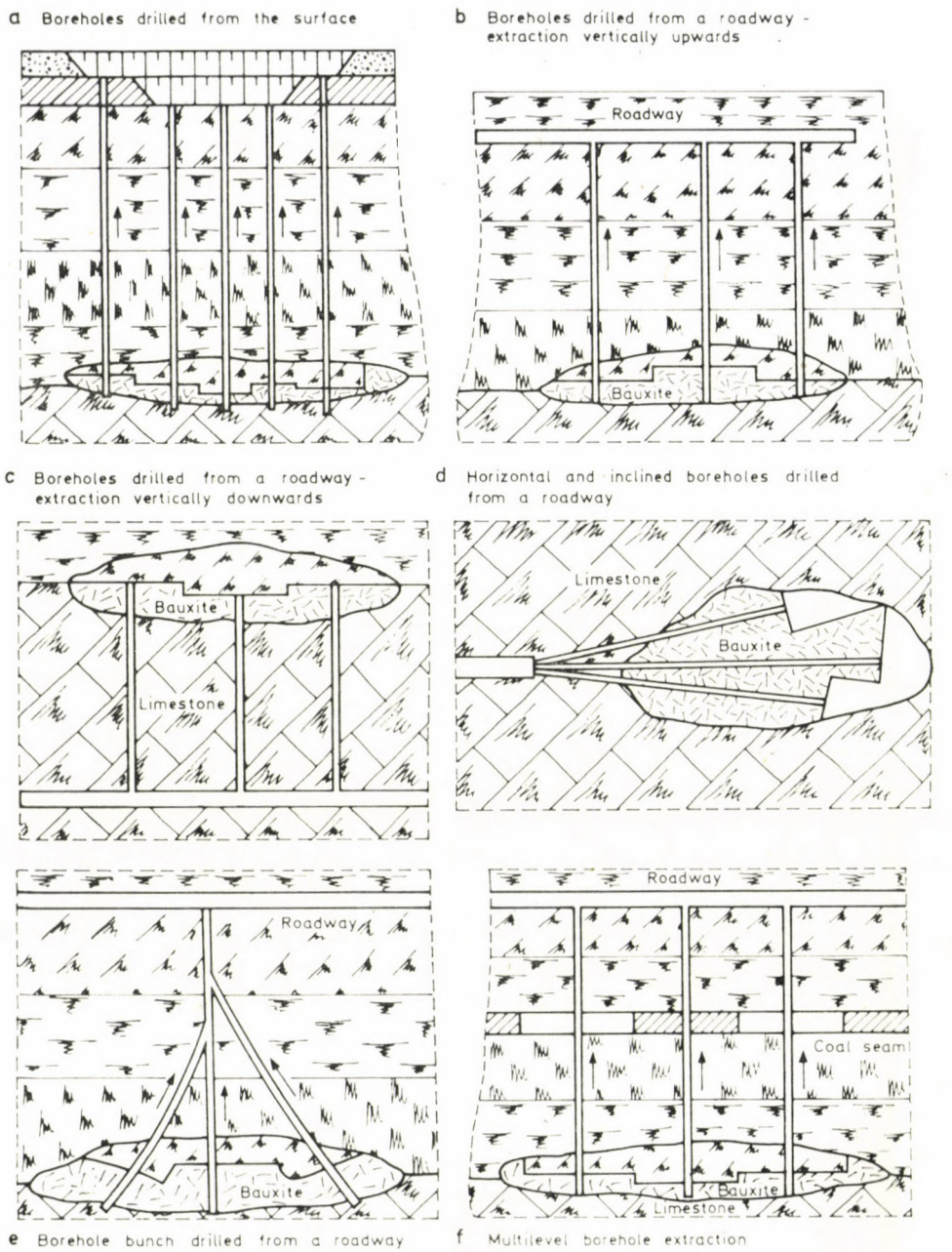


Fig. 5. **Feasibility of various borehole mining technologies in extracting solid mineral bodies**

Example for selecting the optimum combination of mining technological system

In the following, quantities of minerals to be found in a productive massif and the specific profits to be gained by various mining technological systems, are given:

i) Quantity of sand $Q_S = 20 \cdot 10^6$ t
Specific profit of strip mining $e_{SO} = 80$ Ft/t
sub-water mining $e_{SW} = 150$ Ft/t
ii) Quantity of coal to be extracted by underground mining $Q_{CU} = 30 \cdot 10^6$ t
Specific profit of underground mining $e_{CU} = 50$ Ft/t
Quantity of coal to be extracted by borehole method (lessened because of higher losses) $Q_{CB} = 25 \cdot 10^6$ t
Specific profit of borehole hydromechanical method $e_{CB} = 100$ Ft/t
iii) Quantity of bauxite to be extracted by underground mining $Q_{BU} = 15 \cdot 10^6$ t
Specific profit of underground mining $e_{BU} = 50$ Ft/t
Quantity of bauxite to be extracted by borehole method from the same area $Q_{BB} = 10 \cdot 10^6$ t
Specific profit of borehole method $e_{BB} = 120$ Ft/t
iv) Quantity of water to be extracted by underground or borehole mining $Q_W = 300 \cdot 10^6$ m^3
Specific profit of underground water production $e_{WU} = 5$ Ft/m^3
borehole water production $e_{WB} = 10$ Ft/m^3

The results of the calculations carried out with the above data, are shown in Table IV. For the sake of simplicity, the useful mineral components about a given section of mine were supposed to be extracted by only one or another particular

Table IV

Combinations of mining technological systems	Profit when extracting a useful mineral by a particular technological system 10^9 Ft				Total profit 10^9 Ft
	Sand	Coal	Bauxit	Water	
T_1	1.60	1.50	0.75	1.50	$\Sigma K_{T1} = 5.35$
T_2	1.60	1.50	1.20	1.50	$\Sigma K_{T2} = 5.80$
T_3	1.60	1.50	1.20	3.00	$\Sigma K_{T3} = 7.30$
T_4	1.60	2.50	1.20	3.00	$\Sigma K_{T4} = 8.30$
T_5	3.50	1.50	0.75	1.50	$\Sigma K_{T5} = 7.25$
T_6	3.50	1.50	1.20	1.50	$\Sigma K_{T6} = 8.70$
T_7	3.50	1.50	1.20	3.00	$\Sigma K_{T7} = 9.20$
T_8	3.50	2.50	1.02	3.00	$\Sigma K_{T8} = 10.20$

mining technological system. In reality, this condition is not necessarily met or may not be met at all. However, even in that case if the mineral materials about any section of mine can be extracted by various mining methods, the optimum combination of mining technological systems can be selected similarly as shown in Table IV.

According to Table IV, the rank of the mining technological system combinations based on the total profit to be obtained, can be written as follows:

$$\Sigma K_{T8} > \Sigma K_{T7} > \Sigma K_{T6} > \Sigma K_{T4} > \Sigma K_{T3} > \Sigma K_{T5}\, \Sigma K_{T2} > \Sigma K_{T1}$$

Conclusion

The steadily increasing demand for mineral raw materials, the need of efficient protection of the environment and the struggle to achieve the advantages of the industrial concentration, suggest complex production of mineral massifs. The aim of a high degree of economy ensures and requires the use of combined mining technological systems.

On the other hand, the adoption of combined mining technological systems in producing mineral massifs, makes it possible to introduce the newest achievements of scientific research in the possible shortest time. An extremely high level of integrated automation can be utilized in all of the working processes of the extraction and mineral processing which is impossible in the conventional type of technology.

There are many possibilities for adopting combined mining technological systems. Some of these are mentioned below.

i) The possible results of adopting a new technological system (e.g. borehole method) can be investigated in mines which have been claimed to be exhausted while using another method of working (e.g. underground mining).

ii) It can be determined in operating mines which areas are suitable for mono mining systems only, and where can successive or combined mining technological systems supported by each other applied.

iii) While exploring new mineral deposits, all parameters characterizing the quantitative, qualitative and spatial distribution of the useful components have to be investigated thoroughly down to the basement rock. Knowing the data of exploration in detail, the combinations of mining technological systems of practical importance can be outlined and their rank determined. For the technically and economically optimum combination of mining technological systems, the best pattern of starting with the partial systems can be prescribed.

Having sufficient amount of information, the combined mining technological systems must be analysed from the application's point of view, not only for a given basin but for the whole country. This ensures a concentrated and complex location of industry from the economic geology's point of view, based on the mining of a given massif.

REFERENCES

1. Arens, V. Zh.: Geotechnical ways of production of minerals. Nedra, Moscow, 1975.
2. Zambó, J. et al.: The possibility of application of geotechnical mining methods of working in the production of solid mineral deposits in Hungary. Research Report. Technical University for Heavy Industry, Department of Mining, Miskolc, 1975.
3. Tóth, M.: Natural conditions determining the optimum mining method of working in mineral deposits. (Manuscript) 1975.
4. Authors' group: Geotechnical and geochemical production methods of minerals. Report for the National Technical Development Committee, 1976.
5. Patvaros, J.: The possibility of application of a new type of mining technological systems in producing Hungarian bauxite deposits. Publications of the Technical University for Heavy Industry. Ser. 1. Mining. 22 (1976), 237—251. Miskolc, 1976 (In Hungarian).
6. Patvaros, J.: Feasibility of borehole mining method of working in producing Hungarian mineral deposits. Study written for the competition of the Hungarian Academy of Sciences. 1976.
7. Patvaros, J.: Hydraulic extraction of bauxite through boreholes. Competition by the paper Műszaki Élet (Technical Life), 1976.

ПРИМЕНЯЕМОСТЬ КОМБИНИРОВАННЫХ ГОРНЫХ ТЕХНОЛОГИЧЕСКИХ СИСТЕМ ДЛЯ РАЗРАБОТКИ МИНЕРАЛЬНЫХ МАССИВОВ

Й. ПАТВАРОШ

РЕЗЮМЕ

В статье анализируется экономичность комбинированного применения различных горных технологических систем (глубинная разработка, карьером, разработка из под гидроскопии, разработка скважинами) для случая разработки минерального массива. Самые целесообразные возможности соединения в пространстве и во времени различных горных технологических систем показываются на конкретном примере.

Acta Geodaet., Geophys. et Montanist. Acad. Sci. Hung. Tomus 14 (4), pp. 449—472 (1979)

DIE ANWENDUNGSMÖGLICHKEITEN DER BOHRLOCH-ABBAUTECHNOLOGIE BEI DER GEWINNUNG DER HEIMISCHEN BAUXITVORKOMMEN

J. PATVAROS

UNIVERSITÄTSDOZENT, KANDIDAT DER TECHN. WISSENSCHAFTEN, LEHRSTUHL FÜR BERGBAU AN DER TECHNISCHEN UNIVERSITÄT FÜR SCHWERINDUSTRIE, MISKOLC, UNGARN

[Eingegangen am 10. September 1977]

Das Absenken des aktiven Wasserniveaus bürdet immer größere technisch-wirtschaftliche Lasten auf die herkömmlichen Bauxitgewinnungsverfahren. Dieses Hindernis kann durch ein neues hydraulisches Bergbauverfahren — das sog. Bohrlochverfahren — bekämpft oder wesentlich beseitigt werden. Die Studie behandelt ausführlich die bei der Gewinnung der Bauxitlinsen in Frage kommenden hydraulisch-technischen Bohrloch-Einrichtungen, sowie die Bestimmung der für dieses Verfahren kennzeichnenden optimalen Parameter (wie Abbauwirkungsradius und Gewinnungsgrenztiefe).

Kurze vergleichende Analyse der technologischen Abbausysteme für feste Mineralgrundstoffe

Zur Gewinnung der Vorkommen mineralischer Grundstoffe sind zur Zeit die folgenden vier technologischen Systeme bekannt: Tiefbau, Tagebau, Unterwasser-Abbau, und Bohrloch-Abbau. Die ersten beiden Abbautechnologien kommen in erster Linie zur Gewinnung der flöz- oder stockartig ausgebildeten Minerallagerstätten bei mittel- oder hochfestem anstehenden Gestein zum Einsatz. Der Abbau unter dem Wasserspiegel wird vor allem zur Gewinnung von losem, körnigem Material (Sand und Kies) angewendet. Die Bohrloch-Abbautechnologie aber wird meist dazu benützt, um locker gebundene, hydraulisch auswaschbare, bzw. auslaugbare Rohstoffe, wie Schwefel und Steinsalz zu gewinnen.

Um die einzelnen bergbaulichen Abbautechnologien auf realer Grundlage miteinander vergleichen zu können, empfiehlt es sich, folgende Hauptparameter zu prüfen:

1. Mineralvorratsmenge
2. Lagerstättentiefe
3. Gewinnungskapazität
4. Gesamtabbauzeit
5. Betriebsstruktur
6. Anpassungsfähigkeit an die Umweltbedingungen
7. Investitions- und Betriebskosten

8. Erzielbare Leistungen
9. Abbauverluste und Verdünnungen
10. Entwicklungsmöglichkeiten der Technologien

Der Mineralvorrat wird bei Tiefbau-Bergbaubetrieben entweder durch die naturgemäßen und betrieblichen Gegebenheiten oder durch die ökonomischen Anforderungen bestimmt. Die wirtschaftliche Lebensdauer von Tiefbau-Grubenbetrieben beträgt bei der zur Zeit gegebenen Produktionskapazität 25—30 Jahre, und besonders dieser Kennwert bestimmt den zu gewinnenden Mineralvorrat.

Unter den vier grundlegenden Typen der Abbautechnologie ist das *Tiefbauverfahren* allein jene Lösung, die qualitativ und quantitativ geregelt werden kann und das Fördern fester Mineralrohstoffe aus großen Tiefen ermöglicht. Mit diesem technologischen System werden in unserem Land Lagerstätten fester Mineralgrundstoffe bis über 1000 m Tiefe abgebaut. Hingegen werden im Ausland unter günstigeren geologischen und geothermischen Gegebenheiten schon Tiefbaue in 4000 m Tiefe betrieben. Trotz den ungünstigen heimischen Gegebenheiten aber kann auch bei uns nach entsprechender technischer Entwicklung eine wirtschaftliche Gewinnung fester Mineralstoffe aus 2000 m und noch größeren Tiefen erwartet werden.

Die Förderkapazität der Tiefbaugruben wird in erster Linie durch die Leistungsfähigkeit der Schachtförderung begrenzt. Bei neuzeitlichen Kohlenbergwerken erreicht die Förderung im Großbetrieb heute schon 10—15 000 t/Tag, und in naher Zukunft wird es schon zum Anlegen von Bergwerksgroßbetrieben mit 20—25 000 t/Tag Kapazität kommen. In unserem Lande zählen schon Erzbergwerke mit jährlich 5—7 Mill. t Förderung zu den Großbetrieben, während im Ausland bereits Tiefbau-Erzbergwerke mit 20—30 Mill. t Jahresförderung betrieben werden.

Bei einem Tiefbau-Grubenbetrieb dauert die Erkundung des Erzvorrates gewöhnlich 2—3 Jahre. Zur Erarbeitung der konkreten Pläne und zum Entwerfen der Bergwerksanlagen aufgrund der detaillierten Erkundungsdaten ist etwa ein gleicher Zeitraum erforderlich. Die Frist für Erschließung und Ausrichtung der Grube beträgt also 3—8 Jahre. Das Anlaufen der Förderung auf volle Kapazität erfordert etwa weitere 3—5 Jahre und ebenso lange dauert auch die Auslaufszeit der Gewinnung. Da das Abbauen bei voller Kapazität etwa 25—30 Jahre beträgt, sind im Vergleich zu diesem die Zeiten für Vorbereitung und Beendigung des Abbaus unverhältnismäßig lang.

In Abb. 1 ist das technologische Schaubild des Tiefbau-Grubenbetriebes, bzw. sein Struktursystem mit Bezeichnung der Fließrichtung der verschiedenen Kraftquellen dargestellt . Wie man sieht, ist die Struktur des Tiefbaugrubensystems kompliziert und aus Einzelsystemen aufgebaut, die sich meist eng aneinander anschließen. Dies besagt, daß die relative kleinere Betriebs-

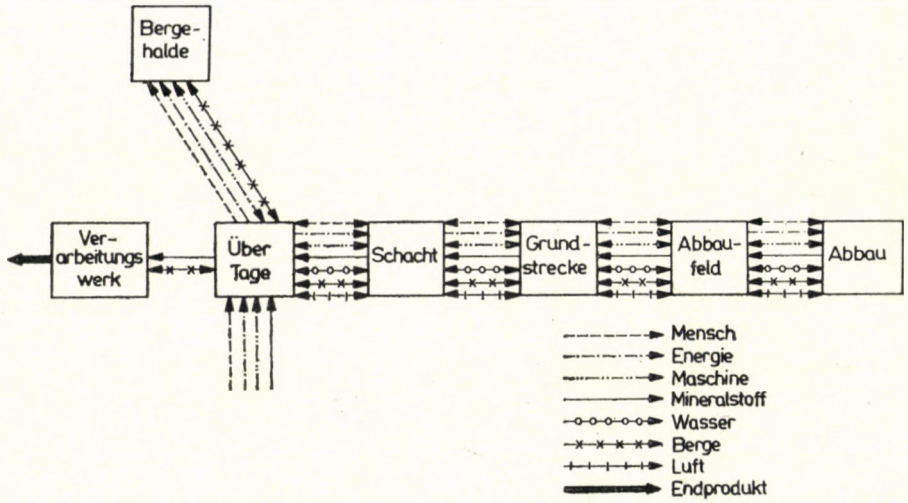


Abb. 1. Technologisches Diagramm des Tiefbau-Abbauverfahrens

zuverlässigkeit des einen oder anderen Teilsystems (Abbaubetrieb, Abbaufeld, usw.) die Arbeitszuverlässigkeit des ganzen Systems in hohem Maße verschlechtert. Der größte strukturelle Mangel des Tiefbau-Technologiesystems aber besteht vielleicht darin, daß im Vergleich zum Abbau (den Abbaubetrieben), als *aktive*, räumlich und zeitlich fortlaufend vorwärtschreitende und das Mineralprodukt liefernde Grubenräume das *inaktive*, zur Grubenförderung, Wetterführung und sonstigen Zwecken dienende, lange Zeit hindurch offen- und instandgehaltene Streckennetz zu groß bemessen ist. Trotzdem in letzter Zeit in den Tiefbaugruben eine sehr intensive Gewinnungskonzentration durchgeführt, und in Extremfällen sogar das Prinzip »ein Abbau — eine Grube« verwirklicht wurde, ist doch im Verhältnis der aktiven zu den inaktiven Grubenräumen eine Änderung nach Größenordnung nicht zu verzeichnen.

Die Entropie einer hochkonzentrierten, stark mechanisierten Tiefbaugrube kann um den Preis materieller und finanzieller Aufwendungen beträchtlich vermindert werden. Ein starkes Senken der Entropie des Grubenbetriebes ist aber auch mit erheblichen Gefahren verbunden, denn die Grube wird dadurch anfälliger gegen unerwartete Ereignisse (Verbruch, Grubenbrand, Wassereinbruch, Schlagwetter- und Gasexplosionen, usw.) bzw. gegen Betriebsstörungen an Maschinen und sonstigen Einrichtungen. Mit dem Bilden einer entsprechenden Betriebsreserve (an Abbauorten, Geräten, Einrichtungen u.dgl.) kann man aber die Störungsanfälligkeit der Grube auf Kosten von zusätzlichen Anschaffungen stark vermindern.

Die Höhe der Investitionskosten hängt von der Förderkapazität des Betriebes ab. Die Investitionskosten für Großleistungs-Grubenbetriebe über 10 000 t/Tag Förderleistung können selbst die Summe von 5—10 Milliarden

Forint erreichen. Hingegen werden die Betriebskosten von der Struktur und Belegung des Grubenbetriebes bestimmt. Doch selbst in günstigem Fall sind die Betriebskosten einer Tiefbaugrube mindestens doppelt so hoch, wie die des Tagebaus.

Im Tiefbau-Kohlenbergbau kann die Abbauleistung selbst 50 t pro Mann und Schicht, im Erzbergbau 100 t/MS erreichen. Die Kopfleistungen für Gesamtbetrieb aber sind je nach der Systemstruktur selbst bei hochgradiger Mechanisierung nicht wesentlich höher als die gegenwärtigen Kennziffern 4 t/MS bzw., 10 t/MS.

Bei den aus immer größeren Teufen fördernden Schächten werden in den Schachtsicherheitspfeilern immer größere, nutzbare Mineralvorräte vorübergehend oder endgültig blockiert. Diese in den Schachtpfeilern gebundenen Vorräte können in manchen Fällen 20—30% oder mehr des gesamten bauwürdigen Mineralvorrates betragen. Durch ein umsichtiges Anlegen der Schächte können zwar die blockierten Mineralvorräte wesentlich verringert werden, doch als Gegenposten steigt dann die Länge der Hauptaufschlußstrecken, ihre Kosten für Ausfahrung und Instandhaltung, sowie die Kosten der Grubenförderung.

Die direkten Abbauverluste der Tiefbaugruben betragen bei Normalbetrieb meist 10—15%. Bei Raubbau können sie sogar 30—40% erreichen. Bei tiefbaumäßigem Abbau flözartiger Lagerstätten beträgt die Verdünnung 5—10%. Bei Vorkommen mit komplizierterem geologischen Aufbau aber, wo eine selektive Gewinnung nicht, oder nur zum Teil zu verwirklichen ist, kann die Verdünnung selbst 15—20% erreichen.

Die technische Entwicklung ist bei Tiefbau in erster Linie durch Erhöhung der Tagesförderung je Abbauort (auf 5000—10 000 t/Tag), durch Verkürzung des inaktiven Streckennetzes, bzw. durch eine verstärkte Verbreitung der teil- oder vollautomatischen Abbaubetriebe zu erwarten.

Die überwiegende Mehrzahl der *Tagebaue* arbeitet in der ganzen Welt meist als Zielbergwerke, d.h. als an einen Großverbraucher (elektrisches Wärmekraftwerk, Zentralaufbereitung, chemisches Kombinat, usw.) eng angeschlossener Großbetrieb. Der im Tagebau gewinnbare Mineralvorrat — der 100—200 Mill. t beträgt, manchmal aber auch mehrere Milliarden Tonnen betragen kann —, wird in erster Linie durch die ökonomische Lebensdauer des verarbeitetenden (verbrauchenden) Zielbetriebes bestimmt.

Die Grenztiefe der Tagebaugewinnung wird durch das sog. Abraumverhältnis bestimmt; in unserem Lande 1:5. Doch im Ausland erreicht dieser Kennwert selbst 1:10. Die Grenztiefe von Tagebauen beträgt in Europa 250—300 m, doch wurden im Kupferbergbau der USA auch Tagebautiefen von 750—800 m erreicht.

Bei Tagebauen zählen die Werke mit 5—10 Mill. t/Jahr Förderung zu den kleinen, die mit 10—20 Mill. t/Jahr Förderung zu den mittleren, und die

Tagebaue mit 20—30 Mill. t/Jahr Förderung zu den Großbetrieben. In naher Zukunft aber wird es schon zum Anlegen solche großer Tagebaue (Hambach, Tscheljabinsk, usw.) kommen, deren Jahresförderung 50—60 Mill. t betragen wird.

Das Erschürfen und Erkunden des Mineralvorrats von Tagebaugruben erfolgt im allgemeinen schablonenhaft und deswegen in kürzerer Zeit als bei den Tiefbaugruben. Die Planungszeit stimmt bei beiden technologischen Typen ungefähr überein. Bei den Tagebauen beträgt die Dauer der Erschließungsphase, das Herstellen des Einbruchgrabens je nach dem Einsatz an Abraum-Großgeräten ca. 1—2 Jahre. Etwa die gleiche Zeit erfordert ihr Anlaufen auf volle Förderkapazität bzw. der Produktionsauslauf bei Erliegen der Grube. Die Laufzeit bei voller Kapazität aber wird durch die ökonomische Lebensdauer des Betriebs bestimmt.

In Abb. 2 ist das technologische Schaubild des Tagebau-Grubenbetriebes zu sehen. Die Struktur dieses Gewinnungssystems ist prinzipiell weniger kompliziert als die des Tiefbaus, da hier weniger Teilsysteme zusammenwirken. Doch auch bei der tagebaumäßigen Produktionsweise wird die Betriebszuverlässigkeit des technologischen Systems in hohem Maße dadurch beeinflußt, daß seine Teilsysteme (Vorentwässerung, Abraum, Haldenausbildung) gleichfalls eng miteinander gekoppelt sind. Infolgedessen wird durch das schwächere Arbeiten des einen oder anderen Teilsystems das resultierende Gesamtergebnis des Tagebaus stark beeinträchtigt.

Der Tagebau-Bergbau beeinflußt durch Absenken des Wasserspiegels und durch das Abräumen regional, vorübergehend oder endgültig auch die natürlichen Umweltsbedingungen. Als Folge hiervon müssen etwa 60—70% der Tagebau-Gesamtkosten für Räume, Abfördern und Auf-Halde-Kippen der

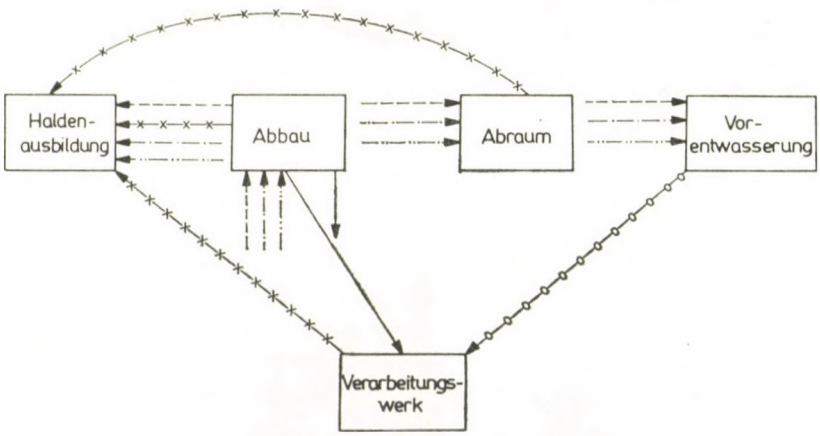


Abb. 2. Technologisches Diagramm des Tagebau-Abbauverfahrens

Abraumberge, für Wiederauffüllung, Planierung und Rekultivierung aufgewendet werden. Durch widrige Witterungsverhältnisse (Regen, Schneefall, Eisbildung, usw.) wird die Arbeit im Tagebau erheblich beeinträchtigt. Allerdings trifft auch zu, daß die in Großtagebauen eingesetzen Großgeräte gegen Leistungsschwankungen durch ungünstige Witterung weniger anfällig sind und bei entsprechender Arbeitsorganisation eventuelle Ausfälle leichter ausgleichen können.

Die Investitionskosten der Tagebaue können wegen der größeren Kapazität und des Einsatzes gewaltiger Großgeräte im Vergleich zu den Tiefbaugruben ein Mehrfaches betragen; hingegen belaufen sich die Betriebskosten nur auf die Hälfte oder ein Drittel.

Bei Tagebauen erreicht die produktive Leistung 100—150 t/MS, die Kopfleistung des ganzen Betriebes aber 10—20 t/MS oder noch mehr. Durch ein besseres Ausnützen der großen Maschinenkapazitäten kann man hier die Leistungen viel elastischer erhöhen, als im Tiefbau.

Tagebau fördern mit nicht mehr als 5—10% Abbauverlusten. Bei tagebaumäßigem Abbau homogener flözartiger Vorkommen bleibt die Verdünnung des Rohmaterials durch Berge meist unter 5%, doch kann bei Vorhandensein starker und zahlreicher Zwischenmittel dieser Kennwert auch 15—20% erreichen.

Die technologische Entwicklungstendenz weist bei Tagebauen in der Richtung der hochleistungsfähigen Großgeräte, z.B. Maschineneinheiten von 100 000—200 000 t/Tag Kapazität, Förderbänder von 3 m Breite und 5—6 m/s Fahrgeschwindigkeit, direkt austragende Abraumabsetzgeräte mit 150—250 m Austragsweite. Andererseits rückt das automatisierte, optimal in Einklang gebrachte Zusammenarbeiten dieser Großgeräte immer mehr in den Vordergrund.

Bei dem *Unterwasser-Bergbau* (auf Sand, Kies, Kohle, u.dgl.) wird der optimal gewinnbare Mineralvorrat eines Betriebes entweder durch die natürlichen Gegebenheiten, oder durch die wirtschaftlichen Anforderungen des Verbrauchers bestimmt.

Dieses abbautechnologische System wird zur Zeit bei den heimischen Vorkommen körniger Mineralgrundstoffe in größeren Abbautiefen als 50—60 m nicht angewendet. Im Ausland aber wird bei einigen marinen Lagerstätten diese Art der Gewinnung sogar bei 100—200 m und noch größeren Lagerungstiefen mit Erfolg angewendet. In letzter Zeit ist international eine sehr intensive Forschungs- und Entwicklungsarbeit im Gange, um das Unterwasser-Abbauverfahren zur Gewinnung der in mehreren tausend Meter Wassertiefe am Meeresgrund gelagerten Mineralvorkommen einzusetzten.

In Abb. 3 ist das technologische Schaubild des Unterwasser-Mineralabbaus dargestellt. Der große Vorteil dieses technologischen Verfahrens besteht darin, daß dabei die direkten Bergbau-Arbeitsprozesse (Gewinnung,

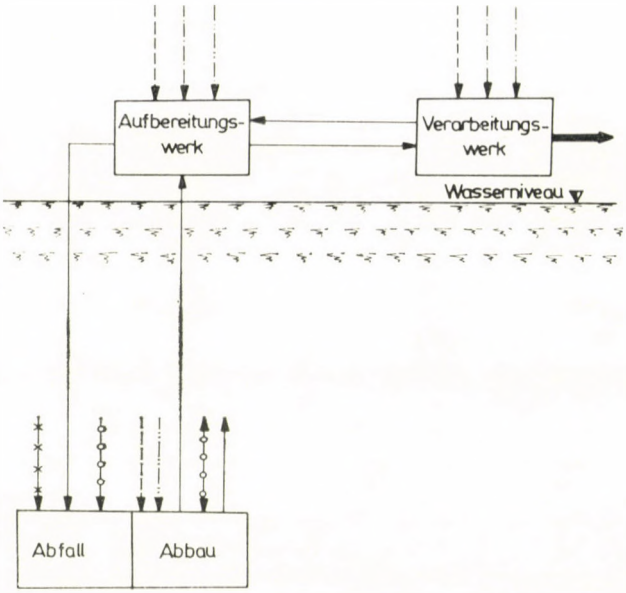


Abb. 3. Technologisches Diagramm des Unterwasser-Abbaus

Ladung, Förderung, usw.) und die Arbeitsprozesse der Aufbereitung (Klassierung, Zerkleinerung, Anreicherung, usw.) nach einem einfachen Stammbau miteinander gekoppelt werden können.

Die Produktionskapazität wird hier in erster Linie von der Maschinenleistung des Schwimmbaggers (1000—2000 t/Tag) bestimmt. Durch den Einsatz weiterer Schwimmbagger und Aufbereitungseinheiten kann die Förderkapazität des Betriebs verhältnismäßig einfach erhöht werden.

Bei dem Unterwasser-Abbau erfolgt die Erkundung meist mit geophysikalischen Methoden, und auch die Projektierung kann relativ einfacher und in kürzerer Zeit durchgeführt werden, als bei den vorerwähnten bergbaulichen Abbausystemen. Die Phasen der Grubenerschließung und Förderung schließen sich eng aneinander an. Infolgedessen beträgt der Gesamtzeitbedarf des Unterwasser-Mineralabbaus — von der Erkundung bis zum Anlauf auf volle Kapazität — nicht mehr als 1,5—3 Jahre. Dabei dauert die An- und Auslaufsperiode nur einige Monate.

Die Betriebsstruktur ist sehr einfach; deswegen sind auch die Fehlermöglichkeiten kleiner als die der anderen abbautechnologischen Systeme.

Der normale Betriebsablauf ist besonders im Winter durch die Witterung behindert. Bei der Mineralgewinnung unter Wasser ist die Umweltschädigung nur gering. Die nach dem Abbau zurückbleibenden Teiche und Seen können zu landwirtschaftlichen Zwecken, als Erholungsstätten oder zur Trinkwasserversorgung ausgenützt werden.

Die Investitionskosten betragen nur einen Bruchteil jener Kosten, die hierfür bei Tiefbau- oder Tagebaugruben aufgewendet werden müssen. Beim Einsatz von Schwimmbaggern oder Schlammpumpen von gutem Wirkungsgrad und einer kleinen Belegschaftszahl können auch die Betriebskosten wesentlich niedriger gehalten werden, als in den Tagebau- und Tiefbaubetrieben.

Die produktive Leistung beträgt beim Unterwasser-Abbau 100—150 t/MS; die Kopfleistung kann selbst 20—25 t/MS erreichen.

Die Abbauverluste sind bei umsichtig geführtem Abbau kleiner als 10%. Die Verdünnung aber kann ganz vernachlässigt werden, da das Trennen der Berge durch verschiedene Mineralaufbereitungsverfahren in direktem Anschluß an die Arbeitsprozesse der Gewinnung sofort erfolgen kann.

Bei dem Unterwasser-Abbau ist die zukünftige technologische Entwicklung in erster Linie auf das Erreichen größerer Abbautiefen, andererseits auf eine Leistungssteigerung der Abbaugeräte (Schwimmbagger) ausgerichtet.

Die *Bohrloch-Abbautechnologie* wird gegenwärtig hauptsächlich zur Gewinnung von fluiden Grundstoffen (Wasser, Erdöl, Erdgas, usw.) angewendet. Hierbei wird die Größe der mit einem Bohrloch gewinnbaren Mineralvorratsmenge in erster Linie durch die naturgegebene oder künstlich intensivierte Schichtenenergie bestimmt.

Bei der Gewinnung *fester Mineralstoffe mittels Bohrungen* muß in der ursprünglichen Lagerstätte der Aggregatzustand des Materials verändert werden. Hierzu kommen in der Praxis gewöhnlich die folgenden Verfahren zur Anwendung: [1, 2, 3, 4, 5, 6, 7].

a) physikalisches Lösen oder Schmelzen (beim Abbau von Steinsalz- und Schwefel-Lagerstätten)

b) hydraulisches Auswaschen und Bilden einer Trübe (zum Abbau von Sand-, Kies-, Kohlenlagerstätten u.dgl.)

c) Auslaugen oder das regulierte Lösen mit Anwendung von physikalischen, chemischen, biologischen Prozessen (z.B. das in situ In-Lösung-Bringen von sulfidischen Erzlagerstätten, Uranvorkommen)

d) Vergasung (Verbrennen von Erdöl, Ölschiefer und Kohlenflözen in ihren ursprünglichen Lagestätten).

Bei dem Bohrloch-Abbau von festen Mineralgrundstoffen durch Umwandlung des Aggregatzustandes beträgt die auf eine Produktionseinheit entfallende Fördermenge 50—100 t/h. Die Gleichmäßigkeit der Sicherung der Förderkapazität wird jedoch durch die natürlichen Gegebenheiten in hohem Maße beeinflußt; deswegen ist es zweckmäßig, mehrere Bohrlöcher gleichzeitig zu betreiben.

Die Gesamtproduktionszeit wird wesentlich dadurch verkürzt, daß die Erkundungsbohrungen bei Fündigkeit in kurzer Zeit (einigen Wochen oder Monaten) zu Fördersonden umgestaltet werden können.

Das technologische Schaubild des Bohrloch-Abbaus fester Mineralgrundstoffe ist in *Abb. 4* zu sehen. In der Struktur stimmt es mit dem des Unterwasser-Abbausystems überein. Diese Technologie kann vor allem dann mit Vorteil zum Einsatz kommen, wenn sich unmittelbar an die Gewinnung die Mineralaufbereitung, bzw. die Verarbeitung zu Endprodukten anschließt:

Ein großer Vorteil des Bohrloch-Abbaues besteht darin, daß sich das Verfahren elastisch den Umweltbedingungen anzupassen vermag. Dies äußert sich nicht nur in der geringeren Wirkung der naturgemäßen Bedingungen auf den Bohrloch-Abbau, sondern in der von dieser Abbauweise auf die Umwelt ausgeübten, gut regulierbaren Wirkung.

Ein großer Teil der Investitionskosten erwächst aus der Herstellung der Bohrlöcher und der Anschaffung der Fördereinrichtungen. Die Armaturen der Bohrlöcher können öfter wiedergewonnen und neuverwendet werden, die notwendige Bohrausrüstung aber macht sich relativ schnell bezahlt. Die direkten Betriebskosten stimmen etwa mit den Betriebskosten des Unterwasser-Abbaus überein.

Wegen des geringen Bedarfs an Bedienungspersonal kann die produktive Leistung 100—150 t/MS, die Gesamtbetrieb-Kopfleistung aber selbst 15—20 t/MS erreichen.

Die Abbauverluste können bei dem Bohrloch-Abbau 30—50% betragen. Diese Kennwerte aber können sich bei dem Abbau solcher Mineralvorräte oder Vorratsteile, die mit keiner der anderen Abbautechnologien technisch real durchgeführt werden könnten, noch immer als rentabel erweisen. Wird die Mineralaufbereitung in der Nähe des Gewinnungsortes angelegt, dann wird

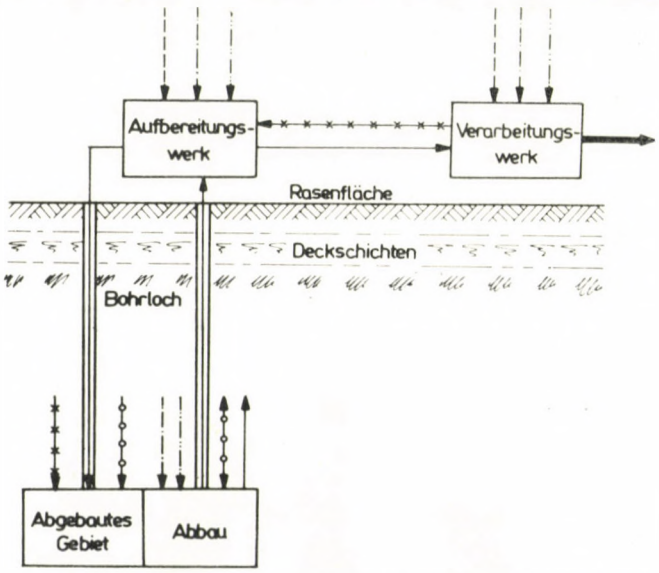


Abb. 4. Technologisches Diagramm des Bohrloch-Mineralabbaus

durch die Verdünnung das technisch-wirtschaftliche Ergebnis, welches mit der Bohrloch-Abbautechnologie und Veränderung des Aggregatzustandes erzielt werden kann, nicht wesentlich beeinflußt.

Zur Verbreitung des Bohrloch-Abbaus fester Mineralgrundstoffe müssen in erster Linie die entsprechenden Bohr-, Gewinnungs- und Fördereinrichtungen entwickelt werden, ferner der mit diesen Geräten erreichbare Wirkungsradius und Wirkungstiefe erhöht werden.

In Ungarn werden von den vier grundlegenden Abbautechnologien zur Zeit der Tiefbau, der Tagebau und der Unterwasser-Abbau in weitem Umfang betrieben. Mit dem Tiefbauverfahren erfolgt der Abbau der meisten Kohle- und Erzvorkommen, während die Tagebau-Technologie zur Gewinnung der Lignitlagerstätten und von Bauindustriestoffen (Kalkstein, Dolomit) zur Anwendung kommt. Der Unterwasser-Abbau wird zur Gewinnung von Sand, Kies und sonstigen Mineralvorkommen von körniger Struktur durchgeführt. Der Bohrloch-Abbau aber wird bei uns nur zur Erdöl-, Erdgas- und Wassergewinnung betrieben.

Bei den am Lehrstuhl für Bergbaukunde an der Technischen Universität für Schwerindustrie (Miskolc) in den vergangenen Jahren durchgeführten umfassenden analytischen Untersuchungen kamen wir zu der Schlußfolgerung, daß sich in Ungarn die reale Möglichkeit bietet, mehrere Varianten des Bohrloch-Abbauverfahrens mit Veränderung des Aggregatzustandes auch zum Abbau fester Mineralgrundstoffe heranzuziehen. Zur in situ-Auslaugung der Erzlagerstätten kann es in Recsk und im Mecsek kommen. Die unterirdische Vergasung von Kohlenflözen kann am einfachsten beim Abbau der jungen Kohlenvorkommen im Bodva-Tal verwirklicht werden. Dort kann nämlich das aus der Kohle gewinnbare Gas in unmittelbarer Nähe des Gewinnungsortes zu chemischen oder energetischen Zwecken verwertet werden [3, 7].

Neben diesen erwähnten Möglichkeiten bin ich der Meinung, daß sich der Bohrloch-Abbau fester Mineralgrundstoffe am wirksamsten bei der hydraulischen Auswaschung unserer unter dem Karstwasserspiegel anstehenden Bauxit-Linsen verwirklichen läßt. Auch in technischer und ökonomischer Hinsicht ist dieses heute und in nächster Zukunft eines unserer brennendsten Probleme, nämlich für den erfolgreichen Abbau der unter dem Wssserspiegel anstehenden beträchtlichen Bauxitvorräte eine gute bergbauliche Lösung zu finden.

Möglichkeiten des Abbaus von Bauxitlinsen mit dem hydraulischen Bohrloch-Abbauverfahren

In Abb. 5 ist die Prinzipskizze des hydraulischen Bohrloch-Abbaus einer Bauxitlinse dargestellt. Bei diesem Verfahren wird in die Bohrlöcher ein doppeltes Rohrsystem eingebaut. Über das eine Rohrsystem gelangt das zur

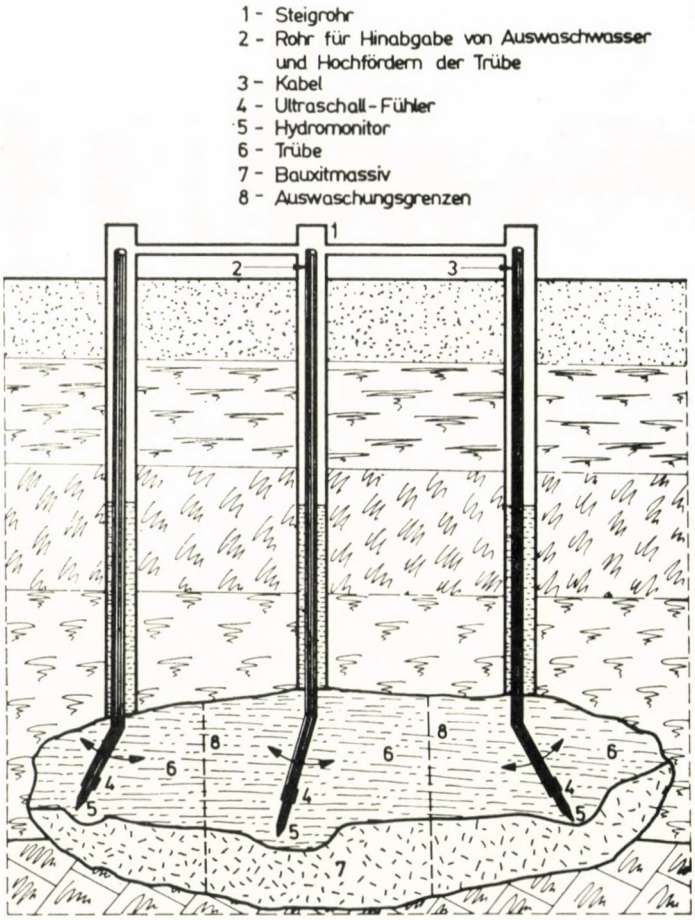


Abb. 5. Prinzipskizze des hydraulischen Bohrloch-Abbaus einer Bauxitlinse

Gewinnung benötigte Waschwasser auf die Bohrlochsohle, während über das andere Leitungssystem der schon gelöste Vorrat als Arbeitstrübe zu Tage gefördert, und der am Bohrloch errichteten Aufbereitungsrichtung aufgegeben wird.

Zur erfolgreichen praktischen Anwendung der mit hydraulischer Auswaschung arbeitenden bohrlochmäßigen Bauxitgewinnung müssen noch folgende grundlegende Aufgaben gelöst werden [3, 7]:

a) Innerhalb der für den Abbau vorgesehenen Bauxitlinse muß die Druckrohrleitung teleskopartig und verdrehbar ausgestaltet werden, um sich bei der Bewegung des, die Gewinnung verrichtenden Hydromonitors der Form der Bauxitlinse anpassen zu können.

b) Die in das Bohrloch niedergelassenen Hydromonitore müssen mit einem Ultraschall-Suchgerät versehen werden, um möglichst viel Bauxit-

material und je weniger Nebengestein hereinzuwaschen. Das schnellere Sedimentieren der sich beim Auswaschen bildenden feinen Kolloidteilchen soll durch Zugabe geeigneter Koagulationsmittel gefördert werden.

Die wichtigsten technischen Vorzüge des hydraulischen Bohrloch-Abbaus von Bauxitlinsen können wie folgt zusammengefaßt werden:

1. Der Abbau des Mineralkörpers kann in seiner ursprünglichen Lagerstätte »mannlos« (ohne Beisein von Bergleuten am Arbeitsstoß) verwirklicht werden.

2. Zur Durchführung des Abbaus ist hier die sehr kostspielige aktive Absenkung des Wasserspiegels nicht erforderlich.

3. Für einen Ausbau des durch Abbau entstandenen Hohlraumes braucht nicht gesorgt zu werden, da das an Stelle des abgeförderten Materials eindringende Wasser die Senkbewegung des Hangendgebirges einigermaßen abschwächt.

4. Aus dem Abbauraum kann das gelöste Fördergut über die Austragsrohre auf kürzestem Wege zu Tage gebracht werden. Mit alledem kann ein sehr einfaches, dem Kohlenwasserstoffbergbau ähnliches abbautechnologisches System geschaffen werden.

5. Das beim Abbau in die geschaffenen Hohlräume eingedrungene Wasser kann man zum Gewinnen, Abfördern und Aufbereiten des nutzbaren Mineralgrundstoffes in geschlossenem Kreislauf verwenden.

6. An das Förderbohrloch können nach Abb. 6 die Mineralaufbereitungseinrichtungen direkt angeschlossen werden, sodaß von diesen nunmehr das Konzentrat zu den Tonerdefabriken befördert werden muß. Das Bergematerial aber kann auf kürzestem Wege in den ausgewaschenen Hohlraum zurückgespeist, und damit auch die Vorschriften für Umweltschutz verhältnismäßig billig erfüllt werden.

In Abb. 7 wird die Möglichkeit für zeitlich und räumlich straffe Kopplung der verschiedenen Arbeitsphasen: Erkundung, Gewinnung und Auflassung des Mineralvorkommens veranschaulicht.

7. Da man die Gewinnungseinrichtungen verhältnismäßig schnell und leicht zu anderen Verwendungsstellen umsetzen kann, können auch räumlich stark gegliederte, oder zerklüftete Bauxitkörper mit kleinem Mineralvorrat wirtschaftlich abgebaut werden. Es kann sogar der sekundäre, mehrmalige Abbau jener Gebiete verwirklicht werden, die schon früher mit herkömmlichen Bergbautechnologien (Tiefbau, Tagebau) in Förderung standen.

8. Die Arbeitsprozesse der Gewinnung, Abförderung und Mineralaufbereitung können komplex automatisiert werden; auch die Betriebslenkung durch Rechenanlagen kann hier einfacher ausgestaltet werden.

Doch auch das Bohrloch-Abbauverfahren hat seine kennzeichnenden Grenzfaktoren, die seine praktische Einsatzmöglichkeit in technischer Hinsicht ziemlich begrenzen.

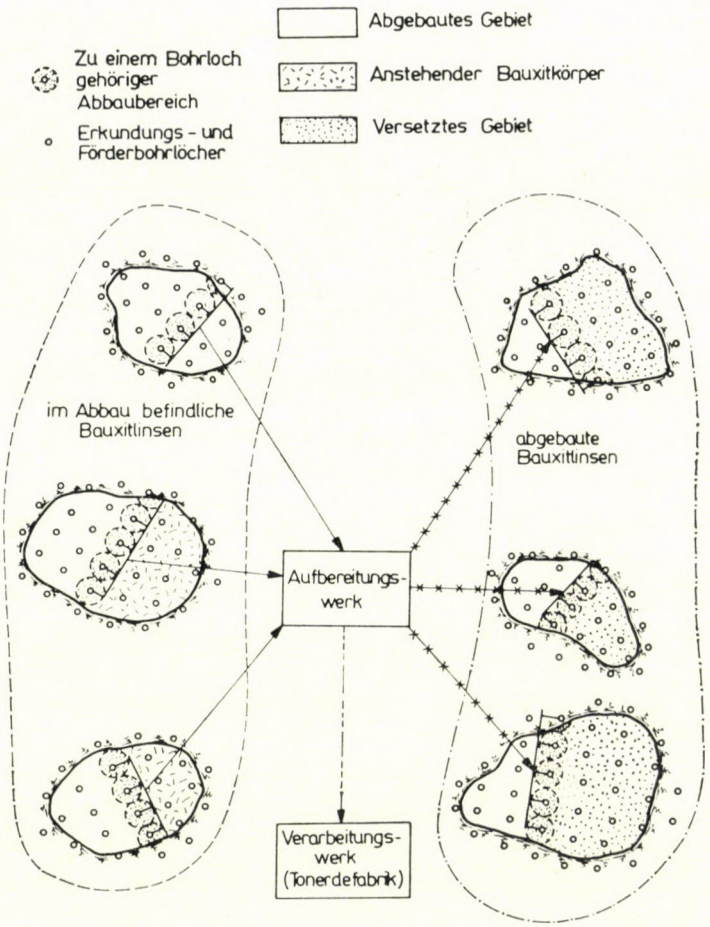


Abb. 6. Das hydraulische Auswaschen und Verarbeiten einer Bauxit-Linsengruppe durch Anlegen einer ortsveränderlichen Aufbereitungseinrichtung

Die wichtigsten dieser Faktoren sind folgende:

a) Mit einem Bohrloch kann nur ein verhältnismäßig kleiner Mineralvorrat gewonnen werden, da der Wirkungsradius des effektiven Abbaus aus technisch-ökonomisch-sicherheitstechnischen Gründen zur Zeit den Wert von 8—15 m nicht überschreitet. Deswegen kommt das Bohrloch-Abbauverfahren nur beim Abbau solcher Bauxitkörper in Frage, deren Mächtigkeit mehr als 5 m beträgt.

b) Bei kleineren Bohrgeschwindigkeiten kann die Zeitquote der Erschließung und Gewinnung der Bauxitlinsen ungünstiger als bei den herkömmlichen Abbauverfahren sein.

c) Da sich auf der Bohrlochsohle, d.h. am Abbaustoß Menschen nicht aufhalten, können die direkten Arbeitsprozesse der Gewinnung und Ab-

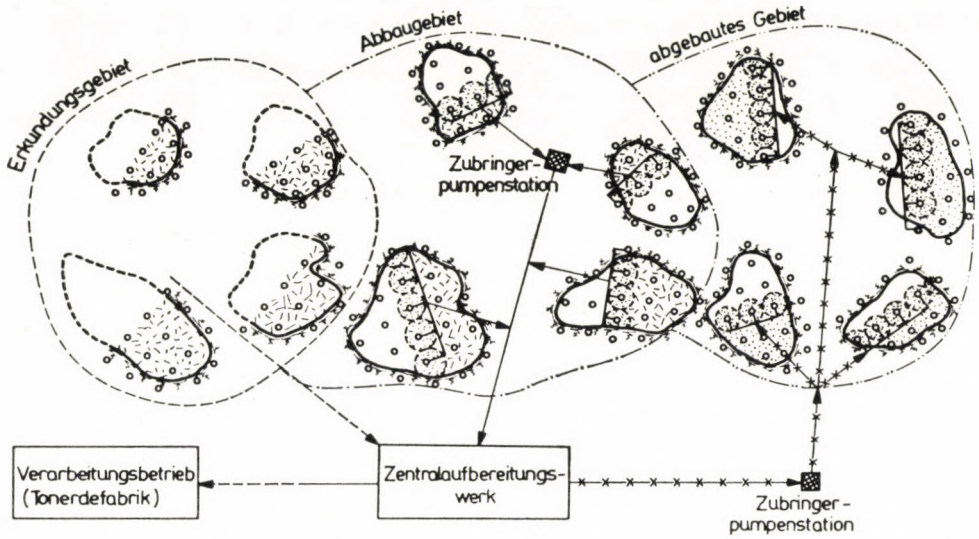


Abb. 7. Das Koppeln verschiedener bergbaulicher Gewinnungsprozesse zum hydraulischen Bohrloch-Abbau einer Bauxitlinsengruppe

förderung schwerer geregelt werden. Als Folge hiervon zeigt die auf die Zeiteinheit entfallende Förderung erhebliche quantitative und qualitative Schwankungen.

Bestimmung der Hauptparameter des Bohrloch-Abbauverfahrens

In der vorliegenden Abhandlung werden die Hauptparameter des Bohrloch-Abbauverfahrens für einen solchen Fall untersucht, bei welchem die anderen Abbauverfahren (Tiefbau, Tagebau, Unterwasser-Abbau) wegen des geringen Mineralvorrates oder der räumlich zerstreuten Lagerung aus technisch-ökonomischen Gründen real nicht in Frage kommen können. In solchen Fällen können die zweckmäßigen (optimalen) Hauptparameter des Bohrloch-Abbauverfahrens durch eine Gegenüberstellung des Wertes (Weltmarktpreises), des geförderten Mineralproduktes, und der beim Abbau erwachsenen Kosten festgestellt werden.

Die wichtigsten Parameter des Bohrloch-Abbauverfahrens sind nach Abb. 8 der Abbau-Wirkungsradius (R) und die Abbautiefe (H). Ihr günstiger (optimaler) Wert kann durch solche technisch-wirtschaftliche Berechnungen ermittelt werden, die sich auf ein Bohrloch, eine Bohrlochgruppe oder auf den Bohrloch-Abbau ganzer Abbaufelder beziehen können. Durch diese Aufteilung wird im Wesen der Kreis der in Rechnung zu stellenden Objekte und Kosten erweitert. In jedem beliebigen Fall zusammengesetzter Lagerung aber können die Kosten in entsprechenden Anteilen auf die einzelnen Bohrlöcher verteilt

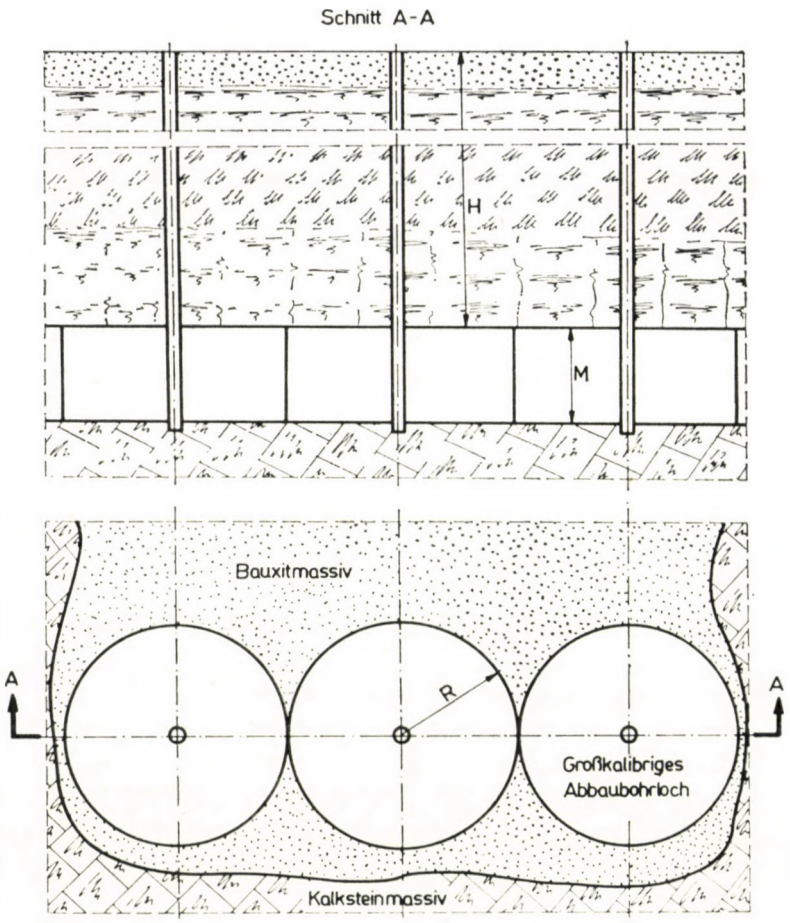


Abb. 8. Skizze zur Bestimmung der Hauptparameter des Bauxitabbaus

werden. Deswegen soll nun, um die grundsätzlichen Zusammenhänge markanter herauszustellen, hier weiterhin nur mit jenen direkten Kosten gerechnet werden, die sich auf die Ausbildung und den Betrieb nur eines Produktions-Bohrloches beziehen [4, 5, 6, 7].

Die Gesamtkosten für Ausgestaltung und Betrieb eines großkalibrigen Förderbohrloches können wie folgt aufgeschrieben werden:

$$K = K_b + K_{\ddot{u}} \qquad \text{(Ft)}$$

Hierin sind die gesamten Investitionskosten:

$$K_b = (H + M) \cdot k_f \quad \text{(Ft)},$$

worin

H Tiefe der Firste des Mineralvorkommens unter der Rasendecke (in m)

M Lagerstättenmächtigkeit (in m)

k_f gesamte spezifische Investitionskosten zur Ausbildung des Förderbohrloches und Ausstattung mit den Einrichtungen für betriebsmäßiges Fördern (in Ft/m) bedeuten.

Die Betriebskosten beim Abbau des gewinnbaren Mineralvorrates innerhalb des Wirkungsradius (R) aber können aus folgender Beziehung errechnet werden:

$$K_{\ddot{u}} = t \cdot q_t \cdot k_{\ddot{u}} = Q \cdot k_{\ddot{u}} = R^2 \cdot \pi \cdot M \cdot \gamma \cdot \zeta_f \cdot k_{\ddot{u}} = R^2 \cdot \delta_f \cdot k_{\ddot{u}} \quad \text{(Ft)}.$$

Hierin sind:

t — Gewinnungszeit (in Tagen)

q_t — Förderkapazität (in t/d)

$k_{\ddot{u}}$ — Selbstkosten des Bohrloch-Mineralabbaus (in Ft/t)

γ — Volumengewicht des gewonnenen Mineralgrundstoffes (in t/m^3)

ζ_f — Gewinnungsfaktor bei Bohrloch-Abbau

$\delta_f = M \cdot \pi \cdot \gamma \cdot \delta_f$ regionaler Produktivitätskennwert des Bohrloch-Abbaus (in t/m^3)
(In der Berechnung wurden der Einfachheit halber die Flözproduktivität und Flözmächtigkeit als vom Abbau-Wirkungsradius unabhängige Größen angenommen, während sie in Wirklichkeit von diesem Parameter abhängig sind.)

Bei der Bestimmung der Hauptparameter des Bohrloch-Abbaus soll von einer einfachen wirtschaftlichen Bedingungen ausgegangen werden, nämlich davon, daß der Wert des gewonnenen Mineralvorrates mindestens gleich sei allen jenen Kosten, die zur Gewinnung des Vorrats erforderlich sind. Diese Bedingung ist eigentlich das Prinzip der Erzielung des Null-Gewinns. In Wirklichkeit trachtet man natürlich danach, den Gewinn zu maximieren, d.h. im Wert des geförderten Vorrates ein Mehrfaches der Ausgaben einzubringen. Wieviel aber letzten Endes der erzielbare Gewinn betragen wird, entscheidet die Gesamtheit der naturgegebenen, technischen, wirtschaftlichen und sicherheitstechnischen Einflußgrößen.

Als einfachster Fall sei angenommen, daß

$$K = K_{\acute{e}} \text{ (in Ft) ist,}$$

wobei

$$K_{\acute{e}} = R^2 \cdot \delta_f \cdot k_{\acute{e}} \text{ (Ft)}$$

den Wert des gewinnbaren Mineralvorrates bedeutet, wobei $k_é$ den Verkaufspreis (Weltmarktpreis) der Einheitsmenge des gegebenen Mineralgrundstoffes (in Ft/t) bedeutet. Der Weltmarktpreis kann aus verschiedenen Gründen erheblich schwanken. Deswegen muß sorgfältig erwogen werden, in welcher Periode der Weltmarktpreis-Schwankung es zweckdienlich ist, den besagten Mineralvorrat abzubauen. In Konjunkturperioden können auch Mineralvorräte von schlechter Güte noch wirtschaftlich abgebaut werden. Bei Dekonjunktur aber kann ein Bremsen der Förderung, eventuell ein Fördern auf Depot die wirtschaftliche Lösung sein.

Die Bedingung für Kostengleichheit kann detailliert wie folgt aufgeschrieben werden:

$$(H + M) \cdot k_f + R^2 \cdot \delta_f \cdot k_ü = R^2 \cdot \delta_f \cdot k_é \quad \text{(in Ft)}.$$

Hieraus ergibt sich der minimale Abbau-Wirkungsradius, bei dem die Kosten für Bohrloch-Abbau eben noch hereingebracht werden können:

$$R_{\min} = \sqrt{\frac{(H + M) \cdot k_f}{\delta_f \cdot (k_é - k_ü)}} \quad \text{(in m)}.$$

Ist der effektive Abbau-Wirkungsradius des Bohrloch-Abbaus $R > R_{\min}$, dann ist auch dieses Abbauverfahren in jeder Hinsicht wirtschaftlich.

Die Grenztiefe des Bohrloch-Abbaus kann wie folgt berechnet werden:

$$H_{\max} = \frac{R^2 \cdot \delta_f (k_é - k_ü) + M \cdot k_f}{k_f} \quad \text{(in m)}.$$

Das Bohrloch-Abbauverfahren ist dann ökonomisch, wenn für die effektive Abbautiefe die Ungleichheit $H < H_{\max}$ besteht.

In der Praxis trachtet man natürlich danach, daß bei dem Bohrloch-Abbau nach Möglichkeiten der Betrag $n \Sigma K$ Kosten hereingebracht werde. Mit Berücksichtigung eines mehrfachen Kostenrücklaufs kann der minimale Abbau-Wirkungsradius und die minimale Abbautiefe mit folgender Formel ausgedrückt werden.

$$R_{\min} \geq \sqrt{\frac{n(H + M) \cdot k_f}{\delta_f \cdot (k_é - k_ü)}} \quad \text{(in m)},$$

beziehungsweise

$$H_{\max} \leq \frac{R^2 \cdot \delta_f \cdot (k_é - k_ü) + n \cdot M \cdot k_f}{n \cdot k_f} \quad \text{(in m)},$$

worin

$n > 1$ Rücklaufsfaktor der Kosten bedeutet.

Um die grundsätzlichen Zusammenhänge besser zu erläutern, wurden in Abb. 9—14 die Diagramme aufgrund von Daten aus der Praxis entworfen. Zu ihrer Anfertigung wurde mit folgenden, für unseren heimischen Bauxitbergbau kennzeichnenden Grunddaten gerechnet:

$$M = 20 \text{ m}; \quad \delta_f = 54 \text{ t/m}^2; \quad k_f = 300 \text{ Ft/t}$$

$$k_{\ddot{u}} = 250 \text{ Ft/t}; \; k_f = 5000 - 30\,000 \text{ Ft/m}.$$

In Abb. 9 ist die Änderung des Abbau-Wirkungsradius des Bohrloch-Abbaus als Funktion der spezifischen Bohrlochausbildungskosten und des Gewinnes dargestellt.

Abb. 10 zeigt den Verlauf der Abbaugrenztiefe in Abhängigkeit vom Abbau-Wirkungsradius und den spezifischen Kosten für Niederbringen des Bohrloches. Es ist gut zu erkennen, daß die Abbautiefe umso größer sein kann, je größer der Abbau-Wirkungsradius und je kleiner die Niederbringungskosten des Bohrloches sind.

Abb. 11 zeigt die Gestaltung des Abbau-Wirkungsradius des Bohrloch-Abbaus als Funktion der Abbaugrenztiefe und des spezifischen Gewinns. Man sieht, daß bei einer gegebenen Abbaugrenztiefe der Abbau-Wirkungsradius um so kleiner sein kann, je größer der Gewinn ist.

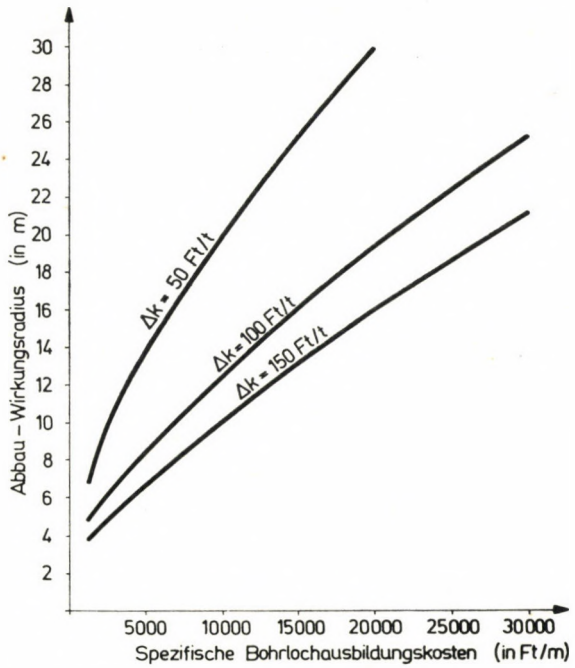


Abb. 9. Änderung des Abbau-Wirkungsradius als Funktion der spezifischen Bohrloch-Ausbildungskosten und des Gewinns

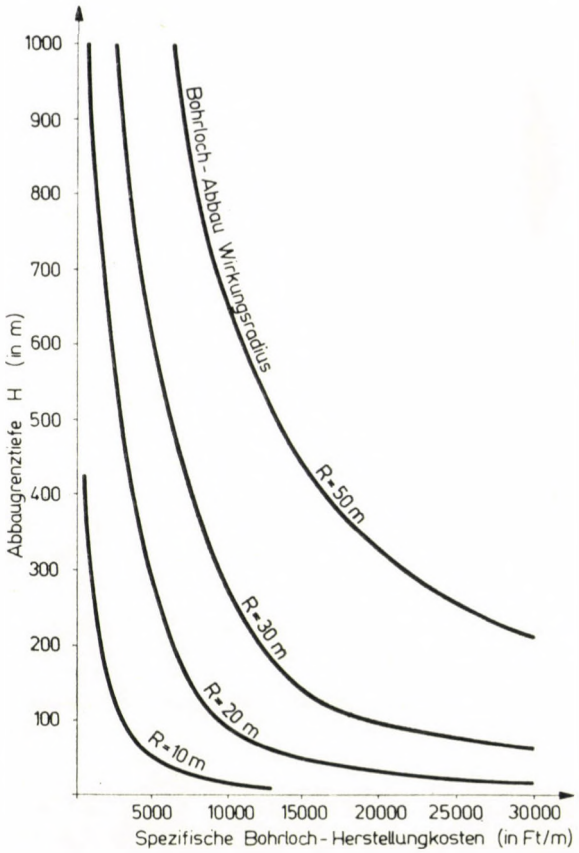
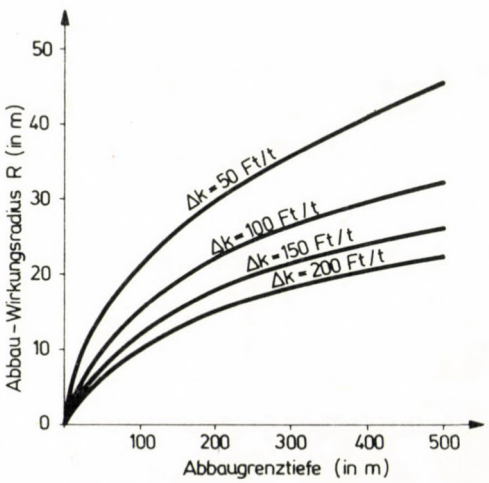


Abb. 10. Änderung der Abbaugrenztiefe als Funktion der spezifischen Kosten für Herstellung des großkalibrigen Bohrloches und des Abbau-Wirkungsradius



k_f = 30000 Ft/m
ξ_f = 0.8
M = 20 m

Abb. 11. Änderung des Wirkungsradius des Bohrloch-Abbaus als Funktion der Abbaugrenztiefe und des spezifischen Gewinns

In Abb. 12 ist die Änderung des Abbau-Wirkungsradius als Funktion der Flözmächtigkeit und des spezifischen Gewinns dargestellt. Hier ist es etwas überraschend, daß bei einem gegebenen spezifischen Gewinn sich der Abbau-Wirkungsradius bis etwa 20 m Flözmächtigkeit schnell ändert, während er darüber praktisch konstant verläuft.

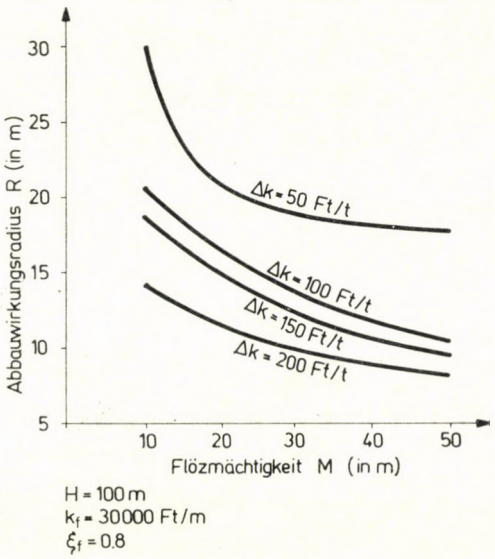


Abb. 12. Änderung des Wirkungsradius des Borhloch-Abbaus als Funktion der Flözmächtigkeit und des spezifischen Gewinns

Abb. 13 zeigt die Änderung des Abbau-Wirkungsradius des Bohrloch-Abbaus als Funktion der Flözmächtigkeit und des Abbaufaktors. Es ist gut zu sehen: Bis $\zeta_f = 0{,}7$ nimmt der Abbau-Wirkungsradius des Bohrloch-Abbaus nur wenig zu. Selbst wenn $\zeta_f = 0{,}5$ ist, muß der Wirkungsradius des Bohrloch-Abbaus nur um 20—30% erhöht werden, um einen minimalen Gewinn zu erzielen.

Bei gegebener Flözmächtigkeit, Lagerungstiefe und Abbau-Wirkungsradius kann der minimale Abbaufaktor aus folgender Beziehung berechnet werden

$$\xi_{f\min} = \frac{(H + M) \cdot k_f}{R^2 \cdot \pi M \cdot \gamma \cdot (k_é - k_ü)},$$

beziehungsweise bei einem n-fachen Kostenrücklauf

$$\xi_{f\min} = \frac{n(H + M) \cdot k_f}{R^2 \cdot \pi M \cdot \gamma \cdot (k_é - k_ü)}.$$

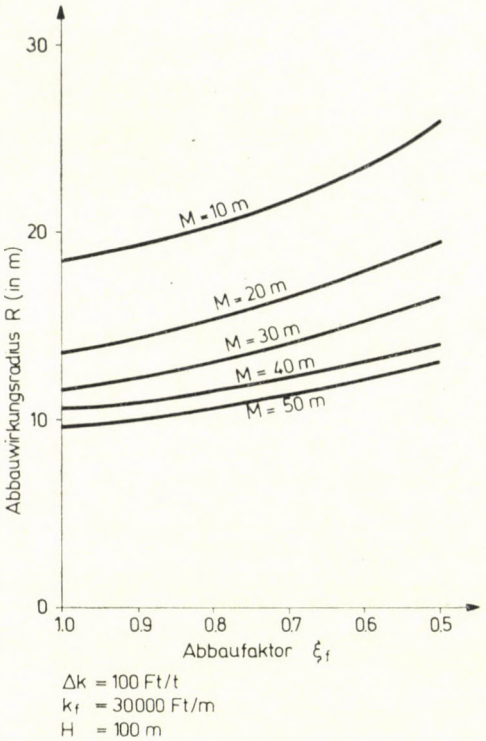


Abb. 13. Änderung des Abbauwirkungsradius des Bohrloch-Abbaus als Funktion der Flözmächtigkeit und des Abbaufaktors

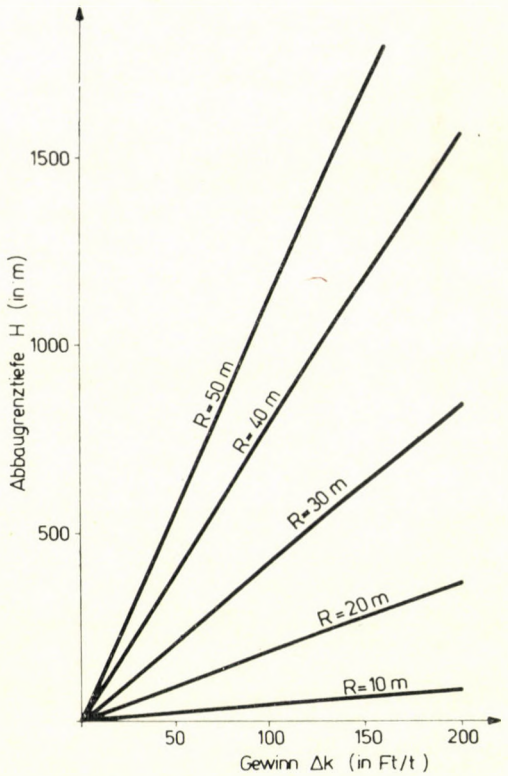
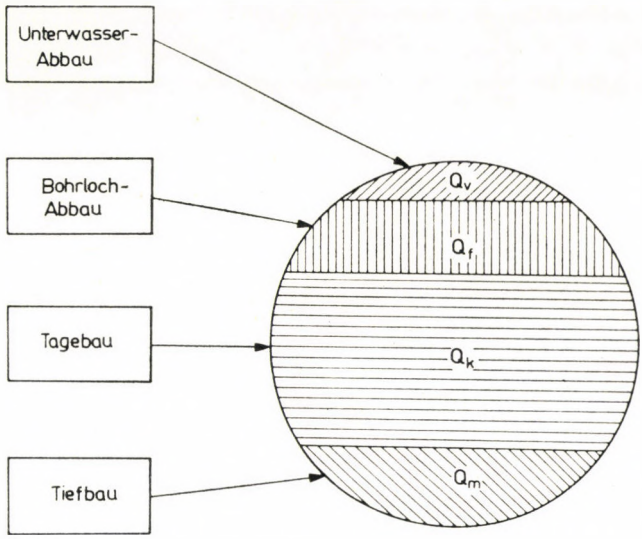


Abb. 14. Änderung der Grenztiefe des Bohrloch-Abbaus als Funktion des Abbauwirkungsradius und des Gewinns

Abb. 14 veranschaulicht die Gestaltung der Grenztiefe des Bohrloch-Abbaus als Funktion des spezifischen Gewinns und des Abbau-Wirkungsradius. Es ist gut zu sehen: Je größer bei einem gegebenen spezifischen Gewinn der Abbau-Wirkungsradius ist, aus umso größerer Tiefe kann mit dem Bohrlochabbauverfahren noch wirtschaftlich gefördert werden.

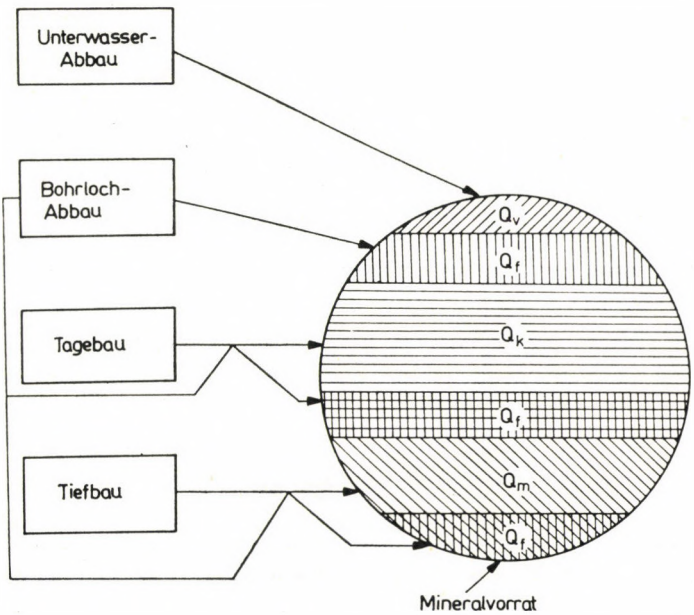
Die Anwendbarkeit kombinierter Abbauverfahren

In unserem Bauxitbergbau besteht auch die Möglichkeit zur Anwendung kombinierter Abbautechnologien. Dies kann beim Abbauen eines gegebenen Vorkommens nach Abb. 15 räumlich und zeitlich getrennt, oder nach Abb. 16 sich aufeinander stützend durchgeführt werden. Die bestentwickelte Variante einer Kopplung bergbaulich-technologischer Abbausysteme ist letztere Lösung; damit kann nämlich ein viel vollständigerer Abbau und wirtschaftlicherer



$$Q_v + Q_f + Q_k + Q_m = \Sigma Q$$

Abb. 15. Skizze der zergliederten Anwendung von Abbausystemen zum Abbau eines gegebenen Mineralvorrates



$$Q_v + \Sigma Q_f + Q_k + Q_m = \sum \Sigma Q$$

Abb. 16. Skizze der Anwendung von sich aufeinander stützenden Abbausystemen zum Abbau eines gegebenen Mineralvorrates

Verbrauch erzielt werden als mit den herkömmlichen Abbauverfahren [3, 4, 5, 6, 7].

Der große Vorzug des Bohrloch-Abbauverfahrens besteht nämlich darin, daß es sich am elastischesten allen anderen bergbau-technologischen Systemen anpassen kann. Der Bohrloch-Abbau kann gleichermaßen von der Tagesoberfläche aus, dem Förderhorizont der Tagebaue, oder von dessen Restmulden, bzw. vom Streckennetz der Tiefbaugruben ausgehend durchgeführt werden. Es besteht auch die Möglichkeit, daß Vorräte, die bei dem herkömmlichen Abbaubetrieb in der Grube verlorengingen, durch neuerlichen Abbau mit dem Bohrloch-Abbauverfahren wirtschaftlich gewonnen werden können.

Bei den bisherigen Darlegungen wurde angenommen, daß die selbständige, oder kombinierte Anwendung der verschiedenen technologischen Abbauverfahren nur auf einen einzigen mineralischen Grundstoff (Bauxit) beschränkt sei. Bei unseren heimischen Bauxitvorkommen aber besteht auch die Möglichkeit, aus mehreren Komponenten (Sand, Wasser, Kohle, Bauxit, Kalkstein, Ton, usw.) bestehende Mineralmassive abzubauen. In solchen Fällen kann dann die Integration der technologischen Systeme, nämlich der Gewinnung, Mineralaufbereitung und Verarbeitung auf höchster Stufe verwirklicht werden.

SCHRIFTTUM

1. Arens, V. Zs.: Geotechnologija. Moskva, 1971.
2. Arens, V. Zs.: Geotechnologitscheskie metodü dobütschi polesnüh iskopaemüh. Isd. »Nyedra«, Moskva, 1975.
3. Zambó, J. u. Mitarb.: Geotechnikai bányaművelési módszerek alkalmazási lehetőségei hazai szilárd ásványelőfordulásaink kitermelésére (Die Anwendungsmöglichkeiten für geotechnische Grubenabbauverfahren zum Abbau heimischer Vorkommen von festen Mineralgrundstoffen). Forschungs-Abschlußbericht. Lehrstuhl für Bergbaukunde an der NME (Techn. Universität für Schwerindustrie). Miskolc, 1975.
4. Patvaros, J.: Új típusú bányászati technológiai rendszer alkalmazási lehetőségei hazai bauxit előfordulásaink kitermelésében (Anwendungsmöglichkeiten neuartiger technologischer Abbausysteme zum Abbau unserer heimischen Bauxit-Vorkommen). *NME-Mitteilungen*, I. Folge: Bergbau. 22 (1976), 237—251.
5. Patvaros, J.: Fúrólyukas bányaművelési rendszer alkalmazási lehetőségei hazai ásványelőfordulásaink kitermelésében (Anwendungsmöglichkeiten des Bohrloch-Abbauverfahrens zum Abbau heimischer Mineralvorkommen). Akademischer Forschungswettbewerb, 1976, 75.
6. Patvaros, J.: Geotechnikai (fúrólyukas) bányaművelési módszerek alkalmazási lehetőségei ércelőfordulások kitermelésére (Anwendungsmöglichkeiten geotechnischer [Bohrloch-] Abbauverfahren zum Abbau von Erzvorkommen). BKL (Berg- u. Hüttenmännische Blätter), Folge: Bergbau, 1976, Heft 9, 589—598.
7. Patvaros, J. u. Mitarb.: Ásványi nyersanyagok geotechnikai és geokémiai termelési módszerei (Geotechnische und geochemische Verfahren zur Gewinnung mineralischer Rohstoffe). OMFB (Landeskommission für Technische Entwicklung). Studie, 1976.

ВОЗМОЖНОСТЬ ПРИМЕНЕНИЯ ТЕХНОЛОГИИ ЭКСПЛУАТАЦИИ СКВАЖИНАМИ ПРИ ДОБЫЧЕ ОТЕЧЕСТВЕННЫХ БОКСИТОВЫХ МЕСТОРОЖДЕНИЙ

Й. ПАТВАРОШ

РЕЗЮМЕ

Традиционные методы добычи боксита из-за понижения активного уровня воды сопровождаются все большими технико-экономическими трудностями. Это препятствие может быть преодолено или существенно уменьшено при помощи одного нового гидравлического горного метода — эксплуатации скважинами. В статье подробно рассматриваются гидравлические технические сборудования при этом методе, а также определение важных для этого метода оптимальных параметров (как радиус действия и предельная глубина разработки).

RECENSIO

H. Moritz—H. Sünkel:

Approximation methods in geodesy

Sammlung Wichmann, Neue Folge Bd. 10. Karlsruhe, 1978.
284 pages, 24 figures. 80.— DM.

The volume comprises the main lectures given at the Second International Summer School in the Mountain on Mathematical Methods in Physical Geodesy, held in Ramsau (Austria) in 1977. The topic of the School was "Geodesy and Approximation Theory". The School gave an introduction to advanced least-squares methods in physical geodesy (least-squares collocation), placing them within the general frame of mathematical approximation theory, to present recent results of collocation and to discuss further developments.

The following lectures are published in the volume:

MORITZ, H.: Introduction to Interpolation and Approximation
BALMINO, G.: Introduction to Least-Squares Collocation
SCHWARZ, K. P.: On the Application of Least-Squares Models to Physical Geodesy
RAPP, R. H.: Results of the Application of Least-Squares Collocation to Selected Geodetic Problems
TSCHERNING, C. C.: Introduction to Functional Analysis with a View to Its Applications in Approximation Theory
KRARUP, T.: Some Remarks about Collocation
BJERHAMMAR, A.: A Review of Discrete Methods in Physical Geodesy
GRAFAREND, E. W.: Operational Geodesy

MORITZ gives the mathematical frame of interpolation and approximation. BALMINO presents the collocation from the point of view of least-squares estimation. SCHWARZ and RAPP discuss the practical aspects of collocation and present a number of recent practical applications. TSCHERNING provides an introduction to the advanced theory of functional analyses. It gives a view on contemporary developments in collocation and related fields. KRARUP discusses the non-standard aspects of collocation. BJERHAMMAR gives a review of an alternative method of the collocation. GRAFAREND's paper discusses the synthesis of different solutions.

We hope that the volume is useful for scientists in the geodesy and in surveying. It is the first introduction in this field and so it will find a great interest by the geodesist.

We have to express our thanks to the authors and to the publishing company Wichmann for the very quick edition and publishing.

Halmos F.

INDEX

Halmos, F.: Some problems of the connection of networks deduced from satellite observations and of terrestrial networks 405

Hristov, W. K.: Ausgleichung einer mehrmals beobachteten Nivellierungsstrecke nach Bedingungen 417

Bobok, E.—Somosvári, Zs.: Mechanical erosion in flow channels of rocks 421

Patvaros, J.: Feasibility of combined mining technological systems in production of mineral massifs 437

Patvaros, J.: Die Anwendungsmöglichkeiten der Bohrloch-Abbautechnologie bei der Gewinnung der heimischen Bauxitvorkommen 449

Recensio

Moritz, H.—Sünkel, H.: Approximation methods in geodesy — *F. Halmos* 473

Printed in Hungary

A kiadásért felel az Akadémiai Kiadó igazgatója. Műszaki szerkesztő: Zacsik Annamária

A kézirat nyomdába érkezett: 1979. II. 8. — Terjedelem: 6,30 (A/5) ív, 29 ábra

79.6790 Akadémiai Nyomda, Budapest — Felelős vezető: Bernát György

Acta Geodaetica, Geophysica et Montanistica, eine Halbjahresschrift der Ungarischen Akademie der Wissenschaften, veröffentlicht Originalbeiträge aus dem Bereich der Geodäsie, Geophysik und des Bergbaus in deutscher, englischer, französischer oder russischer Sprache.

Redaktion: H-9400 Sopron, Múzeum u. 6.

Jahresabonnementspreis: $ 36.00.

Bestellbar bei »Kultura« Außenhandelsunternehmen (1389 Budapest 62, P.O.B. 149) oder seinen Auslandsvertretungen.

Acta Geodaetica, Geophysica et Montanistica est une revue biannuelle de l'Académie Hongroise des Sciences publiant des essais originaux du domaine de la géodésie, géophysique et des sciences minières en français, anglais, allemand ou russe.

Rédaction: H-9400 Sopron, Múzeum u. 6.

Le prix de l'abonnement: $ 36.00 par an.

On peut s'abonner à l'Entreprise du Commerce Extérieur « Kultura » (1389 Budapest 62, P.O.B. 149) ou che ses représentants à l'étranger.

Acta Geodaetica, Geophysica et Montanistica выходят два раза в год в издании Академии наук Венгрии. В журнале публикуются оригинальные исследования по проблемам геодезии, геофизики и горного дела на русском, английском, немецком и французском языках.

Адрес редакции: H-9466 Sopron, Múzeum u 6.

Подписная цена на год: $ 36,00.

Заказать журнал через Внешнеторговое предприятие «Kultura» (1389 Budapest 62, P. O. B. 149) или через его заграничные представительства.

Reviews of the Hungarian Academy of Sciences are obtainable at the following addresses:

AUSTRALIA
C.B.D. LIBRARY AND SUBSCRIPTION SERVICE, Box 4886, G.P.O., *Sydney N.S.W. 2001*
COSMOS BOOKSHOP, 145 Ackland Street, *St. Kilda (Melbourne), Victoria 3182*

AUSTRIA
GLOBUS, Höchstädtplatz 3, *1200 Wien XX*

BELGIUM
OFFICE INTERNATIONAL DE LIBRAIRIE, 30 Avenue Marnix, *1050 Bruxelles*
LIBRAIRIE DU MONDE ENTIER, 162 Rue du Midi, *1000 Bruxelles*

BULGARIA
HEMUS, Bulvar Ruszki 6, *Sofia*

CANADA
PANNONIA BOOKS, P.O. Box 1017, Postal Station "B", *Toronto, Ontario M5T 2T8*

CHINA
CNPICOR, Periodical Department, P. O. Box 50 *Peking*

CZECHOSLOVAKIA
MAD'ARSKÁ KULTURA, Národní třida 22, *115 66 Praha*
PNS DOVOZ TISKU, Vinohradská 46, *Praha 2*
PNS DOVOZ TLAČE, *Bratislava 2*

DENMARK
EJNAR MUNKSGAARD, Norregade 6, *1165 Copenhagen*

FINLAND
AKATEEMINEN KIRJAKAUPPA, P. O.Box 128, *SF-00101 Helsinki 10*

FRANCE
EUROPÉRIODIQUES S. A., 31 Avenue de Versailles, *78170 La Celle St-Cloud*
LIBRAIRIE LAVOISIER, 11 rue Lavoisier, *75008 Paris*
OFFICE INTERNATIONAL DE DOCUMENTATION ET LIBRAIRIE, 48 rue Gay-Lussac, *75240 Paris Cedex 05*

GERMAN DEMOCRATIC REPUBLIC
HAUS DER UNGARISCHEN KULTUR, Karl-Liebknecht-Strasse 9, *DDR-102 Berlin*
DEUTSCHE POST ZEITUNGSVERTRIEBSAMT, Strasse der Pariser Kommüne 3—4, *DDR-104 Berlin*

GERMAN FEDERAL REPUBLIC
KUNST UND WISSEN ERICH BIEBER, Postfach 46, *7000 Stuttgart 1*

GREAT BRITAIN
BLACKWELL'S PERIODICALS DIVISION, Hythe Bridge Street, *Oxford OX1 2ET*
BUMPUS, HALDANE AND MAXWELL LTD., Cowper Works, *Olney, Bucks MK46 4BN*
COLLET'S HOLDINGS LTD., Deningston Estate, *Wellingborough, Northants NN8 2QT*
WM. DAWSON AND SONS LTD., Cannon House, *Folkestone, Kent CT19 5EE*
H. K. LEWIS AND CO., 136 Gower Street, *London WC1E 6BS*

GREECE
KOSTARAKIS BROTHERS, International Booksellers, 2 Hippokratous Street, *Athens-143*

HOLLAND
MEULENHOFF-BRUNA B.V., Beulingstraat 2, *Amsterdam*
MARTINUS NIJHOFF B.V., Lange Voorhout 9—11, *Den Haag*
SWETS SUBSCRIPTION SERVICE, 347b Heereweg, *Lisse*

INDIA
ALLIED PUBLISHING PRIVATE LTD., 13/14 Asaf Ali Road, *New Delhi 110001*
150 B-6 Mount Road, *Madras 600002*
INTERNATIONAL BOOK HOUSE PVT. LTD., Madame Cama Road, *Bombay 400039*
THE STATE TRADING CORPORATION OF INDIA LTS., Books Import Division, Chandralok, 36 Janpath, *New Delhi 110001*

ITALY
EUGENIO CARLUCCI, P.O. Box 252, *70100 Bari*
INTERSCIENTIA, Via Mazzé 28, *10149 Torino*
LIBRERIA COMMISSIONARIA SANSONI, Via Lamarmora 45, *50121 Firenze*
SANTO VANASIA, Via M. Macchi 58, *20124 Milano*
D. E. A., Via Lima 28, *00198 Roma*

JAPAN
KINOKUNIYA BOOK-STORE CO. LTD., 17-7 Shinjuku-ku 3 chome, Shinjuku-ku, *Tokyo 160-91*
MARUZEN COMPANY LTD., Book Department, P.O. Box 5050 Tokyo International, *Tokyo 100-31*
NAUKA LTD. IMPORT DEPARTMENT, 2-30-19 Minami Ikebukuro, Toshima-ku, *Tokyo 171*

KOREA
CHULPANMUL, *Phenjan*

NORWAY
TANUM-CAMMERMEYER, Karl Johansgatan 41—43, *1000 Oslo*

POLAND
WĘGIERSKI INSTYTUT KULTURY, Marszałkowska 80, *Warszawa*
CKP I V ul. Towarowa 28 *00-958 Warszawa*

ROUMANIA
D. E. P., *Bucureşti*
ROMLIBRI, Str. Biserica Amzei 7, *Bucureşti*

SOVIET UNION
SOJUZPETCHATJ — IMPORT, *Moscow*
and the post offices in each town
MEZHDUNARODNAYA KNIGA, *Moscow G-200*

SPAIN
DIAZ DE SANTOS, Lagasca 95, *Madrid 6*

SWEDEN
ALMQVIST AND WIKSELL, Gamla Brogatan 26, *101 20 Stockholm*
GUMPERTS UNIVERSITETSBOKHANDEL AB, Box 346, *401 25 Göteborg 1*

SWITZERLAND
KARGER LIBRI AG, Petersgraben 31, *4011 Basel*

USA
EBSCO SUBSCRIPTION SERVICES, P. O. Box 1943, *Birmingham*, Alabama *35201*
F. W. FAXON COMPANY, INC., 15 Southwest Park, *Westwood, Mass. 02090*
THE MOORE-COTTRELL SUBSCRIPTION AGENCIES, *North Cohocton, N. Y. 14868*
READ-MORE PUBLICATIONS, INC., 140 Cedar Street, *New York, N. Y. 10006*
STECHERT-MACMILLAN, INC., 7250 Westfield Avenue, *Pennsauken N. J. 080110*

VIETNAM
XUNHASABA, 32, Hai Ba Trung, *Hanoi*

YUGOSLAVIA
JUGOSLAVENSKA KNJIGA, Terazije 27, *Beograd*
FORUM, Vojvode Mišica 1, *21000 Novi Sad*

25. X. 1979 HU ISSN 0374—1842 Index: 26.031